

A Thesis Submitted for the Degree of PhD at the University of Warwick

Permanent WRAP URL:

<http://wrap.warwick.ac.uk/163228>

Copyright and reuse:

This thesis is made available online and is protected by original copyright.

Please scroll down to view the document itself.

Please refer to the repository record for this item for information to help you to cite it.

Our policy information is available from the repository home page.

For more information, please contact the WRAP Team at: wrap@warwick.ac.uk

**Investigation of the molecular and cellular
mechanisms of *in vitro* phage therapy in human cells
and the innate immune response against
Escherichia coli K1 and bacteriophage K1F**

Christian Møller-Olsen

Submitted for the degree of Doctor of Philosophy

School of Life Science

University of Warwick

May 2021

Table of Contents

Acknowledgements	<i>i</i>
Declaration	<i>ii</i>
Inclusion of Published Work	<i>iii</i>
Abstract	<i>iv</i>
List of Abbreviations	<i>v</i>
List of Figures	<i>ix</i>
List of Tables	<i>xiv</i>
Chapter 1 Introduction	<i>1</i>
1.1 A brief history of antibiotics	<i>1</i>
1.2 The emergence of antibiotic-resistant bacteria	<i>2</i>
1.3 A brief history of phage therapy	<i>4</i>
1.4 Biology of bacteriophages	<i>5</i>
1.5 Bacteria and phages co-existence	<i>8</i>
1.6 Bacterial resistance to phages	<i>8</i>
1.7 Bacteriophage interactions with mammalian cells	<i>10</i>
1.8 Current standing of phage therapy	<i>12</i>
1.9 Influence of endotoxins in phage therapy	<i>16</i>
1.10 Diseases of interest	<i>17</i>
1.10.1 Urinary tract infections	<i>17</i>
1.10.2 Neonatal bacterial meningitis	<i>19</i>
1.11 The <i>in vitro</i> model system	<i>21</i>
1.11.1 Bacteriophage K1F	<i>22</i>
1.11.2 <i>Escherichia coli</i> K1	<i>23</i>
1.11.3 Transitional epithelial cells.....	<i>24</i>
1.11.4 Cerebral endothelial cells.....	<i>25</i>

1.12	Mechanisms of entry and degradation	26
1.12.1	Bacterial entry into mammalian cells	27
1.12.2	Viral entry into mammalian cells	28
1.12.3	Phage entry into mammalian tissue and cells.....	30
1.12.4	Degradation pathways	31
1.12.5	Molecules involved in degradation.....	34
1.12.6	Cytokines associated with pathogen entry	36
1.12.7	Endothelial barrier integrity.....	37
1.13	A brief history of phage engineering.....	39
1.14	Engineering phages with altered or expanded host tropism	40
1.15	Controlling the release of LPS by phage engineering	41
1.16	The aim of this research project	42
Chapter 2	<i>Materials and Methods</i>.....	43
2.1	Bacterial strains and culture	43
2.2	Determination of bacterial concentration	44
2.3	Antibiotic concentrations	45
2.4	Human cell lines and culture	45
2.5	Growth determination of hCMEC cultures.....	47
2.6	Preparation of human cell cultures for experiments.....	47
2.7	Bacteriophage strains.....	47
2.8	Purification of bacteriophages.....	48
2.9	Bacteriophage enumeration.....	49
2.10	Determination of endotoxins in bacteriophage preparations	50
2.11	Determination of bacteriophage host specificity in liquid culture	50
2.12	Transmission electron microscopy.....	50
2.13	Fluorescent immunocytochemical imaging.....	51
2.14	Flow cytometric analysis of bacteriophage invasion in bacteria.....	52
2.15	Flow cytometric analysis of bacteriophage invasion in human cells	53
2.16	Measurements of planktonic bacteria and free phages over time	54

2.17	Quantitative real-time PCR.....	54
2.18	ELISA.....	55
2.19	xCELLigence.....	56
2.20	Preparation of electrocompetent bacterial cells.....	57
2.21	Transformation by electroporation	58
2.22	Polymerase Chain Reaction	58
2.23	GATC Sequencing	61
2.24	Engineering strategy for modifying the phage host tropism.....	61
2.25	Engineering strategy for a replication-deficient phage.....	65
2.26	Integration of g-blocks into cloning vectors	67
2.27	Homologous recombination	68
2.28	Selection for recombinant phages	69
2.29	Integration of sgRNAs in pCas9 vectors	71
2.30	Statistical analysis	73
Chapter 3 <i>Establishing in vitro model systems for phage therapy</i>.....		74
3.1	Bacteriophage K1F display podoviridae morphology	74
3.2	Bacteriophage K1F strains specifically infect <i>E. coli</i> EV36.....	76
3.3	Bacteriophage K1F-GPF exhibit high fluorescence intensity.....	78
3.4	Bacteriophage K1F induces bacterial cell death	80
3.5	Plasmid-based RFP expression variation in <i>E. coli</i> EV36	83
3.6	<i>E. coli</i> EV36 infection of human cells is time- and concentration-dependent... 84	
3.7	Bacteriophage K1F infects intracellular <i>E. coli</i> EV36.....	89
3.8	Human cells influence phage K1F population dynamics.....	91
3.9	Discussion	94
Chapter 4 <i>Uptake and degradation of bacteriophage by human cells</i>.....		98
4.1	<i>E. coli</i> EV36 and phage K1F are degraded by lysosomal enzymes	98
4.2	<i>E. coli</i> EV36 and phage K1F activates LC3-assisted phagocytosis	103

4.3	Phage K1F activates galectin-8 dependent autophagy in T24 cells but not hCMECs	106
4.4	<i>E. coli</i> EV36 and not phage K1F activate ubiquitin-dependent autophagy	109
4.5	Discussion	116
Chapter 5 Phage interactions with human cells.....		121
5.1	<i>E. coli</i> EV36 but not phage K1F induce inflammatory responses in hCMEC cultures	121
5.2	Phage K1F and T7 temporarily decrease hCMEC barrier integrity.....	128
5.3	Phage K1F and T7 do not affect proliferation or morphology of hCMECs	132
5.4	Bacterial lysis releases large amounts of endotoxins during <i>in vitro</i> phage therapy.....	134
5.5	Endotoxin monitoring in reagents and phage preparations	135
5.6	Discussion	136
Chapter 6 Phage engineering		139
6.1	Chimeric phage T7/K1F is present following homologous recombination	139
6.2	Chimeric phage T7/K1F display reduced viability.....	142
6.3	Selection on <i>E. coli</i> BW25113 Δ trxA reduces concentration of wildtype phage T7	145
6.4	Depletion of wildtype phage T7 in the HR_chimera product by CRISPR/Cas9	150
6.5	Engineering of replication-deficient phage K1F.....	154
6.6	<i>E. coli</i> EV36 introduces mutations in RNAP expressing plasmid.....	159
6.7	Isolating replication-deficient phage K1F.....	160
6.8	Discussion	164
Chapter 7 Final discussion		168
7.1	Establishing <i>in vitro</i> model systems for phage therapy	168
7.2	Phage uptake and processing by human cells	169
7.3	Phage influence on the inflammatory responses of hCMEC cultures.....	171

7.4	Phage influence on the barrier integrity of hCMEC cultures.....	172
7.5	Altering the host tropism of phage T7	173
7.6	Engineering of a replication-deficient phage K1F	174
7.7	Future studies	175
Chapter 8	References	177
Chapter 9	Appendix.....	194

Acknowledgements

Firstly, I would like to thank my supervisor, Dr Antonia Sagona, for giving me the opportunity to be part of her lab, the many discussions about science and experimental data, and her guidance and support throughout my PhD. I would also like to thank my second supervisor, Dr Keith Leppard, for his positive engagement and always thoughtful and thorough suggestions and comments.

I have crossed paths with many people over the course of my PhD, and I would like to thank everyone in c126, the Sagona group, the MIBTP cohort, and prep and core facility technicians who has given helpful advice or suggestions along the way or just been a good lab buddy.

I would also like to thank all the contributors of the published work, especially Dr Tamás Fehér and MRes student Toby Ross who have played a big part in generating and understanding data.

Last but not least, I would like to thank my family for their patience and support through all these years. I cannot guarantee that I will be talking less about phages in the future though.

This has been 4.5 fantastic years of gaining knowledge, doing great science and diving into the incredible world of phages. Thank you all!

Declaration

This thesis is submitted to the University of Warwick in support of my application for the degree of Doctor of Philosophy. Unless explicitly stated below, the experimental data presented and discussed in this thesis has been produced by myself and has not been submitted in any previous application for any degree.

- PhD student Veronica Foisor performed staining of phage K1F-GFP with gold-conjugated GFP probe and subsequent electron microscopy imaging.
- MBio student Stanley Ho and Dr Antonia Sagona performed ICC and subsequent imaging of T24 cultures stained with anti-RAB7, anti-Cathepsin-L, and anti-LC3B antibodies.
- MRes student Toby Ross performed, under the co-supervision and guidance of Christian Møller-Olsen, ICC and subsequent imaging of hCMEC cultures stained with anti-RAB7, anti-Cathepsin-L, anti-LC3B, anti-hGalectin-8, and anti-Ubiquitin antibodies.

Inclusion of Published Work

The majority of the experimental data presented and discussed in this thesis has been published or submitted for publishing at the time of thesis submission. The details of each manuscript are provided below and the full manuscripts are included in the appendix.

- “Engineered K1F bacteriophages kill intracellular *Escherichia coli* K1 in human epithelial cells”. Christian Møller-Olsen, Siu Fung Stanley Ho, Ranti Dev Shukla, Tamás Fehér & Antonia P. Sagona. (Research paper) Published December 2018 in Nature Scientific Reports.

The data presented in this manuscript correlates to Chapters 3 and 4.

- “Bacteriophage K1F targets *Escherichia coli* K1 in cerebral endothelial cells and influences the barrier function”. Christian Møller-Olsen, Toby Ross, Keith N. Leppard, Veronica Foisor, Corinne Smith, Dimitris K. Grammatopoulos & Antonia P. Sagona. (Research paper) Published June 2020 in Nature Scientific Reports.

The data presented in this manuscript correlates to Chapters 3, 4 and 5.

- “Advances in engineering of bacteriophages for therapeutic applications”. Christian Møller-Olsen, Gurneet K. Dhanoa, Tamás Fehér & Antonia P. Sagona. (Book chapter) Accepted for publishing March 2021 in “New Frontiers and Applications of Synthetic Biology” by Elsevier.

- “Analysing parallel strategies to alter the host specificity of bacteriophage T7”. Ákos Avramucz, Christian Møller-Olsen, Aurelija Grigonyte, Yanahan Paramalingam, Andrew Millard, Antonia P. Sagona & Tamás Fehér. (Research paper) Submitted for publishing 2021.

The data presented in this manuscript correlates to Chapter 6.

Abstract

The last few decades have seen bacteria becoming increasingly resistant to antibiotic treatment. This is considered a threat to human health and financial stability by global non-governmental organisations (NGOs) and governments alike. As a result, multiple technologies are being pursued to mitigate the effects of antimicrobial resistance, one of which is phage therapy. Phage therapy is a re-emerging technology that exploits the natural enemy of bacteria, the bacteriophage (phage), to treat bacterial infection in humans. Although phages are used extensively in biotechnology and food security industries, research is needed to advance the clinical potential of the technology. This study uses clinically relevant tripartite *in vitro* model systems to investigate the cellular and molecular processes underpinning phage therapy and the interactions between phages and human cells.

It is demonstrated that phage K1F effectively can locate and infect intracellular *E. coli* EV36 in both epithelial (T24) and endothelial (hCMEC) cell lines. Microscopy and flow cytometry experiments further demonstrated that phage K1F is taken up by T24 cells and hCMECs by the endocytic machinery and processed by non-selective and LC3-assisted phagocytosis. In contrast, *E. coli* EV36 uptake activated galectin-8 and ubiquitin-dependent autophagy. The inflammatory responses of hCMEC cultures were analysed by RT qPCR. The analyses demonstrated that phage K1F does not elicit inflammatory measures, while *E. coli* induced expression of cytokines TNF α , IL-6, IL-8, IL-10, or IFN β . Phage intervention of bacteria-infected hCMEC cultures resulted in reduced expression of TNF α and increased expression of IL-6 and IL-8. Temporal measurements of the barrier integrity of hCMEC cultures, using xCELLigence, demonstrated that phages K1F and T7 decrease the impedance of hCMEC cultures, indicating an increase in barrier permeability. This function has the potential to promote immune cell extravasation through capillaries to a site of infection.

Collectively, this study presents valuable experimental *in vitro* data to further the advancement of phage therapy. The data suggests that while human cell lines recognise phages through PRR activation, the response is non-inflammatory with potentially additional clinical benefits.

List of Abbreviations

ADME	absorption, distribution, metabolism, excretion
AMR	antimicrobial resistance
BAM	bacteriophage adherence to mucus
BAVS	Bacterial and Archaeal Viruses Subcommittee
BBB	blood-brain-barrier
bp	base pair
BRED	bacteriophage recombineering of electroporated DNA
CBA	Cytometric Bead Array
CDC	Centres for Disease Control and Prevention
CFU	colony forming units
CNS	central nervous system
CsCl	Caesium Chloride
DAMPs	danger associated molecular patterns
DNA	deoxyribonucleic acid
dsDNA	double-stranded DNA
ECIS	Electric Cell-substrate Impedance Sensing
<i>E. coli</i>	<i>Escherichia coli</i>
ELISA	enzyme-linked immunosorbent assay
EM	electron microscopy
EU	endotoxin unit
ExPEC	extraintestinal pathogenic <i>E. coli</i>
FBS	foetal bovine serum
FDA	Food and Drug Administration
FGF-2	basic fibroblast growth factor (bFGF)
FMT	faecal microbiota transplant
GFP	green fluorescent protein

gp17	gene product 17
hCMEC	human cerebral microvascular endothelial cells
Hfr	high-frequency
HUVEC	human umbilical vein endothelial cells
ICC	immunocytochemical
ICTV	International Committee of the Taxonomy of Viruses
IFN	interferon beta
IL-10	interleukin 10
IL-6	interleukin 6
IL-8	interleukin 8
LAL	Limulus Amebocyte Lysate
LB	lysogeny broth
LC3	microtubule-associated protein 1A/1B light chain 3
LIR	LC3-interacting region
LPS	lipopolysaccharide
MBC	minimal bactericidal concentration
MDR	multidrug resistant
MFI	mean fluorescent intensity
MIC	minimal inhibitory concentration
MOI	multiplicity of infection
MWCO	molecular weight cut-off
NAC	no amplification control
NCAM	neural cell adhesion molecule
NDP52	Calccoco2/Calcium-binding and coiled-coil domain-containing protein 2
NGO	Non-governmental organisation
NTC	no treatment control
OD	optical density
ORF	open reading frame

PAMPs	pathogen associated molecular patterns
PCR	polymerase chain reaction
PEG	polyethylene glycol
PI	propidium iodide
PRR	pattern recognition receptors
RBP	receptor binding protein
RBS	ribosomal binding site
RNA	ribonucleic acid
RNAP	RNA polymerase
RT	room temperature
RT qPCR	real-time quantitative PCR
SD	standard deviation
sgRNA	single guide RNA
SIR	systemic inflammatory response syndrome
SM	sodium-magnesium
SMURF1	SMAD specific E3 ubiquitin protein ligase 1
STEC	Stx-producing <i>E. coli</i>
Stx	Shiga toxin
T24	human urinary bladder epithelial cell line
TBK-1	tank-binding kinase
TEER	trans-endothelial electrical resistance
TEM	transmission electron microscopy
TLR	toll-like receptor
TNF	tumour necrosis factor alpha
TURP	transurethral resection of prostate
UK	United Kingdom
UN	United Nations
UPEC	uropathogenic <i>E. coli</i>

US	United States
UTI	urinary tract infection
WHO	World Health Organisation
wt	wild type
XDR	extensively drug resistant
H&E	hematoxylin and eosin

List of Figures

Figure 1-1. Timeline showing the clinical introduction of new classes of antibiotics..	2
Figure 1-2. Estimation of global causes of deaths	3
Figure 1-3. Timeline showing the development of phage therapy.....	5
Figure 1-4. The four strategies for phage survival and infection.....	6
Figure 1-5. The life cycle of virulent (lytic) and temperate (lysogenic) phages	7
Figure 1-6. The preclinical antibacterial drug pipeline	15
Figure 1-7. The tripartite in vitro model system.....	22
Figure 1-8. The major components of phages belonging to the Podoviridae family...22	
Figure 1-9. Transmission electron micrographs of K1 E. coli isolates.....	23
Figure 1-10. A histological section of a transitional epithelium	25
Figure 1-11. The structure of continuous and fenestrated capillaries	26
Figure 1-12. The endocytic pathways into mammalian cells of bacterial species	28
Figure 1-13. Viral entry pathways into mammalian cells via the endocytic route ...	29
Figure 1-14. Phage entry pathways into mammalian cells.....	30
Figure 1-15. Pathway for eukaryotic phagocytosis and selective autophagy.....	33
Figure 1-16. Role of LC3 in initiation of phagophore elongation.....	35
Figure 1-17. Cell-cell adherence molecules of the endothelium.....	38
Figure 2-1. Standard curve for bacterial growth	45
Figure 2-2. Genome organisation of phage K1F	62
Figure 2-3. Genome organisation of phage T7	62
Figure 2-4. Comparison of amino acid sequences of phage T7 and K1F	63
Figure 2-5. Design overview of the p7_K1F_chimera plasmid	64
Figure 2-6. Design overview of the pT7_gp17 plasmid	65
Figure 2-7. Design overview of the pK1F_RNAP_deletion plasmid	66
Figure 2-8. Design overview of the pK1F_RNAP_optimised	67
Figure 2-9. Selection strategy for recombinant T7/K1F chimeric phage	69
Figure 2-10. Selection strategy for recombinant replication-deficient phage.....	70
Figure 3-1. Negative staining electron micrographs of bacteriophage K1F.....	75

Figure 3-2. A phage preparation before and after equilibrium of the CsCl density gradient	76
Figure 3-3. Host specificity of bacteriophages K1F, K1F-GFP and T7 in liquid culture	77
Figure 3-4. Host specificity of bacteriophages K1F and T7 on solid media	78
Figure 3-5. Assessment of bacteriophage K1F-GFP fluorophore intensity.....	79
Figure 3-6. Confocal images showing hCMECs and T24 cells incubated with phage K1F-GFP	80
Figure 3-7. Confocal images showing bacterial cell death following phage infection over time	81
Figure 3-8. Bacterial cell death following phage infection as measured by flow cytometry	82
Figure 3-9. Plasmid-driven expression of RFP in E. coli EV36	84
Figure 3-10. Confocal images showing hCMECs and T24 cells following infection by E. coli EV36-RFP	85
Figure 3-11. Infection of bacteria in human cells as quantified by image analysis ..	86
Figure 3-12. Infection rates of bacteria in human cells as quantified by flow cytometry	88
Figure 3-13. Bacteriophage infection of intracellular bacteria.....	90
Figure 3-14. Influence of human cells on phage population dynamics	93
Figure 4-1. Colocalisation assay of T24 cells stained with anti-Rab7 antibodies.....	99
Figure 4-2. Colocalisation assay of hCMECs stained with anti-Rab7 antibodies	100
Figure 4-3. Colocalisation assay of T24 cells stained with anti-Cathepsin-L antibodies	101
Figure 4-4. Colocalisation assay of hCMECs stained with anti-Cathepsin-L antibodies	102
Figure 4-5. LysoTracker MFI of hCMECs as quantified by flow cytometry	103
Figure 4-6. Colocalisation assay of T24 cells stained with anti-LC3B antibodies	104
Figure 4-7. Colocalisation assay of hCMECs stained with anti-LC3B antibodies.....	105
Figure 4-8. hLC3B expression in hCMECs as quantified by flow cytometry.....	106
Figure 4-9. Colocalisation assay of T24 cells stained with anti-hGalactin-8 antibodies	107

Figure 4-10. Colocalisation assay of hCMECs stained with anti-hGalactin-8 antibodies	108
Figure 4-11. Quantification of anti-hGalactin-8 co-localisation assay of T24 cells....	109
Figure 4-12. Colocalisation assay of T24 cells stained with anti-NDP52 antibodies	110
Figure 4-13. Colocalisation assay of hCMECs stained with anti-NDP52 antibodies	111
Figure 4-14. Quantification of anti-NDP52 co-localisation assay of T24 cells	112
Figure 4-15. Colocalisation assay of T24 cells stained with anti-Ubiquitin antibodies	113
Figure 4-16. Colocalisation assay of hCMECs stained with anti-Ubiquitin antibodies	114
Figure 4-17. Quantification of anti-Ubiquitin co-localisation assay of T24 cells.....	115
Figure 4-18. Ubiquitin expression of hCMECs as quantified by flow cytometry	116
Figure 5-1. Expression pattern of TNF α by real-time qPCR.....	122
Figure 5-2. Expression pattern of IL-6 by real-time qPCR.....	124
Figure 5-3. Expression pattern of IL-8 by real-time qPCR.....	125
Figure 5-4. Expression pattern of IL-10 by real-time qPCR.....	126
Figure 5-5. Expression pattern of IFN β by real-time qPCR	127
Figure 5-6. Concentration pattern of IL-6 protein by ELISA.....	128
Figure 5-7. Temporal impedance profiling of hCMEC cultures incubated with E. coli EV36.....	129
Figure 5-8. Temporal impedance profiling of hCMEC cultures incubated with phage K1F.....	130
Figure 5-9. Temporal impedance profiling of hCMEC cultures incubated with phage T7.....	131
Figure 5-10. Temporal impedance profiling of hCMEC cultures incubated with E. coli EV36 and phage K1F in combination.....	132
Figure 5-11. Proliferation of hCMEC cultures incubated with phages K1F or T7....	133
Figure 5-12. Morphology of hCMEC cultures incubated with phage K1F or T7	133
Figure 5-13. Endotoxin levels of hCMEC cultures incubated with E. coli EV36 and phage K1F in combination	134

Figure 6-1. Schematic showing the recombination events for recombinant chimeric phage T7/K1F.....	140
Figure 6-2. PCR of the HR_chimera product using primer sets AS080/AS081 and AS072/AS073.....	141
Figure 6-3. PCR of the HR_chimera product using primer sets AS072/AS081 and AS080/AS073.....	142
Figure 6-4. Phage K1F infection on multiple bacterial hosts on solid media.....	143
Figure 6-5. Phage T7 infection on multiple bacterial hosts on solid media.....	144
Figure 6-6. Plaque assays of HR_chimera product on multiple hosts.	146
Figure 6-7. Plaque PCR following infection with the HR_chimera product using primers AS080/AS081.....	148
Figure 6-8. Plaque PCR following infection with the HR_chimera product using primers AS072/AS073.....	149
Figure 6-9. Plaque PCR following infection with the HR_chimera product using primers AS072/AS081.....	150
Figure 6-10. Validation of sgRNAs complementing gene17 of wt phage T7	151
Figure 6-11. Isolation of chimeric phage T7/K1F using CRISPR/Cas9	152
Figure 6-12. PCR testing of plaques on E. coli EV36 + sgRNS2_5 using primers AS080/AS081.....	153
Figure 6-13. PCR testing of plaques on E. coli EV36 + sgRNS2_5 using primers AS072/AS073.....	153
Figure 6-14. PCR testing of plaques on E. coli EV36 + sgRNS2_5 using primers AS072/AS081.....	154
Figure 6-15. Schematic overview of the recombineering events for recombinant replication-deficient phage K1F.....	155
Figure 6-16. Selection of bacterial host for HR of replication-deficient phage K1F	156
Figure 6-17. PCRs of the HR_RNAP product following infection of E. coli EV36 + pK1F_RNAP_deletion by wt phage K1F using primer sets AS103/AS104, AS105/AS106, and AS113/AS114	158
Figure 6-18. Selection of E. coli EV36 + pK1F_RNAP_optimised colonies	159
Figure 6-19. Overnight cultures of E. coli EV36 + pK1F_RNAP_optimised.	160

Figure 6-20. Phage-derived ampicillin resistance of E. coli EV36 infected with the HR_RNAP product	161
Figure 6-21. E. coli EV36 + pK1F_RNAP_deletion infected with the HR_RNAP product.	162
Figure 6-22. HR_RNAP phage selection on E. coli EV36 or E. coli EV36 + pK1F_RNAP_optimised.....	162
Figure 6-23. CRISPR/Cas9 selection of replication-deficient phage K1F.....	164

List of Tables

Table 1-1. Challenges of phage therapy.	14
Table 1-2. Prevalent bacterial pathogens causing uncomplicated UTIs	18
Table 1-3. Prevalent bacterial pathogens causing neonatal bacterial meningitis	20
Table 2-1. Bacterial strains used in this study.	44
Table 2-2. Antibiotic concentrations for bacterial culture and selection.	45
Table 2-3. Composition of SM-buffers for phage purification.....	49
Table 2-4. Antibodies for immunocytochemistry.....	52
Table 2-5. Quantitative real-time PCR primers.....	55
Table 2-6. Default PCR program.	58
Table 2-7. Amplification and screening primers.....	61
Table 2-8. g-blocks and cloning vectors.....	68
Table 2-9. sgRNA pairs for pCas9 integration.....	72
Table 2-10. pCas9 vector primers for PCR testing.	73
Table 3-1. Infection of E. coli EV36-RFP in T24 cells and hCMECs	85
Table 3-2. Infection rates of E. coli EV36-RFP in hCMECs over time.	87
Table 3-3. Infection of E. coli EV36-RFP in hCMECs across concentrations.....	87
Table 3-4. Influence of human cells on phage population dynamics as measured by the concentration of planktonic E. coli EV36.....	92
Table 3-5. Influence of human cells on phage population dynamics as measured by concentration of free phage K1F.....	94
Table 4-1. Summary of LysoTracker MFI of hCMEC cultures.....	103
Table 4-2. Summary of LC3B MFI of hCMEC cultures.....	106
Table 4-3. Summary of Ubiquitin MFI of hCMEC cultures.....	116
Table 4-4. Summary table for Chapter 4	120
Table 5-1. Endotoxin concentration of example phage preparations	135
Table 5-2. Endotoxin concentration of media and reagents	136
Table 6-1. Primer pairs used for PCR testing for chimeric phage T7/K1F.....	141
Table 6-2. Primer pairs used for PCR testing for replication-deficient phage K1F...155	

Chapter 1 Introduction

1.1 A brief history of antibiotics

In 1928, at St. Mary's Hospital, London, after returning from a holiday in Suffolk, Alexander Fleming found that a mould growing on a discarded culture plate had bactericidal properties against staphylococci. He had, in fact, by chance, discovered what later became known as penicillin¹. By the late 1930s, Howard Florey, director of the Sir William Dunn School of Pathology at Oxford University and biochemist Ernest Chain had managed to successfully purify penicillin from *Penicillium notatum* extracts and demonstrated its effectiveness *in vivo* in mice. In February 1941, the first person, an Oxford policeman, was administered penicillium to treat a serious bacterial infection causing abscesses. Due to procurement issues, he died a few weeks later, however clinical success would soon follow².

Penicillin was not the first antibiotic to be discovered or to receive clinical approval; the discovery did however spark the golden age of antibiotic discovery³. A timeline of antibiotic discovery and their clinical introduction is presented in Figure 1-1. During the Second World War, the development of large-scale penicillin production was launched by the UK and US governments in collaboration with industry scientists from Merck & Co, Pfizer & Co, and E.R. Squibb & Sons among others. By the end of the 1950's, the lessons learned in the discovery and production of penicillin had facilitated the discovery of more than a handful of principal antibiotics still in use today including streptomycin, chloramphenicol and cephalosporins⁴.

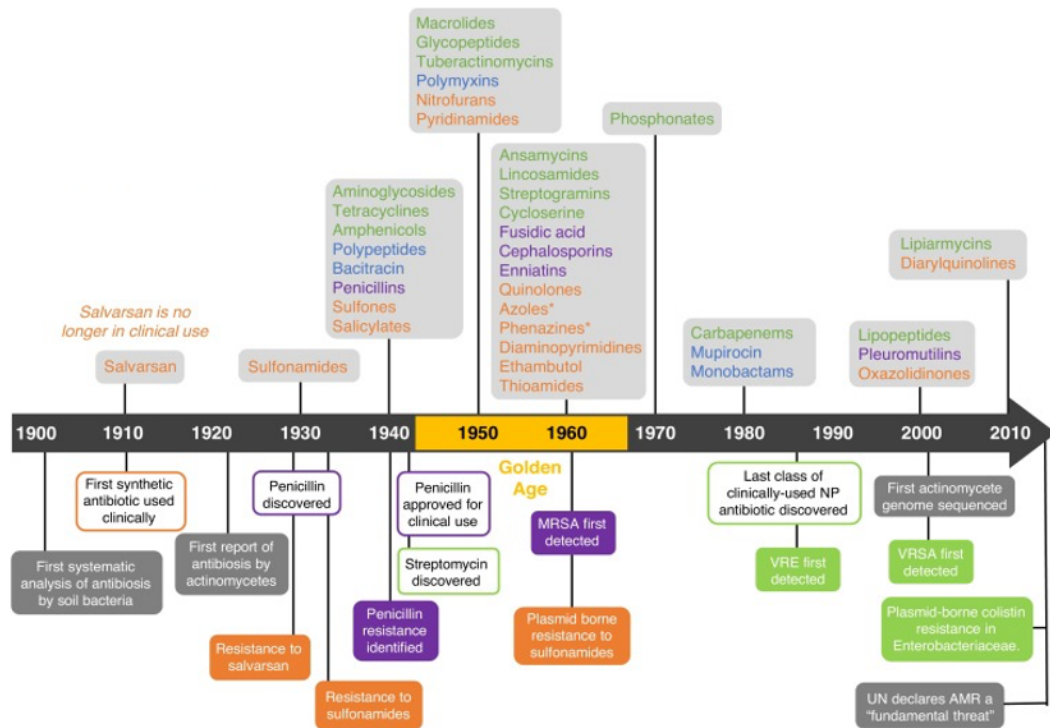


Figure 1-1. Timeline showing the clinical introduction of new classes of antibiotics per decade (above) with key dates in antibiotic discovery and the identification of antimicrobial resistance (below). Actinomycete natural products shown in green, other bacterial natural products in blue, fungal natural products in purple, and synthetic antibiotics in orange. Figure from Hutchings et al. 2019³.

The past century has seen an incredible increase in life expectancy at birth. In the UK, a man born in 1915 could be expected to live up to 48.4 years, whereas a man born in 2015 the life expectancy was increased to 79.3 years⁵. Whilst there are many contributing factors to this increase, huge improvements in medical knowledge, including the development of antibiotics, have changed the causes of death significantly. Today, however, the golden age of antibiotic discovery has dried up leaving what was described by the UN, already in 2010, as a fundamental threat to human health³.

1.2 The emergence of antibiotic-resistant bacteria

The emergence of antibiotic-resistant bacteria was predicted by Alexander Fleming himself, stating: *“The greatest possibility of evil in self-medication is the use of too small doses so that instead of clearing up infection the microbes are educated to resist penicillin and a host of penicillin-fast organisms is bred out, which can be passed to*

other individuals and from them to others until they reach someone who gets a septicæmia or pneumonia which penicillin cannot save”⁶.

In 1940, even before mass distribution of penicillin was a reality, biochemists Ernst Chain and Edward Abraham of Oxford University had documented an enzyme capable of inactivating penicillin, penicillinase. The first clinical cases soon followed in 1944, when the β -lactamase production by a strain of *Staphylococcus aureus* (*S. aureus*) was reported.

The spread of antimicrobial resistance (AMR), hereunder bacterial antibiotic resistance, is driven solely by the use, abuse, misuse and overuse of antimicrobial medicines e.g. antibiotics.

The 2014 O’Neill Report estimated that globally 700,000 deaths could be attributed to AMR annually, predicted to increase to as many as 10 million annual deaths by 2050. This estimation would set AMR as the leading cause of death, surpassing deaths currently related to cancer (Figure 1-2). The accompanying financial burden is estimated to cost up to 100 trillion USD annually and would lead to a reduction in global GDP⁷.

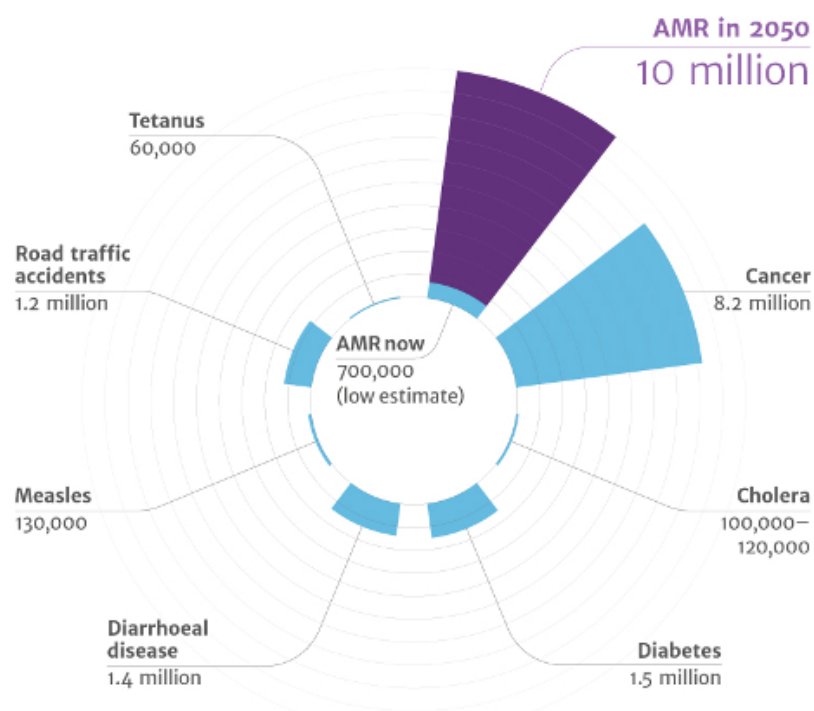


Figure 1-2. Estimation of global causes of deaths. Figure from O’Neil 2014⁷.

In the UK, a 5-year strategy to tackle national AMR covered the period 2013-2018. The initiative promoted, in the period of 2014-2017, a decrease of 7.3% (daily doses/1000 inhabitants) in human antibiotic consumption and of 40% (mg/kg body weight)⁸ in antibiotic sold for food-producing animals. A renewed national UK action plan covering 2019-2024, in addition to an international 20-year vision, has since been commenced. In comparison, the Centres for Disease Control and Prevention (CDC) reported that up to 30% of antibiotics prescribed in the US in 2018 were likely unnecessary and that almost 70% of all antibiotic prescriptions had prolonged durations beyond the recommended 5-7 days⁹. Data published by the US Food and Drug Administration (FDA) on antibiotic use in livestock in 2017 estimated that the US antibiotic use for all food-producing animals was five times greater than the UK¹⁰. A 2020-2025 national action plan for combating antibiotic resistance was set out by the White House and the CDC in 2015 detailing action and monitoring points. Despite the efforts made by some governments, global human consumption and use in agriculture is predicted by the WHO to increase three times from 2018 levels by 2030 with consequent acceleration in AMR. Therefore, in order to avoid reverting back to the pre-antibiotic era, it is essential that we develop novel solutions and technologies or repurpose existing ones.

1.3 A brief history of phage therapy

Bacteriophages, also known as phages, were discovered concurrently by Frederick Twort and Felix d’Herelle in 1915 and 1917 respectively. However, while Twort reported a “transmissible glassy transformation” of bacteria, D’Herelle conceptualised phages as we know them today, as bacterial viruses. The first therapeutic use of phages (phage therapy) is also credited to d’Herelle, who in 1919 successfully treated severe dysentery in a 12-year old boy. It is reported that d’Herelle himself and several hospital staff ingested the phage preparation beforehand to check its safety¹¹. A timeline of the discovery and development of phage therapy is presented in Figure 1-3.

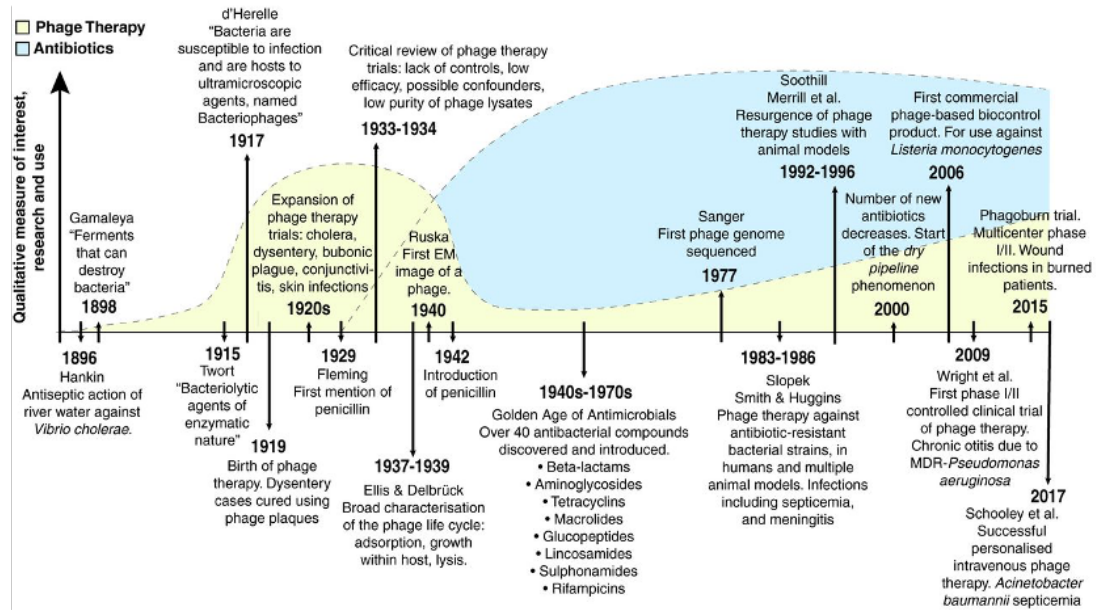


Figure 1-3. Timeline showing the development of phage therapy highlighting major achievements. Figure from Altamirano and Barr 2019 ¹².

Following their discovery, the study of phage biology was picked up in multiple laboratories, albeit in most cases these laboratories worked from the hypothesis of Twort. Phages were not broadly recognised as viruses until the advent of electron microscopy in the late 1930's in Germany. The access to cheap and effective antibiotics soon pushed the development of phage therapy to the wayside in Western medicine. D'Herelle travelled to Tbilisi in Georgia in 1934 and established, with Georg Eliava, an institute to study phage and phage therapy. The Eliava Institute continues its research to this day and is reported to store one of the biggest phage collections in the world ¹¹.

Around the turn of the 21st century, the realisation that AMR is an immediate and potentially devastating threat to global health has re-energised the study of phage biology and therapy. Today, it is studied by scientists and health professionals in thousands of laboratories and private companies around the world.

1.4 Biology of bacteriophages

Evolutionary pressures have generated a rich and diverse repertoire of competitive phages that are present in every known environment on earth, where bacteria exist.

With an estimated number of 10^{31} tailed phage particles in the biosphere, phages are numerically more abundant than any other biological entity on earth and are estimated, depending on the environment, to outnumber bacteria by a factor of around 10^{13} .

Phages have developed a multitude of strategies for survival and infection. The primary distinction of lifecycle lies between obligately lytic (virulent) and lysogenic (temperate) and could include as many as four distinct categories: (I) lytic and non-temperate, (II) chronic and non-temperate, (III) lytic and temperate, and (IV) chronic and temperate (Figure 1-4) ¹⁴.

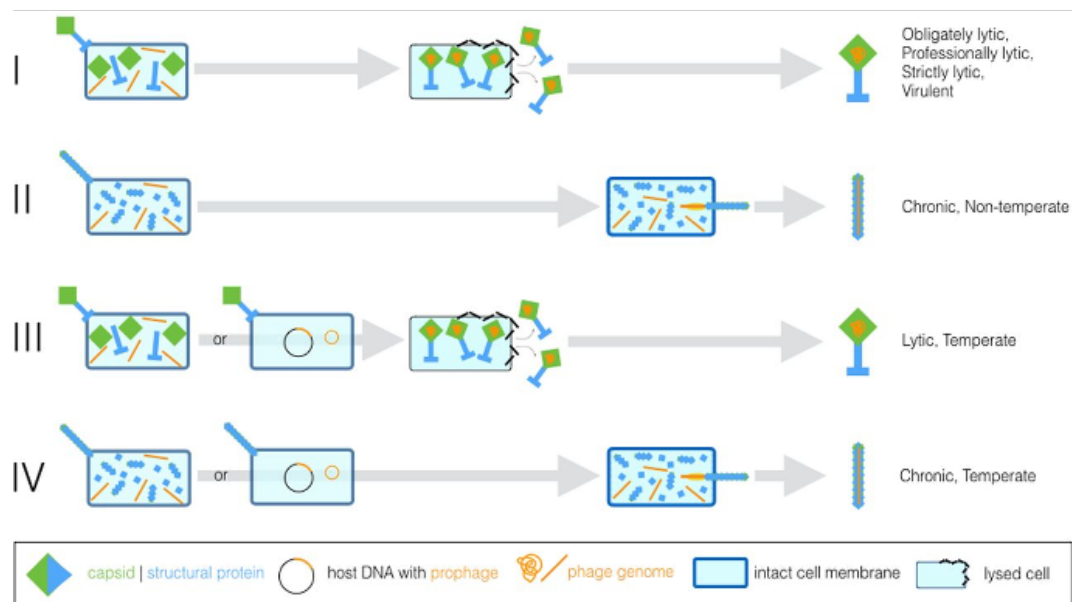


Figure 1-4. The four strategies for phage survival and infection. (I) lytic and non-temperate, (II) chronic and non-temperate, (III) lytic and temperate, and (IV) chronic and temperate. Figure from Hobbs and Abedon 2016 ¹⁴.

Virulent phages infect their bacterial host, replicate their own genetic material (DNA or RNA) using the host machinery, assemble as many as 200 new phage particles per cell, and then lyse the infected bacterial host cell. The virulent life cycle can take as little as 16 minutes ¹⁵. Temperate phages infect their bacterial host and integrate into the host genome as prophages. The host bacterium continues to live and reproduce unaffected by the infection and vertically transferring the prophage(s) to its daughter cells. When certain cues are present, such as a specific chemical, UV or radiation, the prophage is released, replicates its own DNA and then lyses the infected bacterial host cell ¹⁶. These life cycles are presented in Figure 1-5. A third, less studied and

defined life cycle, is the pseudolysogenic life cycle, where phages infect their bacterial host and remain dormant until certain cues are present before entering into either the lytic or lysogenic lifecycle ¹⁷.

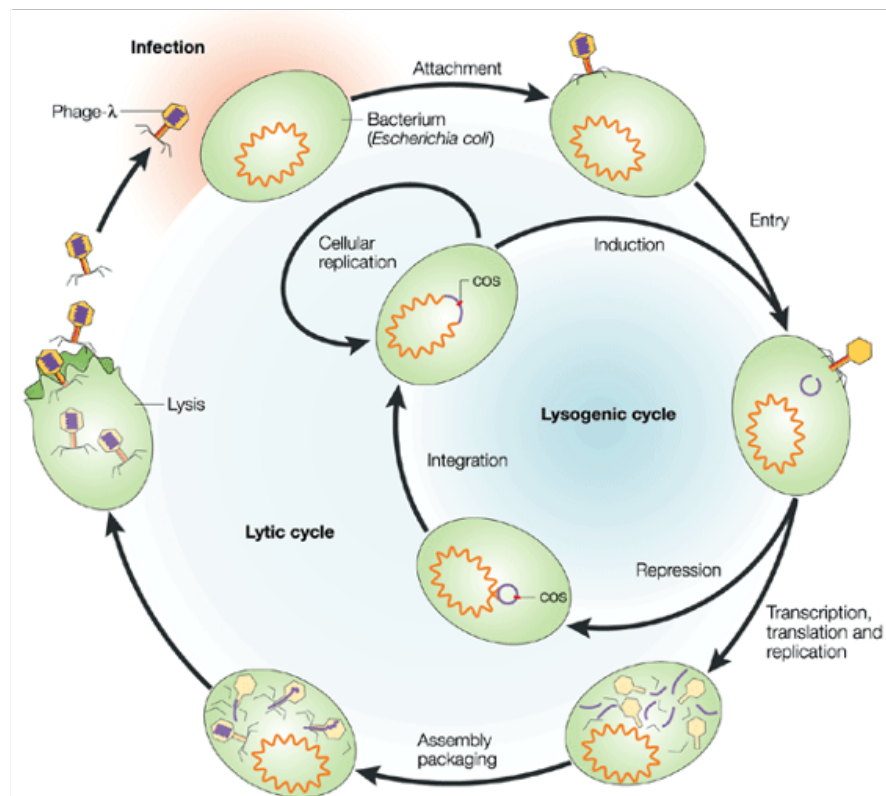


Figure 1-5. The life cycle of virulent (lytic) and temperate (lysogenic) phages. Figure from Campbell 2003 ¹⁸.

Phage classification is the responsibility of the Bacterial and Archaeal Viruses Subcommittee (BAVS), a part of the International Committee of the Taxonomy of Viruses (ICTV). The classification is based on genome composition and morphology, dividing phages into orders, families, subfamilies, genera and species. The discovery, sequencing, and classification of new phages is ever-growing and new taxa are updated accordingly. Current taxonomy of bacterial and archaeal viruses comprises of at least 11 orders, 26 families, and an abundance of subfamilies, genera and species.

1.5 Bacteria and phages co-existence

Bacteria and phages have evolved to co-exist over the past 3 billion years. In comparison, human-restricted bacterial pathogens have evolved to their host within the last 1 million years¹³. It is, therefore, no surprise that phage-bacteria co-existence has a strong and far-reaching influence on everything from global biochemical cycling of organic matter and carbon to eukaryotic fitness to bacterial virulence. In fact, the majority of bacterial pathogens have evolved to include either prophage-encoded virulence or fitness factors to cause diseases, such as the Shiga toxin (Stx) of Stx-producing *E. coli* (STEC) or contain a prophage swarm contributing to lysogen fitness as often observed in *Staphylococcus aureus* strains¹³. In the marine environment, one litre of seawater can contain as many as 2.5×10^8 phage per millilitre and it is estimated that 20-30% of all marine bacteria are infected by phage at any given time¹⁹.

The co-existence of bacteria and phages in an environment occurs in cycles, whereby each population increases or decreases in size opposite to each other, with one being at its peak when the other is in its trough. These relationships become highly complicated in communities comprising of many different genera of bacteria and phages, where the spatial confinement of each bacterium-phage pair may display its own cycling timings. In complex communities, phage-induced bacterial lysis re-releases organic matter into the microbial soup and facilitates the transfer of genetic material between phages and their hosts thus shaping the direction and success of the microbial ecosystem.

1.6 Bacterial resistance to phages

In nature, as in a clinical setting, the driver for bacterial resistance to phages is the actual presence of phages that will pressure bacteria to evolve resistance. This evolutionary pressure has selected for the development of elaborate anti-phage systems in bacteria – and they have evolved an arsenal targeting every single step in the life cycle of a phage²⁰. Mutations identified in a clinical setting are however not

elaborate systems, but often point mutations that cause either the loss or the alteration of host proteins necessary for phage infection or propagation. It is important to note that, while bacterial resistance to phages occurs, it comes at a cost. This cost can, among others, affect fitness, virulence or their susceptibility to antibiotics. To this end, it has been suggested that bacteria becoming resistant to phages, in turn, may become susceptible to antibiotics, giving scope for a combination treatment of phages and antibiotics.

The emergence of phage-resistant bacterial variants has been described in three out of four human clinical trials of phage therapy²¹. *In vivo* studies have shown that using multiple phages in cocktails, which target multiple different bacterial surface receptors, lowers the frequency of phage-resistant bacteria, statistically reduces the chance of co-resistance and creates a synergy, whereby infection efficiency increases²¹.

The potential bacterial trade-off or trade-up between phage- and antibiotic resistance was nicely demonstrated by Burmeister *et al.*²² in a series of evolution experiments. Phage-resistance was observed following infection cycles using *Escherichia coli* (*E. coli*) phage U136B, which, for host entry, relies on two host factors also involved in antibiotic resistance, namely the efflux pump protein *ToIC* and lipopolysaccharide (LPS). It was found that all phage-resistant bacterial *ToIC*-mutants displayed reduced resistance to tetracycline, bacterial resistance to which occurs via the *ToIC*-AcrAB efflux pump, with some also showing reduced resistance to colistin. This antagonistic gene pleiotropy observed is possible when multiple phenotypic traits are associated with a single gene, here phage infection and antibiotic resistance. Additionally, they observed synergistic gene pleiotropy, a trade-up, where phage-resistant bacterial LPS-mutants also displayed increased tetracycline resistance; however, these mutants were outcompeted over time by *ToIC*-mutants²².

1.7 Bacteriophage interactions with mammalian cells

Phages are abundantly present on all body surfaces that are in direct contact with the exterior environment, including the skin, urogenital tract, oral cavity, gut, and lungs²³ and have further been detected in blood, ascitic fluid, and cerebrospinal fluid²⁴. The presence of phages in body niches allows for selective pressure to be exerted on their bacterial hosts and consequent modulation of the human microbiome, while their presence in blood grants direct interaction with vascular endothelial cells and cells of the immune system. The potential influence and significance of phage interactions with human cells, organs and cells of the immune system is largely unknown^{23, 25}.

The unique pharmacological properties of phages, i.e. pharmacokinetics, the movement of a drug through the human body over time, observed as absorption, distribution, metabolism, excretion (ADME), and pharmacodynamics, the biochemical, physiologic, and molecular effects of a drug on the human body, are complicated and should be recognised as such²⁶. This complexity is attributed to their large size, generic diversity, structural complexity, and their potential to replicate within the human body^{26, 27}.

Multiple studies have identified intracellular phages within eukaryotic cells, however, as the focus until recently predominantly has been on phage-bacterial interactions, the mechanisms by which phages enter eukaryotic cells are not well understood^{23, 28}. A 2017 paper by Lehti *et al.*²⁹ described how the *E. coli* phage PK1A2 binds to a surface polysaccharide acid expressed by human neuroblastoma cells as part of the neural cell adhesion molecule (NCAM). The binding of PK1A2 to NCAM enabled the phage to enter the neuroblastoma cells by constitutive endocytosis, where it was found to be associated with both endosomal and lysosomal markers. Dispersal of phages between tissues of an eukaryotic host has been shown to rely on transcytosis whereby phages are transported across epithelial layers by the endomembrane system³⁰. Transcytosis differs from endocytosis as it is solely transcellular transport relying on the endomembrane system to enclose the cargo and ensure separation from the cytoplasm. Transcytosis across epithelial layers is unidirectional, transporting cargo from apical to basolateral plasma membranes³⁰.

Specific adaptive immune response against phages in mammalian cells has been identified. *In vivo* studies have shown that phage-induced antibody production is highly variable between patients and between phage preparations, but the evidence suggests that an adaptive response in the form of phage-specific IgA, IgM and IgG is common and does not affect the clinical outcome ^{23, 31}.

The clearance of circulating phages by adaptive immune responses can be enhanced by inducing a systemic inflammatory response syndrome (SIR) using LPS, thus mimicking a bacterial infection. Therefore, when settling on a suitable dose for phage therapy, it should be considered that the concentration of phages increases over time with each replication cycle therefore leading to enhanced clearance by the human immune system ³². It is believed that phagocytosis by immune cells is the primary process for phage neutralisation and this may result in a specific immune response ^{31, 33}.

The mucosa, encompassing the epithelium and an apical surface lining consisting mainly of mucin glycoproteins and inorganic salts, has long been recognised as a central part of the mammalian immune defence against bacterial infections ³⁴. A non-host derived immunity has been described in these mucosal surfaces, where an increase in phage abundance reduced bacterial infection of the underlying epithelium ^{23, 35, 36}. *In vitro* studies demonstrated a mucosa-dependent increase in phage T4 abundance, which contributed to protection against bacterial infection in cell lines ³⁶. This non-host derived immunity achieved through bacteriophage adherence to mucus (BAM) was associated with specific binding interactions between Ig-like protein domains expressed on phage capsids and mucosa glycan residues, effectively creating an antimicrobial layer. Genomic analysis further demonstrated that the phage-expressed Ig-like proteins were specific to phage strains associated with mucosa environments, suggesting co-evolution with the epithelium to maintain binding and immunity ³⁶. In support of a co-evolution theory, Shan *et al.* ³⁷ demonstrated that phages become more virulent in the presence of both bacteria and human cells than in the presence of bacteria alone ³⁷. In these experiments, phages, specific to *C. difficile*, showed strong adsorption to HT-29 cells thus increasing the spatial proximity to the natural host of *C. difficile* ³⁷.

The BAM model has further been demonstrated *in vivo* in mice, where intranasal delivery of multidrug-resistant *Pseudomonas aeruginosa* was treated with a suitable phage. It was shown that 100% of infected mice survived throughout the 16-day experiment when given a preventative dose of phage four days prior to infection with *Pseudomonas aeruginosa* and 95% of infected mice survived when the phage was given 2 hours after the onset of infection. In comparison, 0% of the control cohort, survived past 2 days post infection^{38, 39}. It is therefore likely that the BAM model has implications for our understanding of humoral immunity as it theorises a phage-derived immunity at the interface of bacterial infection of eukaryotic cells.

Along these lines, increasing attention is also given to phage populations of the human gut microbiota, as research suggests a protective and possibly immunomodulatory role in the immune response of the human gut⁴⁰.

It is also suggested that the continual stimulation of antiviral immune responses by commensal bacteriophage activation of innate immune pathways, could induce low-level cytokine production resulting in continuously activated immune cells conferring protection against pathogenic viral infections^{25, 41}.

Collectively these accounts show that the unique pharmacological properties of phages, their pharmacokinetics and pharmacodynamics, and of phage therapy are complex and point in many different directions. Standard determination of minimal inhibitory concentrations (MICs) and minimal bactericidal concentrations (MBCs) in line with the characterisation of antibiotics will not be sufficient, as over the course of therapy the dynamics more resemble that of a predator-prey model. It is also clear that the human host defences must be taken into consideration as it is conceivable that immune responses can be raised against both predator and prey.

1.8 Current standing of phage therapy

As a re-emerging technology, phage therapy is being explored as a treatment of antibiotic resistant- and non-resistant bacterial infections. Phages display many properties that are considered as advantages in a clinical setting. First, the high host-specificity of phages enables targeting of a small subset of troublesome strains while

leaving an otherwise healthy microbiome unaffected. Second, the lifecycle of virulent phages suggests that low- and single-dose administration is possible as propagation repeats as long as there is a susceptible host present. Third, the sheer abundance and diversity of phages assures that there will be a suitable match for every single bacterial pathogen, multi- or extensively-drug resistant or not.

The technology is being extensively studied both *in vitro* and *in vivo* and has already seen positive clinical results in cases of compassionate use targeting antibiotic-resistant bacterial infections ⁴². The challenge now lies in bridging the gap to the commercial market, which includes scientific questions in relation to manufacturing and to our understanding of bacteriophage interactions with human cells on a cellular and molecular level and questions in relation to legislation and public opinion. The scientific questions can be answered through experimentation, whereas questions relating to legislation and public opinion require a maturation process, which is difficult to predict in terms of direction and timescale. The current challenges of phage therapy are summarised in Table 1-1.

Specificity	The high host-specificity of phages is considered an advantage of phage therapy, however, a narrow host range conversely limits the versatility of individual phage preparations.
Selection	A rigorous phage selection process is needed to provide adequate certainty that no undesirable genes are contained within the phage genome and that the phage is suitably effective.
Pharmacokinetics	The pharmacokinetics of phages as observed through their ADME in the human body over time appear to differ between strains and may influence phage selection.
Pharmacodynamics	The pharmacodynamics of phage therapy is not definitively understood with potentially unknown biochemical, physiological or molecular effects on the human body.
Standardisation	A standardised set of requirements is needed for the production and quality of phage preparations.
Legislation	The current legislation is based on drug pharmacology which does not apply easily to the unique biology of phages.

Table 1-1. Challenges of phage therapy.

The interest in phages is dominated by agriculture and food security industries, while the presence of big pharma is not equally well established so far. The growing focus on phages as therapeutics by academia and small innovative companies is, however, illustrated by a recent review of the global preclinical antibacterial drug pipeline, which showed that 13% (33 of 407 projects) of scientific concepts in the lead generation phase contained a phage or phage-derived component (Figure 1-6)⁴³. These concepts predominantly focus on modulation of the microbiota, engineered probiotics, antibacterial payloads or compounds, and faecal microbiota transplants (FMTs), and are mainly based on wildtype or engineered phage cocktails or

engineered endolysin within a range of gram-positive and -negative bacterial hosts

43

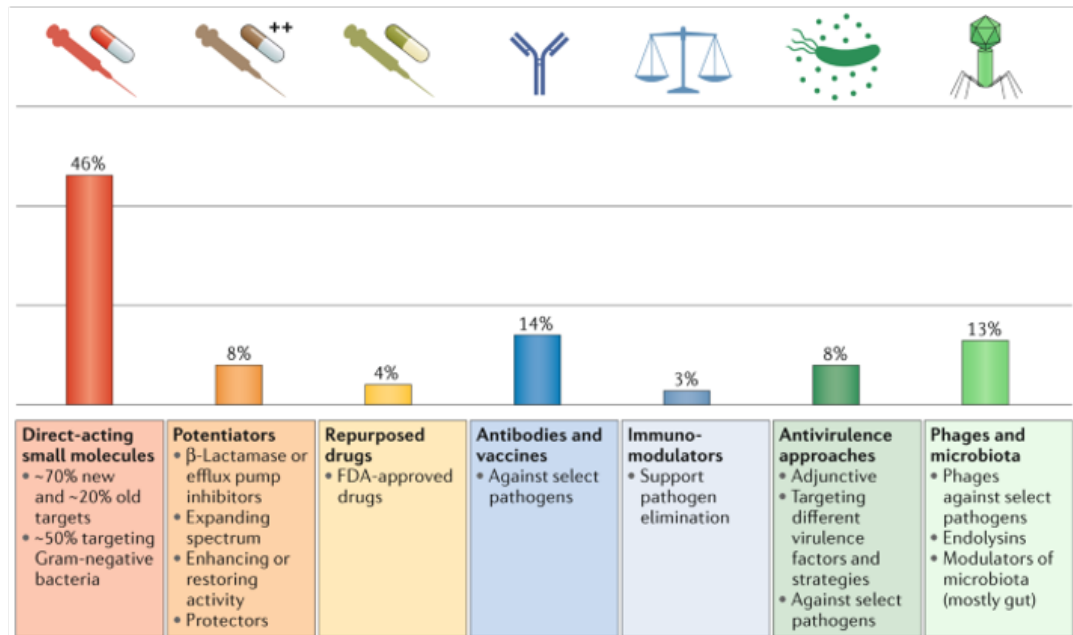


Figure 1-6. The preclinical antibacterial drug pipeline comprising a total of 407 projects from 314 institutions. Figure from Theuretzbacher et al. 2020 ⁴³.

There are, however, translational challenges to overcome before we see most of these novel scientific concepts in the clinical pipeline. A search performed on the 2nd of February 2021 using clinicaltrials.gov, a search engine run by the US National Library of Medicine, returned 13 active phage related studies. This should be viewed in comparison to the 29,398 active cancer-related studies returned in a similar search. The 13 active phage related studies include safety and efficacy studies of bone, joint, implant and wound infections, phase I/II trials of phage therapy for UTIs, diabetic foot ulcers, acute tonsillitis, cystic fibrosis, and studies utilising phages as molecular sensors or biomarkers.

Therapeutic phage preparations contrast with traditional antibiotics on many points and the legislative approval process for phage preparations can therefore not be directly aligned with antibiotics ⁴⁴. The current legislative model used in the Western world, designed for industrially-made pharmaceuticals for implementation in the general population, does not cater well for personalised medicine. Recent years, however, have brought about relaxed regulatory exceptions for compassionate use

in some European countries, where legislation has been introduced to allow quicker access for patients and doctors to phage therapy ⁴⁵. Amendments to the current process of authorisation to allow for widespread use of phage therapy will ultimately rely on robust evidence delivered by randomised clinical trials in a general population demonstrating phage efficacy, immunogenicity and any potential adverse effects ⁴⁶.

1.9 Influence of endotoxins in phage therapy

Phage therapy is further complicated by the release of endotoxins or LPS. LPS is part of the gram-negative bacterial membrane and is important for bacterial membrane organisation and stability ⁴⁷. Disruption of the bacterial membrane, for example by phage-induced lysis, releases LPS into its surroundings. LPS is known for its immunogenic, pro-inflammatory and pyrogenic effects, which have been widely demonstrated both *in vitro* and *in vivo* ⁴⁸. For this reason, a maximum concentration of endotoxin contamination present in pharmaceutical and biological products for intravenous applications is set at 5 endotoxin unit (EU) per kg bodyweight per hour, which is directly related to the minimum endotoxin level of 5 EU per kg bodyweight that could induce a fever in a patient ⁴⁹. The amount of endotoxin per bacterium varies between strains.

The presence of endotoxins may interfere with experimental results in phage biology studies, where interactions with the immune system are studied. Strategies for removal of endotoxin from phage preparations and determination of endotoxin levels are widely used. Endotoxin levels in crude phage lysates can be as high as 10⁵ EU/ml and with the gold standard of phage purification methods, CsCl density centrifugation, up to 99% endotoxins can be removed ⁵⁰. Irrespective of the chosen phage purification strategy, there will always be a loss of phage, so a high starting titre is essential to achieve a final preparation titre of 10⁸ PFU/ml, which is the most common concentration used in phage therapy ⁵¹.

Antibiotic-induced release of endotoxins from bacteria was detected *in vitro* by Crosby *et al.* ⁵², which showed endotoxin levels of *E. coli* cultures treated with 100 x MIC of cefotaxime, ciprofloxacin or piperacillin increase to approximately 4500

EU/ml after three hours. This equates to a 700-fold increase of endotoxin released per bacterium. This illustrates that antibiotic treatment, like phage therapy, has the potential to release large amounts of endotoxins.

1.10 Diseases of interest

In this study, the clinical focus lies on two diseases, urinary tract infections and neonatal bacterial meningitis, in both of which *E. coli* K1 is a primary causative pathogen. An overview of each disease is presented in the following sections.

1.10.1 Urinary tract infections

Urinary tract infections (UTIs) affect the bladder, urethra and kidneys and are among the most frequent human bacterial diseases, chiefly affecting women. In Europe, UTIs may account for up to 35% of hospital-acquired and 25% of community-acquired infections⁵³ and are considered the leading cause of bacteraemia⁵⁴. The distribution of disease causing bacterial pathogens varies across geographical location as illustrated by Table 1-2.

Europe & US ^{54, 55}	Asia-Pacific region ⁵⁶	Uganda, Africa ⁵⁷
<i>E. coli</i> (75-95%)	<i>E. coli</i> (52%)	<i>E. coli</i> (42%)
<i>Proteus mirabilis</i> (7-11%)	<i>Klebsiella pneumonia</i> (7%)	<i>Staphylococcus aureus</i> (31%)
<i>Klebsiella pneumoniae</i> (7-8%)	<i>Staphylococcus saprophyticus</i> (7%)	<i>Klebsiella pneumoniae</i> (12%)
<i>Staphylococcus saprophyticus</i>	<i>Enterococcus faecalis</i> (5.5%)	<i>Klebsiella oxytoca</i> (7%)
<i>Staphylococcus epidermis</i>	<i>Staphylococcus aureus</i> (3.5%)	<i>Proteus mirabilis</i> (3.5%)
<i>Pseudomonas aeruginosa</i>	<i>Staphylococcus warneri</i> (3.5%)	<i>Enterococcus faecalis</i> (3.5%)

Table 1-2. Prevalent bacterial pathogens causing uncomplicated UTIs by region/country and frequency (% of cases).

The symptoms of UTIs vary greatly between individuals and may include a need to urinate more often or more urgently than usual, a burning sensation while urinating, lower abdomen or back pain or temperature change. While the symptoms are often perceived as mild discomfort, they are likely to negatively affect an individual's daily routine.

Bacteria are present everywhere on the human body and the urinary tract is no exception. Diagnosis often includes culturing bacteria from a urine sample. While laboratory practices vary between countries, a bacterial count of $< 10^3$ CFU/ml in adult urine is considered normal, while a bacterial count of $> 10^4$ CFU/ml is indicative of a urinary tract infection ⁵⁸. Culturing may also include an antibiotic susceptibility challenge. Uropathogenic *E. coli* (UPEC) strains have adapted specifically to the environment of the urinary tract and may account for as many as 75-95% of uncomplicated UTIs in Europe and the US ⁵⁵. UPEC strains live alongside commensal *E. coli* strains in the gut environment without causing disease ⁵⁹. UTIs are primarily caused by introducing UPEC bacteria from the external opening of the rectum to the urethra.

Antibiotics are usually the prescribed medical treatment for UTIs, however, this is not always necessary as in many cases the symptoms clear up within a few days with increased water consumption. According to the UK National Institute for Health and Care Excellence (NICE) guidelines, the antibiotics prescribed for simple uncomplicated infections not affecting the kidneys include nitrofurantoin, trimethoprim, beta-lactams and quinolones, while antibiotics prescribed for complicated infection, such as chronic or recurrent infections or infections affecting the kidneys include ciprofloxacin or levofloxacin ⁶⁰.

Phage therapy could be one solution to curb the increasing antibiotic resistance and the emergence of multidrug-resistant (MDR) and extensively drug-resistant (XDR) in UPECs. A study by Ujmajuridze *et al.* ⁶¹, performed in Georgia, enrolled 118 human subjects with a urine bacterial count of $> 10^4$ in a feasibility pilot. They demonstrated that *in vitro* 41% of collected UPEC samples showed sensitivity to a commercially available phage cocktail, Pyo, and that the sensitivity increased to 75% following phage adaptation cycles. This adaptation included titering each individual phage within the cocktail against its bacterial host and determining the lowest concentration cut-off of phages yielding clearance after 24-72 h in both liquid and solid culture. The adapted Pyo phage cocktail was also administered to nine human subjects twice a day over seven days following a transurethral resection of prostate (TURP) via a suprapubic catheter. The phage intervention resulted in a decrease in bacterial titre of 1-5 log₁₀ in 67% of the subjects ⁶¹. While the efficacy of the described treatment is questionable, the study importantly recorded no phage-associated adverse effects.

1.10.2 Neonatal bacterial meningitis

Bacterial meningitis is characterised by severe inflammation of the meninges, a network of connective tissues surrounding the brain and spinal cord. The inflammation is a result of bacterial invasion into the subarachnoid space, between the arachnoid and pia mater and can be caused by numerous bacterial strains ⁶². The distribution of bacterial strains causing neonatal bacterial meningitis varies across geographical regions. In Europe and the US, the two prevailing strains are

Streptococcus agalactiae and *E. coli* K1 which accounts for as many as two-thirds of US cases (Table 1-3) ⁶³.

Neonatal bacterial meningitis ^{62, 63, 64}	Meningitis in 16+ years old ⁶⁵
<i>Streptococcus agalactiae</i> (39-48%)	<i>Streptococcus pneumoniae</i> (51%)
<i>E. coli</i> K1 (30-35%)	<i>Neisseria meningitidis</i> (37%)
<i>Streptococcus pneumoniae</i> (6%)	<i>Listeria monocytogenes</i>
<i>Listeria monocytogenes</i> (5-7%)	<i>Streptococcus agalactiae</i>
<i>Klebsiella pneumoniae</i>	<i>Streptococcus bovis</i>
<i>Serratia marcescens</i>	

Table 1-3. Prevalent bacterial pathogens causing neonatal bacterial meningitis (left) and meningitis in older children over 16 years of age and adults (right), with frequency (% of cases).

Neonates are at increased risk of infection due to their undeveloped immune system and immature microbiome. Pathogenic bacteria can, with little competition, colonise and proliferate in the immature gut and subsequently cross the gastrointestinal barrier into the bloodstream. In the bloodstream, the pathogenic bacteria can continue sustained proliferation unhindered by the neonatal immune system and traverse the blood-brain barrier once a critical mass has been achieved ⁶⁶.

Bacterial meningitis is an acute and potentially life-threatening infection that requires rapid diagnosis and initiation of medical treatment, usually comprising of antibiotics and sometimes corticosteroids. The disease is more common in babies (neonatal meningitis) and young children, with incidence rates reported at 1/5,000 in full-term neonates and 1/500 in low-birth-weight neonates in developed countries. The mortality rate for treated bacterial neonatal meningitis is reported at 5-20%, with significant life-changing implications for 25-50% of survivors that include cognitive impairment, deafness, blindness and seizures ^{67, 68}. Improvements in diagnosis and treatments of bacterial neonatal meningitis have seen a gradual decline in mortality rates in recent decades, while morbidity rates have remained relatively unchanged ⁶⁷. However, the emergence of antibiotic resistance could see a resurgence in mortality rates, as illustrated by an epidemiological study showing

declining antibiotic susceptibility of clinical isolates derived from the cerebrospinal fluid of meningitis patients ⁶⁹. As an increasing number of infections are becoming harder or impossible to treat, the need for the development of new technologies that can complement or replace conventional antibiotics is crucial.

E. coli strains are a prevalent cause of gram-negative bacterial neonatal meningitis worldwide ⁷⁰, in particular strains that express the K1 capsule, α -2,8-linked polysialic acid polymer that covers the surface of the bacteria, thereby hiding many of its antigenic features. This capsule is believed to enhance its ability to evade the human immune system and to traverse the blood-brain-barrier (BBB) ^{71, 72}, highlighting the clinical importance of this particular pathogen. In the US, *E. coli* K1-expressing strains are accounting for at least one-third of annually confirmed cases ⁶⁴.

Phage therapy was reported to successfully treat bacterial meningitis caused by multiple pathogens as early as at the turn of the 21st century ^{73, 74}, demonstrating the ability of bacteriophages to cross physiological barriers, including the BBB ⁷⁵, whereas many antimicrobials, including vancomycin, beta-lactams and other hydrophilic antibiotics have reduced penetration across the BBB ⁷⁶. Studies performed in a rat meningitis model infected with *E. coli* O25b:H4-ST131, a strain producing extended-spectrum beta-lactamase CTx-M-15, showed 100% and 50% survival after 7 hours or 24 hours post-infection respectively following administration of phage EC200^{PP} ⁷⁷.

1.11 The *in vitro* model system

Experimental model systems and model organisms are used extensively in medical research to conduct experiments and to expand our understanding without experimenting on humans. Experimental model systems may be *in vivo* animal models, *ex vivo* models culturing tissue or organs, or *in vitro* cellular models. Tripartite *in vitro* model systems have previously found use in phage research of *Clostridium difficile* infections of a colon environment ³⁷ as well as *E. coli* infection of the epithelium ³⁶.

The tripartite *in vitro* phage therapy model system used in this study was assembled to replicate a clinical setting as much as an *in vitro* model system will allow by

selecting disease-relevant cell lines and well-characterised bacterial and phage strains. The main players in this study are *E. coli* EV36, phage K1F, and the human cell lines T24 and hCMEC (Figure 1-7).

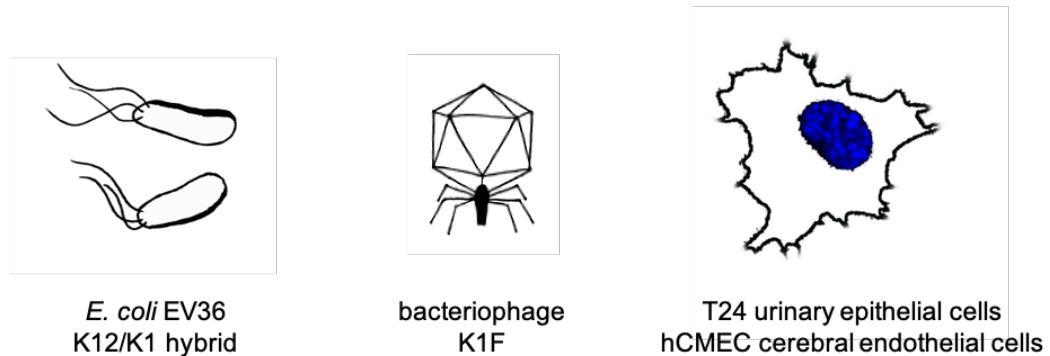


Figure 1-7. The tripartite in vitro model system. Original figure.

1.11.1 Bacteriophage K1F

Phage K1F is a virulent phage belonging to the *Podoviridae* family in the order *Caudovirales*. The *Podoviridae* family includes 147 described species divided into 23 genera ⁷⁸, all displaying a head-tail geometry with icosahedral heads and fixed non-contractile tails (Figure 1-8).

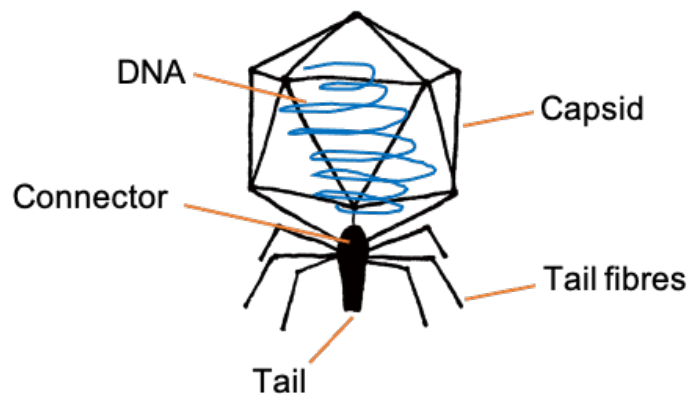


Figure 1-8. The major components of phages belonging to the *Podoviridae* family. Original figure.

Examined in greater detail, the morphological and genomic characteristics show that phage K1F is part of the T7-like supergroup ⁷⁹ and is closely related to phages K1-5 ⁸⁰, K1E ⁸¹ and 63D ⁸², which all share significant sequence similarities with K1F and are

capable of infecting and replicating in *E. coli* strains that express the K1 polysaccharide capsule. Phage K1F has a linear double-stranded DNA (dsDNA) genome of 39.7 kbp encompassing 42 ORFs. The product encoded by *gene17* (gp17), endosialidase, likely enables both recognition and depolymerisation of the K1 polysaccharide capsule⁷⁹. Studies have shown that phage dependent on the K1 capsule for successful infection possess greater fitness, as measured by growth rate and burst size, than non-dependent phage in the same host⁸³.

1.11.2 *Escherichia coli* K1

Many *E. coli* strains express the K1 antigen, a thick capsular polysaccharide, mainly composed of a α -2,8 linked polysialic acid. This capsular polysaccharide gives the bacterial surface a rough appearance (Figure 1-9). Research suggests that the K1 polysaccharide capsule is an important determinant for the invasive capabilities of pathogenic *E. coli*, allowing the bacteria to evade the host immune systems and cross endothelial and epithelial barriers. It also renders the bacteria immune to infection by most known *E. coli* phages⁷¹.

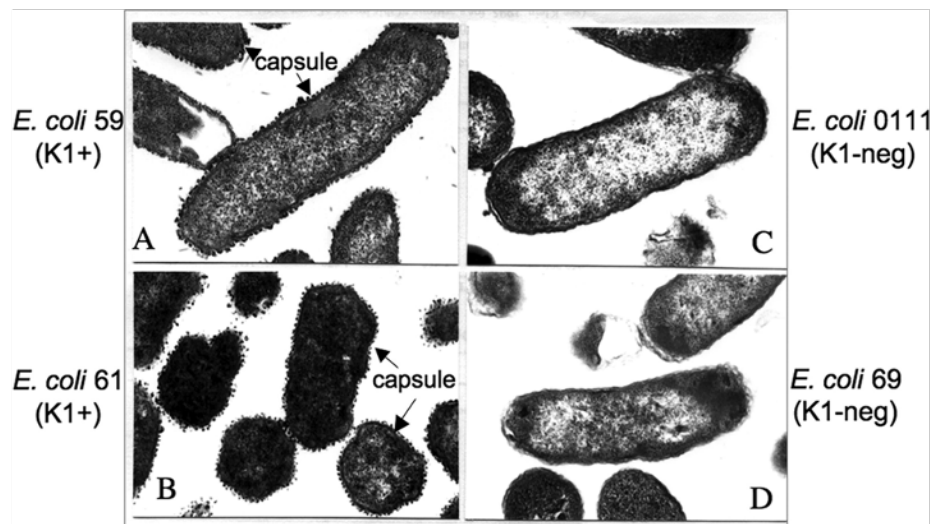


Figure 1-9. Transmission electron micrographs of K1-positive (A-B) and K1-negative (C-D) *E. coli* isolates. The arrows indicate the presence of the K1 capsule stained with ruthenium red. Figure from Metkar et al.⁸⁴.

In general, *E. coli* strains expressing the K1 antigen are associated with higher pathogenicity and are specifically identified with UTIs and meningitis, both of which can ultimately lead to bacteraemia ⁸⁵.

Bacteraemia (septicaemia) is a bloodstream infection that develops when a bacterial infection elsewhere in the body enters the bloodstream. If left untreated, bacteraemia can progress to sepsis, a serious complication of bacteraemia, which is classified as systemic inflammation. Endotoxins released by the bacteria in the bloodstream can cause a sharp drop in blood pressure (septic shock), which may lead to organ or tissue damage. Contracting severe burns or wounds, being an infant, elderly or having a compromised immune system, are associated with increased risk of developing bacteraemia ⁸⁶.

In this present study, *E. coli* EV36 is used as the main model bacterial strain. *E. coli* EV36 is a hybrid K12/K1 strain that displays a K1 polysialic acid capsule morphologically identical to that of natural *E. coli* K1 strains ⁸⁷. *E. coli* EV36 has previously been shown to be susceptible to endosialidase-expressing phages, which can hydrolyse the K1 polysialic acid capsule ⁷².

1.11.3 Transitional epithelial cells

The transitional epithelium (urothelium) is a specialised stratified epithelium, capable of transition through expansion and contraction, which lines the organs of the urinary system such as the ureter, urinary bladder and proximal urethra ⁸⁸. The urothelium sits on the lamina propria and consists of three layers, i.e. the apical-, intermediate-, and basal layer and is further covered by a layer of uroplakin forming an impermeable barrier ⁸⁹. The urothelium is capable of distended stretching and relaxing in response to varying pressures from the apical side without compromising the barrier function and varies in thickness from 2-7 layers of cells ⁹⁰.

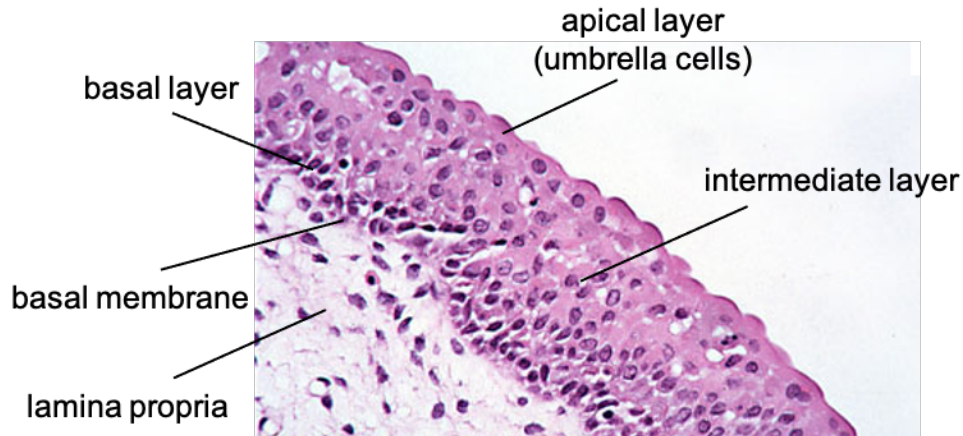


Figure 1-10. A histological section of a transitional epithelium stained with hematoxylin and eosin (H&E). Figure adapted from Khandelwal et al. ⁸⁹.

In this present study, the T24 human urinary bladder epithelial cell line is used as the cellular model system for UTIs. The T24 cell line displays a distinct epithelial morphological phenotype and expresses the epithelial-specific markers desmoglein and cytokeratin-8 ⁹¹. Furthermore, the T24 cell line has been used extensively as a cell model in UTI studies for pathogenesis ⁹² and in studies of chronic and recurrent infections ⁹³. T24 cells display sensitivity to *E. coli* and *E. coli*-derived LPS extracts and will express and secrete IL-8 and IL-6 in response ^{94, 95}.

1.11.4 Cerebral endothelial cells

Endothelial cells are specialised epithelial cells also called simple squamous epithelial cells. The endothelium lines the entire circulatory system, i.e. the cardiovascular and lymphatic systems and is comprised of a single interlocking layer of endothelial cells (Figure 1-11). In larger vessels, such as arteries and veins, the endothelium is attached to a subendothelial layer comprised of mainly collagen, elastic fibres and proteoglycan, which is further enclosed by layers of smooth muscle cells. In capillaries of both the cardiovascular and lymphatic system the endothelium is attached only to the basal lamina, the basement membrane, an extracellular matrix comprised of mainly collagen, elastin, laminin.

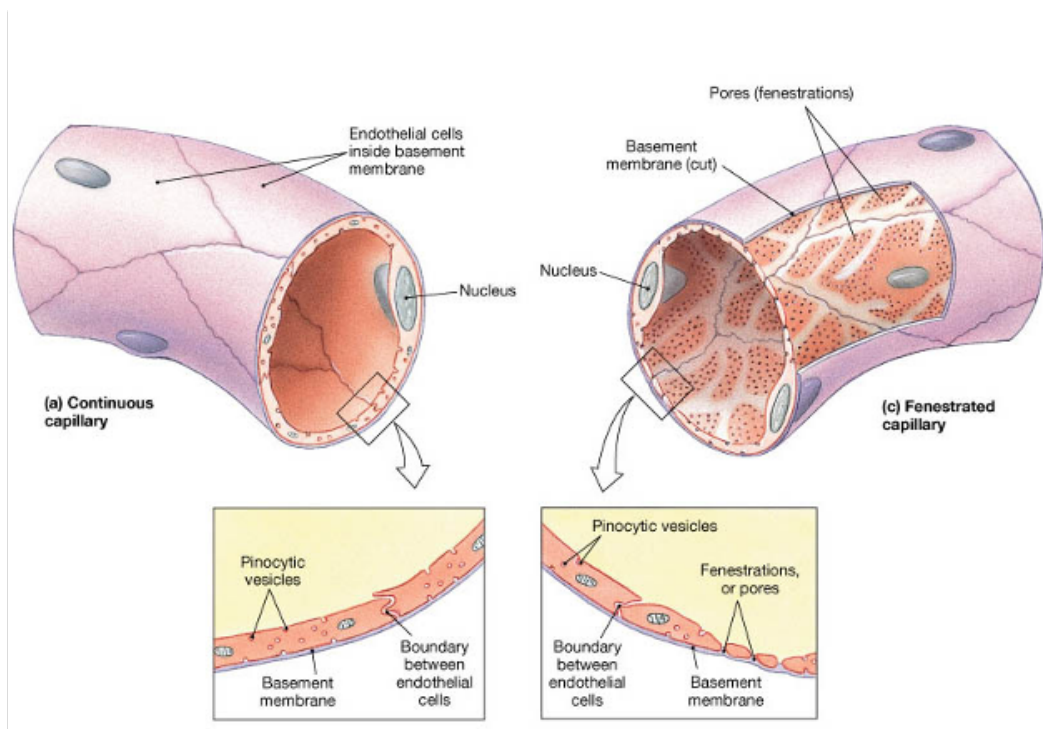


Figure 1-11. The structure of a continuous (left) and a fenestrated (right) capillary. The tubular vessel is formed by interlocking endothelial cells sitting on the basement membrane. Figure by Marieb & Keller ⁹⁶.

Cerebral endothelial cells, the primary constituents of the BBB, form a continuous and active barrier which has key roles in maintaining homeostasis of the central nervous system (CNS). Cerebral endothelial barrier regulation and permeability allow for the selective transport of nutrients and other molecules and for participation in neuroinflammatory processes, such as coordinating trans-endothelial migration of immune cells ⁹⁷.

The human cerebral micro-endothelial cell line (hCMEC/D3) is a well-characterised BBB and cerebral endothelial cell line used extensively in drug transport and CNS studies since its establishment in 2005. hCMECs display a distinct endothelial phenotype and express endothelial-specific markers, such as endoglin and VE-cadherin and will form capillary structures *in vitro* if grown in Matrigel ⁹⁸.

1.12 Mechanisms of entry and degradation

Pinocytosis, endocytosis, and phagocytosis are mechanisms for entry of extracellular material into eukaryotic cells. These mechanisms have an abundance of variations

and share many similarities, while having distinct differences such as size exclusions or preferences for a particular type of cargo. Once the extracellular material has made it successfully across the plasma membrane, different pathways can be initiated and depending on the cargo; these event can be considered as routine recycling of resources or defence against an intruder. In this section, the relevant pathways and players are outlined.

1.12.1 Bacterial entry into mammalian cells

Most bacteria can replicate on their own. Some have, however, evolved to reside and replicate in the intracellular environment of mammalian cells. The protective environment of the cytosol or cytoplasmic vacuoles of non-phagocytic cells offers cloaking from circulating immune cells and potentially favourable conditions for growth. Intracellular bacterial pathogens cause some of the most common and severe bacterial diseases, such as listeriosis and tuberculosis ⁹⁹.

Bacteria can initiate uptake by mammalian cells via several different mechanisms (Figure 1-12), with the underlying pathway being endocytosis whereby the mammalian plasma membrane folds around the extracellular material, ultimately forming an internal vesicle. In general, however, the term endocytosis is reserved for the continual and constitutive uptake of molecules or smaller particles, whereas endocytosis of larger objects, such as bacteria with a size >0.5 μm , is termed phagocytosis or internalisation ¹⁰⁰.

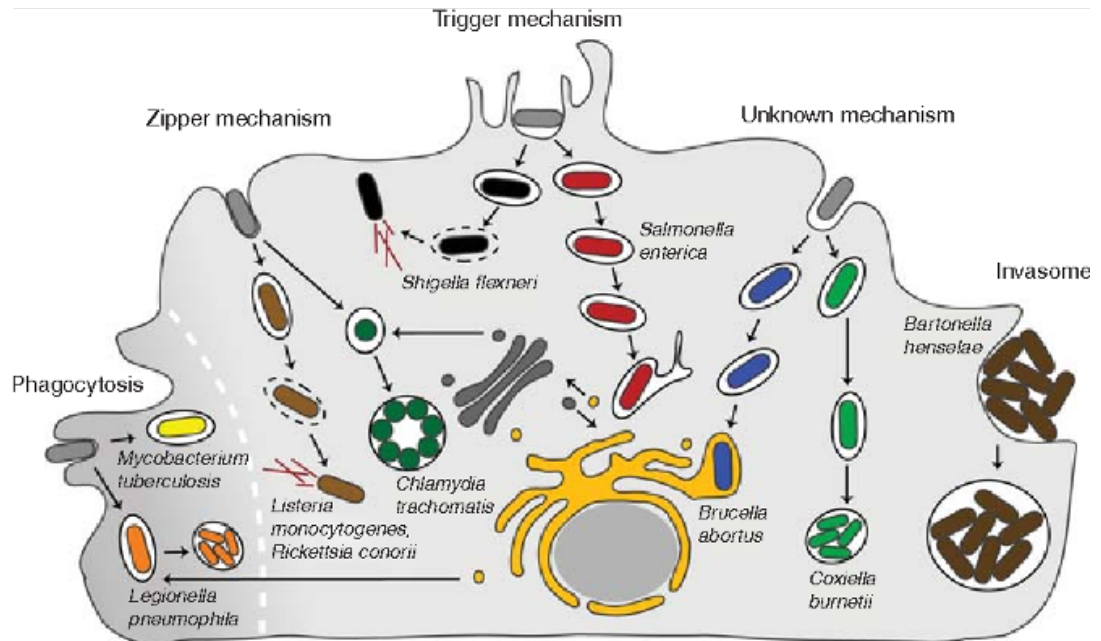


Figure 1-12. The endocytic pathways into mammalian cells of various different bacterial species. Figure by Cossart & Helenius 2014 ¹⁰¹

Following interactions between bacterial adhesins and specific host cell-surface receptors or delivery of active effector molecules, initiation of cytoskeletal remodelling begins ¹⁰⁰. This process can be both clathrin and non-clathrin mediated. Once internalised, the bacterial pathogen must counteract a multitude of cellular defence mechanisms. Bacterial survival strategies within a mammalian host cell include becoming intra-cytosolic by escape from the endosome or secretion of proteins that customise the endosome allowing for an intravacuolar lifestyle ¹⁰².

1.12.2 Viral entry into mammalian cells

Phages and mammalian viruses alike are obligate intracellular parasites requiring a host in order to replicate. In order to produce progeny, they must deliver their genome to the cytosol or nucleus of the infected host. Without the ability to condition the host for entry by the delivery of active effector proteins, viruses rely on indirect manipulation of host signalling pathways from the plasma membrane ¹⁰³. Viruses have evolved diverse strategies for entry into non-phagocytic cells, including inducing membrane lysis and pore generation, however as with bacterial entry, the most common mechanism is endocytosis. Enveloped viruses can release their capsids

into the cytosol following fusion of their envelope with the plasma- or endosomal membrane.

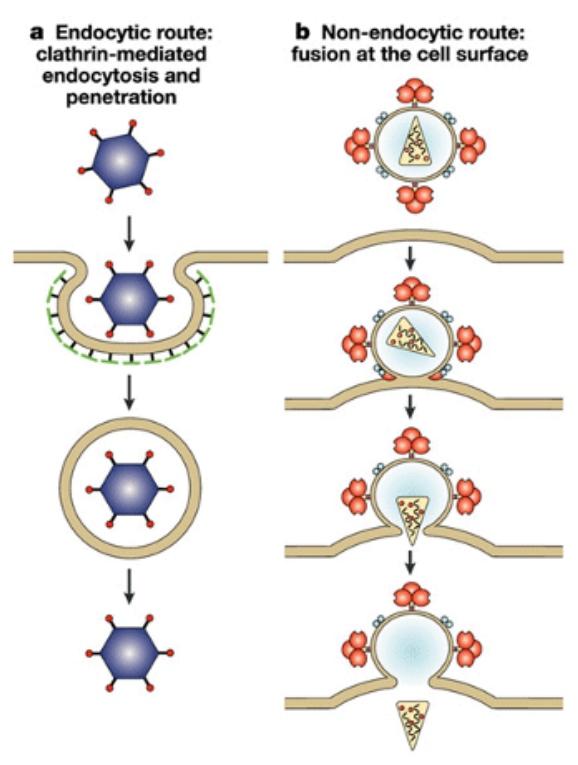


Figure 1-13. Viral entry pathways into mammalian cells via the endocytic route (A) and the non-endocytic route (B). Figure by Dimitrov 2004¹⁰⁴.

Entry by endocytosis is initiated by the attachment of viral capsid or envelope proteins to the host cell and can be via both clathrin and non-clathrin mediated surface receptors. The recognition of host receptors or a change to pH induces conformational change in viral entry proteins, which drives the escape from the internalised endosome by membrane fusion or -penetration¹⁰⁴. Once present in the cytoplasm, the nucleoprotein complex of DNA viruses is transported to the nucleus for transcription using host RNA polymerase, while RNA viruses transcribe mRNA using viral encoded RNA-dependent RNA polymerase within the cytoplasm. As always there are exceptions to the rule, and hence Pox viruses containing DNA replicate in the cytoplasm while influenza A virus containing RNA replicates in the nucleus.

1.12.3 Phage entry into mammalian tissue and cells

Since the discovery of phages, it has been assumed that they would be unable to penetrate the plasma membrane of mammalian cells. Given the precision specificity evolved by an individual phage strain towards a narrow prokaryotic host range, there would be no evolutionary selective pressure for a mechanism that would target or infect mammalian cells. However, while phages possess no natural tropism for mammalian cells ²⁹, it has been demonstrated that phages are capable of translocation across cell layers into tissues via both the para and transcellular routes, and entry into cells via endocytic mechanisms ¹⁰⁵.

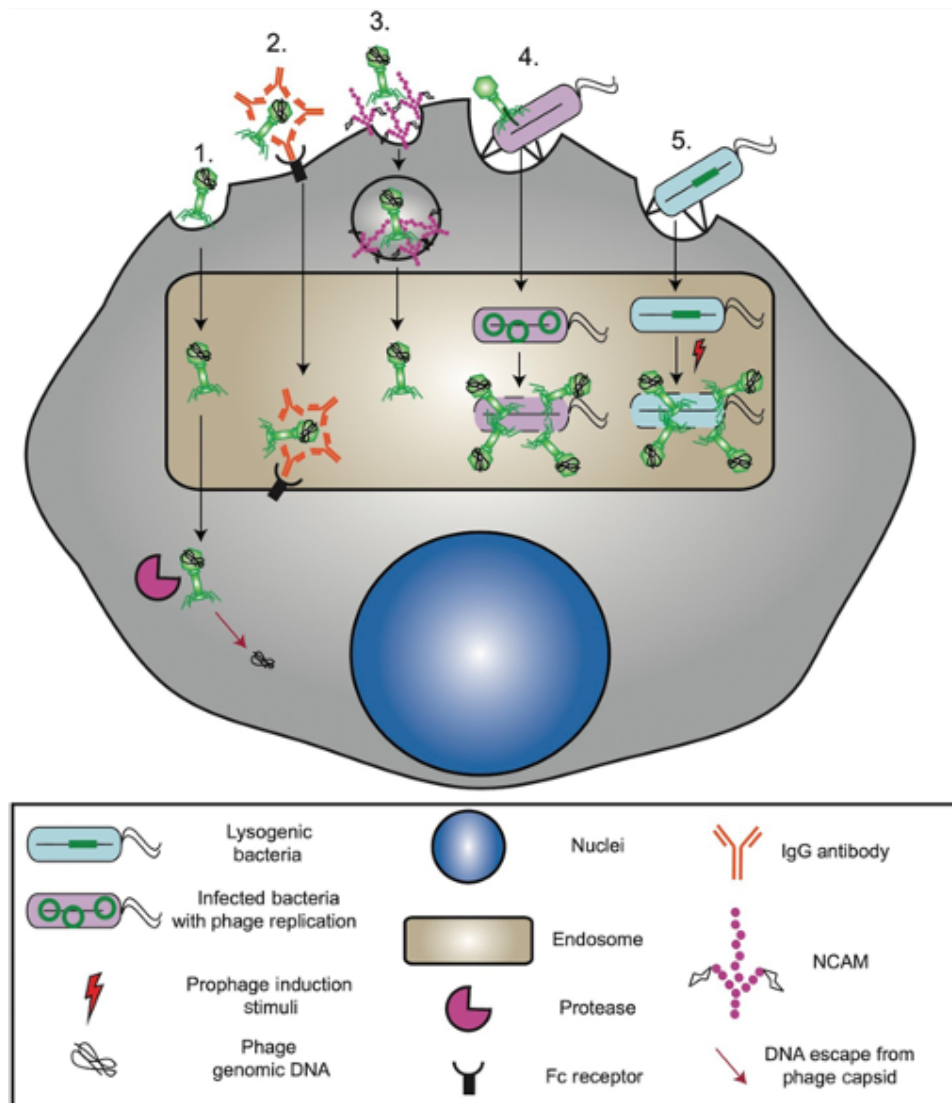


Figure 1-14. Phage entry pathways into mammalian cells. Phage uptake via non-selective endocytosis (1), antibody-dependency (2), molecular mimicry (3), active bacterial infection (4), or by prophage integration. Figure from Bodner et al. 2020 ¹⁰⁶.

Phages are widespread throughout the human body and their persistent and immediate presence has been demonstrated in, among others, epithelial cell layers, internal organs and the bloodstream¹⁰⁷. It has been hypothesised by Wang *et al.*¹⁰⁵ that phages translocate via the bacteria-rich epithelial cell layers, of the gastrointestinal tract in particular, into the bloodstream and other tissues¹⁰⁵. Whether interactions between phages and mammalian cells are directly significant for human health or not, it is clear that their presence is essential for evolution and ongoing maintenance of the bacterial microbiome¹⁰⁸.

While eukaryotic viruses can be either enveloped or non-enveloped, most bacteriophages are non-enveloped. Phage adsorption and infection of a prokaryotic host is initiated by receptor binding proteins (RBPs), membrane penetrating proteins and potentially enzymes degrading bacterial structures. A 2017 paper by Lehti *et al.*²⁹ described how the *E. coli* phage PK1A2 bind to a surface polysaccharide acid expressed by human neuroblastoma (SK-N-AS) cells as part of the neural cell adhesion molecule (NCAM). The binding of phage PK1A2 to NCAM enabled the phage to enter the neuroblastoma cells by endocytosis and after which it was found to be associated with both endosomal and lysosomal markers.

In analogous observations, it has been shown that phages can be transported across a confluent epithelial cell layer by transcytosis. This was demonstrated using *E. coli* phage T4 in both human colon epithelial (CaCo2) cells, human lung epithelial (A549) cells, and human hepatocyte epithelial (Huh-7) cells³⁰ and using a lipid encapsulated *Salmonella* phage UAB_Phi20 in both human colon epithelial (CaCo2) cells, human colon tumorigenic (HT-29) cells, and human lymphoma Raji-B cells¹⁰⁹.

1.12.4 Degradation pathways

Once bacteria or phages have entered a mammalian cell they are vulnerable to a variety of host degradative pathways. The pathways may affect the dynamics of the phage-bacteria interaction and hence impact on the efficacy of phage therapy. Autophagy is an evolutionarily conserved process in eukaryotes that tags and targets cytoplasmic components for elimination by lysosomal degradation. Pleiotropic in

nature, the mechanism of autophagy is a stepwise process comprising at least 30 autophagy-related proteins ¹¹⁰.

Canonical or non-selective autophagy is central for maintaining cellular homeostasis by the degradation of excess or unwanted cytoplasmic particles independently of origin. The process is induced by environmental factors such as nutrient starvation, ER stress, or toxic compounds via the mTOR complex ¹¹⁰.

Selective autophagy or xenophagy, on the other hand, is a key cellular defence mechanism against invading microbes compromising the phagosome membrane and attempting an escape into the cytosol. This mechanism relies on the association of selective autophagy-related cargo receptors with the pathogen, which initiates the formation of a pre-autophagosomal isolation membrane or phagophore and eventually fully enclosing the invading microbe in an autophagosome destined for lysosomal fusion and subsequent degradation. Selective autophagy has been demonstrated to specifically target and degrade intracellular pathogens, including bacteria, viruses, and parasites ¹¹¹. An overview of the stepwise processes of phagocytosis and autophagy are presented in Figure 1-15.

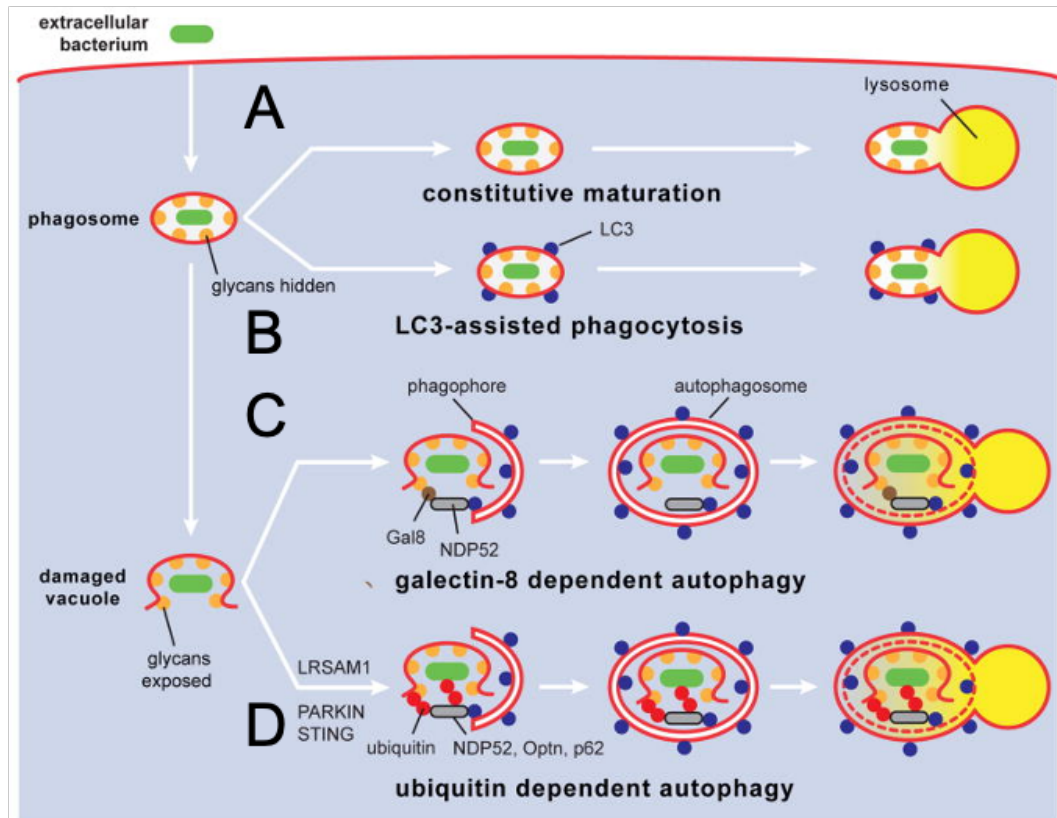


Figure 1-15. Pathway for eukaryotic phagocytosis and selective autophagy. Following entry via the phagocytic pathway the contents are processed and degraded by (A) constitutive phagocytosis, (B) LC3-assisted phagocytosis, (C) galectin-8 dependent autophagy, or (D) ubiquitin-dependent autophagy. Figure from Rando and Youle 2014 ¹¹².

Phagocytosis, the endocytic process of identifying, engulfing, and degrading pathogens or dying host cells, is the hallmark of professional phagocytes such as macrophages, monocytes, neutrophils, specialised dendritic cells, and natural killer cells. Nonetheless, this process can also be performed in a passive form by many non-professional phagocytes, including both epithelial and endothelial cells ¹¹³. In a stepwise process, the internalised phagosome enters a maturation process and, once completed, will fuse with lysosomes so that its contents are degraded. During the phagosome maturation process, cargo activation and signalling via pathogen associated molecular patterns (PAMPs) or damage associated molecular patterns (DAMPs) can recruit L3C, an autophagy-related protein, thus promoting and enhancing lysosomal fusion ¹¹⁴. This process is distinct from autophagy and does not require the formation of an autophagosome.

1.12.5 Molecules involved in degradation

Specific molecules involved in degradation allow for distinction between the four pathways presented in Figure 1-15. Specifically, Rab7 and Cathepsin-L are involved in the constitutive maturation of phagosomes (Figure 1-15A); Rab7 is a small GTPase, which has been demonstrated to be associated with late phagosomes and to be required for regulation of lysosomal-bound phagosomes and their fusion with lysosomes ¹¹⁵. The maturation process from early to late phagosome involves a conversion from Rab5 to Rab7 association allowing for a clear distinction between the two stages ¹¹⁶. Rab7 is also one of a number of Rab GTPases shown to be involved in the biogenesis and maturation of the phagophore by regulating the recruitment of LC3 to the phagophore membrane ¹¹⁷. Cathepsin-L, a cysteine protease, is part of a large family of cathepsins (lysosomal proteases), which includes a variety of nucleases, lipases, and proteases collectively ensuring complete degradation of engulfed extracellular material. Studies have shown that Cathepsin-L alongside Cathepsin-Z are present in all mammalian tissues and are critical proteases for lysosomal protein degradation across different cell lines and in *in vivo* murine models ¹¹⁸. Cathepsin-L is also involved in an assortment of other processes including antigen-processing, tumour invasion, and growth regulation.

Microtubule-associated protein 1A/1B light chain 3 (LC3) is a ubiquitin-like autophagy-related protein recruited to the phagophore double-membrane system for selective and non-selective degradation (Figure 1-16). The cytosolic form of LC3 is designated LC3A and upon conjugation to phosphatidylethanolamine is designated LC3B. During selective autophagy, LC3B provides the docking sites for cargo receptors, e.g. NDP52 ¹¹². Elongation of the phagophore and closure of the autophagosome is dependent on LC3B recruitment. LC3B can also be recruited by single-membrane phagosomes during their maturation process before lysosomal fusion in a process termed LC3-assisted phagocytosis ¹¹⁰ (Figure 1-15B). Studies have shown that LC3-assisted phagocytosis has multiple functions and can be activated by mechanisms governing cellular homeostasis ¹¹⁹ and by phagosome cargo recognition of, among others, bacterial and fungi via TLR1/2, TLR2/6, and TLR4 and antibodies IgG and IgE via Fc receptors ¹¹⁴.

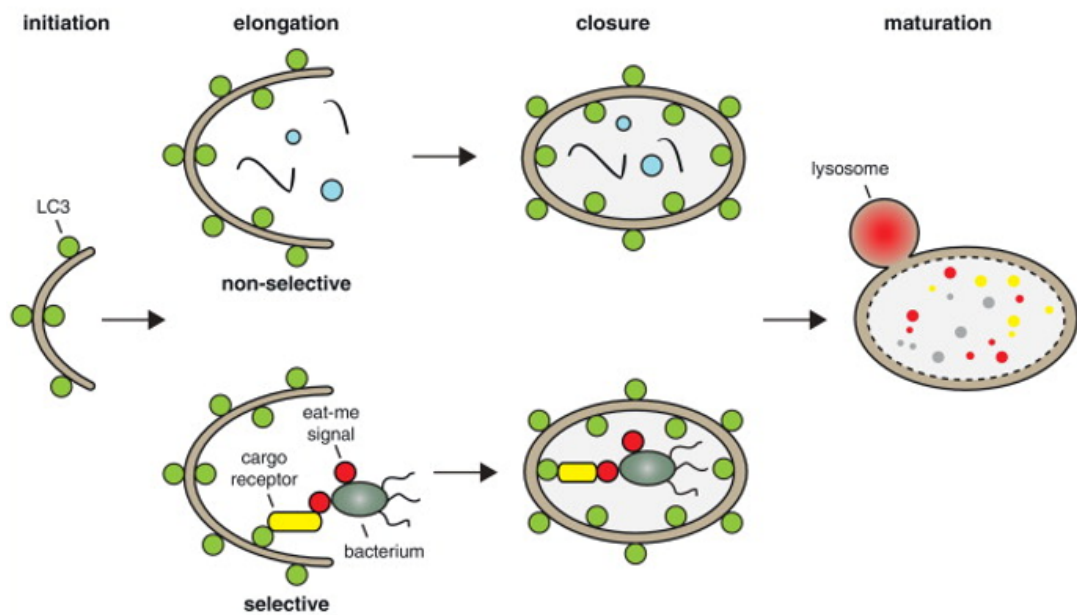


Figure 1-16. Role of LC3. Elongation of the phagophore is initiated by the recruitment of LC3 which also provides docking sites for cargo receptors. The encapsulated cytosolic material is degraded once fused the complete autophagosome is fused with lysosomes. Figure from Boyle and Randow 2013 ¹²⁰.

Galectin-8 is a cytosolic lectin belonging to a small family of autophagy-related galectins, which are able to sense damaged or breached vesicles in the endocytic pathway, such as phagosomes and lysosomes (Figure 1-15C). As a danger receptor, galectin-8 monitors the membrane integrity of these vesicles and detects and binds to exposed membrane-bound host-derived glycans, which are not normally present in the cytosol. The accumulation of galectin-8 provides a signal for cargo receptor NDP52 to mediate autophagosome formation ¹²¹. The underlying principle is that galectin-8 performs pathogen detection, allowing the cells to identify the entry of vastly different vesicle-damaging pathogens, including Gram-negative and Gram-positive bacteria and non-enveloped viruses alike ¹¹².

The intermediate autophagy-related cargo receptor NDP52/Calcoco2 (calcium binding and coiled-coil domain 2), a member of the nuclear dots family, is activated by bacteria-associated eat-me signals by Galectin-8, arising from the detection of damaged vesicles within the cytosol. The activation triggers selective autophagy and initiates the formation of the LC3-interacting region (LIR), an inter-molecular β -sheet, allowing for selective binding to LC3 necessary for phagophore genesis ¹¹². Uniquely, NDP52 is capable of recognising the binding and accumulation of both galectin-8 and

poly-ubiquitin and can function independently by activation from either danger receptor ¹²⁰.

Routine proteasomal degradation of surplus or otherwise unwanted intracellular proteins is initiated through the process of ubiquitin tagging (ubiquitination). In selective autophagy, polyubiquitinated proteins accumulating on and around cytosol-exposed bacteria function as eat-me signals for multiple cargo receptors including NDP52 and restrict bacterial proliferation by induction of TANK-binding kinase (TBK-1) ¹²². Ubiquitination can also activate selective autophagy independently through NDP52 recruitment (Figure 1-15D) or by enhancing Galectin-8 activation. Bacterial coat proteins are believed to serve as recognition signals for the antibacterial E3 ubiquitin ligases, LRSAM1 and Parkin ¹¹², which catalyse ubiquitination, however their exact substrates are unknown ¹¹¹.

Ubiquitination has also been shown to play a role in selective autophagy of some viruses via recognition by E3 ubiquitin ligase SMURF1 and phagophore genesis through cargo receptor p62 ¹¹¹.

1.12.6 Cytokines associated with pathogen entry

The entry of a pathogenic entity into mammalian cells will activate defence pathways of the host. This activation may involve cytokines associated with both innate and adaptive immunity.

Tumour necrosis factor alpha (TNF α) is considered a master regulator of inflammation and is implicated in the pathogenesis of bacterial, viral, and chronic inflammatory disease. In response to TNF α , vascular endothelial cells will increase leukocyte adhesion and transendothelial migration, illustrating its central role as a pro-inflammatory cytokine in clearing an infection ¹²³. hCMECs have been demonstrated to express TNF α in response to LPS as determined by RT qPCR and ELISA ¹²⁴.

Interleukin 6 (IL-6) is a pleiotropic cytokine involved in both innate and adaptive immunity, and also in neural development and function. The cytokine is rapidly produced to stimulate host defences, such as induction of C-reactive protein

expression, the concentration of which is directly related to the severity of infection¹²⁵.

Interleukin 8 (IL-8) is a potent chemokine involved in defensive inflammatory responses, specifically activating vascular endothelial cells, attracting and inducing neutrophils at the site of infection. IL-8 plays an important role in the early stages of angiogenesis by increasing endothelial permeability and has been shown to down-regulate the expression of tight junction proteins¹²⁶. hCMECs have been demonstrated to express and secrete IL-6 and IL-8 in response to stimulation by TNF α as determined by Cytometric Bead Array (CBA) analysis¹²⁷.

Interleukin 10 (IL-10) is an anti-inflammatory cytokine, which plays a central role in preventing autoimmune inflammation, maintaining tissue homeostasis, and limiting excess host activation of pro-inflammatory cytokines in response to pathogenic invasion¹²⁸. While IL-10 expression and activity is mainly considered as associated with immune cells such as leukocytes and monocytes, it has been demonstrated that non-immune cells such as epithelial¹²⁸ and endothelial¹²⁹ cells are capable of expressing this cytokine in response to infection or tissue damage.

Interferon beta (IFN β), an antiviral cytokine, plays an important role in innate and adaptive immunity against viruses. IFN β induction also occurs during bacterial infections, through TLR3/4 activation, albeit this response is considered variable. As antivirals, IFNs, including IFN β , have been demonstrated to be induced in many cell types, including endothelial cells in the early stages of viral infection following the detection of viral DNA and RNA via pattern recognition receptors (PRRs) such as TLR7 and TLR9¹³⁰.

1.12.7 Endothelial barrier integrity

The primary function of the endothelium of the circulatory system is to selectively enable free passage of solutes and small molecules across the barrier, while limiting the extravasation of larger molecules and cells. The endothelium is essential for maintaining proper circulation and lymphatic drainage and displays a differential selectivity depending on the tissue location, e.g. endothelial cells of the BBB form a

strong and tightly regulated barrier, while endothelial cells of the kidney form fenestrae, which are specialised holes for the rapid transport of molecules.

The structural and functional integrity of the endothelial barrier is regulated by an assortment of cell-cell adherence molecules including VE-Cadherin, junctional adhesion molecules (JAMs), occludin, nectins, and claudins (Figure 1-17) ¹³¹. These adherence molecules further enable cell-cell signalling. Experimentally, the endothelial barrier integrity can be characterised *in vitro* by measurements of trans-endothelial electrical resistance (TEER).

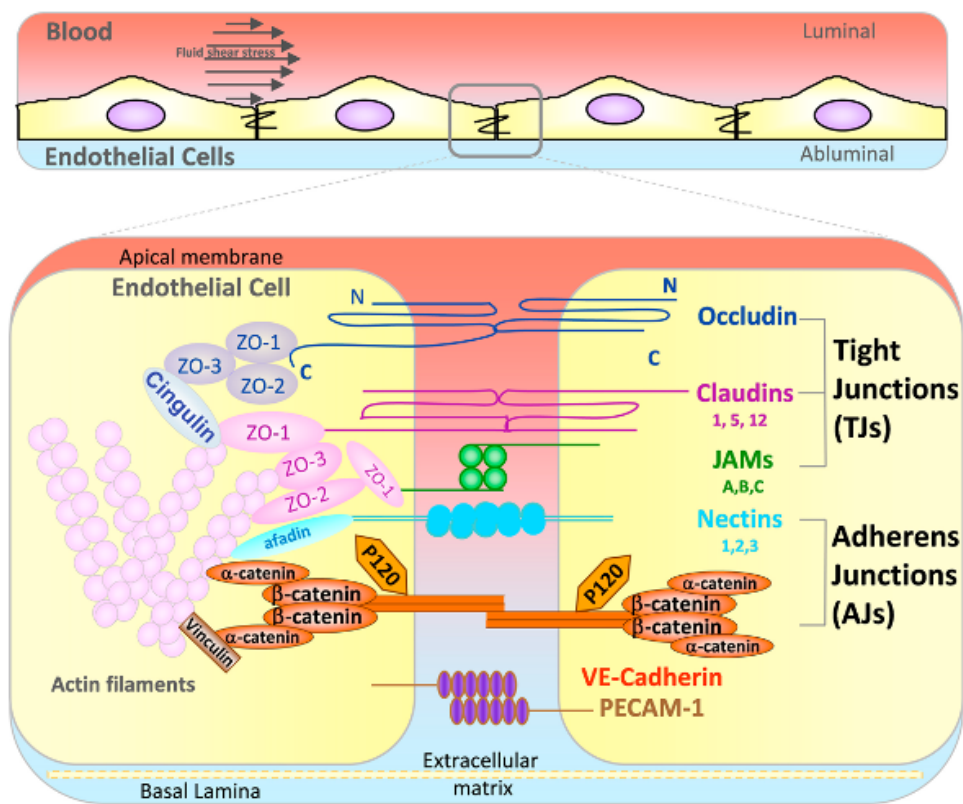


Figure 1-17. Cell-cell adherence molecules of the endothelium. Figure from Carutti & Ridley 2017 ¹³¹.

In many diseases, such as diabetes and in chronic inflammatory conditions, endothelial barrier integrity is compromised resulting in leakage. This phenomenon is also observed in tumour-induced angiogenesis ¹³².

Regulation of endothelial permeability can be induced by activated immune cells, pathogens or inflammatory mediators. Infection by extraintestinal pathogenic *E. coli* (ExPEC) clinical isolates has been demonstrated *in vitro* and *in vivo* to downregulate

the expression of tight junction proteins in brain microvascular endothelial cells, thereby disrupting the BBB and increasing the BBB permeability¹³³.

1.13 A brief history of phage engineering

In light of the biological challenges surrounding the developing phage therapy, genetic engineering of phages is being explored. Phage engineering has undergone considerable advancement over the last decades with novel applications in diverse areas, such as agriculture, food security and human health. This advancement is attributed to the incredible expansion seen in tools available for molecular and synthetic biology, and to the renewed global interest in phages as antimicrobials.

In pursuing clinical improvements, phage engineering is being exploited to tackle some of the challenges facing phage therapy, such as broadening their host range, inhibiting propagation, or enhancing their natural capabilities to enable biofilm degradation or infection of cancerous cells.

The power of phage engineering was significantly demonstrated in 2018 when a 15-year-old British girl with cystic fibrosis was treated with a phage cocktail targeting a disseminated *Mycobacterium abscessus* infection¹³⁴. Multiple antibiotics and immunosuppressant drugs administered following a double lung transplant had allowed for the antibiotic-resistant bacterial infection to take hold and spread. The bacteria formed large colonies in her body resulting in visible skin lesions and a failing liver. As she was discharged from ICU with a palliative care plan, a search for therapeutic phages was commenced. Three phage from the family *Siphoviridae* were identified and following six weeks of twice-daily intravenous and topical application of the phage cocktail a dramatic clinical improvement was observed. This case not only demonstrated to the broader public the potential for clinical applications of phage therapy, but also demonstrated for the first time successful use of engineered phages. In this particular case, two of the three phages were temperate phages engineered to become virulent derivatives by removing their immunity repressor gene (gp45) using the Bacteriophage Recombineering of Electroporated DNA (BRED) technique¹³⁵.

Techniques for engineering synthetic phages are well established and phage are generally considered to be easily manipulated. Practical applications for engineered phages are gaining ground in agriculture and food security industries, where immobilised phages or parts of those are used for bio-detection and pathogen management ¹³⁶. In the life sciences, practical applications for engineered phages are currently at a more conceptual and experimental level. However, the development of phage-based antimicrobials, using only the lytic enzyme of a phage or an engineered analogue, has proven successful in *in vivo* studies ¹³⁷. Another promising application is exploiting phage specificity to create a platform for delivery of antibodies ¹³⁸ or anticancer drugs ¹³⁹, where either the phages actively expresses a peptide or carries a toxic sequence to be translated by the target host.

1.14 Engineering phages with altered or expanded host tropism

The host specificity of individual phages is a double-edged sword as this particular feature can be viewed both as an advantage and as a disadvantage. The high host specificity of individual phage strains, leading them to target only a narrow subset of bacterial strains, allows for directed infection of a specific bacterial pathogen while leaving populations of beneficial commensal bacteria unharmed. This, conversely, constitutes a challenge for clinicians, as therapeutic deployment of such phages firstly requires isolation and identification of the causal pathogen, and secondly, a potentially time-consuming and costly search for a suitable phage strain either from environmental samples or from a library of previously isolated phages that target common bacterial strains.

Synthetic biology tools may be used to design and engineer recombinant phages with an altered or expanded host tropism. Phage specificity is primarily determined by the receptor-binding proteins (RBPs) located on either their tail fibres or tail spikes. These RBPs are the main focus of phage engineering, aiming to alter or expand the host tropism. A modular approach was employed by Ando *et al.* ¹⁴⁰ to reprogram wild-type *E. coli* phage T7 to infect different bacterial species including *Yersinia* and *Klebsiella*. The approach included synthesis of the entire phage genome in fragments

followed by Gibson assembly into artificial yeast chromosomes and subsequent expression and assembly in yeast cells¹⁴⁰. Demonstrating a different approach, Yosef *et al.*¹⁴¹ extended the host range of phage T7 that was intended for DNA transduction rather than phage replication, potentially targeting bacterial species that would not normally support propagation of phage T7. Individual recombinant phage particles were engineered by homologous recombination to incorporate a specific RBP gene into their genome. Multiple *Klebsiella pneumonia* and *Salmonella enterica* strains showed susceptibility towards the recombinant phage¹⁴¹.

1.15 Controlling the release of LPS by phage engineering

Immediately following the successful entry into the host, a virulent phage will commence the synthesis of new phage progeny. The burst size varies greatly between individual phage strains with a single infected bacterium yielding from tens to hundreds of phage progeny. This poses two potential challenges in a clinical setting; firstly, the exponential growth of phages allows for the simultaneous lysis of an increasing number of bacteria resulting in the rapid release of LPS, which in turn activates innate immune responses. Secondly, a preparation of self-propagating phage does not allow for controlled dose administration which is highly desirable in relation to monitoring safety and efficacy of phage preparation and for regulatory affairs.

To counter these difficulties, several design approaches, targeting different aspects of the phage lifecycle, may be pursued to engineer recombinant phages that decrease or slow the release of LPS. Studies have shown that engineered lysis-deficient phages retain the ability to infect and kill bacteria *in vitro* and *in vivo* while reducing the release of endotoxin^{142, 143}. In these studies, bacterial death relied on high multiplicity of infection (MOI), an increase in phage holin proteins that halt bacterial respiration, and a healthy immune system for clearance of the starved bacteria^{143, 144}. However, an *in vitro* study of bacterial starvation by over-expression of holin proteins or bacterial damage by DNase expression of engineered M13

phages showed that growth of *E. coli* cultures resumed following infection at both low and high MOIs ¹⁴⁵.

1.16 The aim of this research project

A deeper understanding of the cellular and molecular processes underpinning phage therapy and of the interactions between phages and human cells is needed to mature and implement the technology of phage therapy in a broader sense and to address the challenges that need to be overcome.

This research project aims to advance the understanding of phage biology in a human cell environment and the interactions between phages, their hosts and human cells. This is achieved by developing and characterising disease-relevant *in vitro* phage therapy model systems and by studying cellular and molecular mechanisms and responses of human cells following phage administration and uptake.

Specifically, what endocytic or phagocytic pathways are involved in the uptake and degradation of phages and bacteria individually and in combination in human cells? How do human cells respond to phage treatment in comparison with bacteria in relation to immune responses? Is phage therapy feasible for urinary tract infections and neonatal meningitis caused by K1-capsule expressing *E. coli*?

Chapter 2 Materials and Methods

2.1 Bacterial strains and culture

A total of six bacterial strains were used for the experimental research in this study. These are listed in Table 2-1.

Strain	Description
<i>E. coli</i> EV36	A K12/K1 hybrid engineered by Drs Eric R. Vimr and Frederic A. Troy ⁸⁷ . This strain was produced by conjugation with a high-frequency (Hfr) <i>kps</i> ⁺ strain and kindly provided by Drs Eric R. Vimr and Susan M. Steenbergen. By selecting this K12/K1 hybrid strain we gained the advantage of performing experiments in a biohazard level 1 laboratory setting while retaining the phenotypic properties of a pathogenic K1-expressing strain.
<i>E. coli</i> EV36-RFP	An EV36 derivative engineered by electroporation with low-copy plasmid pSB6A1 expressing the mRFP1 protein. Design and cloning of pSB6A1 was previously performed by Dr Antonia Sagona. The pSB6A1/pBR322BB1 BioBrick vector was kindly provided by iGEM. <i>E. coli</i> EV36-RFP was cultured under 100 ug/ml ampicillin selection.
<i>E. coli</i> MG1655 (ATCC 47076) (LGC Standards)	A well-characterised K12 strain ¹⁴⁶ , and a natural host for phage T7, was used as a control for phage selectivity.
<i>E. coli</i> BW25113 ΔtrxA	A strain from the Keio collection ¹⁴⁷ which was used for positive selection of recombinant chimeric phage. This strain is deficient of the <i>trxA</i> gene encoding for thioredoxin, a processivity factor for T7 DNA polymerase, which is essential for phage T7

	intracellular growth ^{148, 149, 150} . The strain was kindly provided by Dr Alfonso Jaramillo.
<i>E. coli</i> BW25113	A strain included as control for <i>E. coli</i> BW25113 Δ trxA selection efficiency. The strain was kindly provided by Dr Andrew Millard.
<i>E. coli</i> Top10 (ATCC PTA-10989) (Invitrogen)	A strain used solely, in this study, as an expression vector.

Table 2-1. Bacterial strains used in this study.

All strains were propagated in Lysogeny broth (LB) ¹⁵¹, with 1.5% w/v agar added to prepare solid culture plates. 25% v/v glycerol stock were prepared of all bacterial strains and stored at -80°C. Before experimental use, glycerol stocks were streaked on LB plates and incubated overnight at 37°C. Single bacterial colonies were picked and inoculated in 5 ml LB and cultured overnight at 37°C with shaking at 200 rpm. Overnight cultures were diluted 1:5 in LB and allowed 60 minutes to return to log phase growth before experimental use.

2.2 Determination of bacterial concentration

The concentration of bacteria, in CFU/ml, used in each experiment was estimated by reading the optical density (OD) of the exponentially growing bacterial culture at 600 nm and by interpolating the reading on a standard curve (Figure 2-1) of exponential bacterial growth. Concurrently, in many experiments, the actual bacterial concentration, in CFU/ml, was determined by preparation of a 10-fold dilution series and plating of 2-3 appropriate dilutions in triplicates on LB culture plates. These plates were incubated at 37°C overnight and the actual CFU/ml was determined by colony counting. The determined concentration, in CFU/ml and the associated OD reading were subsequently added to the standard curve to improve accuracy. Separate standard curves were generated for each bacterial strain.

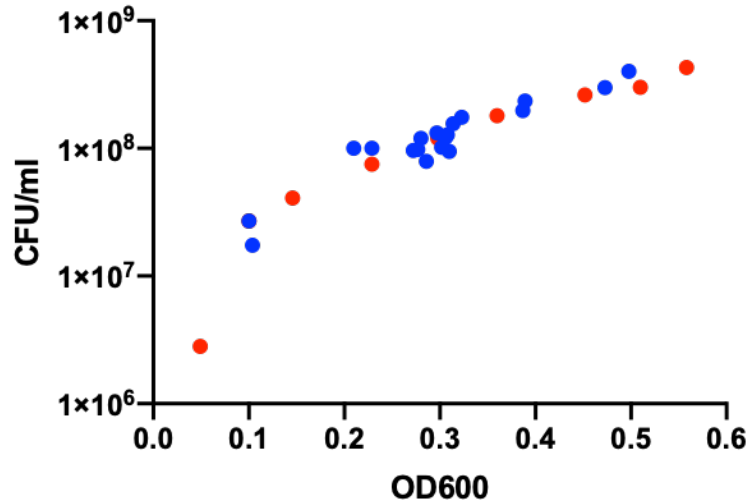


Figure 2-1. Standard curve for bacterial growth. Graph showing *E. coli* EV36 growth as measured by OD600 and CFU/ml. The series of red datapoints corresponds to the standard curve produced initially, while the blue datapoints corresponds to the concentrations determined for individual experiments.

2.3 Antibiotic concentrations

Antibiotics were used, where appropriate, at the concentrations listed in Table 2-2 in order to maintain plasmid expression or for selection purposes.

Antibiotic	Concentration	Reference
Ampicillin	100 $\mu\text{g/ml}$	152
Chloramphenicol	35 $\mu\text{g/ml}$	153
Kanamycin	100 $\mu\text{g/ml}$	153
Tetracycline	10 $\mu\text{g/ml}$	154

Table 2-2. Antibiotic concentrations for bacterial culture and selection.

2.4 Human cell lines and culture

The experimental laboratory research in this study was performed using two distinct cell lines, namely T24 and hCMEC, with distinct phenotypic properties as epithelial and endothelial cell lines respectively:

1. The human urinary bladder epithelial cell line, T24 (HTB-4), was acquired from LGC Standards UK, an ATCC (American Type Culture Collection) affiliate. The cell line was originally established *in vitro* in 1973 from the bladder transitional cell carcinoma of a female patient¹⁵⁵, and permanently expresses tumour-specific antigens (TSA).

The T24 cells were cultured in uncoated T75 flasks containing McCoy's 5A (Modified) Medium¹⁵⁶ supplemented with 10% v/v Foetal Bovine Serum (FBS), 100 units/ml Penicillin, and 100 µg/ml Streptomycin and were maintained at 37°C in 5% CO₂ under a humidified atmosphere.

2. The blood-brain barrier hCMEC/D3 (human cerebral microvascular endothelial cells) cell line was acquired from Merck. The cell line was originally established in 2005 from human temporal lobe micro-vessels and consist of enriched cerebral microvascular endothelial cells immortalised by lentiviral vector transduction with the catalytic subunit of human telomerase (hTERT) and SV40 large T antigen⁹⁸.

The hCMEC/D3 cells were cultured in 5 µg/cm² Collagen Type 1 (Collagen-1) coated T75 flasks containing EndoGRO-MV Complete Media (Merck) supplemented with 1 ng/ml bFGF (FGF-2) (Merck), 100 units/ml Penicillin, and 100 µg/ml Streptomycin and were maintained at 37°C in 5% CO₂ under a humidified atmosphere. All hCMEC culture vessels were coated with 5 µg/cm² Collagen-1 in PBS for 1 hour at 37°C before use.

Frozen stocks were prepared for long-term storage and split between -80°C and liquid nitrogen storage. 10% v/v DMSO was added to 1 million cells suspended in culture media in a cryovial and placed in a Nalgene freezing container to ensure a slow freezing cycle with a gradual decrease of 1°C/min.

Cell cultures being prepared for experimental use were routinely maintained by refreshing spent media and by passaging to ensure a continual supply of healthy cells. In order to retain its phenotype the passage number of hCMEC cultures was kept at 12 or under per supplier recommendation.

2.5 Growth determination of hCMEC cultures

hCMEC cells were seeded in culture medium onto 96-well tissue culture plates at a density of approx. 1.5×10^4 cells/cm² and allowed 24 hours to settle. Phages K1F or T7 were added to corresponding wells with untreated cells included as control. The cell density was determined manually at the time of seeding and at subsequent sampling points by using a haemocytometer on a trypsinised population.

2.6 Preparation of human cell cultures for experiments

For immunocytochemical (ICC) imaging, flow cytometry and real-time qPCR, T24 or hCMEC cells were seeded onto 6-well plates in culture medium and allowed 24 or 48 hours respectively to settle. The seeding density for ICC imaging was 2.1×10^4 cells/cm², and 5.2×10^4 cells/cm² for flow cytometry and real-time qPCR. hCMEC culture vessels were Collagen-1 coated before seeding.

Prior to an experiment, the culture medium was aspirated and replaced with Leibovitz L-15 media, a medium designed to support cell growth in environments lacking CO₂ equilibration, and the cultures were moved to a 37°C incubator suitable for bacterial infections.

2.7 Bacteriophage strains

Three phage strains were used in the experimental work for this study as listed below:

1. Phage K1F was originally isolated from sewage in 1984. The strain shows high specificity towards K1-capsule expressing bacteria⁷⁹. The polysaccharide capsule of *E. coli* K1 is recognised and degraded by the phage K1F-encoded endosialidase allowing for phage invasion⁷². The strain was kindly provided by Dr. Dean Scholl.
2. Phage K1F-GFP, a derivative of wild-type (wt) phage K1F engineered by Stanley Ho and Dr Antonia Sagona in collaboration with Dr Tamas Feher. A

cassette containing the superfolder green fluorescent protein (GFP) gene flanked by two 150 bp homology regions analogous to phage K1F was cloned into plasmid pSB6A1. Using homologous recombination, the gene cassette was integrated in wt phage K1F downstream of gene10, encoding for the minor capsid protein ¹⁵⁷.

3. Phage T7 is a well-characterised phage belonging to the family of Autographviridae in the order of Caudovirales. The exact environment of which it was isolated is unknown, but it first appeared in literature in 1945 simply as one of seven virulent phages of *E. coli*. It is an extensively used phage strain that shows high specificity towards commensal *E. coli* K12 bacterial strains ¹⁵⁸.

2.8 Purification of bacteriophages

A modified Castro-Mejia *et al* ¹⁵⁹ protocol was used to purify single-clone phage preparations to high concentrations. Single-clone preparations of phages were obtained by three consecutive infection cycles on their respective hosts and further selection of single plaques.

The single-clone phage preparations were propagated on bacterial cultures with increasing bacterial concentration increasing the phage concentration. Following bacterial clearance, each culture was centrifuged at 3220 g for 15 minutes at 4°C to remove bacterial debris and was filtered through a 0.22 µm syringe filter. The final propagation culture was incubated with 0.2 M NaCl for 1 hour to ensure phage release from bacterial membrane debris and was centrifuged at 5000 g for 45 minutes at 4°C. The supernatant was recovered and incubated with 10% w/v PEG8000 for 16-18 hours at 4°C to precipitate phage particles. The PEG solution was centrifuged for 25,000 g for 1 hour at 4°C and the pellet was resuspended in a small volume of SM-buffer I (Table 2-3).

A CsCl density gradient was prepared in water with three solutions in densities of 1.7, 1.5 and 1.3 g/ml. CsCl was added to the phage solution to achieve a final density of 1.3 g/ml. The CsCl solutions were added to the centrifuge tube in equal volumes

starting with the heaviest at the bottom and subsequently centrifuged at 125,000 g for 20 hours at 4°C.

The resulting blue/grey band was extracted by piercing a syringe through the centrifuge tube and was transferred to a clamped dialysis tube with MWCO of 14 kDa and dialysed overnight in SM-buffer I followed by 2 times 2 hours in SM-buffer II (Table 2-3). Following dialysis, the purified phages were stored at -20 and -80°C in SM-buffer II.

SM-buffer I		SM-buffer II	
NaCl	1 M	NaCl	100 mM
MgSO ₄ x 7H ₂ O	8 mM	MgSO ₄ x 7H ₂ O	8 mM
Tris-HCl	25 mM	Tris-HCl	25 mM

Table 2-3. Composition of SM-buffers for phage purification.

2.9 Bacteriophage enumeration

Phage enumeration was performed using a standard double agar overlay plaque assay as previously described ¹⁶⁰. A 10-fold dilution series of the phage preparation was prepared. Selecting appropriate dilutions and performed in triplicates, 100 µl phage dilution was added to 300 µl bacterial culture (log phase culture, OD₆₀₀ = 0.3) and incubated for 10 minutes at RT. The phage-bacterial suspension was mixed with 3 ml molten soft agarose (0.75% w/v agarose in LB) and immediately poured onto a pre-warmed LB culture plate. After solidification, the culture plates were incubated at 37°C overnight. The plaque numbers counted the following day were used to calculate the phage concentration in PFU/ml, favouring plates containing 30-300 plaques.

The standard double agar overlay approach was also used to determine phage host specificity and efficacy on solid media.

2.10 Determination of endotoxins in bacteriophage preparations

The concentration of endotoxin was determined using the Limulus Amebocyte Lysate (LAL) Chromogenic Endpoint Assay (Hycult Biotech) following the manufacturer's instructions. The kit is a plate-based ELISA with a lower detection limit of 0.04 EU/ml. Samples were diluted up to 1000 times to remain within range of the highest standard concentration of 10 EU/ml. Briefly, standards, controls and samples were assayed in technical duplicates by incubation with LAL for 20 minutes, then stop solution was added and the absorbance was measured at 405 nm using a FLUOstar Omega (BMG Labtech) plate reader. A standard curve was created with mean absorbance plotted on the y-axis and the corresponding concentration plotted on the x-axis with logarithmic scale. Sample absorbance values were interpolated on the standard curve and presented as the mean concentration of three biological replicates +/- SD.

2.11 Determination of bacteriophage host specificity in liquid culture

Bacterial cultures *E. coli* EV36 or *E. coli* MG1655 were aliquoted in 96-well culture plates and treated with phages K1F, K1F-GFP or T7 at an MOI of 0.001. Untreated cultures and LB alone were included as controls.

The OD at 600 nm was measured over four hours in 5-minute intervals using the FLUOstar Omega plate reader, while maintaining 37 C and orbital shaking between readings.

2.12 Transmission electron microscopy

Transmission electron microscopy (TEM) was performed to visually characterise the morphological properties of phage K1F. 400 mesh copper grids with carbon graphite coating were cleaned and hydrophilized by glow discharge. A 10 μ l drop of CsCl density gradient purified phage K1F was applied to the centre of the mesh and incubated for 1 minute at RT. The mesh washed twice with 10 μ l drops of the water

to remove the sample, and finally negatively stained with 10 μ l 2% uranyl acetate for 1 minute. Image were acquired using the Jeol 2100 transmission electron microscope.

2.13 Fluorescent immunocytochemical imaging

Following experimental treatment, the cultures were fixed in 4% paraformaldehyde for 15 minutes, permeabilised in ice-cold PEM buffer (80 mM PIPES, pH 6.75, 5 mM EGTA, 1 mM $\text{MgCl}_2 \times 6\text{H}_2\text{O}$) with 0.05% (v/v) Saponin for 5 minutes, and quenched with 50 mM NH_4Cl_2 in PBS for 15 minutes. Appropriate PBS wash steps were performed after each step.

For association assays, the fixed cells were stained with primary antibodies (Table 2-4) diluted in 0.05% (v/v) Saponin in PBS for 60 minutes at RT. This was followed by detection with secondary antibodies (Table 2-4) diluted in 0.05% (v/v) Saponin in PBS by incubation for 45 minutes at RT. The signal of GFP tagged phage was further enhanced with 5 μ g/ml GFP-Booster (Chromotek) alongside incubation with secondary antibodies. For invasion assays, the fixed cells were stained only with 5 μ g/ml Phalloidin CF680R conjugate (Biotium) for 40 minutes at RT.

Antibody	Type	Concentration
Anti-RAB7, polyclonal rabbit IgG (Bioss)	Primary	40 µg/ml
Anti-Cathepsin L, polyclonal rabbit IgG (Abcam)	Primary	1 µg/ml
Anti-LC3B, polyclonal rabbit IgG (Sigma-Aldrich)	Primary	5 µg/ml
Anti-CALCOCO2/NDP52, polyclonal rabbit IgG (Abcam)	Primary	1 µg/ml
Anti-hGalectin-8, polyclonal goat IgG (R&D Systems)	Primary	1 µg/ml
Anti-mono- and polyubiquitinated conjugated mAb (FK2) (Enzo Life Science)	Primary	1 µg/ml
Phalloidin conjugate, CF680R (Biotium)	Secondary	5 µg/ml
Cy-5 conjugated AffiniPure donkey anti-goat IgG (H+L) (Jackson Immuno Research)	Secondary	2.5 µg/ml
Cy-5 conjugated AffiniPure goat anti-rabbit IgG (H+L) (Jackson Immuno Research)	Secondary	2.7 µg/ml

Table 2-4. Antibodies for immunocytochemistry.

Stained coverslips were mounted on microscope slides using DAPI-containing Flourosshield Mounting Medium (Abcam) and secured with CoverGrip Coverslip Sealent (Biotium). Finally, the cells were imaged using a Zeiss LSM880 confocal microscope with Airyscan, using the following excitation wavelengths: DAPI at 405 nm, GFP at 488 nm, RFP at 561 nm and far-red (Cy5) at 633 nm.

2.14 Flow cytometric analysis of bacteriophage invasion in bacteria

Log-phase *E. coli* EV36 cultures were stained with either 2 µM propidium iodide (PI) or 3 µM Sytox Green Dead Cell Stain, in biological triplicates, and incubated for 20 minutes before the addition of phage K1F. Untreated *E. coli* EV36 cultures were incubated alongside as controls.

Assessment of GFP fluorophore stability was performed by addition of phage K1F-GFP alone to *E. coli* EV36 cultures.

Data acquisition and analysis was performed using a LSR Fortessa flow cytometer with FACSDiva software. Bacterial populations were initially gated on size via SSC/FCA to exclude cellular debris. 10,000 events were acquired of from sample. The mean fluorescent intensity (MFI) was detected for gated populations using B488-530/30A optics for Sytox Green and phage K1F-GFP, and YG561-586/15 optics for PI.

2.15 Flow cytometric analysis of bacteriophage invasion in human cells

Human cell cultures were incubated with respective treatments in biological triplicates. Sampling was performed by aspiration of spent media, trypsinising, and pelleting by centrifugation at 350g for 5 minutes. MEDIUM A (Fix & Perm Cell Permeabilization Kit), containing fixative and permeabilization agents, was added to the pellet, briefly vortexed, and incubated according to manufacturer's instructions. The cell suspension was diluted in eBioscience Flow Cytometry Staining Buffer and pelleted by centrifugation as above. MEDIUM B (Fix & Perm Cell Permeabilization Kit) containing either 1/100 dilution anti-hLC3B Alexa Fluor 647 Conjugated Ab (R&D Systems), or 1 µg/ml Anti-mono- and polyubiquitinated conjugated monoclonal antibody (FK2) (Enzo Life Sciences), was added to the pellet, briefly vortexed, and incubated for 45 minutes at RT. Following incubation, the cell suspension was diluted in Staining Buffer and pelleted by centrifugation as above.

For ubiquitin staining only, a secondary incubation with MEDIUM B containing 2 µg/ml Goat anti-mouse IgG (H+L) Cross Absorbed Secondary Ab Alexa Fluor 647 (Invitrogen) was performed for 30 minutes. Finally, the cell suspension was resuspended in Staining Buffer and placed on ice until acquisition.

MEDIUM A and MEDIUM B were not supplemented with antibodies for LysoTracker (Invitrogen) staining. Here, 500 nM final concentration LysoTracker was added to cultures 30 minutes prior to trypsinisation.

Data acquisition and analysis was performed using a LSR Fortessa flow cytometer and FACSDiva software. The human cell populations were initially gated on size via

SSC/FCA, excluding cellular debris and planktonic bacteria. 10,000 events were acquired from sample. The mean fluorescent intensity (MFI) was detected for gated populations using the following optics: R640-670/14-A for LysoTracker and Alexa Fluor 647 conjugated Ab, and YG561-586/15 for *E. coli* EV36-RFP.

2.16 Measurements of planktonic bacteria and free phages over time

T24 cells were prepared as previously described. *E. coli* EV36 and phage K1F were added to corresponding wells, in biological triplicates, at final concentrations of 5×10^6 CFU/ml and 3×10^3 PFU/ml respectively. Serial dilutions and plating for CFU determination were performed immediately after sampling, whereas samples taken for PFU determination were centrifuged at 3220 rpm for 15 minutes at 4 °C, immediately after sampling, to remove bacterial debris. The phage containing supernatants were stored at 4 °C for plating collectively, following the two-hour sampling period. CFU concentrations were determined by drop assay, plating 4×20 μ l drops of each 10-fold dilution on LB plates and incubating these for 24 hours at 37 °C. Dilutions selected for CFU quantification accounted for a minimum of 80 colonies of a dilution. PFU concentrations were determined by standard double overlay assay as previously described.

2.17 Quantitative real-time PCR

hCMEC cultures were incubated with *E. coli* EV36, phage K1F or TNF α (Sino Biological) in biological triplicates. RNA was recovered using the GenElute Mammalian Total RNA Miniprep Kit (Sigma-Aldrich) with DNase I Digestion Kit (Sigma-Aldrich) following the manufacturer's protocol.

First-strand DNA synthesis reaction was performed by addition of 1 μ g RNA, 50 nM Random Hexamers (Invitrogen), and 10 μ M dNTP Mix (Thermo Scientific), which was heated to 65°C for 5 minutes and was then rapidly chilled on ice. A reverse transcriptase mastermix consisting of 0.1M DTT, 1U RNaseOUT, and 100 U Superscript III (Invitrogen), was added to the reaction and a single cycle PCR

programme was run; anneal at 25 °C for 5 minutes, extend at 50 °C for 60 minutes and inactivate at 70 °C for 15 minutes. The resulting cDNA was subsequently stored at -20 °C.

Real-time PCR of cDNA samples was performed with Brilliant III SYBR Green qPCR Master Mix with Low ROX (Agilent) using the Stratagene Mx3005P instrument with MxPro v4.10 build 389 software (Agilent Technologies). Each sample was quantified in technical triplicates using primer sets for GAPDH, TNF α , IL-6, IL-8, IL-10 and IFN β (Table 2-5) on a 50-cycle programme consisting of annealing at 95 °C for 10 seconds and extending at 60 °C for 30 seconds followed by a single inactivation cycle.

Genes	Forward 5' → 3'	Reverse 5' → 3'	Ref
GAPDH	GGTCGGAGTCAACGGATTT	CCAGCATCGCCCCACTTG	161
TNF α	GCCAGAATGCTGCAGGACTT	GGCCTAAGGTCCACTTGTGTCA	162
IL-6	AAAGAGGCACTGGCAGAAA	TTTCACCAGGCAAGTCTCCT	163
IL-8	AGGTGCAGTTTTGCCAAGGA	TTTCTGTGTGGCGCAGTGT	164
IL-10	CATCGATTTCTCCCTGTGAA	TCTTGGAGCTTATTAAAGGCATTC	165
IFN β	ATTGCCTCAAGGACAGGATG	GGCCTTCAGGTAATGCAGAA	166

Table 2-5. Quantitative real-time PCR primers.

Data analysis was performed using the Comparative Ct Method ¹⁶⁷. Δ Ct values for each gene of interest were calculated by subtracting the average GAPDH Ct value from the average Ct value obtained for each gene. $\Delta\Delta$ Ct values were calculated by subtracting Δ Ct values of untreated cultures from Δ Ct values of treated cultures. The fold change was calculated by taking the log base 2 of $\Delta\Delta$ Ct values.

2.18 ELISA

The IL-6 protein expression of hCMEC cultures was detected using ELISA. hCMEC cultures were treated with *E. coli* EV36, phage K1F or TNF α in biological triplicates to

capture random biological variation. The cultures were incubated for 6 hours, during which time spent media was recovered at set time points and immediately passed through a 0.22 μm filter and stored at -80°C . Untreated hCMEC cultures were included as controls. Appropriate sample dilution was performed to maintain readings within the assay range of 2-200 pg/ml.

Expression of IL-6 protein was detected using the Human IL-6 Uncoated ELISA kit (Invitrogen). 96-wells plates were coated with capture antibody and were incubated overnight. The capture antibody was aspirated, plates thoroughly washed, and incubated with blocking diluent for 1 hour. Samples and a prepared 2-fold serial diluted human IL-6 standard were added to corresponding wells in technical duplicates and the plate was incubated overnight at 4°C . Following incubation, a series of reagents were added with aspiration and thorough wash between each addition, this included detection antibody, Streptavidin-HRP, TMB solution and finally stop solution. The completed ELISA build was measured at 450 and 570 nm using a FLUOstar Omega plate reader. Analysis was performed by wavelength subtraction of 570 from 450 nm readings and subsequent interpolating of sample values on the standard curve. Graph generation was performed using GraphPad Prism.

2.19 xCELLigence

hCMECs were seeded into Collagen-1 coated E-Plate VIEW 16 PET (ACEA Biosciences) at a concentration of 5×10^4 cells/well in assay media. The plates were inserted into the RTCA DP station and the cells allowed approximately 24 hours to settle before the addition of treatment. Acquisition was performed using the xCELLigence RTCA DP instrument (ACEA Biosciences) housed in a humidified incubator at 37°C with 5% CO_2 . The instrument was set to a single frequency of 10 kHz with 5-minute measuring intervals over the course of 96 hours. Using a fixed frequency of 10 kHz, the current predominantly travels transcellularly allowing for impedance measurements relating to the cell-to-electrode adhesion (focal adhesion) of the cells¹⁶⁸. The focal adhesion of epithelial and endothelial cells represents adhesion to the extracellular matrix and

is a direct contributor to the flexibility and permeability of the vessel. Other systems, such as the Electric Cell-substrate Impedance Sensing (ECIS) uses a lower frequency of <4 kHz by which the current predominantly travels paracellularly thus allowing for measurements representing the cell-to-cell adhesion of the cells.

The xCELLigence VIEW plates contain a gold electrode array onto which the cells adhere. The electrode array mimics an extracellular matrix substrate. The data output returned by the xCELLigence system, the Cell Index, represents the relative changes in frequency-dependent electrode resistance or impedance. The term impedance collectively covers resistance and reactance which is defined as the opposition to a flow of current and the opposition to a change in current¹⁶⁹. The Cell Index is affected by cell interactions with the electrode array, and can therefore be influenced by cell proliferation, cell morphology, cell viability and cell-electrode adhesion.

Data analysis and graph generation was performed in GraphPad Prism 8.2.1, where the data was normalised to a Cell Index of 1 relative to approximately 1 hour before treatment addition.

2.20 Preparation of electrocompetent bacterial cells

Overnight bacterial cultures were refreshed 1:10 with LB and allowed to grow to an OD₆₀₀ of 0.6-0.8. The cultures were poured into prechilled centrifuge bottles and incubated on ice for 30 minutes, before being centrifuged at 2000 g for 15 minutes in a pre-cooled centrifuge at 4 °C. Pellets were gently resuspended over multiple rounds, firstly, in cold sterile water, and secondly, in cold 10% v/v glycerol and were centrifuged as previously between rounds with intermittent incubation periods on ice. Finally, the pellets were resuspended in a small volume of cold 10% v/v glycerol and aliquoted into cold 1.5 ml eppendorfs, which were snap frozen on dry ice and subsequently transferred to -80 °C.

2.21 Transformation by electroporation

1 µl transformation product was added to 50 µl cool electrocompetent bacterial cells on ice and immediately transferred to a 1 mm electroporation cuvette. The cells/product were briefly electroporated with 2.5 kV at 200 Ohms, transferred to 1 ml prewarmed SOC media and incubated for 37 °C for 2 hours with shaking. The cell suspension was centrifuged at 2000 g for 2 minutes, and 800 µl supernatant were discarded. The pellet was gently resuspended in the remaining SOC media and both streaked and poured onto separate LB culture plates with appropriate antibiotics.

2.22 Polymerase Chain Reaction

Polymerase Chain Reaction (PCR) was carried out by preparing 50 µl reactions consisting of 1 µl sample, 25 µl Taq Mix Red (PCRBIO), 2.5 µl 10 µM forward (fwd) primer, 2.5 µl 10 µM reverse (rev) primer, 1.5 µl DMSO, and sterile H₂O. The reactions were run on a thermocycler initially on a default program (Table 2-6), however the annealing temperature and extension time would often need optimisation depending on primers and template.

Cycles	Temperature (°C)	Time	Description
1	95	1 min	Initial denaturation
40	95	15 sec	Denaturation
	55	45 sec	Anneal
	72	30 sec	Extension
1	72	10 min	
1	4	∞	

Table 2-6. Default PCR program.

For screening PCRs, a no template control (NTC) with no sample, a no amplification control (NAC) with no Taq Mix and appropriate positive and negative controls were included in each run.

Primers were designed with the following design stipulations in mind; Melting temperatures should be 52-58°C, close as a pair, and never above 65°C. GC content should be 40-60%. Di-nucleotide repeats and secondary structures should be avoided. Primers used for amplification and screening purposes are listed in Table 2-7.

Primer	Sequence 5' to 3'	Description
AS058	actagatgagcgtcatctct	FWD for K1F RNAP with spel
AS059	ctgcagttaagcgaatgcaaa	REV for K1F RNAP with pst1
AS067	aattcgcggccgcttctaga	FWD seq for chimeric G-BLOCK insert in plasmid
AS072	taacctccactaccgaccga	FWD seq to detect correct insert of chimeric G-BLOCK in T7
AS073	gctacaccggtccaacaat	REV seq to detect correct insert of chimeric G-BLOCK in T7
AS074	tattctagaataaatgtgagcggataacattg	FWD for amp of lac promoter with Xbal
AS075	tatactagttttctctctttctctagtgg	REV for amp of lac promoter with SpeI
AS076	atcagctttcagcacgtcggt	REV seq for chimeric G-BLOCK insert in plasmid
AS077	gtcaataacgatggtcacttggatgc	FWD for amp of the g-block chimeric phage
AS078	ttacttctgttcaagagcagaaagtctgg	REV for amp of the g-block chimeric phage

AS080	atgcaccttacatgggtagc	FWD middle seq for correct insert of chimeric gblock in T7
AS081	atgttactactggctgctggc	REV middle seq for correct insert of chimeric gblock in T7
AS083	tattctagatatttacactcgcctattgtaactgtaa	FWD anti-sense strand with XbaI - complement to AS074
AS084	tatactagtaaagaggagaaagagatcacca	REV sense strand with SpeI - complement to AS075
AS085	ataaatgtgagcggataacattgaca	FWD seq to detect orientation of PLLac0-1
AS086	ccagcaggttaaacggc	REV seq to detect orientation of PLLac0-1
AS097	ccggaattccgactcacggt	FWD amp of RNAP deletion gBlock
AS098	ggactagttgaacgggatgtaagctg	REV amp of RNAP deletion gBlock
AS099	gaattcggccgcttctagataaatg	FWD amp of PLLac + RNAP gBlock
AS100	ctgcagcggccgctactagtatta	REV amp of PLLac + RNAP gBlock
AS101	gccgccgtcattatcctgaa	FWD selection for RNAP gblock insert
AS102	tcaggcgcgtcgtatctttc	REV selection for RNAP gblock insert
AS103	cagtgctgcaatgataccgc	FWD screening for RNAP deletion insert
AS104	agtcccaccattaacgccag	REV screening for RNAP deletion insert
AS105	ctaagattgcgcaagccgtc	FWD screening for wt RNAP in cloned K1F
AS106	ggaaggcaaggcttcaggat	REV screening for wt RNAP in cloned K1F

AS113	ctcaggctggaaggcgatag	FWD for PCR/GATC screen of AmpR insert/wt RNAP in wt K1F
AS114	gagtgctcctagccacaagg	REV for PCR/GATC screen of AmpR insert/wt RNAP in wt K1F

Table 2-7. Amplification and screening primers.

Gel electrophoresis was performed to visualise the bp size of the PCR product. The gel was cast with 1% agarose in 1X TAE buffer and 1X SYBR Safe (Invitrogen). Once completely solidified, the agarose gel was placed into the electrophoresis unit and was fully submerged in 1X TAE buffer. Samples, controls, and a molecular weight ladder were loaded to corresponding wells. Typically, a small 8-well gel was run for 40 minutes at 100 V.

2.23 GATC Sequencing

Overnight GATC sequencing was exploited by dispatching an eppendorf containing 5 μ l 80-100 ng/ μ l template and 5 μ l 5 μ M primer. Templates such as ligation products or phage DNA were purified before dispatch. The data received would cover a sequence upwards of 1000 bases.

2.24 Engineering strategy for modifying the phage host tropism

One of the challenges of phage therapy is the limited host range of individual phage strains. In this study, a chimeric podoviridae phage was sought designed and engineered to address this challenge.

The complete phage K1F sequence was published in 2005 (GenBank: DQ111067.1)⁷⁹. The single double-stranded DNA molecule of 39,704 bp consists of 42 open reading frames (ORFs) with 88% of the sequence predicted to encode for proteins (Figure 2-2). Phage K1F is closely related to the phages of the T7 supergroup which

also include coliphages T7, T3, K1E, and K1-5, yersiniophages phiA1122 and phiYeO3-12, and salmonellaphage SP6 among others ⁷⁹.

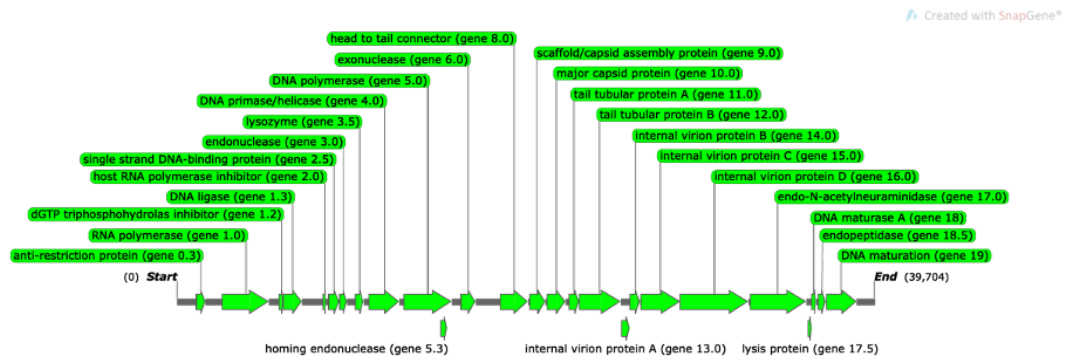


Figure 2-2. Genome organisation of phage K1F. Unknown gene products not shown. Figure generated using SnapGene.

Although phage K1F encodes an endosialidase similar to that of phages in the SP6 subgroup, the overall genome organisation and position of endosialidase is more similar to that of phages in the T7 subgroup ⁷⁹. The complete T7 nucleotide sequence was published in 1983 (GenBank: V01146.1) and was one of the first complete phage genomes ever published ¹⁷⁰. The genome comprises of 39,936 bp with 50+ expressed genes covering 92% of the sequence (Figure 2-3), and both phages K1F and T7 performs a ribosomal frameshift during translation from gene 10A to gene 10B making up the major and minor capsid proteins.

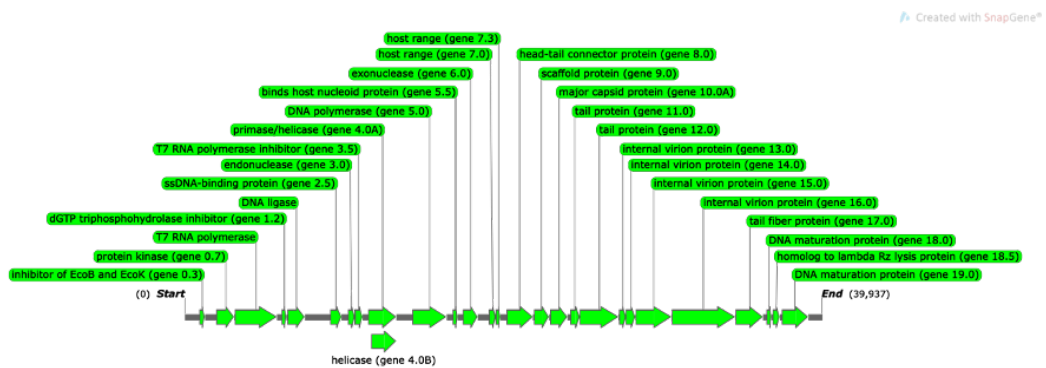
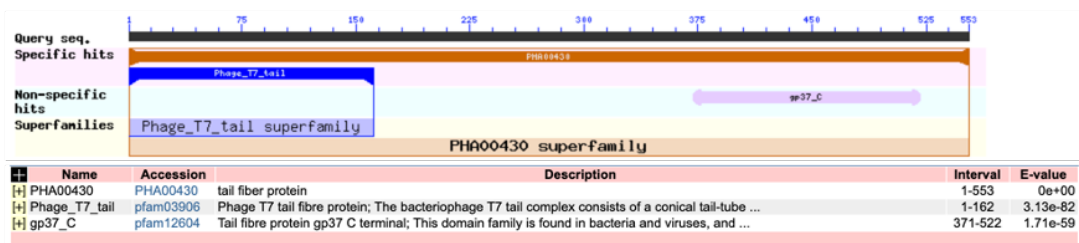


Figure 2-3. Genome organisation of phage T7. Unknown gene products not shown. Figure generated using SnapGene.

The RBP of phage K1F is the phage-bound endo-N-acetylneuraminidase (endosialidase) encoded by *gene17* which enables the phage to recognise, bind to, and degrade the K1 polysaccharide capsule⁷⁹. The K1F endosialidase as an active enzyme generated by auto catalytical truncation of the gene product 152 amino acids from the C-terminus¹⁷¹. The K1F endosialidase also consists of an N-terminal head-binding domain with sequence similarity to the T7 tail fibre (Figure 2-4). Phages K1F and T7 both performs a ribosomal frameshift during translation from gene 10A to gene 10B making up the major and minor capsid proteins.

T7 gp17 protein BLAST



K1F gp17 protein BLAST

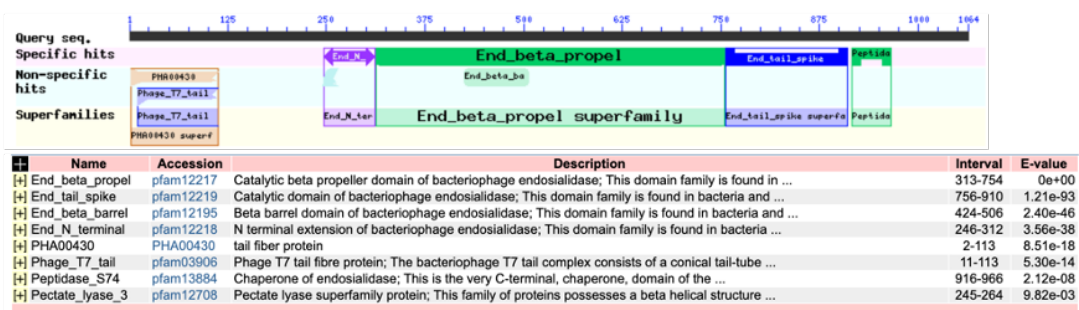


Figure 2-4. Comparison of amino acid sequences of phages T7 (above) and K1F (below) highlighting conserved domains. Figure generated using NCBI protein BLAST.

Based on the similarities in genomic organisation and sequence of phage K1F and T7 a engineering strategy was formed to replace *gene17* of phage T7 with phage K1F endosialidase. A chimeric g-block was designed to incorporate the 2700 bp 3' end of K1F endosialidase and the 120 bp 5' end of phage T7 *gene17*. Cloning vector pBR322 with a pUC replicon and ampicillin resistance through expression of β -lactamase was used as the plasmid backbone. Thioredoxin and a second 91 bp T7 homology region corresponding to the region directly downstream of phage T7 *gene17* was cloned

into the plasmid. Finally, the p7_K1F_chimera plasmid was completed by the integration of the chimeric g-block using Gibson assembly (Figure 2-5).

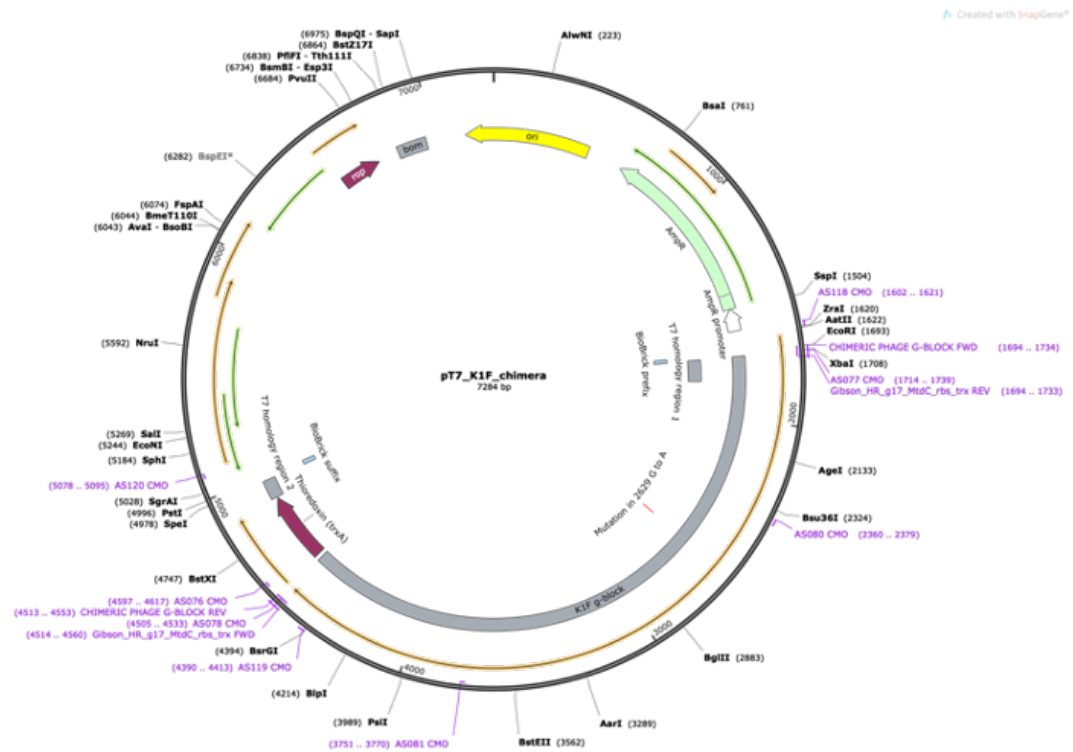


Figure 2-5. Design overview of the p7_K1F_chimera plasmid. Figure generated using SnapGene.

A second plasmid was designed to promote the growth of recombinant phages by expression of phage T7 gene product 17 in trans. A g-block consisting of T7 promoter, ribosomal binding site (RBS), phage T7 *gene17*, and T0 terminator. The g-block was ligated into the pBR322 cloning vector using BioBricks Prefix and Suffix predetermined restriction sites (Figure 2-6).



Figure 2-6. Design overview of the pT7_gp17 plasmid. Figure generated using SnapGene.

2.25 Engineering strategy for a replication-deficient phage

The natural ability of virulent phages to replicate in the presence of a susceptible host results in an uncontrollable rate of bacterial death and the associated release of endotoxins. The ability to control or limit the replication of a phage preparation would enable the death of a known concentration of bacteria more akin to a drug. In this study a replication-deficient phage was sought to be designed and engineered.

A strategy was formed to delete the phage K1F gene 1.0 which encode for RNA polymerase (RNAP) by substitution. A g-block was designed to incorporate two 150 bp regions homologues to phage K1F immediately down- and upstream of gene 1.0 surrounding an ampicillin resistance gene and promoter. The g-block was ligated into the pSB1C3 cloning vector containing the pmb1 replicon and a chloramphenicol acetyltransferase gene conferring chloramphenicol resistance (Figure 2-7).

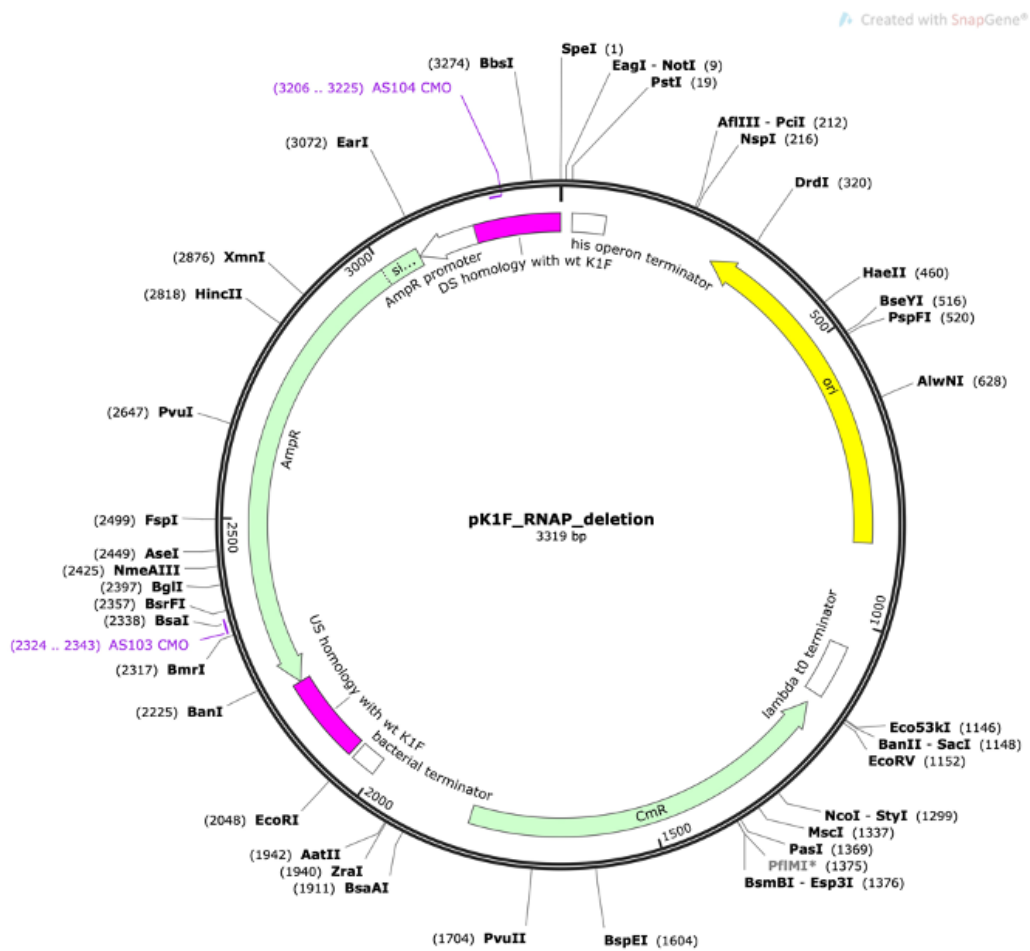


Figure 2-7. Design overview of the pK1F_RNAP_deletion plasmid. Figure generated using SnapGene.

A second plasmid was designed to allow for the replication of recombinant replication-deficient phages by the expression of phage K1F RNAP in trans. A g-block was designed to incorporate the entire phage K1F RNAP gene with RBS and terminator and was ligated into the pSB3T5 cloning vector containing the p15a replicon and a tetracycline efflux gene conferring tetracycline resistance (Figure 2-8). The plasmid-expressed RNAP sequence was codon optimised to allow for the simultaneous expression of codon optimised RNAP in trans while selecting for the wild type RNAP using CRISPR-Cas.

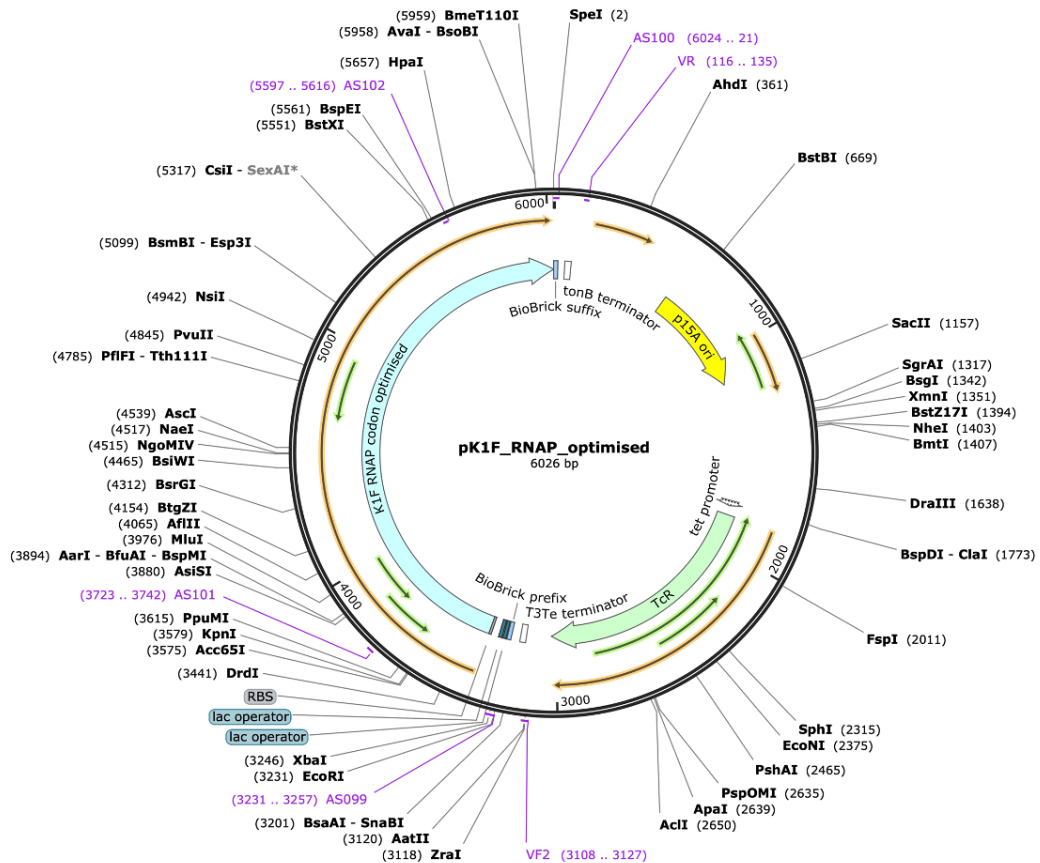


Figure 2-8. Design overview of the *pK1F_RNAP_optimised*. Figure generated using SnapGene.

2.26 Integration of g-blocks into cloning vectors

Upon receipt, g-blocks were PCR amplified as described by the supplier and the was product purified using GeneJET PCR kit (ThermoScientific).

Insert and vector pairs (Table 2-8) were digested in separate 50 μ l reactions consisting of up to 1 μ g DNA (insert or vector), 1 μ l 20,000 U/ml EcoRI (NEB), 1 μ l 10,000 U/ml SpeI (NEB), 5 μ l 10X CutSmart Buffer (NEB), and sterile H₂O. The reactions were incubated for 1 hour at 37 $^{\circ}$ C, and were purified using the DNA clean & concentrator kit (Zymo) eluted in a small volume.

Insert	Description	Amp primers	Vector
g-block_T7_K1F_ chimera	Substitution of phage T7 gp17 with phage K1F endosialidase	AS065 + AS066	pBR322
g-block_T7_gp17	Expression of codon optimised phage T7 gp17 in trans	AS077 + AS078	pBR322
g-block_RNAP_K1F_ deletion	RNAP deletion by insertion	AS097 + AS098	pSB1C3
g-block_RNAP_K1F_CO	RNAP expression in trans	AS099 + AS100	pSB3T5

Table 2-8. g-blocks and cloning vectors.

Ligation of insert into vector was performed by preparing a 20 µl reaction consisting of 150 ng insert, 50 ng vector, 2 µl T4 10X Ligation Buffer (NEB), 1 µl T4 DNA Ligase (NEB), and sterile H₂O. The ligation reaction was incubated overnight at RT and was subsequently stored at -20 °C. Confirmation of correct integration was confirmed by PCR and GATC sequencing before transformation into a bacterial host.

2.27 Homologous recombination

Phage K1F at a MOI of <1 was added to a log phase bacterial culture at an OD₆₀₀ of 0.3 previously transformed with the HR plasmid and incubated at 37 °C with shaking (200 rpm). Following bacterial clearance, the lysate was centrifuged at 3220 g for 15 minutes at 4 °C and subsequently passed through a 0.22 µm pore size filter. Consecutive rounds of HR were performed to enrich the recombinant phage population by allowing further generation of phage progeny.

Generation of recombinant phages during HR was confirmed by PCR directly from the HR lysate or by plaque PCR.

2.28 Selection for recombinant phages

Multiple selection strategies were devised for the selection of recombinant T7/K1F chimeric phages (Figure 2-9). The HR lysate containing wt and recombinant phages was plated on bacterial hosts using the standard double overlay method previously described and incubated overnight at 37 °C. Growth on *E. coli* EV36 should positively favour and enrich for the recombinant K1 phenotype, while marker-based selection on a thioredoxin deficient bacterial host should exclude growth of wt phages. The added expression of either phage T7 *gene17* *in trans* or CRISPR enzymes containing spacers targeting the phage T7 *gene17* should enhance the selection of recombinant T7/K1F chimeric phages. Candidate plaques were picked and prepared for PCR or GATC sequencing.

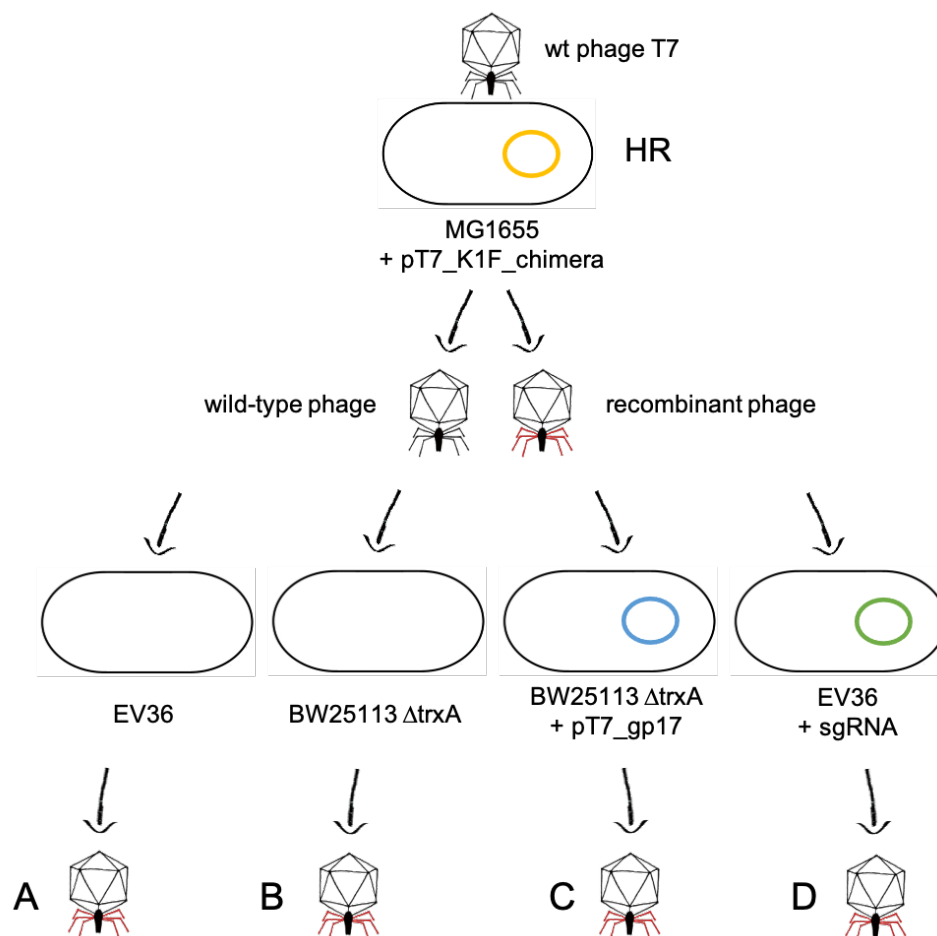


Figure 2-9. Selection strategy for recombinant T7/K1F chimeric phages.. Positive selection on host *E. coli* EV36 (A). Marker-based selection relying on the thioredoxin deficiency of host *E. coli* BW25113 Δ trxA alone (B), in conjunction with either the expression of phage T7 gp17 (C) or negative selection of wt phages using CRISPR-Cas (D). Original figure.

The strategy for selection of recombinant replication-deficient phages relied on phage-derived ampicillin resistance (Figure 2-10). The HR lysate containing wt and recombinant phages was plated on *E. coli* EV36 expressing pK1F_RNAP_optimised using the standard double overlay method previously as per chimeric phage selection. The addition of CRISPR enzymes containing spacers targeting the wt phage K1F RNAP expressed on pCas9_K1F_RNAP further enhanced the selection for recombinant phages.

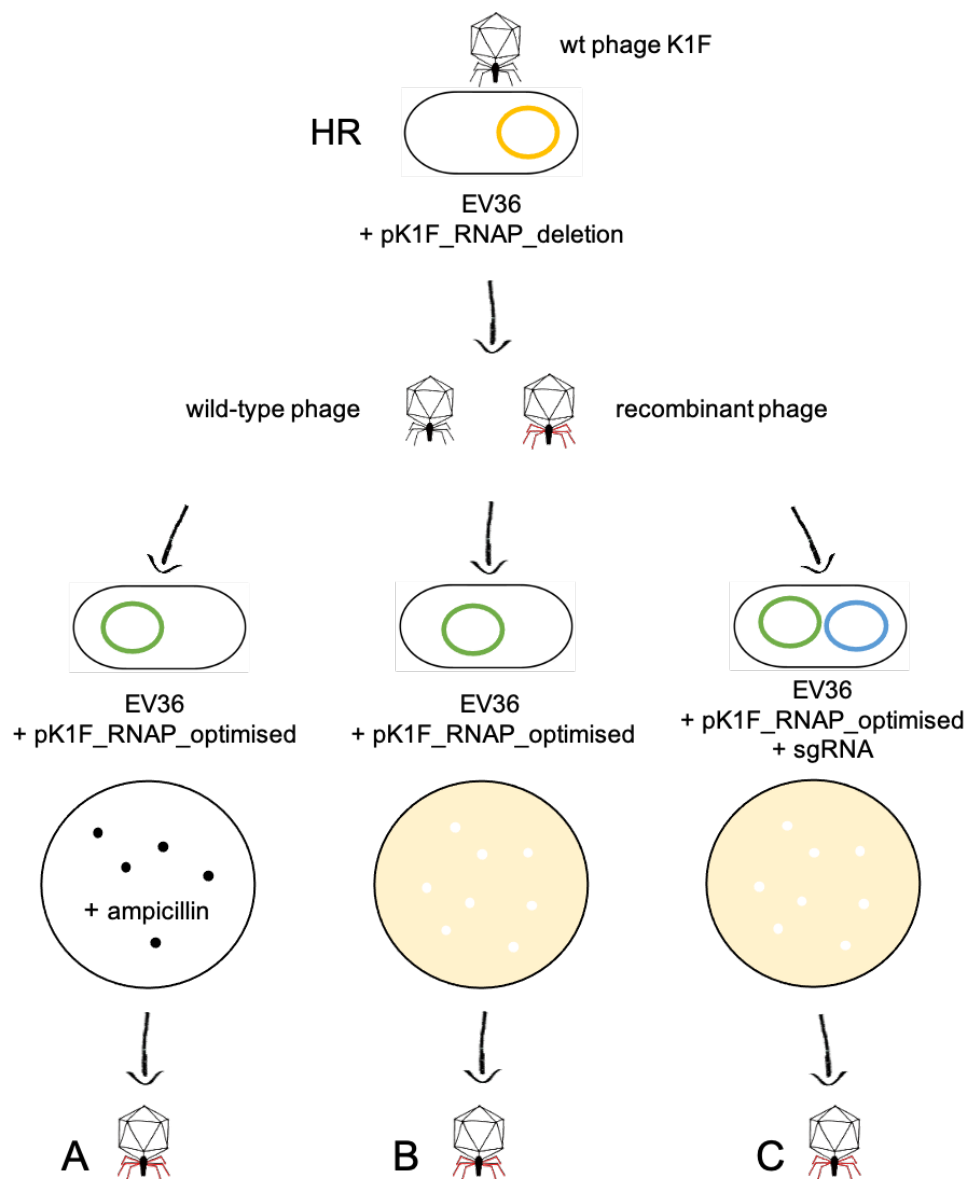


Figure 2-10. Selection strategy for recombinant replication-deficient phage. Following HR of wt phage K1F on EV36 + pK1F_RNAP_deletion, the HR product is plated on various hosts to select for recombinant phage. Ampicillin selection of bacterial host containing intracellular recombinant phage with pK1F_RNAP_optimised relying on

phage-derived ampicillin resistance (A) Selection of recombinant phage on EV36 + pK1F_RNAP_optimised alone (B) or in conjunction with pCas9_K1F_RNAP targeting wt K1F RNAP (C). Original figure.

2.29 Integration of sgRNAs in pCas9 vectors

A 20 μ l digestion reaction of the pCas9 vector ¹⁷² (Addgene 42876, kindly provided by Dr Luciano Marraffini) was prepared with 1 μ g pCas9 vector, 1 μ l Bsal (NEB), 0.5 μ l 100x BSA (NEB), 1 μ l Quick CIP (NEB), 2 μ l 10X CutSmart Buffer (NEB), and ddH₂O. The reaction was incubated for 60 minutes at 37 °C, purified using the DNA clean & concentrator kit (Zymo), and stored at -20 °C.

The spacers were designed using the www.atum.bio cas9 tool, by uploading the target gene sequences to the platform and selecting *E. coli* as expression host, NGG as PAM, and the wtCas9 enzyme. The tool returned spacers with the least off-target effect, i.e. toxicity, in *E. coli*. To minimise the sequence similarity of the spacers with the recombinant sequences, recursive searches were performed continually shortening the PAM-distal end of the spacer.

sgRNA phosphorylation was carried out for each sgRNA pair (Table 2-9) by preparing a 20 μ l reaction consisting of 1 μ l 100 μ M of each sgRNA (fwd and rev) (IDT), 2 μ l 10 mM ATP (NEB), 2 μ l T4 PNK 10X Reaction Buffer (NEB), 1 μ l T4 Polynucleotide Kinase (PNK) (NEB), and ddH₂O. The phosphorylation reaction was incubated for 30 minutes at 37 °C. This was followed by sgRNA annealing, performed by addition of 2.5 μ l 1 M NaCl to each phosphorylated sgRNA pair, incubation for 5 minutes at 95 °C, gradient cooling to RT over 2 hours, purified using the DNA clean & concentrator kit (Zymo), and finally stored at -20 °C.

sgRNA	Sequence 5' to 3'	Description
sgRNA1_gp17_fwd	aaacgagttaccactacgaacttag	FWD pCas9 spacer sequence for T7 gp17 - PAM on antisense
sgRNA1_gp17_rev	aaaactaagttcgtagtggaactc	REV pCas9 spacer sequence for T7 gp17 - PAM on antisense
sgRNA2_gp17_fwd	aaacgatggtcacttggatgctcgg	FWD pCas9 spacer sequence for T7 gp17 - PAM on sense
sgRNA2_gp17_rev	aaaaccgagcatccaagtgaccatc	REV pCas9 spacer sequence for T7 gp17 - PAM on sense
sgRNA5_RNAP_fwd	aaaccgttcgatgggtcctgctctg	FWD pCas9 spacer sequence for K1F RNAP - PAM on sense
sgRNA5_RNAP_rev	aaaacagagcaggacctcgaacg	REV pCas9 spacer sequence for K1F RNAP - PAM on sense
sgRNA6_RNAP_fwd	aaacaccttcgtgccactccttgag	FWD pCas9 spacer sequence for K1F RNAP - PAM on antisense
sgRNA6_RNAP_rev	aaaactcaaggagtggcacgaaggt	REV pCas9 spacer sequence for K1F RNAP - PAM on antisense

Table 2-9. sgRNA pairs for pCas9 integration.

Ligation of sgRNA pairs in pCas9 vector was carried out by preparation of a 20 μ l reaction consisting of 50 ng vector, 150 ng insert, 2 μ l T4 10X Ligation Buffer (NEB), 1 μ l 400 U/ μ l T4 DNA Ligase (NEB), and sterile water. The reaction was incubated overnight at RT and was subsequently stored at -20 °C.

Integration of sgRNAs into pCas9 vectors was confirmed by PCR and GATC sequencing using the primers listed in Table 2-10 .

Primer	Sequence 5' to 3'	Description
pCas9_fwd	cagctaggagggtgactgaag	pCas9 forward PCR and seq primer. Covers DR repeats and spacer insertion site.
pCas9_rev	ggtgatgtcggcgatatagg	pCas9 reverse PCR and seq primer. Covers DR repeats and spacer insertion site.
sgRNA1_gp17_check_rev	gagttaccactacgaactta	Check for inserted spacer.
sgRNA2_gp17_check_fwd	gatggtcacttggatgctcg	Check for inserted spacer.
sgRNA1_RNAP_check_fwd	cgttcgatgggtcctgctct	Check for inserted spacer.
sgRNA2_RNAP_check_rev	tcaaggagtggcacgaagg	Check for inserted spacer.

Table 2-10. pCas9 vector primers for PCR testing.

2.30 Statistical analysis

All quantification and statistical analysis in this study were performed using GraphPad Prism 8.2.1 (San Diego, CA). Probability values were calculated pair-wise where appropriate using the unpaired t-test assuming Gaussian distribution. The level of significance is presented in relevant graphs.

Chapter 3 Establishing *in vitro* model systems for phage therapy

The primary aim of this chapter was to establish model systems for phage therapy that would enable cellular and molecular studies *in vitro*. This was accomplished through characterisation of the relationship between the three legs of the system, namely bacteria, phages, and human cells.

In this context, the suitability of *E. coli* EV36 and phage K1F was assessed in terms of host specificity and efficacy, and their ability to fulfil their roles as prey and predator in a human cell environment.

The experiments performed in this chapter also allowed for an assessment of the versatility and compatibility of the methodologies used in this and subsequent chapters, in that time points and concentrations used would allow infection of both bacteria and phage to be visualised and quantified.

3.1 Bacteriophage K1F display podoviridae morphology

During preliminary method optimisation and characterisation efforts of phage K1F, transmission electron microscopy (TEM) was performed (Figure 3-1). The negatively stained electron micrographs of phage K1F confirmed a phenotype similar to that of the podoviridae family characterised by displaying very short tails, which are non-contractile, and a clear icosahedral capsid structure with a diameter of approximately 60 nm¹⁷³.

TEM was also used for the optimisation and evaluation of each protocol step for purification of phage preparations (Figure 3-1). Purification by consecutive rounds of centrifugation, PEG-precipitation, and CsCl density gradient ultra-centrifugation yielded a high-titre phage preparation visually free of contaminants. The result of the ultra-centrifugation in itself was evident by the observation of a blue-greyish phage-containing band (Figure 3-2).

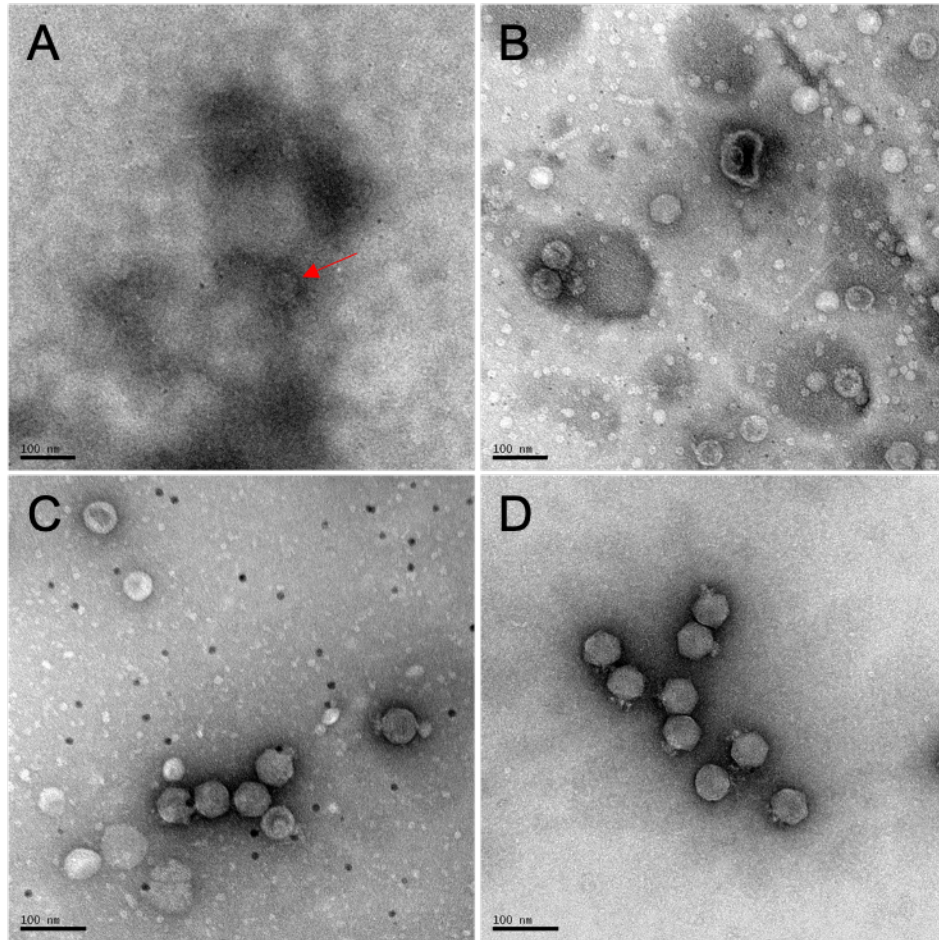


Figure 3-1. Negative staining electron micrographs of bacteriophage K1F showing the optimisation of the phage purification protocol. Micrographs acquired by transmission electron microscopy at 30,000x magnification. (A) Brief centrifugation and sterile filtering. Arrow denotes a potential phage capsid. (B) As A plus high-speed centrifugation. (C) As B plus NaCl addition and PEG8000 precipitation. (D) as C plus CsCl gradient density ultracentrifugation and dialysis.

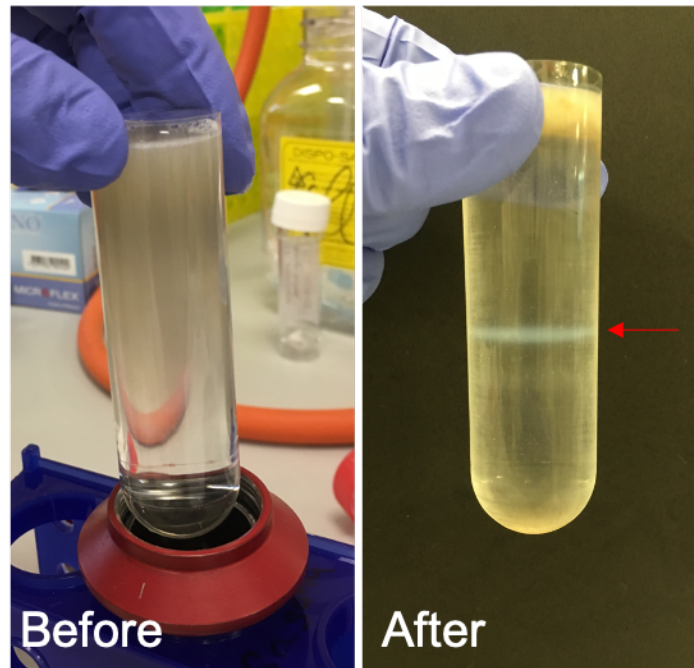


Figure 3-2. Images show a phage preparation before and after equilibrium of the CsCl density gradient. The arrow denote the formation of a phage-containing band.

3.2 Bacteriophage K1F strains specifically infect *E. coli* EV36

The host specificity of phages K1F, K1F-GFP and T7 was tested on bacterial hosts *E. coli* EV36 and *E. coli* MG1655 in liquid culture by measurement of absorbance at an optical density (OD) of 600 nm over four hours (Figure 3-3). The optical density is a measure of bacterial concentration or in this case, bacterial growth. Log phase cultures were treated at 0 hours at an initial OD₆₀₀ of approximately 0.2 with phages at a multiplicity of infection (MOI) of 0.001. The ability of phages K1F and K1F-GFP to infect and lyse *E. coli* EV36 was demonstrated by the decreasing OD₆₀₀ of the bacterial culture starting at 65 and 100 minutes, respectively (Figure 3-3A). The continually decreasing OD₆₀₀ indicated clearance of the *E. coli* EV36 culture at 120 and 180 minutes for phages K1F and K1F-GFP respectively. The difference observed in the rate of decrease in OD₆₀₀ illustrates a difference in fitness between the wild type (wt) phage and its engineered derivative, with the wt phage K1F exhibiting superior fitness. As experimental controls, a no-treatment control (NTC) receiving no addition of phage and *E. coli* EV36 treated with phage T7 was included. *E. coli* EV36 treated with phage T7 showed only a slight reduction of OD₆₀₀ after 160 minutes in

comparison with the NTC. Additionally, *E. coli* MG1655 was treated with phages K1F, K1F-GFP and T7 in a similar manner (Figure 3-3B). In contrast to the infections of *E. coli* EV36, the OD600 of *E. coli* MG1655 cultures decreased after 60 minutes following the addition of phage T7 and cleared within a further 30 minutes, while the OD600 of *E. coli* MG1655 cultures treated with phages K1F and K1F-GFP remained comparable to the NTC throughout the experiment.

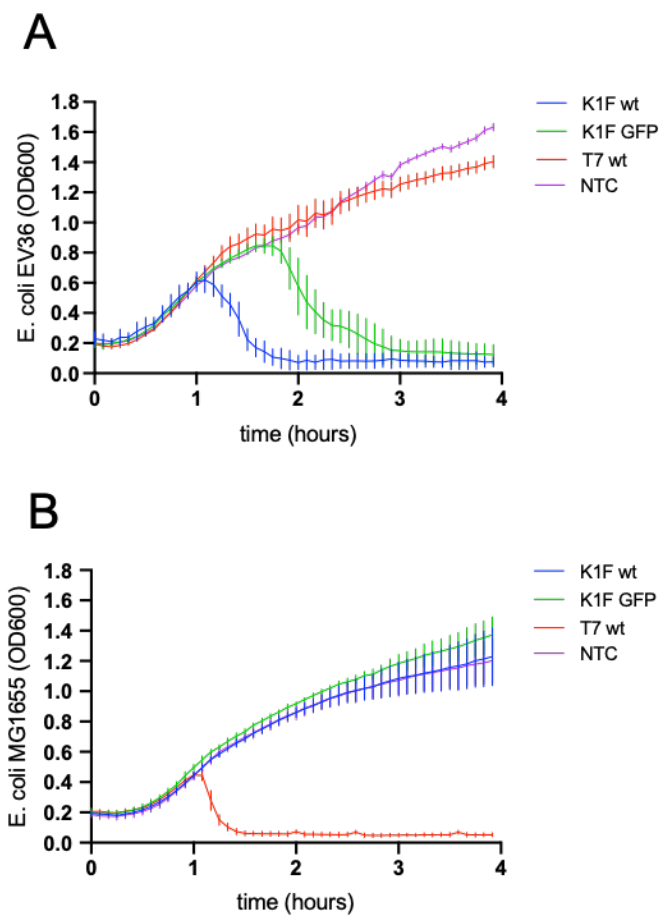


Figure 3-3. Host specificity of bacteriophages K1F, K1F-GFP and T7. The growth of *E. coli* EV36 (A) and *E. coli* MG1655 (B) cultures treated with phages was measured at OD600 over four hours. The phages were added at an MOI of 0.001 with NTC included as a control. All data are shown as mean \pm SD, $n = 4$.

The host specificity of phages K1F and T7 was further assessed on solid media (Figure 3-4). Phage-induced lysis of *E. coli* EV36 by phage K1F result in large circular plaques with a mostly uniform size and shape. In contrast, plaques resulting from phage T7 infection of *E. coli* EV36 are highly irregular in size and shape with some plaques exhibiting a small clear centre surrounded by a diffuse halo, while others are slightly

larger with a more uniform spread. Infection of *E. coli* MG1655 by phage K1F did not result in any plaques, while infection by phage T7 resulted in large plaques mostly uniform in size and shape.

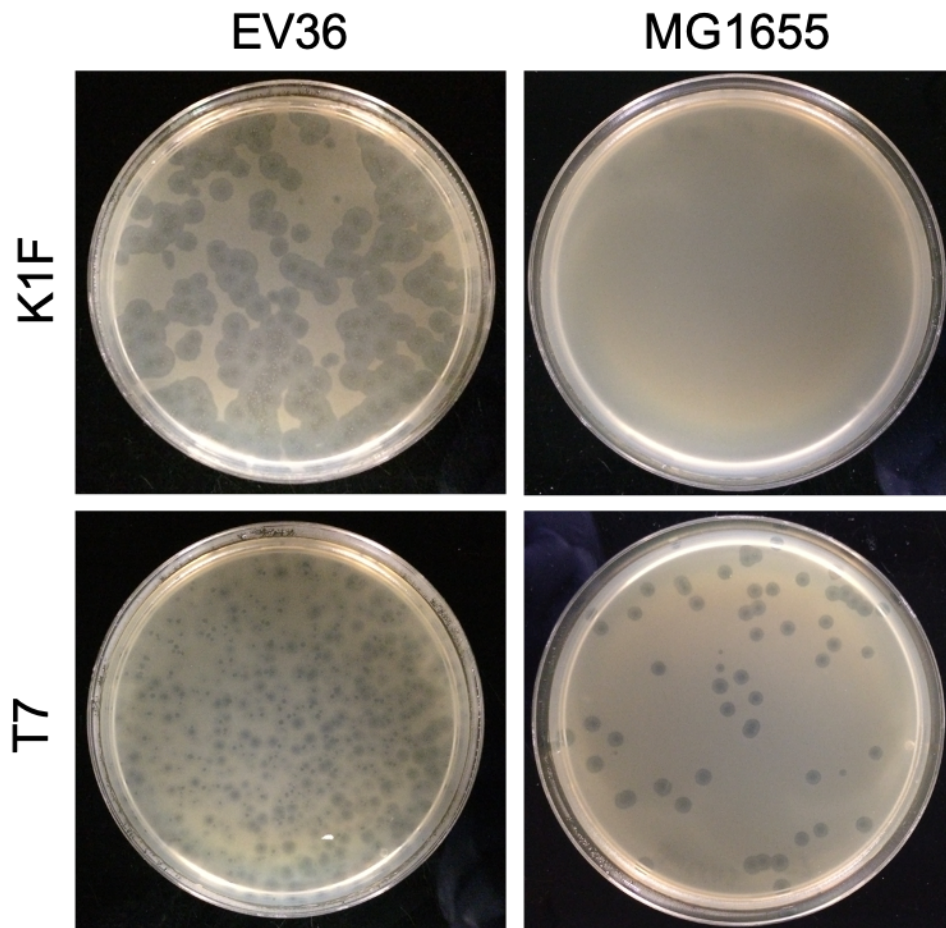


Figure 3-4. Host specificity of bacteriophage K1F and T7 challenged against *E. coli* EV36 and *E. coli* MG1655 on solid media. The plates were prepared using standard double overlay method and incubated overnight before imaging.

3.3 Bacteriophage K1F-GFP exhibit high fluorescence intensity

The intensity of phage K1F-GFP fluorophore and the suitability of flow cytometry as a platform for measuring phage infection was assessed (Figure 3-5). An overlay histogram of phage K1F-GFP infection of *E. coli* EV36 120 minutes after the addition of phage as measured by GFP emission using flow cytometry yielded two distinct populations (Figure 3-5A). The fluorophore intensity was similarly observed over a

two-hour time course (Figure 3-5B), where an increase of GFP MFI was detected after 60 minutes incubation in comparison with NTC.

The GFP MFI continued to increase until the final sampling point at 120 minutes, where an approximately 6-fold difference was observed in comparison with NTC. The distribution of GFP molecules on the capsid of phage K1F-GFP was visualised by negative staining EM (Figure 3-5C) of phages incubated with a gold-conjugated GFP binding probe. The micrograph showed gold particles uniformly distributed across the phage capsid (Figure 3-5C left) in comparison with wt phage K1F exposed to the same probe (Figure 3-5C middle) or K1F-GFP phage incubated with unconjugated gold particles (Figure 3-5C right), which both showed no association of the gold particles with the phage capsid.

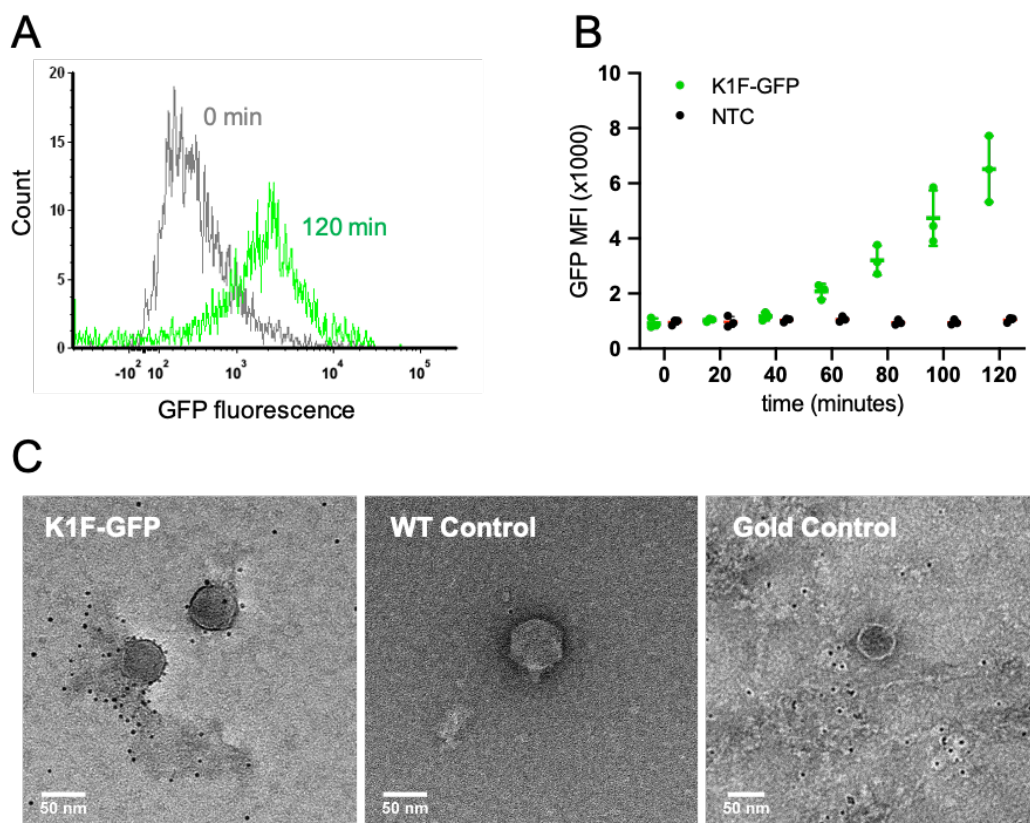


Figure 3-5. Bacteriophage K1F-GFP fluorophore intensity. (A) Flow cytometry overlay histogram of phage K1F-GFP infection of *E. coli* EV36 after 0 minutes (grey) and 120 minutes (green). (B) GFP MFI as measured by flow cytometry of *E. coli* EV36 cultures with and without the addition of phage K1F-GFP. Data are shown as mean \pm SD, $n = 3$. (C) Negative staining electron micrographs of gold-conjugated GFP binding probe with phage K1F-GFP (left), wt phage K1F control (middle), and non-conjugated gold particle control with phage K1F-GFP (right). EM images courtesy of Veronica Foisor.

In order to perform colocalisation imaging experiments it was necessary that phage K1F-GFP would be internalised by human cells and that the GFP could be detected using confocal microscopy. Initial imaging experiments performed with both hCMEC and T24 cultures incubated with phage K1F-GFP showed bright GFP aggregates located in vacuoles situated within the boundaries of the phalloidin stained actin filaments and therefore inside the cell (Figure 3-6). These results demonstrated that hCMEC and T24 cell lines have the ability to internalise phage K1F-GFP and that phage-expressed GFP fluorophores are sufficiently bright to be visualised under a confocal microscope.

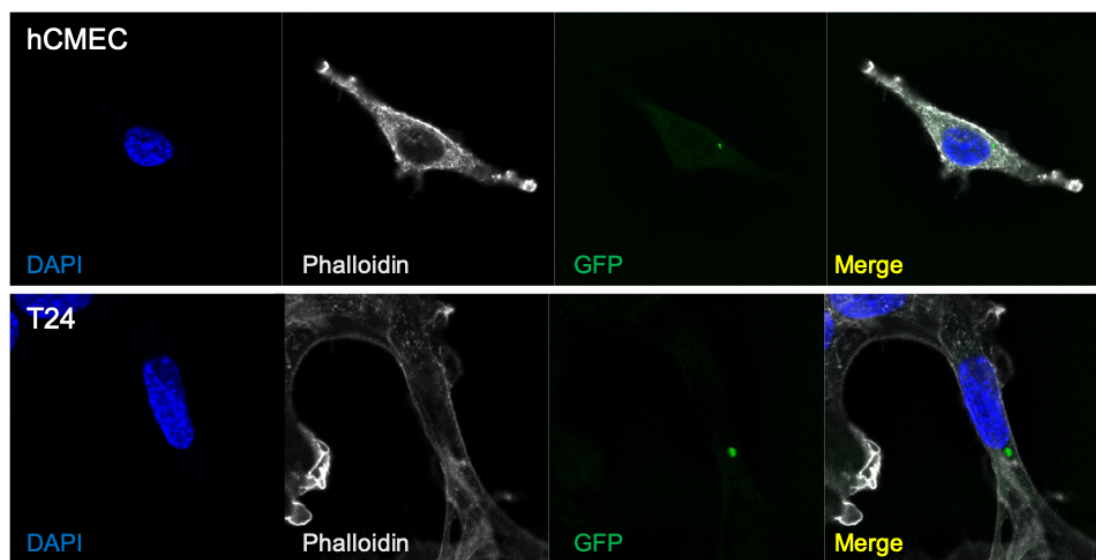


Figure 3-6. Confocal images showing hCMECs (above) and T24 cells (below) following incubation with 10^7 PFU/ml of phage K1F-GFP for one hour. The human cell cultures were fixed and stained with phalloidin shown in grey-scale and DAPI in blue. Phage K1F-GFP is shown in green.

3.4 Bacteriophage K1F induces bacterial cell death

Analysis of bacterial cell death following phage infection was performed using both imaging (Figure 3-7) and flow cytometry (Figure 3-8). Imaging of bacterial cell death was performed using Sytox Green, a nucleic acid stain which can penetrate bacterial cells with compromised cell membranes. Figure 3-7 show an *E. coli* EV36 culture incubated with phage K1F over a time course of five minutes starting from 14 minutes after the addition of phages. The initial image show the phage-induced lysis of a single bacterium in a culture where Sytox Green-stained DNA starts to spill into

the culture media as the bacterial membrane is compromised. Three minutes later, the DNA-containing bacterial cytoplasm also becomes stained with Sytox Green. Five minutes after lysis was initiated all bacterial DNA was spilled into and dispersed in the culture media. These images illustrate the death of bacteria induced by virulent phages.

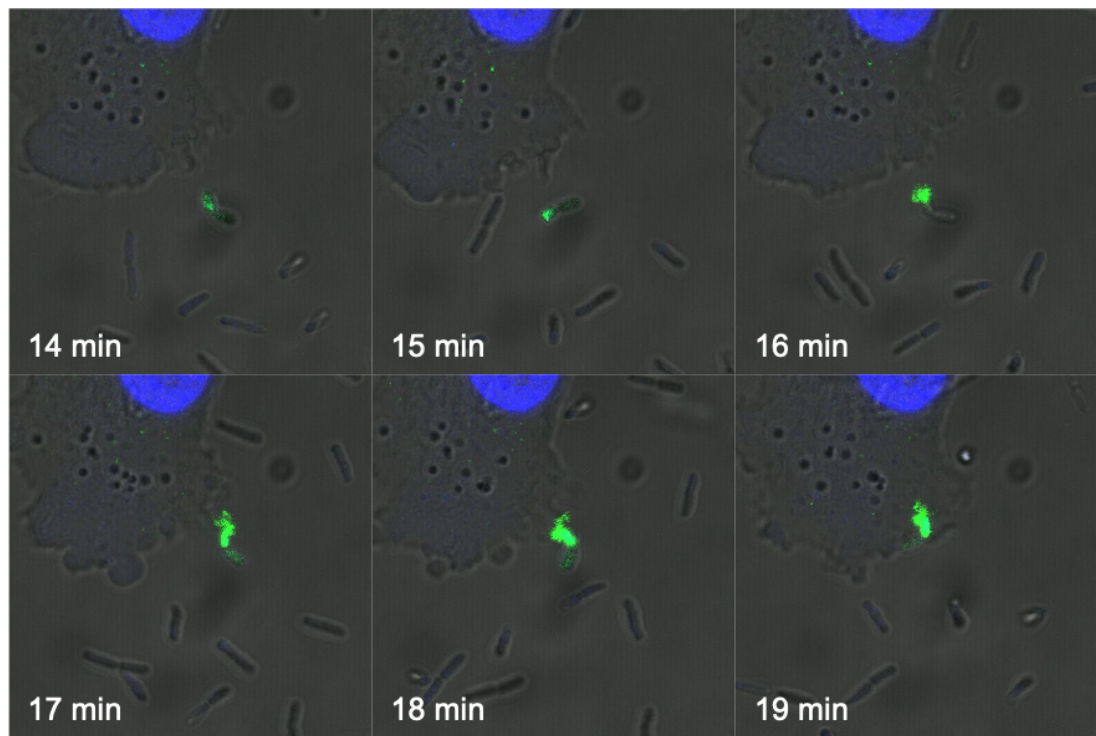


Figure 3-7. Extracellular bacterial cell death following phage infection as visualised over time. The images show *E. coli* EV36 incubated with phage K1F over a time course of five minutes. The culture was stained with Sytox Green and NucBlue Live ReadyProbe. The images were acquired live using fluorescent and bright field microscopy.

Phage-induced bacterial death was examined by measuring Sytox Green and propidium iodide (PI) fluorescence using flow cytometry (Figure 3-8). The mean fluorescence intensity (MFI) of Sytox Green stained *E. coli* EV36 cultures (Figure 3-8A) showed a time-dependent increase following treatment with phage K1F reaching an MFI of 6,678 (SD = 2,486) after two hours incubation. In contrast, the MFI of NTC did not fluctuate over the two-hour time course with an average MFI of 1,004 (SD = 76). Similar observations were made measuring PI stained *E. coli* EV36 cultures (Figure 3-8B), which showed a time-dependent increase of MFI following treatment with phage K1F, however, with delayed onset in comparison to Sytox Green stained cultures. After two hours incubation, an MFI of 18,473 (SD = 2,855) was reached by

E. coli EV36 cultures treated with phage K1F in comparison to NTC which remained steady around an MFI of 1,605 (SD = 28) throughout the experiment.

In experimental setups, staining with either Sytox or PI, a plateau is reached around the 100-minute sampling point, indicating full bacterial lysis.

In flow cytometry experiments, 10,000 events were collected per sample. However, it is worth noting that from 60 minutes post phage infection and onwards, the runs took increasingly longer to complete and/or the flow rate was increased. This was due to the decreasing number of detectable bacterial cells.

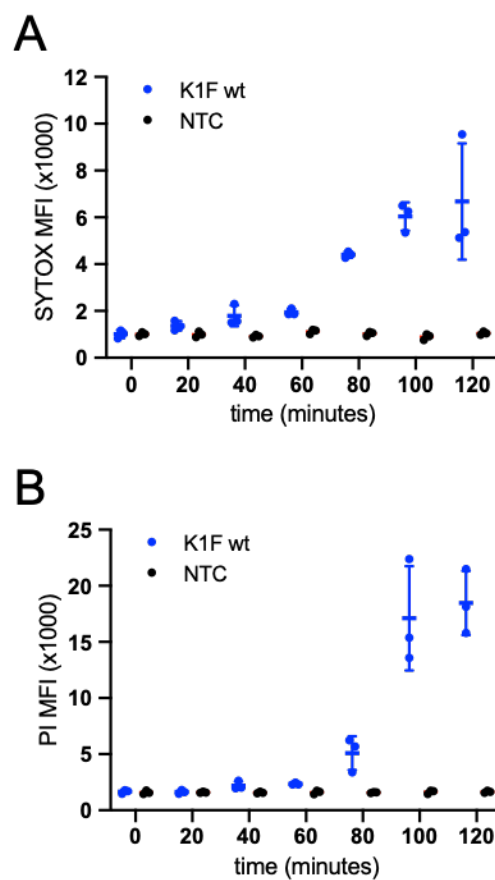


Figure 3-8. Bacterial cell death following phage infection as measured by flow cytometry. Graphs showing *E. coli* EV36 cultures stained with Sytox Green (A) or PI (B) measured over a two-hour incubation period. Bacterial cultures were stained and treated, in biological triplicates, with phage K1F at an MOI of 0.001. Aliquots were aspirated at set time points and analysed by flow cytometry. Stained and untreated bacterial cultures (NTC) were included as a control. Data shown as mean \pm SD, $n = 3$.

3.5 Plasmid-based RFP expression variation in *E. coli* EV36

An IPTG-induced *E. coli* EV36 RFP-expressing strain was previously generated and used in the group. IPTG induction of the RFP expression in this strain proved difficult to manage and as a result cultures did not consistently express RFP with some cultures not expressing RFP at all. This was illustrated by the mix of RFP-expressing red colonies and non-expressing white colonies forming when the strain was grown on solid media (Figure 3-9A). A new RFP-expressing strain, henceforth called *E. coli* EV36-RFP, was generated by electroporation of pSB6A1_RFP (for details see Materials and Methods), a plasmid expressing RFP via an unregulated promoter allowing for continual transcription under ampicillin selection, in *E. coli* EV36. Growing on solid media, *E. coli* EV36-RFP consistently developed red colonies (Figure 3-9B). However, single red colonies, which were picked and grown in overnight liquid cultures, displayed a range of red intensities (Figure 3-9C). As it was evident that the constitutive RFP expression of *E. coli* EV36-RFP visually varied across cultures, flow cytometric analysis was used to ensure the accuracy of quantitative experiments involving the strain. The flow cytometric analysis showed detectable RFP fluorescence in >98% of the total bacteria of individual cultures regardless of the intensity level.

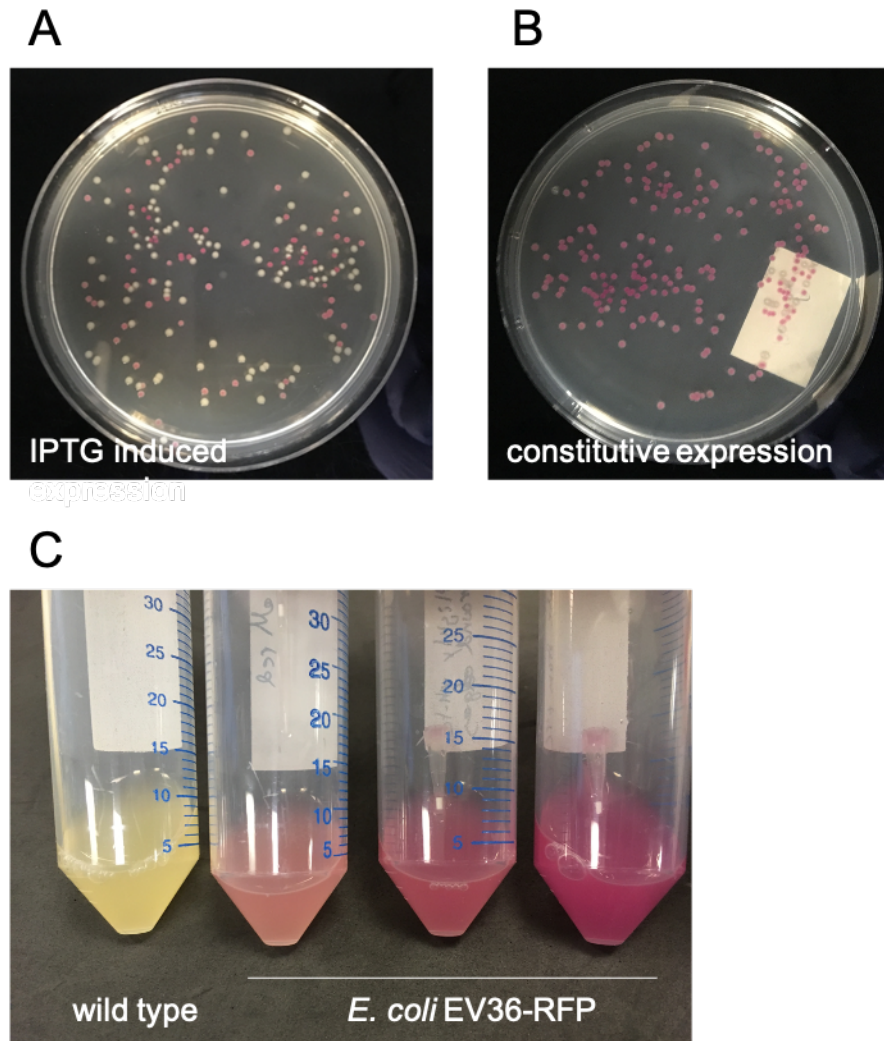


Figure 3-9. Plasmid-driven expression of RFP is assessed in *E. coli* EV36. IPTG-induced RFP-expression of *E. coli* EV36 growing on solid media. Constitutive RFP-expression of *E. coli* EV36 growing on solid media (B) or in overnight liquid cultures (C). The wild type control is *E. coli* EV36 (without RFP plasmids).

3.6 *E. coli* EV36 infection of human cells is time- and concentration-dependent

A series of imaging and flow cytometry experiments were performed to assess and quantify the infection of *E. coli* EV36-RFP in human cells. In Figure 3-10, representative images of fixed and stained hCMEC and T24 cells treated with *E. coli* EV36-RFP are shown. The RFP-tagged bacteria appear intracellular within the boundaries of the phalloidin stained mesh of actin filaments, demonstrating the ability of *E. coli* EV36-RFP to infect these human cell lines.

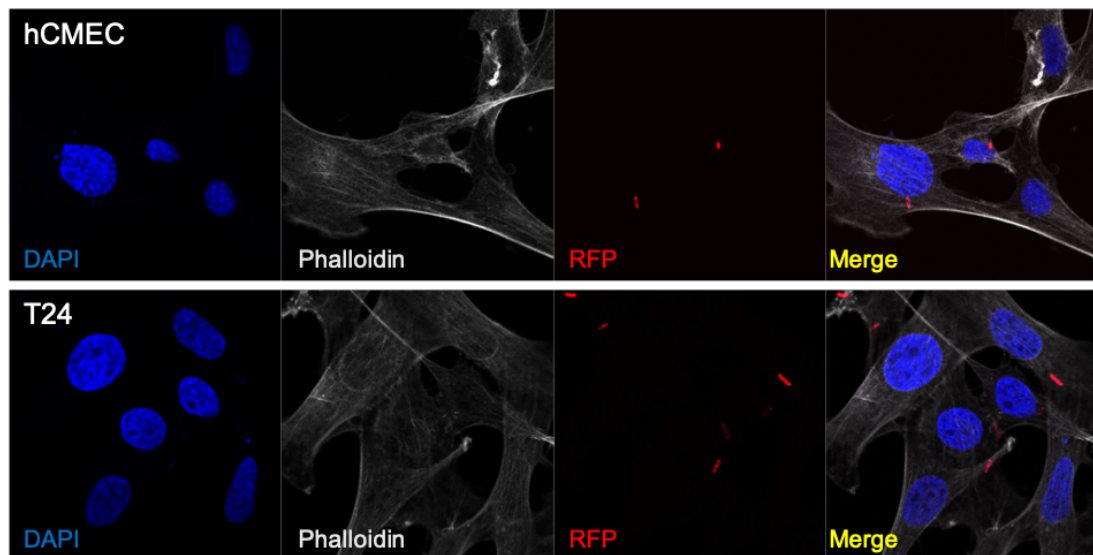


Figure 3-10. Confocal images showing hCMECs (above) and T24 cells (below) following infection by *E. coli* EV36-RFP for one hour. The human cell cultures were fixed and stained with phalloidin shown in grey-scale and DAPI show in blue. *E. coli* EV36-RFP is shown in red.

Manual quantification of microscopy images showed this infection to be concentration-dependent (Figure 3-11B), with increasing *E. coli* EV36-RFP concentrations leading to significantly greater infection of T24 cells (Table 3-1). In comparison, hCMECs treated with *E. coli* EV36-RFP showed a similar concentration-dependent infection albeit with a comparable higher percentage of infected cells (Table 3-1).

Cell type	<i>E. coli</i> EV36-RFP CFU/ml	% intracellular <i>E. coli</i> EV36-RFP	P-value
T24	5×10^6	8.70% (SD = 0.3)	-
T24	1×10^7	12.7% (SD = 0.2)	3.1×10^{-5}
T24	2×10^7	22.7% (SD = 2.2)	1.6×10^{-3}
hCMEC	1×10^6	21.7% (SD = 5.8)	-
hCMEC	1×10^7	49.4% (SD = 10.5)	1.6×10^{-3}

Table 3-1. Infection of *E. coli* EV36-RFP in T24 cells and hCMECs. P-values are presented as pair-wise comparison (student t-test) between a sample and the preceding sample at lower concentration.

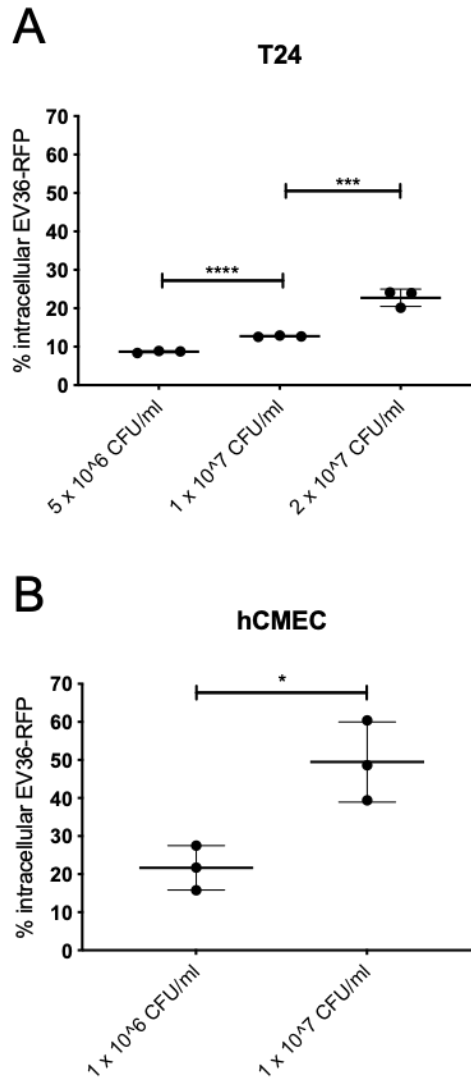


Figure 3-11. Infection of bacteria in human cells as quantified by image analysis. Image quantification showing the percentage of infected human cells, T24 (A) or hCMEC (B) after a one-hour incubation period with *E. coli* EV36-RFP at a range of concentrations. P-values are displayed as $p \leq 0.05$ (*), $p \leq 0.01$ (**), $p \leq 0.001$ (***), $p \leq 0.0001$ (****) and not statistical significant $p \geq 0.05$ (ns).

Flow cytometry was used to complement the imaging efforts and to enable quantitative analysis of a larger population (Figure 3-12). An overlay histogram of *E. coli* EV36-RFP infected- and non-infected hCMEC cultures (Figure 3-12A) demonstrated the shift in signal and clear separation achieved between populations gated on RFP fluorescence. hCMEC cultures treated with *E. coli* EV36-RFP at a concentration of 10^7 CFU/ml (Figure 3-12B) showed a time-dependent increase in RFP fluorescence throughout the time course with indications of a plateau forming towards the end. Gating for size exclusion and RFP fluorescence was performed after the addition of bacteria on samples at time = 0. The population of RFP-fluorescence

positive hCMECs at time = 0 was 0.22% (SD = 0.043) demonstrating the low false-positive rates achieved by the method. By 2 hours after the addition of *E. coli* EV36-RFP, the percentage of RFP-fluorescence positive hCMECs had increased to 66% (SD = 2.5) (Table 3-2).

Sampling point (min)	Invaded hCMECs (%)
0	0.22% (SD = 0.043)
30	37% (SD = 2.5)
60	55% (SD = 4.5)
120	66% (SD = 2.5)

Table 3-2. Infection rates of *E. coli* EV36-RFP in hCMECs over time.

In a similar experiment, the percentage of RFP-positive, i.e. *E. coli* EV36-RFP infected, hCMEC cells was found to be concentration-dependent (Figure 3-12C). hCMEC cultures treated with *E. coli* EV36-RFP at a range of concentrations showed a significantly increasing percentage of infection with increasing bacterial concentration (Table 3-3). The biggest increase was observed between bacterial concentrations of 10^5 and 10^7 CFU/ml which resulted in a 390% increase (p-value = 0.0006).

<i>E. coli</i> EV36-RFP CFU/ml	Invaded hCMECs (%)
10^3	3.4% (SD = 2.0)
10^5	13% (SD = 6.0)
10^7	51% (SD = 3.1)

Table 3-3. Infection of *E. coli* EV36-RFP in hCMECs across concentrations.

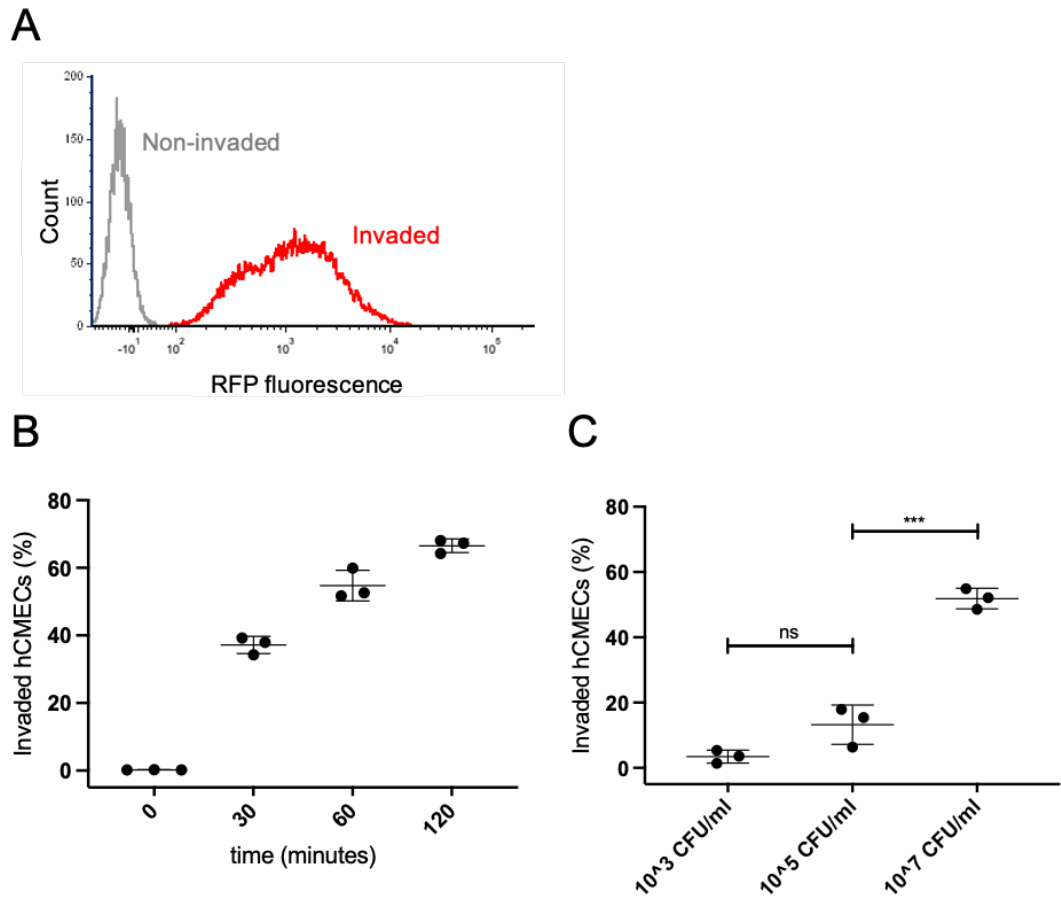


Figure 3-12. Infection rates of bacteria in human cells as quantified by flow cytometry. (A) Overlay histogram showing population separation between hCMECs infected with *E. coli* EV36-RFP in red and non-infected hCMECs in grey as detected by RFP fluorescence. (B-C) Graphs showing the percentage of *E. coli* EV36-RFP infected hCMECs. (B) hCMEC cultures were treated with *E. coli* EV36-RFP at a single concentration of 10^7 CFU/ml and measured over time. (C) hCMEC cultures were treated with *E. coli* EV36-RFP at concentrations ranging from 10^3 to 10^7 CFU/ml and incubated for 1 hour before sampling. P-values are displayed as $p \leq 0.05$ (*), $p \leq 0.01$ (**), $p \leq 0.001$ (***), $p \leq 0.0001$ (****) and not statistical significant $p \geq 0.05$ (ns). Data shown as mean \pm SD, $n = 3$.

3.7 Bacteriophage K1F infects intracellular *E. coli* EV36

The ability of phage K1F to infect intracellular *E. coli* EV36 was assessed by microscopy imaging where colocalisation between the predator and prey was assessed (Figure 3-13). This is illustrated by representative microscopy images (Figure 3-13A) showing intracellular colocalisation of phage K1F-GFP and *E. coli* EV36-RFP encapsulated by the phalloidin stained actin filaments of hCMECs.

The efficiency of the phage-mediated reduction of intracellular bacteria was determined by image quantification (Figure 3-13B). The quantification of T24 cultures treated with *E. coli* EV36-RFP alone showed that 26.1% (SD = 2.7) of the total T24 cell population contained intracellular bacteria. In comparison, T24 cultures treated with *E. coli* EV36-RFP and phage K1F-GFP only had an invaded T24 cell population of 16.7% (SD = 1.3), yielding a reduction of 37% (p-value 0.005) over the course of one hour. While the bacteria-containing media is removed before the addition of phage, it is likely that a small percentage of membrane-bound extracellular bacteria becomes infected with phage before uptake.

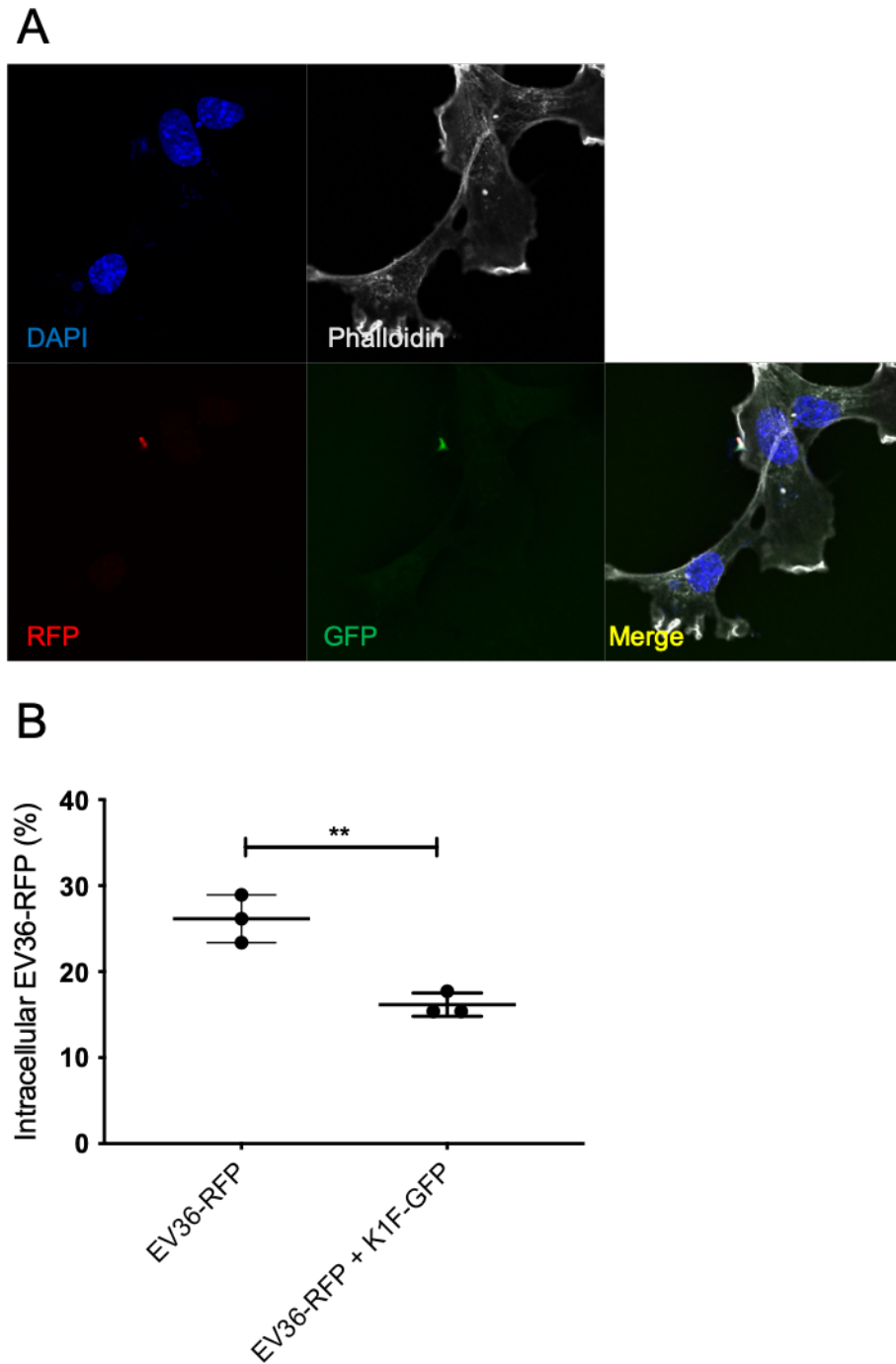


Figure 3-13. Bacteriophage infection of intracellular bacteria. (A) Representative microscopy images show hCMECs treated with *E. coli* EV36-RFP and phage K1F-GFP. DAPI nuclear stain shown in blue, phalloidin in grey-scale, *E. coli* EV36-RFP in red, and phage K1F-GFP in green. (B) The graph shows the percentage of intracellular *E. coli* EV36-RFP of T24 cells with and without the addition of phage K1F-GFP as determined by image quantification. T24 cells were treated with *E. coli* EV36-RFP at a concentration of 10^7 CFU/ml and either incubated for 2 hours alone or incubated for 1 hour before removal of media and subsequent addition of fresh media containing phage K1F-GFP at a concentration of 10^3 PFU/ml and then incubated for an additional hour. P-values are displayed as $p \leq 0.05$ (*), $p \leq 0.01$ (**), $p \leq 0.001$ (***), $p \leq 0.0001$ (****) and not statistical significant $p \geq 0.05$ (ns). Data shown as mean \pm SD, $n = 3$.

3.8 Human cells influence phage K1F population dynamics

The influence of human cells on the phage population dynamics was assessed (Figure 3-14). The concentration of *E. coli* EV36 (Figure 3-14A, Table 3-4) was determined over time under various conditions by colony counting. All four conditions, *E. coli* EV36 alone or in the presence of T24 cells with or without phage K1F addition, were in exponential phase for EV36 growth with similar trajectories for the first 60 minutes of the experiments at which time phage K1F was added. Once phage K1F was added to *E. coli* EV36 cultures with or without the presence of T24 cells, the bacterial concentration showed a slight decline at the 90 minutes sampling point followed by a sharp decline up to the final 120-minute sampling point. A non-significant reduction was observed at the 90-minute sampling point between cultures of phage K1F treated *E. coli* EV36 grown in the presence of T24 cells in comparison with cultures grown in the absence of T24 cells. Ultimately, the addition of phage K1F almost entirely cleared the *E. coli* EV36 cultures with or without the presence of T24 cells. *E. coli* EV36 control cultures remained in exponential growth phase throughout the time course with an average generation time of 22.1 minutes (SD = 0.36). In the absence of added phage, a reduction was seen in concentration of *E. coli* EV36 in cultures growing in the presence of T24 cells in comparison with control cultures at time points 90 and 120 minutes, with a reduction of 78.2% (SD = 3.4, p-value = 2.2×10^{-5}) and 67.2% (SD = 13.9, p-value = 1.3×10^{-3}).

Sampling point (min)	<i>E. coli</i> EV36 (CFU/ml)	<i>E. coli</i> EV36 + T24 (CFU/ml)	<i>E. coli</i> EV36 + phage K1F (CFU/ml)	<i>E. coli</i> EV36 + phage K1F + T24 (CFU/ml)
0	5.7×10^6 , SD = 1.2×10^5	5.7×10^6 , SD = 1.2×10^5	5.7×10^6 , SD = 1.2×10^5	5.7×10^6 , SD = 1.2×10^5
30	1.4×10^7 , SD = 2.1×10^5	1.1×10^7 , SD = 2.8×10^6	6.6×10^6 , SD = 2.2×10^6	1.4×10^7 , SD = 8.1×10^5
60	3.8×10^7 , SD = 1.0×10^6	4.9×10^7 , SD = 1.2×10^7	5.1×10^7 , SD = 7.8×10^6	4.4×10^7 , SD = 4.7×10^6
90	1.0×10^8 , SD = 4.4×10^6	2.3×10^7 , SD = 4.2×10^6	1.1×10^7 , SD = 2.2×10^6	4.0×10^6 , SD = 9.8×10^5
120	2.5×10^8 , SD = 1.3×10^7	8.2×10^7 , SD = 3.4×10^7	1.8×10^2 , SD = 8.7×10^1	3.1×10^2 , SD = 2.3×10^2

Table 3-4. Influence of human cells on phage population dynamics as measured by the concentration of planktonic *E. coli* EV36.

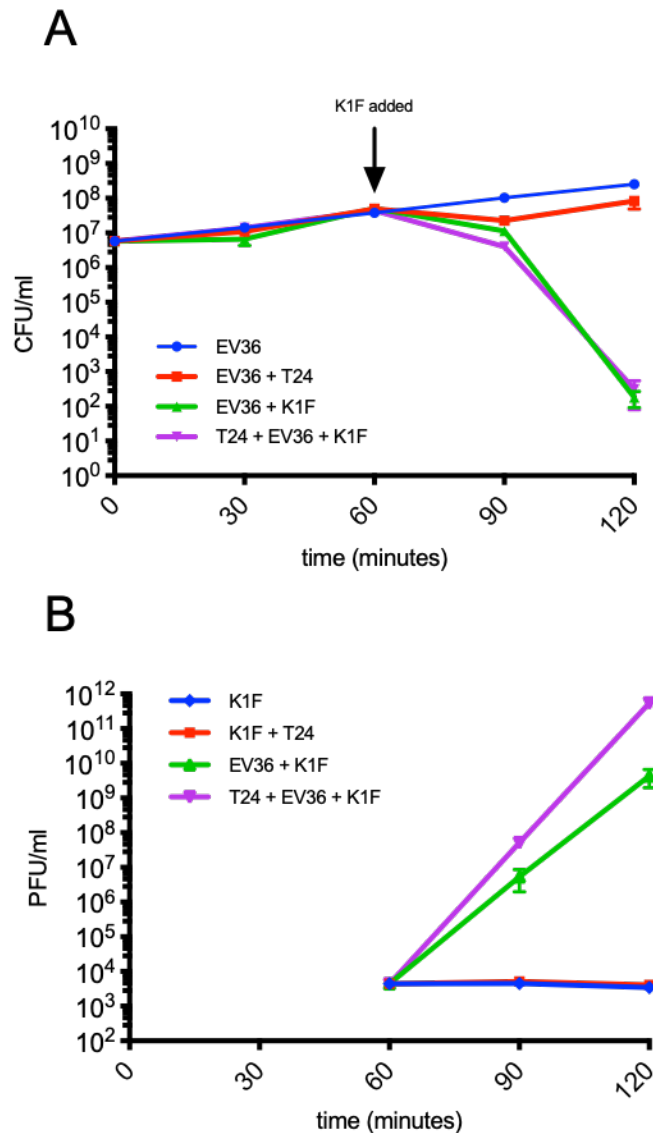


Figure 3-14. Influence of human cells on phage population dynamics. Graphs showing growth of planktonic *E. coli* EV36 as illustrated by CFU/ml (A) and free phage K1F as illustrated by PFU/ml (B) over a two-hour time course. Phage K1F was added to corresponding samples after one hour at an MOI of 0.001. Data shown as mean \pm SD, $n = 3$.

As part of the same experiment, the concentration of free phage K1F (Figure 3-14B) was determined from the time of addition at time = 60 minutes, covering the final hour of the time course. Sampling for CFU and PFU determination was performed from identical wells to allow for direct comparison of the concentrations of bacteria and phage. An acute increase of phage K1F concentration was observed in cultures containing *E. coli* EV36 from phage addition until the final sampling point, with the highest trajectory for cultures grown in the presence of T24 cells. After 90 and 120 minutes, K1F phage titres in cultures containing T24 cells showed a fold increase of

8.6 (p-value = 5.1×10^{-4}) and 125 (p-value = 5.0×10^{-4}) respectively in comparison with cultures not containing human cells. No difference was observed in phage K1F concentration in cultures not containing bacteria.

Sampling point (min)	Phage K1F (PFU/ml)	Phage K1F + T24 (PFU/ml)	<i>E. coli</i> EV36 + phage K1F (PFU/ml)	<i>E. coli</i> EV36 + phage K1F + T24 (PFU/ml)
60	4.4×10^3 , SD = 8.3×10^2	4.4×10^3 , SD = 8.3×10^2	4.4×10^3 , SD = 8.3×10^2	4.4×10^3 , SD = 8.3×10^2
90	4.5×10^3 , SD = 1.0×10^2	5.2×10^3 , SD = 7.1×10^2	5.3×10^6 , SD = 3.3×10^6	5.2×10^7 , SD = 7.1×10^6
120	3.5×10^3 , SD = 5.1×10^2	4.1×10^3 , SD = 4.9×10^3	4.2×10^9 , SD = 2.3×10^9	5.5×10^{11} , SD = 9.1×10^{10}

Table 3-5. Influence of human cells on phage population dynamics as measured by concentration of free phage K1F.

3.9 Discussion

TEM was performed early on in the project as part of optimising the phage purification protocol. A phage preparation devoid of contaminants, such as bacterial residues, was essential to ensure that any responses found in subsequent human cell experiments were directly related to phage interactions and not influenced by bacterial remnants. Multiple purification arrangements were trialled with the best result achieved using a modified Castro-Mejia *et al.*¹⁵⁹ protocol (See Materials and Methods for details). The high-quality TEM images acquired clearly showed that phage K1F has the expected structural phenotype of the podoviridae family, with its icosahedral capsid structure and short tail fibres, as previously described by Ackermann¹⁷³. The diameter of the phage K1F capsid of approximately 60 nm was comparable to that of its close relatives in the genus of T7-like phages^{79, 174}.

The high host specificity of phage K1F and its derivative phage K1F-GFP towards K1-capsule expressing bacteria was demonstrated by liquid culture experiments using the hybrid K12/K1 *E. coli* EV36 strain. *E. coli* EV36 expresses a K1 capsule which is morphologically similar to that of *E. coli* K1 clinical isolates⁸⁵. Phages K1F and K1F-GFP both exhibited high specificity towards *E. coli* EV36 and were unable to replicate on the non-K1 capsule expressing control strain, *E. coli* MG1655. Phage K1F-GFP showed slightly lower efficacy in killing *E. coli* EV36 than its wt counterpart, which is likely due to reduced fitness e.g. longer replication time and/or smaller burst size as a result of carrying the 26.9 kDa GFP gene. Phage T7, used as a control for comparison, showed high specificity towards *E. coli* MG1655, a K12 stain, as expected, with only a slight reduction observed of *E. coli* EV36 growth. This small reduction is due to the nature of the hybrid strain where an unknown fraction of the bacterial cells retains the K12 phenotype. This was also evidenced by phage T7 infection of *E. coli* EV36 on solid media which yielded irregular plaques where killed K12 phenotype cells were overgrown by the K1 phenotype.

During the four-hour time course in liquid culture, no bacterial regrowth was observed, indicating that no bacterial resistance to phage evolved during this time. The emergence of phage-resistant bacteria in liquid culture experiments such as these is however common, and was observed in separately performed experiments where cleared cultures were left in an incubator overnight (data not shown).

GFP measurements of *E. coli* EV36 cultures treated with phage K1F-GFP using flow cytometry demonstrated the high fluorescent intensity and robustness of the engineered phage. Due to the size of phage K1F-GFP, it was not possible to detect individual phage particles as the lower limit of the flow cytometry system used was 200nm. Overlay histogram of individually recorded events showed overlap between treated and non-treated bacterial cultures which means that direct gating of the populations was not possible. This is caused by the intrinsic fluorescence, or background, of the bacterial culture. However, *E. coli* EV36 cultures treated with phage K1F showed a 6-fold increase of GFP MFI after two hours incubation in comparison with non-treated cultures. This sufficiently demonstrated the stability of the engineered phage construct and the usefulness of the method for detection of

bacteria invaded by GFP-tagged phage. The presence and physical distribution of GFP particles along the exterior of the phage capsid were shown by electron microscopy, albeit the dispersion of particles appeared variable. Phage K1F-GFP was previously engineered by the integration of the GFP gene to the 3' end of gp10b encoding for the minor capsid protein. The phage T7 capsid is comprised of a total of 415 capsid proteins¹⁷⁵ in ratio of major and minor capsid proteins under normal conditions of 9:1¹⁷⁶ suggesting that approximately 41.5 GFP proteins could be present on the capsid of phage K1F-GFP.

Attempts to characterise the progression from phage uptake by human cells to lysis of intracellular bacteria were performed using imaging and flow cytometry. Initial confocal imaging showed the presence of phage K1F located in vacuoles within the boundaries of the cytoplasm of the human cell lines, demonstrating the ability of these to internalise the phage. Given the size of the vacuole it is evident that this GFP signal is delivered by a large number of phages. Whether the phages form aggregates in the extracellular space before internalisation or are assembled in vacuoles by human cell machinery is unknown.

The fate of bacteria following phage-induced lysis was illustrated by Sytox Green staining, highlighting the difficulties experienced in examining the progression of *in vitro* phage therapy using end-point assays, as the interval in which the bacteria were Sytox-positive lasted only minutes. Experiments using Sytox Green or PI were therefore set up over time to quantify the concentration of infected bacteria. A direct correlation was found between increasing Sytox-positive bacteria and GFP expression from phage. Based on the accelerating increase of Sytox- and PI MFI of phage K1F treated *E. coli* EV36 after 60 minutes incubation and in combination with the onset of a reduced bacterial abundance, a one-hour phage-treatment incubation period was adopted going forward.

Once the host specificity and efficacy of phage K1F towards *E. coli* EV36 had been clarified and the two established as a pair, the focus was shifted towards the third leg of the *in vitro* model system, the human cell lines. Invasion rates of *E. coli* EV36-RFP in both T24 and hCMEC cells were concentration-dependent with a markedly

greater rate achieved in the latter. Live imaging demonstrated the ability of *E. coli* EV36 quickly, within a few hours, to overrun the adherent layer of human cells resulting in their release from the growth surface. For this reason, a two-hour bacterial incubation period was settled upon for microscopy purposes.

This type of image quantification presents three pitfalls; 1) Unconscious bias arising from manually panning across a cell layer choosing which areas to acquire images, 2) missing positive events as they are in another plane or shielded by other objects, and 3) capturing enough images to warrant a meaningful analysis. These concerns were offset by quantification using flow cytometry of a larger population of human cells. This analysis of *E. coli* EV36-RFP invasion rate of hCMECs generated reliable data, with full separation between invaded and non-invaded population enabling gating. The invasion rate, as quantified by two distinct methods, imaging and flow cytometry, was found to be similar, thus illustrating the complementarity of these methodologies.

The ability of phage K1F to enter the cytosol of human cells and to identify and infect intracellular *E. coli* EV36 was essential for the value of the model. This ability was demonstrated in T24 cells, which showed a phage-mediated reduction of 37% of the intracellular bacterial concentration after one hour.

Using the experimental setup determined in this chapter i.e. bacterial and phage concentrations and incubation periods, it was found that the abundance of free phage K1F increased at a higher rate in the presence of human cells than in their absence. Interestingly, the higher concentration of free phage only slightly influenced the rate of phage-induced clearance of *E. coli* EV36. It has been observed previously that human cells can influence the phage dynamics *in vitro*. One particular study found phages targeting *C. difficile* were more virulent in the presence of human cells leading to an increase in phage concentration and decrease in bacterial concentration³⁷. This observation was attributed to strong phage binding to the human cells and thereby bringing phage and bacteria into closer contact.

Chapter 4 Uptake and degradation of bacteriophage by human cells

The characterisation experiments of the tripartite *in vitro* model system demonstrated the uptake of phage K1F by human cells and the ability of phage K1F to infect intracellular *E. coli* EV36 (Chapter 3). The experiments presented in this chapter were therefore designed to examine the mechanisms involved in phage uptake and degradation in T24 cells and hCMECs.

Several studies have identified intracellular phages within eukaryotic cells^{23, 29, 30, 105}. Multiple mechanisms of internalisation have been demonstrated, including transport via the para- and transcellular routes^{30, 105} and entry via the endocytic pathways²⁹. In order to further identify the molecular pathways involved in the uptake and degradation of phages by human cells via endocytic mechanisms, a panel of phagosomal, lysosomal, and autophagy markers were selected. The panel was used in microscopy compartment colocalisation studies and flow cytometric quantification and consisted of six markers: Rab7, Cathepsin-L, LC3B, galectin-8, NDP52, and ubiquitin.

4.1 *E. coli* EV36 and phage K1F are degraded by lysosomal enzymes

Early phagosomes containing newly engulfed extracellular material undergo a maturation process to late phagosomes. Rab7 association is indicative of this maturation process having occurred^{116, 177}. T24 cell and hCMEC cultures were incubated with either *E. coli* EV36-RFP, phage K1F-GFP, or both in combination. The treated cells were subsequently fixed and stained for Rab7, Cathepsin-L or LC3B. Microscopy images for both cell lines showed co-localisation of Rab7 with *E. coli* EV36-RFP (Figure 4-1A, Figure 4-2A), phage K1F-GFP (Figure 4-1B, Figure 4-2B) and *E. coli* EV36-RFP and phage K1F-GFP in combination (Figure 4-1C, Figure 4-2C), suggesting that *E. coli* EV36-RFP and phage K1F-GFP are taken up by both T24 cells and hCMECs via the phagocytic pathway.

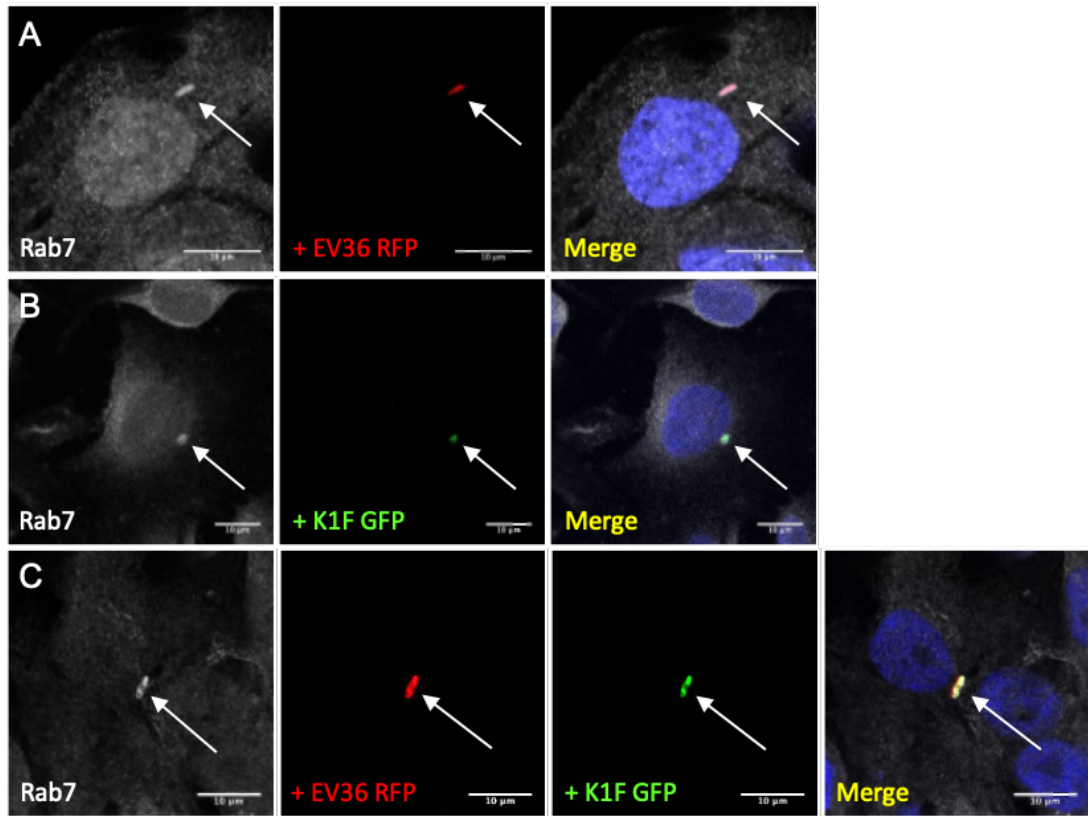


Figure 4-1. Colocalisation assay of T24 cells stained with anti-Rab7 antibodies. (A-C) Microscopy images showing T24 cells following a 1-hour incubation period with 10^7 CFU/ml *E. coli* EV36-RFP (A) or 10^7 PFU/ml phage K1F-GFP (B) alone, or a 1 hour incubation with 10^7 CFU/ml *E. coli* EV36-RFP followed by 1 hour incubation with 10^4 PFU/ml phage K1F-GFP (C). Images are representative of three independently performed experiments.

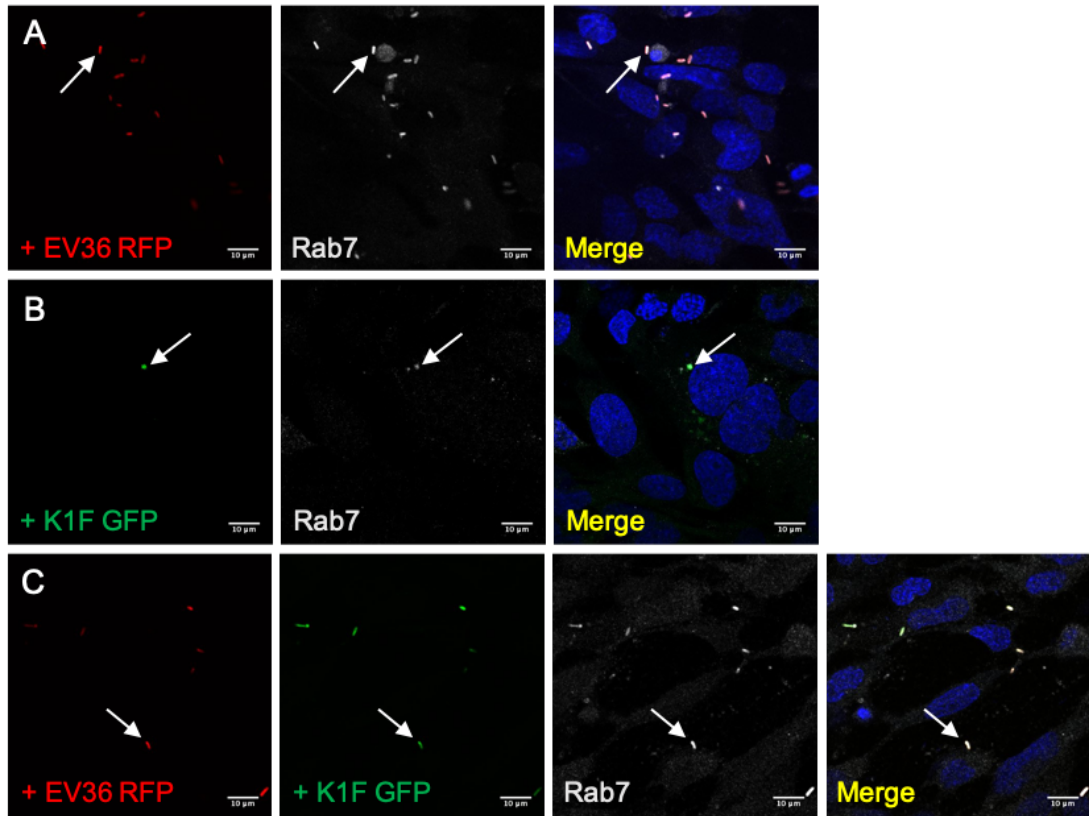


Figure 4-2. Colocalisation assay of hCMECs stained with anti-Rab7 antibodies. (A-C) Microscopy images showing hCMECs following a 1-hour incubation period with 10^7 CFU/ml *E. coli* EV36-RFP (A) or 10^7 PFU/ml phage K1F-GFP (B) alone, or a 1 hour incubation with 10^7 CFU/ml *E. coli* EV36-RFP followed by 1 hour incubation with 10^4 PFU/ml phage K1F-GFP (C). Images are representative of three independently performed experiments.

Fusion of late phagosomes with lysosomes initiates the degradation process of the phagosome-contained extracellular material. The association of Cathepsin-L is suggestive of lysosomal degradation¹¹⁸. Microscopy imaging for both cell lines showed co-localisation of Cathepsin-L with *E. coli* EV36-RFP (Figure 4-3A, Figure 4-4A), phage K1F-GFP (Figure 4-3B, Figure 4-4B), and *E. coli* EV36-RFP and phage K1F-GFP in combination (Figure 4-3C, Figure 4-4C), suggesting, in both T24 cells and hCMECs, that *E. coli* EV36-RFP and phage K1F-GFP are delivered to lysosomes for degradation following the phagosome maturation process.

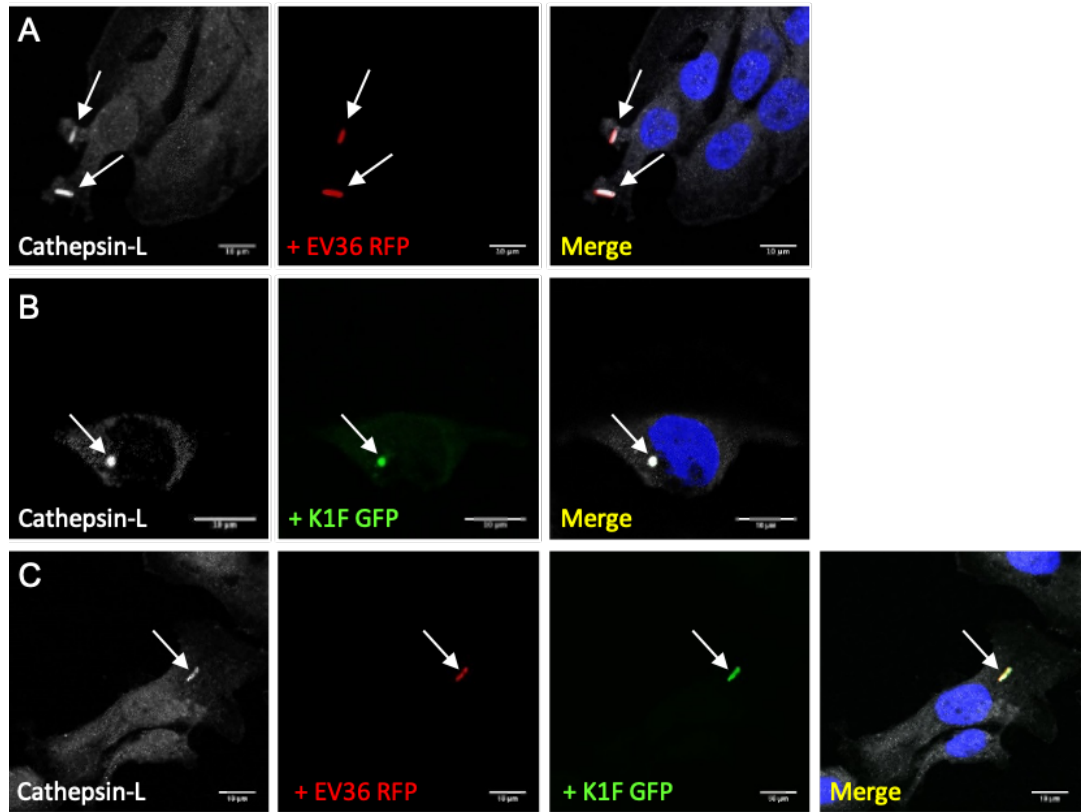


Figure 4-3. Colocalisation assay of T24 cells stained with anti-Cathepsin-L antibodies. (A-C) Microscopy images showing T24 cells following a 1 hour incubation period with 10^7 CFU/ml *E. coli* EV36-RFP (A) or 10^7 PFU/ml phage K1F-GFP (B) alone, or a 1 hour incubation with 10^7 CFU/ml *E. coli* EV36-RFP followed by 1 hour incubation with 10^4 PFU/ml phage K1F-GFP (C). Images are representative of three independently performed experiments.

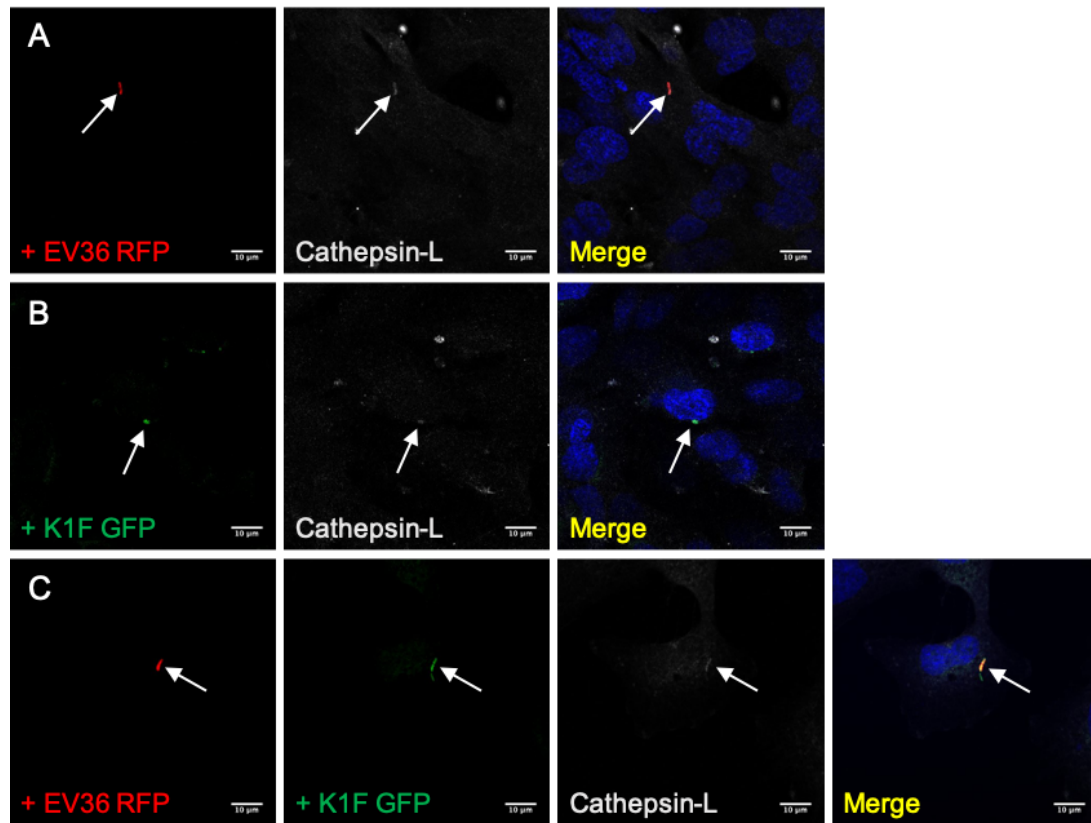


Figure 4-4. Colocalisation assay of hCMECs stained with anti-Cathepsin-L antibodies. (A-C) Microscopy images showing hCMECs following a 1 hour incubation period with 10^7 CFU/ml *E. coli* EV36-RFP (A) or 10^7 PFU/ml phage K1F-GFP (B) alone, or a 1 hour incubation with 10^7 CFU/ml *E. coli* EV36-RFP followed by 1 hour incubation with 10^4 PFU/ml phage K1F-GFP (C). Images are representative of three independently performed experiments.

This conclusion was further tested by quantitative flow cytometry of LysoTracker-stained hCMEC cultures (Figure 4-5). LysoTracker is a membrane permeable dye, the MFI of which is directly related to the pH of its surroundings and as such the probe is highly selective for acidic organelles such as lysosomes¹⁷⁸. Flow cytometry data showed a sharp increase of LysoTracker MFI of hCMEC cultures treated with *E. coli* from the 60-minute timepoint, suggesting a shift in endosomal activity towards increased lysosomal activity (Figure 4-5A, Table 4-1). In comparison, hCMEC cultures treated with phage K1F showed a decrease from the 60-minute timepoint albeit less pronounced (Figure 4-5B, Table 4-1). In a separate experiment measuring LysoTracker MFI at a single timepoint, hCMEC cultures treated with *E. coli* EV36 and phage K1F in combination (MFI of 1180, SD = 18) showed an increase in lysosome activity in comparison with cells treated with *E. coli* EV36 alone (MFI of 1069, SD = 13), $P = .0012$ (Figure 4-5C).

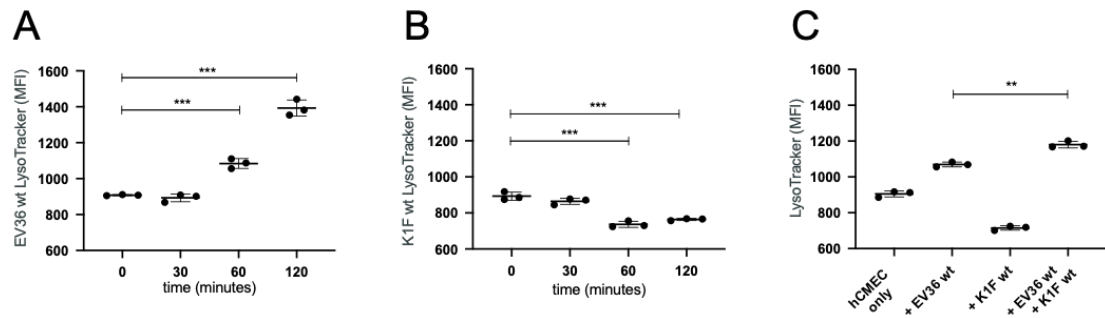


Figure 4-5. LysoTracker MFI of hCMECs as quantified by flow cytometry. (A-C) Graphs showing LysoTracker MFI of hCMEC cultures treated with 10^7 CFU/ml *E. coli* EV36 (A) or 10^7 PFU/ml phage K1F (B) as measured over time, or after a set incubation period of 1 hour (C). Combination treatment was performed in succession with 1 hour incubation each (C). P-values are calculated as a pairwise comparison and displayed as $P \leq .05$ (*), $P \leq .01$ (**), $P \leq .001$ (***) . Data shown as mean \pm SD, $n = 3$.

Sampling point (minutes)	<i>E. coli</i> EV36 (LysoTracker MFI)	Phage K1F (LysoTracker MFI)
0	908 (SD = 3.0)	893 (SD = 22)
30	893 (SD = 22, $P = .306$)	864 (SD = 17, $P = .152$)
60	1084 (SD = 27, $P < .001$)	736 (SD = 17, $P < .001$)
120	1392 (SD = 45, $P < .001$)	763 (SD = 5.8, $P < .001$)

Table 4-1. Summary of LysoTracker MFI of hCMEC cultures treated with *E. coli* EV36 or phage K1F alone as measured over time using flow cytometry. P-values are presented as a pairwise comparison against the 0 minute sampling point.

4.2 *E. coli* EV36 and phage K1F activates LC3-assisted phagocytosis

The involvement of the autophagy machinery in the degradation of phages taken up by phagocytosis was assessed by microscopy compartment colocalisation studies. LC3B has multiple functions in phagophore formation and in phagocytosis upon the recognition of foreign material by TLRs or Fc receptors in a process termed LC3-assisted phagocytosis^{110, 114, 179}. Microscopy imaging of T24 cells and hCMECs showed colocalisation of LC3B with *E. coli* EV36-RFP (Figure 4-6A, Figure 4-7A), phage K1F-GFP (Figure 4-6B, Figure 4-7B), and *E. coli* EV36-RFP and phage K1F-GFP in combination (Figure 4-6C, Figure 4-7C) indicating that these are degraded via LC3-assisted phagocytosis.

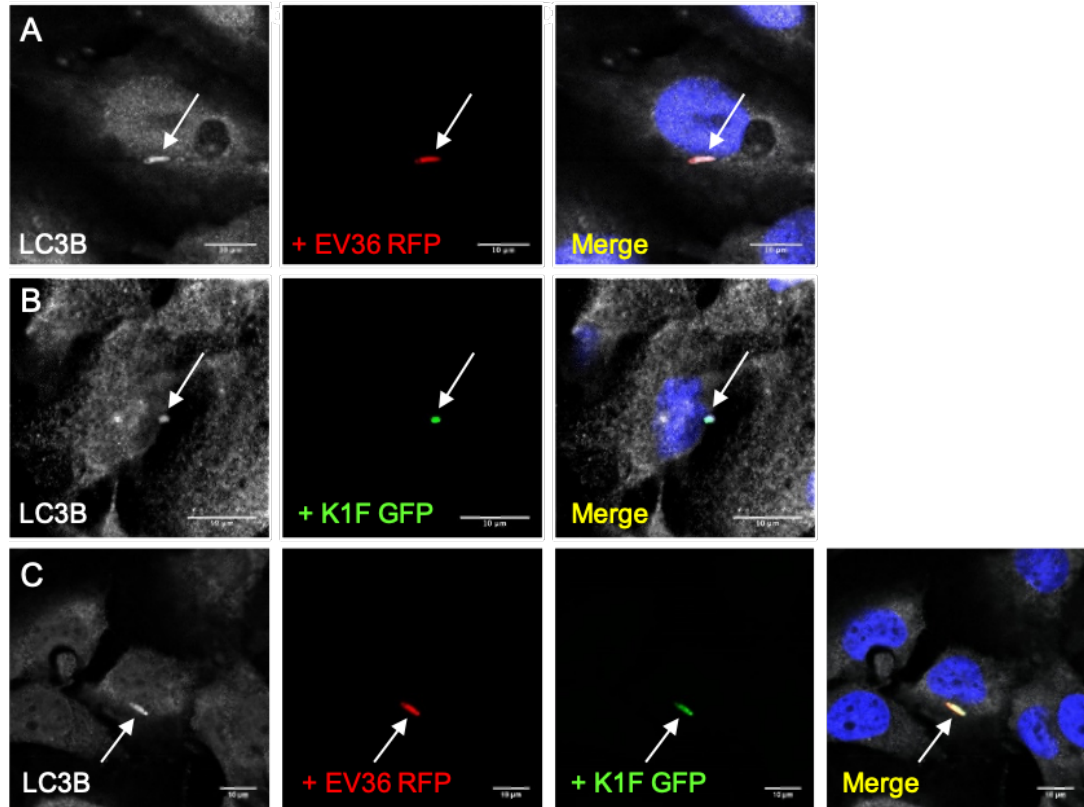


Figure 4-6. Colocalisation assay of T24 cells stained with anti-LC3B antibodies. (A-C) Microscopy images showing T24 cells following a 1-hour incubation period with 10^7 CFU/ml *E. coli* EV36-RFP (A) or 10^7 PFU/ml phage K1F-GFP (B) alone, or a 1 hour incubation with 10^7 CFU/ml *E. coli* EV36-RFP followed by 1 hour incubation with 10^4 PFU/ml phage K1F-GFP (C). Images are representative of three independently performed experiments.

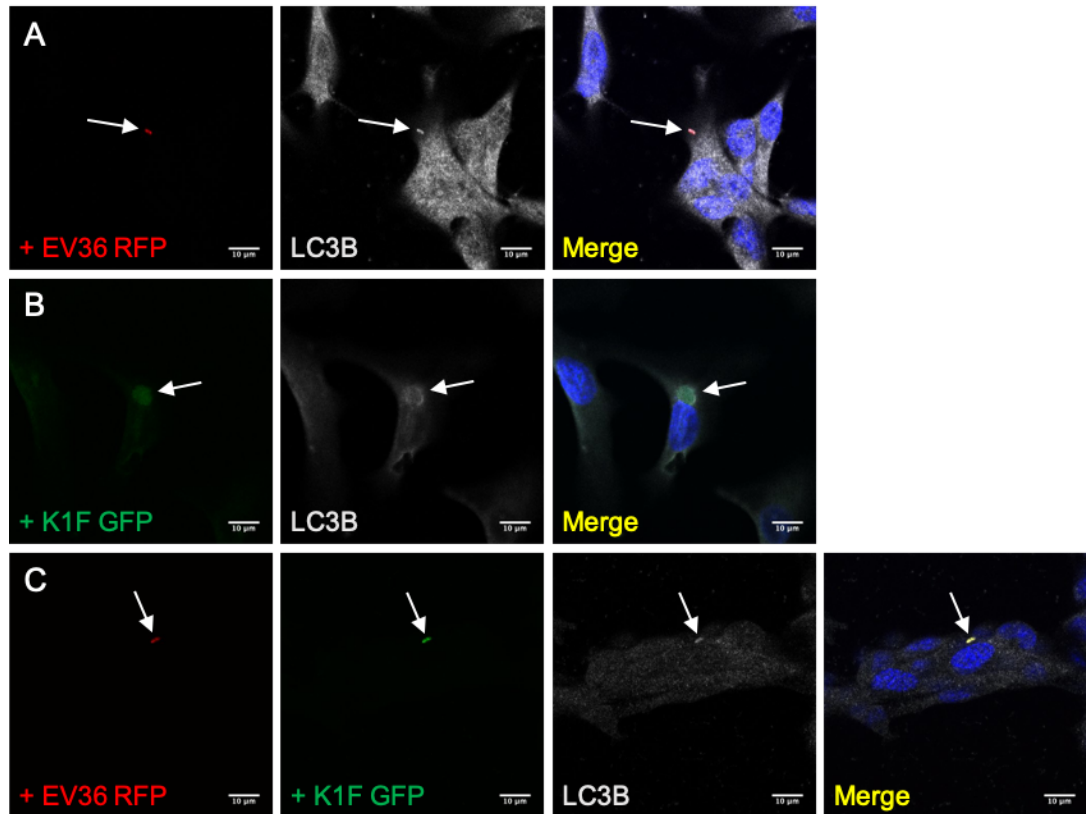


Figure 4-7. Colocalisation assay of hCMECs stained with anti-LC3B antibodies. (A-C) Microscopy images showing hCMECs following a 1-hour incubation period with 10^7 CFU/ml *E. coli* EV36-RFP (A) or 10^7 PFU/ml phage K1F-GFP (B) alone, or a 1 hour incubation with 10^7 CFU/ml *E. coli* EV36-RFP followed by 1 hour incubation with 10^4 PFU/ml phage K1F-GFP (C). Images are representative of three independently performed experiments.

The expression of LC3B under these same treatments was analysed in a larger population of hCMECs by quantitative flow cytometry. The data showed a marked increase in LC3B MFI of hCMECs initiated 60 minutes after the addition of *E. coli* EV36 (Figure 4-8A). In comparison, hCMECs treated with phage K1F show a comparably small constant reduction of LC3B MFI throughout the time course (Figure 4-8B). Interestingly, the LC3B MFI of hCMECs treated with both *E. coli* EV36 and phage K1F in succession (MFI 546, SD = 14) showed a decrease in comparison with *E. coli* EV36 treatment alone (MFI 653, SD = 17), $P = .0011$ (Figure 4-8C). This is in contrast to the behaviour of LysoTracker where combination treatment lead to an increase in fluorescence.

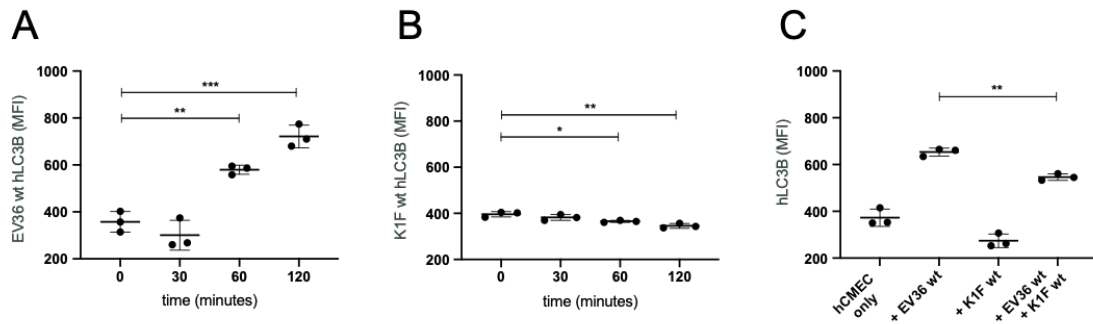


Figure 4-8. LC3B expression in hCMECs as quantified by flow cytometry. (A-C) Graphs showing anti-hLC3B MFI of hCMEC cultures treated with 10^7 CFU/ml *E. coli* EV36 (A) or 10^7 PFU/ml phage K1F (B) as measured over time, or after a set incubation period of 1 hour (C). Combination treatment was performed in succession with 1 hour incubation each (C). P-values are calculated as a pairwise comparison and displayed as $P \leq .05$ (*), $P \leq .01$ (**), $P \leq .001$ (***). Data shown as mean \pm SD, $n = 3$.

Sampling point (minutes)	<i>E. coli</i> EV36 (hLC3B MFI)	Phage K1F (hLC3B MFI x1000)
0	357 (SD = 44)	396 (SD = 11)
30	300 (SD = 63, $P = .271$)	382 (SD = 12, $P = .228$)
60	579 (SD = 19, $P = .0013$)	365 (SD = 4.5, $P = .012$)
120	721 (SD = 48, $P < .001$)	345 (SD = 10, $P = .0048$)

Table 4-2. Summary of LC3B MFI of hCMEC cultures treated with *E. coli* EV36 or phage K1F alone as measured over time using flow cytometry. P-values are presented as a pairwise comparison against the 0 minute sampling point.

4.3 Phage K1F activates galectin-8 dependent autophagy in T24 cells but not hCMECs

The attempted escape of pathogens from the phagosome into the cytosol will activate xenophagy, pathogen-directed autophagy, through selective autophagy-related receptors^{111, 112}. The exposure of host-derived membrane-bound glycans recruits galectin-8 which provides signals for the formation of a phagophore to encapsulate the escaping pathogen¹²¹. Microscopy imaging of T24 cells and hCMECs showed differential patterns of galectin-8 colocalisation. In T24 cells, intracellular *E. coli* EV36-RFP (Figure 4-9A) only colocalised with galectin-8 in some cells, while this was always observed with intracellular *E. coli* EV36-RFP in hCMECs (Figure 4-10A).

This differential activation of galectin-8 dependent autophagy was also observed with intracellular phage K1F of T24 cells which showed incidences of both colocalisation (Figure 4-9C) and of no colocalisation (Figure 4-9B) with galectin-8. In contrast, intracellular phage K1F of hCMECs showed no colocalisation with galectin-8 (Figure 4-10B). However, in both cell types intracellular *E. coli* EV36-RFP and phage K1F-GFP in combination (Figure 4-9D, Figure 4-10C) always showed colocalisation with galectin-8 suggesting consistent activation of galectin-8 dependent autophagy.

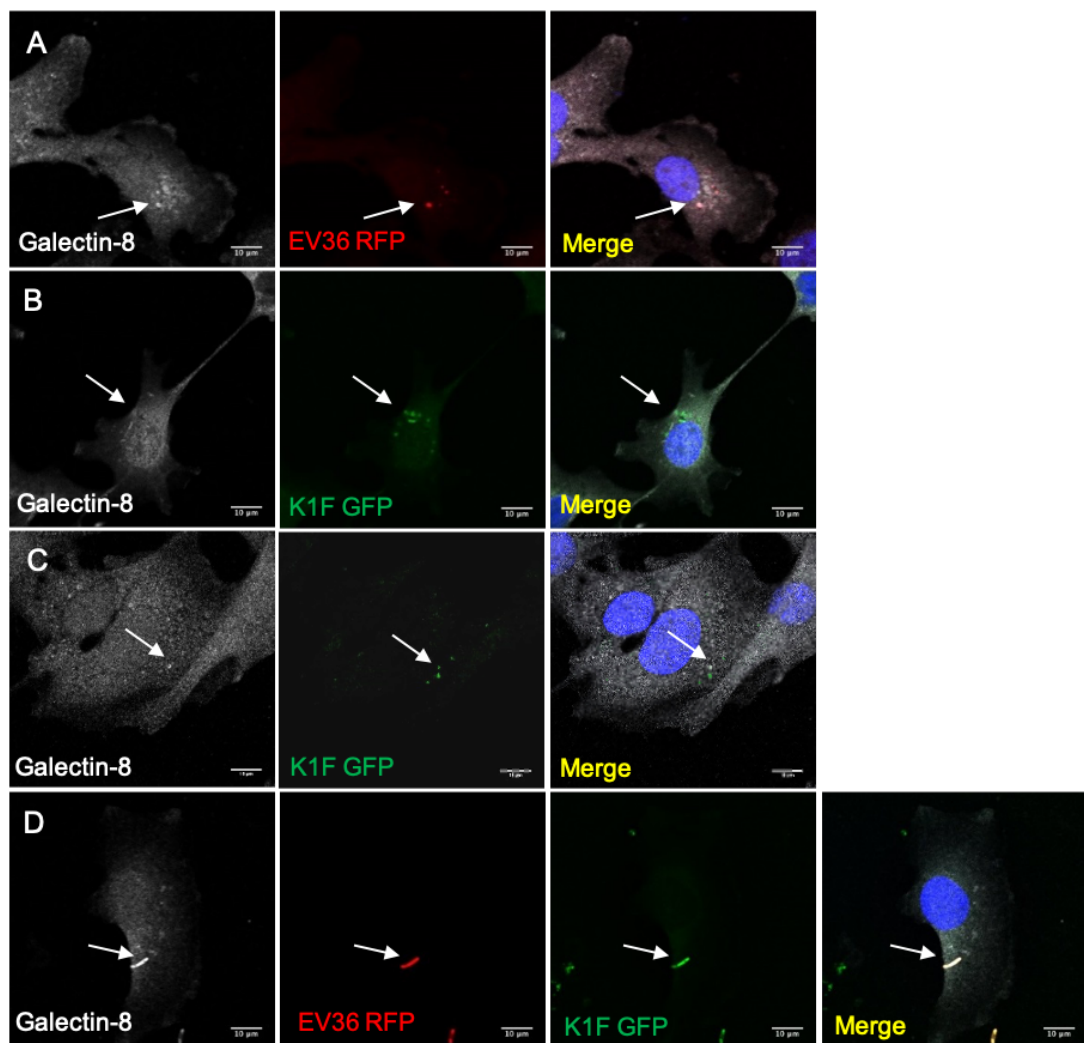


Figure 4-9. Colocalisation assay of T24 cells stained with anti-hGalactin-8 antibodies. (A-D) Microscopy images showing T24 cells following a 1-hour incubation period with 10^7 CFU/ml *E. coli* EV36-RFP (A) or 10^7 PFU/ml phage K1F-GFP (B-C) alone, or a 1 hour incubation with 10^7 CFU/ml *E. coli* EV36-RFP followed by 1 hour incubation with 10^4 PFU/ml phage K1F-GFP (D). Images are representative of three independently performed experiments.

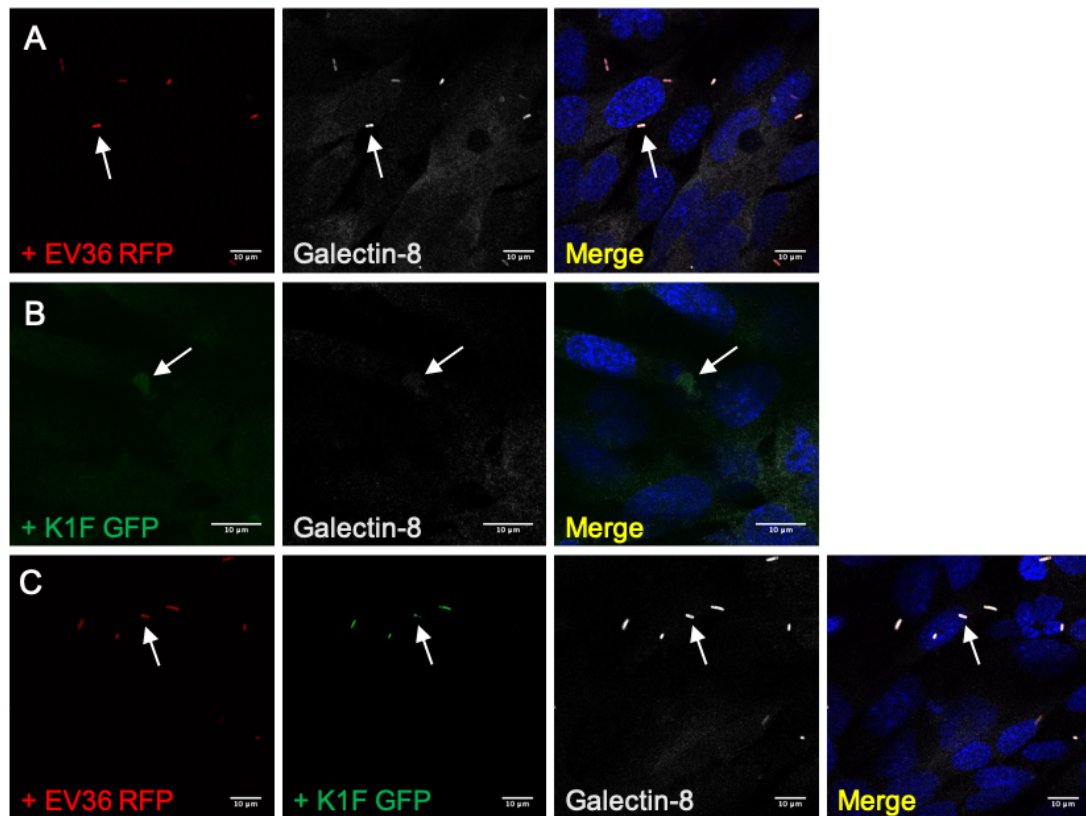


Figure 4-10. Colocalisation assay of hCMECs stained with anti-hGalectin-8 antibodies. (A-C) Microscopy images showing hCMECs following a 1- hour incubation period with 10^7 CFU/ml *E. coli* EV36-RFP (A) or 10^7 PFU/ml phage K1F-GFP (B) alone, or a 1 hour incubation with 10^7 CFU/ml *E. coli* EV36-RFP followed by 1 hour incubation with 10^4 PFU/ml phage K1F-GFP (C). Images are representative of three independently performed experiments.

Intrigued by the potential differences between the two cell types, imaging quantification was performed on the T24 cell data sets (Figure 4-11). The data show colocalisation of galectin-8 with 50.6% of intracellular *E. coli* EV36-RFP and 24.4% of intracellular phage K1F-GFP, giving a reduction of 51.8% ($P = .012$). *E. coli* EV36-RFP and phage K1F-GFP in combination on the other hand increased the colocalisation to 100.0%, an increase from phage K1F-GFP alone of 309% ($P = .0002$) and from *E. coli* EV36-RFP alone of 97.6% ($P < .001$).

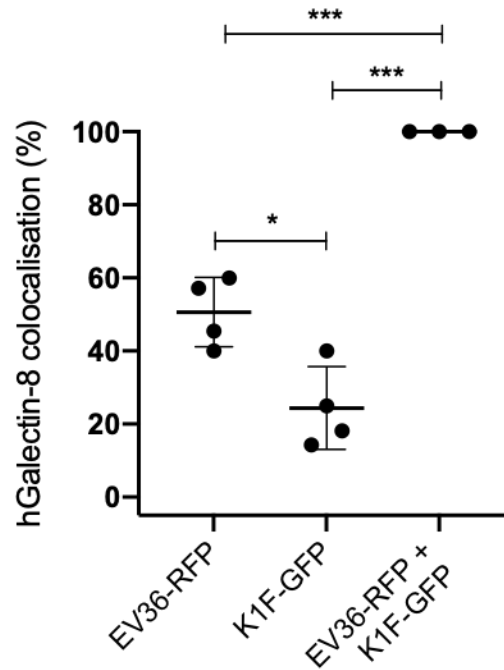


Figure 4-11. Quantification of anti-hGalectin-8 co-localisation assay of T24 cells. T24 cells were incubated for 1 hour with 10^7 CFU/ml *E. coli* EV36-RFP or 10^7 PFU/ml phage K1F-GFP alone, or a 1-hour incubation with 10^7 CFU/ml *E. coli* EV36-RFP followed by 1 hour incubation with 10^4 PFU/ml phage K1F-GFP. P-values are calculated as a pairwise comparison and displayed as $P \leq .05$ (*), $P \leq .01$ (**), $P \leq .001$ (***). Data shown as mean \pm SD, $n = 3$. Each data point represents an independently performed experiment comprising of > 200 imaged T24 cells.

4.4 *E. coli* EV36 and not phage K1F activate ubiquitin-dependent autophagy

The accumulation of galectin-8 to exposed membrane-bound glycans sequesters autophagy-related cargo receptor, NDP52, to these sites, bridging the gap to phagophore-bound LC3B and ultimately resulting in autolysosomal degradation^{112, 121}. Microscopy imaging of T24 cells showed colocalisation of NDP52 with *E. coli* EV36-RFP (Figure 4-12A), and *E. coli* EV36-RFP and phage K1F-GFP in combination only in some cells (Figure 4-12C) indicating that the phagosome progression towards autolysosomal degradation is not guaranteed within this timeframe. In contrast, in hCMECs, intracellular *E. coli* EV36-RFP (Figure 4-13A), and *E. coli* EV36-RFP and phage K1F-GFP in combination (Figure 4-13C) always showed colocalisation with NDP52. Intracellular phage K1F-GFP within either T24 cells or hCMECs showed no colocalisation with NDP52 (Figure 4-12B, Figure 4-13B), suggesting that the phage-containing phagosome does not assemble with phagophore-bound LC3B.

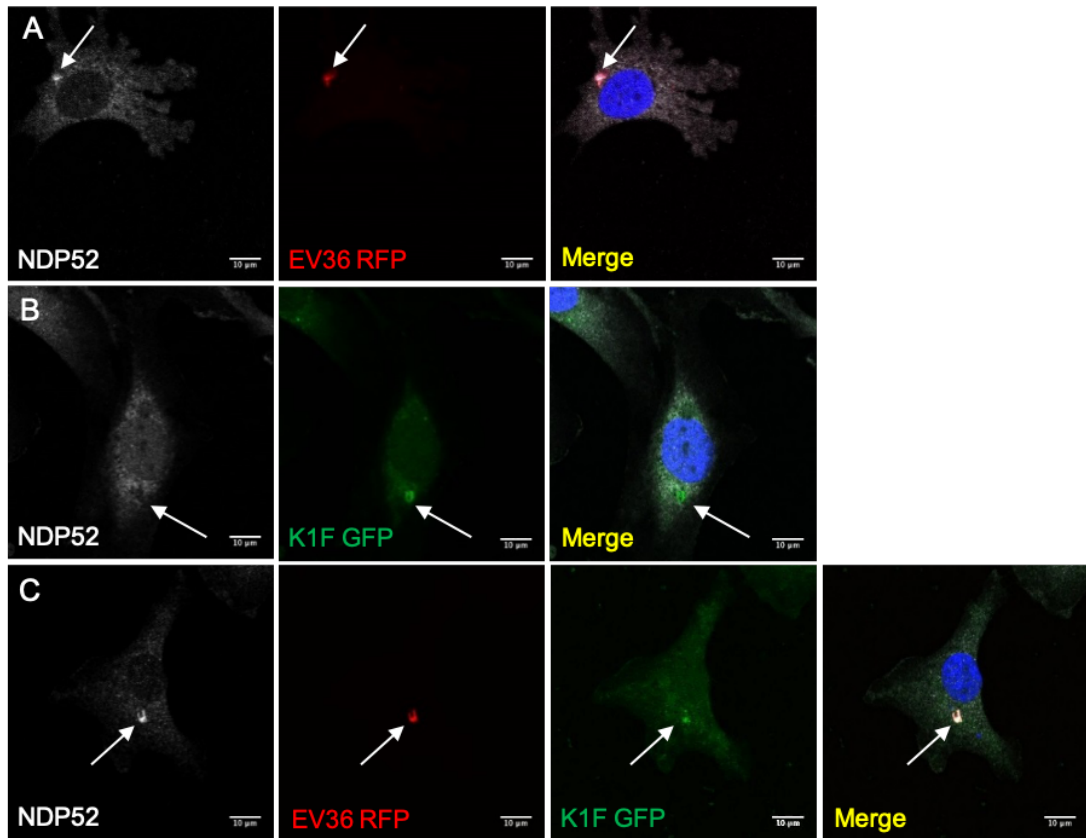


Figure 4-12. Colocalisation assay of T24 cells stained with anti-NDP52 antibodies. (A-C) Microscopy images showing T24 cells following a 1-hour incubation period with 10^7 CFU/ml *E. coli* EV36-RFP (A) or 10^7 PFU/ml phage K1F-GFP (B) alone, or a 1 hour incubation with 10^7 CFU/ml *E. coli* EV36-RFP followed by 1 hour incubation with 10^4 PFU/ml phage K1F-GFP (C). Images are representative of three independently performed experiments.

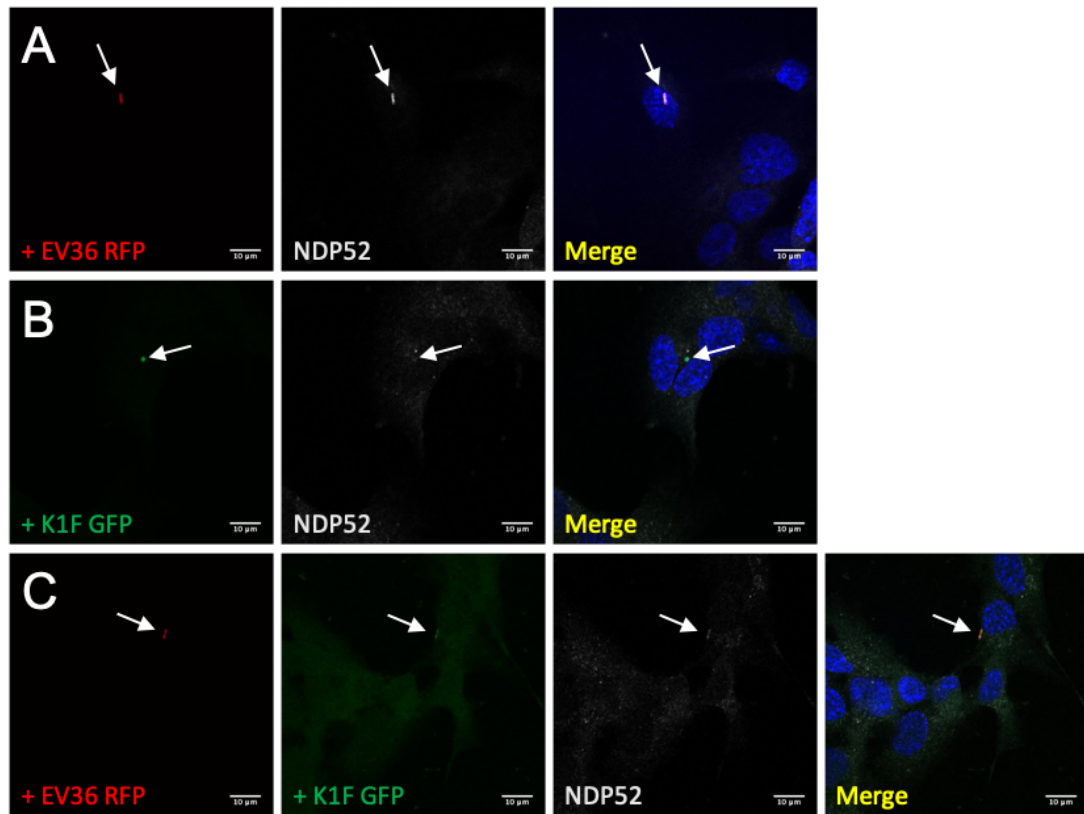


Figure 4-13. Colocalisation assay of hCMECs stained with anti-NDP52 antibodies. (A-C) Microscopy images showing hCMECs following a 1 hour incubation period with 10^7 CFU/ml *E. coli* EV36-RFP (A) or 10^7 PFU/ml phage K1F-GFP (B) alone, or a 1 hour incubation with 10^7 CFU/ml *E. coli* EV36-RFP followed by 1 hour incubation with 10^4 PFU/ml phage K1F-GFP (C). Images are representative of three independently performed experiments.

Image quantification was performed on the T24 cell data sets as previously (Figure 4-14). The analysis showed that NDP52 colocalised with 47.8% of intracellular *E. coli* EV36-RFP which was reduced to 24.9% when intracellular *E. coli* EV36-RFP and phage K1F was observed in combination. No colocalisation of intracellular phage K1F-GFP with NDP52 was observed in T24 cells.

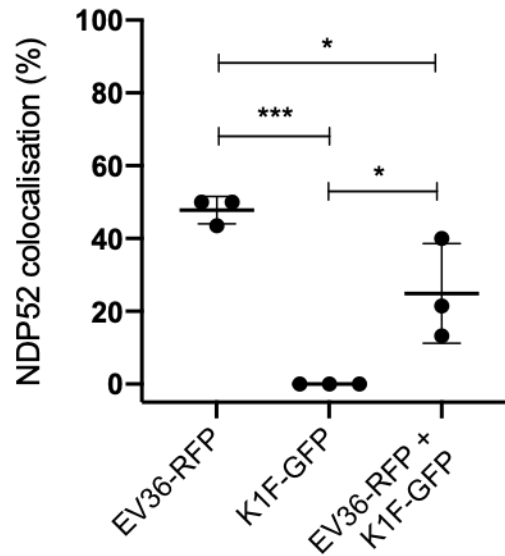


Figure 4-14. Quantification of anti-NDP52 co-localisation assay of T24 cells. T24 cells were incubated for 1 hour with 10^7 CFU/ml *E. coli* EV36-RFP or 10^7 PFU/ml phage K1F-GFP alone, or a 1-hour incubation with 10^7 CFU/ml *E. coli* EV36-RFP followed by 1 hour incubation with 10^4 PFU/ml phage K1F-GFP. P-values are calculated as a pairwise comparison and displayed as $P \leq .05$ (*), $P \leq .01$ (**), $P \leq .001$ (***). Data shown as mean \pm SD, $n = 3$. Each data point represents an independently performed experiment comprising of > 200 imaged T24 cells.

In selective autophagy, the accumulation of polyubiquitinated proteins on and around the cytosol-exposed pathogen has antimicrobial effects and can enhance NDP52 recruitment ¹²². Ubiquitination has been shown to be associated with recognition of both bacteria and viruses ¹¹¹ and can be activated independently though NDP52 or enhance galectin-8 activation ¹¹². Microscopy imaging performed with an ubiquitin antibody, a marker for ubiquitinated proteins, showed colocalisation with most, but not all, intracellular *E. coli* EV36-RFP in T24 cells (Figure 4-15A-B) while all intracellular *E. coli* EV36-RFP in hCMECs showed colocalisation (Figure 4-16A). No colocalisation was observed of ubiquitin with intracellular phage K1F alone in either T24 cells (Figure 4-15C) or hCMECs (Figure 4-16B). In contrast, *E. coli* EV36-RFP in combination with phage K1F showed colocalisation with ubiquitin in both cell types (Figure 4-15D, Figure 4-16C). Collectively, this indicates that *E. coli* EV36-RFP, and not phage K1F, associate with ubiquitin and activates ubiquitin dependent autophagy.

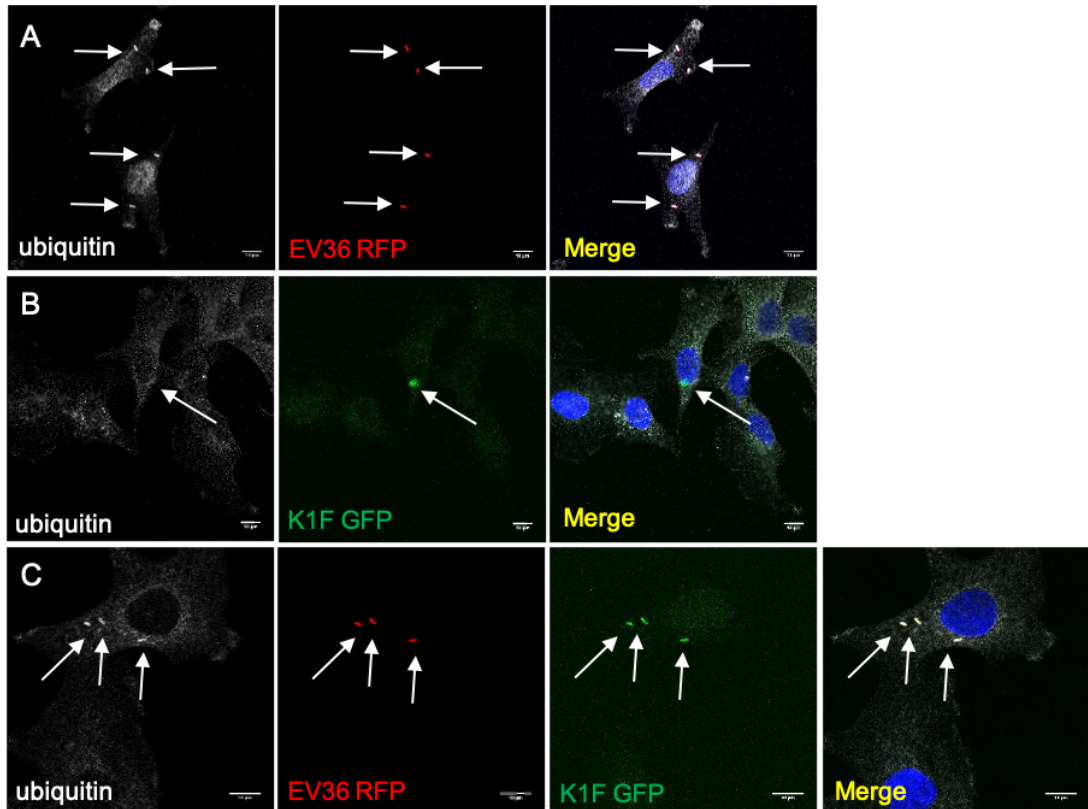


Figure 4-15. Colocalisation assay of T24 cells stained with anti-Ubiquitin antibodies. (A-C) Microscopy images showing T24 cells following a 1-hour incubation period with 10^7 CFU/ml *E. coli* EV36-RFP (A) or 10^7 PFU/ml phage K1F-GFP (B) alone, or a 1 hour incubation with 10^7 CFU/ml *E. coli* EV36-RFP followed by 1 hour incubation with 10^4 PFU/ml phage K1F-GFP (C). Images are representative of three independently performed experiments.

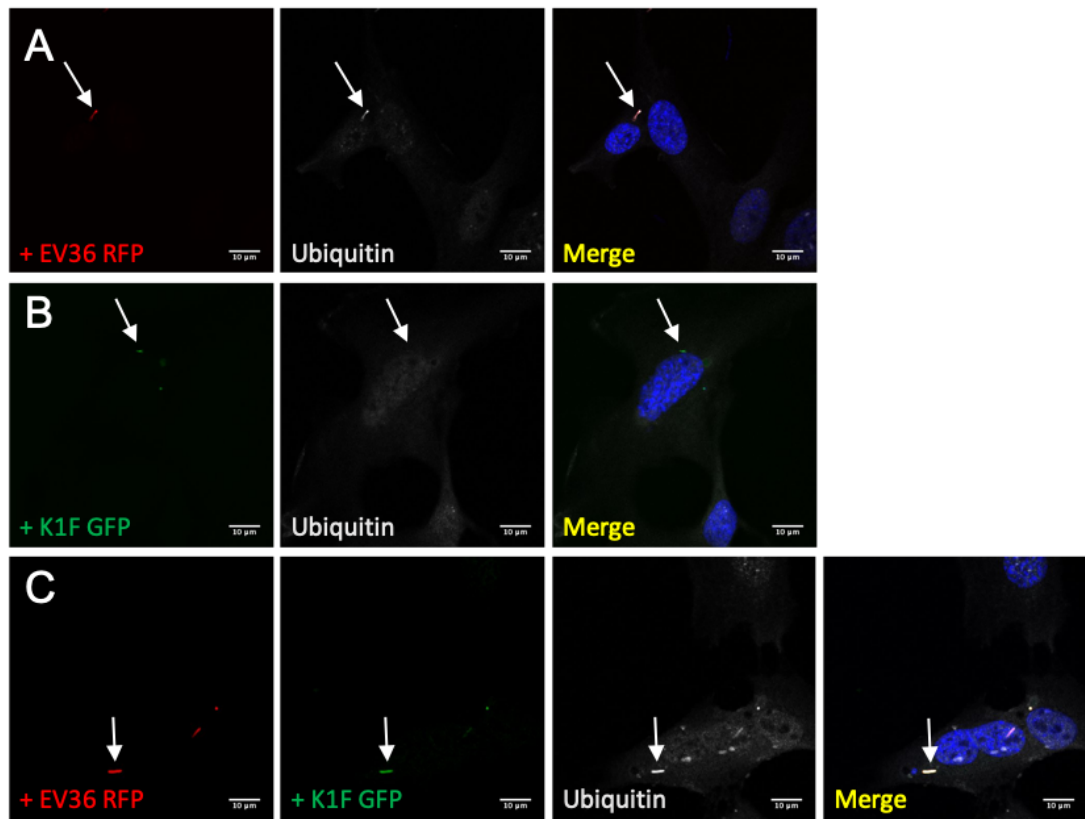


Figure 4-16. Colocalisation assay of hCMECs stained with anti-Ubiquitin antibodies. (A-C) Microscopy images showing hCMECs following a 1-hour incubation period with 10^7 CFU/ml *E. coli* EV36-RFP (A) or 10^7 PFU/ml phage K1F-GFP (B) alone, or a 1-hour incubation with 10^7 CFU/ml *E. coli* EV36-RFP followed by 1 hour incubation with 10^4 PFU/ml phage K1F-GFP (C). Images are representative of three independently performed experiments.

Image quantification was performed of the T24 image set to clarify the variation observed in ubiquitin colocalisation (Figure 4-17). The analysis showed that 89.2% of intracellular *E. coli* EV36-RFP colocalised with ubiquitin. The percentage of colocalisation increased to 97.8% for intracellular *E. coli* EV36 and phage K1F in combination. As before, no colocalisation was observed with intracellular phage K1F.

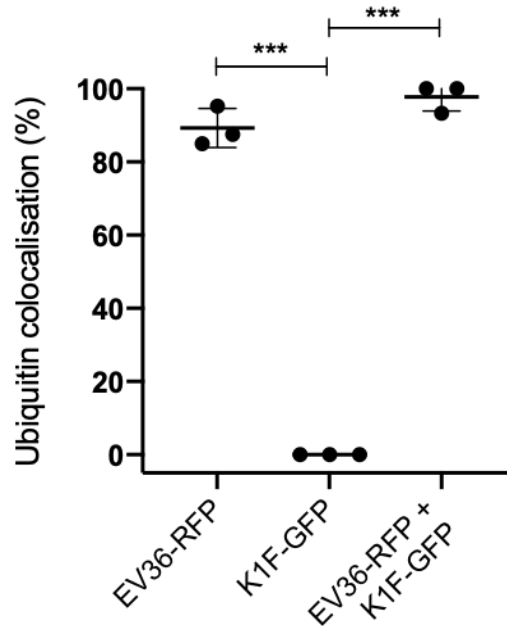


Figure 4-17. Quantification of anti-Ubiquitin co-localisation assay of T24 cells. T24 cells were incubated for 1 hour with 10^7 CFU/ml *E. coli* EV36-RFP or 10^7 PFU/ml phage K1F-GFP alone, or a 1-hour incubation with 10^7 CFU/ml *E. coli* EV36-RFP followed by 1 hour incubation with 10^4 PFU/ml phage K1F-GFP. P-values are calculated as a pairwise comparison and displayed as $P \leq .05$ (*), $P \leq .01$ (**), $P \leq .001$ (***). Data shown as mean \pm SD, $n = 3$. Each data point represents an independently performed experiment comprising of > 200 imaged T24 cells.

Ubiquitin abundance was quantified on a larger population of hCMECs using flow cytometry (Figure 4-18). In flow cytometry, the ubiquitin signal is averaged from whole cells rather than being focused on intracellular vacuoles of individual cells. This format ensures detection of any smaller cellular compartments containing ubiquitin. hCMEC cultures incubated with *E. coli* EV36 showed an increase in ubiquitin MFI over time reaching a plateau 60 minutes after addition of bacteria (Figure 4-18A). In contrast, hCMEC cultures incubated with phage K1F alone exhibited no difference in ubiquitin levels over the time course (Figure 4-18B), nor did *E. coli* EV36 and phage K1F in combination (Figure 4-18C).

The numbers obtained in quantification of ubiquitin expression in T24 cells and hCMECs resembled imaging data and emphasised that the presence of bacteria alone and not phage K1F, increases ubiquitination and activates ubiquitin-dependent autophagy.

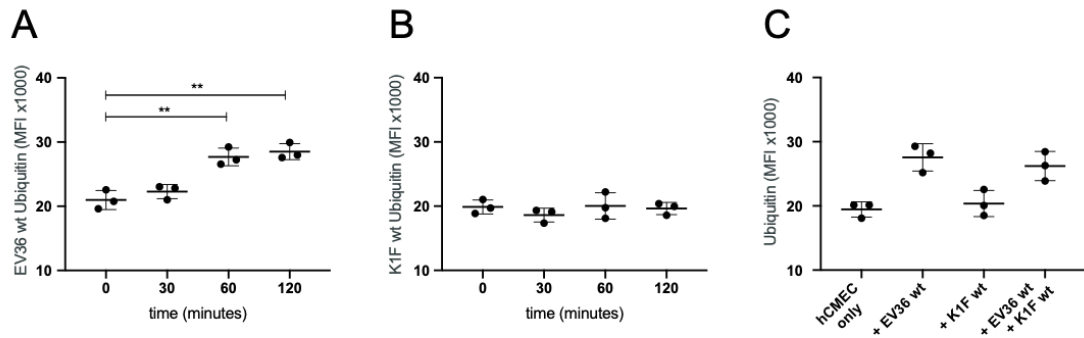


Figure 4-18. Ubiquitin expression of hCMECs as quantified by flow cytometry. (A-C) Graphs showing anti-Ubiquitin MFI of hCMEC cultures treated with 10^7 CFU/ml *E. coli* EV36 (A) or 10^7 PFU/ml phage K1F (B) as measured over time, or after a set incubation period of 1 hour (C). Combination treatment was performed in succession with 1 hour incubation each (C). P-values are calculated as a pairwise comparison and displayed as $P \leq .05$ (*), $P \leq .01$ (**), $P \leq .001$ (***) . Data shown as mean \pm SD, $n = 3$.

Sampling point (minutes)	<i>E. coli</i> EV36 (Ubiquitin MFI x1000)	Phage K1F (Ubiquitin MFI x1000)
0	20.9 (SD = 1.5)	19.9 (SD = 1.1)
30	22.3 (SD = 1.1, $P = .289$)	18.6 (SD = 1.1, $P = .227$)
60	27.7 (SD = 1.4, $P = .0046$)	20.0 (SD = 2.0, $P = .878$)
120	28.5 (SD = 1.2, $P = .0025$)	19.6 (SD = 0.9, $P = .791$)

Table 4-3. Summary of Ubiquitin MFI of hCMEC cultures treated with *E. coli* EV36 or phage K1F alone as measured over time using flow cytometry. P-values are presented as a pairwise comparison against the 0-minute sampling point.

4.5 Discussion

The data presented in this chapter illustrates similarities and differences in the mechanisms employed for the degradation of bacteria and phage between epithelial and endothelial cell lines.

Studies has demonstrated that Rab7-association is characteristic for maturation of the early phagosome^{116,177} and that Cathepsin-L is present in lysosomes of all tissues¹¹⁸. In experiments in both T24 cells and hCMECs, colocalisation of both Rab7 and Cathepsin-L was observed with *E. coli* EV36-RFP and phage K1F-GFP alone and in combination. This suggest that, independently of cell type, these bacteria and phages

are taken up by the endocytic machinery and are then degraded in part by non-selective constitutive phagocytosis.

This suggestion was confirmed by flow cytometry of hCMECs following bacterial or combination treatment, which showed a clear time-dependent increase of LysoTracker fluorescence, a proxy for acidic organelles ¹⁷⁸. However, the flow cytometry data showed a decrease of LysoTracker fluorescence over time following phage treatment, down to below basal level. This observation would seem contradictory with the imaging data that demonstrated colocalisation of phages and lysosome-associated Cathepsin-L. It is worth noting that while phage treatment was found to greatly reduce the percentage of human cells harbouring intracellular bacteria and thus must be present in most if not all human cells of a culture, phage-containing vacuoles were only observed in 1-2% of human cells of a culture. The light microscope used in these studies has a separation resolution of 200nm and the size of phage K1F is approximately 50 nm. While it is theoretically possible to detect a single GFP molecule, this would be incredibly challenging considering inherent background of human cells and media and the sheer difference in scale. Observation of individual phages is therefore not easily performed with this setup and the colocalisation studies must rely on the aggregation of phages. It is unknown if the phages aggregate extracellularly or are bundled together in vacuoles intracellularly. Further analysis of the flow cytometry data suggests that upon phage treatment, the cytosolic store of lysosomes is spent over time, suggesting that a degradation process is ongoing, and that the hCMECs are not replenishing the lysosome store over the time course. This analysis ties in with the previous imaging observations, that phages are degraded by non-selective constitutive phagocytosis.

Interestingly, comparison of hCMECs treated with bacteria alone and in combination with phages showed an increase in lysosome abundance. This could be facilitated by phage-induced bacterial lysis resulting in breakage of the bacterial cell envelope, causing either debris to be degraded in increased amounts of individual lysosomes or an increasing host-recognition of LPS intensifying the overall lysosomal activity.

Both epithelial and endothelial cells express an array of PRRs enabling detection of a wide range of PAMPs and DAMPs. During phagosome maturation autophagy-related

proteins are recruited in response to cargo activation and signalling of PRRs ^{110, 114}. In this manner, LC3 can be recruited to the late phagosome and participate in selective LC3-assisted phagocytosis. Colocalisation of LC3B was observed with *E. coli* EV36-RFP and phage K1F-GFP alone and in combination in both T24 cells and hCMECs. This demonstrated that bacteria and phages alike are recognised by phagosome-bound PRRs.

Until now, the data had showed coherence between the T24 epithelial cells and endothelial hCMECs in their mechanisms for uptake and degradation of both bacteria and phages. However, phenotypic differences were observed in the activation of xenophagy. Exposure of host-derived membrane-bound glycans following the attempted escape of pathogen from a pathogen-containing phagosome recruits galectin-8 ^{112, 121}. The cytosolic association of galectin-8 initiates xenophagy through autophagy-related receptors, one of which being NDP52. In T24 cells, colocalisation of galectin-8 was observed with about half of intracellular *E. coli* EV36-RFP and about a quarter of intracellular phage K1F-GFP. This suggests firstly that only half of the phagosome-contained bacteria manages to breach the phagosomal membrane before the harsh lysosomal environment hinders further attempts, and secondly, that a quarter of phagosome-contained phages somehow manages to damage the phagosomal membrane, by an unknown mechanism. In contrast, in hCMECs, all intracellular *E. coli* EV36-RFP and none of intracellular phage K1F-GFP was found to colocalise with galectin-8. Interestingly, all intracellular *E. coli* EV36-RFP and phage K1F-GFP in combination colocalised with galectin-8 in both hCMECs and T24. This suggests, that in T24 cells, *E. coli* EV36-RFP and phage K1F-GFP in combination more often leads to a breached phagosome than *E. coli* EV36-RFP alone. The unknown mechanism for this is intriguing, and hints that the bacteria become more vigilant or desiring an escape when infected with phages. Collectively this illustrates phenotypic differences between epithelial and endothelial cells likely relating to their natural and distinct environments; epithelial cells are typically more exposed to the environment and therefore might intrinsically respond differently to pathogens.

Additional colocalisation studies confirmed the differentiated response of T24 cells towards intracellular *E. coli* EV36-RFP as only about half of the bacteria showed colocalisation with NDP52 and about 90% with ubiquitin. NDP52, as a mediator between the cytosolic pathogen-associated galectin-8 or ubiquitin and phagophore-bound LC3B, signals the further progression of xenophagy¹²⁰. Galectin-8 association alone cannot lead to xenophagy; for this NDP52 is required. On the contrary, ubiquitin association can lead to phagophore formation and xenophagy with or without NDP52. It is believed that ubiquitin association is derived from a host-perceived higher level of virulence¹¹². Intuitively, bacteria would present a bigger threat than phages. This assumption is confirmed by the absence of colocalisation of NDP52 and ubiquitin with intracellular phage K1F in both cell types. The galectin-8 colocalisation observed in T24 with intracellular phage K1F is therefore demonstrated not to progress to xenophagy. Further studies could examine the temporal relationship of galectin-8, NDP52, and ubiquitin association with intracellular bacteria or phages at a single-cell level to elucidate the progression of the various pathways observed here.

In these experiments, image quantification provided insights into the level of involvement of galectin-8, NDP52, and ubiquitin in T24 cells beyond the simple observations of colocalisation. Flow cytometric quantification provided temporal insights of the level of involvement of lysosomes by proxy, LC3B, and ubiquitin in a larger population of hCMECs. These quantitative data sets add value to the qualitative imaging data and illustrates that these methodologies are comparable in identifying the level of involvement of various proteins in molecular mechanisms. A summary table of these results are presented in Table 4-4.

Treatment / Antibody	T24 – ICC			hCMEC – ICC			hCMEC – Flow cytometry		
	EV36	K1F	EV36 + K1F	EV36	K1F	EV36 + K1F	EV36	K1F	EV36 + K1F
Rab7	+	+	+	+	+	+	N/A	N/A	N/A
Cathepsin-L	+	+	+	+	+	+	N/A	N/A	N/A
LysoTracker	N/A	N/A	N/A	N/A	N/A	N/A	+	-	+
LC3B	+	+	+	+	+	+	+	-	-
Galectin-8	+/-	+/-	+	+	-	+	N/A	N/A	N/A
NDP52	+/-	-	+/-	+	-	+	N/A	N/A	N/A
Ubiquitin	+/-	-	+	+	-	+	+	No diff.	No diff.

Table 4-4. Summary table for Chapter 4. Immunocytochemistry was performed with both T24 cells and hCMECs, while flow cytometry was performed with hCMECs only. Definitions: + indicates a positive (present) colocalisation for ICC and an increasing MFI over time for flow cytometry, - indicates a negative (absent) colocalisation for ICC and a decreasing MFI over time for flow cytometry. Note that for flow cytometry analysis of cultures receiving a single treatment (EV36 or K1F) the comparison is against an untreated control culture, while cultures receiving a combination treatments (EV36 + K1F) the comparison is against a culture receiving EV36 treatment alone .

Chapter 5 Phage interactions with human cells

The colocalisation experiments demonstrated that phage K1F, taken up by human cells, was recognised by human PRRs during phagosome maturation and degraded, in part, by selective LC3-assisted phagocytosis. Additionally, *in vitro* phage therapy demonstrated an increase in lysosomal activity hinting at a potential effect of inflammatory progression.

The experiments in this chapter were therefore designed to determine if recognition of phages would induce an inflammatory response in human cells and what influence phage therapy would have on the progression of bacterial-induced inflammation. In this context, the inflammatory response of hCMECs to *E. coli* EV36 and phage K1F individually and in combination was investigated by measuring the induction of inflammatory markers. The markers used in real-time qPCR studies consisted of: TNF α , IL-6, IL-8, IL-10, and IFN β .

A fundamental function of endothelial cells is to regulate the transport of nutrients and other molecules across the endothelium and to coordinate migration of immune cells ⁹⁷. Experiments assessing the influence of phage alone and phage therapy on the endothelium membrane permeability were therefore included.

5.1 *E. coli* EV36 but not phage K1F induce inflammatory responses in hCMEC cultures

In the following experiments, hCMEC cultures were incubated with *E. coli* EV36 and/or phage K1F and specific mRNA levels were measured by real-time qPCR. hCMEC cultures treated with TNF α were included as a positive control for induction of expression and untreated hCMEC cultures (NTC) as a control of basal expression.

TNF α is considered a master regulator with many roles in inflammation through signalling, from regulation of immune cells to induction of fever and apoptotic cell

death¹²³. hCMEC cultures incubated with *E. coli* EV36 showed a significant and sharp increase of TNF α expression over time from 2 hours and beyond, reaching a plateau of an approximately 100- fold increase over control after 4 hours (Figure 5-1A). In contrast, hCMEC cultures incubated with phage K1F showed no change in the expression levels of TNF α during the time course (Figure 5-1B). TNF α induction of TNF α expression, monitored as a control, was observed with an early onset and subsequent decrease, but with large variability between replicate samples (Figure 5-1C). Combined treatment with both *E. coli* EV36 and K1F (*in vitro* phage therapy) showed that *E. coli* EV36-induced TNF α expression was reduced by approximately 50% by the addition of phage K1F compared to *E. coli* EV36 alone (Figure 5-1D). The addition of phages 1 hour before in comparison with 1 hour after the addition of bacteria gave an average reduction of 22.6 % ($P = .043$).

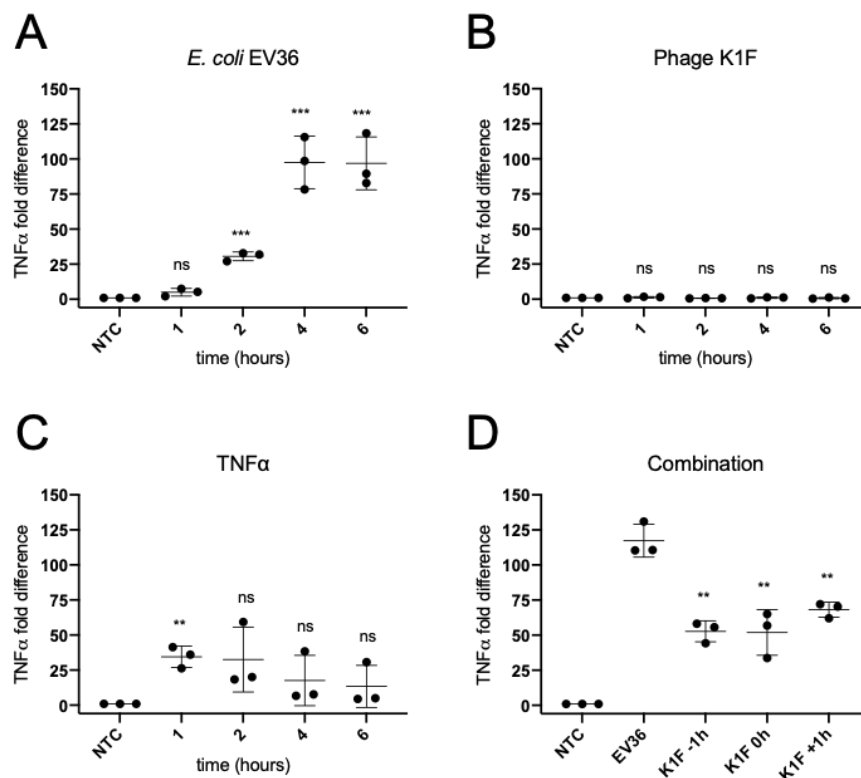


Figure 5-1. Expression pattern of TNF α by real-time qPCR. hCMEC cultures were incubated with either 10^7 CFU/ml *E. coli* EV36 (A), 10^7 PFU/ml phage K1F (B), or 500 pg/ml TNF α (C) with mRNA levels measured over time or incubated with 10^4 PFU/ml phage K1F 1 h before, simultaneously, or after the addition of 10^7 CFU/ml *E. coli* EV36 with mRNA levels measured after 6 h (D). The data is presented as expression relative to GAPDH and normalised to NTC. P-values are calculated as a pairwise comparison to NTC (A-C) or EV36 (D) and displayed as $P \leq .05$ (*), $P \leq .01$ (**), $P \leq .001$ (***).

IL-6 is produced to stimulate host defences early in infection and the concentration is directly related to the severity of the infection^{125 180}. Over time, hCMEC cultures incubated with *E. coli* EV36 showed a steep increase in IL-6 expression peaking at the 4-hour time point (Figure 5-2A), while cultures incubated with phage K1F showed no change in expression levels (Figure 5-2B). Control cultures incubated with TNF α showed a stable gradual time-dependent increase in IL-6 expression throughout the incubation period (Figure 5-2C). Contrary to the observed reduction in TNF α induction when combining phages and bacteria, the *in vitro* phage therapy combination scenario in hCMEC cultures increased IL-6 expression by more than 200% as compared with *E. coli* EV36 alone (Figure 5-2D). The observed increase was independent of whether the phages were added before, simultaneously, or after bacteria.

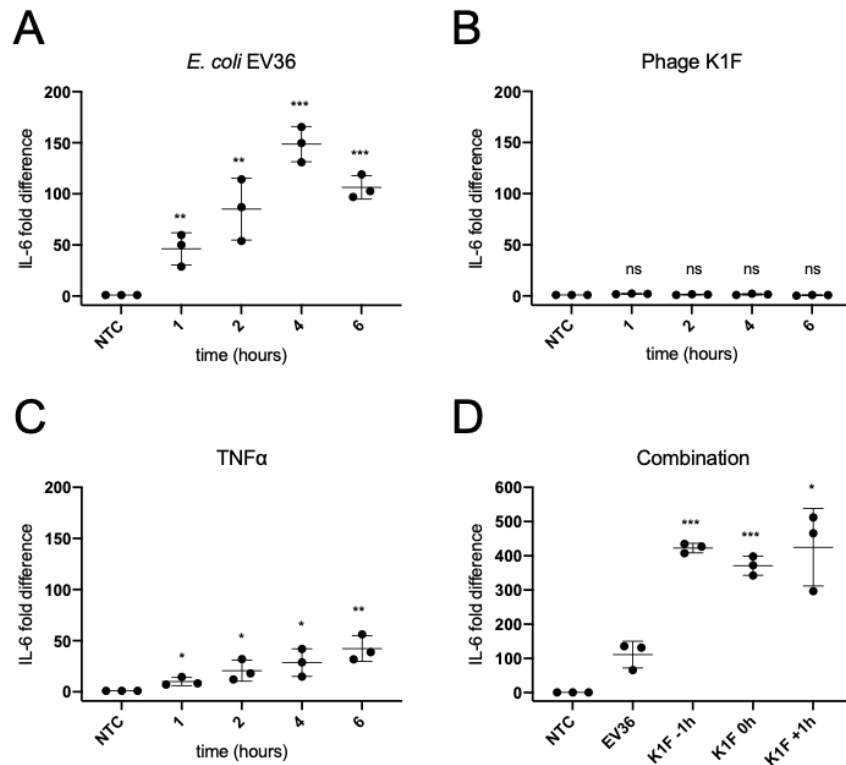


Figure 5-2. Expression pattern of IL-6 by real-time qPCR. hCMEC cultures were incubated with either 10^7 CFU/ml *E. coli* EV36 (A), 10^7 PFU/ml phage K1F (B), or 500 pg/ml TNF α (C) with mRNA levels measured over time or incubated with 10^4 PFU/ml phage K1F 1 h before, simultaneously, or after the addition of 10^7 CFU/ml *E. coli* EV36 with mRNA levels measured after 6 h (D). The data is presented as expression relative to GAPDH and normalised to NTC. P-values are calculated as a pairwise comparison to NTC (A-C) or EV36 (D) and displayed as $P \leq .05$ (*), $P \leq .01$ (**), $P \leq .001$ (***).

As a potent chemokine, IL-8 is involved in anti-inflammatory regulation of immune cells, specifically attracting and activating neutrophil granulocytes, while inhibiting leukocyte adhesion to endothelial cells^{28, 126}. hCMEC cultures incubated with *E. coli* EV36 induced IL-8 expression with a kinetic profile similar to the induction of TNF α (Figure 5-3A), showing a slow onset increase of expression reaching a plateau after 4 hours (Figure 5-3A). On the other hand, hCMEC cultures incubated with phage K1F showed no change in IL-8 expression during the time course (Figure 5-3B), again resembling the effect phage K1F had on TNF α expression (Figure 5-3B). The control treatment with TNF α gave more rapid induction of IL-8 expression, plateauing after 2 hours (Figure 5-3C). The induced expression profile of IL-8 following *in vitro* phage therapy of *E. coli* EV36 – infected hCMEC cultures was comparable to that of IL-6 rather than TNF α , showing an increase of more than 150% following phage K1F

addition in relation to *E. coli* EV36 treated cultures alone (Figure 5-3D). No difference was observed between the three timepoints of phage K1F addition.

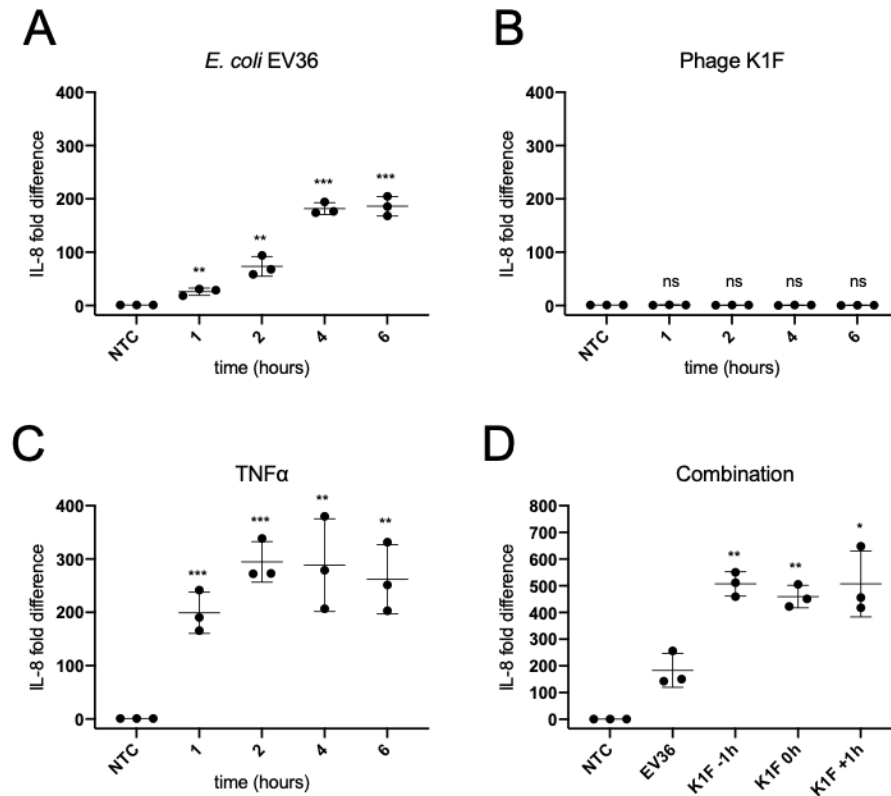


Figure 5-3. Expression pattern of IL-8 by real-time qPCR. hCMEC cultures were incubated with either 10^7 CFU/ml *E. coli* EV36 (A), 10^7 PFU/ml phage K1F (B), or 500 pg/ml TNF α (C) with mRNA levels measured over time or incubated with 10^4 PFU/ml phage K1F 1 h before, simultaneously, or after the addition of 10^7 CFU/ml *E. coli* EV36 with mRNA levels measured after 6 h (D). The data is presented as expression relative to GAPDH and normalised to NTC. P-values are calculated as a pairwise comparison to NTC (A-C) or EV36 (D) and displayed as $P \leq .05$ (*), $P \leq .01$ (**), $P \leq .001$ (***).

In response to infection or tissue damage, endothelial cells can express IL-10 in order to limit excess activation of pro-inflammatory cytokines¹²⁹. The induction of IL-10 expression in hCMEC cultures by *E. coli* EV36 or phage K1F alone and in combination, or by TNF α , was minimal and not significant during the time course (Figure 5-4A-D).

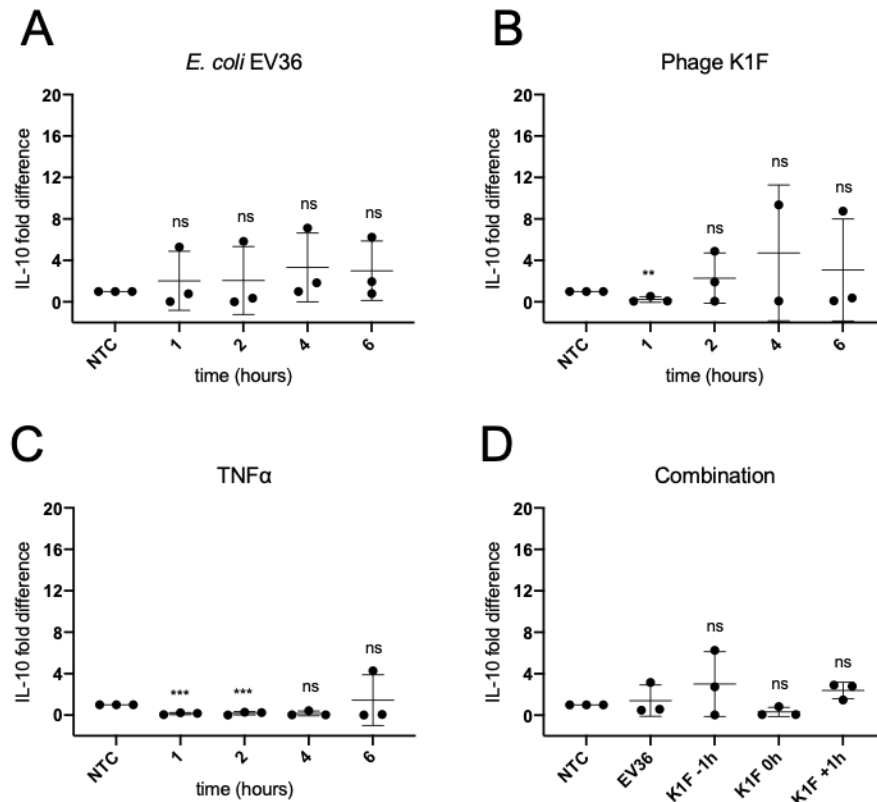


Figure 5-4. Expression pattern of IL-10 by real-time qPCR. hCMEC cultures were incubated with either 10^7 CFU/ml *E. coli* EV36 (A), 10^4 PFU/ml phage K1F (B), or 500 pg/ml TNF α (C) with mRNA levels measured over time or incubated with 10^4 PFU/ml phage K1F 1 h before, simultaneously, or after the addition of 10^7 CFU/ml *E. coli* EV36 with mRNA levels measured after 6 h (D). The data is presented as expression relative to GAPDH and normalised to NTC. P-values are calculated as a pairwise comparison to NTC (A-C) or EV36 (D) and displayed as $P \leq .05$ (*), $P \leq .01$ (**), $P \leq .001$ (***)

In these experiments, analysis of IFN β induction was included to complement the study of inflammatory cytokines as IFN β is known to be virus-inducible¹³⁰. hCMEC cultures incubated with *E. coli* EV36 showed a small time-dependent increase in IFN β expression (Figure 5-5A), while cultures incubated with phage K1F showed no induced expression of IFN β during the time course (Figure 5-5B). hCMEC cultures incubated with TNF α showed a barely significant induction of IFN β (Figure 5-5C). The responses of hCMEC cultures incubated with *E. coli* EV36 and phage K1F in combination (Figure 5-5D) showed greater variation between experiments of induced expression of IFN β with no significant differences between treatments.

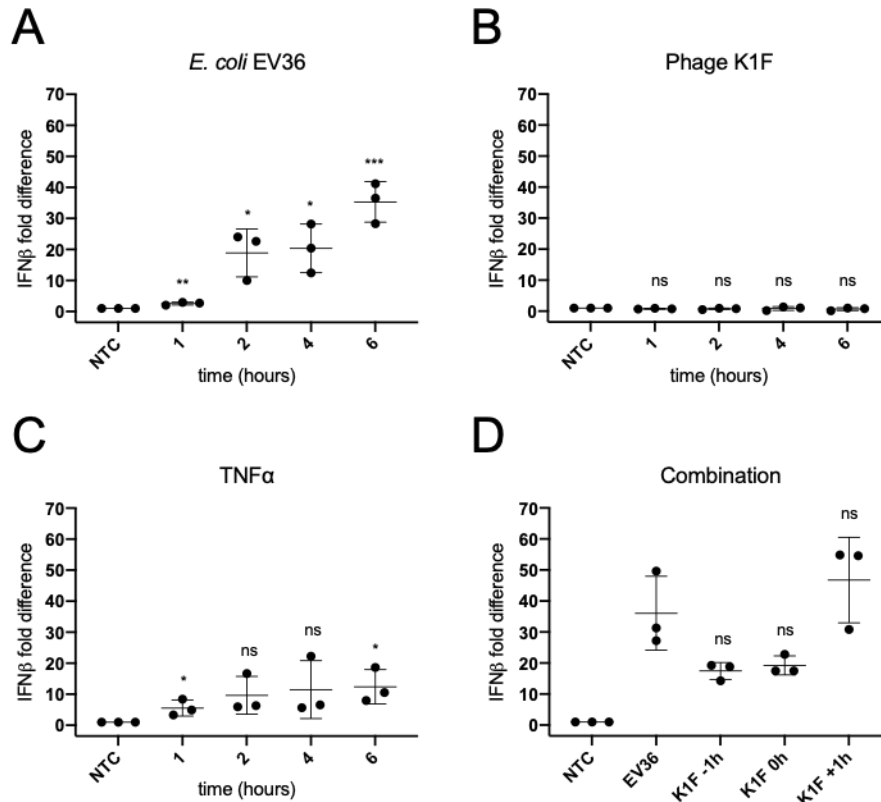


Figure 5-5. Expression pattern of *IFNβ* by real-time qPCR. The hCMEC cultures were incubated with either 10^7 CFU/ml *E. coli* EV36 (A), 10^4 PFU/ml phage K1F (B), or 500 pg/ml *TNFα* (C) with mRNA levels measured over time or incubated with 10^4 PFU/ml phage K1F 1 h before, simultaneously, or after the addition of 10^7 CFU/ml *E. coli* EV36 with mRNA levels measured after 6 h (D). The data is presented as expression relative to GAPDH and normalised to NTC. P-values are calculated as a pairwise comparison to NTC (A-C) or EV36 (D) and displayed as $P \leq .05$ (*), $P \leq .01$ (**), $P \leq .001$ (***)

The correlation between induced mRNA transcription and protein accumulation was assessed by ELISA measuring the concentration of IL-6 protein in hCMEC cultures (Figure 5-6A-D). The data showed, across all conditions, a striking correlation between the concentration of IL-6 protein and the expression level of IL-6 mRNA (Figure 5-2A-D), suggesting that the hCMEC cytokine response is mediated mainly through new transcription leading to cytokine expression. The increase in IL-6 protein following *in vitro* phage therapy (Figure 5-6D) exhibited an even greater increase, than that observed at mRNA level, of approximately 3.5 fold, in comparison with *E. coli* EV36 incubation alone. The difference observed in concentrations of IL-6 protein and IL-6 mRNA is likely due to protein stabilisation versus mRNA destabilisation. The

absence of IL-6 mRNA expression of NTCs suggests that the increases observed in either condition is driven solely in response to the condition itself.

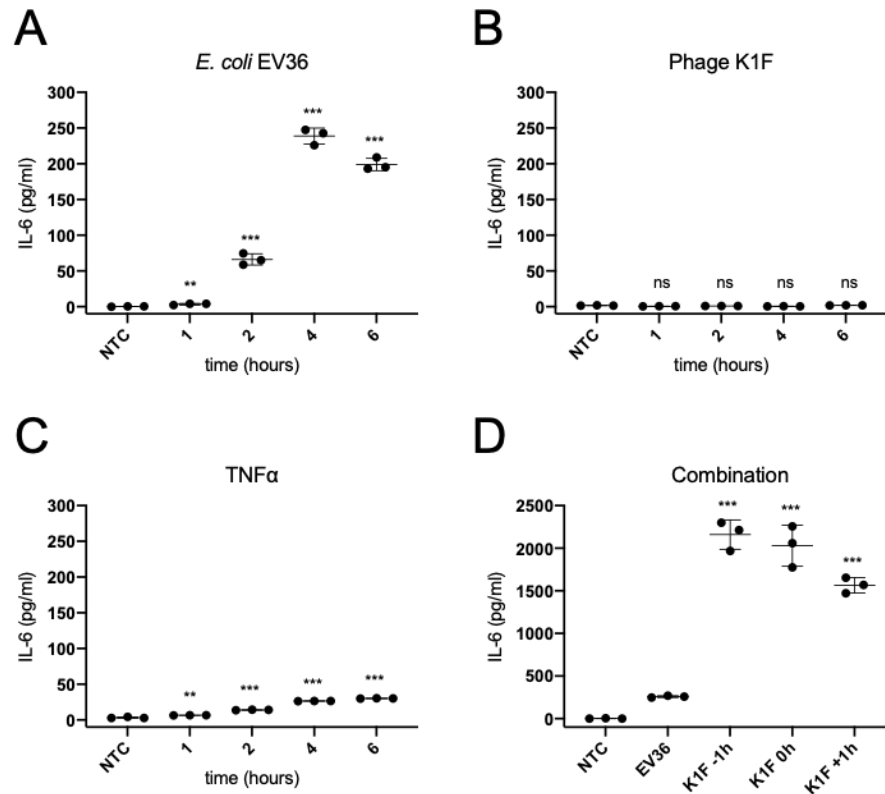


Figure 5-6. Concentration pattern of IL-6 protein by ELISA. The hCMEC cultures were incubated with either 10^7 CFU/ml *E. coli* EV36 (A), 10^7 PFU/ml phage K1F (B), or 500 pg/ml TNF α (C) with protein levels measured over time, or incubated with 10^4 PFU/ml phage K1F 1 h before, simultaneously, or after the addition of 10^7 CFU/ml *E. coli* EV36 with protein levels measured after 6 h (D). P-values are calculated as a pairwise comparison to NTC (A-C) or EV36 (D) and displayed as $P \leq .05$ (*), $P \leq .01$ (**), $P \leq .001$ (***).

5.2 Phage K1F and T7 temporarily decrease hCMEC barrier integrity

Endothelial barrier integrity can be assessed experimentally *in vitro* by measurements of TEER. The exact TEER-related properties measured depend on system parameters, such as composition of the electrode array, frequency and signal post-processing. In these experiments, the xCELLigence system, measuring impedance at a fixed frequency, was used. The arbitrary system output, the Cell Index, is mainly influenced by focal adhesions and to a smaller extent by adherence junctions.

The temporal influence of *E. coli* EV36 on the barrier function of hCMEC cultures was determined using the xCELLigence system (Figure 5-7). The data showed an immediate and dramatic decrease in Cell Index over the course of the initial 10 hours for all bacterial concentrations (Figure 5-7A). The detrimental effect of *E. coli* EV36 incubation on hCMEC cultures is clear with no sign of sustained recovery during the 72-hour experiment (Figure 5-7B), ultimately ending at a decrease in Cell Index of >95% across all bacterial concentrations.

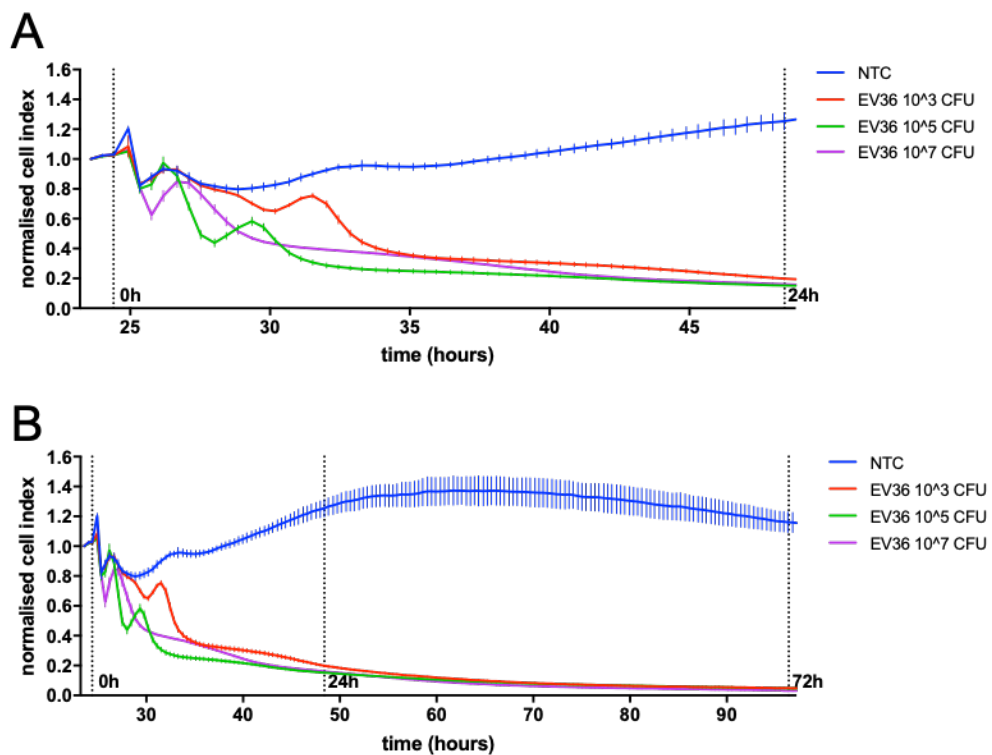


Figure 5-7. Temporal impedance profiling of hCMEC cultures incubated with *E. coli* EV36. The hCMEC cultures were incubated with *E. coli* EV36 at a concentration range of 10³ to 10⁷ CFU/ml with impedance measured by xCELLigence (A-B). The x-axis show time from cell seeding with the first vertical line denoting the addition of treatment at 0 h, and second and third line denoting 24 and 72 h post treatment respectively. The data is presented as the average normalized cell index across the acute (A) and long-term (B) incubation period (+/- SD, n => 3).

The temporal impedance profile of hCMEC cultures incubated with phage K1F (Figure 5-8) showed a slow divergence between phage-containing cultures and NTC. The divergence was detectable after approximately 12 hours after treatment addition in

hCMEC cultures incubated with phages at the highest concentrations of 10^7 and 10^9 PFU/ml (Figure 5-8A). The phage-induced decrease in Cell Index was sustained long-term (Figure 5-8B), reaching maximum divergence after approximately 35 hours from treatment addition, whereafter a gradual reduction in divergence was observed throughout towards the end of the experiment after 72-hour of incubation. This suggests that phage K1F, at high concentrations, directly influence the barrier integrity of hCMECs, but only temporarily and never to the same extent as observed for incubation with *E. coli* EV36.

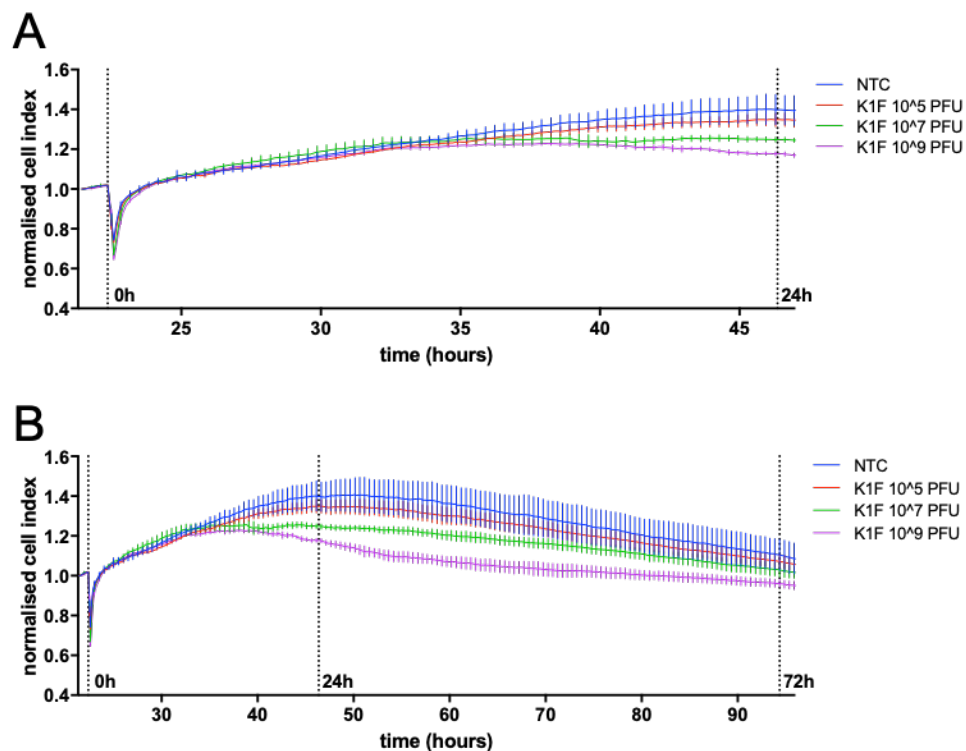


Figure 5-8. Temporal impedance profiling of hCMEC cultures incubated with phage K1F. The hCMEC cultures were incubated with phage K1F at a concentration range of 10^5 to 10^9 PFU/ml with impedance measured by xCELLigence (A-B). The x-axis show time from cell seeding with the first vertical line denoting the addition of treatment at 0 h, and second and third line denoting 24 and 72 h post treatment respectively. The data is presented as the average normalised cell index across the acute (A) and long-term (B) incubation period (+/- SD, $n \Rightarrow 3$).

With the aim to determine if these observations were specific to phage K1F or phages in general, a similar experiment was performed incubating hCMEC cultures with phage T7 (Figure 5-9). This experiment showed a strikingly similar concentration-

dependent profile of divergence in Cell Index as with phage K1F incubation. This suggests that these observations could be relevant to responses to phages in general.

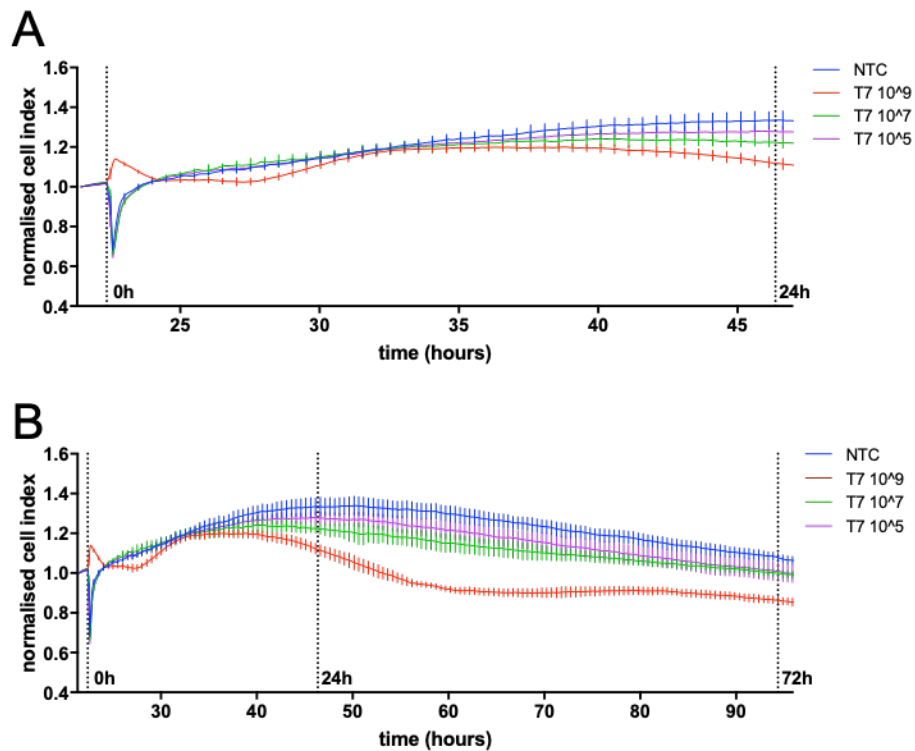


Figure 5-9. Temporal impedance profiling of hCMEC cultures incubated with phage T7. The hCMEC cultures were incubated with phage T7 at a concentration range of 10^5 to 10^9 PFU/ml with impedance measured by xCELLigence (A-B). The x-axis show time from cell seeding with the first vertical line denoting the addition of treatment at 0 h, and second and third line denoting 24 and 72 h post treatment respectively. The data is presented as the average normalised cell index across the acute (A) and long-term (B) incubation period (+/- SD, $n > 3$).

The effect of phages on the dramatic disruption of hCMEC barrier function was investigated next. *In vitro* phage therapy was performed by the addition of phage K1F to hCMEC cultures 1 hour before, simultaneously, or 1 hour after the addition of *E. coli* EV36 (Figure 5-10). As observed, the immediate and dramatic influence of bacterial incubation on the Cell Index is similar to experiments without the addition of phages. However, the addition of phage K1F 1 hour prior to or simultaneously with *E. coli* EV36 addition, allowed the impedance of hCMEC cultures to transiently recover (Figure 5-10A) in the initial 10 hours of bacterial infection. As observed with bacterial incubation alone, this transient recovery occurs in bouts. Nonetheless, despite phage intervention, the Cell Index was not maintained in the quasi-normal

range beyond the initial 10 hours of incubation and a decrease of >95% across all treatments was eventually observed (Figure 5-10B).

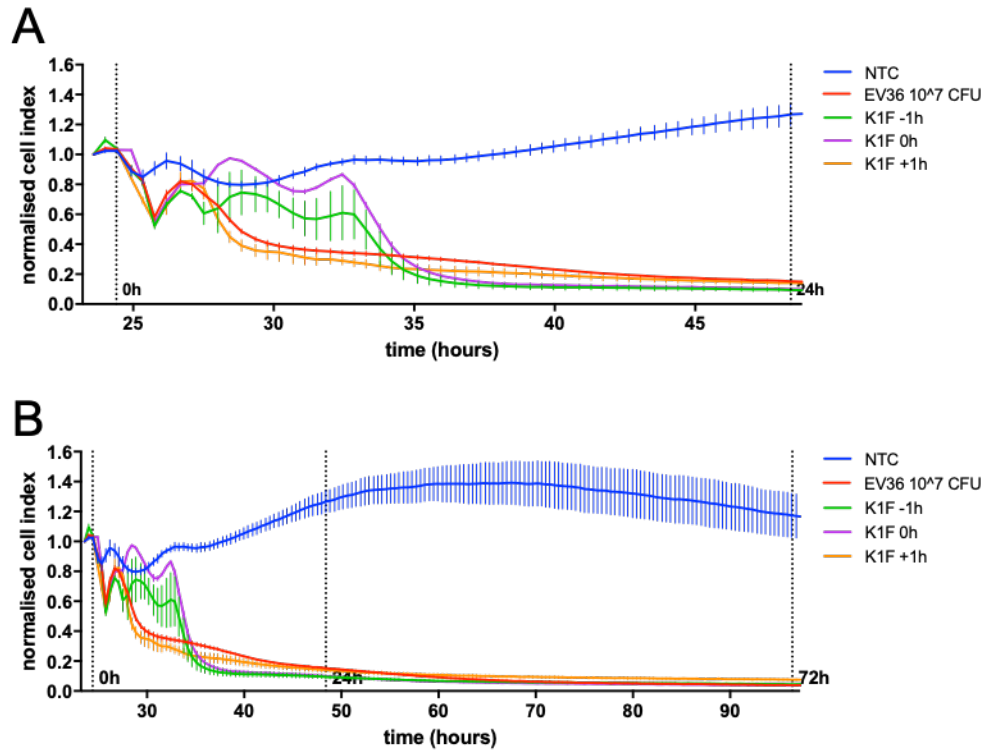


Figure 5-10. Temporal impedance profiling of hCMEC cultures incubated with *E. coli* EV36 and phage K1F in combination. The hCMEC cultures with incubated with 10⁴ PFU/ml phage K1F 1 h before, simultaneously, or after the addition of 10⁷ CFU/ml *E. coli* EV36 with impedance measured by xCELLigence (A-B). The x-axis show time from cell seeding with the first vertical line denoting the addition of treatment at 0 h, and second and third line denoting 24 and 72 h post treatment respectively. The data is presented as the average normalised cell index across the acute (A) and long-term (B) incubation period (+/- SD, n => 3).

5.3 Phage K1F and T7 do not affect proliferation or morphology of hCMECs

The xCELLigence measured Cell Index is influenced, not only by cell-to-electrode adhesion, but also by cell proliferation and cell morphology. Control experiments designed to assess the proliferation and morphology of hCMEC incubated with phages K1F and T7 were therefore performed.

hCMEC cultures incubated with phages K1F or T7 at identical concentrations showed no difference in cell concentration over time when compared to control cultures

(NTC) (Figure 5-11), suggesting that the proliferation of hCMECs is not influenced by phage addition.

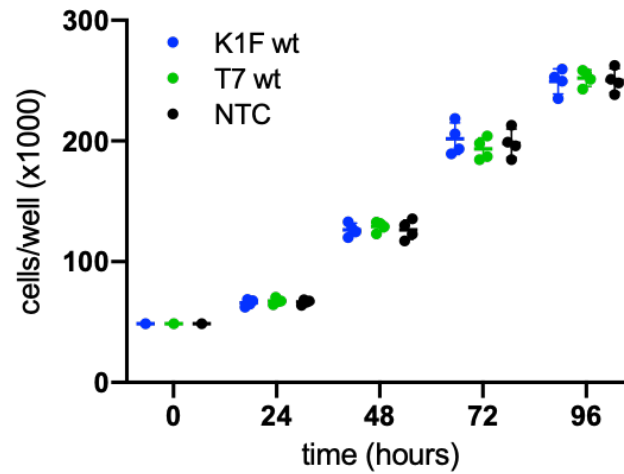


Figure 5-11. Proliferation of hCMEC cultures incubated with phages K1F or T7. hCMEC cultures were incubated with phage K1F or T7 at a concentration of 10^9 PFU/ml and cell concentration determined by manual haemocytometer counting (\pm SD, $n \geq 3$).

The morphology of hCMECs was visually assessed in relation to the shape and size of their nucleus and network of actin filaments. Image analysis of hCMEC cultures incubated with phages K1F or T7 at identical concentrations and stained to reveal the actin cytoskeleton showed healthy, well-structured stretched out cells with no obvious differences when compared to control cultures (Figure 5-12), suggesting that the overall health of hCMECs is not affected by the addition of phages.

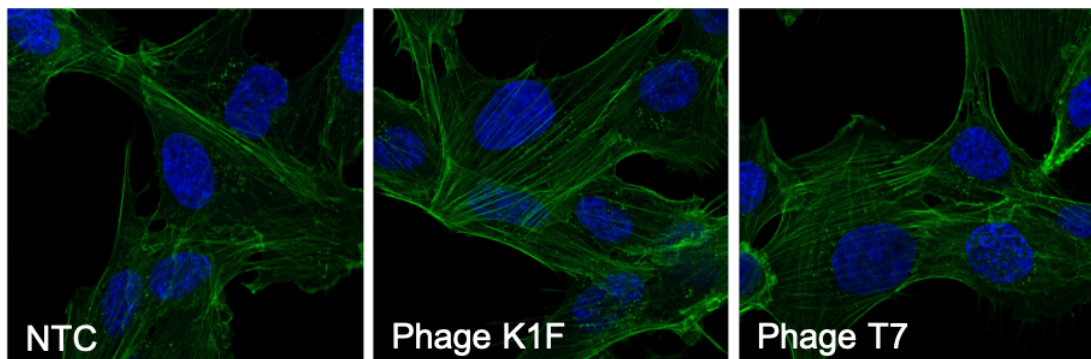


Figure 5-12. Morphology of hCMEC cultures incubated with phages K1F or T7. hCMEC cultures were incubated with phages K1F or T7 at a concentration of 10^9 PFU/ml for 72 hours. The cultures were subsequently fixed and stained with phalloidin and DAPI. Representative images are shown.

5.4 Bacterial lysis releases large amounts of endotoxins during *in vitro* phage therapy

LPS has known immunogenic, pro-inflammatory and pyrogenic effects, which have been extensively demonstrated both *in vitro* and *in vivo* ⁴⁸. In order to better understand the scale of endotoxin influence on the expression on cytokines of hCMECs cultures treated with *E. coli* EV36 and phage K1F in combination, the endotoxin concentration was determined over time using an Limulus Amebocyte Lysate (LAL) assay (Figure 5-13). The LAL assay is a chromogenic assay based on an aqueous extract of blood cells (amebocytes) from the horseshoe crab which is synthetically bound to a yellow colorant, p-nitroaniline. The presence of bacterial lipopolysaccharides induces an enzymatic reaction releasing the yellow colorant into the solution allowing for specific and sensitive detection of endotoxins. During *in vitro* phage therapy where hCMEC cultures were incubated with *E. coli* and phage K1F in combination, a sharp increase in endotoxin concentration was observed from 1 to 2 hours of incubation, followed by plateauing from 4 hours of incubation. This suggests that the bulk of endotoxins are released between the 1 and 2-hour timepoints, with the release being completed before the 4-hour timepoint.

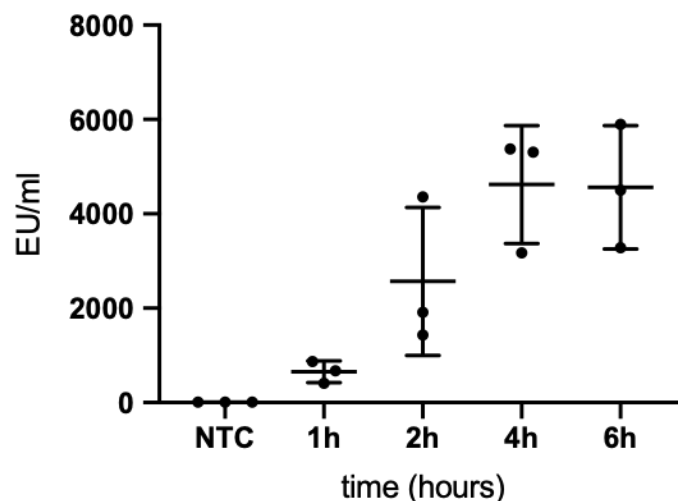


Figure 5-13. Endotoxin levels of hCMEC cultures incubated with *E. coli* EV36 and phage K1F in combination. The hCMEC cultures with incubated 10^7 CFU/ml *E. coli* EV36 and 10^4 PFU/ml phage K1F and endotoxin concentration measured by LAL assay (\pm SD, $n = 3$).

5.5 Endotoxin monitoring in reagents and phage preparations

The concentration of endotoxin was monitored in reagents and phage preparations for the purpose of ensuring that undesirable LPS contamination could be linked to any of the effects observed in the experiments described above.

An extensive phage purification protocol was applied to generate experimental stocks and this proved pivotal in reducing the endotoxin concentration of phage preparations. The endotoxin concentration of purified phage stock was reduced by 92.5% in comparison with crude phage K1F lysate as determined using an LAL assay (Table 5-1). The high titre of the phage stocks allowed for further reduction of endotoxin introduction into experiments by dilution to a suitable experimental phage concentration. Therefore, in experiments where a phage concentration of 10^7 PFU/ml was used, the endotoxin concentration was as low as 0.0060 - 0.086 EU/ml. This is well below the threshold of 0.1 ug/ml LPS (5-10 EU/ml) required to stimulate cytokine signalling in endothelial cell cultures¹⁸¹.

Preparation	Phage lysate (EU/ml)	Phage stock (EU/ml)	10^7 PFU/ml (EU/ml)	10^9 PFU/ml (EU/ml)
Phage K1F-GFP	-	846	0.086	-
Phage K1F	28036	303	0.0060	0.60
Phage T7	-	523	0.013	1.3

Table 5-1. Endotoxin concentration of example phage preparations. The endotoxin concentrations presented for phage dilutions are calculated from the concentrations of undiluted phage stock.

The endotoxin concentration in reagents and media used routinely in this study remained extremely low and quite close to the assay detection limit of 0.04 EU/ml (Table 5-2).

Reagent	EU/ml
EndoGRO medium	0.15
Leibovitz	0.12
DEPC water	0.14
SM-buffer	< 0.04
LB	0.19

Table 5-2. Endotoxin concentration of media and reagents. Detection limit for LAL Assay used was 0.04 EU/ml.

5.6 Discussion

Real-time qPCR analysis demonstrated that *E. coli* EV36 induces a substantial upregulation of inflammatory cytokines, in particular TNF α , IL-6, and IL-8 and to some degree IFN β . This observation correlates with previously published patterns of bacterial infection of the human endothelium¹⁸². *E. coli* EV36-induced IL-6 and IL-8 expression was observed already after 1 hour incubation, while a slower onset was observed for TNF α expression, detected after 2 hours incubation.

In sharp contrast, the real-time qPCR analysis demonstrated that phage K1F does not induce expression of inflammatory cytokines TNF α , IL-6, IL-8, IL-10, or IFN β in hCMEC cultures. Previous studies have shown phage-induced upregulation of TNF α and IL-6 expression *in vitro* in peripheral blood monocytes (PBMCs)¹⁸³. The inflammatory responses of PBMCs, a collection of immune cells with specific roles in innate and adaptive immunity, is however likely to differ from that of hCMECs as each cell type conforms to the nature of their function and environment. The expression of IFN β has been shown to be induced by the activation of PRRs in the early stages of viral infection^{184 185}. While colocalisation experiments demonstrated that phage K1F was recognised by PRRs, no increase was observed in IFN β expression of hCMEC cultures following incubation with phages.

In the context of *in vitro* phage therapy, the addition of phage K1F to *E. coli* EV36-infected hCMEC cultures resulted in a reduction of TNF α expression of approximately 50% compared to *E. coli* EV36 infection alone. As demonstrated previously (Figure 3-3) bacterial lysis occurs within 2 hours of phage addition. The reduction observed in TNF α expression is therefore likely to be directly related to the reduction in live bacteria as a result of phage intervention. This correlates well with the function of TNF α as a central pro-inflammatory cytokine in bacterial infection¹²³. Conversely, a steep increase was observed following *in vitro* phage therapy in the expression of IL-6 and IL-8, increasing expression levels by more than 200% and 150% respectively compared to bacteria alone. The outcome of phage intervention is bacterial lysis leading to a high concentration of bacterial debris and LPS, as illustrated by the determination of endotoxin concentration over time. The observed increase in cytokine expression correlates well with studies showing LPS induction of IL-6 and IL-8 expression in lymphatic microvascular endothelial cells (LECs)¹⁸⁶. Collectively, this suggests that, in the context of phage therapy, the inflammation measured as the expression of IL-6 and IL-8 of hCMEC cultures is primarily induced by the influx of bacterial endotoxins released by bacterial lysis, whereas the inflammation measured as the expression of TNF α is mainly related to the bacterial infection itself.

xCELLigence experiments showed that *E. coli* EV36 infection of hCMEC cultures results in a rapid and complete reduction in Cell Index, indicative of complete disruption of barrier integrity. The observed reduction is in line with previous *in vivo*¹⁸⁷ and *in vitro*¹⁸⁸ studies of endothelial barrier integrity during infection. The frequency of 10 kHz used in these experiments principally favours the measurement of cellular focal adhesion¹⁶⁸. Changes in impedance of a confluent endothelial cell layer is a direct reflection of changes to the barrier integrity and therefore illustrates an increase or reduction of the permeability of the cell layer¹⁸⁹. However, in this case of complete reduction in impedance, the cause is likely rounding of the hCMECs followed by complete detachment from the electrode array.

The increase observed in the Cell Index of untreated control cultures during the first 24 hours is related to cell proliferation. As the confluent layer is formed, space for

further proliferation is hindered and the Cell Index reaches a plateau. Thereafter a decrease is observed starting at approximately 55-65 hours and beyond, relating to the gradual depletion of nutrients which affects the overall health and therefore also adhesion and function. The proliferation experiment showed unhindered growth of untreated controls, however this experiment is not directly comparable with xCELLigence, as it was performed in 6-well plates, whereas xCELLigence is performed in a 16-well plate with 96-well format.

hCMEC cultures incubated with phage K1F at concentrations of 10^7 PFU/ml and above showed a reduction in impedance over a considerable length of time. Similar temporal profiles were observed in hCMEC cultures incubated with phage T7. Control experiments assessing the influence of phages demonstrated that these observations were unrelated to hCMEC proliferation and morphology or presence of endotoxins. The cellular change indicated by a decrease in Cell Index is a decrease in focal adhesion to the extracellular matrix, suggesting that the endothelial barrier integrity is decreased and thus the endothelium is becoming more permeable in the presence of high concentrations of phages. Circulating free phages are rapidly degraded once the host bacteria have been cleared in *in vivo*^{77, 190} and *in vitro*³⁷ studies of phage intervention, which suggests that the recovery of hCMEC impedance observed here following prolonged incubation could be directly linked to a reduction in phage concentration. While no phage-only control experiments were performed in absence of human cells, it is highly unlikely that phages would have any influence on measurements performed with the xCELLigence system as it relies on changes in impedance at the electrode/solution interface.

Interestingly, phage intervention in bacterial-infected hCMEC cultures only conferred a short-lived recovery of barrier integrity. By correlating this observation with the phage-induced lysis of bacteria in the first 2 hours of incubation and the substantial increase observed in endotoxin concentration during therapy within this period of time, it suggests that while phage intervention may alleviate the bacterial infection itself, the resulting bacterial debris ultimately leaves the hCMEC culture to perish.

Chapter 6 Phage engineering

Two of the prevailing and widely discussed challenges of clinical phage therapy is the high host specificity of individual phage strains and the release of bacterial endotoxins induced by lytic phages. The experiments in this chapter were designed to address these two challenges.

Alteration of host tropism of phage T7 by replacing part of its tail fibres with that of phage K1F creates a new receptor binding protein (RBP) allowing infection on K1-capsule expressing bacterial hosts. These experiments were intended to advance our understanding of the possibilities of modulating phage tropism.

Engineering a replication-deficient derivative of phage K1F by deletion of its RNAP gene allows for dose-controlled administration and a controlled release of bacterial endotoxins. These experiments were intended to provide a proof-of-principle and address the potential obstacles experienced by novel phage engineering.

6.1 Chimeric phage T7/K1F is present following homologous recombination

Engineering of phage T7/K1F was based on homologous recombination (HR) using *E. coli* MG1655 expressing a donor plasmid containing the chimeric sequence of phages T7 and K1F (Figure 2-9). HR was performed over two consecutive rounds using *E. coli* MG1655 expressing pT7_K1F_chimera as host and wild-type (wt) phage T7 in the first round and the HR product from the first round in the second round. Successful HR would result in the insertion of a fusion *gene17* in the place of wt *gene17* of phage T7, enabling the chimeric phage T7/K1F to infect *E. coli* strains expressing the K1 capsule. The individual contributions of phages T7 and K1F to the fusion *gene17* are illustrated in Figure 6-1. The efficiency of HR is variable, and before any purification steps was performed it was assumed that the final HR product (henceforth referred to as the HR_chimera product) contained a mix of wt phage T7 and recombinant phage T7/K1F.

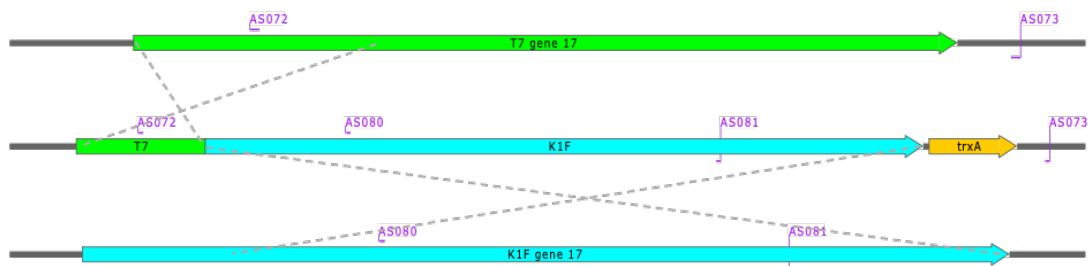


Figure 6-1. Schematic showing the recombination event between T7 gene17 (green, above) and K1F gene17 (blue, below) and the resulting fusion gene (middle). The fusion gene is incorporated into pT7_K1F_chimera. The position of primers used in PCR and GATC screening are annotated in purple with feet above the gene indicating a forward primer and feet below a reverse primer. Homology arms are indicated with dotted lines.

Phage DNA isolation was performed on the HR_chimera product. This was followed by PCRs to determine if the HR was successful. Four primer pairs were used to enable detection of and distinction between wt and fusion phage genomes (Table 6-1). Phage K1F was used as a control for *gene17* of phage K1F alongside phage T7, a No Template Control (NTC) without any sample and a No Amplification Control (NAC) without any DNA polymerase.

The initial PCRs (Figure 6-2) used primer pairs AS080/AS081 or AS072/AS073, complementary to sequences within the *gene17* of phage K1F and immediately outside the plasmid homology regions of phage T7 respectively. PCR with AS080/AS081 showed the presence of *gene17* of phage K1F in the HR_chimera product as illustrated by a band at 1440 bp correlating with wt phage K1F control (Figure 6-2A). This product is present in both pT7_K1F_chimera and recombinant phage T7/K1F. PCR with AS072/AS073 showed the presence of wt phage T7 in the form of a band at 1553 bp correlating with wt phage T7 control (Figure 6-2B). Although not a quantitative comparison, by the intensity of bands on these two gels it appears, visually, that the T7 sequence is present in greater quantities than the K1F sequence in the HR_chimera product. However, no band was observed around the 3431 bp mark, which would have otherwise indicated the presence of a T7/K1F fusion product (Figure 6-2A).

Primer pair	Wt phage product size (bp)	Chimeric phage product size (bp)	Primer binding site
AS080/AS081	1440	1440	Positioned on K1F <i>gene17</i>
AS072/AS073	1553	3431	Positioned towards T7 5' end of <i>gene17</i> and downstream of <i>gene17</i>
AS072/AS081	NA	2191	Positioned towards 5' end of T7 <i>gene17</i> and 3' end of K1F <i>gene17</i>
AS080/AS073	NA	2651	Positioned towards 5' end of K1F <i>gene17</i> and downstream of T7 <i>gene17</i>

Table 6-1. Primer pairs used for PCR testing for wt and chimeric phage products, their sizes and complementary binding sites. NA denotes that the product does not exist.

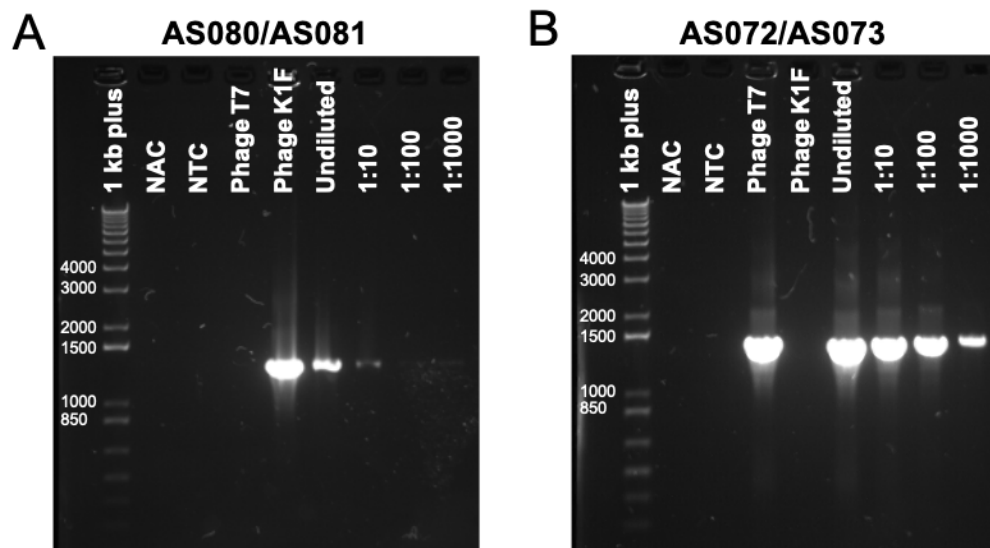


Figure 6-2. PCR testing of the HR_chimera product using primer sets AS080/AS081 (A) and AS072/AS073 (B). NAC, NTC and phage T7 and K1F was included as controls.

Further PCRs were run to assess the presence of a T7/K1F fusion in the HR_chimera product. By using the same primers, but in different combinations, only fusion sequences would be detected. Primer pairs AS072/AS081 and AS080/AS073 are

complementary to one position in phage T7 and one position in the phage K1F insert. The respective gels showed the presence of a band in the undiluted sample at 2191 bp from PCR using AS072/AS081 (Figure 6-3A) and a band at 2651 bp from PCR using AS080/AS073 (Figure 6-3B). This demonstrated that homologous recombination was successful and that a chimeric phage T7-K1F is present in the HR_chimera product. The lack of bands in wt phage controls further supports that only fusion products are detected with these primer pairs. It is noteworthy that the intensity of these bands is much lower than observed with wt phage sequences (Figure 6-2), suggesting that the concentration of chimeric phage is much lower.

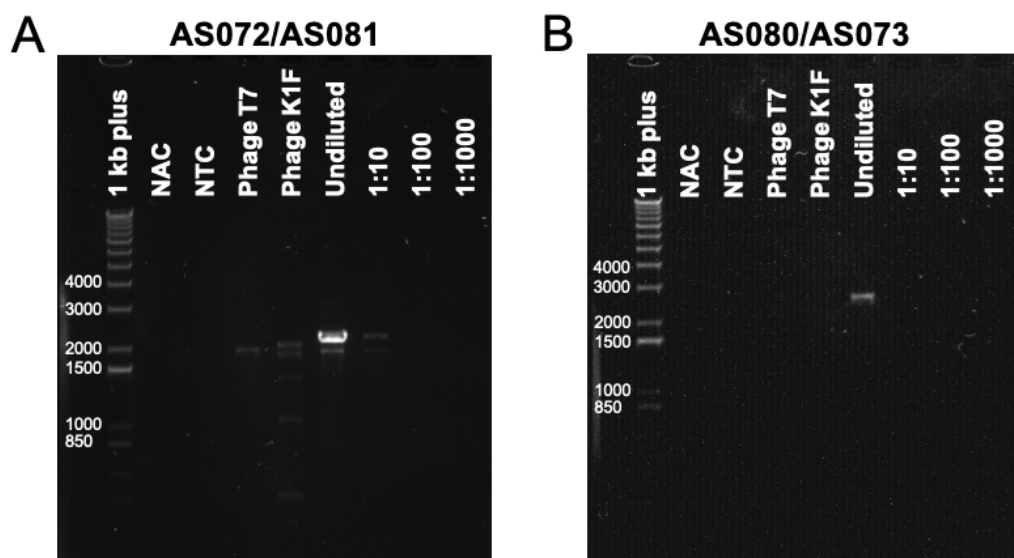


Figure 6-3. PCR testing of the HR_chimera product using primer sets AS072/AS081 (A) and AS080/AS073 (B). NAC, NTC and phage T7 and K1F was included as controls.

6.2 Chimeric phage T7/K1F display reduced viability

The selection efforts of recombinant T7/K1F were initially based on the inability of phage T7 to infect EV36 (Strategy A, Figure 2-9). Therefore, the HR_chimera product was incubated on solid agar with *E. coli* EV36 and candidate plaques were picked. 40 candidate plaques were picked and used to infect liquid cultures of *E. coli* EV36. Nine cultures cleared and were DNA purified and sent for GATC sequencing with primer AS073. Three samples returned a sequence corresponding to the chimeric phage T7/K1F with a length of approximately 600-900 bp. Further confirmation of correct

insertion of the full fusion gene in these was subsequently obtained by GATC sequencing using primers AS072, AS080 and AS081.

Consecutive infection rounds were performed to amplify the chimeric phage population by plating the three recombinant phage samples on individual *E. coli* EV36 lawns and transferring the resulting plaques to new plates the following day, while in parallel, testing the infection of phage samples in liquid *E. coli* EV36 cultures. None of the three confirmed recombinant phage samples could clear liquid cultures of *E. coli* EV36 again, and it was observed that the phage samples lost the ability to form plaques on *E. coli* EV36 lawns after 1-3 rounds of infection. This suggested that the recombinant phages were not stable. Interestingly, PCR testing of plaques following the 1st or 2nd rounds of infection using primers AS072/AS073 revealed the presence of wt phage T7. Plaque assays were therefore performed to determine if phage T7 could potentially piggyback on an infection by chimeric phage T7/K1F and so passively persist in the culture, or if phage T7 could infect *E. coli* EV36 on its own.

Plaque assays of phage K1F on bacterial hosts *E. coli* EV36 and *E. coli* BW25113, a natural phage T7 host, (Figure 6-4) showed that phage K1F readily infected *E. coli* EV36 but was unable to infect *E. coli* BW25113 even at very high concentrations of approximately 10^9 PFU/ml.

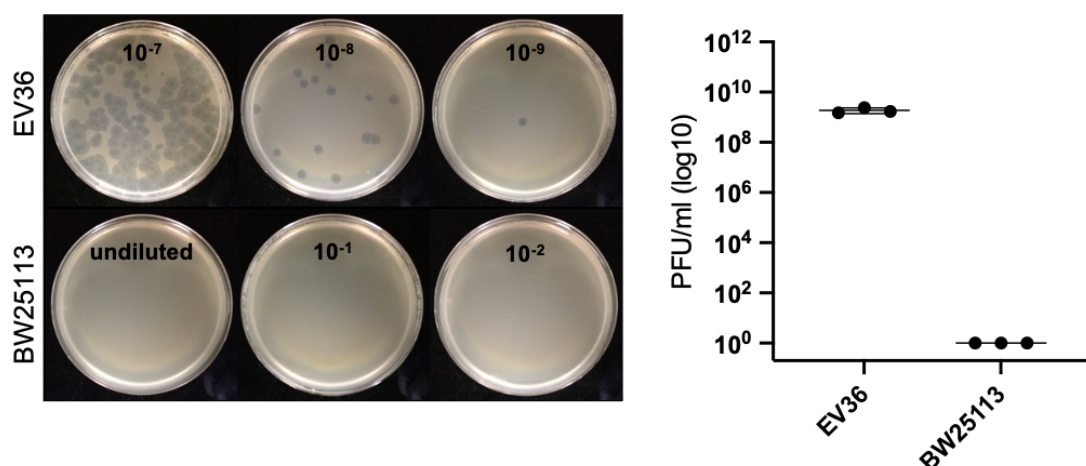


Figure 6-4. Phage K1F infection on multiple bacterial hosts on solid media. A single preparation of phage K1F was diluted in a 10-fold series and plated using double overlay on all hosts simultaneously. Plaque quantification was performed by manual counting ($n = 3$).

Plaque assays of phage T7 on bacterial hosts *E. coli* EV36, *E. coli* BW25113, and *E. coli* BW25113 Δ trxA, (Figure 6-5) showed that phage T7 infection on *E. coli* EV36 and *E. coli* BW25113 achieved similar infectious titres of 3.6×10^9 PFU/ml (SD = 6.6×10^8) and 2.1×10^{10} PFU/ml (SD = 4.0×10^9) respectively. However, the plaque morphology and size varied greatly between the two bacterial strains; on *E. coli* BW25113 phage T7 produced large uniformly circular plaques as expected, whereas on *E. coli* EV36 the plaques were small, diffuse, and irregular in size and circularity. *E. coli* BW25113 Δ trxA, here included as a control, is a derivative of *E. coli* BW25113 which is restrictive to phage T7 replication as it has been engineered to not express the essential host factor thioredoxin (trx). Phage T7 infection on *E. coli* BW25113 Δ trxA did not result in the formation of plaques, however at the highest concentration of phage of approximately 10^{10} PFU/ml (undiluted sample) disruption of the bacterial lawn was observed to become slightly more opaque.

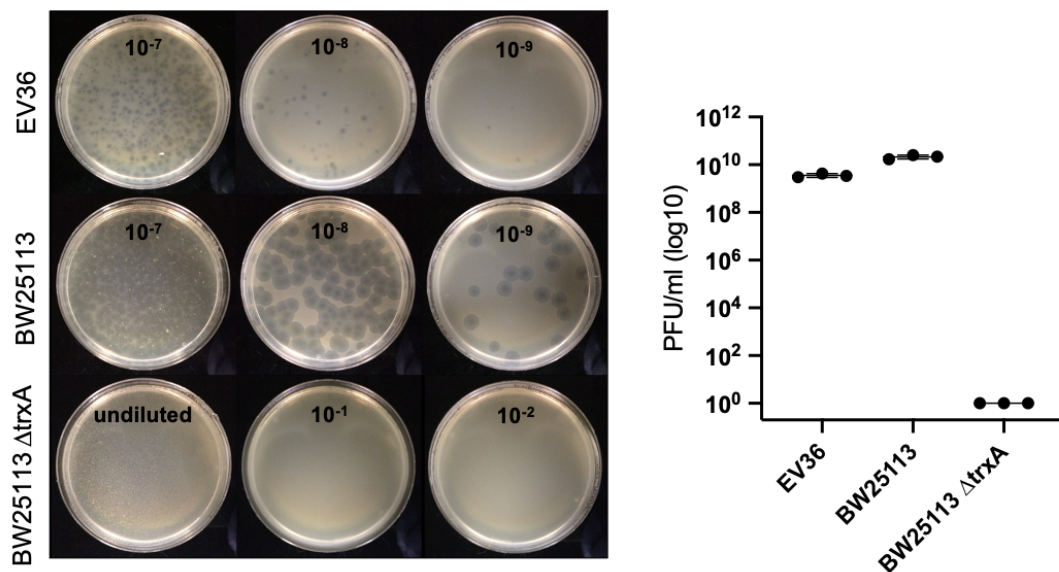


Figure 6-5. Phage T7 infection on multiple bacterial hosts on solid media. A single preparation of phage T7 was diluted in a 10-fold series and plated using double overlay on all hosts simultaneously. Plaque quantification was performed by manual counting ($n = 3$).

6.3 Selection on *E. coli* BW25113 Δ trxA reduces concentration of wildtype phage T7

Infection of *E. coli* EV36 with the HR_ chimera product proved inadequate for the selection of pure recombinant phage (Strategy A, Figure 2-9). Multiple strategies were therefore employed in parallel, using *E. coli* BW25113 Δ trxA as host with and without the support of phage T7 *gene17* transcribed *in trans* (Strategy B and C, Figure 2-9).

The phage titre of the HR_ chimera product on *E. coli* BW25113 was determined to be 6.5×10^8 PFU/ml (SD = 1.0×10^8) by plaque assays (Figure 6-6). This titre decreased to 2.2×10^3 PFU/ml (SD = 1.6×10^2) when plated on *E. coli* BW25113 Δ trxA. It was previously demonstrated that wt phage T7 was unable to replicate on *E. coli* BW25113 Δ trxA (Figure 6-5), suggesting that any replication observed here (formation of plaques) must be attributed to recombinant phage T7/K1F. This was promising for improved isolation of recombinant phage T7/K1F. Differences in plaque morphology and size were observed, with plaques on *E. coli* BW25113 appearing larger and more uniform in size and circularity than plaques observed on *E. coli* BW25113 Δ trxA.

Expression of phage T7 *gene17 in trans* on plasmid pT7_gp17 in host *E. coli* BW25113 Δ trxA yielded an approximately 100-fold increase in phage titre to 2.3×10^5 PFU/ml (SD = 4.6×10^3) in comparison with *E. coli* BW25113 Δ trxA (Figure 6-6). This suggests that supplying this gene product increases phage replication, however, this is more likely associated with wt phage T7 than recombinant phage T7/K1F as *E. coli* BW25113 is a K12 strain.

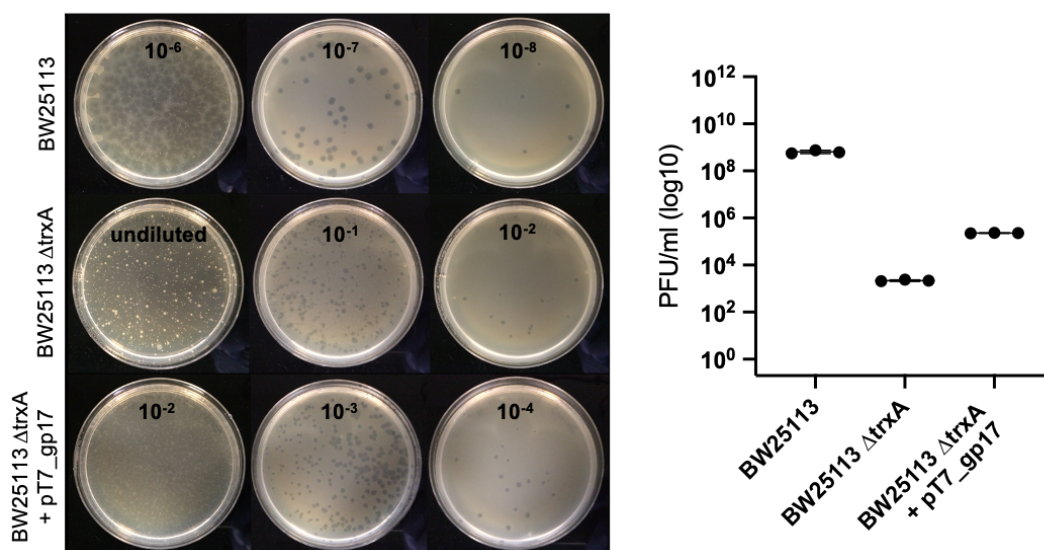


Figure 6-6. Plaque assays of the HR_chimera product on *E. coli* BW25113, *E. coli* BW25113 $\Delta trxA$ and *E. coli* BW25113 $\Delta trxA$ expressing gene17 of phage T7 in trans. The HR_chimera product was diluted in a 10-fold series and plated using double overlay on all hosts simultaneously. Plaque quantification was performed by manual counting ($n = 3$).

The presence and composition of both wt and recombinant phages in plaques were determined by plaque PCRs (Figure 6-7, Figure 6-8, Figure 6-9). 24 plaques were picked in total: 12 plaques on *E. coli* BW25113 $\Delta trxA$ plates and 12 plaques on *E. coli* BW25113 $\Delta trxA$ + pT7_gp17 plates. PCRs using primer pair AS080/AS081 show the presence of phage K1F *gene17* in all plaques (Figure 6-7A + B) as illustrated with bands at 1440 bp, suggesting insertion of the chimeric sequence in some form in wt phage T7.

Interestingly, a divergence was observed in phage composition between the two bacterial hosts using primer pair AS072/AS073. This primer pair produces PCR product of 1553 bp in wt phage T7 and of 3431 bp in recombinant phage T7/K1F. Plaques picked on host *E. coli* BW25113 $\Delta trxA$ (Figure 6-8A) showed a predominant presence of wt phage T7 with bands at 1553 bp, while no samples showed bands at 3431 bp, a couple of samples showed additional bands of variable size suggesting that only part of the chimeric sequence was integrated. In contrast, only 1 of 12 plaques picked on *E. coli* BW25113 $\Delta trxA$ + pT7_gp17 plates showed a clear band correlating with wt phage T7 (Figure 6-8B). The remaining 11 samples showed single or multiple bands of varying size, but none correlating with the size of phage T7/K1F.

Finally, PCR was performed with primer pair AS072/AS081 (Figure 6-9) which showed the presence of recombinant phage T7/K1F in all 24 plaques as illustrated by a clear band at 2191 bp. While the band intensity varied and 2 samples had additional bands, this demonstrates that HR was overall successful.

Candidate plaques grown on *E. coli* BW25113 $\Delta trxA$ + pT7_gp17 plates with no phage T7 detected (Plaques 14, 17, 19 and 22 of Figure 6-8B) were selected for further culturing in liquid and on solid media using *E. coli* EV36 as host. Similarly with previous observations, only one of the four recombinant phage candidates was able to clear a liquid bacterial culture and only for one round of infection, while on solid media the formation of plaques ceased after 1-2 rounds of infection. Following the first round of infection on *E. coli* EV36 several plaques were picked and sent for GATC sequencing with primers AS072 or AS073. The returned sequences demonstrated the presence of both chimeric phage T7/K1F and wt phage T7.

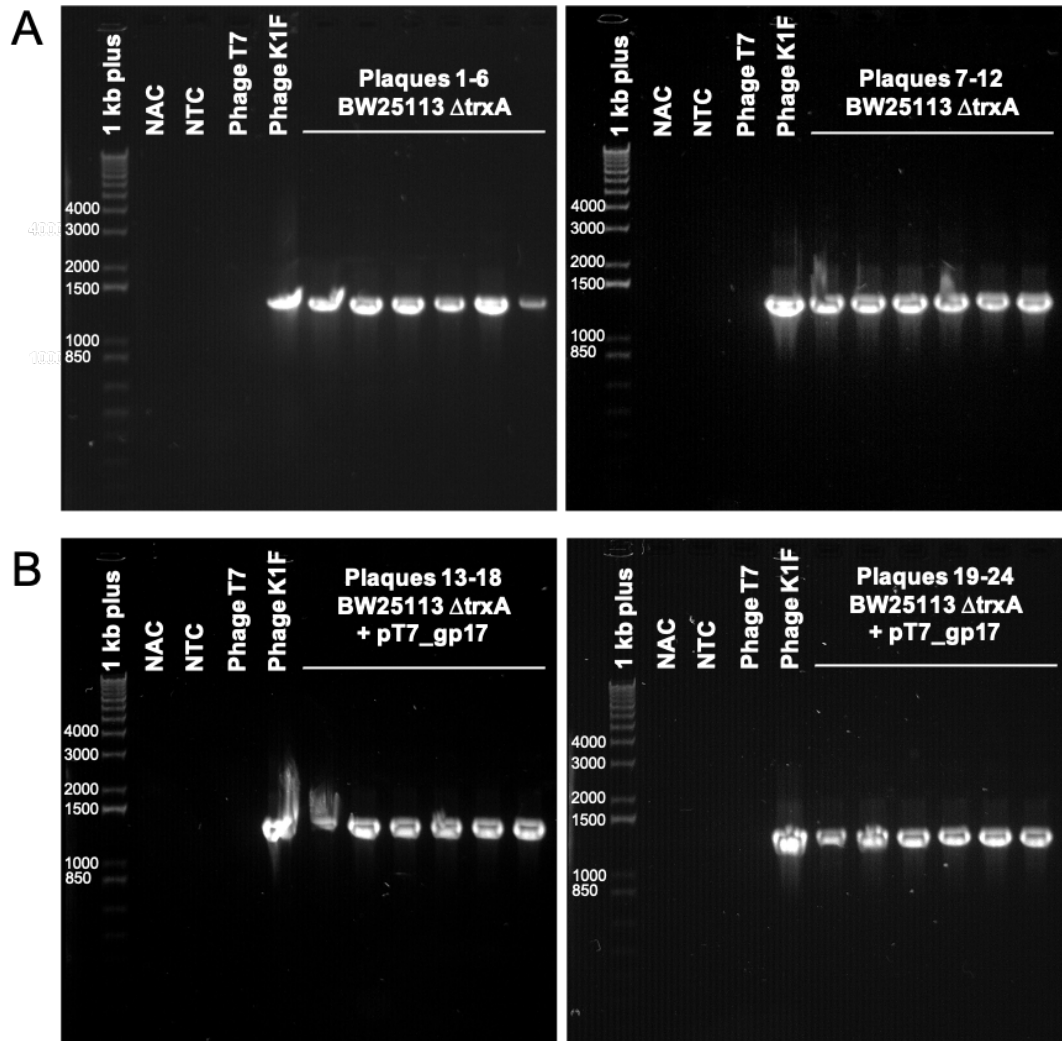


Figure 6-7. Plaque PCR following infection by chimeric HR product using primers AS080/AS081. Plaques were picked from *E. coli* BW25113 Δ trxA (A) and *E. coli* BW25113 + T7_gp17 (B). NAC, NTC and phage T7 and K1F were included as controls.

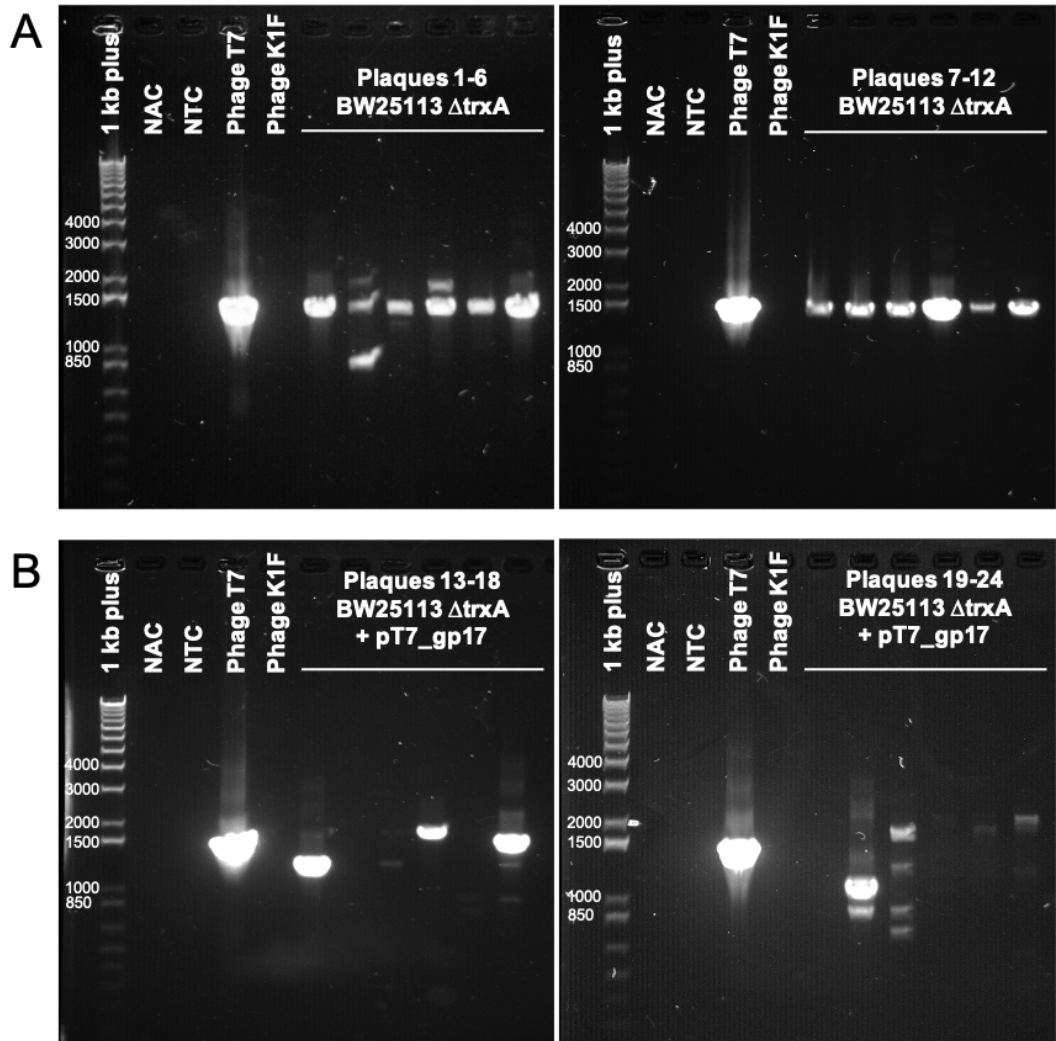


Figure 6-8. Plaque PCR following infection by chimeric HR product using primers AS072/AS073. Plaques were picked from *E. coli* BW25113 Δ trxA (A) and *E. coli* BW25113 + T7_gp17 (B). NAC, NTC and phage T7 and K1F were included as controls.

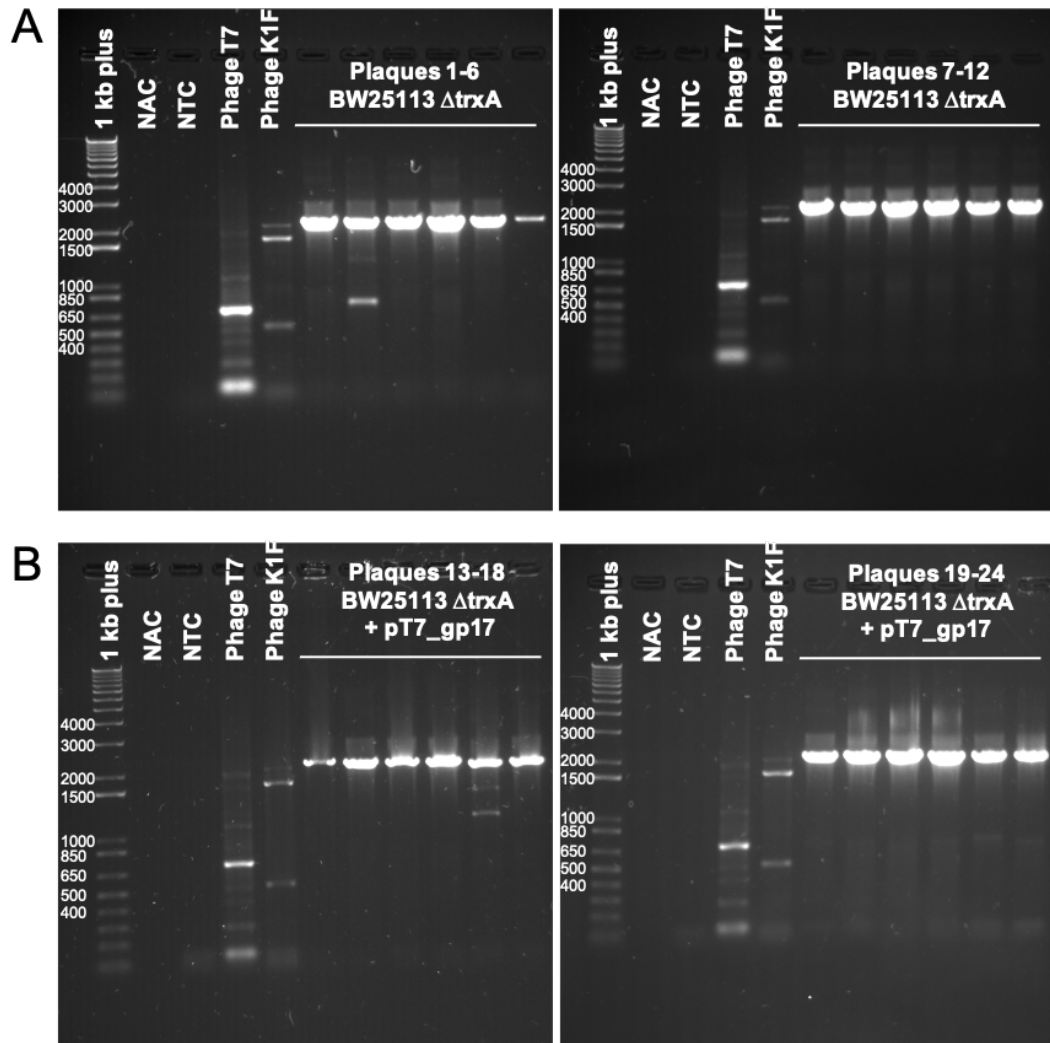


Figure 6-9. Plaque PCR following infection by chimeric HR product using primers AS072/AS081. Plaques were picked from *E. coli* BW25113 Δ trxA (A) and *E. coli* BW25113 + T7_gp17 (B). NAC, NTC and phage T7 and K1F were included as controls.

6.4 Depletion of wildtype phage T7 in the HR_chimera product by CRISPR/Cas9

A final endeavour to isolate a pure preparation of chimeric phage T7/K1F was performed using CRISPR/Cas9 (Strategy D, Figure 2-9). Two single guide RNAs (sgRNAs) were designed to specifically complement *gene17* of wt phage T7, targeting sequences that would be deleted from the desired chimeric phage. The sgRNAs were ligated into pCas9 vectors and subsequently electroporated into *E. coli* EV36 individually. Several candidate colonies were sent for GATC sequencing to confirm the correct sequence. The ability of each sgRNA to facilitate cleavage of *gene17* of wt phage T7 was validated by plaque assays (Figure 6-10). Both sgRNAs were able to

mediate specific Cas9 cleavage of wt phage T7 as demonstrated by the reduction of phage titre: *E. coli* EV36 expressed plasmids sgRNA1_6 and sgRNA2_5 achieved approximately 2- and 5-log₁₀ reductions in comparison with the control respectively (Figure 6-10D). Interestingly, in contrast to plaques formed on *E. coli* EV36 (Figure 6-10A) the plaques formed on *E. coli* EV36 + sgRNA1_6 (Figure 6-10B) appeared more angular with a substantially larger cleared area as well as larger halo. The plaques formed on *E. coli* EV36 + sgRNA2_5 (Figure 6-10C) appeared more similar in size to the plaques formed on *E. coli* EV36, however these presented no apparent halos.

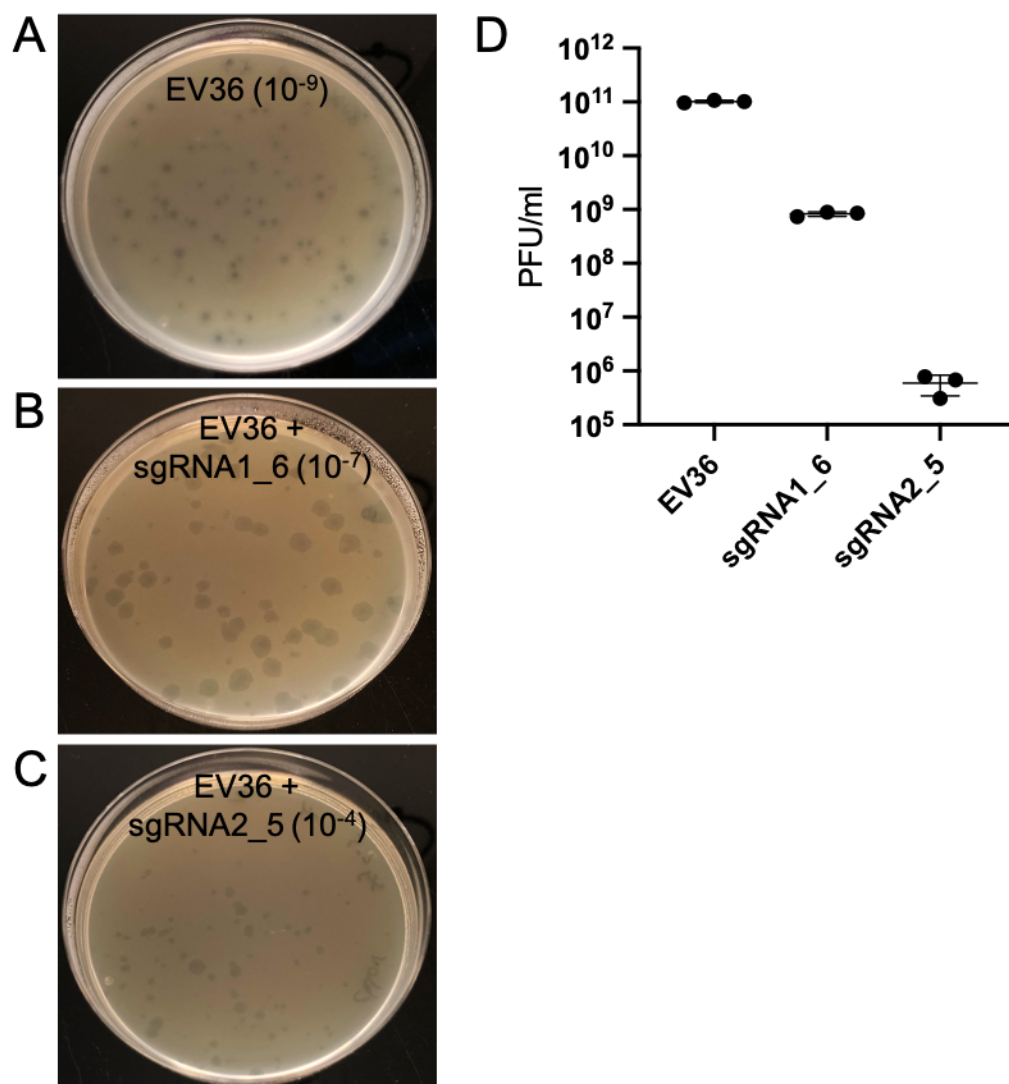


Figure 6-10. Validation of sgRNAs complementing gene17 of wt phage T7. Plaque assays showing wt phage T7 infection on *E. coli* EV36 as control (A), *E. coli* EV36 expressing plasmid sgRNA1_6 (B), and *E. coli* EV36 expressing plasmid sgRNA2_5 (C). Plaque quantification was performed by manual counting ($n = 3$) (D). The phage dilution used is shown in parentheses.

Based on these findings, *E. coli* EV36 expressing plasmid sgRNA2_5 was selected as host for further isolation of chimeric phage T7/K1F. Plaque assays performed with the HR_chimera product showed an approximately one log₁₀ reduction in phage titre (Figure 6-11) on *E. coli* EV36 + sgRNA2_5 as host in comparison with *E. coli* EV36. The reduction in phage titre was considerably lower than observed for wt T7 (Figure 6-10) suggesting a high concentration of recombinant phage in the HR_chimera product mix. Plaques on each bacterial host showed similar morphological characteristics to previous experiments.

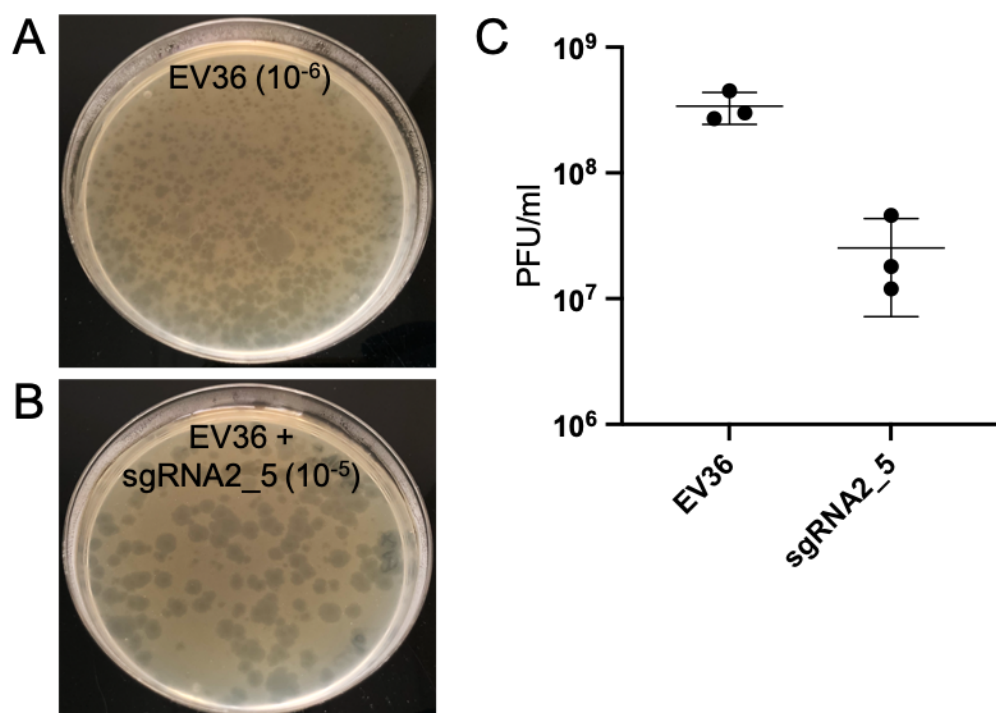


Figure 6-11. Isolation of chimeric phage T7/K1F using CRISPR/Cas9. Plaque assays showing infection of chimeric HR product on *E. coli* EV36 as control (A) and *E. coli* EV36 expressing plasmid sgRNA2_5 (B). Plaque quantification was performed by manual counting ($n = 3$) (C).

12 plaques, 6 large and 6 small, were picked from *E. coli* EV36 + sgRNA2_5 plates and plaque PCRs were performed to determine the composition of phage. Surprisingly, PCR performed using primer set AS080/AS081 (Figure 6-12) showed that phage K1F *gene17* sequence was not present in any of the 12 samples. Furthermore, PCR performed with primer set AS072/AS073 (Figure 6-13) showed that phage T7 *gene17* was present in all 12 samples. The absence of chimeric phage following CRISPR/Cas9

selection was further confirmed by PCR performed with primer set AS072/AS081 which showed no bands in any of the 12 plaques.

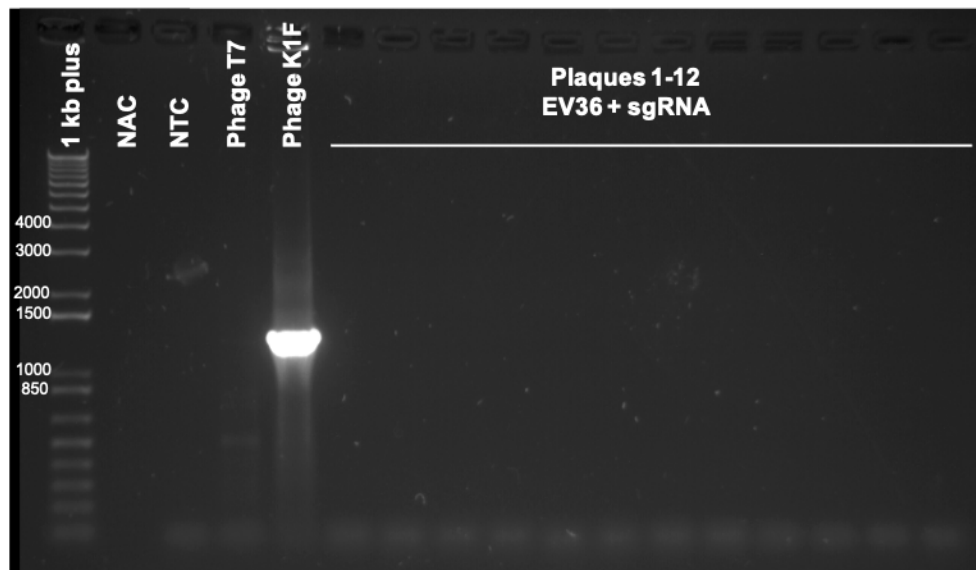


Figure 6-12. PCR testing of plaques on *E. coli* EV36 expressing plasmid *sgRNS2_5* using primers AS080/AS081. Plaques were picked following infection with the HR_chimera product. NAC, NTC and phage T7 and K1F were included as controls.

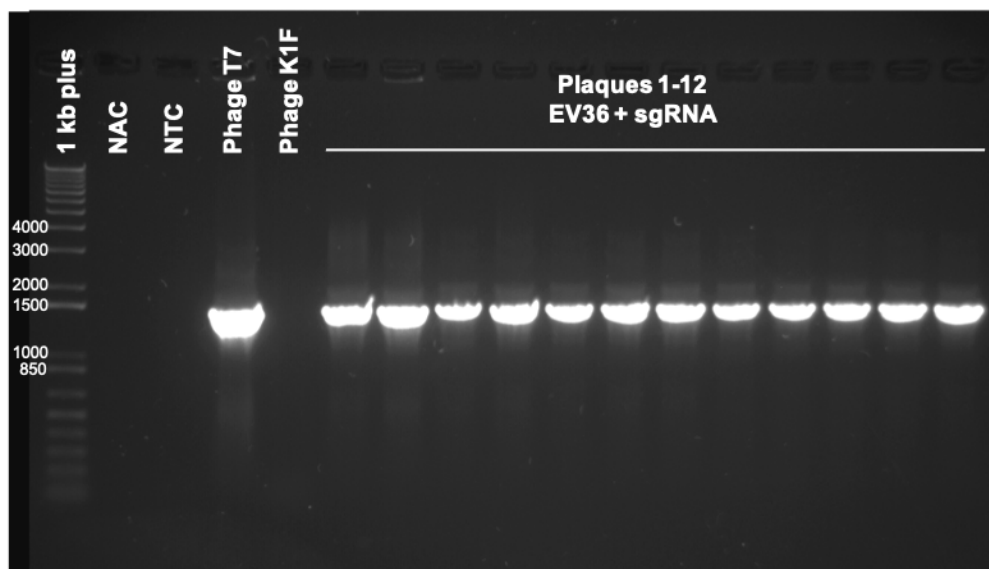


Figure 6-13. PCR testing of plaques on *E. coli* EV36 expressing plasmid *sgRNS2_5* using primers AS072/AS073. Plaques were picked following infection with the HR_chimera product. NAC, NTC and phage T7 and K1F were included as controls.

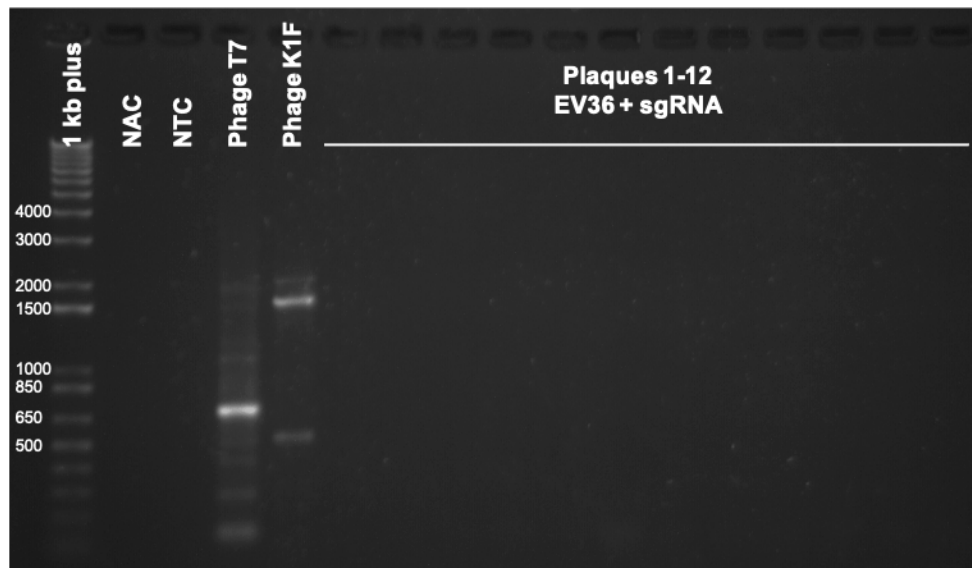


Figure 6-14. PCR testing of plaques on *E. coli* EV36 expressing plasmid sgRNS2_5 using primers AS072/AS081. Plaques were picked following infection with the HR_chimera product. NAC, NTC and phage T7 and K1F were included as controls.

6.5 Engineering of replication-deficient phage K1F

Previous studies have attempted to engineer phage which would enable dose-controlled administration by deletion of endolysin or holin genes. This approach would produce a phage capable of infection and replication but unable to lyse and escape the host bacterium. In either scenario of deleting endolysin or holin genes individually or in combination, phage T7 has been shown to restore fitness by re-evolving known or unknown genes¹⁹¹.

Without the ability of replication, a virulent replication-deficient phage would need other means of killing than bacterial lysis. In this respect, two scenarios were considered: lysis-from-without where the sheer scale of phage adsorption leads to bacterial death¹⁹², or abortive infection where the infected bacterial cell commits suicide¹⁹³.

The engineering strategy to generate a replication-deficient phage K1F was designed to delete the RNA polymerase (RNAP) gene in its entirety by substitution with a β -lactamase gene conferring ampicillin resistance (Figure 6-15). Homology regions positioned immediately up- and downstream of the RNAP gene were used for HR.

Primers were designed to identify the presence or sequence of original and recombinant genome structures using PCR or GATC sequencing respectively (Figure 6-15 and Table 6-2).

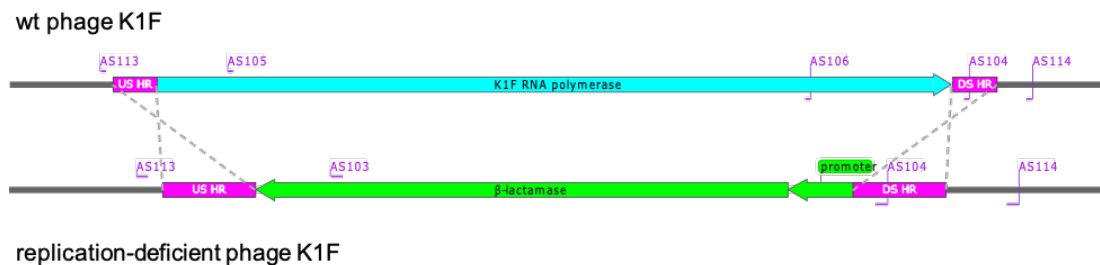


Figure 6-15. Schematic overview of the recombineering event showing wt phage K1F (blue, above) and recombinant replication-deficient phage K1F (green, below) with primer complement sites. US = upstream, DS = downstream, HR = homology region.

Primer pair	Wt phage K1F product size (bp)	RNAP-deficient phage K1F product size (bp)	Primer binding site
AS103/AS104	902	NA	Positioned on β -lactamase gene and DS homology region.
AS105/AS106	1666	NA	Positioned towards the 5' and 3' ends of RNAP of phage K1F.
AS113/AS114	3144	1428	Positioned immediately outwards of US homology region and DS homology region.

Table 6-2. Primer pairs used for PCR testing for wt and RNAP-deficient phage products, their sizes and complementary binding sites. NA denote that DNA product does not exist.

Identification of *E. coli* EV36 colonies containing the pK1F_RNAP_deletion HR donor plasmid was initially based on a cloning selection marker indicating successful ligation into cloning vector pSB1C3 (Figure 6-16A). White colonies were individually

transferred to corresponding grids on solid media with either chloramphenicol alone (Figure 6-16B) or chloramphenicol and ampicillin (Figure 6-16C). Plasmid pK1F_RNAP confers chloramphenicol resistance off vector pSB1C3 and ampicillin resistance off the insert sequence. Colonies that were able to grow on both antibiotics were presumed to contain a full and functioning donor plasmid conferring resistance to both antibiotics. Five such colonies were identified (marked with red circles) and transferred to liquid culture for overnight incubation. GATC sequencing using primers AS113 or AS114 individually subsequently confirmed that all 5 cultures contained the full pK1F_RNAP_deletion plasmid.

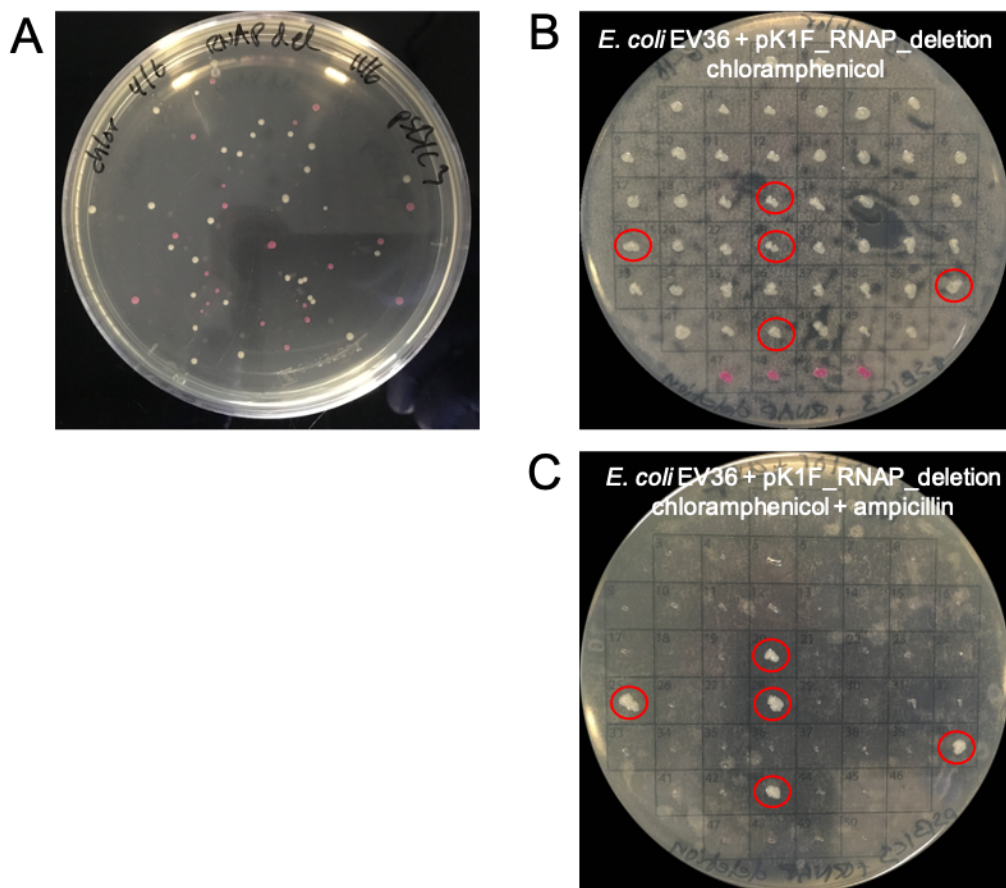


Figure 6-16. Selection of bacterial host for HR of replication-deficient phage K1F. Selection based on (A) cloning selection marker where the red protein gene is deleted by substitution suggesting successful ligation, and on resistance against (B) chloramphenicol suggesting the presence of vector pSB1C3 and (C) chloramphenicol and ampicillin suggesting the presence of vector pSB1C3 and insert sequence. Red circles denotes desired colonies containing vector and insert.

HR was performed over two consecutive rounds of infection on host *E. coli* EV36 + pK1F_RNAP_deletion with wt phage K1F in the first round, and the HR product from

round 1 in the second round (Figure 2-10). Complete clearance was not observed as per usual when infecting *E. coli* EV36 with wt phage K1F with the *E. coli* EV36 + pK1F_RNAP_deletion cultures remaining a little hazy. This suggested a high proportion of recombinant phage was produced as wt phage K1F is shown to readily infect and proliferate on *E. coli* EV36 and would therefore clear the culture completely.

Following phage DNA purification, PCRs were performed to identify the composition of phage in the final HR product (henceforth referred to as the HR_RNAP product) (Figure 6-17). As controls were included: phage K1F (positive control), the original gblock containing the β -lactamase gene and homology regions (positive control), phage T7, a No Template Control (NTC) without any sample and a No Amplification Control (NAC) without any DNA polymerase.

PCR using primer set AS103/AS104 complementary to the β -lactamase gene and the downstream homology region present on both pK1F_RNAP_deletion and the putative recombinant phage, demonstrated the presence of a DNA product of identical in size to the original gblock (Figure 6-17A). The presence of wt phage K1F was demonstrated by PCR using primer set AS105/AS106 complementary to the RNAP gene of phage K1F (Figure 6-17B). Here, bands of similar size were observed in both the HR_RNAP product and wt phage K1F, acting as positive control. Finally, PCR using primer set AS113/AS114 complementary to phage K1F immediately upstream and downstream of the homology regions resulted in multiple product sizes of the HR_RNAP product (Figure 6-17C). The predominant product size from the HR_RNAP product was comparable to that from phage K1F, around 3144 bp, with no visible band corresponding to a putative recombinant phage around 1428 bp. This suggests that recombinant replication-deficient phages were not present. Further purification of phage DNA of the HR_RNAP product and GATC sequencing using primers AS113 or AS114 was inconclusive.

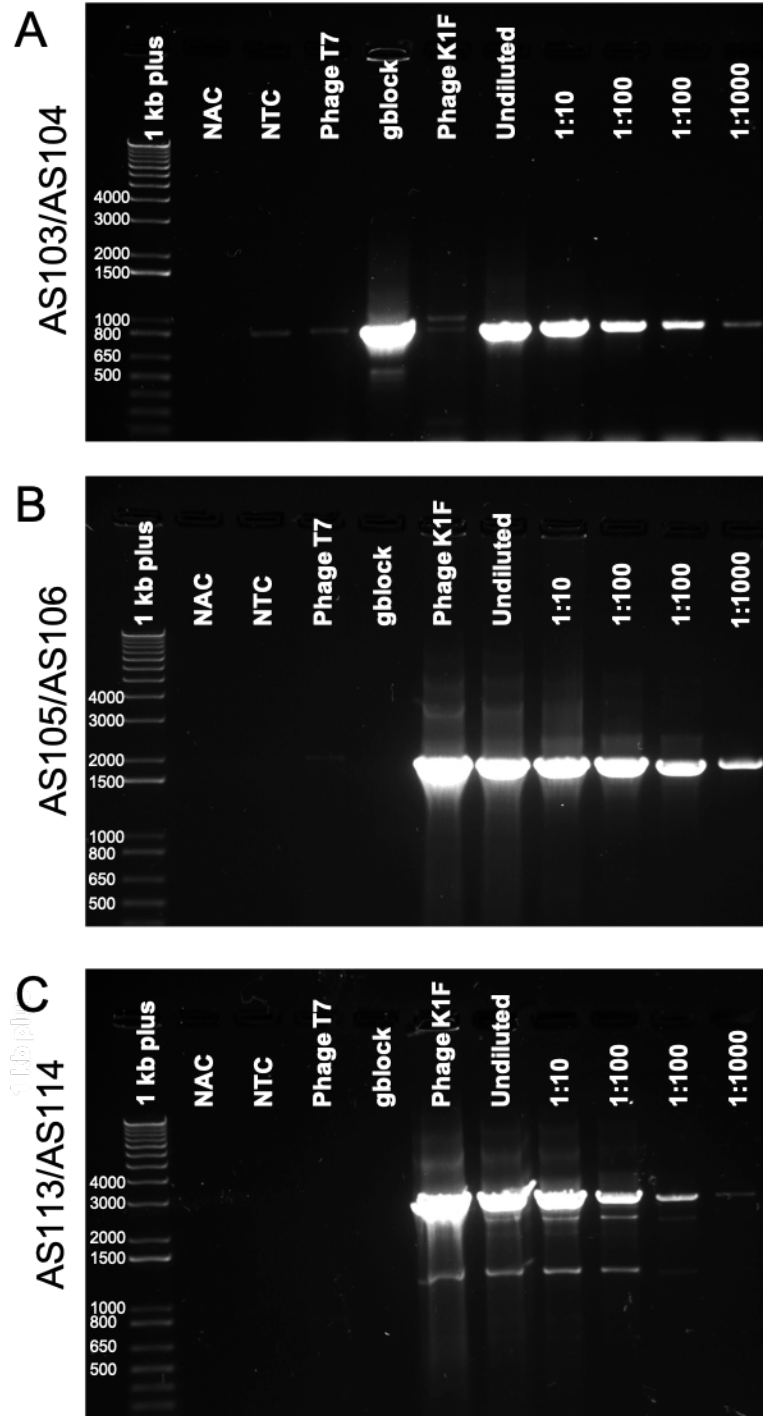


Figure 6-17. PCRs of the HR_RNAP product following infection of *E. coli* EV36 expressing plasmid pK1F_RNAP_deletion by wt phage K1F using primer sets AS103/AS104 (A), AS105/AS106 (B), and AS113/AS114 (C). Controls included: NAC, NTC, phage T7 (negative control), and original gblock containing the β -lactamase gene and homology regions and phage K1F (positive controls).

6.6 *E. coli* EV36 introduces mutations in RNAP expressing plasmid

In order to support a putative proliferation-deficient phage, a bacterial host was designed to express the missing RNAP *in trans*. The pSB3T5 cloning vector with medium copy number for constitutive expression was selected. Ligation of a codon-optimised RNAP gene of phage K1F into the pSB3T5 cloning vector, electroporation, and subsequent isolation of *E. coli* EV36 colonies containing plasmid pK1F_RNAP_optimised for expression of RNAP of phage K1F *in trans* required many attempts. Eventually, 14 colonies were identified based on cloning markers (Figure 6-18A). Colony PCR screening with primer set AS101/AS102 revealed a product of similar size to the positive control of 1894 bp in 7 of the 14 identified colonies (Figure 6-18B-C).

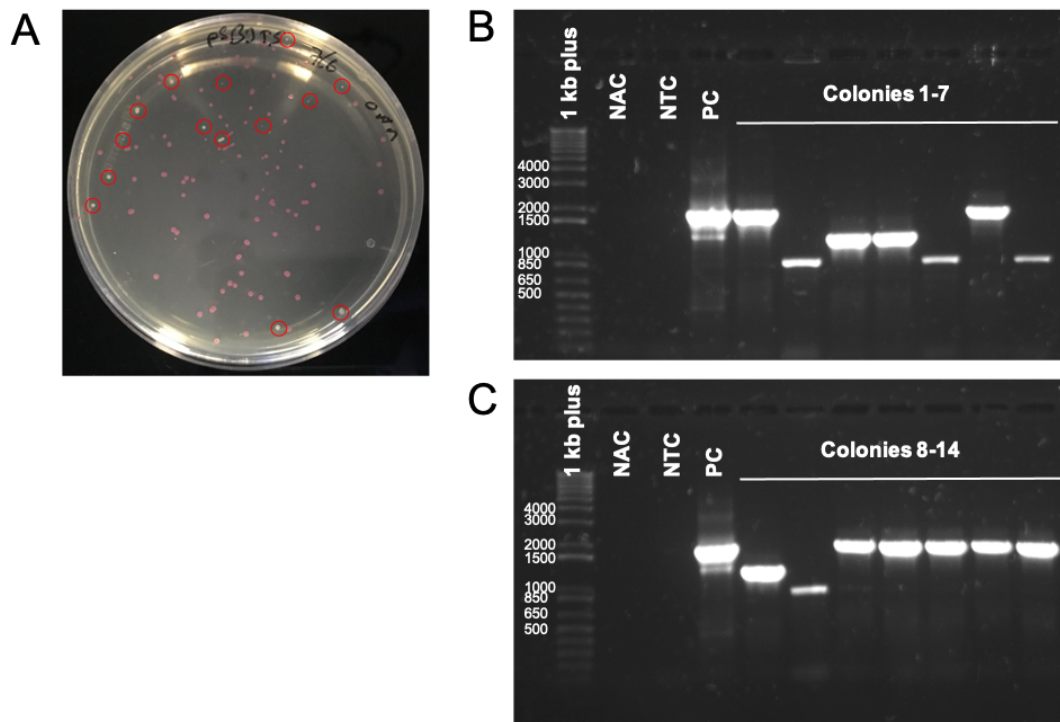


Figure 6-18. Selection of *E. coli* EV36 + pK1F_RNAP_optimised colonies. Selection based on cloning marker where the red protein gene is deleted by substitution during ligation yielding white colonies (A) and PCR based using primer set AS101/AS102 (B-C). NAC, NTC, and original gblock gblock containing the β -lactamase gene and homology regions included as positive control (PC) for each PCR.

The 7 *E. coli* EV36 + pK1F_RNAP_optimised colonies identified by PCR screening were transferred to liquid culture for overnight incubation (Figure 6-19). All 7 cultures

grew, but achieved different levels of turbidity; cultures 1 and 11 were dense, culture 12 was cloudy, while the rest were only a little hazy but evidently contained bacteria. Plasmid miniprep and GATC sequencing later revealed that cultures 1, 11, and 12 all contained multiple different point mutations suggesting that these were introduced during bacterial growth. The plasmid sequence of culture 11 contained only two silent mutations and it was therefore assumed that a functional RNAP protein would be expressed in this culture. Culture 11 was therefore used in subsequent experiments.

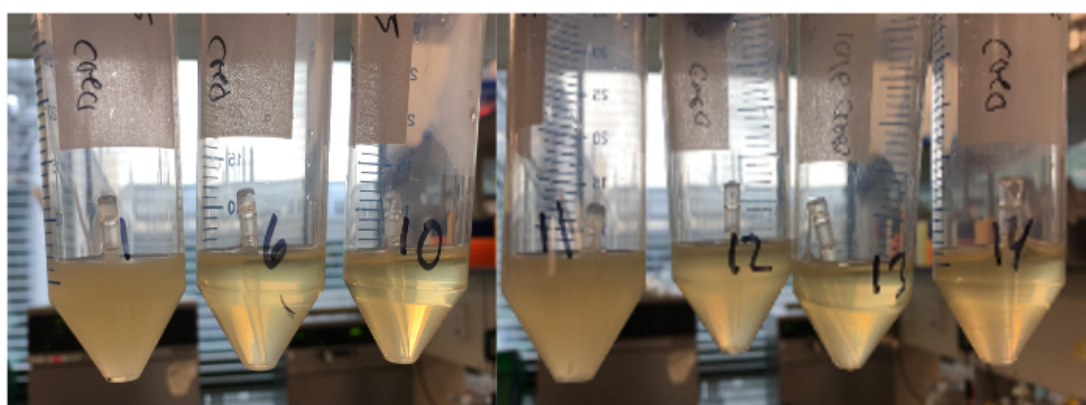


Figure 6-19. Overnight cultures of *E. coli* EV36 expressing plasmid pK1F_RNAP_optimised.

6.7 Isolating replication-deficient phage K1F

The first strategy for isolation of replication-deficient phage K1F (Strategy A, Figure 2-10) was based on phage-derived resistance towards ampicillin. Previously it was demonstrated that plasmid-driven ampicillin resistance was achieved in *E. coli* EV36 expressing pK1F_RNAP_deletion, and during HR the β -lactamase gene and promoter would be integrated into the recombinant phage. Therefore, *E. coli* EV36 + pK1F_RNAP_optimised was infected with the HR_RNAP product and plated on solid media containing ampicillin (Figure 6-20). It was hoped that infection with recombinant phages would confer resistance to ampicillin and that the phages could subsequently be extracted from the bacterial colony. However, this experiment demonstrated that phage-derived resistance did not occur at any concentration as evident by the absence of a single colony on any plate.

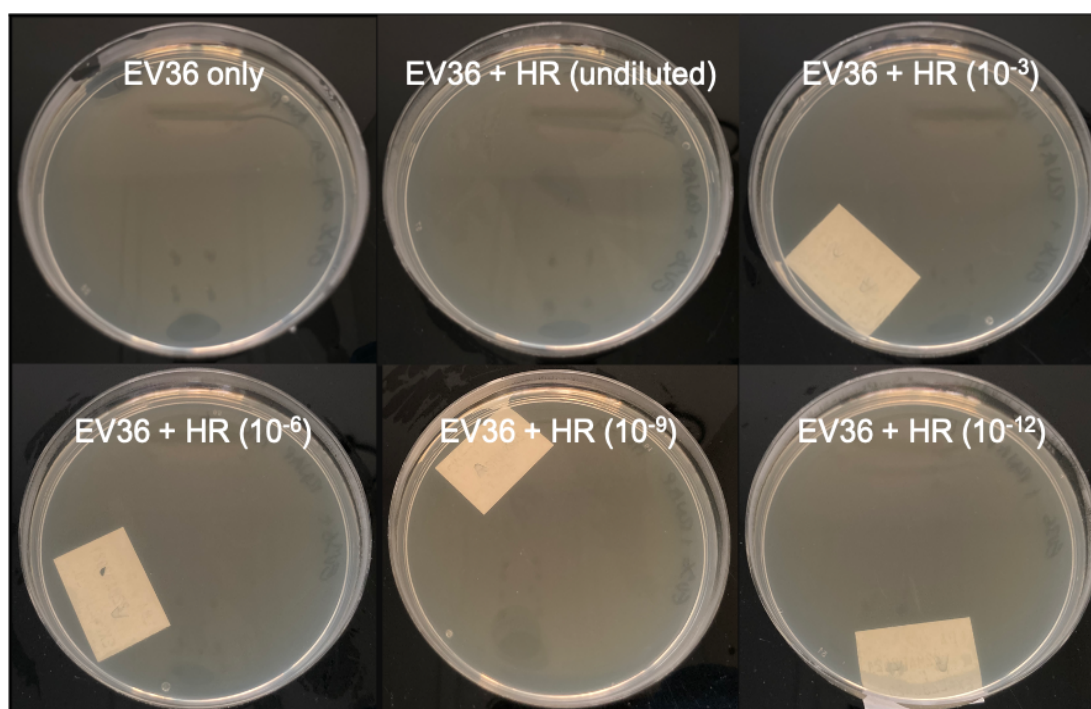


Figure 6-20. *E. coli* EV36 + pK1F_RNAP_optimised infected with the HR_RNAP product and plated over a range of dilutions on solid media containing ampicillin.

The second strategy (Strategy B, Figure 2-10) was based on the recombinant phages relying on expression of RNAP *in trans* in order to replicate and therefore being unable to replicate and form plaques on *E. coli* EV36 alone.

A plaque assay was performed using the HR_RNAP product to infect *E. coli* EV36 + pK1F_RNAP_deletion (Figure 6-21). The observed plaque morphology showed high resemblance to that of wt phage K1F infection of *E. coli* EV36. 150 individual plaques were picked from these plates and each plaque was transferred in parallel onto two grid plates in corresponding grids (Figure 6-22). One grid plate contained a lawn of *E. coli* EV36 and the other a lawn of *E. coli* EV36 + pK1F_RNAP_optimised. All 150 plaques picked were able to replicate and form a plaque on both hosts suggesting that a replication-deficient phage was not present.

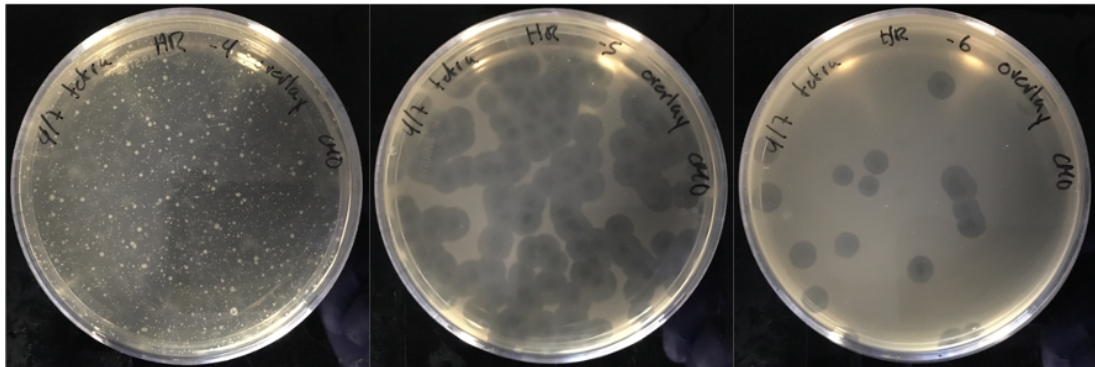


Figure 6-21. *E. coli* EV36 + pK1F_RNAP_deletion infected with the HR product and plated using the double overlay method.

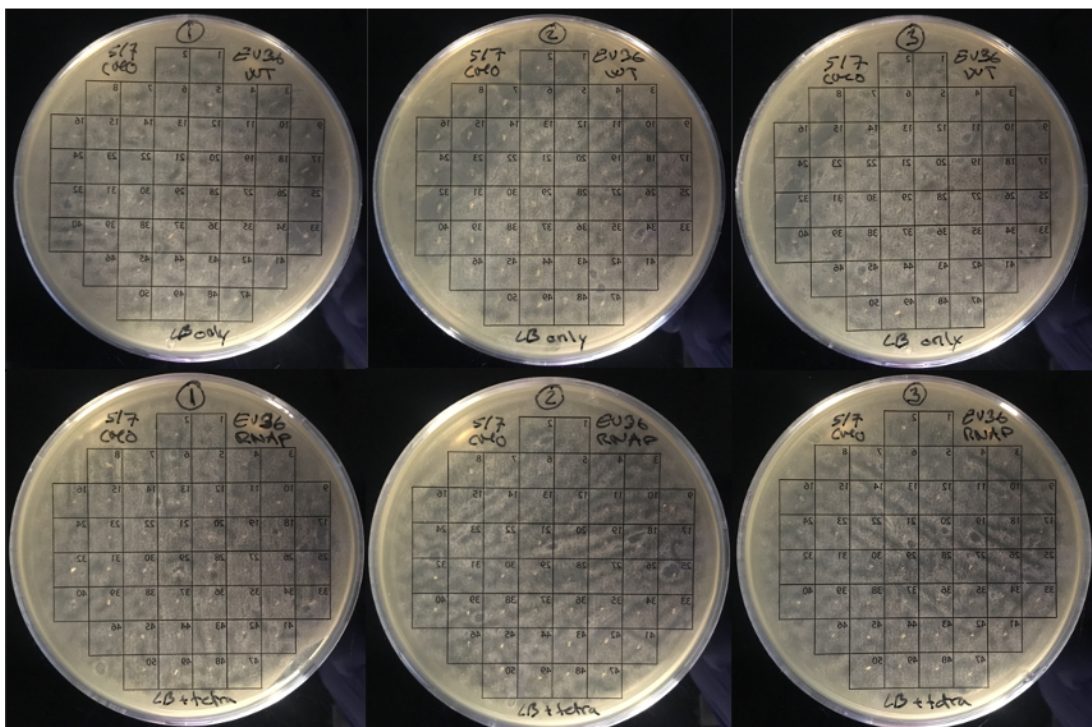


Figure 6-22. Plaques picked on plates with the HR_RNAP infecting *E. coli* EV36 + pK1F_RNAP_deletion and transferred onto a lawn of *E. coli* EV36 (above) and *E. coli* EV36 + pK1F_RNAP_optimised (below) in parallel.

In a final attempt to isolate recombinant phages from the heterogenous HR_RNAP product, two sgRNAs, identified as sgRNA5 and sgRNA6, were designed for Cas9-mediated cleavage of wt RNAP of phage K1F (Strategy C, Figure 2-10). Codon optimisation of the RNAP gene contained on plasmid pK1F_RNAP_optimised used for *in trans* expression ensured that the sequence of each sgRNAs would only complement wt RNAP present in wt phage K1F. The two sgRNAs were ligated into pCas9 vectors individually and subsequently electroporated into *E. coli* EV36 + pK1F_RNAP_optimised. Several colonies were selected and cultured whereafter the

plasmid DNA was purified and sent for GATC sequencing. *E. coli* EV36 + pK1F_RNAP_optimised cultures expressing a Cas9 vector with the correct sequence of each sgRNA were identified. These and *E. coli* EV36 + pK1F_RNAP_optimised without sgRNAs were infected with the HR_RNAP product (Figure 6-23) and plated. Both sgRNA demonstrated the ability to mediate cleavage of RNAP gene of wt phage K1F as evident by the reduction in phage titre. sgRNA5_1 and sgRNA6_1 achieved similar reductions of phage titre of approximately 1 log₁₀ in comparison with *E. coli* EV36 control (Figure 6-23D). While plaques formed on *E. coli* EV36 + pK1F_RNAP_optimised showed similar morphology as in previous experiments (Figure 6-23A), plaques formed on *E. coli* EV36 + pK1F_RNAP_optimised + sgRNA5_1 were large circular plaques with jagged edges (Figure 6-23B). Interestingly, plaques formed on *E. coli* EV36 + pK1F_RNAP_optimised + sgRNA6_1 were either large circular with jagged edges or tiny and diffuse (Figure 6-23C). Though the two sgRNAs mediated a similar reduction in phage titre, it appears that sgRNA6_1 also has an effect on phage morphology. As a phage plaque is formed outwards from a central starting point, the tiny plaques observed on *E. coli* EV36 + pK1F_RNAP_optimised + sgRNA6_1 could suggest that phage proliferation was impeded. Finally, 20 plaques were transferred from *E. coli* EV36 + pK1F_RNAP_optimised + sgRNA5_1 plate alongside 30 plaques from *E. coli* EV36 + pK1F_RNAP_optimised + sgRNA6_1 to a grid plate containing a lawn of *E. coli* EV36. As observed before, all plaques were able to form large circular plaques suggesting that these plaques did not contain replication-deficient phage K1F.

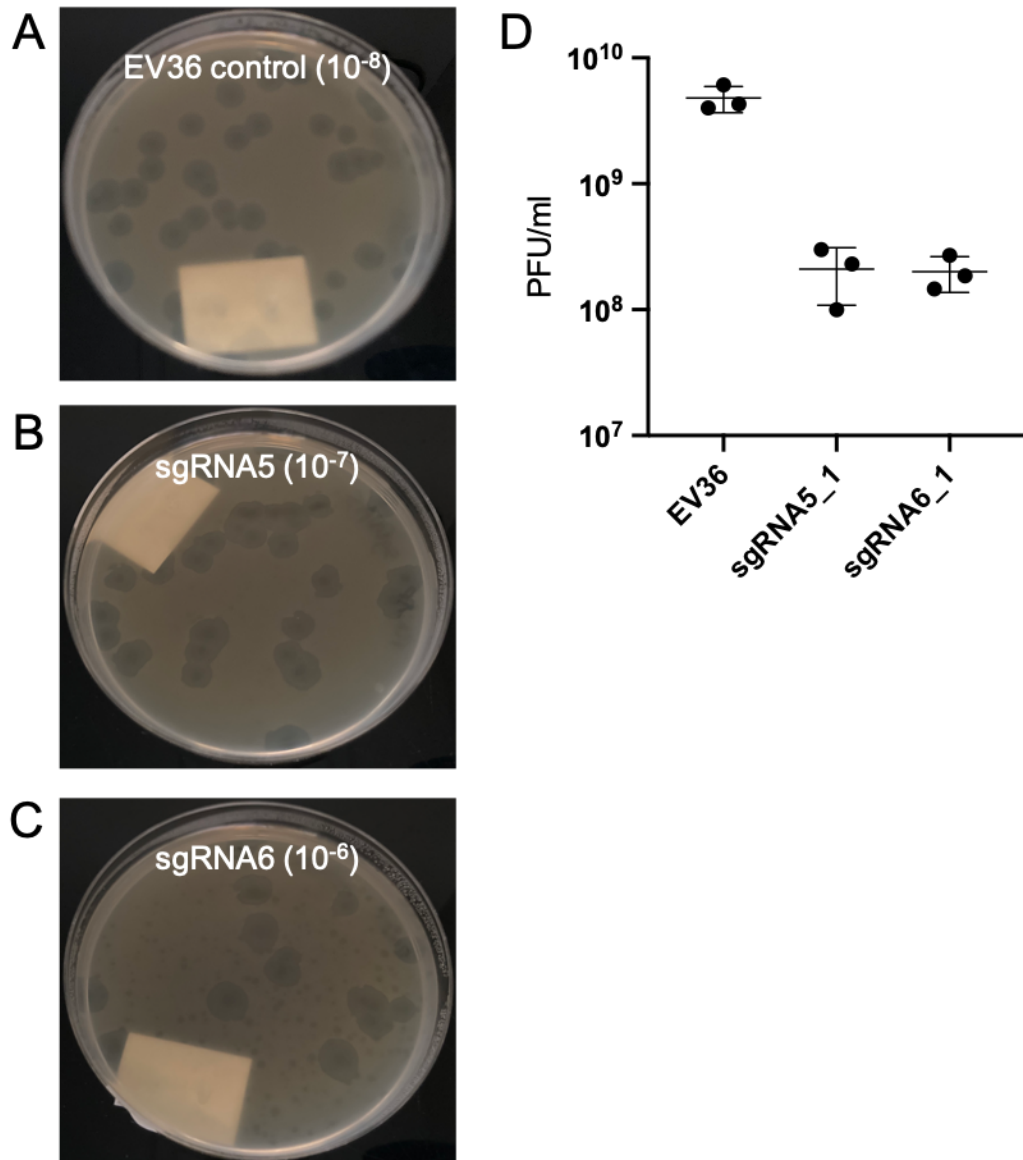


Figure 6-23. CRISPR/Cas9 selection of replication-deficient phage K1F. Plaque assays showing infection of the HR_RNAP product on *E. coli* EV36 + pK1F_RNAP_optimised as control (A), *E. coli* EV36 + pK1F_RNAP_optimised + sgRNA5_1 (B), and *E. coli* EV36 + pK1F_RNAP_optimised + sgRNA6_1 (C). Plaque quantification was performed by manual counting ($n = 3$) (D).

6.8 Discussion

The efforts to produce a chimeric T7/K1F phage culminated with PCR and GATC sequencing confirming the presence of recombinant phage T7/K1F following HR, albeit PCR band intensity suggested that the abundance of recombinant phages was lower than wt phages. This however demonstrated successful genomic modification of the RBP of phage T7. The genomic modification was achieved by substitution of the native RBP of phage T7 with that of phage K1F thus allowing the chimeric phage

T7/K1F to infect K1-capsule expressing bacterial strains. The ability of chimeric phage T7/K1F to infect and proliferate was demonstrated by its ability to clear liquid *E. coli* EV36 cultures, which, in contrast, phage T7 is not capable of doing.

Despite the clear evidence of successful phage engineering, issues arose in regards to obtaining a pure preparation of viable chimeric phage T7/K1F. The observation that chimeric phage preparations lost the ability both to clear liquid cultures and to form plaques on solid media after only one to three rounds of infection was initially considered to be a purification issue, the rationale being that in a heterogenous mix of wt and recombinant phages, the superior fitness of wt phages would suppress recombinant phages. This notion was substantiated by the revelation that phage T7 was able to efficiently infect *E. coli* EV36 with only one log reduction in plaque formation on solid media as compared with a fully permissive host. This observation concurrently invalidated Strategy A.

Strategy B and C exploited the *E. coli* BW25113 $\Delta trxA$ strain lacking host factor thioredoxin (*trx*) which renders it non-permissive to replication by many phage T7 strains¹⁹⁴. This enabled positive selection of phage T7/K1F by inclusion of the *trx* gene in the HR incorporated recombinant sequence. Strategy C furthermore involved the expression of *gene17* of phage T7 *in trans*. Plaque assays demonstrated that phages T7 and K1F were unable to form plaques on *E. coli* BW25113 and *E. coli* BW25113 $\Delta trxA$ respectively. It was therefore conceivable that any plaques formed following infection of the HR product on *E. coli* BW25113 $\Delta trxA$ would consist of phage T7/K1F. PCR testing confirmed the presence of phage T7/K1F recombinant sequence in all analysed plaques. Interestingly, while phage T7 was present in all analysed plaques grown on *E. coli* BW25113 $\Delta trxA$ in the absence of expression of phage T7 *gene17*, plaques grown on *E. coli* BW25113 $\Delta trxA$ with expression of T7 *gene17* did contain stretches of DNA associated with wt phage T7. This could suggest that in the presence of *gene17* of phage T7 the ratio of wt and recombinant phage in the HR product is maintained, whereas in the absence of *gene17* of phage T7 the wt phage is favoured and the recombinant phage is ultimately suppressed.

However, despite the apparent efficiency of selection and promising PCR data obtained, the viability of phage T7/K1F did not improve and wt phage T7 still persisted in plaques. At this point it had become clear that the chimeric phage could

not compete successfully with wt phage T7. In a final attempt to increase the ratio of chimeric phage against wt, CRISPR/Cas9 was used to target *gene17* of phage T7 (Strategy D). The designed sgRNAs efficiently reduced the titre of phage T7 by up to 5-log₁₀ in control cultures. Nonetheless, sgRNA-mediated cleavage only resulted in a 1-log reduction of phage titre of HR product, initially presumed to indicate that the concentration of recombinant phages was high. However, plaque PCR confirmed that none of the analysed plaques contained DNA matching the chimeric phage T7/K1F or wt phage K1F. sgRNAs used in these experiments were designed with 20 bases complementary to the target gene in phage T7. However, a complementary sequence of 8 bases was also identified adjacent to a PAM in *gene17* of phage K1F, and while studies has shown that even lowering the complementary target sequence to 17 bases reduces the efficiency of cleavage by 20%¹⁹⁵, it is possible that the sgRNA used also facilitated cleavage of phage T7/K1F. Additionally, Cas9 nucleases have been shown to tolerate mismatch of complementary target sequence resulting in off-target cleavage¹⁹⁶.

The strategy for engineering and producing a stock of a replication-deficient phage K1F, by deleting the RNAP gene essential for its replication, hinged on the ability to supply the RNAP by other means. However, *E. coli* EV36 cultures expressing codon-optimised RNAP off plasmid pK1F_RNAP_optimised showed reduced growth in liquid culture and readily introduced point mutations within the optimised RNAP gene. These mutations were varied and found to be silent, nonsense and amino acid altering mutations. Altogether this indicated that RNAP in this form and concentration was toxic to *E. coli* EV36 and thus potentially affected the outcome of the strategy.

Success of the recombination event to produce a replication-deficient phage K1F was evaluated by means of PCRs. It was demonstrated that DNA products were present following HR that matched the β -lactamase gene and the downstream homology region of a recombinant phage and plasmid pK1F_RNAP_deletion. The HR_RNAP product was centrifuged, sterile filtered and run a through phage DNA purification column (keeping the flow-through, discarding any plasmid) prior to PCRs, and so it is unlikely that remnants of plasmid pK1F_RNAP_deletion would remain in the sample.

An overwhelming presence of phage K1F in the HR_RNAP product was demonstrated by efforts to isolate recombinant phages. Hundreds of phage plaques picked from plating on *E. coli* EV36 + pK1F_RNAP_optimised as host following infection with the HR_RNAP product all demonstrated the ability to replicate and form plaques on *E. coli* EV36 with and without expression of RNAP *in trans*. The final push to isolate recombinant phages using sgRNAs complementary to the wt RNAP gene did not have the intended result. However, interestingly, sgRNA6_1 mediated a clear reduction in plaque size that could be correlated with a reduced ability to replicate as growth was impeded.

Chapter 7 Final discussion

In this study, the cellular and molecular processes underpinning phage therapy and the interactions between phages and human cells were investigated. By establishing *in vitro* phage therapy model systems, the similarities and differences in uptake and degradation of bacteria and phages by human cell lines were determined individually and in combination. The presented data advance and reinforce the existing knowledge of phage uptake and degradation, complemented by analysis of expression patterns of inflammatory cytokines during *in vitro* phage therapy and the temporal influence of phages on the barrier permeability of human endothelial cells.

In a separate series of experiments, phage engineering was used to address two prevailing clinical challenges of phage therapy, namely the endotoxin release associated with phage-induced lysis of bacteria and the absence of dosage control of administering virulent phages.

7.1 Establishing *in vitro* model systems for phage therapy

Phage-bacteria interactions have been characterised extensively by *in vitro* experimentation and modelling. However, in order to release the full potential of phage therapy, it is imperative that solid pharmacokinetic and pharmacodynamic data are generated from *in vivo* animal models and from tripartite *in vitro* models. Tripartite *in vitro* model systems comprise of phages, bacteria and human cell lines and have previously been used to study phage infection of *Clostridium difficile* in a colon environment using the HT-29 cell line³⁷ and phage T4 infection of *E. coli* in the mucosal surfaces of the epithelium³⁶.

In this study, clinically relevant *in vitro* model systems for phage therapy were established employing *E. coli* EV36, phage K1F and two distinct cell lines; the human urinary bladder epithelial cell line, T24, and the blood-brain barrier cell line, hCMEC. *E. coli* K1 was selected as the model bacterium because of its clinical relevance. It is

identified as a primary causal pathogen for conditions such as UTIs^{54, 55} and neonatal bacterial meningitis⁶³, with strains expressing the K1 capsule being associated with higher pathogenicity⁷⁰. The two human cell lines were selected for their individual relevance in previous epithelial^{92, 93} or endothelial⁹⁸ studies to link back with the environment of UTIs and neonatal bacterial meningitis, respectively.

The characterisation experiments of *E. coli* EV36 and phage K1F illustrated the high specificity and efficacy of phage K1F towards K1-capsule expressing *E. coli* EV36. The suitability of *E. coli* EV36 and phage K1F in the tripartite model system was demonstrated by the capability of *E. coli* EV36 to invade human cells and the capability of phage K1F to invade and lyse intracellular *E. coli* EV36 of the selected cell lines.

The methodologies of microscopy imaging and flow cytometry were enabled by the use of the derivatives *E. coli* EV36-RFP containing an RFP expression vector and the phage K1F-GFP containing genome-based expression of GFP. Both derivatives were demonstrated to express stable and readily detectable fluorophores. The experimental variables e.g. the concentrations of bacteria and phages and incubation periods with human cell lines, were based on the early characterisation experiments. These variables were set with bacteria-phage dynamics in mind, giving adequate time for the bacteria to cause inflammation without killing all the human host cells and for the phages to infect and replicate without killing all the bacterial host cells. The subsequent microscopy experiments allowed for the study of interactions between human cells, phages, and bacteria, individually and in combination. Flow cytometry was used in parallel with microscopy to support the data and proved to be valuable in generating quantitative data of larger populations.

7.2 Phage uptake and processing by human cells

The uptake of phages by human cells has been observed to occur via receptor-mediated^{29, 36} and non-specific^{31, 33, 106} endocytic pathways although the mechanisms are not well understood^{23, 28}. It is worth noting that several of these

studies equate transcellular transport, where the phages are passed through the cell, with uptake. In this study, a clear distinction was observed between the way human cell lines handle the uptake of bacteria and of phages and their subsequent processing.

The uptake and processing of *E. coli* EV36 by T24 cells and hCMECs were consistent with previously published observations of bacterial uptake by mammalian cells^{100, 102, 112}. In this study, colocalisation of intracellular *E. coli* EV36-RFP with multiple phagosomal-, lysosomal- and autophagy-associated proteins illustrated that the bacteria were phagocytosed and induced xenophagy either by galectin-8 dependency following the attempted escape from the phagosomes or by ubiquitin dependency independently.

These observations were in contrast to the uptake and processing of phage K1F-GFP. In both T24 cells and hCMECs, observations of colocalisation of phage K1F-GFP with Rab7, a protein associated with maturation of the early phagosome^{116, 177} and Cathepsin-L, a cysteine protease associated with lysosomes, indicated uptake by the endocytic machinery and processing by non-selective constitutive phagocytosis. Following phage treatment, the LysoTracker fluorescence of hCMECs, a proxy for acidic organelles¹⁷⁸, was shown to decrease over time. This observation suggested that the cytosolic store of lysosomes is spent during the process of phage degradation and not readily replenished suggesting a lack of urgency. Interestingly, intracellular phage K1F-GFP was recognised by PRRs during the late phagosome maturation as indicated LC3 colocalisation. The absence of galectin-8 and ubiquitin colocalisation in hCMECs suggested that the phage was subsequently degraded by selective LC3-assisted phagocytosis without inducing xenophagy. In T24 cells, however, a quarter of intercellular phage K1F-GFP colocalised with galectin-8 without initiating xenophagy through NDP52 recruitment, suggesting that phages can compromise the phagosome membrane. The recognition of phages by phagosomes-associated PRRs is novel and could foster a rethink of phage interaction with human cells.

In situ, endothelial cells are exposed to shear stress at the apical side from the continual flow of blood, whereas in these experiments, the culture is static. This difference could have implications for phage uptake; however, a recent study

observed no difference in the uptake of T4 phage between static or shear stress-exposed of HUVEC cultures ¹⁹⁷.

During *in vitro* phage therapy, where human cell cultures were treated with *E. coli* EV36 and phage K1F in succession, tentative molecular effects of the therapy were revealed. This included an increased lysosomal activity of hCMECs, illustrated by an increase in LysoTracker fluorescence and fewer bacteria-containing phagosomes progressing to xenophagy. In T24 cells, the therapy resulted in an increase in galectin-8 colocalisation and a decrease in NDP52 colocalisation.

The differential recognition and response to bacteria and phages between cell lines illustrate the phenotypic differences between epithelial and endothelial cells. Specifically, as illustrated by galectin-8 colocalisation, T24 cells were found to degrade a higher proportion of intracellular bacteria before they were able to compromise the phagosomal membrane than hCMECs. Additionally, Galectin-8 colocalisation with intracellular phages was only observed in T24 cells and not hCMECs.

7.3 Phage influence on the inflammatory responses of hCMEC cultures

The inflammatory responses of hCMEC cultures elicited by *E. coli* EV36 infection were potent and immediate and increased the expression of multiple cytokines, including TNF α , IL-6, and IL-8. These inflammatory responses correlate with previous observations of *E. coli* infection in multiple human cell types, including endothelial cells ^{198, 199}. Importantly, phage K1F did not induce inflammation of hCMEC cultures as illustrated by the absence of expression of all tested inflammatory cytokines. This suggests that phage treatment does not induce inflammatory measures in hCMECs and tie in with the theory of phages being taken up and degraded by non-specific constitutive phagocytosis.

In vitro phage therapy of *E. coli* EV36-infected hCMEC cultures demonstrated a reduction in bacteria-induced TNF α expression and an increase in bacteria-induced IL-6 and IL-8 expression. These effects are likely linked to the reduction in live bacteria following phage-induced lysis and the associated increase in endotoxin

concentration. LPS is a known inducer of both TNF α , IL-6 and IL-8 expression in endothelial cell lines ^{124, 200}, however, TNF α is also itself an inducer of IL-6 and IL-8 expression ¹²⁷, which could therefore amplify the expression of these and explain the differential expression observed with these three cytokines following *in vitro* phage therapy.

7.4 Phage influence on the barrier integrity of hCMEC cultures

E. coli EV36 infection initiated a dramatic and immediate decrease of the barrier impedance of hCMEC cultures as measured by xCELLigence. This observation is indicative of disruption of the barrier integrity and correlates with studies of endothelial barrier integrity during infection ^{187, 188} and with previous observations of bacterial initiation of autophagy and induction of inflammatory cytokines in this study. The likely effect observed in these experiments is a morphological change induced by the bacterial infection and a change in the expression of adhesion proteins, ultimately leading to the release of hCMECs from the electrode array.

Intervention using phage K1F did not lead to a sustained recovery of the barrier impedance of bacteria-infected hCMEC cultures, although the bacterial and phage concentrations used resulted in clearance of bacteria in previous experiments in this study. However, from this data alone, it is not possible to deduce if the bacterial infection had caused irreparable damage to the hCMECs or if the increasing endotoxin concentration caused by phage-induced bacterial lysis hindered recovery. Additionally, considering the extended timeframe of these experiments, it is not unlikely that phage-resistant bacterial escape mutants could grow and cause further infection.

hCMEC cultures incubated with phage K1F and T7 at concentrations of 10⁷ PFU/ml and above, showed a reduction in impedance over a considerable length of time before regressing to a similar level of non-treated cells. Regulation of microvascular permeability by cytokines is a well-known regulatory measure allowing for the extravasation of immune cells at a site of infection ²⁰¹. It is known that continual stimulation of antiviral immune responses by phage activation of innate immune

pathways induces low-level cytokine production, resulting in continuously activated immune cells that confer protection against pathogenic viral infections ^{25, 41}. Additionally, a non-host-derived layer of immunity is theorised to result from phages residing in mucosal layers (BAM model), whereby the presence of phages at the site-of-entry for pathogenic bacteria confers immunity as well as impacting the mucosal-resident community of commensal bacteria ³⁵. The implications of phage regulation of membrane integrity are many, and this observation potentially give hints of a new inflammatory mechanism that could support the immune system in clearing infections.

7.5 Altering the host tropism of phage T7

The engineering of phages with altered host tropism has previously been achieved by the expression of a fully synthesised phage genome using yeast-based assembly ¹⁴⁰. In this study, homologous recombination was used to alter the host tropism of phage T7 by replacing part of the RBP, *gene17*, with the corresponding part of phage K1F, a phage that is similar in phenotype and genomic organisation.

The success of using HR as the engineering approach of a recombinant chimeric phage T7/K1F was demonstrated by PCR testing and GATC sequencing. However, due to selection challenges and the potential of reduced fitness of phage T7/K1F, it was not possible to produce a purified phage preparation. The selection strategies relied on infection of the HR product, containing a mixed population of wt phage T7 and chimeric phage T7/K1F, of various bacterial hosts. Initial selection on *E. coli* EV36, the “new” host of phage T7/K1F, resulted in phage preparations that were unable to sustain infection over consecutive rounds of infection on both solid and in liquid media. While discouraging, this observation confirmed the successful engineering of a chimeric phage with lytic capabilities, albeit the phage not being viable long term. Further selection efforts based on *E. coli* BW25113 Δ *trxA*, a strain engineered to be non-permissive to T7 replication by deletion of host factor *trx*, with and without the added expression of *gene17* of phage T7 *in trans*, allowed for the replication of phage T7/K1F as this host factor was incorporated into the genome of phage T7/K1F.

However, wt *E. coli* BW25113 is a natural host to phage T7 and not phage T7/K1F, which means that the chimeric phage would need to piggyback phage T7 for entry into the host. Phage T7/K1F replication is therefore not favoured, and as a result this does not increase the ratio of phage T7/K1F in the mix. The concept of using a non-permissive/permissive model is great, in this situation, nonetheless, an *E. coli* EV36 strain being non-permissive to phage T7 should have been engineered, or the original chimeric design should have been inverted so that *gene17* of phage T7 was incorporated into the genome of phage K1F.

Reduced viability of the engineered phage and the selection challenges has been experienced by other research groups ^{140, 202} highlighting the difficulties in commandeering phage evolution. In this study, only part of *gene17* of phage K1F was used to replace the counterpart of phage T7. This decision was made because of the sequence similarities between the two phages, though it is feasible that incorporating a longer sequence, possibly covering several genes, would produce a more stable and viable phage.

7.6 Engineering of a replication-deficient phage K1F

The ability to administer a controlled dose of a virulent phage for therapeutic purposes could potentially reduce the phage-induced release of endotoxin and thereby remove an argument against phage therapy, as well as potentially benefitting public opinion and easing legislative affairs.

In this study, efforts were made to engineer a replication-deficient phage K1F. In the design, the RNAP gene was replaced with a β -lactamase gene using the approach of deletion by substitution by HR. PCR testing of the product following HR illustrated the presence of both wt phage K1F and recombinant replication-deficient phage K1F. The evidence for successfully engineering a replication-deficient phage K1F in this study was not definite. The main challenge lies with enabling replication of the replication-deficient phage with the chosen approach of expression of a codon-optimised RNAP *in trans* in *E. coli* EV36. When expressed in *E. coli* EV36, the plasmid contained codon-optimised RNAP would present with multiple mutations once

extracted from the culture, which suggested that the RNAP, at least in this form, was toxic to the bacteria. While many of these mutations were found to be silent, it is unknown if a functional RNAP protein was expressed. Ultimately, the efforts to isolate a recombinant phage was abandoned for this reason.

7.7 Future studies

There are many interesting avenues future research could explore based on the work in this study - In many ways, this study raises more questions than it answers.

All experiments performed in this study are performed *in vitro* using immortalised cell lines and not primary cell lines or *in vivo* animal models. To solidify the findings in this study, *in vivo* experiments are needed. Similarly, in the bulk of experiments in this study, only one phage strain is used, namely phage K1F. In order to generalise about the mechanisms of phage uptake and processing by human cells, future studies could incorporate a wider selection of phages such as filamentous phages, ssDNA or RNA phages. It has also been demonstrated that smaller phages are taken up at higher rates than larger phages¹⁹⁷, suggesting that phage size and potentially shape is a factor.

Intracellular phage K1F was observed to colocalise with LC3 in both T24 cells and hCMECs. PRR activation is required for the recruitment of LC3¹¹⁴. Further studies could identify specifically which DAMPs or PAMPs are involved in phage recognition. Currently, we know very little about direct interactions between phages and the mammalian immune system, and if the PRR could be identified, it would be a first.

Phages K1F and T7 were observed to decrease the impedance of hCMEC cultures over a sustained period of time. This suggests that the endothelial barrier integrity is decreased, resulting in increased permeability of the endothelial monolayer. Further studies, using a panel of diverse adherent cell types, could determine if phage regulation of barrier integrity is a specific or a general trait. It would be very exciting

if the trait is specific to a particular cell type as it would demonstrate an auxiliary process of phage therapy; e.g. if specific to the endothelium, it would support the theory of phage involvement in the delivery and extravasation of immune cells at the site of infection, and if specific to the epithelium it would solidify the theorised BAM model.

Microscopy imaging is an incredibly powerful methodology giving almost tangible evidence to the storytelling. However, single timepoint data as presented in this study does not give justice to the complexity of phage-bacteria-human cell dynamics. Future studies using automated live-cell imaging could obtain real-time data over a longer period of time yielding valuable in-depth dynamic data.

Chapter 8 References

1. Bennett, J.W. & Chung, K.-T. Alexander Fleming and the discovery of penicillin. (2001).
2. Gaynes, R. The Discovery of Penicillin—New Insights After More Than 75 Years of Clinical Use. *Emerg Infect Dis* **23**, 849-853 (2017).
3. Hutchings, M.I., Truman, A.W. & Wilkinson, B. Antibiotics: past, present and future. *Current Opinion in Microbiology* **51**, 72-80 (2019).
4. Davies, J. Where have All the Antibiotics Gone? *Can J Infect Dis Med Microbiol* **17**, 287-290 (2006).
5. (Office for National Statistics, Causes of death over 100 years <https://www.ons.gov.uk/peoplepopulationandcommunity/birthsdeathsandmarriages/deaths/articles/causesofdeathover100years/2017-09-18>; 2017).
6. Levy, S.B. *The antibiotic paradox: how miracle drugs are destroying the miracle*. (Springer, 2013).
7. O'Neill, J. Review on antimicrobial resistance. *Antimicrobial resistance: tackling a crisis for the health and wealth of nations* **2014** (2014).
8. (HM Government, Global and Public Health Group, Tackling antimicrobial resistance 2019-2024
https://assets.publishing.service.gov.uk/government/uploads/system/uploads/attachment_data/file/784894/UK_AMR_5_year_national_action_plan.pdf; 2019).
9. (US Centers for Disease Control and Prevention, Antibiotic use in the United States, Progress and Opportunities <https://www.cdc.gov/antibiotic-use/stewardship-report/pdf/stewardship-report-2018-508.pdf>; 2018).
10. (ASOAntibiotics, Farm antibiotic use in the United States <https://www.saveourantibiotics.org/media/1834/farm-antibiotic-use-in-the-united-states-a-threat-to-uk-standards.pdf>; 2020).
11. Summers, W.C. The strange history of phage therapy. *Bacteriophage* **2**, 130-133 (2012).

12. Gordillo Altamirano, F.L. & Barr, J.J. Phage Therapy in the Postantibiotic Era. *Clinical microbiology reviews* **32**, e00066-00018 (2019).
13. Brüssow, H., Canchaya, C. & Hardt, W.-D. Phages and the Evolution of Bacterial Pathogens: from Genomic Rearrangements to Lysogenic Conversion. *Microbiology and Molecular Biology Reviews* **68**, 560-602 (2004).
14. Hobbs, Z. & Abedon, S.T. Diversity of phage infection types and associated terminology: the problem with 'Lytic or lysogenic'. *FEMS Microbiology Letters* **363** (2016).
15. Wang, I.-N. Lysis Timing and Bacteriophage Fitness. *Genetics* **172**, 17-26 (2006).
16. Howard-Varona, C., Hargreaves, K.R., Abedon, S.T. & Sullivan, M.B. Lysogeny in nature: Mechanisms, impact and ecology of temperate phages. *ISME Journal* **11**, 1511-1520 (2017).
17. Clokie, M.R.J., Millard, A.D., Letarov, A.V. & Heaphy, S. Phages in nature. *Bacteriophage* **1**, 31-45 (2011).
18. Campbell, A. The future of bacteriophage biology. *Nature Reviews Genetics* **4**, 471-477 (2003).
19. Suttle, C.A. Marine viruses — major players in the global ecosystem. *Nature Reviews Microbiology* **5**, 801-812 (2007).
20. Hampton, H.G., Watson, B.N.J. & Fineran, P.C. The arms race between bacteria and their phage foes. *Nature* **577**, 327-336 (2020).
21. Oechslin, F. Resistance Development to Bacteriophages Occurring during Bacteriophage Therapy. *Viruses* **10**, 351 (2018).
22. Burmeister, A.R. *et al.* Pleiotropy complicates a trade-off between phage resistance and antibiotic resistance. *Proceedings of the National Academy of Sciences* **117**, 11207-11216 (2020).
23. Barr, J.J. A bacteriophages journey through the human body. *Immunological Reviews* **279**, 106-122 (2017).
24. Blanco-Picazo, P. *et al.* Unravelling the consequences of the bacteriophages in human samples. *Scientific Reports* **10**, 6737 (2020).

25. Van Belleghem, J.D., Dąbrowska, K., Vaneechoutte, M., Barr, J.J. & Bollyky, P.L. Interactions between bacteriophage, bacteria, and the mammalian immune system. *Viruses* **11** (2019).
26. Danis-Włodarczyk, K., Dąbrowska, K. & Abedon, S.T. Phage Therapy: The Pharmacology of Antibacterial Viruses. *Curr Issues Mol Biol* **40**, 81-164 (2020).
27. Dąbrowska, K. & Abedon, S.T. Pharmacologically Aware Phage Therapy: Pharmacodynamic and Pharmacokinetic Obstacles to Phage Antibacterial Action in Animal and Human Bodies. *Microbiology and Molecular Biology Reviews* **83**, e00012-00019 (2019).
28. Aranda, F. *et al.* Trial watch: Adoptive cell transfer for anticancer immunotherapy. *Oncolimmunology* **3** (2014).
29. Lehti, T.A., Pajunen, M.I., Skog, M.S. & Finne, J. Internalization of a polysialic acid-binding Escherichia coli bacteriophage into eukaryotic neuroblastoma cells. *Nature Communications* **8**, 1915 (2017).
30. Nguyen, S. *et al.* Bacteriophage Transcytosis Provides a Mechanism To Cross Epithelial Cell Layers. *mBio* **8**, e01874-01817 (2017).
31. Gorski, A. *et al.* Phage as a modulator of immune responses: practical implications for phage therapy. *Advances in virus research* **83**, 41-71 (2012).
32. Hodyra-Stefaniak, K. *et al.* Mammalian Host-Versus-Phage immune response determines phage fate in vivo. *Scientific Reports* **5**, 14802 (2015).
33. Dąbrowska, K. Phage therapy: What factors shape phage pharmacokinetics and bioavailability? Systematic and critical review. *Medicinal Research Reviews* **39**, 2000-2025 (2019).
34. Sansonetti, P.J. War and peace at mucosal surfaces. *Nature Reviews Immunology* **4**, 953-964 (2004).
35. Barr, J.J., Youle, M. & Rohwer, F. Innate and acquired bacteriophage-mediated immunity. *Bacteriophage* **3**, e25857 (2013).
36. Barr, J.J. *et al.* Bacteriophage adhering to mucus provide a non-host-derived immunity. *Proceedings of the National Academy of Sciences* **110**, 10771-10776 (2013).

37. Shan, J. *et al.* Bacteriophages are more virulent to bacteria with human cells than they are in bacterial culture; insights from HT-29 cells. *Scientific reports* **8**, 5091-5091 (2018).
38. Morello, E. *et al.* Pulmonary Bacteriophage Therapy on *Pseudomonas aeruginosa* Cystic Fibrosis Strains: First Steps Towards Treatment and Prevention. *PLoS ONE* **6**, e16963 (2011).
39. Hraiech, S., Brégeon, F. & Rolain, J.-M. Bacteriophage-based therapy in cystic fibrosis-associated *Pseudomonas aeruginosa* infections: rationale and current status. *Drug Design, Development and Therapy* **9**, 3653-3663 (2015).
40. Łusiak-Szelachowska, M., Weber-Dąbrowska, B., Jończyk-Matysiak, E., Wojciechowska, R. & Górski, A. Bacteriophages in the gastrointestinal tract and their implications. *Gut Pathogens* **9**, 44 (2017).
41. Duerkop, B.A. & Hooper, L.V. Resident viruses and their interactions with the immune system. *Nature Immunology* **14**, 654-659 (2013).
42. McCallin, S., Sacher, J.C., Zheng, J. & Chan, B.K. Current State of Compassionate Phage Therapy. *Viruses* **11**, 343 (2019).
43. Theuretzbacher, U., Outterson, K., Engel, A. & Karlén, A. The global preclinical antibacterial pipeline. *Nature Reviews Microbiology* (2019).
44. Furfaro, L.L., Payne, M.S. & Chang, B.J. Bacteriophage Therapy: Clinical Trials and Regulatory Hurdles. *Frontiers in Cellular and Infection Microbiology* **8** (2018).
45. Fauconnier, A. Phage Therapy Regulation: From Night to Dawn. *Viruses* **11**, 352 (2019).
46. Nikolich, M.P. & Filippov, A.A. Bacteriophage Therapy: Developments and Directions. *Antibiotics (Basel)* **9**, 135 (2020).
47. Rietschel, E.T. *et al.* Bacterial endotoxin: molecular relationships of structure to activity and function. *The FASEB Journal* **8**, 217-225 (1994).
48. Aderem, A. & Ulevitch, R.J. Toll-like receptors in the induction of the innate immune response. *Nature* **406**, 782-787 (2000).
49. Daneshian, M., Guenther, A., Wendel, A., Hartung, T. & von Aulock, S. In vitro pyrogen test for toxic or immunomodulatory drugs. *Journal of Immunological Methods* **313**, 169-175 (2006).

50. Van Belleghem, J.D., Merabishvili, M., Vergauwen, B., Lavigne, R. & Vaneechoutte, M. A comparative study of different strategies for removal of endotoxins from bacteriophage preparations. *Journal of Microbiological Methods* **132**, 153-159 (2017).
51. Merabishvili, M. *et al.* Quality-Controlled Small-Scale Production of a Well-Defined Bacteriophage Cocktail for Use in Human Clinical Trials. *PLOS ONE* **4**, e4944 (2009).
52. Crosby, H.A., Bion, J.F., Penn, C.W. & Elliott, T.S. Antibiotic-induced release of endotoxin from bacteria in vitro. *J Med Microbiol* **40**, 23-30 (1994).
53. Al-Badr, A. & Al-Shaikh, G. Recurrent Urinary Tract Infections Management in Women: A review. *Sultan Qaboos University Medical Journal* **13**, 359-367 (2013).
54. J., W. *et al.* Trends among pathogens reported as causing bacteraemia in England, 2004–2008. *Clinical Microbiology and Infection* **17**, 451-458 (2011).
55. Gupta, K. *et al.* International Clinical Practice Guidelines for the Treatment of Acute Uncomplicated Cystitis and Pyelonephritis in Women: A 2010 Update by the Infectious Diseases Society of America and the European Society for Microbiology and Infectious Diseases. *Clinical Infectious Diseases* **52**, e103-e120 (2011).
56. Bitew, A., Molalign, T. & Chanie, M. Species distribution and antibiotic susceptibility profile of bacterial uropathogens among patients complaining urinary tract infections. *BMC Infectious Diseases* **17**, 654 (2017).
57. Odoki, M. *et al.* Prevalence of Bacterial Urinary Tract Infections and Associated Factors among Patients Attending Hospitals in Bushenyi District, Uganda. *International Journal of Microbiology* **2019**, 4246780 (2019).
58. Wilson, M.L. & Gaido, L. Laboratory Diagnosis of Urinary Tract Infections in Adult Patients. *Clinical Infectious Diseases* **38**, 1150-1158 (2004).
59. Johnson, J.R. Virulence factors in Escherichia coli urinary tract infection. *Clinical microbiology reviews* **4**, 80-128 (1991).
60. (NICE Guidance, Urinary tract infection (lower): antimicrobial prescribing <https://www.nice.org.uk/guidance/ng109>; 2018).

61. Ujmajuridze, A. *et al.* Adapted Bacteriophages for Treating Urinary Tract Infections. *Frontiers in Microbiology* **9** (2018).
62. Barichello, T. *et al.* Pathophysiology of neonatal acute bacterial meningitis. *Journal of Medical Microbiology* **62**, 1781-1789 (2013).
63. Hoffman, O. & Weber, J.R. Review: Pathophysiology and treatment of bacterial meningitis. *Therapeutic Advances in Neurological Disorders* **2**, 401-412 (2009).
64. Gaschignard, J. *et al.* Neonatal Bacterial Meningitis: 444 Cases in 7 Years. *The Pediatric Infectious Disease Journal* **30**, 212-217 (2011).
65. van de Beek, D. *et al.* Clinical Features and Prognostic Factors in Adults with Bacterial Meningitis. *New England Journal of Medicine* **351**, 1849-1859 (2004).
66. Khan, N.A. & Goldsworthy, G.J. Novel Model To Study Virulence Determinants of Escherichia coli K1. *Infection and Immunity* **75**, 5735-5739 (2007).
67. Heath, P.T. & Okike, I.O. Neonatal bacterial meningitis: an update. *Paediatrics and Child Health* **20**, 526-530 (2010).
68. Ku, L.C., Boggess, K.A. & Cohen-Wolkowicz, M. Bacterial Meningitis in Infants. *Clinics in Perinatology* **42**, 29-45 (2015).
69. Jiang, H. *et al.* Prevalence and antibiotic resistance profiles of cerebrospinal fluid pathogens in children with acute bacterial meningitis in Yunnan province, China, 2012-2015. *PLoS One* **12**, e0180161 (2017).
70. Okike, I.O. *et al.* Incidence, Etiology, and Outcome of Bacterial Meningitis in Infants Aged <90 Days in the United Kingdom and Republic of Ireland: Prospective, Enhanced, National Population-Based Surveillance. *Clinical Infectious Diseases* **59**, e150-e157 (2014).
71. Bingen, E. *et al.* Phylogenetic Analysis of Escherichia coli Strains Causing Neonatal Meningitis Suggests Horizontal Gene Transfer from a Predominant Pool of Highly Virulent B2 Group Strains. *The Journal of infectious diseases* **177**, 642-650 (1998).
72. Scholl, D., Adhya, S. & Merrill, C. Escherichia coli K1's Capsule Is a Barrier to Bacteriophage T7. *Applied and Environmental Microbiology* **71**, 4872-4874 (2005).

73. Weber-Dabrowska, B., Mulczyk, M. & Gorski, A. Bacteriophage therapy of bacterial infections: an update of our institute's experience. *Arch Immunol Ther Exp (Warsz)* **48**, 547-551 (2000).
74. Strój, L., Weber-Dabrowska, B., Partyka, K., Mulczyk, M. & Wójcik, M. Successful treatment with bacteriophage in purulent cerebrospinal meningitis in a newborn. *Neurologia i neurochirurgia polska* **33**, 693-698 (1999).
75. Ghose, C. *et al.* The Virome of Cerebrospinal Fluid: Viruses Where We Once Thought There Were None. *Frontiers in Microbiology* **10** (2019).
76. Kim, K.S. Acute bacterial meningitis in infants and children. *The Lancet Infectious Diseases* **10**, 32-42 (2010).
77. Pouillot, F. *et al.* Efficacy of bacteriophage therapy in experimental sepsis and meningitis caused by a clone O25b:H4-ST131 Escherichia coli strain producing CTX-M-15. *Antimicrob Agents Chemother* **56**, 3568-3575 (2012).
78. (ICTV), I.C.o.T.o.V. Virus Taxonomy: 2017 Release. (2017).
79. Scholl, D. & Merril, C. The Genome of Bacteriophage K1F, a T7-Like Phage That Has Acquired the Ability To Replicate on K1 Strains of Escherichia coli. *Journal of bacteriology* **187**, 8499-8503 (2005).
80. Scholl, D., Rogers, S., Adhya, S. & Merril, C.R. Bacteriophage K1-5 encodes two different tail fiber proteins, allowing it to infect and replicate on both K1 and K5 strains of Escherichia coli. *Journal of Virology* **75**, 2509-2515 (2001).
81. Long, G.S., Bryant, J.M., Taylor, P.W. & Luzio, J.P. Complete nucleotide sequence of the gene encoding bacteriophage E endosialidase: Implications for K1E endosialidase structure and function. *Biochemical Journal* **309**, 543-550 (1995).
82. MacHida, Y. *et al.* Structure and function of a novel coliphage-associated sialidase. *FEMS Microbiology Letters* **182**, 333-337 (2000).
83. Stummeyer, K. *et al.* Evolution of bacteriophages infecting encapsulated bacteria: lessons from Escherichia coli K1-specific phages. *Molecular microbiology* **60**, 1123-1135 (2006).

84. Metkar, S. *et al.* Role of CD14 in Responses to Clinical Isolates of Escherichia coli: Effects of K1 Capsule Expression. *Infection and Immunity* **75**, 5415-5424 (2007).
85. Silver, R.P. & Vimr, E.R. Polysialic acid capsule of Escherichia coli K1. *The bacteria* **11**, 39-60 (1990).
86. Angus, D.C. & van der Poll, T. Severe Sepsis and Septic Shock. *New England Journal of Medicine* **369**, 840-851 (2013).
87. Vimr, E.R. & Troy, F.A. Identification of an inducible catabolic system for sialic acids (nan) in Escherichia coli. *Journal of bacteriology* **164**, 845-853 (1985).
88. Walz, T. *et al.* Towards the molecular architecture of the asymmetric unit membrane of the mammalian urinary bladder epithelium: a closed "twisted ribbon" structure. *J Mol Biol* **248**, 887-900 (1995).
89. Khandelwal, P., Abraham, S.N. & Apodaca, G. Cell biology and physiology of the uroepithelium. *American journal of physiology. Renal physiology* **297**, F1477-F1501 (2009).
90. Abelson, B. *et al.* Sex differences in lower urinary tract biology and physiology. *Biol Sex Differ* **9**, 45 (2018).
91. Suda, K., Rothen-Rutishauser, B., Günthert, M. & Wunderli-Allenspach, H. Phenotypic characterization of human umbilical vein endothelial (ECV304) and urinary carcinoma (T24) cells: endothelial versus epithelial features. *In Vitro Cellular & Developmental Biology-Animal* **37**, 505-514 (2001).
92. Toval, F. *et al.* Characterization of Urinary Tract Infection-Associated Shiga Toxin-Producing *Escherichia coli*. *Infection and Immunity* **82**, 4631-4642 (2014).
93. Horsley, H. *et al.* Enterococcus faecalis Subverts and Invades the Host Urothelium in Patients with Chronic Urinary Tract Infection. *PLOS ONE* **8**, e83637 (2013).
94. Bäckhed, F., Söderhäll, M., Ekman, P., Normark, S. & Richter-Dahlfors, A. Induction of innate immune responses by Escherichia coli and purified lipopolysaccharide correlate with organ- and cell-specific expression of Toll-

- like receptors within the human urinary tract. *Cell Microbiol* **3**, 153-158 (2001).
95. Hunstad, D.A., Justice, S.S., Hung, C.S., Lauer, S.R. & Hultgren, S.J. Suppression of Bladder Epithelial Cytokine Responses by Uropathogenic *Escherichia coli*. *Infection and Immunity* **73**, 3999-4006 (2005).
 96. E. Marieb, S.K. *Essentials of Human Anatomy & Physiology*. (Pearson Education, 2017).
 97. Nagyószzi, P. *et al.* Expression and regulation of toll-like receptors in cerebral endothelial cells. *Neurochemistry International* **57**, 556-564 (2010).
 98. Weksler, B., Romero, I.A. & Couraud, P.O. The hCMEC/D3 cell line as a model of the human blood brain barrier. *Fluids Barriers CNS* **10**, 16 (2013).
 99. Theriot, J.A. The Cell Biology of Infection by Intracellular Bacterial Pathogens. *Annual Review of Cell and Developmental Biology* **11**, 213-239 (1995).
 100. Cossart, P. & Sansonetti, P.J. Bacterial invasion: the paradigms of enteroinvasive pathogens. *Science* **304**, 242-248 (2004).
 101. Cossart, P. & Helenius, A. Endocytosis of viruses and bacteria. *Cold Spring Harbor perspectives in biology* **6** 8 (2014).
 102. Kumar, Y. & Valdivia, R.H. Leading a sheltered life: intracellular pathogens and maintenance of vacuolar compartments. *Cell host & microbe* **5**, 593-601 (2009).
 103. Danthi, P. *et al.* From touchdown to transcription: the reovirus cell entry pathway. *Curr Top Microbiol Immunol* **343**, 91-119 (2010).
 104. Dimitrov, D.S. Virus entry: molecular mechanisms and biomedical applications. *Nature Reviews Microbiology* **2**, 109-122 (2004).
 105. Żaczek, M., Górski, A., Skaradzińska, A., Łusiak-Szelachowska, M. & Weber-Dąbrowska, B. Phage penetration of eukaryotic cells: practical implications. *Future Virology* **14**, 745-760 (2019).
 106. Bodner, K., Melkonian, A.L. & Covert, M.W. The Enemy of My Enemy: New Insights Regarding Bacteriophage–Mammalian Cell Interactions. *Trends in Microbiology* (2020).
 107. Pacífico, C. *et al.* Natural Occurrence of *Escherichia coli*-Infecting Bacteriophages in Clinical Samples. *Frontiers in Microbiology* **10** (2019).

108. Thannesberger, J. *et al.* Viruses comprise an extensive pool of mobile genetic elements in eukaryote cell cultures and human clinical samples. *The FASEB Journal* **31**, 1987-2000 (2017).
109. Otero, J. *et al.* Biodistribution of Liposome-Encapsulated Bacteriophages and Their Transcytosis During Oral Phage Therapy. *Frontiers in Microbiology* **10** (2019).
110. Lai, S.-c. & Devenish, R.J. LC3-Associated Phagocytosis (LAP): Connections with Host Autophagy. *Cells* **1**, 396 (2012).
111. Schreiber, A. & Peter, M. Substrate recognition in selective autophagy and the ubiquitin–proteasome system. *Biochimica et Biophysica Acta (BBA) - Molecular Cell Research* **1843**, 163-181 (2014).
112. Randow, F. & Youle, Richard J. Self and Nonself: How Autophagy Targets Mitochondria and Bacteria. *Cell host & microbe* **15**, 403-411 (2014).
113. Rosales, C. & Uribe-Querol, E. Phagocytosis: A Fundamental Process in Immunity. *BioMed Research International* **2017**, 9042851 (2017).
114. Heckmann, B.L. & Green, D.R. LC3-associated phagocytosis at a glance. *Journal of Cell Science* **132**, jcs222984 (2019).
115. Guerra, F. & Bucci, C. Multiple Roles of the Small GTPase Rab7. *Cells* **5**, 34 (2016).
116. Ng, E.L., Gan, B.Q., Ng, F. & Tang, B.L. Rab GTPases regulating receptor trafficking at the late endosome-lysosome membranes. *Cell Biochem Funct* **30**, 515-523 (2012).
117. Chua, C.E.L., Gan, B.Q. & Tang, B.L. Involvement of members of the Rab family and related small GTPases in autophagosome formation and maturation. *Cellular and Molecular Life Sciences* **68**, 3349 (2011).
118. Bhutani, N., Piccirillo, R., Hourez, R., Venkatraman, P. & Goldberg, A.L. Cathepsins L and Z are critical in degrading polyglutamine-containing proteins within lysosomes. *Journal of Biological Chemistry* **287**, 17471-17482 (2012).
119. Florey, O., Kim, S.E., Sandoval, C.P., Haynes, C.M. & Overholtzer, M. in *Nat Cell Biol*, Vol. 13 1335-1343 (2011).

120. Boyle, K.B. & Randow, F. The role of 'eat-me' signals and autophagy cargo receptors in innate immunity. *Current Opinion in Microbiology* **16**, 339-348 (2013).
121. Thurston, T.L.M., Wandel, M.P., von Muhlinen, N., Foeglein, Á. & Randow, F. Galectin 8 targets damaged vesicles for autophagy to defend cells against bacterial invasion. *Nature* **482**, 414 (2012).
122. Thurston, T.L., Ryzhakov, G., Bloor, S., von Muhlinen, N. & Randow, F. The TBK1 adaptor and autophagy receptor NDP52 restricts the proliferation of ubiquitin-coated bacteria. *Nat Immunol* **10**, 1215-1221 (2009).
123. Bradley, Jr. in *J. Pathol.*, Vol. 214 149-160 (2008).
124. Li, J. *et al.* (-)-Epigallocatechin gallate inhibits endotoxin-induced expression of inflammatory cytokines in human cerebral microvascular endothelial cells. *Journal of Neuroinflammation* **9**, 161 (2012).
125. Tanaka, T., Narazaki, M. & Kishimoto, T. IL-6 in inflammation, immunity, and disease. *Cold Spring Harbor perspectives in biology* **6**, a016295-a016295 (2014).
126. Yu, H. *et al.* Interleukin-8 regulates endothelial permeability by down-regulation of tight junction but not dependent on integrins induced focal adhesions. *Int J Biol Sci* **9**, 966-979 (2013).
127. O'Carroll, S.J. *et al.* Pro-inflammatory TNF α and IL-1 β differentially regulate the inflammatory phenotype of brain microvascular endothelial cells. *Journal of Neuroinflammation* **12**, 1-18 (2015).
128. Iyer, S.S. & Cheng, G. Role of interleukin 10 transcriptional regulation in inflammation and autoimmune disease. *Crit Rev Immunol* **32**, 23-63 (2012).
129. Gunnett, C.A., Heistad, D.D., Berg, D.J. & Faraci, F.M. IL-10 deficiency increases superoxide and endothelial dysfunction during inflammation. *American Journal of Physiology-Heart and Circulatory Physiology* **279**, H1555-H1562 (2000).
130. Nagarajan, U. Induction and function of IFN β during viral and bacterial infection. *Crit Rev Immunol* **31**, 459-474 (2011).
131. Cerutti, C. & Ridley, A.J. Endothelial cell-cell adhesion and signaling. *Experimental Cell Research* **358**, 31-38 (2017).

132. Rahimi, N. Defenders and Challengers of Endothelial Barrier Function. *Frontiers in Immunology* **8** (2017).
133. Yang, R. *et al.* Induction of VEGFA and Snail-1 by meningitic Escherichia coli mediates disruption of the blood-brain barrier. *Oncotarget* **7**, 63839-63855 (2016).
134. Dedrick, R.M. *et al.* Engineered bacteriophages for treatment of a patient with a disseminated drug-resistant Mycobacterium abscessus. *Nature Medicine* **25**, 730-733 (2019).
135. Dedrick, R.M. *et al.* Mycobacteriophage Zoel: A broad host-range close relative of mycobacteriophage TM4. *Tuberculosis* **115**, 14-23 (2019).
136. Sagona, A.P., Grigonyte, A.M., MacDonald, P.R. & Jaramillo, A. Genetically modified bacteriophages. *Integrative biology : quantitative biosciences from nano to macro* **8**, 465-474 (2016).
137. Schmelcher, M., Donovan, D.M. & Loessner, M.J. Bacteriophage endolysins as novel antimicrobials. *Future Microbiology* **7**, 1147-1171 (2012).
138. Frenkel, D. & Solomon, B. Filamentous phage as vector-mediated antibody delivery to the brain. *Proc Natl Acad Sci U S A* **99**, 5675-5679 (2002).
139. Bar, H., Yacoby, I. & Benhar, I. Killing cancer cells by targeted drug-carrying phage nanomedicines. *BMC Biotechnology* **8**, 37 (2008).
140. Ando, H., Lemire, S., Pires, Diana P. & Lu, Timothy K. Engineering Modular Viral Scaffolds for Targeted Bacterial Population Editing. *Cell Systems* **1**, 187-196 (2015).
141. Yosef, I., Goren, M.G., Globus, R., Molshanski-Mor, S. & Qimron, U. Extending the Host Range of Bacteriophage Particles for DNA Transduction. *Mol Cell* **66**, 721-728.e723 (2017).
142. Matsuda, T. *et al.* Lysis-deficient bacteriophage therapy decreases endotoxin and inflammatory mediator release and improves survival in a murine peritonitis model. *Surgery* **137**, 639-646 (2005).
143. Paul, V.D. *et al.* Lysis-deficient phages as novel therapeutic agents for controlling bacterial infection. *BMC Microbiology* **11**, 195 (2011).
144. Young, R. Bacteriophage holins: Deadly diversity. *Journal of Molecular Microbiology and Biotechnology* **4**, 21-36 (2002).

145. Hagens, S. & Blasi, U. Genetically modified filamentous phage as bactericidal agents: a pilot study. *Letters in applied microbiology* **37**, 318-323 (2003).
146. Blattner, F.R. *et al.* The complete genome sequence of Escherichia coli K-12. *Science* **277**, 1453-1462 (1997).
147. Johnson, L.A. *et al.* An inflammation- induced mechanism for leukocyte transmigration across lymphatic vessel endothelium. *The Journal of experimental medicine* **203**, 2763 (2006).
148. Qimron, U., Marintcheva, B., Tabor, S. & Richardson, C.C. Genomewide screens for Escherichia coli genes affecting growth of T7 bacteriophage. *Proceedings of the National Academy of Sciences of the United States of America* **103**, 19039-19044 (2006).
149. Mark, D.F. & Richardson, C.C. Escherichia coli thioredoxin: a subunit of bacteriophage T7 DNA polymerase. *Proc Natl Acad Sci U S A* **73**, 780-784 (1976).
150. Tabor, S., Huber, H.E. & Richardson, C.C. Escherichia coli thioredoxin confers processivity on the DNA polymerase activity of the gene 5 protein of bacteriophage T7. *The Journal of biological chemistry* **262**, 16212-16223 (1987).
151. Sambrook, H.C. *Molecular cloning : a laboratory manual*. Cold Spring Harbor, NY. (1989).
152. Jensen, K.F. The Escherichia coli K-12 "wild types" W3110 and MG1655 have an rph frameshift mutation that leads to pyrimidine starvation due to low pyrE expression levels. *Journal of bacteriology* **175**, 3401-3407 (1993).
153. Huang, Y. (2017).
154. Larsson, E.M., McManus, J.B. & Murray, R.M. Construction of an inducible amyloid expression circuit in Bacillus megaterium: A case study with CsgA and TasA. *BioRxiv*, 858266 (2019).
155. Bubenik, J. *et al.* Established cell line of urinary bladder carcinoma (T24) containing tumour-specific antigen. *Int J Cancer* **11**, 765-773 (1973).
156. McCoy, T.A., Maxwell, M. & Kruse Jr, P.F. Amino acid requirements of the Novikoff hepatoma in vitro. *Proceedings of the Society for Experimental biology and Medicine* **100**, 115-118 (1959).

157. Møller-Olsen, C., Ho, S.F.S., Shukla, R.D., Feher, T. & Sagona, A.P. Engineered K1F bacteriophages kill intracellular Escherichia coli K1 in human epithelial cells. *Scientific Reports* **8**, 17559 (2018).
158. Studier, F.W. The genetics and physiology of bacteriophage T7. *Virology* **39**, 562-574 (1969).
159. Castro-Mejía, J.L. *et al.* Optimizing protocols for extraction of bacteriophages prior to metagenomic analyses of phage communities in the human gut. *Microbiome* **3**, 64 (2015).
160. Kropinski, A.M., Mazzocco, A., Waddell, T.E., Lingohr, E. & Johnson, R.P. Enumeration of bacteriophages by double agar overlay plaque assay. *Methods Mol Biol* **501**, 69-76 (2009).
161. Vestergaard, A.L., Knudsen, U.B., Munk, T., Rosbach, H. & Martensen, P.M. Transcriptional expression of type-I interferon response genes and stability of housekeeping genes in the human endometrium and endometriosis. *Molecular Human Reproduction* **17**, 243-254 (2010).
162. Chege, D. *et al.* Evaluation of a quantitative real-time PCR assay to measure HIV-specific mucosal CD8+ T cell responses in the cervix. *PloS one* **5**, e13077-e13077 (2010).
163. Jeong, J.B., Shin, Y.K. & Lee, S.-H. Anti-inflammatory activity of patchouli alcohol in RAW264.7 and HT-29 cells. *Food and Chemical Toxicology* **55**, 229-233 (2013).
164. Romero, D.G. *et al.* Interleukin-8 Synthesis, Regulation, and Steroidogenic Role in H295R Human Adrenocortical Cells. *Endocrinology* **147**, 891-898 (2006).
165. Stordeur, P. *et al.* Cytokine mRNA quantification by real-time PCR. *Journal of Immunological Methods* **259**, 55-64 (2002).
166. Shi, H.-X. *et al.* Positive Regulation of Interferon Regulatory Factor 3 Activation by Herc5 via ISG15 Modification. *Molecular and Cellular Biology* **30**, 2424-2436 (2010).
167. Schmittgen, T.D. *et al.* Quantitative Reverse Transcription–Polymerase Chain Reaction to Study mRNA Decay: Comparison of Endpoint and Real-Time Methods. *Analytical Biochemistry* **285**, 194-204 (2000).

168. Kho, D. *et al.* Application of xCELLigence RTCA Biosensor Technology for Revealing the Profile and Window of Drug Responsiveness in Real Time. *Biosensors* **5**, 199-222 (2015).
169. Xi, B., Yu, N., Wang, X., Xu, X. & Abassi, Y. The application of cell-based label-free technology in drug discovery. *Biotechnology Journal* **3**, 484-495 (2008).
170. Dunn, J.J., Studier, F.W. & Gottesman, M. Complete nucleotide sequence of bacteriophage T7 DNA and the locations of T7 genetic elements. *Journal of Molecular Biology* **166**, 477-535 (1983).
171. Muhlenhoff, M., Stummeyer, K., Grove, M., Sauerborn, M. & Gerardy-Schahn, R. Proteolytic processing and oligomerization of bacteriophage-derived endosialidases. *The Journal of biological chemistry* **278**, 12634-12644 (2003).
172. Jiang, W., Bikard, D., Cox, D., Zhang, F. & Marraffini, L.A. RNA-guided editing of bacterial genomes using CRISPR-Cas systems. *Nature biotechnology* **31**, 233-239 (2013).
173. Ackermann, H.-W. Phage classification and characterization, in *Bacteriophages* 127-140 (Springer, 2009).
174. Leiman, P.G. *et al.* The structures of bacteriophages K1E and K1-5 explain processive degradation of polysaccharide capsules and evolution of new host specificities. *J Mol Biol* **371**, 836-849 (2007).
175. Guo, F. *et al.* Capsid expansion mechanism of bacteriophage T7 revealed by multistate atomic models derived from cryo-EM reconstructions. *Proceedings of the National Academy of Sciences* **111**, E4606-E4614 (2014).
176. Deng, X., Wang, L., You, X., Dai, P. & Zeng, Y. Advances in the T7 phage display system (Review). *Mol Med Rep* **17**, 714-720 (2018).
177. Chua, C.E., Gan, B.Q. & Tang, B.L. Involvement of members of the Rab family and related small GTPases in autophagosome formation and maturation. *Cell Mol Life Sci* **68**, 3349-3358 (2011).
178. Dolman, N.J., Kilgore, J.A. & Davidson, M.W. A review of reagents for fluorescence microscopy of cellular compartments and structures, part I: BacMam labeling and reagents for vesicular structures. *Curr Protoc Cytom* **Chapter 12**, Unit 12.30 (2013).


179. Randow, F. & Youle, R.J. Self and nonself: how autophagy targets mitochondria and bacteria. *Cell Host Microbe* **15**, 403-411 (2014).
180. Damas, P. *et al.* Cytokine serum level during severe sepsis in human IL-6 as a marker of severity. *Ann Surg* **215**, 356-362 (1992).
181. Dayang, E.-Z. *et al.* Identification of LPS-Activated Endothelial Subpopulations With Distinct Inflammatory Phenotypes and Regulatory Signaling Mechanisms. *Frontiers in Immunology* **10** (2019).
182. Valbuena, G. & Walker, D.H. in *Annual Review of Pathology*, Vol. 1 171-198 (2006).
183. Van Belleghem, J.D., Clement, F., Merabishvili, M., Lavigne, R. & Vanechoutte, M. Pro- and anti-inflammatory responses of peripheral blood mononuclear cells induced by *Staphylococcus aureus* and *Pseudomonas aeruginosa* phages. *Scientific Reports* **7**, 8004 (2017).
184. Bedsaul, J.R., Zaritsky, L.A. & Zoon, K.C. Type I Interferon-Mediated Induction of Antiviral Genes and Proteins Fails to Protect Cells from the Cytopathic Effects of Sendai Virus Infection. *J Interferon Cytokine Res* **36**, 652-665 (2016).
185. Hiscott, J., Nguyen, H. & Lin, R. Molecular mechanisms of interferon beta gene induction. *Seminars in Virology* **6**, 161-173 (1995).
186. Sawa, Y. *et al.* LPS-induced IL-6, IL-8, VCAM-1, and ICAM-1 Expression in Human Lymphatic Endothelium. *Journal of Histochemistry & Cytochemistry* **56**, 97-109 (2007).
187. Shifflett, D.E., Clayburgh, D.R., Koutsouris, A., Turner, J.R. & Hecht, G.A. Enteropathogenic *E. coli* disrupts tight junction barrier function and structure in vivo. *Laboratory Investigation* **85**, 1308-1324 (2005).
188. Spitz, J. *et al.* Enteropathogenic *Escherichia coli* adherence to intestinal epithelial monolayers diminishes barrier function. *American Journal of Physiology-Gastrointestinal and Liver Physiology* **268**, G374-G379 (1995).
189. Atienza, J.M. *et al.* Dynamic and label-free cell-based assays using the real-time cell electronic sensing system. *Assay Drug Dev Technol* **4**, 597-607 (2006).
190. Kutter, E. *et al.* Phage therapy in clinical practice: Treatment of human infections. *Current Pharmaceutical Biotechnology* **11**, 69-86 (2010).

191. Heineman, R.H., Bull, J.J. & Molineux, I.J. Layers of evolvability in a bacteriophage life history trait. *Mol Biol Evol* **26**, 1289-1298 (2009).
192. Abedon, S.T. Lysis from without. *Bacteriophage* **1**, 46-49 (2011).
193. Lopatina, A., Tal, N. & Sorek, R. Abortive Infection: Bacterial Suicide as an Antiviral Immune Strategy. *Annual Review of Virology* **7**, 371-384 (2020).
194. Grigonyte, A.M. *et al.* Comparison of CRISPR and Marker-Based Methods for the Engineering of Phage T7. *Viruses* **12**, 193 (2020).
195. Zhang, J.-P. *et al.* Different Effects of sgRNA Length on CRISPR-mediated Gene Knockout Efficiency. *Scientific Reports* **6**, 28566 (2016).
196. Hsu, P.D. *et al.* DNA targeting specificity of RNA-guided Cas9 nucleases. *Nature Biotechnology* **31**, 827-832 (2013).
197. Bichet, M.C. *et al.* Bacteriophage uptake by mammalian cell layers represents a potential sink that may impact phage therapy. *iScience* **24**, 102287 (2021).
198. Agace, W. *et al.* Selective cytokine production by epithelial cells following exposure to Escherichia coli. *Infection and Immunity* **61**, 602-609 (1993).
199. Bielaszewska, M. & Karch, H. Consequences of enterohaemorrhagic Escherichia coli infection for the vascular endothelium. *Thrombosis and haemostasis* **94** **2**, 312-318 (2005).
200. Sawa, Y. *et al.* LPS-induced IL-6, IL-8, VCAM-1, and ICAM-1 expression in human lymphatic endothelium. *J. Histochem. Cytochem.* **56**, 97-109 (2008).
201. Sedgwick, J.B., Menon, I., Gern, J.E. & Busse, W.W. Effects of inflammatory cytokines on the permeability of human lung microvascular endothelial cell monolayers and differential eosinophil transmigration. *J Allergy Clin Immunol* **110**, 752-756 (2002).
202. Pires, D.P., Cleto, S., Sillankorva, S., Azeredo, J. & Lu, T.K. Genetically Engineered Phages: a Review of Advances over the Last Decade. *Microbiology and Molecular Biology Reviews* **80**, 523-543 (2016).

Chapter 9 Appendix

1. Engineered K1F bacteriophages kill intracellular *Escherichia coli* K1 in human epithelial cells.
2. Bacteriophage K1F targets *Escherichia coli* K1 in cerebral endothelial cells and influences the barrier function.
3. Advances in engineering of bacteriophages for therapeutic applications.
4. Analysing parallel strategies to alter the host specificity of bacteriophage T7.

SCIENTIFIC REPORTS



OPEN

Engineered K1F bacteriophages kill intracellular *Escherichia coli* K1 in human epithelial cells

Christian Møller-Olsen ¹, Siu Fung Stanley Ho¹, Ranti Dev Shukla^{2,3}, Tamas Feher ² & Antonia P. Sagona ¹

Bacterial infections can be treated with bacteriophages that show great specificity towards their bacterial host and can be genetically modified for different applications. However, whether and how bacteriophages can kill intracellular bacteria in human cells remains elusive. Here, using CRISPR/Cas selection, we have engineered a fluorescent bacteriophage specific for *E. coli* K1, a nosocomial pathogen responsible for urinary tract infections, neonatal meningitis and sepsis. By confocal and live microscopy, we show that engineered bacteriophages K1F-GFP and *E. coli* EV36-RFP bacteria displaying the K1 capsule, enter human cells via phagocytosis. Importantly, we show that bacteriophage K1F-GFP efficiently kills intracellular *E. coli* EV36-RFP in T24 human urinary bladder epithelial cells. Finally, we provide evidence that bacteria and bacteriophages are degraded by LC3-associated phagocytosis and xenophagy.

Bacteriophages or phages are viruses that infect bacteria and are the most abundant organisms on earth¹. Bacteriophages present significant diversity and play an important role in the evolution of their host². Bacteriophages have also been found inside the human body^{3–6} and more recently have been shown to enter via different mechanisms in human cells^{7,8}. Bacteriophages are used to treat bacterial infections (phage therapy) and the interest in phage therapy has grown increasingly in recent years due to the emerging problem of antibiotic resistance of many bacterial pathogens^{9–12}. Due to the recent advances of molecular and synthetic biology, bacteriophages can be easily genetically modified to obtain preferable characteristics for different applications^{13,14}. A recently established efficient strategy applies the CRISPR/Cas System for the selection of recombinant bacteriophages^{15–17}. This has opened new perspectives for phage therapy, by making genetically modified bacteriophages more easily attainable¹⁸. Such an approach could provide solutions to naturally resistant nosocomial bacterial pathogens, such as *Escherichia coli* K1. *E. coli* K1 is a gram-negative pathogen, responsible for a wide range of diseases, including sepsis, neonatal meningitis, urinary tract infections and inflammatory bowel syndrome^{19–21}.

The virulence of *E. coli* K1 (*E. coli* O18:K1:H7) is attributed to its K1 polysaccharide capsule. The K1 capsular polysaccharide (K1 antigen) is an α -2-8-linked homopolymer of sialic acid (NeuNAc), which is responsible for the virulence and pathogenicity of these strains. The K1 antigen acts as a natural antiphagocytic barrier for the bacteria²². In addition, structural similarities between K1 and human tissue components indicate that immune tolerance may also be a factor of capsular *E. coli* pathogenesis²³. Due to these characteristics, *E. coli* O18:K1:H7 is able to invade human endothelial and epithelial cells and cause the corresponding diseases referred to above^{21,24–26}.

Phage K1F is a T7-like phage, which was first isolated in sewage and specifically infects *E. coli* strains that such as *E. coli* O18:K1:H7²⁷. Despite its similarities to phage T7 at the genome scale, phage K1F incorporates the endosialidase enzyme within its tail structure instead of the T7 tail fiber protein, which enables the attachment to- and degradation of the K1 polysaccharide capsule²⁷. The K1 polysaccharide capsule has therefore been shown to be a barrier to T7²⁸ and a receptor for phage K1F.

Here we have developed a novel *in vitro* model system for studying phage therapy for *E. coli* K1 in T24 human urinary bladder epithelial cells. We have applied the CRISPR/Cas system to engineer fluorescent phage K1F that are able to infect the *E. coli* EV36 strain, an *E. coli* K12/K1 hybrid derivative with the ability to display a K1

¹School of Life Sciences, University of Warwick, Gibbet Hill Road, CV4 7AL, Coventry, UK. ²Synthetic and Systems Biology Unit, Biological Research Centre of the Hungarian Academy of Sciences, Szeged, Hungary. ³Doctoral School in Biology, Faculty of Science and Informatics, University of Szeged, Szeged, Hungary. Correspondence and requests for materials should be addressed to A.P.S. (email: A.Sagona@warwick.ac.uk)

polysaccharide capsule morphologically similar to that of *E. coli* K1 clinical isolates²⁹. This system has enabled us to observe that both bacteria and bacteriophages invade T24 cells and that phage K1F kill intracellular *E. coli* EV36. We also show that upon being phagocytosed, bacteria and phages are degraded via different pathways: phage K1F is degraded mostly via LC3-assisted phagocytosis, whereas *E. coli* EV36 strain activates xenophagy. In the presence of both bacteria and bacteriophages, xenophagy is activated, indicating that the pathogen is sufficient to activate autophagy, whereas the bacteriophages on their own cannot activate autophagy to the same extent.

Results

Phage K1F targets *E. coli* EV36-RFP strain. We initially confirmed the specificity of phage K1F for *E. coli* cells displaying a K1 capsule. For our experiments, we used the *E. coli* EV36 strain, an *E. coli* K-12-K1 hybrid derivative with the ability to express a K1 polysaccharide capsule morphologically similar to that of *E. coli* K1 clinical isolates²⁹. We first compared in liquid culture the specificity of phage K1F and phage T7 for targeting the K1 capsule of the *E. coli* EV36 strain (Suppl. Fig. S1A left panel). By measuring the optical density at 600 nm over a period of 3.5 hours, we observed a drop in optical density in *E. coli* EV36 liquid culture only upon phage K1F addition. When no phage was added or when phage T7 was added, the *E. coli* EV36 bacteria continued to grow, indicating that solely phage K1F was capable of lysing them. We further tested phage K1F specificity towards an *E. coli* K-12 strain (MG1655 cells) (Suppl. Fig. S1A right panel) and we observed that in the presence of phage K1F or when no phage was added, *E. coli* MG1655 bacteria continued to grow and only upon T7 phage addition did the optical density of the liquid culture drop, indicating that T7 is specific to K-12 strains but not phage K1F. These results were further confirmed by plaque assays (Suppl. Fig. S1B). The phage K1F selected from a single plaque was further purified with a CsCl column and we performed transmission electron microscopy to reveal the exact pattern and structure of phage K1F (Suppl. Fig. S1C). This purified phage K1F was used for all our phage-related experiments and was the basis of the genetically engineered fluorescent phage K1F. In order to make *E. coli* EV36 bacteria easily visualized by microscopy, we transformed them with an RFP-expressing plasmid to provide them with a red colour (Suppl. Fig. S1D). Upon successfully obtaining *E. coli* EV36-RFP bacteria, we tested both in liquid culture (Suppl. Fig. S1E left panel) and with plaque assays (Suppl. Fig. S1E right panel) the ability of phage K1F to efficiently kill *E. coli* EV36-RFP. Our results showed that expression of RFP in *E. coli* EV36 did not seem to affect phage K1F's ability to infect this strain, when compared with empty *E. coli* EV36 (Suppl. Fig. S1E left panel). All together our results confirm that phage K1F targets *E. coli* EV36-RFP.

Genome engineering of fluorescent phage K1F-GFP followed by CRISPR/Cas selection. To engineer a fluorescent phage K1F, we decided to integrate the superfolder green fluorescent protein (GFP) gene into the phage's genome. Our primary aim was to generate translational fusions of GFP with *gene10* (or *g10*), which encodes the major capsid protein gp29. It is worth noting, that *gene10* can undergo a -1 translational frameshift in its 3' region, resulting in the addition of 44 triplets. The protein encoded by this extended ORF (referred to as *gene10b* or *g10b*) functions as the minor capsid protein of the virion. For phage genome editing, we relied on the strategy of providing the donor DNA on a plasmid residing in the bacterial strain used to grow the targeted phage on (Fig. 1A), combined with the CRISPR/Cas selection of recombinant phages (Suppl. Fig. S2A,B)^{16,17}. In our case, the strain hosting the donor DNA was *E. coli* EV36²⁹. The donor DNA cassette, consisting of the GFP gene flanked by appropriate homology arms, was cloned into the pSB6A1 plasmid. We attempted the engineering of three different recombinant phages: phage K1Fg10::gfp would carry the *gfp* gene fused to the 3' end of *gene10*, making a C-terminal GFP fusion of the major capsid protein (Fig. 1A,B); analogously, phage K1Fgfp::g10 would express the N-terminal GFP fusion of the major capsid protein (Fig. 1C) and phage K1Fg10b::gfp would harbour the *gfp* gene fused to the 3' end of *gene10b*, making a C-terminal GFP fusion of the minor capsid protein (Fig. 1D). Plasmid and phage constructs are summarized in Table S3.

Growing phage K1F on *E. coli* EV36 carrying either of the three donor DNA molecules (Table S1) permitted the generation of phage mixtures containing both wild-type and recombinant phages. The presence of recombinants was indeed PCR-verified in each phage lysate using the GFPfw-g11rev primer pair (Suppl. Fig. S2C). However, the PCR-screening of plaques generated from these phage mixes did not result in the identification of recombinant plaques, thereby prohibiting the isolation of pure recombinant phage suspensions. To enrich recombinant phages within the phage mix, we applied CRISPR/Cas selection by growing the phage mix on *E. coli* EV36 harbouring various pCas9 plasmid derivatives. The CRISPR/Cas9 machineries on these selection plasmids were engineered to cleave the wild-type *gene10*, but leave the *gfp*-fusion construct intact (Suppl. Fig. S2A,B). CRISPR/Cas selection of phages K1Fg10::gfp using the plasmid pCas9g10 however, did not yield recombinant plaques, nor did it increase the fraction of recombinants within the mix (data not shown). Next, the CRISPR/Cas selection process was applied to the phage mix of phages K1Fg10b::gfp. We used two different selection plasmids: pCas9K1FC1 and pCas9K1FC2, differing only in the encoded crRNA spacer sequences. After two rounds of growth of the phage mix on the two selection strains, recombinant plaques were observed with a frequency of 4/20, but only when using pCas9K1FC2 for selection. Phages retrieved from the positive plaques were further grown on *E. coli* EV36 cells and exposed to plaque assays to re-test for GFPfw-g11rev PCR fragment positivity. For all the four phage lysates, 5/5 plaques displayed the correct PCR product, verifying that the four original plaques of phages K1Fg10b::gfp were homogenous and that the C-terminal minor capsid gene fusions were stably maintained in the phage genomes. PCR analysis with primers g9fw-g11rev from all the four recombinant plaques yielded a single product of 2591 bp, as opposed to the 1831 bp obtained from phage K1F (Suppl. Fig. S2D), again supporting successful *gfp* integration and the clonal nature of the phages K1Fg10b::gfp. Sequencing the g9fw-g11rev region also verified correct integration, apart from a C to T transition at 22829, leading to Thr to Ile change in the C terminal region of the minor capsid protein. Each of the four phage K1Fg10b::gfp lines underwent

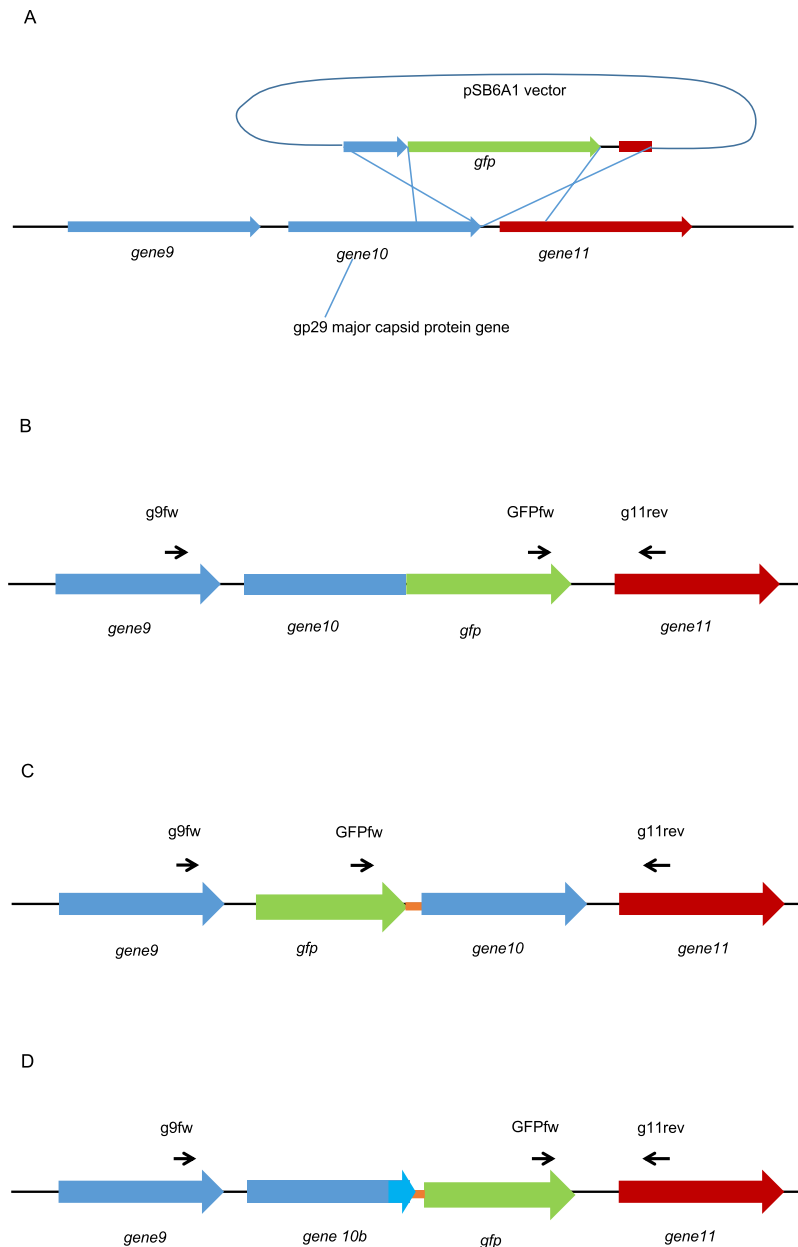


Figure 1. Construction of fluorescent phages K1F. (A) The engineering of three different constructs was attempted using *in vivo* recombination between a plasmid-borne donor DNA and *gene10* of the phage, encoding the major and minor capsid proteins. The double crossover required for recombination is shown for the process generating the C-terminal GFP fusion of the major capsid protein. (B–D) The expected results of the three engineering strategies are displayed: *g10::gfp*, the C-terminal GFP fusion of the major capsid protein-encoding gene (B), *gfp::g10*, the N-terminal GFP fusion of the major capsid protein-encoding gene (C) and *g10b::gfp*, the C-terminal GFP fusion of the minor capsid protein-encoding gene, i.e. *gene10b* (D). Linker peptide-encoding sequences used for the two latter constructs are depicted by orange lines. Thin arrows represent PCR primers used for screening and validation of recombinant phages.

fluorescent microscopic analysis (Fig. 2G,H,I and J). The stable fluorescent phages K1F (K1Fg10b::gfp) were used in the downstream experiments to detect phage K1F localisation in human cells.

K11-displaying *E. coli* EV36-RFP bacteria and engineered phage K1F-GFP invade T24 human urinary bladder epithelial cells. We next examined whether engineered phage K1F-GFP (approximately 1×10^8 PFU/ml) and *E. coli* EV36-RFP bacteria (approximately 2×10^7 CFU/ml) can invade T24 human urinary bladder epithelial cells. It has been shown previously that *E. coli* O18:K1:H7 can enter T24 cells via microtubule and microfilament dependent pathways²⁴. We infected T24 cells with *E. coli* EV36-RFP and stained them with phalloidin (for the actin cytoskeleton) and DAPI (for the nucleus) (Fig. 2A,B). Using confocal microscopy, we observed that *E. coli* EV36-RFP could invade T24 cells. This was further confirmed with live time-lapse

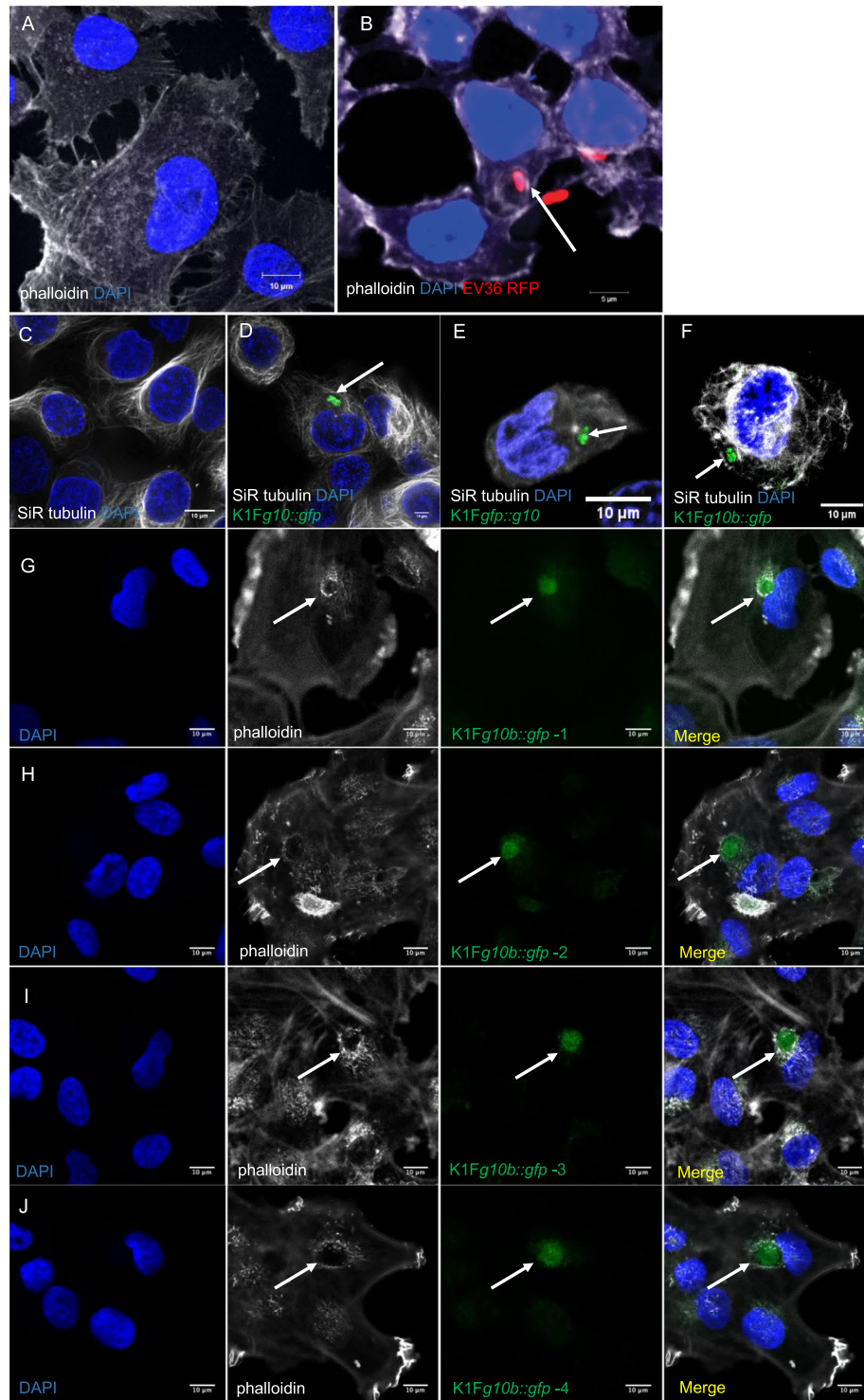


Figure 2. Image analysis of *E. coli* EV36-RFP bacteria and phage K1F-GFP constructs inside epithelial human cells. (A,B) Fluorescent images showing human epithelial T24 cells alone (A) and infected with *E. coli* EV36-RFP (B). DAPI stain is shown in blue. Phalloidin stain is shown in grey. (C–F) Fluorescent images showing human epithelial T24 cells alone (C) and infected with different constructs of fluorescent phages K1F: *g10::gfp* (D), *gfp::g10* (E), *g10b::gfp* (F). Arrows annotate the location of fluorescent phage K1F accumulation in vacuoles. DAPI stain is shown in blue. SiR-tubulin stain is shown in grey. (G–J) Fluorescent images showing T24 cells infected with the four pure fluorescent *g10b::gfp* phages K1F upon *in vivo* CRISPR/Cas selection (Suppl. Fig. S2D). Arrows annotate the location of pure fluorescent *g10b::gfp* phages K1F accumulation in vacuoles. DAPI stain is shown in blue. Phalloidin is shown in grey.

microscopy (Supplementary Fig. S7A). We then stained T24 cells with SiR-tubulin, a live cell microtubule probe and NucBlue Live ReadyProbes for nuclear staining in live cells (Fig. 2C) and we further incubated with C-terminal major capsid protein-labelled phage K1F-GFP mix (K1Fg10::gfp) (Fig. 2D), N-terminal major capsid protein-labelled phage GFP-K1F mix (K1Fgfp::g10) (Fig. 2E) and C-terminal minor capsid protein-labelled pure phage K1F-GFP (K1Fg10b::gfp) (Fig. 2F). In all the above cases, it was shown that phage K1F-GFP invaded T24 cells and localised inside vacuoles. Additionally, it was further confirmed by confocal microscopy (Suppl. Fig. S6A,B) and live time-lapse microscopy (Suppl. Fig. S7B), that phage K1F-GFP co-localised with *E. coli* EV36-RFP (Suppl. Fig. S6B) with great specificity (Suppl. Fig. S6A), indicating that the phage can target the bacteria in a human cell environment. We then continued analysing *in vivo* in more detail the pattern and localisation of the CRISPR-Cas selected four fractions (Suppl. Fig. S2D) of stable phage K1Fg10b::gfp (K1Fg10b::gfp-1 to -4, Fig. 2G–J). It was clearly shown that all the fractions of stable phage K1Fg10b::gfp could invade T24 cells and localise inside vacuoles, as pinpointed with arrows in the phalloidin staining (actin cytoskeleton) (Fig. 2G–J). Collectively these results show that both phage K1F-GFP and *E. coli* EV36-RFP bacteria can invade T24 human urinary bladder epithelial cells.

Engineered phage K1F-GFP efficiently kills intracellular *E. coli* EV36-RFP bacteria in T24 human urinary bladder epithelial cells.

Next, we applied SYTOX Red Dead Cell staining to investigate the ability of phage K1F-GFP to efficiently target and kill both intracellular and extracellular *E. coli* EV36-RFP bacteria. We found that upon phage addition, the percentage of intracellular dead bacteria (Fig. 3A,C) increases significantly (Fig. 3B,C). *E. coli* EV36-RFP showed 29.1% co-localisation with SYTOX ($n = 3$ experiments), whereas upon phage K1F addition, this was increased to 77.6% co-localisation with SYTOX ($n = 3$ experiments). Additionally, we observed co-localisation between bacteria (red), phage (green) and SYTOX (grey), indicating that the bacteria infected by bacteriophage were dying. These results were further confirmed with live time-lapse microscopy (Suppl. Fig. S8A,B). T24 cells were infected with *E. coli* EV36-RFP (Suppl. Fig. S8A) and in the absence of phage K1F-GFP, the bacteria continued to grow and damaged the human cells. In the presence of phage K1F-GFP (Suppl. Fig. S8B), the *E. coli* EV36-RFP infection cleared over time and dead *E. coli* EV36-RFP began to float in the medium and made aggregates that moved via Brownian motions. In order to further confirm that the reduction in the intracellular bacteria is a consequence of phage infection, we performed again the SYTOX assay, this time applying phage K1F on *E. coli* MG1655 bacteria ($n = 3$ experiments), which as shown previously are not sensitive to phage K1F (Suppl. Fig. S8B) and phage T7 on *E. coli* EV36 bacteria ($n = 3$ experiments), which as shown previously are not sensitive to phage T7 (Suppl. Fig. S1A). Our results (Suppl. Fig. S3), present that upon phage addition, in both cases, there was no statistical significant increase in the percentage of intracellular dead bacteria, measured by co-localisation with SYTOX. These results enhance our observations that the increase in intracellular *E. coli* EV36 dead bacteria upon K1F phage addition is due to phage specificity to its host and phage infectivity rather than degradation of the bacteria by the T24 epithelial human cells. We next incubated the culture with gentamycin^{21,24} in order to clear it from extracellular bacteria and subsequently quantified the amount of intracellular *E. coli* EV36-RFP in T24 cells (Fig. 3D,F) to be 26.1% ($n = 3$ experiments). Upon bacteriophage addition, it was observed that phage K1F-GFP could co-localise with intracellular *E. coli* EV36-RFP (Fig. 3E,F) and could target more than half (16.2%, $n = 3$ experiments) of the intracellular *E. coli* EV36-RFP (of 26.1% as above). These results show that engineered phage K1F-GFP can kill intracellular *E. coli* EV36-RFP in T24 human urinary bladder epithelial cells. To estimate the concentration of bacteria to be added to T24 epithelial cells and further understand the correlation between concentration of bacteria added for incubation to human cells and the fraction of cells containing intracellular bacteria, we incubated T24 human cells as previously with *E. coli* EV36-RFP at concentrations ranging from 5×10^6 to 2×10^7 CFU (Suppl. Fig. S4). Based on our observations upon quantification, the concentration of added bacteria strongly correlates with the fraction of human cells harbouring intracellular bacteria. More specifically, when incubated with *E. coli* EV36-RFP (5.65×10^6 CFU/ml), 8.7% ($n = 3$ experiments) of T24 epithelial human cells were invaded, when incubated with *E. coli* EV36-RFP (1.13×10^7 CFU/ml), 12.74% ($n = 3$ experiments) of human cells were invaded, whereas, when incubated with *E. coli* EV36-RFP (2.26×10^7 CFU/ml), 22.74% ($n = 3$ experiments) of T24 epithelial human cells were invaded. Most of the invaded human cells (>95%) carried only a single bacterial cell within. The experiment was performed in biological triplicates and quantified by manually counting a minimum of 125 cells of each experimental condition. For the microscopy observation purposes, it was decided that bacterial concentration higher to 2.26×10^7 CFU/ml on our experimental setting was not preferred, due to defects caused to human cells soon after incubation, and thus causing difficulties to properly quantify the internalised bacteria in single cells. Equally, bacterial concentrations lower to 5.65×10^6 CFU/ml, resulted to a very small amount of intracellular bacteria and thus were not preferred either due to difficulties to identify intracellular bacteria in our microscopic observations.

To assess the dependence of the fraction of phage-containing human cells on the phage concentration, T24 cells were incubated with phage K1F-GFP, with PFUs ranging from approximately 1×10^5 to 1×10^7 (1.4×10^5 , 1.28×10^6 and 1.27×10^7). The samples were observed on the confocal microscope and the number of human cells containing phage-vacuoles were quantified and were further divided by the number of total cells imaged. Upon confocal observation and quantification of internalized phages K1F-GFP, it was estimated that final PFU of approximately 1.28×10^6 resulted in 13.8% ($n = 3$ experiments) of phage K1F-GFP internalized in T24 human cells. PFU approx. 1×10^5 gave weak GFP signal, which we had difficulty to quantify and at PFU 1.27×10^7 , we did not observe any difference compared to PFU 1.28×10^6 , apart from the fact that the GFP signal looked brighter, possibly indicating a higher number of intracellular phages/higher number of phage virions in these cells.

We therefore concluded that the concentration of phages added to the cell culture did not influence the fraction of human cells that have up-taken them, but most probably affected the number of phages per human cell.

Based on previous observations, showing that *C. difficile* bacteriophages are more virulent to their host in the presence of human cells³⁰, we performed similar experiments in our system to investigate whether this is also

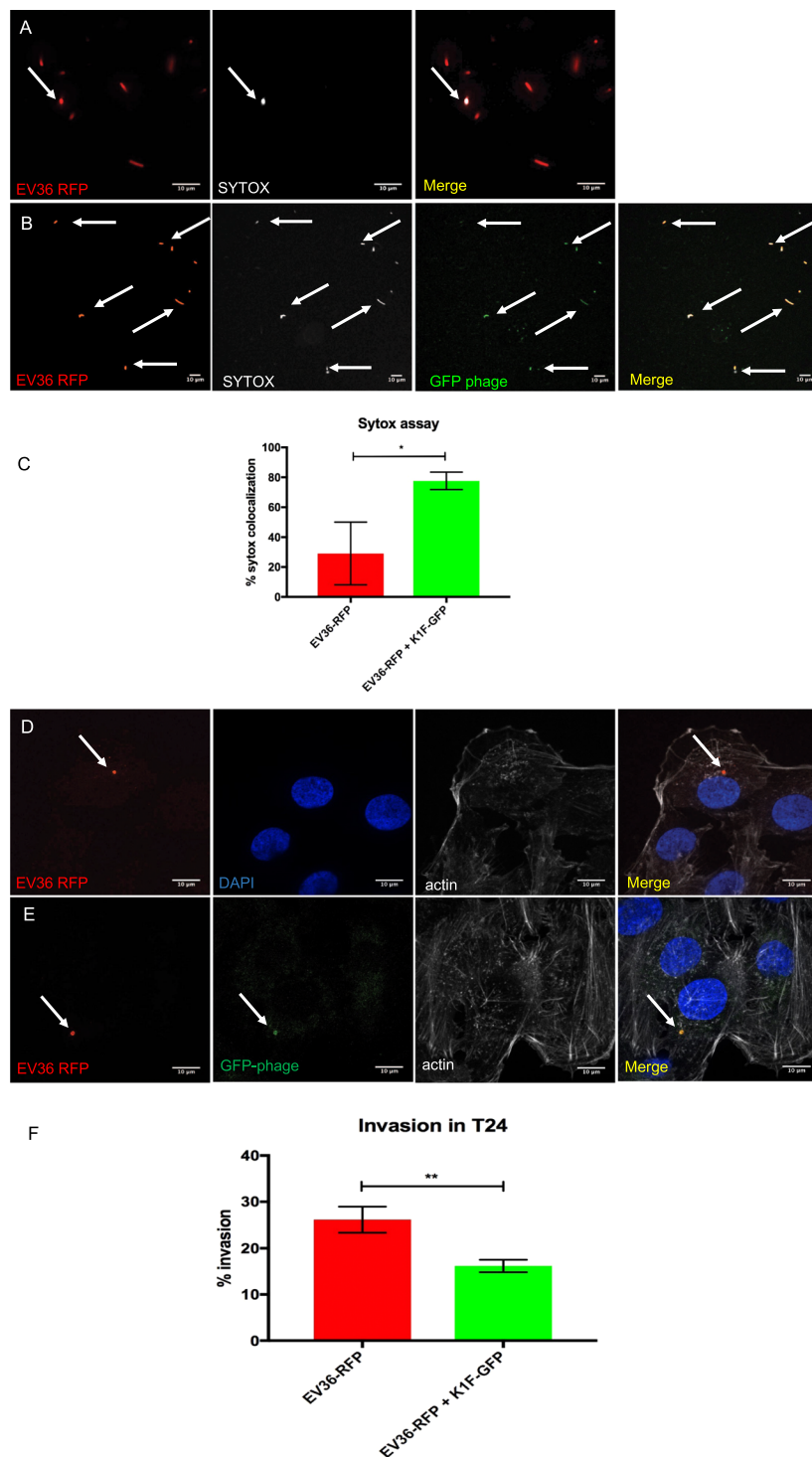


Figure 3. Phage K1F targets extracellular and intracellular bacteria in epithelial human cells. **(A,B)** Live confocal microscopy imaging of *E. coli* EV36-RFP bacteria stained with SYTOX Red Dead Cell stain (here shown in grey). Arrows refer to SYTOX stained cells. **(A)** Negative control sample containing *E. coli* EV36-RFP without phage K1F. **(B)** Sample containing *E. coli* EV36-RFP infected with fluorescent phage K1Fg10b::gfp. **(C)** Quantification of SYTOX stained cells from live confocal imaging showing the percentage of *E. coli* EV36-RFP cells stained with SYTOX prior (29.1%) or upon fluorescent phage K1F addition (77.6%). Comparisons of means were carried out using a Student's t-test with error bars representing \pm SD. Calculated probability values are $p = 0.018$ (*), $n = 3$. **(D-F)** Confocal imaging and quantification of intracellular *E. coli* EV36-RFP and fluorescent phage K1F in human epithelial cells. T24 cells have been stained with Phalloidin as a marker for F-actin and DAPI for DNA-rich nucleus. Each panel represents one channel of a single image. 'Merge' panel shows all channels merged into one image. Each set of panels come from a single image. **(D)** T24 cells have been infected with *E. coli* EV36-RFP and further incubated with gentamycin to ensure the clearance of extracellular bacteria. The arrow indicates intracellular *E. coli* EV36-RFP bacteria. **(E)** T24 cells have been infected with

E. coli EV36-RFP and fluorescent phage K1Fg10b::gfp has been added. The arrows indicate intracellular *E. coli* EV36-RFP and intracellular fluorescent phage K1F co-localising. (F) Quantification of invasion experiments, showing that 26.1% (SD = 2.8) of T24 cells were invaded by intracellular bacteria and above half of those bacteria in total (16.2%, SD = 1.4) were targeted by fluorescent phage K1Fg10b::gfp. Error bars indicate Standard Deviation. Comparisons of means were carried out using a Student's t-test with error bars representing \pm SD. Calculated probability values are $p \leq 0.01$ (**), $n = 3$.

the case with phage K1F and *E. coli* EV36 in the presence of T24 epithelial human cells. Indeed, it was observed (Suppl. Fig. S5A), that the concentration of planktonic bacteria upon phage K1F addition and in the presence of T24 human epithelial cells decreased more rapidly compared to the same conditions in the absence of human cells (at 90 min, 30 min after phage K1F addition, the concentration of planktonic bacteria in the presence of human cells dropped to 1.09×10^8 CFU/ml (SD = 7.22×10^5) compared to 3.13×10^8 CFU/ml (SD = 2.16×10^7) in the absence of human cells, with a statistical significance of $p = 0.00008$). Additionally, the PFU of phage K1F was higher in the presence of human cells when this was compared to the PFU of phage K1F in the absence of human cells (at 120 min, the PFU/ml of phage K1F in the presence of human cells was 5.13×10^{11} (SD = 1.46×10^{11}), whereas in the absence of human cells was estimated 5.65×10^9 (SD = 7.78×10^8), with a statistical significance of $p = 0.018$) (Suppl. Fig. S5B). Interestingly, even when phage K1F was not added, the concentration of planktonic *E. coli* EV36 in the presence of human cells was shown to drop initially (at 90 min, the concentration of planktonic bacteria in the presence of human cells dropped to 6.21×10^8 CFU/ml (SD = 5.91×10^7) compared to 2.92×10^9 CFU/ml (SD = 7.32×10^8) in the absence of human cells (Suppl. Fig. S5A) possibly due to the process of invasion to the T24 epithelial human cells. Overall, these results confirm the previous observation³⁰ that bacteriophages become more efficient in killing their host, in a human cell environment.

Engineered phage K1F-GFP and *E. coli* EV36-RFP bacteria enter T24 human urinary bladder epithelial cells via phagocytosis and are degraded via LC3-associated phagocytosis. Our results obtained up to this point indicated that both bacteria and bacteriophage enter human cells via their engulfment into vacuoles (Fig. 2). To examine this further, we incubated T24 human urinary bladder epithelial cells with either *E. coli* EV36-RFP bacteria (approximately 2×10^7 CFU/ml), phage K1F-GFP (approximately 1×10^8 PFU/ml) or both. The treated cells were subsequently fixed and stained with phagosomal markers, starting with an Rab7 antibody, which has been shown to localise on phagosomes and to be required for phagosomal maturation³¹. We showed that Rab7 co-localises with *E. coli* EV36-RFP (Fig. 4A), phage K1F-GFP (Fig. 4B) and both *E. coli* EV36-RFP and phage K1F-GFP in combination (Fig. 4C), suggesting that *E. coli* EV36-RFP and phage K1F-GFP enter T24 cells via phagocytosis.

It is known that phagosomes are fused with lysosomes where their content is degraded³². To this end, we next tested lysosomal markers to identify whether these co-localise with bacteria and bacteriophage that were previously phagocytosed. Using the same conditions as previously, treated T24 cells were stained with a Cathepsin-L antibody, a marker for lysosomes³³. We observed that Cathepsin-L co-localised with *E. coli* EV36-RFP (Fig. 4D), phage K1F-GFP (Fig. 4E) and both *E. coli* EV36-RFP and phage K1F-GFP in combination (Fig. 4F), suggesting that both bacteria and bacteriophage are delivered upon phagosome maturation into lysosomes to be degraded. Additionally, live imaging of T24 cells stained with LysoTracker Deep Red stain, was performed to track lysosomes based on their acidic properties. We observed that *E. coli* EV36-RFP, phage K1F-GFP and the two in combination co-localise with lysosomes (Fig. 5A).

It has been shown that cells use some components of the autophagy machinery to process extracellular cargo, in a process called LC3-associated phagocytosis^{32,34}. To test this, we treated T24 cells as previously and stained with an LC3 antibody³⁵. It was indeed confirmed that both *E. coli* EV36-RFP (Fig. 5B), phage K1F-GFP (Fig. 5C) and both *E. coli* EV36-RFP and phage K1F-GFP in combination (Fig. 5D), co-localise with LC3, suggesting that these are degraded via LC3-assisted phagocytosis.

***E. coli* EV36-RFP bacteria are degraded by xenophagy.** It has been shown previously that intracellular bacteria can escape the initial phagosome and activate xenophagy (anti-bacterial autophagy) through selective autophagy receptors³². To test this, we incubated T24 human urinary bladder epithelial cells with either *E. coli* EV36-RFP bacteria (approximately 2×10^7 CFU/ml), phage K1F-GFP (approximately 1×10^8 PFU/ml) or both. The treated T24 cells were fixed and initially stained with a Galectin-8 antibody, which has been found to participate in xenophagy via the targeting of damaged vesicles upon bacterial invasion³⁶. Here, Galectin-8 was found to co-localise with 50.6% ($n = 4$ experiments) of intracellular *E. coli* EV36-RFP (Fig. 6A), but only with 24.4% ($n = 4$ experiments) of intracellular phage K1F-GFP (Fig. 6B,C). When intracellular *E. coli* EV36-RFP was infected with phage K1F-GFP, the co-localisation with Galectin-8 was increased to 100.0% ($n = 3$ experiments) (Fig. 6D).

We then repeated the same sets of experiments, this time staining with an NDP52³⁷ antibody, a xenophagy receptor. Upon performing the experiment, we could see NDP52 co-localised with 47.8% ($n = 3$ experiments) of intracellular *E. coli* EV36-RFP (Fig. 6E), suggesting that cytosolic *E. coli* EV36-RFP are degraded via xenophagy. In cells incubated with phage K1F-GFP, it was observed that intracellular bacteriophages alone do not co-localise with NDP52 ($n = 3$ experiments) (Fig. 6F). In the presence of both bacteria and phages (Fig. 6G), the co-localisation of NDP52 with intracellular *E. coli* EV36-RFP infected with phage K1F-GFP, quantified from three different experiments, was found to be 24.9% ($n = 3$ experiments).

Finally, we repeated the same sets of experiments, this time staining with an ubiquitin antibody, as a marker for ubiquitinated proteins³⁴. Ubiquitin was found to co-localise with 89.2% ($n = 3$ experiments) of intracellular *E. coli* EV36-RFP (Fig. 7A), but no co-localisation ($n = 3$ experiments) was observed with intracellular phage

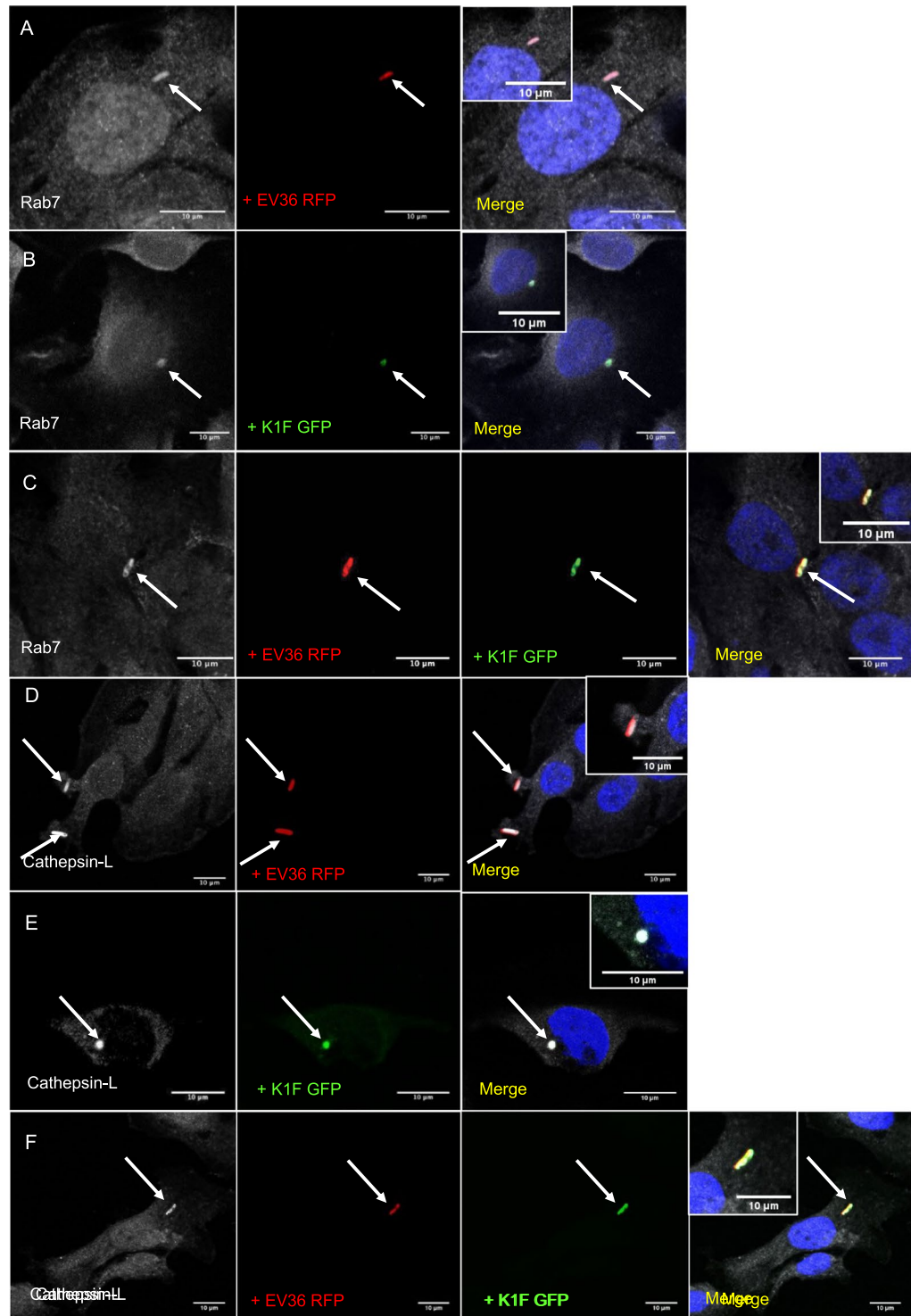


Figure 4. *E. coli* EV36 and phage K1F enter epithelial human cells via phagocytosis and are directed to lysosomes. (A–C) T24 cells infected with *E. coli* EV36-RFP (A), fluorescent phage K1F (B) or both (C), were fixed and stained with anti-RAB7 antibody, a marker for phagosomes. DAPI stain is shown in blue and anti-RAB7 antibody in grey. (D–F) T24 cells infected with *E. coli* EV36 RFP (D), fluorescent phage K1F (E) or both (F), were fixed and stained with anti-Cathepsin-L antibody, a marker for lysosomes. DAPI stain is shown in blue and anti-Cathepsin-L antibody in grey. Arrows represent the RFP-expressing bacteria, GFP-labelled phage and their co-localisation with the corresponding antibody.

K1F-GFP (Fig. 7B). On the contrary, in the presence of both phage and bacteria (Fig. 7C) the co-localisation with ubiquitin increased to 97.8% (n = 3 experiments), indicating that the sole presence of bacteria increases ubiquitination dramatically.

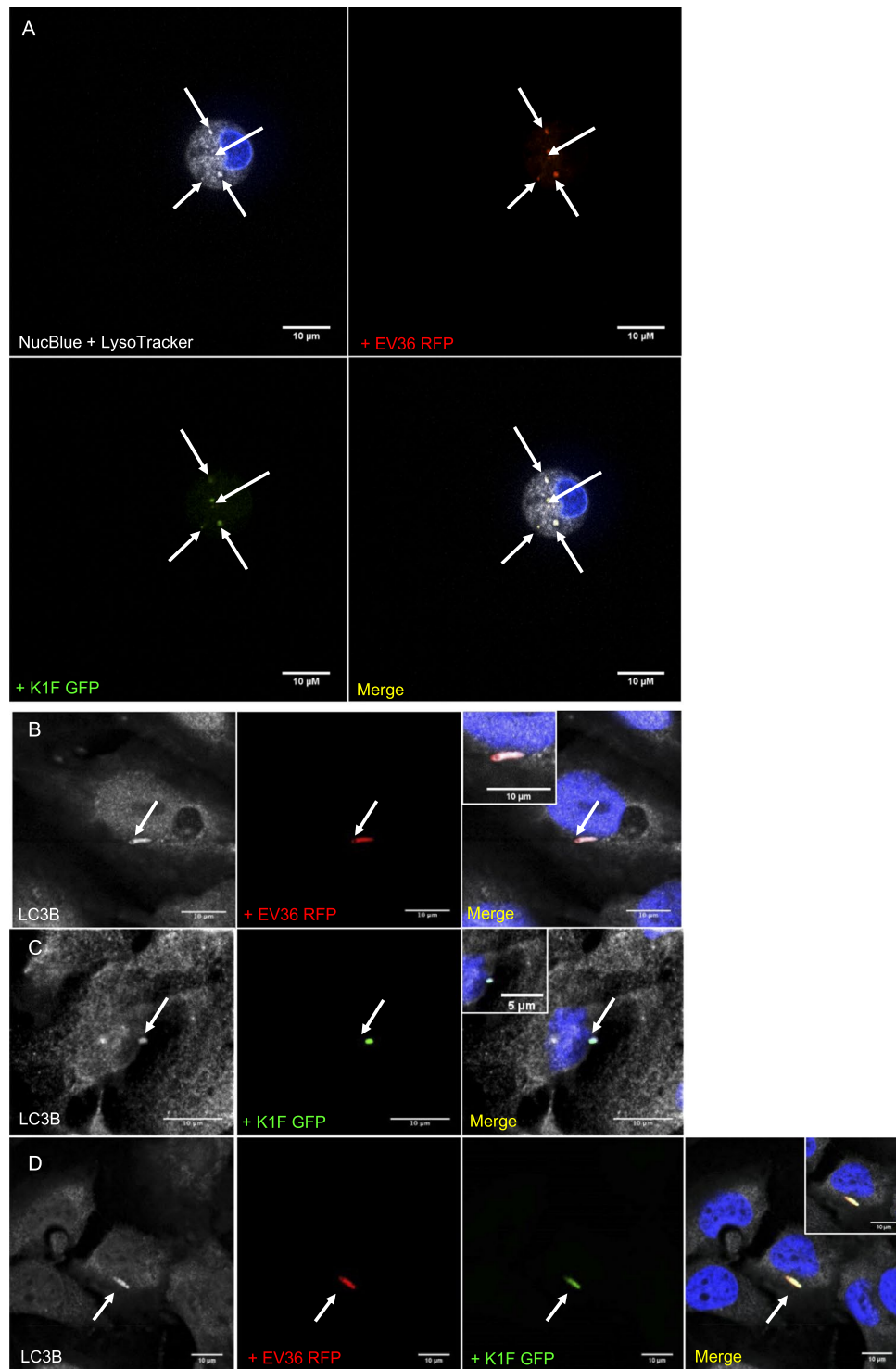


Figure 5. Degradation of *E. coli* EV36 and phage K1F via LC3-assisted phagocytosis. **(A)** Z-stack of live T24 cells infected with *E. coli* EV36-RFP bacteria and fluorescent phage K1F, stained with NucBlue Live ReadyProbes Reagent for the nucleus and LysoTracker Deep Red stain, a marker of acidic organelles in live cells. Shown here is a single image taken from a z-stack. **(B–D)** T24 cells infected with *E. coli* EV36-RFP **(B)**, fluorescent phage K1F **(C)** or both **(D)**, were fixed and stained with anti-LC3B antibody, a marker for LC3-assisted phagocytosis. DAPI stain is shown in blue and anti-LC3B antibody in grey. Arrows represent the RFP-expressing bacteria, GFP-labelled phage and their co-localisation with the corresponding stain/antibody.

These experiments were repeated in triplicates at minimum and the quantification corresponds to the average co-localisation with intracellular bacteria or bacteriophage across all experiments (Fig. 7D). Negative controls for all the secondary antibodies used for the co-localisation assays, verify the validity of these results (Suppl.

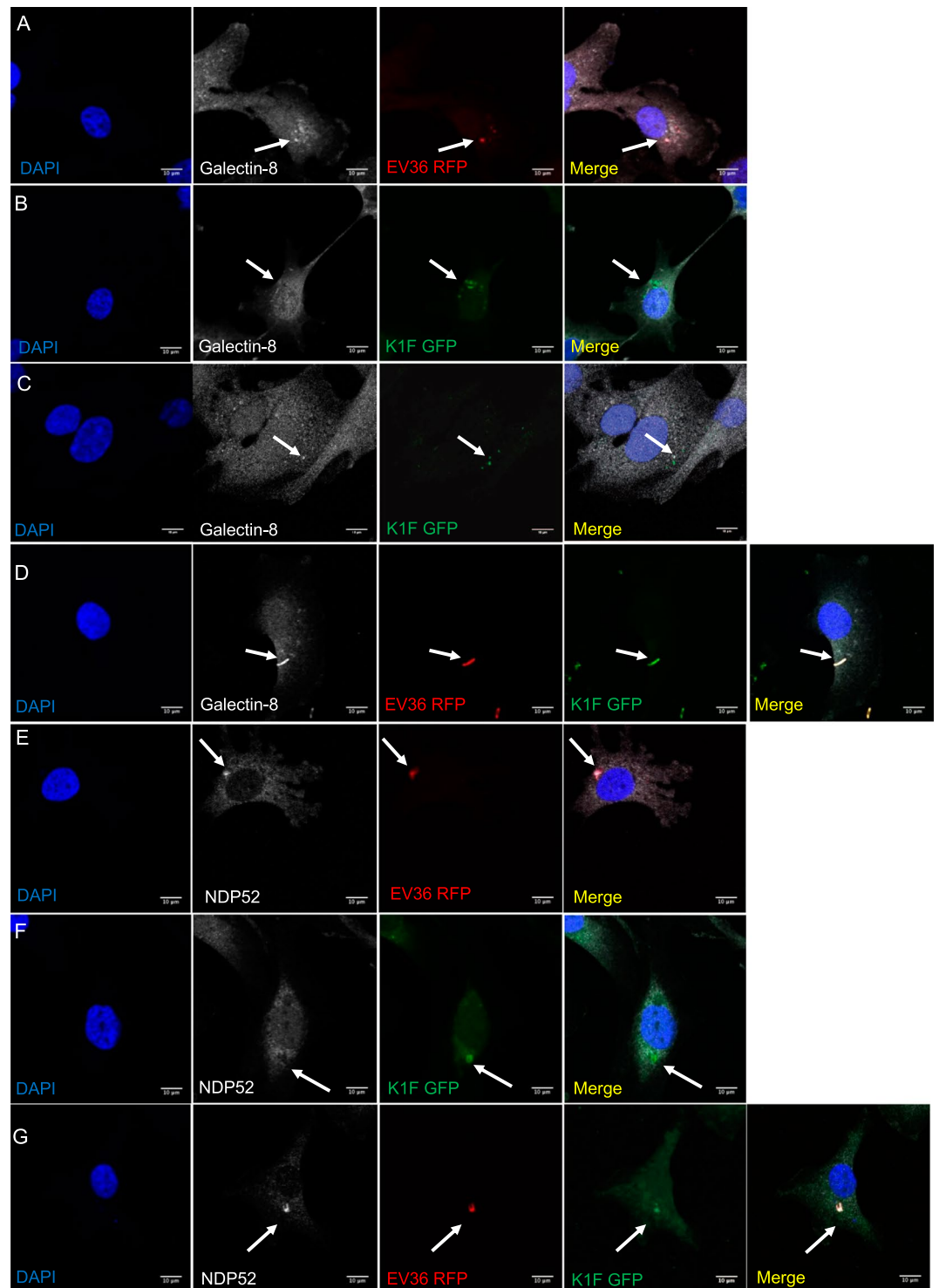
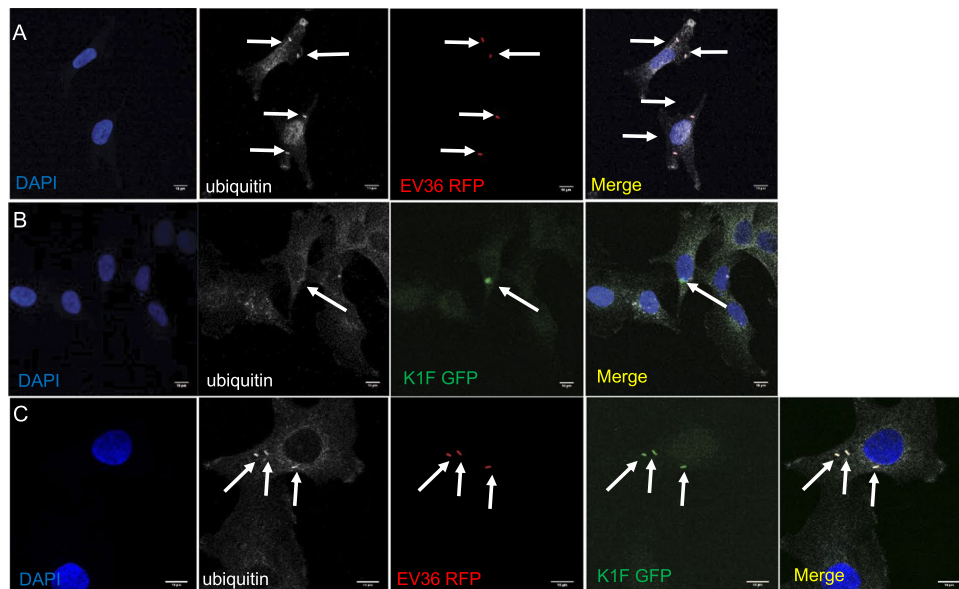


Figure 6. *E. coli* EV36 activates Galectin-8 dependent autophagy. (A–C) T24 cells were incubated with *E. coli* EV36-RFP alone (A), phage K1F-GFP alone (B), or *E. coli* EV36-RFP and subsequently with phage K1F-GFP (C). The cells were then fixed and stained with anti-Galectin-8/LGALS8 antibody as an autophagy marker. Arrows annotate *E. coli* EV36-RFP bacteria, fluorescent phage K1F and co-localisation with anti-Galectin-8 antibody. Images are representative of three independently performed experiments. D–G. T24 cells were incubated with *E. coli* EV36-RFP alone (D), phage K1F-GFP alone (E,F), or *E. coli* EV36-RFP and subsequently added phage K1F-GFP (G). The cells were then fixed and stained with anti-NDP52/CALCOCO2 antibody as an autophagy marker. Arrows annotate *E. coli* EV36-RFP bacteria, fluorescent phage K1F and co-localisation with anti-NDP52 antibody. Images are representative of three independently performed experiments.



D

Colocalization with intracellular endosomal markers

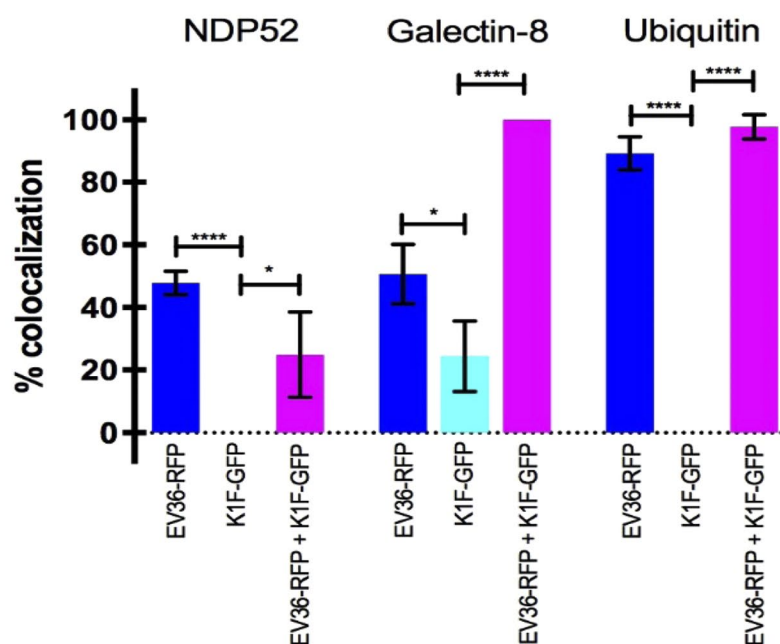


Figure 7. Phage K1F in the absence of *E. coli* EV36 cannot activate autophagy. (A–C) T24 cells were incubated with *E. coli* EV36-RFP alone (A), phage K1F-GFP alone (B), or *E. coli* EV36-RFP and subsequently added phage K1F-GFP (C). The cells were then fixed and stained with anti-ubiquitin antibody as an autophagy marker. Arrows annotate *E. coli* EV36-RFP bacteria, fluorescent phage K1F and co-localisation with anti-ubiquitin antibody. Images are representative of three independently performed experiments. (D) Quantification of co-localisation of endosomal markers with *E. coli* EV36-RFP and phage K1F-GFP alone and in combination. A Student's t-test corrected for multiple comparisons using the Holm-Sidak method was performed using GraphPad Prism 7. The calculated probability values (p-values) are displayed as $p \leq 0.05$ (*), $p \leq 0.01$ (**), $p \leq 0.001$ (***), $p \leq 0.0001$ (****) and not statistical significant $p \geq 0.05$ (ns). $n \geq 3$.

Fig. S6C,D and E). Based on the above results, we propose that both *E. coli* EV36-RFP and phage K1F-GFP invade T24 epithelial human cells via phagocytosis and they can be degraded via LC3-assisted phagocytosis. When *E. coli* EV36-RFP escape the phagosome and become cytosolic they can activate xenophagy, whereas the bacteriophage alone cannot activate xenophagy. In the presence of both phage and bacteria, xenophagy is activated.

Discussion

Bacteriophages are the most abundant viruses residing in the human body even in the absence of disease^{38–40}. In various instances, the presence of bacteriophages within the human body and especially in the gut^{41–45} and in the bladder⁴¹, is regarded to function as a protective mechanism to the human body in the control of pathogens^{46,47}. Recent studies have shown that bacteriophages can even invade human cells, either randomly, via transcytosis across epithelial cell layers⁷, via direct cellular interactions the bacteriophages might have with mammalian cells^{6,8,48,49} or via phagocytosis by macrophages⁵⁰. In this study, we have engineered a fluorescent phage K1F that specifically targets the K1 polysaccharide capsule of *E. coli* EV36. We inserted a *gfp* gene into the phage genome by combining *in vivo* homologous recombination with CRISPR/Cas-selection. The engineering of fluorescent bacteriophages with the insertions of a fluorescent gene in their genome has been applied before, using various methodologies and different bacteriophages, such as T7⁵¹, PP01⁵², T4⁵³, P22^{54,55} as well as the mycobacteriophages D29⁵⁶ and DS6A⁵⁷, where the fluorescent protein is either expressed in the capsid of the phage or in a non-essential region of its genome. We report for the first time the engineering of a fluorescent phage K1F and we have applied for the first time CRISPR/Cas to select for fluorescent bacteriophages. Even though we initially tried to integrate the *gfp* gene into the *gene 10* (*g10*) of the phage's genome, encoding for the major capsid protein of phage K1F, we were not able to isolate recombinant phage due to its fitness defect. This was confirmed by the observation of the formation of very small plaques obtained by plating the phage mix. Plaques with a ten-fold reduced diameter were found in frequencies of 1/94 and 1/135. PCR analysis of these plaques however yielded fragments of unexpected size, indicating the incorrect genomic integration of *gfp*. Our inability to fuse GFP to the C-terminal of gp29 may have resulted from at least two factors. First, the fusion of *gfp* to the 3' of *gene10* interrupts the ORF of *gene10b*. The lack of isolated plaques harbouring the correct construct most likely indicates that infective virions cannot assemble without the minor capsid protein. The presence of both wild type and recombinant phage genomes in the same cell however may allow the packaging of the recombinant DNA into wild type heads, explaining the existence and PCR-positivity of the phage K1F + phage K1Fg10::gfp mix. Second, the lack of a linker peptide between the capsid protein and GFP in the *g10::gfp* construct could severely reduce the fitness of the phage by inhibiting proper capsid protein folding⁵⁸. To avoid these caveats, we attempted to fuse the *gfp* to gene 10b (*g10b*), resulting from a -1 translational frameshift in the 3' region of *g10*, encoding for the minor capsid protein of the phage and the two remaining constructs were designed in a way to harbour a 3xGGGGGS flexible linker connecting the fused proteins. For phage genome editing, we relied on the strategy of providing the donor DNA on a plasmid residing in the bacterial strain used to grow the targeted phage, combined with the CRISPR/Cas selection of recombinant phages^{16,17}. With the above methodology, we managed to generate a stable recombinant fluorescent phage K1F. This has enabled us to observe the invasion of this phage into T24 human epithelial cells via phagocytosis, which was confirmed after our initial observations of invasion of fluorescent phage K1F into vacuoles, with the co-localisation of phage K1F with anti-Rab7 antibody, a protein known to localise into phagosomes and to participate in phagosome maturation³¹. The same was observed also for the *E. coli* EV36-RFP strain, which was also shown to invade T24 epithelial cells via phagocytosis and co-localise with anti-Rab7. It has been shown previously that *E. coli* K1 invades epithelial cells in a process depending on cytoskeletal rearrangements²⁴ and regulated by the expression of the K1 capsule²¹ or via transcytosis⁵⁹, assisted by the outer membrane protein expressed in *E. coli* K1⁶⁰. We clearly present here that the phage K1F by this invasion mechanism can efficiently kill the host bacteria in human cellular environment and importantly can also target intracellular *E. coli* EV36 bacteria. In order to further verify that the killing of the intracellular *E. coli* EV36 is attributed to the efficiency and specificity of phage K1F rather than the potential bacterial degradation by T24 epithelial cells, we performed control experiments with phage T7 and phage K1F coupled with bacterial strains non-sensitive to these phages (*E. coli* EV36 and *E. coli* MG1655 respectively) and upon these conditions we did not observe any increase in the killing of the bacterial strains upon addition of the aforementioned phages. These results confirmed that phage K1F is able to target intracellular host bacteria in human cell environment. This is a novel finding and very informative on the *in vitro* mechanism of phage therapy, providing knowledge that can accelerate this field in the future. Previous observations suggest that phage phiCDHS1 is more virulent to its host *C. difficile* bacteria in epithelial cell environment³⁰. Our results enhance this finding, since we also observed that phage K1F presented higher killing efficiency towards its host *E. coli* EV36 bacteria in the presence of T24 epithelial human cells. Taken together, these results further confirm the hypothesis that there are specific interactions between phages and human cells, possibly in forms of recognition receptors present in phages and human cells, which facilitate the bacterial clearance further during phage treatment³⁰.

Lysosomes (phagolysosomes) are considered the endpoint in the phagocytosis where the mature phagosome fuses with a lysosome and any particles that are contained inside are completely degraded. We showed that both the phage and the bacteria upon phagocytosis, co-localise with Cathepsin-L, an endopeptidase enzyme that plays an important role in lysosome function³³ and this was further confirmed with their co-localisation with LysoTracker Deep Red stain, which also a marker for lysosomes. This is indicative that phage K1F and *E. coli* EV36 bacteria enter the lysosomal degradative pathway, possibly as the result of constitutive maturation of phagosomes. In all the above cases, we showed that bacteria and phage together and independently were found in phagosomes and lysosomes. Uropathogenic *E. coli* bacteria have been shown to subvert the human innate immune system by escaping the phagosome⁶¹. When this vacuole is damaged by effectors released by the bacterium the glycan molecules that are typically enclosed within the cell compartment are exposed to the cytosol. The cell combats this via antibacterial autophagy (xenophagy) mechanisms³². This is typically via galectin-8 or ubiquitin dependent autophagy which both recruit the microtubule-associated protein 1A/1B-light chain (LC3). Our results suggests that *E. coli* EV36 bacteria and phage K1F are able to escape the phagosome and are targeted by autophagy mechanisms. On the contrary, in the presence of phage K1F alone, co-localisation was observed only with Galectin-8 in approximately 20% of the internalized phage, whereas 50% of bacteria alone were shown to co-localise with Galectin-8 and in the presence of both bacteria and phage this was increased to 100%. Phage K1F alone was not

shown to co-localise at all neither with ubiquitin nor NDP52, both further down on the xenophagy pathway, indicating that bacteriophage alone cannot activate autophagy³². From these results, it seems that bacteriophage is degraded via LC3-assisted phagocytosis, rather than autophagy. This would suggest that the bacteriophage does not have the necessary machinery to escape the phagosome in which it was contained. Bacteriophages are found not to be toxic to human cells³⁰ and thus we hypothesize based on our results that unlike their bacterial hosts, bacteriophages are not considered to be harmful for the human body. This hypothesis could explain the differential activation of mechanisms of degradation between phages and bacteria. The host pathogenic bacteria are known to be harmful for the human body and thus activate autophagy³². To our knowledge, there are no reports to this date on the mechanisms that bacteriophages are degraded by. This is the first report presenting a mechanism of bacteriophages' degradation.

Our results overall reveal for the first time the mechanism via which bacteriophages that invade T24 human cells get degraded in comparison to the mechanism of invasion and degradation of their host bacteria. The fluorescent phage K1F that we have engineered provides an excellent tool to discover the pathway that bacteriophages follow in their interaction with bacteria and human cells. Finally, the engineering of this human tissue model system of phage therapy in *E. coli* EV36, mimicking the *E. coli* O18:K1:H7²⁹, a well-defined bacterial strain accountable for a multitude of conditions, has enabled us to unfold the cellular processes underpinning phage therapy. Our study provides an essential platform for engineering synthetic phages against *E. coli* or other antibiotic resistant bacteria as an innovative tool in the AMR fight.

Methods

Tissue cell culture. The human urinary bladder epithelial cell line, T24 (HTB-4), was acquired from LGC Standards (UK) an ATCC (American Type Culture Collection) affiliate. This cell line was originally derived from a bladder transitional cell carcinoma of a female patient.

The T24 cells were cultured in uncoated T75 flasks containing McCoy's 5A (Modified) Medium (Gibco, MA) supplemented with 10% v/v Foetal Bovine Serum (FBS) (Labtech International, UK) and 1% v/v Penicillin-Streptomycin and were maintained at 37 °C in 5% CO₂ under a humidified atmosphere.

Purification of bacteriophages. A single-clone preparation of phage K1F (kindly provided by Dr Dean Scholl²⁷) was obtained by three consecutive infections of *E. coli* EV36 which is a K12/K1 hybrid developed by conjugation of Hfr kps + strain²⁹ (kindly provided by Dr Eric R. Vimr). *E. coli* EV36 was used as an *E. coli* O18:K1:H17 analogue host to grow and purify phage K1F from a single plaque.

The single-clone phage K1F preparation was propagated to a high concentration over many infection cycles of cultures with increasing *E. coli* EV36 concentration. Each propagation culture was centrifuged at 3220 g for 15 minutes at 4 °C after bacterial clearance. The final culture was incubated with 0.2 M NaCl on ice for 1 hour to release phage particles from bacterial membranes and centrifuged at 5000 g for 45 minutes at 4 °C. The supernatant was recovered and incubated with 10% w/v PEG8000 for 16–18 hours at 4 °C to precipitate phage particles. The PEG solution was centrifuged for 25,000 g for 1 hour at 4 °C and the pellet was resuspended in a small volume SM-buffer⁶².

A CsCl density gradient was prepared in water with three solutions in densities of 1.7, 1.5 and 1.3 g/ml. CsCl was added to phage solution to achieve a density of 1.3 g/ml. The CsCl solutions were added to the centrifuge tube in equal volumes starting with the heaviest and subsequently were centrifuged at 125,000 g for 20 hours at 4 °C.

The resulting blue/grey band was extracted and transferred to a clamped dialysis tube with MWCO of 14 kDa and dialysed for 16–18 hours in a SM-buffer with high concentration of NaCl (1 M) followed by 2 times 2 hours in a SM-buffer with low concentration of NaCl (100 mM). Following dialysis the purified bacteriophage was stored at –20 °C.

Determination of phage infection efficiency in liquid culture. The phage infection efficiency and host selectivity were determined in a liquid culture assay. Bacterial cultures of *E. coli* EV36 strain and *E. coli* K-12 MG1655 (ATCC-47076) wild-type⁶³, were inoculated in lysogeny broth (LB)⁶⁴ and incubated in a rotating incubator at 37 °C.

The optical density was measured at 600 nm in 30 minute intervals. Cultures were inoculated with 1 µl wild type phage K1F (PFU 10⁸) or 1 µl T7⁶⁵ (PFU 10¹⁰) phages once they reached their exponential phase after approximately two hours.

Transmission electron microscopy (TEM). 400 mesh copper grids with carbon graphite coating were cleaned and hydrophilized by glow discharge. A 10 µl drop of purified phage K1F was applied to the centre of the mesh and was incubated for 1 minute. The sample was removed and the mesh washed twice with 10 µl drops of water and finally negatively stained with 10 µl 2% uranyl acetate for 1 minute. Images were acquired using the Jeol 2100 transmission electron microscope.

Construction of *E. coli* EV36-RFP bacteria. In order to visualise the location and concentration of bacteria in a human cell environment, fluorescent *E. coli* EV36-RFP bacteria were constructed. *E. coli* EV36 bacteria were made electrocompetent as shown previously⁶⁶ and were transformed with plasmid pSB1C3 (Registry of Standard Biological Parts. http://parts.igem.org/Main_Page) expressing the mRFP1 protein. Cells containing RFP were selected for with chloramphenicol (Cm: 25 µg/ml) and IPTG induction (0.5 mM).

Construction of genetically modified fluorescent bacteriophages. *Strains, buffers and media.* Phage dilutions were made in buffer Φ80 + containing 0.1 M NaCl, 0.01 M Tris (pH 7.9), 0.01 M CaCl₂ and 0.01 M MgCl₂⁶⁷. TBE buffer contained 45 mM Tris, 45 mM boric acid and 1 mM EDTA⁶⁴. Bacteria were grown

in lysogeny broth (LB)⁶⁴. To make soft agarose for phage titering and plaque assays, LB-agar plates were overlain with 0.5% Seakem LE agarose (Lonza, Basel, Switzerland) containing 5 mM CaCl₂ and 5 mM MgCl₂. Antibiotics (Sigma-Aldrich, St. Louis, MO, USA) were used in the following concentrations: ampicillin (Ap): 50 µg/ml, chloramphenicol (Cm): 25 µg/ml.

Plasmid construction. Plasmid pSB6A1 was obtained from Registry of Standard Biological Parts. (http://parts.igem.org/Main_Page). Plasmid pCas9 (Addgene #42876) was the kind gift of Luciano Marraffini (The Rockefeller University), obtained via Addgene. The three donor plasmids used for phage K1F genome editing, pSBGFP, pSBN and pSBC3 were constructed by digesting a synthetic gene cassette ordered from Integrated DNA Technologies (Leuven, Belgium) with EcoRI and PstI and ligating to the corresponding restriction sites of the pSB6A1 plasmid. The synthetic gene cassettes comprised the superfolder Green Fluorescent Protein (GFP) gene flanked by two 150 bp-long homology boxes corresponding to segments of the phage K1F genome in the gene 10 region (for exact DNA sequences, see Table S1).

The three selection plasmids, pCas9g10, pCas9K1FC1 and pCas9K1FC2 were constructed by ligating the respective CRISPR spacers into the BsaI site of pCas9, as described previously⁶⁸. The CRISPR spacers were designed by manually searching for 30 nt long stretches of the wild type phage K1F genome that span the integration site of GFP and end with an NGG. The spacers were synthesized as pairs of complementary oligonucleotides carrying the ends required for cloning (Table S2).

Phage propagation and titering. Routine bacteriophage procedures were conducted as described previously⁶⁹. Briefly, for phage propagation, *E. coli* EV36 cells were grown by agitating at 37 °C in LB medium supplemented with 5 mM CaCl₂ and 5 mM MgCl₂ and were mixed with 10⁶ plaque forming units (PFU) of phage K1F upon reaching an OD₆₀₀ value of 0.5. Complete bacterial lysis was usually observed within 1–2 h of further shaking. At this point, 50 µl of chloroform was added and the lysate was shaken for 5 min, followed by pelleting of the cell debris and filtration of the supernatant with a 0.22 µm Millex GP PES filter (Merck-Millipore, Carrigtwohill, Ireland) to obtain a cell-free phage lysate.

For phage titering and plaque assays, LB plates were overlain with 3 ml of molten soft agarose (cooled to 42 °C) containing 100 µl of midlog-phase *E. coli* EV36 cells. After solidification, 10 µl samples from each member of a dilution series of the phage lysate, ranging from the concentrated solution to 10⁻⁹ dilution was pipetted on top and let to dry. Individual plaques were already visible within the *E. coli* lawn at the appropriate dilutions after 4 h of incubation at 37 °C. The appropriately diluted phage lysate was then mixed with 100 µl of midlog-phase *E. coli* EV36 cells, mixed with 3 ml of molten soft agarose (cooled to 42 °C) and immediately poured onto LB plates at room temperature. After solidification, plates were incubated overnight at 37 °C. The plaque numbers counted the next day were used to calculate phage titers in PFU/ml. To estimate the fraction of recombinant phages in a phage mix, PCRs using primers GFPfw and g11rev were carried out on 1 µl samples from the dilution series of the phage mix. The ratio of the highest dilution factor still yielding a positive PCR and the phage titer (expressed as PFU/µl) gave the approximate fraction of recombinants within the phage mix.

Phage genome engineering via in vivo homologous recombination. To integrate the GFP gene into the genome of phage K1F, wild-type (wt) phages were propagated on *E. coli* EV36 cells harboring the appropriate donor plasmid for 1–3 rounds, as described above. The presence of recombinant phages in the obtained mixed lysate was verified by PCR analysis of the 1000-fold diluted lysate using primers GFPfw and g11rev (Table S2). To acquire pure recombinant phage cultures, the mixed lysate was propagated on *E. coli* EV36 carrying the appropriate selection plasmid. The obtained phage lysate was titered and the appropriate dilution was plated on *E. coli* EV36 to obtain individual plaques. In a plaque-assay, 10–20 plaques were aspirated with cut-off pipette tips as agarose plugs and released each into 40 µl of TBE buffer. After 4 h of incubation at 42 °C and a short vortexing, 0.5 µl of each sample was used as a template in PCR reactions using primers GFPfw and g11rev. The phage suspensions yielding a correct PCR product were titered and plated again on *E. coli* EV36 for a second round of plaque assay to warrant their purity. Positive phage suspensions obtained this way were propagated on *E. coli* EV36 to generate recombinant phage stocks to be further used in infection assays analyzed by microscopy.

Sequencing of recombinant bacteriophages. The sequence of the engineered K1Fg10b::gfp phage genome in the vicinity of the gfp insertion was verified by Sanger capillary sequencing using the ABI Big Dye Terminator v3.1 kit and a 3500 Series Genome Analyzer (Life Technologies-Thermo Fisher Scientific, Waltham, MA, USA). First, the region of interest was PCR-amplified using primers g9fw and g11rev. This 2591 bp-long PCR product was purified using the PCR Advanced PCR Cleanup System (Viogene, Taiwan, China) and sequenced with primers g9fw, g10fw, AS504 and g11rev. The obtained reads were aligned with the expected phage sequence using the Serial Cloner v2.6.1 (Serial Basics Inc.) to assemble to empirical g10b::gfp sequence map. The empirical sequence matched the expected sequence except for a C > T transition at 22264, resulting in a Thr377Ile mutation in the C terminal of g10b.

Immunofluorescence and confocal microscopy. Fluorescent immunocytochemistry was performed to identify the association of bacteria and phage with biological markers of the endolysosomal and autophagy pathways.

For invasion assays, the T24 cells were seeded onto uncoated 22 × 22 mm coverslips in 6-well plates at a density of approximately 4 × 10⁴ cells/cm² in McCoy's 5A (Modified) Medium (supplemented with 10% v/v FBS only, without antibiotics at 37 °C) and were allowed to settle for 24 hours.

The culture media were aspirated and replaced with Leibovitz media (Lonza, Switzerland) that sustain cell viability in the absence of CO₂ equilibrium and the cells were moved to an incubator appropriate for bacterial infections. While maintaining the confluent cultures at 37 °C, the cultures were incubated with *E. coli* EV36-RFP at OD 600 nm of approximately 0.4 to 0.6, which were added to 1 ml of Leibovitz media^{21,24} for 60 minutes following incubation with phages at PFU 1×10^8 for 60 minutes. In parallel, control cultures were incubated with bacteria or phage alone for 60 minutes. For the assays estimating the number of intracellular bacteria, upon infection, the cells were washed with PBS and fresh medium containing 100 µg/ml gentamycin was added for further 2 hours to kill the extracellular bacteria, prior to bacteriophage addition^{21,24}. Phage K1F-GFP was then added as previously for 60 minutes. Immediately thereafter, the cultures were fixed in 4% paraformaldehyde (PFA) (ThermoFisher Scientific, MA), permeabilised in ice-cold PEM buffer with 0.05% Saponin and quenched with 50 mM NH₄Cl in PBS. Appropriate wash step with PBS was performed between each step⁷⁰. In order to estimate further the correlation between the number of intracellular bacteria and the concentration of bacteria added in human cells, T24 human cells were incubated with *E. coli* EV36-RFP at approximate concentrations ranging from 5×10^6 to 2×10^7 CFU/ml for 2 hours. The cells were fixed and further treated as described above.

The fixed cells were stained with the following primary antibodies diluted in 0.05% Saponin in PBS for 45 minutes at room temperature; 40 µg/ml Anti-RAB7 (Bioss Inc, MA), 1 µg/ml Anti-Cathepsin L (Abcam, UK), 5 µg/ml Anti-LC3B (Sigma-Aldrich, MO), 1 µg/ml Anti-CALCOCO2/NDP52 (Abcam, UK), 1 µg/ml Anti-Galectin-8 (R&D Systems, MN) or 1 µg/ml Anti-Mono- and polyubiquitinated conjugates monoclonal antibody (FK2) (Enzo Life Sciences).

This was followed by conjugation with secondary Cy5 Affinipure Donkey Anti-Goat, Anti-Rabbit or Anti-mouse (Jackson ImmunoResearch, PA). Finally, the stained cells were mounted on microscope slides using Fluoroshield Mounting Medium (Abcam, UK) containing DAPI nuclear stain.

Cultures containing GFP tagged bacteriophages were further enhanced with a GFP-Booster (Chromotek, Germany) at a concentration of 5 µg/ml alongside with the conjugation with secondary antibodies. In the context of visualising bacteria and phage in the cell environment without endolysosomal markers, an actin filament stain, Phalloidin CF680R Conjugate (Biotium, CA), was used at a concentration of 5 µg/ml.

All fixed cells were imaged using the Zeiss LSM 880 confocal microscope with Airyscan, with fluorophore excitation at the following wavelengths: DAPI at 405 nm, GFP at 488 nm, RFP at 561 nm and far-red (Cy-5) at 633 nm.

Quantification was performed by manually counting 10–20 images of each experimental condition. A minimum of 200 cells were counted of each experimental condition.

Live cell imaging. The T24 cells were seeded onto uncoated 35 mm glass bottom microscope dishes (ThermoFisher Scientific, MA) at a density of approximately 4×10^4 cells/cm² in McCoy's 5A (Modified) Medium (supplemented with 10% v/v FBS only) and were allowed to settle for 24 hours.

The culture media were aspirated and replaced with Leibovitz medium (Lonza, Switzerland) that sustain cell viability in the absence of CO₂ equilibrium. While maintaining the confluent cultures at 37 °C, the cultures were incubated with *E. coli* EV36-RFP bacteria and phage K1F-GFP as previously. For the SYTOX Bacterial Death Assay, *E. coli* EV36-RFP at OD 600 nm of approximately 0.4 to 0.6, were added to 1 ml of Leibovitz media for 60 minutes. Fluorescent phage K1F was added, at PFU 1×10^8 for another 60 minutes. SYTOX Red dead cell stain (final conc. 5 nM) and 2 drops of NucBlue Live (ThermoFisher Scientific, MA) per 1 ml of Leibovitz medium was added to both samples for the last 20 minutes of the incubation. After the 20 minutes of SYTOX incubation, the cells were ready to be visualized under the Andor/Nikon Spinning Disk Confocal Laser Microscope.

Quantification was performed by manually counting 30–50 images of each experimental condition. A minimum of 200 cells were counted of each experimental condition.

For the live cell imaging with SiR tubulin (SPIROCHROME, Cytoskeleton, Inc.), T24 cells were seeded as previously onto uncoated 35 mm glass bottom microscope dishes (ThermoFisher Scientific, MA). 1 µL of SiR-tubulin and 1 µL Verapamil were added to 1 ml of McCoy's 5A (Modified) Medium (supplemented with 10% v/v FBS only, free from Pen/Strep). This was added to the glass dishes containing confluent T24 cells to stain them for tubulin. After 1-hour of incubation the media were aspirated off to decrease the background of the SiR-tubulin staining and were infected with *E. coli* EV36-RFP bacteria and/or phage K1F-GFP as previously. In the last 20 minutes of infection, NucBlue Live (ThermoFisher Scientific, MA) was added as previously to stain for the nucleus. The samples were then visualized under the Andor/Nikon Spinning Disk Confocal Laser Microscope. In the live cell imaging provided in Supplementary Figures/Videos 7 and 8, when timing was different, it is mentioned on the corresponding figure legends.

***E. coli* EV36-RFP and phage K1F-GFP concentration dependent infection in T24 cells.** T24 cells were seeded on uncoated coverslips in 6-well plates as described previously.

T24 cells maintained in Leibovitz media at 37 °C were incubated with *E. coli* EV36-RFP at approximate concentrations ranging from 5×10^6 to 2×10^7 CFU/ml and incubated for 2 hours. The cells were gently washed twice in PBS to remove planktonic bacteria and were subsequently fixed and permeabilised and stained with Phalloidin CF680R Conjugate as described in immunofluorescence and confocal microscopy section. The same process was repeated with phage K1F-GFP: 1 µl, 10 µl and 100 µl of phage K1F-GFP (stock PFU 1.4×10^8) was added in wells containing T24 cells (corresponding final PFUs/ml: 1.4×10^5 , 1.28×10^6 and 1.27×10^7) and incubated for 1 h. The cells were then treated as previously and were consequently observed with confocal microscopy.

Time course measurements of planktonic bacteria and free phages. T24 cells were seeded in 6-well plates at a density of approximately 2.2×10^4 cells/cm² in McCoy's 5A (Modified) Medium supplemented with 10% v/v FBS and were allowed 48 hours to settle. The culture media was aspirated and replaced with Leibovitz

media and maintained at 37 °C before commencing the experiment. *E. coli* EV36 and phage K1F were added to corresponding wells at approximate final concentrations of 5×10^6 CFU/ml and 3×10^3 PFU/ml respectively. Sampling was performed at 30 minutes intervals over a period of two hours.

Serial dilutions and plating for CFU determination was performed immediately after sampling, whereas samples taken for PFU determination were centrifuged at 3220 rpm for 15 minutes at 4 °C, immediately after sampling, to remove bacterial debris. The phage containing supernatant was stored at 4 °C for plating collectively, following the two-hour sampling period. CFU concentrations were determined by drop assay, plating $4 \times 20 \mu\text{l}$ drops of each 10-fold dilution on LB plates and incubating these for 24 hours at 37 °C. Dilutions selected for CFU quantification accounted for a minimum of 80 colonies of a dilution. PFU concentrations were determined by overlay assay, plating 100 μl phage of each 10-fold dilution with 300 μl host log-phase bacteria in soft agar as described previously under phage propagation and titering. Dilutions selected for PFU quantification accounted for a minimum of 35 plaques of a dilution.

Each experiment was performed in biological triplicates and presented in graphs as the average \pm standard deviation of these.

Statistical analysis. Values are shown as the mean \pm SD of a minimum of three independent experiments in all figures. In liquid infection assays (Suppl. Fig. S1A), comparisons of means were carried out using a student t-test on the SPSS platform. In imaging quantification (Fig. 3C,F, 7D and Suppl. Fig. S4), a Student's t-test corrected for multiple comparisons using the Holm-Sidak method was performed using GraphPad Prism 7. The calculated probability values (p-values) are displayed as $p \leq 0.05$ (*), $p \leq 0.01$ (**), $p \leq 0.001$ (***), $p \leq 0.0001$ (****) and not statistical significant $p \geq 0.05$ (ns).

Data Availability

All data generated or analysed during this study are included in this published article and its supplementary information files. The datasets generated during the current study are available from the corresponding author on reasonable request.

References

- Suttle, C. A. Viruses in the sea. *Nature* **437**, 356–361, <https://doi.org/10.1038/nature04160> (2005).
- Clokic, M. R., Millard, A. D., Letarov, A. V. & Heaphy, S. Phages in nature. *Bacteriophage* **1**, 31–45, <https://doi.org/10.4161/bact.1.1.14942> (2011).
- Wahida, A., Ritter, K. & Horz, H. P. The Janus-Face of Bacteriophages across Human Body Habitats. *PLoS Pathog* **12**, e1005634, <https://doi.org/10.1371/journal.ppat.1005634> (2016).
- Navarro, F. & Muniesa, M. Phages in the Human Body. *Front Microbiol* **8**, 566, <https://doi.org/10.3389/fmicb.2017.00566> (2017).
- Bakhshinejad, B. & Ghiasvand, S. Bacteriophages in the human gut: Our fellow travelers throughout life and potential biomarkers of health or disease. *Virus Res* **240**, 47–55, <https://doi.org/10.1016/j.virusres.2017.07.013> (2017).
- Barr, J. J. A bacteriophages journey through the human body. *Immunol Rev* **279**, 106–122, <https://doi.org/10.1111/imr.12565> (2017).
- Nguyen, S. *et al.* Bacteriophage Transcytosis Provides a Mechanism To Cross Epithelial Cell Layers. *MBio* **8**, <https://doi.org/10.1128/mBio.01874-17> (2017).
- Lehti, T. A., Pajunen, M. I., Skog, M. S. & Finne, J. Internalization of a polysialic acid-binding Escherichia coli bacteriophage into eukaryotic neuroblastoma cells. *Nat Commun* **8**, 1915, <https://doi.org/10.1038/s41467-017-02057-3> (2017).
- Chan, B. K. *et al.* Phage treatment of an aortic graft infected with *Pseudomonas aeruginosa*. *Evol Med Public Health* **2018**, 60–66, <https://doi.org/10.1093/emph/eoy005> (2018).
- Forti, F. *et al.* Design of a broad-range bacteriophage cocktail that reduces *Pseudomonas aeruginosa* biofilms and treats acute infections in two animal models. *Antimicrob Agents Chemother*. <https://doi.org/10.1128/AAC.02573-17> (2018).
- Khalifa, L. *et al.* Defeating Antibiotic- and Phage-Resistant *Enterococcus faecalis* Using a Phage Cocktail *In Vitro* and in a Clot Model. *Front Microbiol* **9**, 326, <https://doi.org/10.3389/fmicb.2018.00326> (2018).
- Burrowes, B., Harper, D. R., Anderson, J., McConville, M. & Enright, M. C. Bacteriophage therapy: potential uses in the control of antibiotic-resistant pathogens. *Expert Rev Anti Infect Ther* **9**, 775–785, <https://doi.org/10.1586/eri.11.90> (2011).
- Sagona, A. P., Grigonyte, A. M., MacDonald, P. R. & Jaramillo, A. Genetically modified bacteriophages. *Integr Biol (Camb)* **8**, 465–474, <https://doi.org/10.1039/c5ib00267b> (2016).
- Pires, D. P., Cleto, S., Sillankorva, S., Azeredo, J. & Lu, T. K. Genetically Engineered Phages: a Review of Advances over the Last Decade. *Microbiol Mol Biol Rev* **80**, 523–543, <https://doi.org/10.1128/MMBR.00069-15> (2016).
- Manor, M. & Qimron, U. Selection of Genetically Modified Bacteriophages Using the CRISPR-Cas System. *Bio Protoc* **7**, <https://doi.org/10.21769/BioProtoc.2431> (2017).
- Martel, B. & Moineau, S. CRISPR-Cas: an efficient tool for genome engineering of virulent bacteriophages. *Nucleic Acids Res* **42**, 9504–9513, <https://doi.org/10.1093/nar/gku628> (2014).
- Kiro, R., Shitrit, D. & Qimron, U. Efficient engineering of a bacteriophage genome using the type I-E CRISPR-Cas system. *RNA Biol* **11**, 42–44, <https://doi.org/10.4161/rna.27766> (2014).
- Bardy, P., Pantucek, R., Benesik, M. & Doskar, J. Genetically modified bacteriophages in applied microbiology. *J Appl Microbiol* **121**, 618–633, <https://doi.org/10.1111/jam.13207> (2016).
- Vimr, E. R. & Steenbergen, S. M. Mobile contingency locus controlling Escherichia coli K1 polysialic acid capsule acetylation. *Mol Microbiol* **60**, 828–837, <https://doi.org/10.1111/j.1365-2958.2006.05158.x> (2006).
- Krishnan, S., Chang, A. C., Stoltz, B. M. & Prasadarao, N. V. Escherichia coli K1 Modulates Peroxisome Proliferator-Activated Receptor gamma and Glucose Transporter 1 at the Blood-Brain Barrier in Neonatal Meningitis. *J Infect Dis* **214**, 1092–1104, <https://doi.org/10.1093/infdis/jiw306> (2016).
- King, J. E., Aal Owaif, H. A., Jia, J. & Roberts, I. S. Phenotypic Heterogeneity in Expression of the K1 Polysaccharide Capsule of Uropathogenic Escherichia coli and Downregulation of the Capsule Genes during Growth in Urine. *Infect Immun* **83**, 2605–2613, <https://doi.org/10.1128/IAI.00188-15> (2015).
- Silver, R. P., Aaronson, W. & Vann, W. F. The K1 capsular polysaccharide of Escherichia coli. *Rev Infect Dis* **10**(Suppl 2), S282–286 (1988).
- Vimr, E. & Lichtensteiger, C. To sialylate, or not to sialylate: that is the question. *Trends Microbiol* **10**, 254–257 (2002).
- Meier, C., Oelschlaeger, T. A., Merkert, H., Korhonen, T. K. & Hacker, J. Ability of Escherichia coli isolates that cause meningitis in newborns to invade epithelial and endothelial cells. *Infect Immun* **64**, 2391–2399 (1996).

25. Huang, S. H. *et al.* Identification and characterization of an *Escherichia coli* invasion gene locus, *ibeB*, required for penetration of brain microvascular endothelial cells. *Infect Immun* **67**, 2103–2109 (1999).
26. Kim, K. J., Elliott, S. J., Di Cello, F., Stins, M. F. & Kim, K. S. The K1 capsule modulates trafficking of *E. coli*-containing vacuoles and enhances intracellular bacterial survival in human brain microvascular endothelial cells. *Cell Microbiol* **5**, 245–252 (2003).
27. Scholl, D. & Merrill, C. The genome of bacteriophage K1F, a T7-like phage that has acquired the ability to replicate on K1 strains of *Escherichia coli*. *J Bacteriol* **187**, 8499–8503, <https://doi.org/10.1128/JB.187.24.8499-8503.2005> (2005).
28. Scholl, D., Adhya, S. & Merrill, C. *Escherichia coli* K1's capsule is a barrier to bacteriophage T7. *Appl Environ Microbiol* **71**, 4872–4874, <https://doi.org/10.1128/AEM.71.8.4872-4874.2005> (2005).
29. Vimr, E. R. & Troy, F. A. Regulation of sialic acid metabolism in *Escherichia coli*: role of N-acetylneuraminidase pyruvate-lyase. *J Bacteriol* **164**, 854–860 (1985).
30. Shan, J. *et al.* Bacteriophages are more virulent to bacteria with human cells than they are in bacterial culture; insights from HT-29 cells. *Sci Rep* **8**, 5091, <https://doi.org/10.1038/s41598-018-23418-y> (2018).
31. Chua, C. E., Gan, B. Q. & Tang, B. L. Involvement of members of the Rab family and related small GTPases in autophagosome formation and maturation. *Cell Mol Life Sci* **68**, 3349–3358, <https://doi.org/10.1007/s00018-011-0748-9> (2011).
32. Randow, F. & Youle, R. J. Self and nonself: how autophagy targets mitochondria and bacteria. *Cell Host Microbe* **15**, 403–411, <https://doi.org/10.1016/j.chom.2014.03.012> (2014).
33. Bhutani, N., Piccirillo, R., Hourez, R., Venkatraman, P. & Goldberg, A. L. Cathepsins L and Z are critical in degrading polyglutamine-containing proteins within lysosomes. *J Biol Chem* **287**, 17471–17482, <https://doi.org/10.1074/jbc.M112.352781> (2012).
34. Lai, S. C. & Devenish, R. J. LC3-Associated Phagocytosis (LAP): Connections with Host Autophagy. *Cells* **1**, 396–408, <https://doi.org/10.3390/cells1030396> (2012).
35. Klionsky, D. J. *et al.* Guidelines for the use and interpretation of assays for monitoring autophagy (3rd edition). *Autophagy* **12**, 1–222, <https://doi.org/10.1080/15548627.2015.1100356> (2016).
36. Thurston, T. L., Wandel, M. P., von Muhlinen, N., Foeglein, A. & Randow, F. Galectin 8 targets damaged vesicles for autophagy to defend cells against bacterial invasion. *Nature* **482**, 414–418, <https://doi.org/10.1038/nature10744> (2012).
37. Thurston, T. L., Ryzhakov, G., Bloor, S., von Muhlinen, N. & Randow, F. The TBK1 adaptor and autophagy receptor NDP52 restricts the proliferation of ubiquitin-coated bacteria. *Nat Immunol* **10**, 1215–1221, <https://doi.org/10.1038/ni.1800> (2009).
38. Rascovan, N., Duraisamy, R. & Desnues, C. Metagenomics and the Human Virome in Asymptomatic Individuals. *Annu Rev Microbiol* **70**, 125–141, <https://doi.org/10.1146/annurev-micro-102215-095431> (2016).
39. Breitbart, M. & Rohwer, F. Method for discovering novel DNA viruses in blood using viral particle selection and shotgun sequencing. *Biotechniques* **39**, 729–736, <https://doi.org/10.2144/000112019> (2005).
40. Moustafa, A. *et al.* The blood DNA virome in 8,000 humans. *PLoS Pathog* **13**, e1006292, <https://doi.org/10.1371/journal.ppat.1006292> (2017).
41. Malki, K. *et al.* Seven Bacteriophages Isolated from the Female Urinary Microbiota. *Genome Announc* **4**, <https://doi.org/10.1128/genomeA.01003-16> (2016).
42. De Sordi, L., Khanna, V. & Debarbieux, L. The Gut Microbiota Facilitates Drifts in the Genetic Diversity and Infectivity of Bacterial Viruses. *Cell Host Microbe* **22**, 801–808, <https://doi.org/10.1016/j.chom.2017.10.010> (2017).
43. Lusiak-Szelachowska, M., Weber-Dabrowska, B., Jonczyk-Matysiak, E., Wojciechowska, R. & Gorski, A. Bacteriophages in the gastrointestinal tract and their implications. *Gut Pathog* **9**, 44, <https://doi.org/10.1186/s13099-017-0196-7> (2017).
44. Mirzaei, M. K. & Maurice, C. F. Menage a trois in the human gut: interactions between host, bacteria and phages. *Nat Rev Microbiol* **15**, 397–408, <https://doi.org/10.1038/nrmicro.2017.30> (2017).
45. Dalmaso, M., Hill, C. & Ross, R. P. Exploiting gut bacteriophages for human health. *Trends Microbiol* **22**, 399–405, <https://doi.org/10.1016/j.tim.2014.02.010> (2014).
46. Gorski, A. & Weber-Dabrowska, B. The potential role of endogenous bacteriophages in controlling invading pathogens. *Cell Mol Life Sci* **62**, 511–519, <https://doi.org/10.1007/s00018-004-4403-6> (2005).
47. Barr, J. J. *et al.* Bacteriophage adhering to mucus provide a non-host-derived immunity. *Proc Natl Acad Sci USA* **110**, 10771–10776, <https://doi.org/10.1073/pnas.1305923110> (2013).
48. Aalto, J., Pelkonen, S., Kalimo, H. & Finne, J. Mutant bacteriophage with non-catalytic endosialidase binds to both bacterial and eukaryotic polysialic acid and can be used as probe for its detection. *Glycoconj J* **18**, 751–758 (2001).
49. Dabrowska, K., Switala-Jelen, K., Opolski, A., Weber-Dabrowska, B. & Gorski, A. Bacteriophage penetration in vertebrates. *J Appl Microbiol* **98**, 7–13, <https://doi.org/10.1111/j.1365-2672.2004.02422.x> (2005).
50. Hodyra-Stefaniak, K. *et al.* Mammalian Host-Versus-Phage immune response determines phage fate *in vivo*. *Sci Rep* **5**, 14802, <https://doi.org/10.1038/srep14802> (2015).
51. Sloatweg, E. J. *et al.* Fluorescent T7 display phages obtained by translational frameshift. *Nucleic Acids Res* **34**, e137, <https://doi.org/10.1093/nar/gkl600> (2006).
52. Oda, M., Morita, M., Unno, H. & Tanji, Y. Rapid detection of *Escherichia coli* O157:H7 by using green fluorescent protein-labeled PP01 bacteriophage. *Appl Environ Microbiol* **70**, 527–534 (2004).
53. Kazmierczak, Z. *et al.* Molecular imaging of T4 phage in mammalian tissues and cells. *Bacteriophage* **4**, e28364, <https://doi.org/10.4161/bact.28364> (2014).
54. Vinay, M. *et al.* Phage-Based Fluorescent Biosensor Prototypes to Specifically Detect Enteric Bacteria Such as *E. coli* and *Salmonella enterica* Typhimurium. *PLoS One* **10**, e0131466, <https://doi.org/10.1371/journal.pone.0131466> (2015).
55. O'Neil, A., Prevelige, P. E., Basu, G. & Douglas, T. Coconfinement of fluorescent proteins: spatially enforced communication of GFP and mCherry encapsulated within the P22 capsid. *Biomacromolecules* **13**, 3902–3907, <https://doi.org/10.1021/bm301347x> (2012).
56. da Silva, J. L. *et al.* Application of BRED technology to construct recombinant D29 reporter phage expressing EGFP. *FEMS Microbiol Lett* **344**, 166–172, <https://doi.org/10.1111/1574-6968.12171> (2013).
57. Mayer, O. *et al.* Fluorescent Reporter DS6A Mycobacteriophages Reveal Unique Variations in Infectibility and Phage Production in Mycobacteria. *J Bacteriol* **198**, 3220–3232, <https://doi.org/10.1128/JB.00592-16> (2016).
58. Werner, S., Marillonnet, S., Hause, G., Klimyuk, V. & Gleba, Y. Immunoabsorbent nanoparticles based on a tobamovirus displaying protein A. *Proc Natl Acad Sci USA* **103**, 17678–17683, <https://doi.org/10.1073/pnas.0608869103> (2006).
59. Burns, J. L., Griffith, A., Barry, J. J., Jonas, M. & Chi, E. Y. Transcytosis of gastrointestinal epithelial cells by *Escherichia coli* K1. *Pediatr Res* **49**, 30–37, <https://doi.org/10.1203/00006450-200101000-00010> (2001).
60. Fagan, R. P. & Smith, S. G. The Hek outer membrane protein of *Escherichia coli* is an auto-aggregating adhesin and invasin. *FEMS Microbiol Lett* **269**, 248–255, <https://doi.org/10.1111/j.1574-6968.2006.00628.x> (2007).
61. Dikshit, N. *et al.* Intracellular Uropathogenic *E. coli* Exploits Host Rab35 for Iron Acquisition and Survival within Urinary Bladder Cells. *PLoS Pathog* **11**, e1005083, <https://doi.org/10.1371/journal.ppat.1005083> (2015).
62. Castro-Mejía, J. L. *et al.* Optimizing protocols for extraction of bacteriophages prior to metagenomic analyses of phage communities in the human gut. *Microbiome* **3**, 64, <https://doi.org/10.1186/s40168-015-0131-4> (2015).
63. Savalia, D., Robins, W., Nechaev, S., Molineux, I. & Severinov, K. The role of the T7 Gp2 inhibitor of host RNA polymerase in phage development. *J Mol Biol* **402**, 118–126, <https://doi.org/10.1016/j.jmb.2010.07.012> (2010).
64. Sambrook, J. *Molecular cloning: a laboratory manual*. (Third edition. Cold Spring Harbor, N.Y.: Cold Spring Harbor Laboratory Press, [2001] ©2001, 2001).
65. Molineux, I. J. The T7 group (2006).

66. Gonzales, M. F., Brooks, T., Pukatzki, S. U. & Provenzano, D. Rapid protocol for preparation of electrocompetent *Escherichia coli* and *Vibrio cholerae*. *J Vis Exp*, <https://doi.org/10.3791/50684> (2013).
67. Blattner, F. R., Fianndt, M., Hass, K. K., Twose, P. A. & Szybalski, W. Deletions and insertions in the immunity region of coliphage lambda: revised measurement of the promoter-startpoint distance. *Virology* **62**, 458–471 (1974).
68. Jiang, W., Bikard, D., Cox, D., Zhang, F. & Marraffini, L. A. RNA-guided editing of bacterial genomes using CRISPR-Cas systems. *Nat Biotechnol* **31**, 233–239, <https://doi.org/10.1038/nbt.2508> (2013).
69. Feher, T., Karcagi, I., Blattner, F. R. & Posfai, G. Bacteriophage recombineering in the lytic state using the lambda red recombinases. *Microb Biotechnol* **5**, 466–476, <https://doi.org/10.1111/j.1751-7915.2011.00292.x> (2012).
70. Sagona, A. P. *et al.* PtdIns(3)P controls cytokinesis through KIF13A-mediated recruitment of FYVE-CENT to the midbody. *Nat Cell Biol* **12**, 362–371, <https://doi.org/10.1038/ncb2036> (2010).

Acknowledgements

This work was supported by the BBSRC Future Leader Fellowship (ref. BB/N011872/1) to A.P.S. and a MIBTP DTP PhD studentship to C.M.O. S.F.S.H was supported by a MBio Master's Program in the University of Warwick. T.F. was supported by the National Research, Development, and Innovation Office of Hungary (NKFIH) Grant No. K119298 and the GINOP-2.3.2-15-2016-00001 grant. We want to acknowledge Dr Dean Scholl, AvidBiotics Corporation, for providing us with the phage K1F and Drs Eric R. Vimr and Susan M. Steenbergen for giving us the *E. coli* EV36 strain. We also want to acknowledge WISB (Warwick Integrative Synthetic Biology Centre), for letting us use their Microscopy Equipment.

Author Contributions

C.M.O. performed experiments, helped in the writing of the manuscript and revised the manuscript, S.F.S.H. performed experiments, R.D.S. performed experiments, T.F. performed experiments, helped in the writing of the manuscript and revised the manuscript and A.P.S. conceived and designed the research, performed experiments and wrote the manuscript. All the authors approved the manuscript.

Additional Information

Supplementary information accompanies this paper at <https://doi.org/10.1038/s41598-018-35859-6>.

Competing Interests: The authors declare no competing interests.

Publisher's note: Springer Nature remains neutral with regard to jurisdictional claims in published maps and institutional affiliations.



Open Access This article is licensed under a Creative Commons Attribution 4.0 International License, which permits use, sharing, adaptation, distribution and reproduction in any medium or format, as long as you give appropriate credit to the original author(s) and the source, provide a link to the Creative Commons license, and indicate if changes were made. The images or other third party material in this article are included in the article's Creative Commons license, unless indicated otherwise in a credit line to the material. If material is not included in the article's Creative Commons license and your intended use is not permitted by statutory regulation or exceeds the permitted use, you will need to obtain permission directly from the copyright holder. To view a copy of this license, visit <http://creativecommons.org/licenses/by/4.0/>.

© The Author(s) 2018



OPEN

Bacteriophage K1F targets *Escherichia coli* K1 in cerebral endothelial cells and influences the barrier function

Christian Møller-Olsen¹, Toby Ross¹, Keith N. Leppard¹, Veronica Foisor³, Corinne Smith¹, Dimitris K. Grammatopoulos^{2,4} & Antonia P. Sagona^{1,5}✉

Bacterial neonatal meningitis results in high mortality and morbidity rates for those affected. Although improvements in diagnosis and treatment have led to a decline in mortality rates, morbidity rates have remained relatively unchanged. Bacterial resistance to antibiotics in this clinical setting further underlines the need for developing other technologies, such as phage therapy. We exploited an *in vitro* phage therapy model for studying bacterial neonatal meningitis based on *Escherichia coli* (*E. coli*) EV36, bacteriophage (phage) K1F and human cerebral microvascular endothelial cells (hCMECs). We show that phage K1F is phagocytosed and degraded by constitutive- and PAMP-dependent LC3-assisted phagocytosis and does not induce expression of inflammatory cytokines TNF α , IL-6, IL-8 or IFN β . Additionally, we observed that phage K1F temporarily decreases the barrier resistance of hCMEC cultures, a property that influences the barrier permeability, which could facilitate the transition of immune cells across the endothelial vessel *in vivo*. Collectively, we demonstrate that phage K1F can infect intracellular *E. coli* EV36 within hCMECs without themselves eliciting an inflammatory or defensive response. This study illustrates the potential of phage therapy targeting infections such as bacterial neonatal meningitis and is an important step for the continued development of phage therapy targeting antibiotic-resistant bacterial infections generally.

Bacterial meningitis is characterised by severe inflammation of the meninges, a network of connective tissues surrounding the brain and spinal cord. The inflammation is a result of bacterial invasion into the subarachnoid space, between the arachnoid and pia mater and can be caused by numerous bacterial species with meningococci, pneumococci, Group B streptococci and *Escherichia coli* being the most prevailing species^{1,2}. These acute and potentially life-threatening infections require rapid diagnosis and initiation of treatment, usually administration of antibiotics and sometimes corticosteroids. The disease is more common in neonates and young children as their immune systems are relatively immature, with incidence rates of 1/5,000 in full-term neonates and 1/500 in low-birth-weight neonates in developed countries. The mortality rate for treated bacterial neonatal meningitis is reported at 5–20%, with significant life-changing neurological sequelae for 25–50% of survivors that include cognitive impairment, deafness, blindness and seizures^{3,4}. *E. coli* strains are a prevalent cause of bacterial neonatal meningitis⁵, in particular, strains that express the K1 capsule⁶, an α -2,8-linked polysialic acid polymer, that covers the surface of the bacteria thus hiding many of its antigenic features. This capsule is believed to enhance its ability to evade the human immune system and to traverse the blood-brain-barrier (BBB)^{5,6}, highlighting the clinical importance of this particular pathogen as a therapeutic target.

Improvements in diagnosis and treatment of bacterial neonatal meningitis have seen a gradual decline in mortality rates in recent decades, while long term post-infection morbidity rates have remained relatively unchanged³. However, the emergence of antibiotic resistance is a major cause of concern and could lead to a resurgence in mortality rates; this is supported by recent epidemiological studies showing declining antibiotic susceptibility of

¹School of Life Sciences, University of Warwick, Gibbet Hill Road, CV4 7AL, Coventry, UK. ²Warwick Medical School, University of Warwick, Gibbet Hill Road, CV4 7AL, Coventry, UK. ³Department of Chemistry, University of Warwick, Gibbet Hill Road, CV4 7AL, Coventry, UK. ⁴Institute of Precision Diagnostics and Translational Medicine, Dept of Pathology, UHCW NHS Trust, Clifford Bridge Road, CV2 2DX, Coventry, UK. ⁵Warwick Integrative Synthetic Biology Centre, University of Warwick, Coventry, CV4 7AL, UK. ✉e-mail: A.Sagona@warwick.ac.uk

clinical isolates derived from the cerebrospinal fluid of meningitis patients⁷. As an increasing number of infections are becoming harder or impossible to treat, there is an urgent need for the development of technologies that can complement or replace conventional antibiotics.

As a re-emerging technology, phage therapy holds great potential for the treatment of resistant and non-resistant bacterial infections, and promising results have been achieved in cases of compassionate use⁸. Virulent bacteriophages (or phages) propagate within a suitable host at the site of infection, ultimately lysing that host and repeating the cycle, allowing for the potential of single-dose administration to eradicate a large number of bacterial cells⁹. Phage therapy was reported to successfully treat meningitis caused by multiple pathogens as early as at the turn of the 21st century^{10,11} manifesting the ability of phages to cross physiological barriers, including the BBB¹², whereas many antimicrobials, including vancomycin, beta-lactams and other hydrophilic antibiotics have reduced penetration across the BBB¹³. Studies performed in a rat meningitis model infected with *E. coli* O25b:H4-ST131, a strain producing extended-spectrum beta-lactamase CTx-M-15, showed 100% and 50% rat survival following administration of phage EC200^{PP} 7 or 24 h post-infection respectively¹⁴.

A comprehensive understanding of phage interactions with human cells on a cellular and molecular level is desired to be able to accurately substantiate the efficacy of the approach. Phages are present on all body surfaces that are in direct contact with the exterior environment, including the skin, urogenital tract, oral cavity, gut and lungs¹⁵, in addition to the blood¹⁶. While their presence in body niches allows them to exert selective pressure on their bacterial hosts and hence to modulate the human microbiome, their presence in the blood allows for direct interaction with mammalian immune cells and the potential for induction of innate and adaptive immune responses¹⁷. Furthermore, the presence of phages in the blood might allow for direct contact with vascular endothelial cells with unknown biological consequences, yet the potential influence and significance of such interactions are yet to be explored.

We present a robust *in vitro* phage therapy model system of neonatal bacterial meningitis based on *E. coli* EV36, phage K1F and hCMECs allowing for a wide range of cellular and molecular analyses. We show that, in hCMEC cultures, phage K1F is phagocytosed and degraded by constitutive- and inducible PAMP-dependent LC3-assisted phagocytosis, does not initiate selective autophagy, and does not induce expression of inflammatory cytokines TNF α , IL-6, IL-8 or IFN β . Conversely, *E. coli* EV36 is degraded by selective autophagy, and a potent inflammatory response is mounted towards the infection in the form of expression of inflammatory cytokines. Additionally, we show that phage K1F temporarily decrease the impedance of hCMEC cultures. This decrease in focal adhesion influences the endothelial barrier function by increasing the barrier permeability and this might represent a mechanism allowing for the transition of immune cells across the endothelial vessel.

Results

***E. coli* EV36 infects human cerebral microvascular endothelial cells in culture.** Infection rates of hCMECs by *E. coli* EV36-RFP were determined by confocal microscopy and flow cytometry (Fig. 1).

The proportion of hCMECs containing intracellular bacteria, as quantified by confocal imaging, was increased in a concentration-dependent manner (Fig. 1A & Suppl. Figure 1). Estimates of infection rates in larger cell populations were obtained by complementary approaches using flow cytometry (Fig. 1B–D). Full separation of RFP fluorescence signals from infected and non-infected cultures was achieved (Fig. 1B). The proportion of infected hCMECs increased in a concentration-dependent manner with increasing bacterial input (Fig. 1C). Additionally, a clear time-dependence of infection was observed in cultures infected at a single concentration (Fig. 1D).

The comparable results obtained by confocal imaging and flow cytometry demonstrated that both methods are applicable for quantifying *E. coli* infection of cultured hCMEC and that this infection is both concentration- and time-dependent.

Bacteriophage K1F host specificity. The host specificity of phages K1F and K1F-GFP towards K1 capsule-expressing bacteria was confirmed by liquid culture growth assays (Fig. 2A,B).

The addition of phages caused the optical density of *E. coli* EV36 cultures to plateau and then to decrease, indicating successful infection (Fig. 2A), with phage K1F-GFP showing some delay in infection in comparison with phage K1F, whereas growth continued unhindered after addition of phage T7. In contrast, phages K1F and K1F-GFP were unable to infect *E. coli* MG1655 as no decrease in optical density was observed (Fig. 2B) whereas phage T7 successfully infected this strain. These data confirmed the high specificity of phages K1F and K1F-GFP towards *E. coli* strains such as EV36, which express the K1 capsule, and also suggest that GFP expression by phage K1F-GFP has some small fitness cost as it kills its host more slowly than phage K1F.

Effect of bacteriophage K1F on the viability and cell wall integrity of *E. coli* EV36. The effect of phage K1F infection on the viability and cell wall integrity of *E. coli* EV36 (Fig. 2C,D) was investigated using flow cytometry.

The addition of phage K1F decreased viability and cell wall integrity of *E. coli* EV36 cultures over time as indicated by an increasing mean fluorescence intensity (MFI) of the membrane-impermeant nucleic acid dyes Sytox (Fig. 2C) and propidium iodide (PI) (Fig. 2D). The temporal differences observed between the two dyes are likely due to the properties and intensities of the dyes themselves. It is noteworthy that a decreasing rate of events was detected from 80 minutes onwards due to bacterial lysis, and that no events were detectable after 140 minutes, suggesting that no live bacteria were present.

Stability of phage K1F-GFP. The stability of phage K1F-GFP was further investigated using flow cytometry (Fig. 2E,F) and electron microscopy (EM) (Fig. 2G).

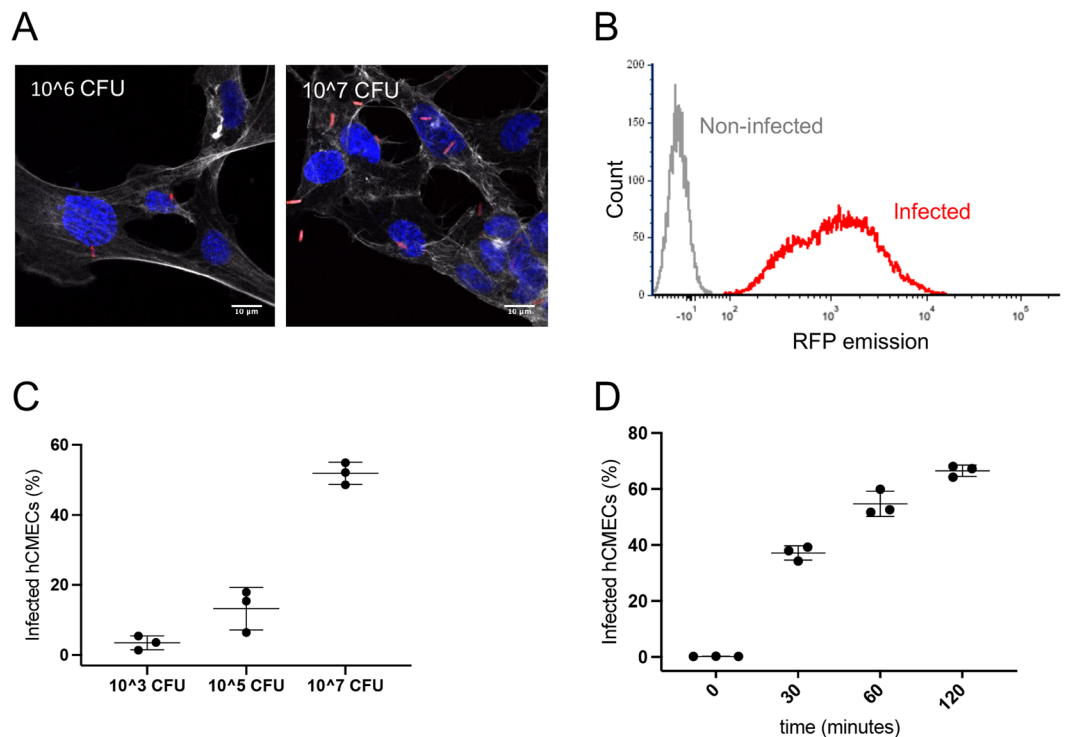


Figure 1. Infection by *E. coli* EV36-RFP of hCMEC cultures. (A) Representative fluorescent images showing *E. coli* EV36-RFP infection of hCMEC cultures at concentrations of 10^6 CFU/ml (left) and 10^7 CFU/ml (right). *E. coli* EV36-RFP fluorescence shown in red, DAPI in blue, and phalloidin in white (B) Flow cytometry histogram showing *E. coli* EV36-RFP infected hCMECs in red and non-infected hCMECs in grey, as detected by RFP fluorescence. (C,D) Mean percentages of *E. coli* EV36-RFP infected hCMECs (RFP-positive by flow cytometry) after a 1 h incubation period with concentrations of 10^3 to 10^7 CFU/ml (C), or 10^7 CFU/ml sampled over time (D); + / - SD, $n = 3$ in each case.

Increasing GFP fluorescence was observed of *E. coli* EV36 cultures infected with phage K1F-GFP (Fig. 2F) over time. No events were recorded after 140 minutes incubation due to bacterial lysis. Two distinguishable populations were observed when comparing the GFP-tagged phage at 0 h and 2 h (Fig. 2E).

Additionally, EM imaging showed that the gold-conjugated probe for GFP binds to phage K1F-GFP in a unique pattern (Fig. 2G); the phages are decorated with the probe in a ring-like shape surrounding the capsid, suggesting that there is enhanced binding of the probe to phage K1F-GFP in comparison with the controls, which showed no specific binding of the probe. This data confirmed the presence and high stability of the GFP fluorophore located on the capsid of phage K1F-GFP.

Endotoxin concentration of phage preparations. The concentration of endotoxin, LPS, in phage preparations used to treat human cell cultures was determined using a Limulus Amebocyte Lysate assay. This was performed to ensure that the molecular and cellular changes observed was caused by phage interactions rather than bacterial remains. Supplementary Fig. 4 shows that phage added to cultures at 10^7 PFU/ml contained 0.0060–0.086 EU/ml and cultures with phage added at 10^9 PFU/ml contained 0.60–1.3 EU/ml. Endotoxin concentrations in this range would enable intravenous administration of phage at a high titre while being well below the recommended 5 EU per kg of body weight per hour¹⁸. While the experimental concentration of endotoxins in this study is very low, the potential effect of trace bacterial contaminants is not accounted for. Therefore, interpretation of data could be skewed by currently unknown effects of trace bacterial debris or interactions of these with phage particles.

Internalisation and degradation of bacteria and phages in human cerebral microvascular endothelial cells. The internalisation and degradation of phage K1F-GFP and *E. coli* EV36 in T24 human urinary epithelial cells has previously been studied in the context of *in vitro* phage therapy¹⁹. Here we expanded on this study using qualitative confocal microscopy and quantitative flow cytometry to examine the internalization and processing of phage K1F in human cerebral microvascular endothelial cells (hCMECs).

Assessment of internalisation and degradation was initially performed as a co-localisation assay between bacteria or phage and phagosomal and lysosomal markers. hCMEC cultures were fixed and stained with antibodies for either RAB7, a GTPase required for the normal progression of late endosomes to lysosomal fusion^{20,21} (Fig. 3A–C), cathepsin-L, a cysteine protease important for lysosomal degradation of engulfed extracellular material²² (Fig. 3D–F), or LC3B, a microtubule-associated protein that is recruited by toll-like receptors for LC3-associated phagocytosis and autophagosome formation²³ (Fig. 4A–C).

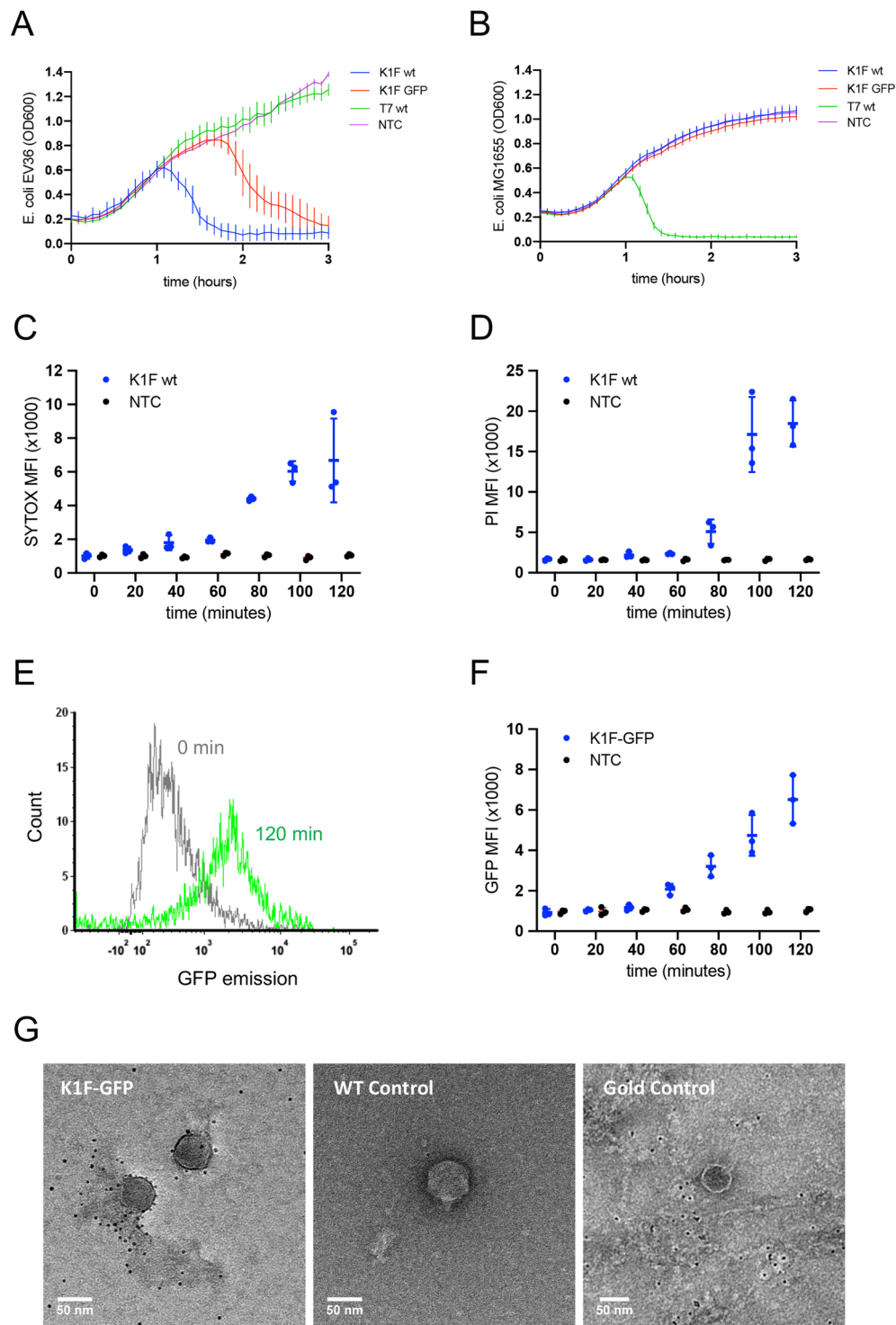
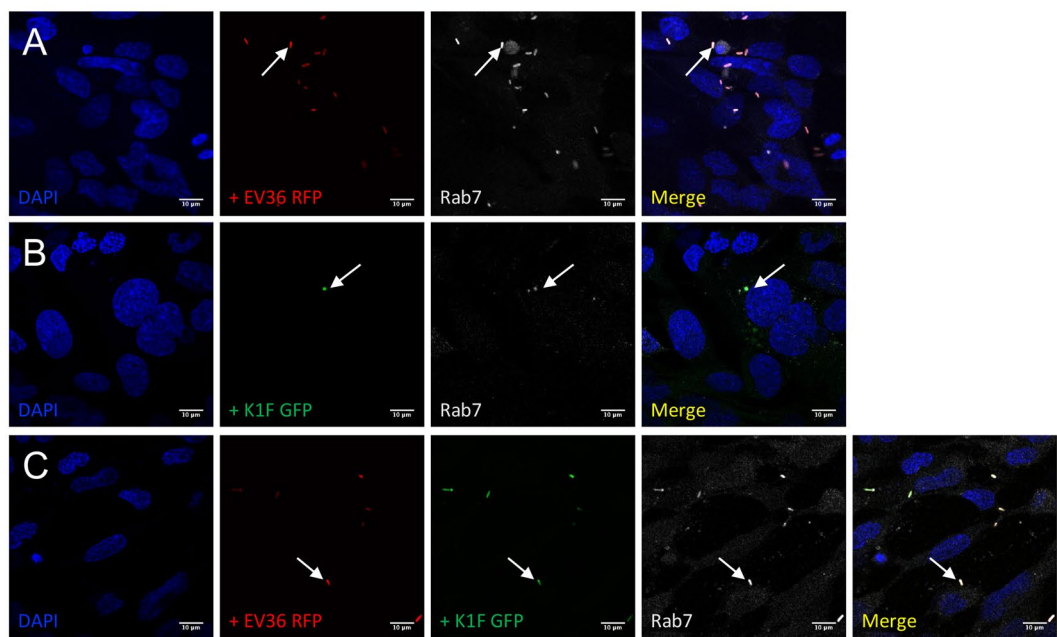


Figure 2. Bacteriophage K1F infection of *E. coli* EV36. **(A,B)** Growth of *E. coli* EV36 **(A)** and *E. coli* MG1655 **(B)** cultures infected by phages K1F, K1F-GFP or T7 at a MOI of 0.001 in comparison with uninfected control cultures, NTC (\pm SD, $n > 3$). **(C–E)** Analysis of bacterial cell death in phage-infected cultures by flow cytometry; *E. coli* EV36 cultures were infected with phage at a MOI of 0.001; NTC = uninfected control **(C)** Sytox Green Dead Cell Stain MFI (\pm SD, $n = 3$) of phage K1F infected *E. coli* EV36. **(D)** Propidium iodide (PI) MFI (\pm SD, $n = 3$) of phage K1F infected *E. coli* EV36. **(E)** Flow cytometry histogram of phage K1F-GFP infected *E. coli* EV36 at 0 min following infection (grey) or 120 min (green). **(F)** GFP MFI (\pm SD, $n = 3$) of phage K1F-GFP infected *E. coli* EV36; NTC = uninfected control. **(G)** Negative staining EM images of sample (Gold-conjugated GFP binding probe with phage K1F-GFP) and controls. Wild-type control is represented by phage K1F incubated with the probe; Gold control was performed using only the 5 nm gold incubated with phage K1F-GFP.

Rab7



Cathepsin-L

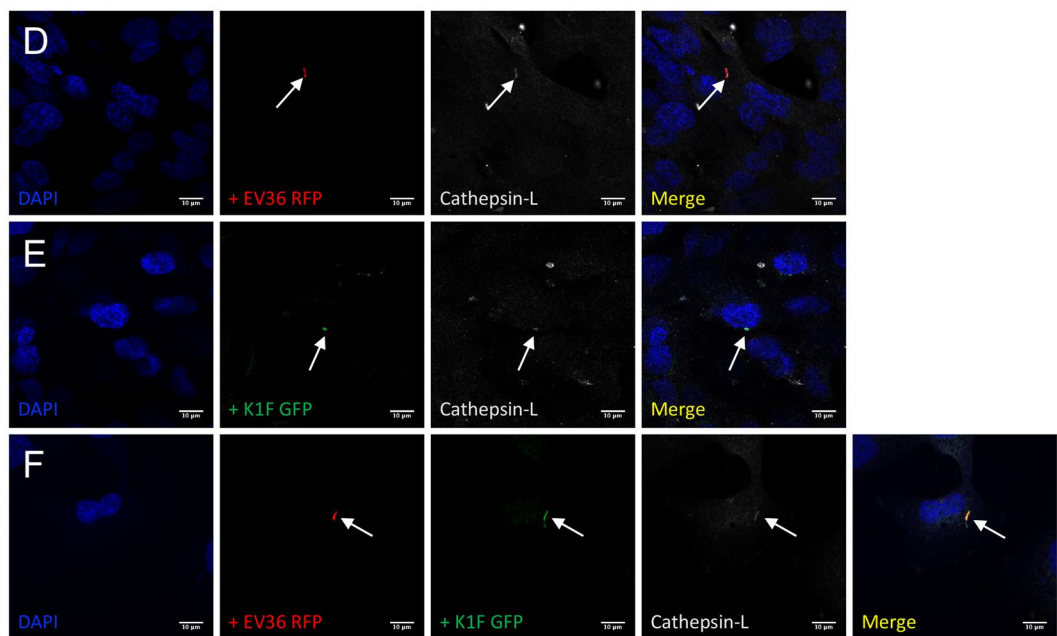


Figure 3. Lysosomal- and phagosomal markers of constitutive phagocytosis. (A–F) Immunofluorescent images showing hCMC cultures fixed and stained with anti-RAB7 (A–C) and anti-Cathepsin-L (D–F) antibodies following a 1 h incubation with 10^7 CFU/ml *E. coli* EV36-RFP alone (A + D) or 10^7 PFU/ml phage K1F-GFP alone (B + E), or a 1 h incubation with 10^7 CFU/ml *E. coli* EV36-RFP followed by a 1 h incubation with 10^4 PFU/ml phage K1F-GFP (C + F). DAPI stain is shown in blue and anti-RAB7/anti-Cathepsin-L antibodies in white. $n = 3$ in each case.

Co-localisation assays in hCMC cultures showed that RAB7, cathepsin-L, and LC3B, all co-localise with *E. coli* EV36-RFP (Fig. 3A,D & 4A), phage K1F-GFP (Fig. 3B,E & 4B), or *E. coli* EV36-RFP and phage K1F-GFP in combination (Fig. 3C,F & 4C). RAB7 and cathepsin-L co-localisation suggested that *E. coli* EV36-RFP and phage K1F-GFP alike are internalised by constitutive phagocytosis and following a maturation process, these vesicles fuse with lysosomes. Constitutive phagocytosis is a continual process whereby the human cells sample the extracellular space and uptake inert particles such as some nutrients²⁴. Additionally, LC3B co-localisation suggests that components of the autophagy pathway are activated via inducible LC3-assisted phagocytosis²⁵.

LC3B

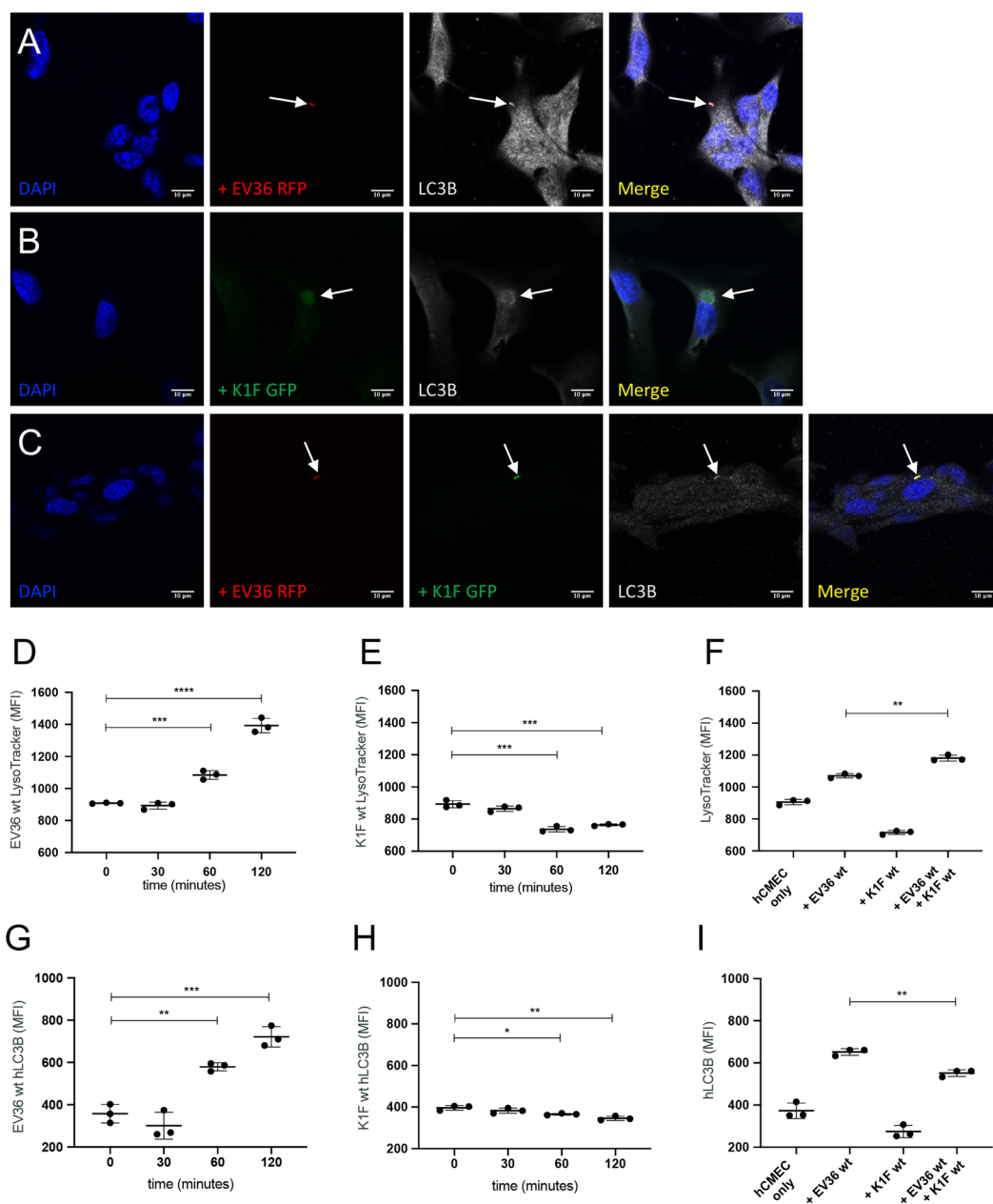


Figure 4. Markers of LC3-assisted phagocytosis and lysosomal activity. (A–C) Immunofluorescent images showing hCMEC cultures fixed and stained with anti-LC3B antibody following a 1 h incubation with 10^7 CFU/ml *E. coli* EV36-RFP alone (A) or 10^7 PFU/ml phage K1F-GFP alone (B), or a 1 h incubation with 10^7 CFU/ml *E. coli* EV36-RFP followed by a 1 h incubation with 10^4 PFU/ml phage K1F-GFP (C). DAPI stain is shown in blue and anti-LC3B antibody in white. $n = 3$ in each case. (D,E) Analysis by flow cytometry. (D–F) Graphs showing LysoTracker MFI (\pm SD, $n = 3$) of hCMEC cultures incubated with 10^7 CFU/ml *E. coli* EV36 alone (D) or 10^7 PFU/ml phage K1F alone (E) over time, or in combination after 1 h incubation (F). (G,H) Graphs showing anti-hLC3B MFI (\pm SD, $n = 3$) of hCMEC cultures treated with 10^7 CFU/ml *E. coli* EV36 (G) or 10^7 PFU/ml phage K1F (H) over time, or in combination after 1 h incubation (I). Probability values (p-values) are displayed as $p \leq 0.05$ (*), $p \leq 0.01$ (**), $p \leq 0.001$ (***), $p \leq 0.0001$ (****).

Confocal microscopy image analysis also confirmed observations of previous studies performed in T24 human urinary epithelial cells¹⁹, showing the ability of phage K1F-GFP to locate and infect *E. coli* EV36-RFP in a human cell environment and the formation of intracellular vacuoles containing phage-aggregates in human cells.

In addition, quantitative flow cytometry was used to measure the MFI of LysoTracker (Fig. 4D–F) and hLC3B (Fig. 4G,H). The LysoTracker is a pH-sensitive, membrane-permeable dye that labels acidic organelles with high selectivity²⁶. The data showed a sharp increase over time of LysoTracker MFI of hCMEC cultures treated with *E. coli* (Fig. 4D), suggesting a shift in endosomal pathway activity towards an increased lysosomal activity, whilst

hCMEC cultures treated with phage K1F showed a lesser gradual decrease (Fig. 4E). hCMEC cultures treated with *E. coli* EV36 and phage K1F in combination showed a small increase of LysoTracker MFI in comparison with cells treated with *E. coli* EV36 alone (Fig. 4F). This increased LysoTracker activity observed, is likely the result of an increase in bacterial debris, in the form of lipopolysaccharides (LPS), released by phage lysis.

Similarly, staining of hCMEC cultures stained with an hLC3B antibody showed a sharp increase over time following incubation with *E. coli* EV36 (Fig. 4G), while hCMEC cultures treated with phage K1F showed a lesser gradual decrease (Fig. 4H). hCMEC cultures treated with *E. coli* EV36 and phage K1F in combination (Fig. 4I) showed a small but significant decrease of hLC3B MFI in comparison with *E. coli* EV36 treatment alone. This observed decrease could translate to a quicker progression from phagosome maturation to lysosome degradation induced by the release of endotoxins following phage lysis.

Degradation of bacteria and phages by xenophagy. Alongside LC3-assisted phagocytosis, anti-bacterial selective autophagy (xenophagy) can occur when bacteria, internalised by phagocytosis, attempt to escape into the cytosol by rupturing the encapsulating membrane²⁵. A further three antibodies were selected to distinguish between LC3-assisted phagocytosis and xenophagy: Galectin-8, a cytosolic lectin which monitors endosomal membrane integrity and responds to membrane damage by binding to exposed glycans²⁷ (Fig. 5A–C), NDP52, a cargo-receptor that, when recruited by Galectin-8, initiates the formation of an autophagosome which triggers selective autophagy²⁸ (Fig. 5D–F) and ubiquitin, the deposition of which on exposed cytosolic bacteria is sensed by a range of receptors, including NDP52, and ultimately restricting bacterial proliferation and initiating xenophagy²⁹ (Fig. 6A–C).

Intracellular *E. coli* EV36-RFP in hCMEC cultures co-localised with antibodies for Galectin-8 (Fig. 5A), NDP52 (Fig. 5D) and ubiquitin (Fig. 6A), suggesting that *E. coli* EV36-RFP is capable of rupturing the phagosomal membrane and initiating xenophagy. In contrast, image data showed no co-localisation between intracellular vacuoles containing phage K1F-GFP and either Galectin-8 (Fig. 5B), NDP52 (Fig. 5E), or ubiquitin (Fig. 6B), suggesting that phage K1F-GFP is solely degraded by constitutive- and LC3-assisted phagocytosis and does not initiate xenophagy. Additionally, hCMEC cultures infected with *E. coli* EV36-RFP and phage K1F-GFP in combination displayed identical co-localisation patterns to that of *E. coli* EV36-RFP infection alone, with co-localisation of both bacterial and phage signals with antibodies for Galectin-8 (Fig. 5C), NDP52 (Fig. 5F) and ubiquitin (Fig. 6C), indicative of xenophagy.

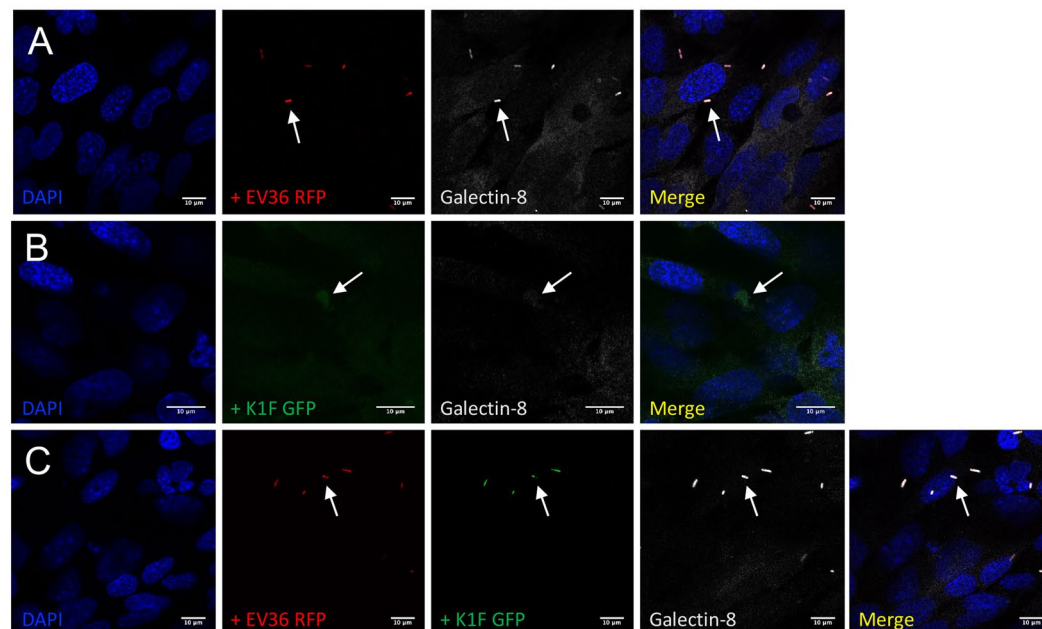
Additionally, flow cytometry was performed to quantify the ubiquitin-mediated contribution to degradation (Fig. 6D–F). hCMEC cultures incubated with *E. coli* EV36 showed an increase in ubiquitin MFI over time eventually reaching a plateau (Fig. 6D), while no difference was observed of hCMEC cultures incubated with phage K1F alone (Fig. 6E) or *E. coli* EV36 and phage K1F in combination (Fig. 6F). These data replicated the results obtained by imaging, suggesting that *E. coli* EV36 alone and not phage K1F, can initiate xenophagy.

Expression pattern of inflammatory markers of hCMEC cultures. The inflammatory response of human cerebral endothelial cells to *E. coli* EV36 and phage K1F individually and in combination was investigated by measuring the induction of inflammatory markers TNF α , IL-6, IL-8, IL-10 and IFN β using real-time qPCR. hCMEC cultures treated with TNF α was included as a positive control for induction of expression (Fig. 7). TNF α is considered a master regulator of inflammation and is implicated in the pathogenesis of bacterial, viral, and chronic inflammatory disease. In response to TNF α , vascular endothelial cells will increase leucocyte adhesion and trans-endothelial migration illustrating its central role as a pro-inflammatory cytokine in clearing an infection³⁰. While hCMEC cultures treated with phage K1F showed no change in the expression levels of TNF α over time (Fig. 7A), cultures treated with *E. coli* EV36 showed a significant and sharp increase (Fig. 7B). The TNF α expression induced by *E. coli* EV36 infection was reduced by approximately 50% with the addition of phage K1F (Fig. 7D). The onset of measurable TNF α induction occurs from 2 hours incubation with bacteria and beyond (Fig. 7B), which correlated with bacterial clearance (Fig. 2), suggesting that the measured expression at the 6-hour endpoint is independent of the presence of live bacteria.

During infections, IL-6, a pleiotropic cytokine involved in both acute and acquired immunity, and also in neural development and function, is rapidly produced to stimulate host defences such as induction of C-reactive protein expression, the concentration of which is directly related to the severity of infection^{31–33}. Over time, hCMECs treated with phage K1F showed no statistically significant change in the expression levels of IL-6 (Fig. 7E), while cultures treated with *E. coli* EV36 (Fig. 7F) showed a gradual time-dependent increase. Control cultures treated with TNF α (Fig. 7G) showed a weaker response characterised by a gradual time-dependent increase throughout the incubation period. Contrary to TNF α , IL-6 expression induced by *E. coli* EV36 treatment (Fig. 7H) was increased more than 200% with the addition of phage K1F, whilst no difference was observed between phage K1F incubation time points. This suggests that, in the context of phage therapy, the inflammation measured as the expression of IL-6 of hCMEC cultures is mainly induced by the influx of bacterial endotoxins released by phage lysis rather than the bacterial infection itself. TNF α and IL-6 are typically both induced by such a stimulus, often attributed to the action of NF- κ B; however, the TNF α response to NF- κ B is complex and negatively affected by the action of other cell type-specific factors that compete for its binding to the promoter³⁴ which may explain the discordance in activation of TNF α and IL-6 in our experiments.

IL-8 is a potent chemokine involved in the inflammatory response, specifically attracting and activating neutrophils at the site of infection, and is associated with many chronic inflammatory conditions³⁵. hCMEC cultures incubated with phage K1F showed no difference in IL-8 expression over time (Fig. 7I). *E. coli* EV36 treatment, on the contrary, induced a time-dependent increase of IL-8 expression of hCMEC cultures (Fig. 7J). A faster onset of increased IL-8 expression was observed in hCMEC cultures treated with TNF α (Fig. 7K). The induced expression of IL-8 following *in vitro* phage therapy of hCMEC cultures (Fig. 7L), was comparable to that of IL-6 expression, showing an average increase above 150% following phage K1F addition in relation to *E. coli* EV36 treated cultures

Galectin-8



NDP52

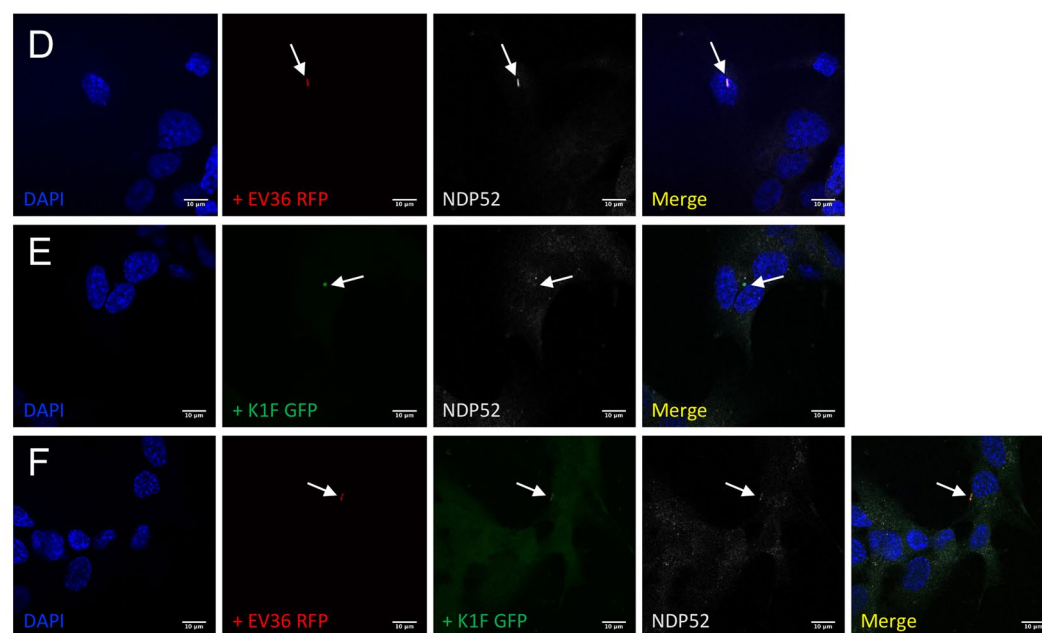


Figure 5. Markers of xenophagy. (A–F) Immunofluorescent images showing hCMCEC cultures fixed and stained with anti-Galectin-8 (A–C) and anti-NDP52/CALCOCO2 (D–F) antibodies following a 1 h incubation with 10^7 CFU/ml *E. coli* EV36-RFP alone (A + D) or 10^7 PFU/ml phage K1F-GFP alone (B + E), or a 1 h incubation with 10^7 CFU/ml *E. coli* EV36-RFP followed by a 1 h incubation with 10^4 PFU/ml phage K1F-GFP (C + F). DAPI stain is shown in blue and anti-Galectin-8/anti-NDP52 antibodies in white. $n = 3$ in each case.

alone. No difference was observed between the three time points of phage K1F addition. As with IL-6 induction, the data suggests that the hCMCECs respond in a higher degree to bacterial endotoxins released by bacterial clearance following phage therapy than the actual bacterial infection itself.

The production of inflammatory cytokines in response to a stimulus is mediated mainly through new transcription of cytokine genes³⁶ and indeed levels of cytokine mRNA were close to zero in the absence of a stimulus. We confirmed mRNA induction by stimulus was reflected in protein levels for IL-6 as an exemplar, using ELISA (Fig. 7Q–T). For all conditions, there was a striking correlation between IL-6 protein levels over time and their respective mRNA expression profiles.

Ubiquitin

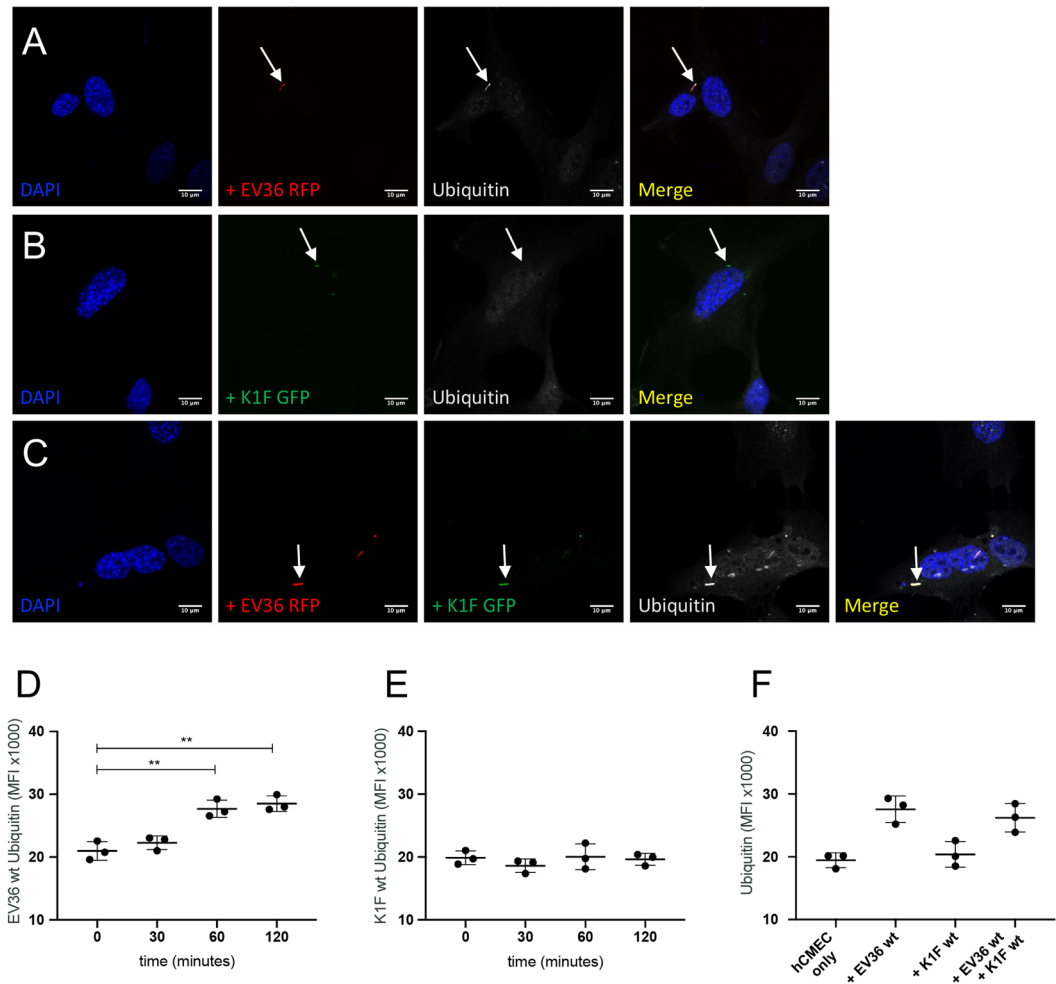


Figure 6. Ubiquitin targeted degradation. (A–C) Immunofluorescent images showing hCMCEC cultures fixed and stained with anti-Ubiquitin antibody following a 1 h incubation with 10^7 CFU/ml *E. coli* EV36-RFP alone (A) or 10^7 PFU/ml phage K1F-GFP alone (B), or a 1 h incubation with 10^7 CFU/ml *E. coli* EV36-RFP followed by a 1 h incubation with 10^4 PFU/ml phage K1F-GFP (C). DAPI stain is shown in blue and anti-Ubiquitin antibody in white. $n = 3$ in each case. (D–F) Graphs showing anti-Ubiquitin MFI (\pm SD, $n = 3$) obtained by flow cytometry of hCMCEC cultures incubated with 10^7 CFU/ml *E. coli* EV36 alone (D) or 10^7 PFU/ml phage K1F alone (E) over time, or in combination after 1 h incubation (F). Probability values (p-values) are displayed as $p \leq 0.05$ (*), $p \leq 0.01$ (**), $p \leq 0.001$ (***), $p \leq 0.0001$ (****).

The anti-inflammatory cytokine, IL-10, is known to play a role in limiting host immune responses towards pathogens³⁷. In these experiments, the data showed no change in IL-10 expression over time following incubation with *E. coli* EV36 or phage K1F alone or in combination (Suppl. Figure 5).

IFN β was included in these experiments to complement the broadly inflammatory cytokines already measured with a cytokine that has a known virus inducible expression. Expression of IFNs, including IFN β , has been shown to be induced by activation of pattern recognition receptors in the early stages of viral infection^{38,39}.

hCMCEC cultures incubated with phage K1F showed no induced expression of IFN β over time (Fig. 7M), however, cultures incubated with *E. coli* EV36 showed a small time-dependent increase of IFN β expression (Fig. 7N). hCMCEC cultures incubated with TNF α showed a barely significant induction of IFN β (Fig. 7O). hCMCEC cultures treated with both *E. coli* EV36 and phage K1F exhibited responses characterised by a greater variation within and between experiments of induced expression of IFN β yielding no statistically significant differences between treatments. Collectively, the IFN β data suggest that phage K1F does not induce inflammatory responses of IFN β in hCMCEC cultures and that the IFN β expression induced by *E. coli* EV36 is more variable and smaller than the induced expression of TNF α , IL-6 and IL-8.

Temporal impedance profiles of hCMCEC cultures. The temporal influence of *E. coli* EV36 and phage K1F alone and in combination on the barrier function of hCMCEC cultures was determined using the xCELLi-gence system (Fig. 8). The temporal impedance profile of hCMCEC cultures treated with phage K1F showed a slow

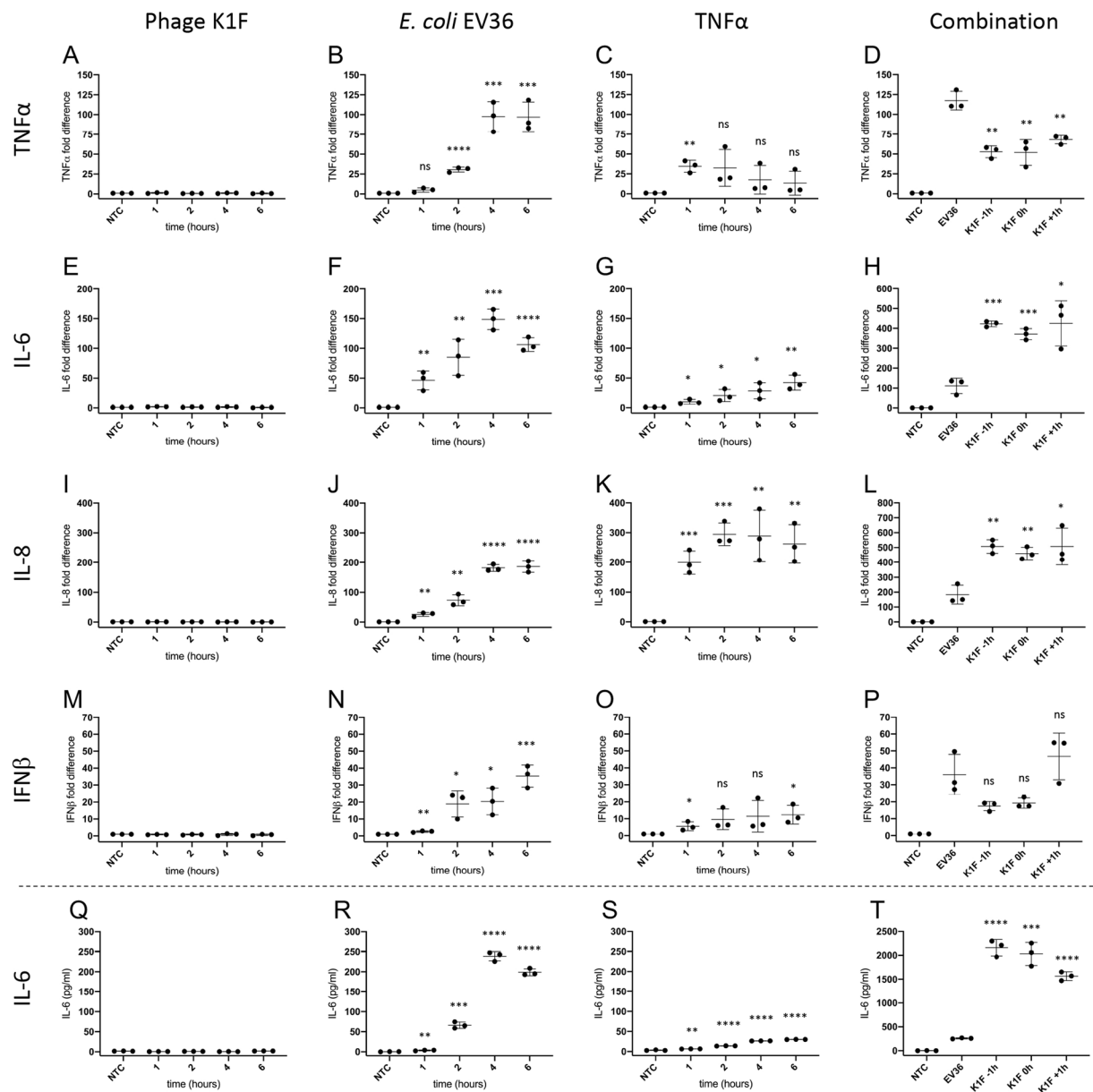


Figure 7. Expression pattern of inflammatory markers by real-time qPCR (A–P). hCMEC cultures were incubated with 10^7 CFU/ml *E. coli* EV36, 10^7 PFU/ml phage K1F or 500 pg/ml $TNF\alpha$ and specific mRNA levels measured over time, or incubated with 10^7 CFU/ml *E. coli* EV36 having 10^4 PFU/ml phage K1F added 1 h before-, simultaneously-, or 1 h after bacterial addition, and incubated for 6 h before RNA harvest. Real-time qPCR was performed with primer pairs specific for $TNF\alpha$ (A–D), IL-6 (E–H), IL-8 (I–L) and $IFN\beta$ (M–P). Data were expressed relative to internal control (GAPDH) and then normalised to the untreated control value. Expression of IL-6 protein as measured by ELISA (Q–T). hCMEC cultures were incubated with 10^7 PFU/ml phage K1F, 10^7 CFU/ml *E. coli* EV36 or 500 pg/ml $TNF\alpha$, or incubated with 10^7 CFU/ml *E. coli* EV36 having 10^4 PFU/ml phage K1F added 1 h before-, simultaneously-, or 1 h after bacterial addition, and incubated for 6 h. NTC = Untreated cultures. \pm SD, $n = 3$ in each case. Probability values (p-values) are displayed as $p \leq 0.05$ (*), $p \leq 0.01$ (**), $p \leq 0.001$ (***) and $p \leq 0.0001$ (****) and not statistically significant $p \geq 0.05$ (ns). P-values are relative to NTC for single treatments experiments and relative to *E. coli* EV36 for combination treatment experiments.

divergence between NTC and phage K1F treated cultures at the highest concentrations of 10^7 and 10^9 PFU with detectable signal after approx. 12 hours incubation (Fig. 8B). The decrease in impedance due to phage K1F was sustained long-term (Fig. 8A), and reached maximum levels after approx. 35 hours incubation; a reduced response was detected by around 72-hour of incubation. To assess if these observations were specific to phage K1F, a similar experiment was performed using phage T7. This experiment showed a similar concentration-dependent decrease (Suppl. Figure 2), suggesting that these observations could be relevant to responses to phage in general.

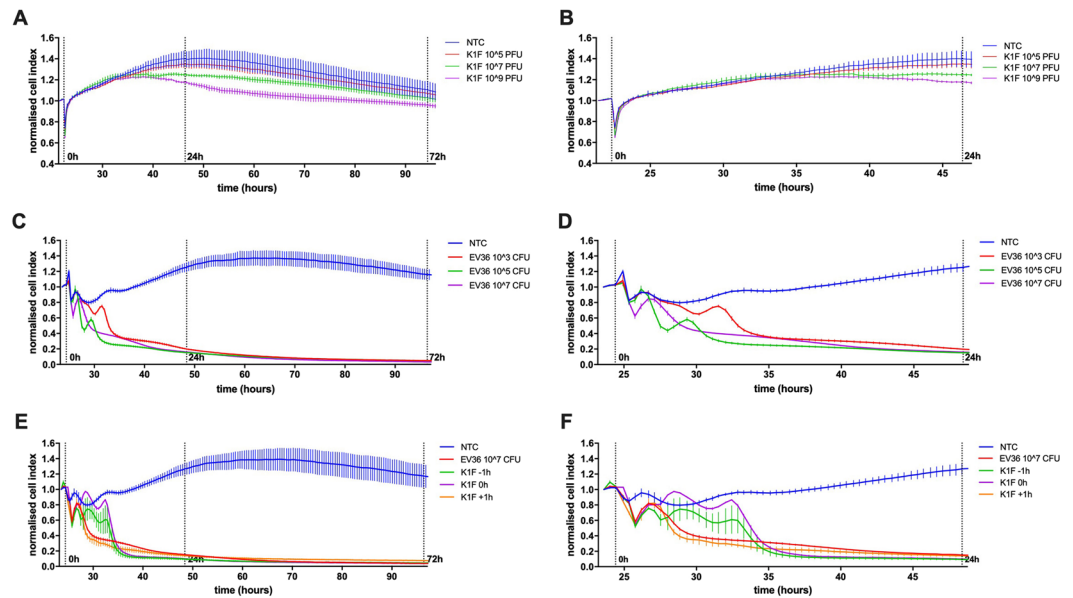


Figure 8. Temporal impedance profiling as measured using the xCELLigence system (A–F). Graphs displaying the barrier resistance over time of hCMEC cultures treated with phage K1F at a concentration range of 10^5 to 10^9 PFU/ml (A,B), *E. coli* EV36 at a concentration range of 10^3 to 10^7 CFU/ml (C,D), or combination treatment of 10^7 CFU/ml *E. coli* and 10^4 PFU/ml phage K1F added 1 h before-, simultaneously-, or 1 h after bacterial addition (E,F). NTC = Untreated hCMEC cultures. X-axis show time from cell seeding. Vertical lines denote the addition of treatment at 0 h, and 24- and 72 h post treatment. The data is presented as the average normalised cell index across the acute (24 hours) and long-term (72 hours) incubate period (\pm SD, $n > 3$).

Additionally, as the impedance measurement is affected not only by cell-to-electrode adhesion but also cell proliferation, a control experiment was performed measuring the proliferation of hCMEC cultures treated with phage K1F or T7 at identical concentrations. This experiment showed no difference in cell proliferation over time between NTC and cultures treated with phages (Suppl. Figure 3), suggesting that the proliferation of hCMEC cultures is not influenced by phage addition.

The impedance of hCMEC cultures treated with *E. coli* EV36 showed an immediate and dramatic decrease over the initial 10 hours for all concentrations (Fig. 8D). The detrimental effect of *E. coli* EV36 infection on the hCMEC cultures is clear with no recovery during the experiment (Fig. 8C), ending at a decrease of $>95\%$ across all bacterial concentrations.

In modelling several *in vitro* phage therapy intervention protocols, phage K1F was added to hCMEC cultures 1 hour before, simultaneously, and 1 hour after the addition of *E. coli* EV36 (Fig. 8E,F). The immediate and dramatic influence of bacterial infection is similar to experiments without phage addition, however, the addition of phage K1F 1 hour prior to or simultaneously with *E. coli* EV36 addition, allowed the impedance of hCMEC cultures to transiently recover (Fig. 8F) in the initial hours of infection. Ultimately, however, despite phage intervention, the impedance was not recovered beyond the initial 10 hours of incubation and similar effects with a decrease of $>95\%$ across all treatments were observed.

Discussion

In this study, we have aimed to develop an *in vitro* phage therapy model for studying bacterial neonatal meningitis. As part of this process, we initially infected hCMEC cultures with *E. coli* EV36. We present that the infection rate of hCMEC cultures is time and concentration-dependent. The percentage of individual hCMECs containing intracellular bacteria was quantified by microscopy and flow cytometry. The two methods of quantification yielded very similar time and concentration-dependent results validating their application. hCMEC cultures incubated with 10^7 CFU *E. coli* EV36-RFP for 1 h showed infection rates of approx. 50%. This is considerably higher than the infection rate previously obtained of approx. 20% in human urinary bladder epithelial cells (T24)¹⁹. This highlighted inherent tissue-specific properties and the necessity for unique tissue-specific model systems to study the mechanism of bacterial infection and phage intervention. We further tested the bacteriophage K1F which we found to display high host specificity towards *E. coli* EV36. The specificity of phage K1F against its bacterial host *E. coli* EV36 was confirmed in liquid cultures, where phages K1F and K1F-GFP were shown to lyse *E. coli* EV36 cultures and not *E. coli* MG1655. Conversely, Phage T7 was shown to lyse *E. coli* MG1655 and not *E. coli* EV36. This demonstrates the high host specificity of the phages used in this study. Infection dynamics assessed by flow cytometry in the form of bacterial viability and cell wall integrity by Sytox⁴⁰ and Propidium Iodide (PI)⁴¹ staining respectively, showed a population Mean Fluorescence Intensity (MFI) increase of over time of both Sytox and PI culminating immediately before bacterial clearance. It is notable that both stains are membrane-impermeable and thus the fluorescent signal is only present in the brief interval from initial lysing to complete dismantlement of the bacterial membrane.

The ability and efficiency of phage K1F-GFP to locate and infect intracellular *E. coli* EV36 in a human cell environment has been confirmed in previous studies¹⁹, however, the signal stability of GFP is often a point for discussion. We therefore initially assessed the fluorescent signal emitted by phage K1F-GFP during infection in *E. coli* EV36 using flow cytometry. We show that bacterial cultures infected with phage K1F-GFP for two hours have a distinctly different fluorescent profile than non-infected bacterial cultures. The fluorescence emitted was time-dependent with a continual increase until bacterial clearance. The location of individual GFP molecules was confirmed by electron microscopy, showing the unequivocal presence of individual GFP molecules across the capsid in alignment with the engineering design of bacteriophage K1F-GFP which places it on the minor capsid protein. These results are in accordance with a previous study⁴², which demonstrated that the gp10b minor capsid protein is present in a limited number of copies, around 15 copies per capsid, in comparison with the major gp10a protein, which forms most of the capsid and is expressed in around 429 copies.

In support of previous results obtained in urinary epithelial cells (T24)¹⁹, our initial imaging data show that *E. coli* EV36 and phage K1F individually and in combination co-localise with antibodies for RAB7, Cathepsin-L and LC3B in hCMEC cultures. The protein targets of these antibodies are involved in phagosome maturation^{20,21}, lysosomal degradation²² and autophagosome formation²³ respectively. Collectively, this illustrates a path of internalisation and degradation of phage K1F by constitutive phagocytosis succeeded by lysosomal degradation along the pathway of LC3-assisted phagocytosis.

LC3-assisted phagocytosis is dependent on the recognition of Pathogen Associated Molecular Patterns (PAMPs) by Toll-like Receptors (TLRs)⁴³, suggesting that mammalian cells recognise phages via TLRs in order to degrade via them via this pathway. Multiple intracellular TLRs are able to recognise viral nucleic acids, specifically, TLR3 recognises dsRNA, TLR7 and TLR8 recognises ssRNA and TLR9 recognises DNA⁴⁴.

The concentration of acidic organelles, including lysosomes, as measured by LysoTracker, decreases over time following phage K1F invasion in hCMEC cultures. It is feasible that the accessible pool of lysosomes is being exhausted during phage degradation, while the cells are not immediately replenishing this store. This is seen in sharp contrast to the substantial increase of lysosome concentration following *E. coli* EV36 infection in hCMEC cultures. Interestingly, phage addition to *E. coli* EV36 infected hCMECs increases the lysosomal activation additionally. This is likely linked to the increase in bacterial debris following bacterial lysis, as the presence of LPS from gram-negative bacteria is a known inducer of autophagy⁴⁵ leading to increased lysosome activity.

While we show that phage K1F and *E. coli* EV36 are degraded by constitutive and LC3-assisted phagocytosis in hCMEC cultures, it is evident that *E. coli* strains can transit from the phagosome into the cytosol in an attempt to evade the innate immune response of lysosomal degradation^{25,46}. In line with previous observations in T24 cells¹⁹, our imaging efforts show that *E. coli* EV36 and not phage K1F co-localise with antibodies for Galectin-8, NDP52 and Ubiquitin in hCMEC cultures. These antibodies target proteins involved in the initiation- and progression of xenophagy, which is pathogen-selective autophagy^{25,47}. Specifically, breaches to the phagosomal membrane are sensed by cytosolic Galectin-8 which binds to exposed membrane-bound glycans²⁷ and interacts with cytosolic NDP52 to mediate autophagosome formation²⁸ thus triggering selective autophagy. Ubiquitination of the escaped bacterium⁴⁷ and the Galectin-8-NDP52 complex²⁵ further promote pathogen degradation. This finding is substantiated by quantitative flow cytometry data showing an increase of ubiquitin abundance over time in hCMEC cultures infected with *E. coli* EV36, whereas hCMEC cultures invaded with phage K1F show no difference of ubiquitin abundance over time.

Real-time qPCR analysis demonstrated that phage K1F does not induce the expression of inflammatory cytokines TNF α , IL-6, IL-8 or IFN β by hCMEC cultures. In contrast, phage upregulation of TNF α and IL-6 expression has been observed *in vitro* in peripheral blood monocytes (PBMCs)⁴⁸. The inflammatory response of PBMCs conforms to the nature of this collection of immune cells, whereas the absence of an inflammatory response of hCMEC cultures is compatible with the nature and function of the endothelium⁴⁹ despite their known involvement in immune processes⁵⁰. Expression of Type I interferons, including IFN β , can be induced by nucleic acid-recognising TLRs⁴⁴ and PAMPs such as LPS. While this study found phages were degraded, in part, by PAMP-recognition dependent LC3-assisted phagocytosis, no increase was observed in IFN β expression of hCMEC cultures following phage invasion. Further studies would be required to investigate which TLR(s) is associated with phage degradation via the LC3-assisted phagocytic pathway. The absence of induction of inflammatory cytokines by phage K1F is seen in sharp contrast to the substantial upregulation of expression induced by *E. coli* EV36 in particular TNF α , IL-6 and IL-8. This is in line with previously published bacterial infection patterns of the human endothelium⁵¹. Interestingly, *in vitro* phage therapy using bacteriophage K1F against *E. coli* EV36 infection of hCMEC cultures resulted in a reduction in TNF α expression of approximately 50% compared to bacterial infection alone. As a central pro-inflammatory cytokine in bacterial infection³⁰, the reduction observed in TNF α expression is likely related directly to the reduction in bacterial concentration as a result of phage intervention.

Conversely, a steep increase was observed following *in vitro* phage therapy in the expression of IL-6 and IL-8. The outcome of phage intervention is bacterial lysis and a high concentration of bacterial debris, LPS. This increase in cytokine expression correlates well with results showing LPS induction of IL-6 and IL-8 expression in lymphatic microvascular cells (LECs)⁵².

Finally, we present that bacteriophage K1F decreases the barrier function of hCMEC cultures.

hCMEC cultures incubated with phage K1F at concentrations of approximately 10⁷ PFU/ml and above showed a temporal reduction of impedance over a considerable length of time.

As far as we are aware this is the first time this has been reported. Similar temporal profiles were observed for incubation with phage T7. Further control experiments showed that these observations were unrelated to hCMEC proliferation.

The frequency of 10 kHz used in these experiments principally favours the measurement of cellular focal adhesion⁵³. The cellular change indicated by a decrease in impedance is weaker focal adhesion to the extracellular

matrix, suggesting that the endothelial barrier function is decreased and thus the endothelium is becoming more permeable in the presence of high concentrations of phage. Circulating free phage is rapidly degraded once the host bacteria have been cleared in *in vivo*^{9,14} and *in vitro*⁵⁴ tests of phage intervention, which suggests that the recovery of hCMEC impedance observed here following prolonged incubation was directly linked to a reduction in bacteriophage concentration. *E. coli* EV36 infection in hCMEC cultures resulted in a rapid and total reduction in barrier resistance in line with previous *in vivo*⁵⁵ and *in vitro*⁵⁶ studies of endothelial barrier function during infection. Interestingly, phage intervention only conferred a short-lived recovery of barrier resistance, ultimately leaving the hCMEC culture to perish due to increasing concentration of LPS.

Continual stimulation of antiviral immune responses by commensal bacteriophage activation of innate immune pathways has been shown to induce low-level cytokine production, resulting in continuously activated immune cells that confer protection against pathogenic viral infections^{17,57}. Additionally, a non-host-derived layer of immunity is theorised to result from phages residing in mucosal layers (BAM model), whereby the presence of phages at the site-of-entry for pathogenic bacteria confers immunity as well as impacting the mucosal-resident community of commensal bacteria⁵⁸. We hypothesise that modulation of endothelial adhesion could be added to the list as an inflammatory mechanism supporting the delivery and extravasation of immune cells to a site of infection.

Overall, the model we propose here to study the interaction between K1F phage, its host bacteria and hCMEC human cells, even though it is in initial steps in terms of directly approaching a clinical phage therapy intervention, can give us useful information to be used when phage therapy is considered. Based on our results, K1F phage is safe to be used as it does not increase inflammation in hCMEC cells and targets successfully its host *Escherichia coli* K1. More studies are required to provide further proof that the current model can be linked even more accurately with real phage therapy examples of neonatal meningitis.

Conclusion

Collectively, the presented results expand the growing understanding of interactions between phages and human cells, reinforce the existing knowledge of phage internalisation and degradation, complemented by an analysis of expression patterns of inflammatory cytokines during *in vitro* phage therapy and results showing the temporal influence of phages on the barrier permeability of human endothelial cells. While there is evidence of interactions between bacteriophage and human cells, it is clear that the responses mounted by the human cells are not inflammatory or defensive. The contribution of this study is valuable in the continued development of phage therapy for bacterial neonatal meningitis and the ongoing war against antibiotic-resistant bacterial infections.

Materials and Methods

Human cell culture. The blood-brain barrier hCMEC/D3⁵⁹ (human cerebral microvascular endothelial cells) cell line (Merck, UK) consists of enriched cerebral microvascular endothelial cells immortalised by lentiviral vector transduction with the catalytic subunit of human telomerase (hTERT) and SV40 large T antigen.

hCMECs were cultured in EndoGRO-MV Complete Media (Merck) supplemented with 1 ng/ml bFGF (FGF-2) (Merck), 100 IU/ml Penicillin (Sigma-Aldrich), and 100 µg/ml Streptomycin (Sigma-Aldrich) and maintained under a humidified atmosphere at 37 C in 5% CO₂. All culture vessels were coated with 5 µg/cm² Collagen Type 1 (Collagen-1) (Merck) in PBS for 1 h at 37 C before use.

Preparation of hCMEC cultures for experiments. For immunocytochemical (ICC) imaging, flow cytometry and real-time qPCR hCMECs were seeded onto 6-well plates in culture medium and allowed 48 h to settle. The seeding density for ICC imaging was approx. 2.1×10^4 cells/cm², and approx. 5.2×10^4 cells/cm² for flow cytometry and real-time qPCR.

Prior to an experiment, the culture medium was replaced with Leibovitz L-15 media (Lonza), a medium designed to support cell growth in environments lacking CO₂ equilibration, and the cultures were moved to a 37 C incubator suitable for bacterial infections.

Growth determination of hCMEC cultures. hCMEC cells were seeded in culture medium onto 96-well tissue culture plates at a density of approx. 1.5×10^4 cells/cm² and allowed 24 hours to settle. Phages T7 or K1F were added to corresponding wells with untreated cells included as a control. The cell density was determined at the time of seeding and at subsequent sampling points by manually using a haemocytometer on a trypsinised population.

Bacterial culture. Three bacterial strains were used in this study: 1) *E. coli* EV36, a K12/K1 hybrid derivative⁶⁰, was kindly provided by Drs Eric R. Vimr and Susan M. Steenbergen. This hybrid strain allowed for work to be performed in a biohazard level 1 laboratory while retaining the phenotypic properties of a pathogenic K1 strain. 2) *E. coli* EV36-RFP, an EV36 derivative constructed by electroporation with low-copy plasmid pSB6A1 constitutively expressing the mRFP1 protein and cultured under 100 µg/ml ampicillin selection. 3) *E. coli* MG1655 (ATCC 47076) (LGC Standards, UK), a well-documented K12 strain, that was included as a control for phage selectivity.

Bacteriophage propagation and purification. Three phage strains were used in this study: 1) Phage K1F, a well-characterised strain that shows high specificity towards K1-capsule expressing bacteria⁶¹, was kindly provided by Dr Dean Scholl. The K1 polysaccharide capsule of *E. coli* is recognised and degraded by a phage K1F-encoded endosialidase allowing phage infection⁶. 2) Phage K1F-GFP, a phage K1F derivative engineered by genome integration of GFP as previously described¹⁹. 3) Phage T7⁶², an extensively used strain showing high specificity towards commensal *E. coli* K12 strains.

Single-clone phage preparations were obtained from cleared bacterial cultures following a modified Castro-Mejia *et al.*⁶³ protocol previously published¹⁹. Briefly, this comprised the release of phage particles from bacterial membranes by NaCl addition, phage precipitation by PEG8000 addition, followed by CsCl gradient column separation, and size exclusion by dialysis. The concentration of endotoxins (LPS) in purified phage preparations were determined using the Limulus Amebocyte Lysate (LAL) Chromogenic Endpoint Assay (Hycult Biotech) following the manufacturer's protocol. Endotoxin concentrations in phage preparations, media and diluents used in this study are presented in Suppl. Figure 4.

Phage host selectivity was assessed by phage infection of liquid bacterial cultures. Phages K1F, K1F-GFP or T7 were added to *E. coli* EV36 or *E. coli* MG1655 in a 96-well plate and the optical density at 600 nm was measured using FLUOstar Omega (BMG Labtech). Uninfected cultures and LB alone were included as controls.

Flow cytometry analysis of phage infection in bacteria. Log-phase *E. coli* EV36 cultures were stained with 2 μ M final concentration propidium iodide (PI) (Invitrogen) or 3 μ M final concentration Sytox Green Dead Cell Stain (Invitrogen), and incubated for 20 min before the addition of phage K1F.

Assessment of fluorophore stability was performed by the addition of phage K1F-GFP alone to a separate bacterial culture.

Data acquisition and analysis were performed using the LSR Fortessa flow cytometer and FACSDiva software (BD Biosciences). Bacterial populations were initially gated on size via SSC/FCA to exclude cellular debris. 10,000 events were detected of each population. The mean fluorescent intensity (MFI) was detected for gated bacterial populations using B488-530/30 A optics for Sytox Green and phage K1F-GFP detection, and YG561-586/15 for propidium iodide detection.

Electron microscopy of phage K1F-GFP. The probe was generated using 5 nm gold functionalized with maleimide groups (Sigma-Aldrich) conjugated to a GFP binding nanobody which has been proven to bind with a high efficiency to GFP proteins⁶⁴, while similar approaches of nanobodies conjugated to gold have shown to be able to track GFP proteins in cells⁶⁵. This approach allows tracking of the GFP protein present on the gp10b capsid protein, as the nanobody binds to the GFP and the gold allows visualization with EM. For the binding of the probe to phage K1F-GFP, 2 μ L of 10^8 PFU/ml phage was incubated with 1 μ L of the probe (1.8×10^{-6} mol/L concentration) at room temperature for 1 hr. Following this, 5 μ L of 1% PBS was added and the total volume was incubated on a formvar/carbon-coated grid (EMResolutions) that was previously glow discharged for 1 min. After 10 minutes, the grid was washed 3 times with 1% PBS, followed by 4 minutes incubation with 2% uranyl acetate staining. The grid was imaged using a Jeol 2100Plus TEM microscope fitted with a Gatan OneView IS camera at 200 kV. Gold controls and wild-type controls were generated using the same protocol, with phage K1F-GFP incubated with only 5 nm gold functionalized with maleimide groups or phage K1F incubated with the probe, respectively. The acquired images were then processed using Fiji (imageJ) software.

Immunofluorescent confocal microscopy. hCMC cultures were fixed in 4% paraformaldehyde (ThermoFisher Scientific) for 15 min, permeabilised in ice-cold PEM buffer (80 mM PIPES pH 6.75, 5 mM EGTA, 1 mM MgCl₂) with 0.05% (v/v) Saponin for 5 min, and quenched with 50 mM NH₄Cl in PBS for 15 min. PBS washes were performed after each step.

For association assays, the fixed cells were stained with the following primary antibodies diluted in 0.05% Saponin in PBS for 60 min at room temperature, as described also previously¹⁹: 40 μ g/ml anti-RAB7 (Bioss Inc, MA); 1 μ g/ml anti-Cathepsin L (Abcam); 5 μ g/ml anti-LC3B (Sigma-Aldrich); 1 μ g/ml anti-CALCOCO2/NDP52 (Abcam); 1 μ g/ml anti-Galectin-8 (R&D Systems); or 1 μ g/ml anti-mono- and polyubiquitinated conjugated monoclonal antibody (FK2) (Enzo Life Sciences). This was followed by detection with secondary antibodies by incubation for 45 min at room temperature with Cy5 Affinipure Donkey Anti-goat, Anti-rabbit or Anti-mouse IgG (Jackson ImmunoResearch, PA). The signal from GFP tagged phage was further enhanced with 5 μ g/ml GFP-Booster (Chromotek, Germany) during incubation with secondary antibodies. For invasion assays, the fixed cells were stained only with 5 μ g/ml Phalloidin CF680R Conjugate (Biotium) for 40 min.

Stained coverslips were mounted on microscope slides using DAPI-containing Fluoroshield Mounting Medium (Abcam, UK) and secured with CoverGrip Coverslip Sealent (Biotium). Finally, the cells were imaged using a Zeiss LSM880 confocal microscope with Airyscan, using the following excitation wavelengths: DAPI at 405 nm, GFP at 561 nm, RFP at 561 nm and far-red (Cy5) at 633 nm.

Flow cytometry analysis of infection in human cells. Sampling was performed by aspirating spent media, trypsinising and centrifuging each the suspension. MEDIUM A (Fix & Perm Cell Permeabilization Kit) (Life Technologies) was added to the pellet and incubated according to the manufacturer's instructions. The cell suspension was diluted in eBioscience Flow Cytometry Staining Buffer (Invitrogen) and pelleted by centrifugation. MEDIUM B (Fix & Perm Cell Permeabilization Kit) (Life Technologies) containing either 1/100 dilution anti-hLC3B Alexa Fluor 647 Conjugated Ab (R&D Systems), or 1 μ g/ml Anti-mono- and polyubiquitinated conjugated monoclonal antibody (FK2) (Enzo Life Sciences), was added to the sample and incubated for 45 minutes. Following incubation, the cell suspension was diluted in Staining Buffer and pelleted by centrifugation as above. For ubiquitin staining only, a secondary incubation with MEDIUM B containing 2 μ g/ml Goat anti-mouse IgG (H + L) Cross Absorbed Secondary Ab Alexa Fluor 647 (Invitrogen) was performed for 30 minutes. Finally, the cell suspension was resuspended in Staining Buffer and placed on ice until acquisition.

MEDIUM A and MEDIUM B were not supplemented with antibodies for LysoTracker (Invitrogen, UK) staining. LysoTracker was added to samples 30 minutes prior to trypsinisation at a final concentration of 500 nM. The endocytic pathway follows a pH gradient ranging from ~6.3 in early endosomes, ~5.5 in late endosomes, to ~4.6

in lysosomes⁶⁶. An observed increase of LysoTracker MFI indicates a downstream shift in endosomal pathway activity towards increased lysosomal activity.

hCMECs treated with *E. coli* EV36-RFP alone were analysed both fixed and live. For fixed cells, the Fix & Perm Cell Permeabilization Kit was used as above. For live cells, the trypsinised cells were diluted in PBS and Sphero Beads AccuCount Fluorescent Particles (SpheroTech, IL) were added according to the manufacturer's instructions, and data acquired immediately thereafter.

Acquisition and analysis were performed using the LSR Fortessa flow cytometer and FACSDiva software (BD Biosciences). 10,000 events were detected of each population. The hCMEC populations were initially gated on size via SSC/FCA, excluding cellular debris and planktonic bacteria. The mean fluorescent intensity (MFI) was detected for gated hCMEC populations using the following optics: R640-670/14-A for LysoTracker and Alexa Fluor 647 conjugated Abs, and YG561-586/15 for *E. coli* EV36-RFP.

Quantitative real-time PCR. hCMEC cultures were incubated with *E. coli* EV36, phage K1F or TNF α (Sino Biological, China) in biological triplicates. RNA was recovered using the GenElute Mammalian Total RNA Miniprep Kit (Sigma-Aldrich) with DNase I Digestion Kit (Sigma-Aldrich) following the manufacturer's protocol.

1 μ g RNA samples were used for cDNA synthesis using 100 U Superscript III (Invitrogen) primed by 50 nM Random Hexamers (Invitrogen) and 10 μ M dNTP Mix (Thermo Scientific).

Real-time PCR of cDNA samples was performed with Brilliant III SYBR Green qPCR Master Mix with Low ROX (Agilent) using the Stratagene Mx3005P instrument with MxPro v4.10 build 389 software (Agilent Technologies). Each sample was quantified in technical triplicate using primer sets for GAPDH⁶⁷, TNF α ⁶⁸, IL-6⁶⁹, IL-8⁷⁰, IL-10⁷¹ and IFN β ⁷².

Data analysis was performed using the Comparative Ct Method⁷³. Δ Ct values for TNF α , IL-6, IL-8, IL-10 and IFN β were calculated by subtracting the average GAPDH Ct value from the average Ct value obtained for each gene. $\Delta\Delta$ Ct values were calculated by subtracting Δ Ct values of untreated cultures from Δ Ct values of treated cultures. The fold change was calculated by taking the log base 2 of $\Delta\Delta$ Ct values.

Detection of IL-6 protein expression using ELISA. hCMEC cultures were incubated with *E. coli* EV36, phage K1F or TNF α (Sino Biological, China) in biological triplicates. Spent media was recovered, centrifuged, sterile filtered and stored at -80°C until analysis. Expression of IL-6 protein was detected using the Human IL-6 Uncoated ELISA kit (Invitrogen) following the manufacturer's instructions.

Temporal impedance measurements of human cells. hCMECs were seeded into Collagen-1 coated E-Plate VIEW 16 PET (ACEA Biosciences) at a concentration of 5×10^4 cells/well in assay media. The plates were then inserted into the RTCA DP station and the cells allowed approx. 24 h to settle before the addition of bacteria or phage. The acquisition was performed using the xCELLigence RTCA DP instrument (ACEA Biosciences) housed in a humidified incubator at 37 C with 5% CO₂. The instrument was set to a single frequency of 10 kHz with 5 min measuring intervals over the course of 96 h. Using a fixed frequency of 10 kHz, the current predominantly travels paracellularly allowing for impedance measurements relating to the cell-to-electrode adhesion (focal adhesion) of the cells⁵³. The parameter measured by the xCELLigence system, the Cell Index, represents the relative changes in frequency-dependent electrode resistance or impedance. Changes observed in impedance of confluent endothelial cells reflect changes in barrier function⁷⁴. The Cell Index was normalised to 1 relative to approx. 1 h before the addition of treatments.

Quantification and statistical analysis. All quantification and statistical analysis were performed using GraphPad Prism 8.2.1 (San Diego, CA). Probability values for flow cytometry- and qPCR datasets were calculated using the unpaired t-test assuming Gaussian distribution. Level of significance is presented in relevant graphs.

Received: 21 January 2020; Accepted: 7 May 2020;

Published online: 01 June 2020

References

- Barichello, T. *et al.* Pathophysiology of neonatal acute bacterial meningitis. *Journal of Medical Microbiology* **62**, 1781–1789 (2013).
- Hoffman, O. & Weber, J. R. Review: Pathophysiology and treatment of bacterial meningitis. *Therapeutic Advances in Neurological Disorders* **2**, 401–412 (2009).
- Heath, P. T. & Okike, I. O. Neonatal bacterial meningitis: an update. *Paediatrics and Child Health* **20**, 526–530 (2010).
- Ku, L. C., Boggess, K. A. & Cohen-Wolkowicz, M. Bacterial Meningitis in Infants. *Clinics in Perinatology* **42**, 29–45 (2015).
- Bingen, E. *et al.* Phylogenetic Analysis of Escherichia coli Strains Causing Neonatal Meningitis Suggests Horizontal Gene Transfer from a Predominant Pool of Highly Virulent B2 Group Strains. *The Journal of infectious diseases* **177**, 642–650 (1998).
- Scholl, D., Adhya, S. & Merril, C. Escherichia coli K1's Capsule Is a Barrier to Bacteriophage T7. *Applied and Environmental Microbiology* **71**, 4872–4874 (2005).
- Jiang, H. *et al.* Prevalence and antibiotic resistance profiles of cerebrospinal fluid pathogens in children with acute bacterial meningitis in Yunnan province, China, 2012–2015. *PLoS One* **12**, e0180161 (2017).
- McCallin, S., Sacher, J. C., Zheng, J. & Chan, B. K. Current State of Compassionate Phage Therapy. *Viruses* **11**, 343 (2019).
- Kutter, E. *et al.* Phage therapy in clinical practice: Treatment of human infections. *Current Pharmaceutical Biotechnology* **11**, 69–86 (2010).
- Weber-Dabrowska, B., Mulczyk, M. & Gorski, A. Bacteriophage therapy of bacterial infections: an update of our institute's experience. *Arch Immunol Ther Exp (Warsz)* **48**, 547–551 (2000).
- Strój, L., Weber-Dabrowska, B., Partyka, K., Mulczyk, M. & Wójcik, M. Successful treatment with bacteriophage in purulent cerebrospinal meningitis in a newborn. *Neurologia i neurochirurgia polska* **33**, 693–698 (1999).
- Ghose, C. *et al.* The Virome of Cerebrospinal Fluid: Viruses Where We Once Thought There Were None. *Frontiers in Microbiology* **10** (2019).
- Kim, K. S. Acute bacterial meningitis in infants and children. *The Lancet Infectious Diseases* **10**, 32–42 (2010).

14. Pouillot, F. *et al.* Efficacy of bacteriophage therapy in experimental sepsis and meningitis caused by a clone O25b:H4-ST131 *Escherichia coli* strain producing CTX-M-15. *Antimicrob Agents Chemother* **56**, 3568–3575 (2012).
15. Barr, J. J. A bacteriophages journey through the human body. *Immunological Reviews* **279**, 106–122 (2017).
16. Moustafa, A. *et al.* The blood DNA virome in 8,000 humans. *PLOS Pathogens* **13**, e1006292 (2017).
17. Van Belleghem, J. D., Dąbrowska, K., Vanechoutte, M., Barr, J. J. & Bollyky, P. L. Interactions between bacteriophage, bacteria, and the mammalian immune system. *Viruses* **11** (2019).
18. Daneshian, M., Guenther, A., Wendel, A., Hartung, T. & von Aulock, S. *In vitro* pyrogen test for toxic or immunomodulatory drugs. *Journal of Immunological Methods* **313**, 169–175 (2006).
19. Møller-Olsen, C., Ho, S. F. S., Shukla, R. D., Feher, T. & Sagona, A. P. Engineered K1F bacteriophages kill intracellular *Escherichia coli* K1 in human epithelial cells. *Scientific Reports* **8**, 17559 (2018).
20. Chua, C. E. L., Gan, B. Q. & Tang, B. L. Involvement of members of the Rab family and related small GTPases in autophagosome formation and maturation. *Cellular and Molecular Life Sciences* **68**, 3349 (2011).
21. Gutierrez, M. G., Munafó, D. B., Berón, W. & Colombo, M. I. Rab7 is required for the normal progression of the autophagic pathway in mammalian cells. *Journal of Cell Science* **117**, 2687–2697 (2004).
22. Bhutani, N., Piccirillo, R., Hourez, R., Venkatraman, P. & Goldberg, A. L. Cathepsins L and Z are critical in degrading polyglutamine-containing proteins within lysosomes. *Journal of Biological Chemistry* **287**, 17471–17482 (2012).
23. Lai, S.-c & Devenish, R. J. LC3-Associated Phagocytosis (LAP): Connections with Host Autophagy. *Cells* **1**, 396 (2012).
24. Rengarajan, M., Hayer, A. & Theriot, J. A. Endothelial Cells Use a Formin-Dependent Phagocytosis-Like Process to Internalize the Bacterium *Listeria monocytogenes*. *PLoS Pathog* **12**, e1005603 (2016).
25. Randow, F. & Youle, R. J. Self and Nonself: How Autophagy Targets Mitochondria and Bacteria. *Cell host & microbe* **15**, 403–411 (2014).
26. Dolman, N. J., Kilgore, J. A. & Davidson, M. W. A review of reagents for fluorescence microscopy of cellular compartments and structures, part I: BacMam labeling and reagents for vesicular structures. *Curr Protoc Cytom* **Chapter 12**, Unit 12.30 (2013).
27. Thurston, T. L. M., Wandel, M. P., von Muhlinen, N., Foeglein, Á. & Randow, F. Galectin 8 targets damaged vesicles for autophagy to defend cells against bacterial invasion. *Nature* **482**, 414 (2012).
28. von Muhlinen, N., Thurston, T., Ryzhakov, G., Bloor, S. & Randow, F. NDP52, a novel autophagy receptor for ubiquitin-decorated cytosolic bacteria. *Autophagy* **6**, 288–289 (2010).
29. Thurston, T. L., Ryzhakov, G., Bloor, S., von Muhlinen, N. & Randow, F. The TBK1 adaptor and autophagy receptor NDP52 restricts the proliferation of ubiquitin-coated bacteria. *Nat Immunol* **10**, 1215–1221 (2009).
30. Bradley, Jr. TNF-mediated inflammatory disease. *The Journal of pathology* **214**, 149–160 (2008).
31. Tanaka, T., Narazaki, M. & Kishimoto, T. IL-6 in inflammation, immunity, and disease. *Cold Spring Harbor perspectives in biology* **6**, a016295–a016295 (2014).
32. Damas, P. *et al.* Cytokine serum level during severe sepsis in human IL-6 as a marker of severity. *Ann Surg* **215**, 356–362 (1992).
33. Spooren, A. *et al.* Interleukin-6, a mental cytokine. *Brain Res Rev* **67**, 157–183 (2011).
34. Falvo, J. V., Tsytsykova, A. V. & Goldfeld, A. E. Transcriptional control of the TNF gene. *Curr Dir Autoimmun* **11**, 27–60 (2010).
35. Baggiolini, M. & Clark-Lewis, I. Interleukin-8, a chemotactic and inflammatory cytokine. *FEBS Letters* **307**, 97–101 (1992).
36. Smale, S. T. & Natoli, G. Transcriptional control of inflammatory responses. *Cold Spring Harb Perspect Biol* **6**, a016261 (2014).
37. Couper, K. N., Blount, D. G. & Riley, E. M. IL-10: The Master Regulator of Immunity to Infection. *The Journal of Immunology* **180**, 5771–5777 (2008).
38. Bedsaul, J. R., Zaritsky, L. A. & Zoon, K. C. Type I Interferon-Mediated Induction of Antiviral Genes and Proteins Fails to Protect Cells from the Cytopathic Effects of Sendai Virus Infection. *J Interferon Cytokine Res* **36**, 652–665 (2016).
39. Hiscott, J., Nguyen, H. & Lin, R. Molecular mechanisms of interferon beta gene induction. *Seminars in Virology* **6**, 161–173 (1995).
40. Roth, B. L., Poot, M., Yue, S. T. & Millard, P. J. Bacterial viability and antibiotic susceptibility testing with SYTOX green nucleic acid stain. *Applied and Environmental Microbiology* **63**, 2421–2431 (1997).
41. Riccardi, C. & Nicoletti, I. Analysis of apoptosis by propidium iodide staining and flow cytometry. *Nature Protocols* **1**, 1458–1461 (2006).
42. Kemp, P., Garcia, L. R. & Molineux, I. J. Changes in bacteriophage T7 virion structure at the initiation of infection. *Virology* **340**, 307–317 (2005).
43. Martinez, J. *et al.* Microtubule-associated protein 1 light chain 3 alpha (LC3)-associated phagocytosis is required for the efficient clearance of dead cells. *Proceedings of the National Academy of Sciences* **108**, 17396–17401 (2011).
44. Blasius, A. L. & Beutler, B. Intracellular Toll-like Receptors. *Immunity* **32**, 305–315 (2010).
45. Han, C. *et al.* The Role of Probiotics in Lipopolysaccharide-Induced Autophagy in Intestinal Epithelial Cells. *Cellular Physiology and Biochemistry* **38**, 2464–2478 (2016).
46. Dupont, N. *et al.* Shigella Phagocytic Vacuolar Membrane Remnants Participate in the Cellular Response to Pathogen Invasion and Are Regulated by Autophagy. *Cell host & microbe* **6**, 137–149 (2009).
47. Sharma, V., Verma, S., Seranova, E., Sarkar, S. & Kumar, D. Selective Autophagy and Xenophagy in Infection and Disease. *Frontiers in Cell and Developmental Biology* **6** (2018).
48. Van Belleghem, J. D., Clement, F., Merabishvili, M., Lavigne, R. & Vanechoutte, M. Pro- and anti-inflammatory responses of peripheral blood mononuclear cells induced by *Staphylococcus aureus* and *Pseudomonas aeruginosa* phages. *Scientific Reports* **7**, 8004 (2017).
49. Mai, J., Virtue, A., Shen, J., Wang, H. & Yang, X.-F. An evolving new paradigm: endothelial cells—conditional innate immune cells. *J Hematol Oncol* **6**, 61–61 (2013).
50. Sumpio, B. E., Timothy Riley, J. & Dardik, A. Cells in focus: endothelial cell. *The International Journal of Biochemistry & Cell Biology* **34**, 1508–1512 (2002).
51. Valbuena, G. & Walker, D. H. in *Annual Review of Pathology* **1**, 171–198 (2006).
52. Sawa, Y. *et al.* LPS-induced IL-6, IL-8, VCAM-1, and ICAM-1 Expression in Human Lymphatic Endothelium. *Journal of Histochemistry & Cytochemistry* **56**, 97–109 (2007).
53. Kho, D. *et al.* Application of xCELLigence RTCA Biosensor Technology for Revealing the Profile and Window of Drug Responsiveness in Real Time. *Biosensors* **5**, 199–222 (2015).
54. Shan, J. *et al.* Bacteriophages are more virulent to bacteria with human cells than they are in bacterial culture; insights from HT-29 cells. *Scientific reports* **8**, 5091–5091 (2018).
55. Shifflett, D. E., Clayburgh, D. R., Koutsouris, A., Turner, J. R. & Hecht, G. A. Enteropathogenic *E. coli* disrupts tight junction barrier function and structure *in vivo*. *Laboratory Investigation* **85**, 1308–1324 (2005).
56. Spitz, J. *et al.* Enteropathogenic *Escherichia coli* adherence to intestinal epithelial monolayers diminishes barrier function. *American Journal of Physiology-Gastrointestinal and Liver Physiology* **268**, G374–G379 (1995).
57. Duerkop, B. A. & Hooper, L. V. Resident viruses and their interactions with the immune system. *Nature Immunology* **14**, 654–659 (2013).
58. Barr, J. J., Youle, M. & Rohwer, F. Innate and acquired bacteriophage-mediated immunity. *Bacteriophage* **3**, e25857 (2013).
59. Weksler, B., Romero, I. A. & Couraud, P. O. The hCMEC/D3 cell line as a model of the human blood brain barrier. *Fluids Barriers CNS* **10**, 16 (2013).

60. Vimr, E. R. & Troy, F. A. Identification of an inducible catabolic system for sialic acids (nan) in Escherichia coli. *Journal of bacteriology* **164**, 845–853 (1985).
61. Scholl, D. & Merrill, C. The Genome of Bacteriophage K1F, a T7-Like Phage That Has Acquired the Ability To Replicate on K1 Strains of Escherichia coli. *Journal of bacteriology* **187**, 8499–8503 (2005).
62. Studier, F. W. The genetics and physiology of bacteriophage T7. *Virology* **39**, 562–574 (1969).
63. Castro-Mejía, J. L. *et al.* Optimizing protocols for extraction of bacteriophages prior to metagenomic analyses of phage communities in the human gut. *Microbiome* **3**, 64 (2015).
64. Kubala, M. H., Kovtun, O., Alexandrov, K. & Collins, B. M. Structural and thermodynamic analysis of the GFP:GFP-nanobody complex. *Protein Sci* **19**, 2389–2401 (2010).
65. Leduc, C. *et al.* A Highly Specific Gold Nanoprobe for Live-Cell Single-Molecule Imaging. *Nano Letters* **13**, 1489–1494 (2013).
66. Chen, J.-W., Chen, C.-M. & Chang, C.-C. A fluorescent pH probe for acidic organelles in living cells. *Organic & Biomolecular Chemistry* **15**, 7936–7943 (2017).
67. Vestergaard, A. L., Knudsen, U. B., Munk, T., Rosbach, H. & Martensen, P. M. Transcriptional expression of type-I interferon response genes and stability of housekeeping genes in the human endometrium and endometriosis. *Molecular Human Reproduction* **17**, 243–254 (2010).
68. Chege, D. *et al.* Evaluation of a quantitative real-time PCR assay to measure HIV-specific mucosal CD8+ T cell responses in the cervix. *PLoS one* **5**, e13077–e13077 (2010).
69. Jeong, J. B., Shin, Y. K. & Lee, S.-H. Anti-inflammatory activity of patchouli alcohol in RAW264.7 and HT-29 cells. *Food and Chemical Toxicology* **55**, 229–233 (2013).
70. Romero, D. G. *et al.* Interleukin-8 Synthesis, Regulation, and Steroidogenic Role in H295R Human Adrenocortical Cells. *Endocrinology* **147**, 891–898 (2006).
71. Stordeur, P. *et al.* Cytokine mRNA quantification by real-time PCR. *Journal of Immunological Methods* **259**, 55–64 (2002).
72. Shi, H.-X. *et al.* Positive Regulation of Interferon Regulatory Factor 3 Activation by Herc5 via ISG15 Modification. *Molecular and Cellular Biology* **30**, 2424–2436 (2010).
73. Schmittgen, T. D. *et al.* Quantitative Reverse Transcription–Polymerase Chain Reaction to Study mRNA Decay: Comparison of Endpoint and Real-Time Methods. *Analytical Biochemistry* **285**, 194–204 (2000).
74. Atienza, J. M. *et al.* Dynamic and label-free cell-based assays using the real-time cell electronic sensing system. *Assay Drug Dev Technol* **4**, 597–607 (2006).

Acknowledgements

This work was supported by the BBSRC Future Leader Fellowship (ref. BB/N011872/1) to A.P.S. and a MIBTP DTP PhD studentship to C.M.O. T.R. was supported by an MBio Master's Program in the University of Warwick. The authors would like to thank Dr Dean Scholl, AvidBiotics Corporation, for providing the bacteriophage K1F strain, Professor Eric R. Vimr and Dr Susan M. Steenbergen for providing the *E. coli* EV36 strain, Dr Paul J. Brighton for assistance with the xCELLigence setup, Dr Ian Hands-Portman and Dr Saskia Bakker for their guidance and training in the operation of the Jeol 2100 plus TEM. We also acknowledge WISB (Warwick Integrative Synthetic Biology Centre), a BBSRC/EPSC Synthetic Biology Research Centre (grant ref: BB/M017982/1) funded under the UK Research Councils' Synthetic Biology for Growth programme, for use of their flow cytometry system, and the Midlands Regional Cryo-EM Facility, hosted at the Warwick Advanced Bioimaging Research Technology Platform, for use of the JEOL 2100Plus, supported by MRC award reference MC_PC_17136.

Author contributions

C.M.-O. designed and performed experiments, wrote and revised the manuscript. T.R. performed experiments. K.N.L. advised on the experimental setup and the interpretation of data, and revised the manuscript. V.F. performed experiments. C.S. revised the manuscript. D.K.G. revised the manuscript. A.P.S. Conceived the idea, designed experiments, participated in the writing and correction of the manuscript, supervised the study and organized the team. All the authors approved the manuscript.

Competing interests

The authors declare no competing interests.

Additional information

Supplementary information is available for this paper at <https://doi.org/10.1038/s41598-020-65867-4>.

Correspondence and requests for materials should be addressed to A.P.S.

Reprints and permissions information is available at www.nature.com/reprints.

Publisher's note Springer Nature remains neutral with regard to jurisdictional claims in published maps and institutional affiliations.



Open Access This article is licensed under a Creative Commons Attribution 4.0 International License, which permits use, sharing, adaptation, distribution and reproduction in any medium or format, as long as you give appropriate credit to the original author(s) and the source, provide a link to the Creative Commons license, and indicate if changes were made. The images or other third party material in this article are included in the article's Creative Commons license, unless indicated otherwise in a credit line to the material. If material is not included in the article's Creative Commons license and your intended use is not permitted by statutory regulation or exceeds the permitted use, you will need to obtain permission directly from the copyright holder. To view a copy of this license, visit <http://creativecommons.org/licenses/by/4.0/>.

© The Author(s) 2020

Advances in engineering of bacteriophages for therapeutic applications

Christian Møller-Olsen ¹, Gurneet K. Dhanoa ¹, Tamas Feher ² & Antonia P. Sagona ^{1*}

¹ School of Life Sciences, University of Warwick, United Kingdom

² Synthetic and Systems Biology Unit, Biological Research Centre of the Hungarian Academy of Sciences, Szeged, Hungary

* Corresponding author:

Antonia P. Sagona,
School of Life Sciences, University of Warwick,
Gibbet Hill Campus
Coventry, CV4 7AL, UK
Phone: +44(0)2476523102
[Email: A.Sagona@warwick.ac.uk](mailto:A.Sagona@warwick.ac.uk)

Keywords: phage engineering, phage therapy, engineering techniques, therapeutic applications

1. Abstract

Synthetic biology has experienced an incredible advancement over the last decades with applications influencing every aspect of our daily lives. The capacity of synthetic biology has been instrumental in the life sciences and is now crossing into clinical settings.

Driven by the accelerating evolution of antibiotic resistant bacteria, the development of phages and phage-derived particles as antimicrobials is receiving renewed attention. In this chapter, we present the current tools and approaches for engineering synthetic bacteriophages, the therapeutic applications for which they are being used and highlight the potential risks and rewards.

A wealth of tools and technologies have been and are being developed for the design and engineering of synthetic bacteriophages for therapeutic applications. While homologous recombination still underpins many recombineering approaches, modern technologies such as CRISPR-Cas gene-editing and cell-free assembly are making an appearance, enabling a higher success rate.

The therapeutic applications for which engineered phage and phage-derived particles can be used are numerous. These range from exploiting the antimicrobial properties of phage-expressed endolysins, or modifying a temperate phage to a virulent lifecycle, to exploiting phages as vectors transporting anticancer compounds or utilising the high host-specificity for pathogen detection. In short, the opportunities are endless and we discuss some of those here.

2. Phage therapy

2.1. Introduction

Bacteriophages (phages) were first discovered in the early 20th century and were instantly recognised for their potential as antimicrobial agents; however, the discovery of antibiotics left phage research on the side line of Western medicine ¹. In recent years, phage therapy, the use of phages to treat bacterial infections, is experiencing a renaissance driven by the developing health and economic burden of bacterial antibiotic resistance.

Controlled randomised clinical trials of phage therapy have so far failed to produce robust irrefutable results; however, numerous reports of compassionate use demonstrate that successful phage therapy is achievable ². Additionally, an impressive 13% of projects in the global preclinical antibacterial pipeline are based on phage or phage-related products ³, illustrating the growing confidence in this technology.

Developing phage therapy to meet future medical needs presents some challenges, which modern molecular and synthetic biology tools may have the power to match. In 2018 a 15-year-old patient with cystic fibrosis was treated with a phage cocktail targeting a disseminated *Mycobacterium abscessus* infection⁴. The cocktail, consisting of three *Siphoviridae* phages, was administered twice daily intravenously and topically and following six weeks of treatment a dramatic clinical improvement was observed. This case showed successful therapeutic use of an engineered phage for the first time, as two of the three phages were virulent derivatives engineered from temperate progenitors ⁵.

In this chapter, we broadly outline current approaches to phage engineering and the novel therapeutic applications of which they are or can be used.

2.2. Design considerations

The challenges of phage therapy are multifaceted and should ideally be considered early in the process of designing phage preparations intended for therapeutic applications.

The unique pharmacological properties of phages, i.e. pharmacokinetics, the movement of a drug through the human body over time, observed as absorption, distribution, metabolism, and excretion; and pharmacodynamics, the biochemical, physiologic and molecular effects of a drug on the human body, are complicated and should be recognised as such. This complexity is contributed to their large size, structural complexity and to their potential to replicate within the human body ^{6, 7}.

Therapeutic phage preparations contrast traditional antibiotics on many points and the legislative approval process of phage preparations can therefore not be directly aligned with antibiotics⁸. The current legislative model used in the Western world, designed for industrially made pharmaceuticals for implementation in the general population, does not cater well for individualised medicines. Recent years, however, have brought about relaxed regulatory exceptions for compassionate use in some European countries, where legislation has been introduced to allow quicker access for patients and doctors to phage therapy ⁹. Amendments to the current process of authorisation to allow for widespread use of phage therapy will ultimately rely on robust evidence delivered by randomised clinical trials in a general population demonstrating phage efficacy, immunogenicity and any potential adverse effects ¹⁰.

Despite the challenges at hand, phage engineering has undergone considerable advancement over the last decade with novel applications in diverse areas such as agriculture, food security and drug development. This advancement is mainly due to the incredible expansion seen in tools available for the field of molecular and synthetic biology and to the renewed global interest in phages as antimicrobials.

Phages can be divided into two primary groups depending on their choice of lifecycle: the lytic lifecycle of virulent phages culminates in lysis of the host bacterium after viral replication, while temperate phages will initially integrate into the host genome as a prophage and only initiate viral replication and lysis following induction cues ¹¹. Generally, virulent phages are preferred for therapeutic purposes since, unlike temperate phages, they do not alter the phenotype of the host and do not mediate horizontal gene transfer, which is a mechanism for the spread of antimicrobial resistance genes (ARGs) and bacterial virulence factors ¹². The natural abundance of temperate over virulent phages is, however, appealing and as such engineered virulent variants of temperate phages appear ¹³.

Long-circulating phages are capable of remaining active and avoiding degradation by the mammalian immune system for longer, making them favourable for therapeutic purposes ¹⁴. Long circulating phages have been engineered by fusing lysine or arginine peptides onto the phage capsid ¹⁵. Similarly, phage encapsulation has the potential to protect phages against chemical stress and to disguise them from the immune system allowing for prolonged circulation ¹⁶.

Regardless of the choice of phage, it is advisable to perform full genome sequencing and annotation to identify any potentially problematic gene products. Identification of genes associated with the lysogenic cycle, such as integrases or recombinases, would suggest undesirable temperate phage traits¹⁷. Genomic analysis also allows for the identification of potentially toxic gene products and antimicrobial resistance elements¹⁸. Additionally, the presence of endonucleases is essential to ensure that the bacterial DNA is degraded before bacterial lysis, as intact bacterial DNA or bacterial plasmids could enter other microorganisms by transduction and would therefore mediate the spread of ARGs and bacterial virulence genes¹⁹.

The most advantageous trait of a phage is possibly its host specificity. This specificity can be exploited in phage therapy to directly target pathogenic bacterial strains, without damaging commensal bacterial strains²⁰. Healthy microbiota are vital to our overall health and protecting those during treatment could potentially accelerate recovery and minimise secondary infections. However, due to the cost of phage isolation and engineering, it may be preferable to use phages that can target a range of pathogenic strains within a genus.

The relationship between bacteria and phages has been fine-tuned during their co-evolution over billions of years. This co-evolution has led to a dependency on multiple levels from both bacteria and phages to sustain the local coexistence dynamics and studies suggest that disrupting the status-quo by broadening the host range of a phage can lead to a decreased infection efficiency of the said phage²¹.

A standard option for therapeutic applications is to use a cocktail of multiple phages able to target different variations of the problematic pathogen. In addition to broadening the host range of the therapy, studies have suggested that the synergy of using multiple phages increase the infection efficacy of the individual phages²² and importantly, decrease the emergence of phage resistance²³.

Consideration should also be placed on the bacterial host strain used for propagation. Selecting a surrogate bacterial strain, that does not contain prophages, ARGs or virulence genes, as propagation host could exclude undesirable genetic transfer, is important²⁴. Furthermore, choosing a host strain with low pathogenicity is practical as it can be handled in laboratories with a low biological safety rating.

2.3. Bacterial resistance to phage

The emergence of antibiotic-resistant bacteria is driven by bacterial exposure to antibiotics. Similarly, bacterial resistance to phage can evolve by exposure to phages, potentially affecting multiple elements of the phage's lifecycle²⁵. It is essential for the success of phage therapy to understand the bacterial defence mechanisms against phage infection and how phages can adapt to counter these defences.

Phage-resistant bacterial variants have been identified in multiple studies as well as clinical trials, however, phage-resistance often leads to a fitness cost²³. Manipulation of resource availability has been demonstrated to affect the co-evolutionary dynamics between phage and bacterial host, where increased resource availability leads to increased bacterial resistance to phage²⁶. While bacterial resistance to phage can arise, it is generally not

perceived to present concern in long-term therapeutic use, as the resistance is often only against the co-evolved phage strain ²⁷.

While phages can exploit several different lifecycles to reproduce, adsorption to the bacterial cell surface by binding to extracellular receptors is universally necessary for infection. Bacteria have developed a number of adsorption-blocking mechanisms with the aim of avoiding the initial adsorption altogether, including altering, disguising, modifying or concealing the surface binding receptors ²⁸, as well as deploying outer membrane vesicles (OMVs), thus decreasing the pool of available surface receptors ²⁹.

Bacterial restriction-modification systems allow the bacterium to distinguish self-DNA from non-self-DNA and can recognise specific restriction-sites and destroy the phage DNA upon injection into the cytoplasm ³⁰. Multiple types of restriction-modification systems have been described, with the most simple form consisting of only two proteins, a methyltransferase and an endonuclease, which will methylate DNA and facilitate cleavage of unmethylated DNA, respectively ³¹.

Similar to restriction-modification systems, bacterial CRISPR-Cas systems allow for sequence-specific cleavage of phage DNA, albeit, CRISPR-Cas systems additionally afford adaptive immunity to future bacterial generations in the creation of new phage derived spacer sequences ³².

Abortive infection anti-phage systems can reduce the number of phage progeny produced and confer protection to the bacterial population as a whole, rather than individually. These systems can disrupt phage propagation following entry by altruistic suicide of the host bacterium, caused by leakage and loss of membrane potential via the formation of membrane channels ³³, by deactivation of essential host genes by kinase phosphorylation³⁴ or by activation of a toxin-antitoxin mechanism designed to disrupt essential cellular processes ³⁵.

Phages can tackle many of these bacterial resistance mechanisms through their own evolution due to their short replication cycle and genomic plasticity, which allow for the exchange of genetic material via both horizontal and vertical transmission ³⁶. By observing naturally occurring phage evolution and by utilising current molecular tools, it is possible to engineer recombinant phage variants or screen for phages with natural forming mutations, to counteract developing bacterial phage resistance mechanisms. Design or selection of phages that contain specific queuosine biosynthesis genes confers protection by genome modification of phage DNA to degradation by some restriction-modification systems ^{37 38}.

The generation of recombinant phages to counteract bacterial phage-resistance has the potential to be more economical and considerably faster than developing new antibiotics to counteract and offset bacterial antibiotic-resistance.

3. Engineering techniques

3.1. Homologous recombination

Homologous recombination is possibly the most well-established and generally used method for the engineering of phage genomes in their bacterial hosts. It is a natural phenomenon, which happens between two homologous DNA sequences as short as 23 bp and this allows cells to recombine introduced heterologous DNA with their genomic DNA, if both sequences share homology regions³⁹. Phage cross was one of the original methods developed using this

technique, to create a recombinant phage with specific phenotypes by combining or separating mutations from parental phages⁴⁰. Bacterial hosts were coinfecting with two phages with at least two phenotypes, and homologous recombination would occur between the two genomes, creating mutant progeny. This method was used to exchange or combine parental phage phenotypes, but was unable to do specific site targeted modification to the genome, limiting its use⁴¹.

Homologous recombination between a phage genome and plasmid has now been developed and this mechanism can be used to introduce genes into a phage's genome, outlined in Figure 1. The gene to be introduced, flanked by two regions of DNA homologous to the DNA segments flanking the targeted locus of the genome⁴², is first cloned into a replicative plasmid and transformed into the phage's bacterial host. The host is infected with the phage to be engineered, allowing homologous recombination to occur between the plasmid and genome, potentially integrating the heterologous gene into the genome and eventually packaging it with the phage particle and future progeny⁴².

Homologous recombination systems are extremely useful for introducing mutations and genes into the bacterial chromosome. However, applying these systems for phage editing requires extensive *in vitro* engineering of plasmids, making it time-consuming and sometimes difficult with phage genome sequencing being necessary to verify successful constructs⁴³. A small proportion of the resulting phage will be recombinant, with reported rates ranging from only 10^{-4} to 10^{-10} ^{42, 44}. Finding the desired clone can be labour-intensive, without an efficient phage screening system; therefore, a reporter gene, such as a luciferase or a fluorescent protein, is often cloned alongside the gene of interest to facilitate identifying mutants by detecting the reporter^{42, 45}. Since recombination rates with this technique are low, it is unlikely that targeting multiple loci within the genome at the same time will give rise to a phage with all the desired mutations. This means that when various modifications are desired, each mutation is often made independently, which is time-consuming³⁹.

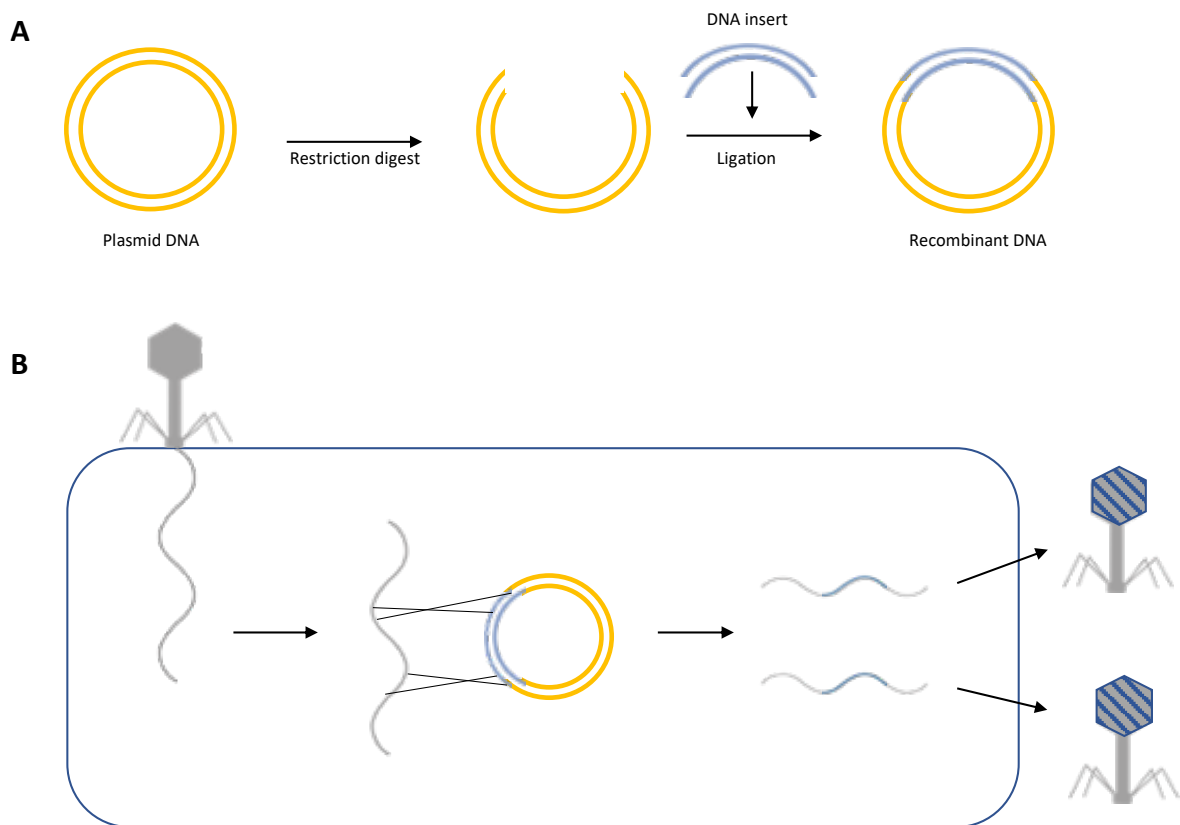


Figure 1: Homologous recombination

A) A recombinant double stranded DNA plasmid is first created by cutting the plasmid DNA and the gene to be inserted (synthetically designed to be flanked with regions homologous to the phage genome) using restriction enzymes; these are then ligated together.

B) Inside a host bacterial cell that has been transformed with the recombinant plasmid, the phage genome undergoes homologous recombination during infection with the plasmid and the gene is incorporated into the genome and packaged into new phage particles.

3.2. Bacteriophage Recombineering of Electroporated DNA

Bacteriophage recombineering of electroporated DNA or BRED, is another commonly used strategy to engineer phage genomes. The technique was first used by Marinelli *et al.* to modify mycobacteriophages⁴⁶ and has since been developed to engineer phages specific to other hosts, such as *Escherichia* and *Salmonella* species⁴⁷. BRED can be used to insert, replace and delete genes, and can create point mutations in genomes^{39, 48}. It is a homologous recombination-based technique, but takes advantage of a recombination system, such as the λ -Red system or the RecE/RecT system in the host, to enhance the frequency of recombination⁴¹.

The technique requires a linear DNA substrate comprising the DNA fragment to be flanked by regions of homology corresponding to those lying upstream and downstream of the region of the phage genome to be modified⁴⁶. This substrate is co-electroporated with phage genomic DNA into electrocompetent bacterial hosts, carrying an expression plasmid encoding recombinases for promoting high levels of homologous recombination, such as the RecE/RecT-like proteins^{46, 49}. The electroporated bacterial cells are then recovered and mixed

with wild-type host and plated. After 24 hours the plates are checked for phage plaques where bacterial cell lysis has occurred and these plaques are screened by PCR to identify phages with the mutated genome ^{46, 48}.

By using BRED, recombinant phages have been obtained at increased frequencies of 10-15% ⁴⁶. It has been suggested that recombination occurs after genome replication has started ⁴⁶, meaning wild-type phages will also be recovered along with the mutant phages so the generated plaques will contain a mixture of both. As a consequence, positive plaques need to be re-suspended and re-plated for a second round of PCR screening to obtain pure recombinant plaques. A potentially high background of wild-type phages can be expected, so extensive screening for recombinants is required ⁴¹. Since the technique relies on co-electroporation of phage DNA and donor DNA, it requires highly competent bacterial hosts. This makes the method more difficult in Gram-positive bacterial hosts which exhibit low transformation efficiencies ⁴¹.

Another similar phage engineering method based on electroporation of substrate is the *in vivo* recombineering. This technique relies on *E. coli* cells carrying a defective λ prophage that contains the *pL*-driven operon (involved in site-specific recombination) under the control of the *cI857* repressor. After infecting these cells with the phage to be engineered ⁵⁰, the culture is transiently heated to induce the recombination system. The cells are then electroporated with the DNA substrate containing the desired mutation or transgene and the phage lysate is recovered and screened for recombinants ⁵⁰. Recombination rates for this method are around 0.5 to 2%, which is higher than traditional homologous recombination, but still low compared to newer techniques like BRED, making screening for mutants challenging ⁴⁹.

3.3. CRISPR-Cas

Classic engineering strategies using homologous recombination between a phage genome and DNA vector are time-consuming and have low recombination rates and alternative strategies relying on the transformation of a synthetic phage genome into a bacterial host are problematic in hosts that exhibit no competence ⁵¹. This obstacle is circumvented with the help of clustered regularly interspaced short palindromic repeats (CRISPR) and CRISPR-associated (Cas) proteins. The CRISPR/Cas system was discovered in the 1990s as a prokaryote immune system, but more recently has been modified for genome engineering across many organisms, including phages ⁴¹.

The CRISPR/Cas system is based on a natural RNA-directed DNA endonuclease mechanism, that provides bacteria with adaptive immunity against invading nucleic acids ⁵², for example, plasmids and phage genomes, by storing sequences (called spacers) corresponding to past encounters on the host chromosome. These spacers are used by Cas proteins to detect and cleave any nucleic acid in the cell that has the same sequence. Engineered CRISPR-Cas systems contain effector complexes comprised of Cas proteins and guide RNA (gRNA) expressed from a single plasmid, shown in Figure 2. The gRNA is composed of spacer and scaffold RNA and the region complementary to the target DNA will specifically bind the effector complex to the target, where the Cas proteins then cleave the DNA and create a double-stranded break ⁵³.

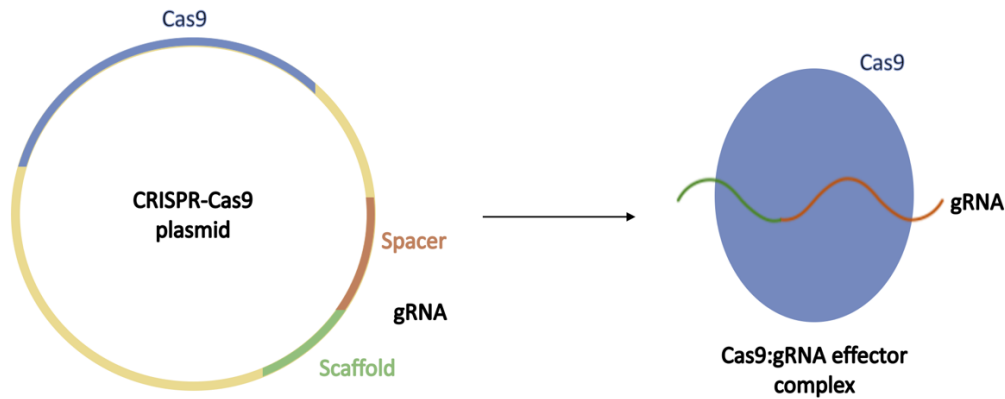


Figure 2: CRISPR-Cas9 effector complex

The CRISPR-Cas9 effector complex is made of the Cas9 protein bound to guide RNA (gRNA), comprised of spacer and scaffold components, all expressed from a single plasmid transformed into a host cell.

CRISPR-Cas systems are currently divided into two classes, with a further division into several subtypes⁵⁴, summarised in Table 1. Class 1 systems (including types I, III, IV) utilise effector complexes comprised of multiple Cas proteins, whereas class 2 systems (including types II, V, VI) use a single Cas protein to cleave target DNA⁵⁵. While CRISPR is useful for editing phage genomes, research still needs to be done to find the most efficient system; for example, three different groups have engineered T4 phage with this method, but with contrasting efficiency for type II⁵⁶. It is known that using different gRNAs can affect the efficiency of CRISPR selection, and the most efficient gRNAs for the type II system have a higher GC content, which is an essential factor to consider during design of new gRNAs⁵⁶.

Class	Type	Number of Cas proteins	Details
Class 1	I	Multiple Cas proteins in an effector complex.	Most commonly found type, signature protein is Cas3 ⁵⁴ .
	III		Present in numerous archaea, but rare in bacteria ⁵⁵ , signature protein is Cas10 ⁵⁴ .
	IV		A rare type with loci lacking the adaptation molecule ⁵⁵ .
Class 2	II	Single Cas protein in effector complex.	Signature protein is Cas9 ⁵⁴ , which is the most widely used in genome editing.
	V		Cpf1 RNA-guided endonuclease, which does not require additional tracrRNA ⁵⁷ .
	VI		Exclusively targets RNA, Cas13 is the signature protein ⁵⁵ .

Table 1: Summary of CRISPR-Cas system types

During phage infection, homologous recombination can occur between the phage genome and plasmid DNA to delete a phage gene. The resulting population will be mixed, but CRISPR-Cas selection can target wild-type particles if the gene has not been deleted to counter select the wild type and retain the recombinant phages. Thus, this method overcomes the issues of having to find a small percentage of successful recombinant phages from the pool of wild-type phages³⁹. Martel *et al.* used the endogenous type II-A CRISPR/Cas system of *Streptococcus termophilus* to engineer the genome of virulent phage 2972. Engineering multiple types of mutations of the phage *gp33* gene was demonstrated by growing the phage on a *S. termophilus* strain, harbouring a chromosomal *gp33*-targeting protospacer and a donor plasmid carrying the desired mutation⁵⁸.

A potential issue that could arise through CRISPR-Cas engineering is off-target cleavage by the nucleases causing undesired mutations⁵¹. However, this can be overcome by whole phage genome sequencing of the recovered mutants to rule out off-target effects. Some phages encode CRISPR-Cas inhibitors, which could make it challenging to find a system to work against such a phage, although not impossible since CRISPR-Cas systems are diverse and widespread⁵¹.

3.4. Yeast-based assembly

When propagating phage genomes in their host, the process can be toxic to the bacterial cell, which limits the efficiency of engineering methods such as homologous recombination and BRED³⁹. This can be overcome by replacing bacteria with the yeast *Saccharomyces cerevisiae* as an intermediate cloning host. *S. cerevisiae* not only provides more efficient homologous recombination machinery, but is also less prone to the toxicity of phage genomes, thereby allowing their more stable maintenance⁵⁹. This method has been used to modify the genomes of phages such as T7 and *Klebsiella* phage K11⁶⁰.

In this technique, the phage genome is captured into a yeast artificial chromosome (YAC) and to allow for the genome and YAC to join by recombination, the plasmid must contain overhangs homologous to the phage genome ends⁵⁹. Phage genomes that have been assembled, modified and propagated in yeast can then be isolated and introduced into the bacterial host to create functional phage particles. Because of this, the yeast-based assembly can be restricted by bacterial transformation efficiencies and while some bacteria such as *E. coli* have efficient transformation protocols, there are many other bacterial species that are difficult to transform³⁹.

Yeast based assembly has been used to expand phage host ranges by engineering genomes in *S. cerevisiae*. In 2015, Ando *et al.* created synthetic phages by redirecting *E. coli* phage to target pathogenic *Yersinia* and *Klebsiella* strains by modular swapping of phage tail components⁶⁰. The technique involved PCR-amplification of the appropriate segments of two different phage genomes to provide the viral scaffold and the heterologous tail fibre. PCR primers were designed to furnish overhangs that connect the fragments with each other, as well as with the termini of a YAC vector. Upon transformation of the fragment mix into yeast, gap repair joined them to create a full phage genome cloned into a replicative yeast plasmid⁶⁰. The YAC-phage DNA could then be extracted from the yeast and be transformed into bacterial hosts to assemble the phage particles. After screening, they found that over 25% of

yeast clones contained correctly assembled phage genomes⁶⁰. The engineered phages were efficient at killing their new targets and could selectively remove bacteria from multi-species communities⁶⁰.

3.5. Cell-free assembly

Cell-free transcription-translation (TXTL) systems utilise the endogenous transcription and translation machinery harvested from bacteria such as *E. coli*, and combines this with a metabolite pool and an ATP-regenerating system to allow for gene expression in a single reaction⁶¹. A popular and commercially available cell-free TXTL system is the hybrid phage-*E. coli* system created in the 1990s, and in this system protein synthesis can reach over 1 mg/ml of reaction⁶². It combines a bacteriophage RNA polymerase to perform transcription, usually T7 phage due to its high specificity and strength, with a cytoplasmic extract from *E. coli* to provide the translation machinery.

Cell-free systems have been adapted for numerous applications across the field of synthetic biology, including assembling whole phage particles in a cell-free environment⁶³. The ability to express phages from their isolated genome allows control over how and when phages are utilised and offers a way to identify genes necessary for assembly through iterative gene knockouts⁶³.

In 2011, Shin *et al.* showed that T7 phage (dsDNA) and Φ X174 phage (ssDNA) could be fully synthesised *in vitro* from their genomes using the cell-free toolbox 1.0, creating more than a billion infectious T7 particles per millilitre of reaction after just hours of incubation⁶⁴. In 2016, Garamella *et al.* developed an all *E. coli* TXTL toolbox 2.0, which integrated a novel mechanism for ATP regeneration into the system and this increased protein synthesis by a factor of 2 to 3 depending on the sigma factor expressed⁶⁵. The new system also showed that the synthesis of the two phages previously assembled increased by several orders of magnitude.

Cell-free TXTL systems may offer a potential solution to the disadvantages seen for other phage engineering methods, such as the toxicity of the donor DNA during homologous recombination or the requirement of high transformation efficiencies for BRED and yeast-based assembly. Testing this technique for a broader range of phage genomes is essential to see if it is universally applicable³⁹.

3.6 Engineering techniques summary

Technique	Description	Advantages	Disadvantages
Homologous recombination	A plasmid containing the gene to be introduced flanked by regions of homology is transformed into a bacterial host and this then integrates into the phage genome by recombination during infection.	A commonly used and well-established protocol, which is useful for introducing genes and mutations.	Needs extensive <i>in vitro</i> engineering of plasmids, which is time-consuming and recombination rates are often low.
BRED	A DNA substrate flanked by regions of homology is co-electroporated with phage DNA into a host cell, containing a plasmid to promote high levels of recombination.	Higher recombination rate and less screening required.	High background of wild-type phage and requires highly competent bacterial hosts.
CRISPR-Cas	A plasmid encoding an effector complex containing guide RNA, which binds to the target sequence and a Cas protein, which cleaves the target DNA, is transformed into a host cell containing phage genome.	Counter selects wild-type phages, so the population only contains recombinant phages and less screening is required.	Potential for off-target cleavage and undesired mutations and some phages may encode Cas inhibitors.
Yeast-based assembly	Phage genome is assembled during its recombination into a yeast artificial chromosome, where it is modified and assembled in the yeast cell, then transformed into a bacterial host to form functional particles.	Phage genomes are not toxic to a yeast host and can be maintained stably.	Requires highly competent bacterial hosts.
Cell-free assembly	Whole phage particles can be assembled in a cell-free environment containing extracted transcription and translation machinery from bacteria mixed with an amino acid and energy solution.	No host needed and it gives extensive control over how and when phage particles are assembled.	A limited number of phages tested so not yet confident if universally applicable.

Table 2: Summary of phage engineering techniques

4. Isolation, purification and characterisation

Following successful phage engineering, the *de novo* phage variant must be isolated, impurities of the preparation must be removed and the phage's characteristics must be assessed. When considering the delivery of the final product, it is vital to keep in mind the rigorous assessment requirements of pharmaceutical-grade phage products. Good manufacturing practice (GMP) certification represents the gold-standard of pharmaceutical classification and provides a guarantee of a well-defined production, purification and quality control protocol, which should be an integral part of the development ⁶⁶.

4.1. Isolation

Isolation of recombinant bacteria is often performed by positive selection, where an antibiotic resistance cassette is expressed by the recombinant bacteria to exclude non-recombinants on selective media. However, isolation of recombinant phages using a similar positive selection is not always suitable, as phage propagation ultimately results in lysis of the host bacterium.

Marker-based selection exploits a bacterial host, which is deficient of a gene that is non-essential for the host, but essential for phage propagation. Selection is performed by designing the recombinant phage to encode the missing gene, thus allowing for phage propagation ⁶⁷. Marker-based selection has been demonstrated to engineer knockout mutants for a number of phage T7 genes ⁶⁸.

Counterselection using CRISPR-Cas allows for selection against phage variants that have not been modified while enriching the recombinant phage, providing that the recombination included a deletion or interruption of a PAM-proximal sequence. This method overcomes the issues of having to find a small percentage of recombinant phages from a large pool of wild-type phages ³⁹. This was used by Kiro *et al.* ⁶⁹ to enhance the engineering of T7 phage genome with the type I-E CRISPR-Cas system. Homologous recombination was used to delete gene 1.7, resulting in a mixed population of wild-type phages and recombinant phages lacking the gene. The phage lysate was plated on host bacteria carrying three plasmids needed for CRISPR-Cas counterselection: a spacer targeting gene 1.7, the targeting cascade complex and the Cas3 degradation machinery ⁶⁹. This resulted in the selective cleavage of wild-type phage genomes still carrying the gene, leaving an enriched population of recombinant phages ⁶⁹. A comparative study by Grigonyte *et al.* ⁵⁶ in engineering of phage T7 demonstrated that the Type II CRISPR-Cas system was superior in efficiency and ease of use than the Type I CRISPR-Cas system.

Regardless of the choice of isolation approach, it is advisable to seek to achieve the greatest concentration of recombinant phages in relation to wild-type phages. This can be achieved by using an effective engineering protocol, through optimisation of the said protocol or through enrichment cycles.

4.2. Purification

Rapid purification can be achieved by the use of single-step ion-exchange monolithic chromatography. The approach is generally fast and has high resolving power, albeit this efficiency is highly dependable on the size of the phage, as well as the dynamic binding

capacity of the media. This was demonstrated by Smrekar *et al.* ⁷⁰, who used Convective Interaction Media (CIM) monolithic columns to purify phage T4 at a high recovery rate of 70%, while maintaining phage infectivity. Purification of filamentous phage M13, commonly used for phage display, was demonstrated by Monjezi *et al.* ⁷¹ using SepFast SuperQ columns, achieving similar recovery rates. It is, however, important to note that effective removal of endotoxins has proven difficult by some chromatography approaches ⁷².

Aqueous two-phase extractions (ATPE) and salting-out extractions (SOE) are effectively used for the purification of various biomolecules, including viruses and virus-like particles ⁷³, with the benefit of being time- and energy-saving as well as inexpensive methods ⁷⁴. Using a two-step SOE with salts and organic solvents, Zhang *et al.* ⁷⁵, determined the optimal purification condition of Klebsiella phage phiKpS2 as a sodium citrate and ethyl acetate-mix in the first step and transfer of bottom phase with the addition of n-propanol in the second step. Their protocol resulted in 77% phage recovery, while 83% of endotoxins were removed.

The gold-standard for purification of phage preparations is still considered to be caesium chloride (CsCl) density gradient separation. The methods consist of successive rounds of high-speed and ultracentrifugation, initially capturing phages using PEG precipitation followed by density gradient separation at 125,000 g and finally dialysis ^{76, 77}. Despite being time consuming and laborious, this approach delivers a highly concentrated phage preparation, while ensuring effective removal of impurities, such as endotoxins.

4.3. Characterisation

In order for a phage preparation to be considered appropriate for therapeutic use, there are a series of important properties that must be determined as these can vary greatly between phage strains. These properties include, but are not limited to: virulence, generation time, burst size and especially host range or specificity. Additionally, a full genome sequencing and annotation should be performed as discussed earlier.

The virulence of a phage is related to generation time and burst size displaying its ability to outcompete the bacterial host and completely clear a culture. While high virulence is desirable, it is likely that in a clinical setting, administration of phage would not be the sole means of reducing the bacterial concentration, as generally, patients will have a functioning immune system or the treatment could be combined with antibiotics ⁷⁸.

The narrow host range of individual phage strains, often limiting infection to a single bacterial species or a few strains, is desirable as it leaves the remaining microbiome intact. However, for the usefulness of phage therapy, it is possible that phages with broader host range, e.g. including most strains within a bacterial species, would lead to fewer treatment failures and limit the need for direct isolation and susceptibility testing of the bacterial pathogen ⁷⁹.

5. Therapeutic applications

In this section, we highlight examples of phage engineering and their potential applications.

5.1. Phage-based antimicrobial agents

During the final stages of virulent phage infection, phage-encoded endolysins degrade the peptidoglycan layer of the bacterial cell wall eventually causing the bacterial cell to rupture and thus release the phage progeny. Phage derived endolysins have been successfully exploited in industrial applications, predominantly targeting gram-positive bacterial strains lacking a second outer membrane ⁸⁰. The peptidoglycan layer consists of a matrix of alternating N-acetylglucosamine (GlcNAc) and N-acetylmuramic acid (MurNAc) residues, which are cross-linked by D- and L-amino acids. Based on their catalytic activity, phage endolysins can be separated into three overall groups.

5.2. Phage host expansion

The continual evolutionary arms race between phages and their bacterial hosts may in part explain the often limited host range of phages ³⁶. Altering the tropism of a particularly efficient phage or expanding the host range on a modular platform seems an appealing thought.

Ando *et al.* ⁶⁰ used a modular approach to engineer *Escherichia coli* phages capable of infecting *Yersinia* and *Klebsiella* bacteria and *Klebsiella* phages capable of infecting *Escherichia coli*. It was achieved by synthesising the entire phage genome in segments containing YAC homology end and electroporating these into *S. cerevisiae*. The yeast-based assembly joined each fragment together by gap repair delivering a full phage genome to be enzymatically excised from the YAC-phage DNA ⁶⁰.

Yosef *et al.* ⁶⁸ sought to extend the host range of phages for DNA transduction rather than phage replication. Transducing phage particles could prove more controllable and may receive a more relaxed approval procedure from regulatory agencies than virulent phages. Fifteen plasmids each containing the tail gene product of an individual phage, as well as an antibiotic resistance cassette and packaging signal, were transformed into a propagation host alongside T7 phage lacking its tail genes (gp11, gp12 and gp17). The resulting lysate contained recombinant T7 phage particles, which could be screened for by incubation with previously unsusceptible hosts on selective media ⁶⁸.

5.3. Virulent derivatives of temperate phages

The natural abundance of temperate phages vastly outnumbers their virulent siblings, these are, however, not suitable for therapeutic use. To overcome this, multiple engineering strategies have been employed to produce virulent derivatives of temperate parents.

By annotation of the 57 kbp genome of the mycobacterium phage ZoeJ, Dedrick *et al.* ⁵ identified gp43 and gp45 as candidate integrase and immunity repressor genes, respectively. Wild-type phage ZoeJ, was shown to be temperate and formed turbid plaques yielding lysogens, which were immune to superinfection. The group used BRED to engineer ZoeJΔ45, which showed deletion of gp45 and was presented as a virulent derivative forming clear plaques with no stable lysogen ⁵.

A different approach was employed by Kilcher *et al.* ⁸¹ to engineer a virulent derivative of *Listeria* phage B025. Phage genomes were assembled *in vitro* from synthesised DNA fragments using Gibson assembly and were transformed into *Listeria monocytogenes* L-form bacterial cells, which allowed for the phage DNA constructs to reboot into replicating phages. The approach was used to assemble *Listeria* phage B025Δrep *in vitro* lacking the 2.7 kb

lysogeny control region, effectively engineering a virulent derivative from its temperate parent⁸¹.

5.4. Enhanced bactericidal activity of antibiotics

The evolution of antibiotic resistance in bacteria is increasingly outpacing the development of new antimicrobial drugs. Edgar *et al.*⁸² demonstrated an approach that re-sensitises resistant bacteria to approved antibiotics. Plasmids containing the genes *rpsL* and *tehAB*, conferring sensitivity to streptomycin and resistance to tellurite respectively, were constructed by standard digestion and ligation protocol and recombinant phages were engineered by homologous recombination. Mutations in the *rpsL* gene of streptomycin-resistant *Mycobacterium tuberculosis* is common and restoring this gene allowing expression of the gene product, S12, re-sensitises the bacteria to streptomycin. Resistant clinical isolates of *M. tuberculosis* infected with the engineered temperate phage λ -*rpsL*-wt-tell were demonstrated to be re-sensitised to streptomycin under the selective pressure of tellurite⁸². Similarly, in a study by Lu *et al.*⁸³, the non-lytic filamentous M13 phage was engineered to carry the *lexA3* gene in order to make targeted *E. coli* cells more susceptible to antibiotic treatment. Bactericidal antibiotics cause DNA damage in bacteria through the formation of hydroxyl-radicals, which is repaired by the bacterial SOS response induced by *recA*. This can be mitigated by knockout of *recA* or by overexpression of *lexA*, the key repressor of the SOS regulon. In the specific example, the gene product of *lexA3*, encoding a repressor non-cleavable by RecA, was transduced by the modified phages to make the SOS system of target cells uninducible and thereby to reduce bacterial survival⁸³.

5.5. Vaccine platforms

The phage display technology has been essential in studies of protein-protein interaction for decades and in this sense, the ease of fusing and displaying exogenous recombinant polypeptides on the phages' surface has been documented. Numerous phage-displayed peptide immunogens have been developed and in some cases have been shown to elicit antibody production. However, recombinant and live attenuated vaccines have so far proven more efficient and easier to produce⁸⁴.

In Alzheimer's disease, amyloid- β (A β) peptides accumulate and form fibrils. Using phage M13 as a scaffold, Tanaka *et al.*⁸⁵, displayed the B6-C15 mimotope on the phage surface. B6-C15 is a peptide with known sequence similarities to B6 scFv, an antibody that binds to A β 42 fibrils but is not soluble to A β and inhibits fibril formation. The group demonstrated that the phage-displayed B6-C15, was capable of inhibiting A β 42 fibril formation and A β 42-induced cytotoxicity. Additionally, mice immunised with the phage exhibited reduced amyloid plaque formation and induction of anti-A β 42 conformer IgG antibody response, suggesting the potential for the future use of phage-derived vaccines in Alzheimer's disease prevention⁸⁵.

The filamentous phage has also been used as a platform for vaccination against infectious diseases. Mascolo *et al.*⁸⁶ demonstrated that phage-displaying the Ovalbumin₂₅₇₋₂₆₄ cytotoxic T-cell epitope, could induce a long-term peptide-specific CD8 cytotoxicity with or without the use of a T-helper epitope⁸⁶. The potential of the filamentous phage as a vaccine scaffold is underlined by its apparent intrinsic immunogenicity and the proven phage display technology.

5.6. Drug delivery systems

Analogous to using phages as a vaccine scaffold by fusing a peptide externally to the capsid or coat protein, phages are being designed to carry anticancer drugs or toxic compounds such as ligands or CRISPR cassettes internally³⁹.

Bar *et al.*⁸⁷ utilised the filamentous fUSE5-ZZ phage vector to enable stable complex formation with target-specific antibodies, including chFRP5, demonstrating strong specific binding towards the ErbB2 overexpressing human breast adenocarcinoma SKBR3 cells. Using confocal microscopy, they showed that engineered phage fUSE5-ZZ-chFRP5 was internalised through receptor-mediated endocytosis and was degraded by lysosomal activity. This was followed by chemical conjugation of anticancer drugs, hygromycin or doxorubicin, using EDC chemistry forming covalent bonds between the major coat protein and the drug. Once internalised, the lysosomal degradation would mediate drug release intracellularly in SKBR3 cells, resulting in a 50% inhibition of cell growth. Such phage mediated drug release yielded a >1000-fold improvement *in vitro* in comparison with corresponding free drugs⁸⁷.

CRISPR-Cas9 was used as a gene-specific antimicrobial delivered by engineered temperate phage ϕ SaBov, targeting methicillin-resistant *Staphylococcus aureus* (MRSA)⁸⁸. A plasmid, pKS4, was constructed to include CRISPR/Cas machinery, spacer sequence specific to the *nuc* gene and was subsequently integrated into the non-coding region of ϕ SaBov using homologous recombination. Phage ϕ SaBov-Cas9-nuc displayed significantly enhanced efficacy towards MRSA, resulting in nearly complete decolonisation *in vitro* and in a two orders of magnitude reduction of CFU in an *in vivo* murine skin model⁸⁸.

In a similar work carried out earlier, Bikard *et al.*⁸⁹ used phage Φ NM1 to deliver a CRISPR/Cas-expressing phagemid to *S. aureus* cells. They demonstrated the selective reduction of MRSA cell count in a mixed bacterial population by nearly three orders of magnitude when targeting a chromosomal locus. If the targeted locus resided on a plasmid, they achieved plasmid loss in 99.99% of the cell population, with the retained phagemid providing immunity against future acquirement of the targeted gene⁸⁹. Such selective killing of pathogenic strains or selective elimination of their virulence plasmids using modified phages is often referred to as "smart antibiotic" treatment, because it leaves the commensal flora otherwise intact.

5.7. Biofilm degradation

In general, bacteria that are capable of forming capsules or biofilms are associated with higher resistance towards antibiotics, as well as phages. While some phages express their own biofilm-degrading enzymes, such as phages UPMK_1 and UPMK_2 targeting methicillin-resistant *Staphylococcus aureus* (MRSA)⁹⁰, engineering of novel phages with similar characteristics has also been demonstrated.

For example, *E. coli* phage T7 was engineered to express Dispersin B (DspB), a glycoside hydrolase capable of disrupting biofilm formation intracellularly during infection, for the enzyme to spread into the extracellular environment upon lysis of the host⁹¹. The T7_{DspB} phage was constructed by integrating the *DspB* gene driven by the potent T7 ϕ 10 promoter into the commercially available phage T7select415-1. Gene 1.2 of phage T3 was also inserted to allow phage propagation in F-plasmid carrying targets, like *E. coli* TG1, which forms a thick biofilm. Using a crystal violet assay to determine the effect of phage T7_{DspB} versus T7_{Control}, the group found that engineered phage T7_{DspB} reduced bacterial cell counts by 4.5 orders of

magnitude, equal to 99.997% removal, which was two orders of magnitude better than phage T7_{Control}⁹¹.

5.8. Pathogen detection

Phages are ideal diagnostic tools for pathogen detection because of their intrinsic high host specificity and signal-amplifying properties and can these be engineered to express reporter genes following infection of a target host bacterium⁹². Multiple stages of the life cycle of a virulent phage can be harnessed for this use in addition to phage derived particles⁹³.

The *Wβ::luxAB-2* reporter phage was engineered by targeted homologous recombination using the temperate *Bacillus anthracis* phage *Wβ* and a *luxAB* expression cassette containing the *Vibrio harveyi luxA* and *luxB* genes, an upstream *Bacillus* promoter and downstream transcriptional terminator TL17⁹⁴. Detection of a bioluminescent signal was possible after 16 minutes following infection of vegetative *B. anthracis* cells⁹⁴ and a bacterial concentration as low as 10 CFU/ml could be detected in water within 8 hours⁹⁵. The bioluminescent *Wβ::luxAB-2* reporter phage also enabled detection of *B. anthracis* spores⁹⁴.

Hinkley *et al.*⁹⁶ engineered a T7 coliphage to express NanoLuc (NLuc), a luciferase from the deep-sea shrimp *Oplophorus gracilirostris*, fused with a carbohydrate-binding module (CBM). The *nluc::cbm* construct included a custom ribosome binding site, designed to optimise translation as well as a N-terminal leader sequence (*pelB*) intended to direct newly made proteins to the periplasmic space. Standard restriction digestion and ligation was used to assemble the construct, while homologous recombination was used for integration. During a diagnostic run, the reporter phage was added to water samples containing *E. coli* cells. The NLuc enzyme released during cell lysis was captured on a cellulose filter and was quantified in a luminometer after addition of the NanoGlo substrate. A detection limit of <10 CFU/ml in 3 hours was achieved in water samples⁹⁶.

6. Conclusion

Bacteriophages were discovered at the beginning of the 20th century, preceding the first antibiotics by more than a decade. Later, with the discovery of low cost and effective antibiotics, the development of phages as antimicrobials, was halted in Western medicine. Today, however, with the spread and evolution of antibiotic-resistant bacteria, we are again turning towards phages as antimicrobials. As described in this chapter, the advancement of technology and the applications for phages as therapeutics are diverse and progressive. This can, in part, be attributed to the efforts achieved in using phage technology in food security, right from the beginning of cultivation of plants and livestock, to the end of the process of preserving food products by reducing spoilage and bacterial contaminants. In the clinical setting, phage therapy is being explored as a treatment of both resistant- and non-resistant bacterial infections and the numerous successful cases of compassionate use demonstrate the capabilities and advantages of phages as therapeutics. The versatility is illustrated by the current global preclinical antibacterial drug pipeline, containing concepts employing phage or phage-derived components in diverse areas such as modulation of the microbiota, engineered probiotics and antibacterial compounds targeting a wide range of gram-positive and -negative bacterial hosts. Changes in legislation for the approval process of phage-derived therapeutics is well underway and will hopefully ensure the continued development of their application in clinical care in as many forms and areas as possible.

7. References

1. Wittebole, X., De Roock, S. & Opal, S.M. A historical overview of bacteriophage therapy as an alternative to antibiotics for the treatment of bacterial pathogens. *Virulence* **5**, 226-235 (2014).
2. McCallin, Sacher, Zheng & Chan Current State of Compassionate Phage Therapy. *Viruses* **11**, 343 (2019).
3. Theuretzbacher, U., Outtersson, K., Engel, A. & Karlén, A. The global preclinical antibacterial pipeline. *Nature Reviews Microbiology* **18**, 275-285 (2020).
4. Dedrick, R.M. *et al.* Engineered bacteriophages for treatment of a patient with a disseminated drug-resistant Mycobacterium abscessus. *Nature Medicine* **25**, 730-733 (2019).
5. Dedrick, R.M. *et al.* Mycobacteriophage ZoeJ: A broad host-range close relative of mycobacteriophage TM4. *Tuberculosis* **115**, 14-23 (2019).
6. Danis-Włodarczyk, K., Dąbrowska, K. & Abedon, S.T. Phage Therapy: The Pharmacology of Antibacterial Viruses. *Curr Issues Mol Biol* **40**, 81-164 (2020).
7. Dąbrowska, K. & Abedon, S.T. Pharmacologically Aware Phage Therapy: Pharmacodynamic and Pharmacokinetic Obstacles to Phage Antibacterial Action in Animal and Human Bodies. *Microbiology and Molecular Biology Reviews* **83**, e00012-00019 (2019).
8. Furfaro, L.L., Payne, M.S. & Chang, B.J. Bacteriophage Therapy: Clinical Trials and Regulatory Hurdles. *Frontiers in Cellular and Infection Microbiology* **8** (2018).
9. Fauconnier, A. Phage Therapy Regulation: From Night to Dawn. *Viruses* **11**, 352 (2019).
10. Nikolich, M.P. & Filippov, A.A. Bacteriophage Therapy: Developments and Directions. *Antibiotics (Basel)* **9**, 135 (2020).
11. Du Toit, A. Phage induction in different contexts. *Nature Reviews Microbiology* **17**, 126-127 (2019).
12. Brown-Jaque, M., Calero-Cáceres, W. & Muniesa, M. Transfer of antibiotic-resistance genes via phage-related mobile elements. *Plasmid* **79**, 1-7 (2015).
13. Monteiro, R., Pires, D.P., Costa, A.R. & Azeredo, J. Phage Therapy: Going Temperate? *Trends in Microbiology* **27**, 368-378 (2019).
14. Merrill, C.R. *et al.* Long-circulating bacteriophage as antibacterial agents. *Proceedings of the National Academy of Sciences of the United States of America* **93**, 3188-3192 (1996).
15. Sokoloff, A.V., Bock, I., Zhang, G., Sebestyén, M.G. & Wolff, J.A. The interactions of peptides with the innate immune system studied with use of T7 phage peptide display. *Mol Ther* **2**, 131-139 (2000).
16. Malik, D.J. *et al.* Formulation, stabilisation and encapsulation of bacteriophage for phage therapy. *Advances in Colloid and Interface Science* **249**, 100-133 (2017).
17. Principi, N., Silvestri, E. & Esposito, S. Advantages and Limitations of Bacteriophages for the Treatment of Bacterial Infections. *Frontiers in Pharmacology* **10** (2019).
18. Verheust, C., Pauwels, K., Mahillon, J., Helinski, D.R. & Herman, P. Contained use of Bacteriophages: Risk Assessment and Biosafety Recommendations. *Applied Biosafety* **15**, 32-44 (2010).
19. Keen, E.C. *et al.* Novel "Superspreader" Bacteriophages Promote Horizontal Gene Transfer by Transformation. *mBio* **8** (2017).

20. Fernández, L., Gutiérrez, D., García, P. & Rodríguez, A. The Perfect Bacteriophage for Therapeutic Applications-A Quick Guide. *Antibiotics (Basel)* **8**, 126 (2019).
21. Duffy, S., Turner, P.E. & Burch, C.L. Pleiotropic Costs of Niche Expansion in the RNA Bacteriophage Φ 6. *Genetics* **172**, 751-757 (2006).
22. Schmerer, M., Molineux, I.J. & Bull, J.J. Synergy as a rationale for phage therapy using phage cocktails. *PeerJ* **2**, e590-e590 (2014).
23. Oechslin, F. Resistance Development to Bacteriophages Occurring during Bacteriophage Therapy. *Viruses* **10**, 351 (2018).
24. Gill, J.J. & Hyman, P. Phage choice, isolation, and preparation for phage therapy. *Curr Pharm Biotechnol* **11**, 2-14 (2010).
25. Allen, R.C., Pfrunder-Cardozo, K.R., Meinel, D., Egli, A. & Hall, A.R. Associations among Antibiotic and Phage Resistance Phenotypes in Natural and Clinical *Escherichia coli* Isolates. *mBio* **8** (2017).
26. Gómez, P., Bennie, J., Gaston, K.J. & Buckling, A. The Impact of Resource Availability on Bacterial Resistance to Phages in Soil. *PLOS ONE* **10**, e0123752 (2015).
27. Örmälä, A.-M. & Jalasvuori, M. Phage therapy. *Bacteriophage* **3**, e24219 (2013).
28. Seed, K.D. Battling Phages: How Bacteria Defend against Viral Attack. *PLoS pathogens* **11**, e1004847-e1004847 (2015).
29. Reyes-Robles, T. *et al.* *Vibrio cholerae* Outer Membrane Vesicles Inhibit Bacteriophage Infection. *Journal of bacteriology* **200** (2018).
30. Ofir, G. *et al.* DISARM is a widespread bacterial defence system with broad anti-phage activities. *Nature Microbiology* **3**, 90-98 (2018).
31. Loenen, W.A., Dryden, D.T., Raleigh, E.A., Wilson, G.G. & Murray, N.E. Highlights of the DNA cutters: a short history of the restriction enzymes. *Nucleic Acids Res* **42**, 3-19 (2014).
32. Barrangou, R. *et al.* CRISPR provides acquired resistance against viruses in prokaryotes. *Science* **315**, 1709-1712 (2007).
33. Parma, D.H. *et al.* The Rex system of bacteriophage lambda: tolerance and altruistic cell death. *Genes Dev* **6**, 497-510 (1992).
34. Depardieu, F. *et al.* A Eukaryotic-like Serine/Threonine Kinase Protects *Staphylococci* against Phages. *Cell host & microbe* **20**, 471-481 (2016).
35. Page, R. & Peti, W. Toxin-antitoxin systems in bacterial growth arrest and persistence. *Nat Chem Biol* **12**, 208-214 (2016).
36. Hampton, H.G., Watson, B.N.J. & Fineran, P.C. The arms race between bacteria and their phage foes. *Nature* **577**, 327-336 (2020).
37. Šimoliūnas, E. *et al.* *Pantoea* Bacteriophage vB_PagS_Vid5: A Low-Temperature Siphovirus That Harbors a Cluster of Genes Involved in the Biosynthesis of Archaeosine. *Viruses* **10**, 583 (2018).
38. Hutinet, G. *et al.* 7-Deazaguanine modifications protect phage DNA from host restriction systems. *Nat Commun* **10**, 5442 (2019).
39. Pires, D.P., Cleto, S., Sillankorva, S., Azeredo, J. & Lu, T.K. Genetically Engineered Phages: a Review of Advances over the Last Decade. *Microbiology and Molecular Biology Reviews* **80**, 523 (2016).
40. Karam, J.D., Drake, J. W., Kreuzer, K. N., Mosig, G., Hall, D. H., Eiserling, F. A Molecular biology of bacteriophage T4. *American Society for Microbiology* (1994).
41. Chen, Y. *et al.* Genetic Engineering of Bacteriophages Against Infectious Diseases. *Frontiers in microbiology* **10**, 954-954 (2019).

42. Loessner, M.J., Rees, C.E., Stewart, G.S. & Scherer, S. Construction of luciferase reporter bacteriophage A511::luxAB for rapid and sensitive detection of viable *Listeria* cells. *Applied and Environmental Microbiology* **62**, 1133 (1996).
43. Court, D.L., Sawitzke, J.A. & Thomason, L.C. Genetic Engineering Using Homologous Recombination. *Annual Review of Genetics* **36**, 361-388 (2002).
44. Mahichi, F., Synnott, A.J., Yamamichi, K., Osada, T. & Tanji, Y. Site-specific recombination of T2 phage using IP008 long tail fiber genes provides a targeted method for expanding host range while retaining lytic activity. *FEMS Microbiol Lett* **295**, 211-217 (2009).
45. Sarkis, G.J., Jacobs, W.R., Jr. & Hatfull, G.F. L5 luciferase reporter mycobacteriophages: a sensitive tool for the detection and assay of live mycobacteria. *Mol Microbiol* **15**, 1055-1067 (1995).
46. Marinelli, L.J. *et al.* BRED: a simple and powerful tool for constructing mutant and recombinant bacteriophage genomes. *PLoS one* **3**, e3957-e3957 (2008).
47. Shin, H., Lee, J.-H., Yoon, H., Kang, D.-H. & Ryu, S. Genomic Investigation of Lysogen Formation and Host Lysis Systems of the *Salmonella* Temperate Bacteriophage SPN9CC. *Applied and Environmental Microbiology* **80**, 374 (2014).
48. Marinelli, L.J., Piuri, M. & Hatfull, G.F. Genetic Manipulation of Lytic Bacteriophages with BRED: Bacteriophage Recombineering of Electroporated DNA, in *Bacteriophages: Methods and Protocols, Volume IV.* (eds. M.R.J. Clokie, A. Kropinski & R. Lavigne) 69-80 (Springer New York, New York, NY; 2019).
49. Marinelli, L.J., Hatfull, G.F. & Piuri, M. Recombineering: A powerful tool for modification of bacteriophage genomes. *Bacteriophage* **2**, 5-14 (2012).
50. Oppenheim, A.B., Rattray, A.J., Bubunencko, M., Thomason, L.C. & Court, D.L. In vivo recombineering of bacteriophage lambda by PCR fragments and single-strand oligonucleotides. *Virology* **319**, 185-189 (2004).
51. Hatoum-Aslan, A. Phage Genetic Engineering Using CRISPR-Cas Systems. *Viruses* **10**, 335 (2018).
52. Sorek, R., Kunin, V. & Hugenholtz, P. CRISPR--a widespread system that provides acquired resistance against phages in bacteria and archaea. *Nat Rev Microbiol* **6**, 181-186 (2008).
53. Westra, E.R., Buckling, A. & Fineran, P.C. CRISPR-Cas systems: beyond adaptive immunity. *Nat Rev Microbiol* **12**, 317-326 (2014).
54. Makarova, K.S. & Koonin, E.V. Annotation and Classification of CRISPR-Cas Systems. *Methods Mol Biol* **1311**, 47-75 (2015).
55. Koonin, E.V., Makarova, K.S. & Zhang, F. Diversity, classification and evolution of CRISPR-Cas systems. *Current Opinion in Microbiology* **37**, 67-78 (2017).
56. Grigonyte, A.M. *et al.* Comparison of CRISPR and Marker-Based Methods for the Engineering of Phage T7. *Viruses* **12**, 193 (2020).
57. Zetsche, B. *et al.* Cpf1 is a single RNA-guided endonuclease of a class 2 CRISPR-Cas system. *Cell* **163**, 759-771 (2015).
58. Martel, B. & Moineau, S. CRISPR-Cas: an efficient tool for genome engineering of virulent bacteriophages. *Nucleic Acids Res* **42**, 9504-9513 (2014).
59. Lu TK, K.M., Chevalier B, Holder J, McKenzie G, Brownell D Recombinant phage and methods. *US patent* (2013).
60. Ando, H., Lemire, S., Pires, D.P. & Lu, T.K. Engineering Modular Viral Scaffolds for Targeted Bacterial Population Editing. *Cell Syst* **1**, 187-196 (2015).



61. Sun, Z.Z., Hayes, C. A., Shin, J., Caschera, F., Murray, R. M. & Noireaux, V. Protocols for implementing an Escherichia coli based TX-TL cell-free expression system for synthetic biology. *J Vis Exp* (2013).
62. Nevin, D.E. & Pratt, J.M. A coupled in vitro transcription-translation system for the exclusive synthesis of polypeptides expressed from the T7 promoter. *FEBS Lett* **291**, 259-263 (1991).
63. Joseph P. Wheatley, S.B.W.L., Richard Amaee, Antonia P. Sagona, Vishwesh Kulkarni Synthetic Biology for the Rapid, Precise and Compliant Detection of Microbes, in *Advances in synthetic biology* 289-306 (2020).
64. Shin, J., Jardine, P. & Noireaux, V. Genome Replication, Synthesis, and Assembly of the Bacteriophage T7 in a Single Cell-Free Reaction. *ACS Synthetic Biology* **1**, 408-413 (2012).
65. Garamella, J., Marshall, R., Rustad, M. & Noireaux, V. The All E. coli TX-TL Toolbox 2.0: A Platform for Cell-Free Synthetic Biology. *ACS Synthetic Biology* **5**, 344-355 (2016).
66. Bretaudeau, L., Tremblais, K., Aubrit, F., Meichenin, M. & Arnaud, I. Good Manufacturing Practice (GMP) Compliance for Phage Therapy Medicinal Products. *Frontiers in Microbiology* **11** (2020).
67. Baba, T. *et al.* Construction of Escherichia coli K-12 in-frame, single-gene knockout mutants: the Keio collection. *Mol Syst Biol* **2**, 2006.0008-2006.0008 (2006).
68. Yosef, I., Goren, M.G., Globus, R., Molshanski-Mor, S. & Qimron, U. Extending the Host Range of Bacteriophage Particles for DNA Transduction. *Mol Cell* **66**, 721-728.e723 (2017).
69. Kiro, R., Shitrit, D. & Qimron, U. Efficient engineering of a bacteriophage genome using the type I-E CRISPR-Cas system. *RNA Biol* **11**, 42-44 (2014).
70. Smrekar, F., Ciringer, M., Peterka, M., Podgornik, A. & Štrancar, A. Purification and concentration of bacteriophage T4 using monolithic chromatographic supports. *Journal of Chromatography B* **861**, 177-180 (2008).
71. Monjezi, R., Tey, B.T., Sieo, C.C. & Tan, W.S. Purification of bacteriophage M13 by anion exchange chromatography. *J Chromatogr B Analyt Technol Biomed Life Sci* **878**, 1855-1859 (2010).
72. Bourdin, G. *et al.* Amplification and purification of T4-like escherichia coli phages for phage therapy: from laboratory to pilot scale. *Applied and environmental microbiology* **80**, 1469-1476 (2014).
73. Ladd Effio, C. *et al.* Downstream processing of virus-like particles: Single-stage and multi-stage aqueous two-phase extraction. *Journal of Chromatography A* **1383**, 35-46 (2015).
74. Su, C.-K. & Chiang, B.H. Partitioning and purification of lysozyme from chicken egg white using aqueous two-phase system. *Process Biochemistry* **41**, 257-263 (2006).
75. Zhang, Z.-R. *et al.* Separation and purification of Klebsiella phage by two-step salting-out extraction. *Separation and Purification Technology* **242**, 116784 (2020).
76. Møller-Olsen, C., Ho, S.F.S., Shukla, R.D., Feher, T. & Sagona, A.P. Engineered K1F bacteriophages kill intracellular Escherichia coli K1 in human epithelial cells. *Scientific Reports* **8**, 17559 (2018).
77. Castro-Mejía, J.L. *et al.* Optimizing protocols for extraction of bacteriophages prior to metagenomic analyses of phage communities in the human gut. *Microbiome* **3**, 64 (2015).

78. Levin, B.R. & Bull, J.J. Population and evolutionary dynamics of phage therapy. *Nature Reviews Microbiology* **2**, 166-173 (2004).
79. Ross, A., Ward, S. & Hyman, P. More Is Better: Selecting for Broad Host Range Bacteriophages. *Frontiers in Microbiology* **7** (2016).
80. Drulis-Kawa, Z., Majkowska-Skrobek, G. & Maciejewska, B. Bacteriophages and phage-derived proteins--application approaches. *Current medicinal chemistry* **22**, 1757-1773 (2015).
81. Kilcher, S., Studer, P., Muessner, C., Klumpp, J. & Loessner, M.J. Cross-genus rebooting of custom-made, synthetic bacteriophage genomes in L-form bacteria. *Proceedings of the National Academy of Sciences* **115**, 567-572 (2018).
82. Edgar, R., Friedman, N., Molshanski-Mor, S. & Qimron, U. Reversing Bacterial Resistance to Antibiotics by Phage-Mediated Delivery of Dominant Sensitive Genes. *Applied and Environmental Microbiology* **78**, 744 (2012).
83. Lu, T.K. & Collins, J.J. Engineered bacteriophage targeting gene networks as adjuvants for antibiotic therapy. *Proceedings of the National Academy of Sciences of the United States of America* **106**, 4629-4634 (2009).
84. Henry, K.A., Arbabi-Ghahroudi, M. & Scott, J.K. Beyond phage display: non-traditional applications of the filamentous bacteriophage as a vaccine carrier, therapeutic biologic, and bioconjugation scaffold. *Front Microbiol* **6**, 755 (2015).
85. Tanaka, K. *et al.* A mimotope peptide of A β 42 fibril-specific antibodies with A β 42 fibrillation inhibitory activity induces anti-A β 42 conformer antibody response by a displayed form on an M13 phage in mice. *Journal of Neuroimmunology* **236**, 27-38 (2011).
86. Mascolo, D., Barba, P., De Berardinis, P., Di Rosa, F. & Del Pozzo, G. Phage display of a CTL epitope elicits a long-term in vivo cytotoxic response. *FEMS Immunology & Medical Microbiology* **50**, 59-66 (2007).
87. Bar, H., Yacoby, I. & Benhar, I. Killing cancer cells by targeted drug-carrying phage nanomedicines. *BMC Biotechnology* **8**, 37 (2008).
88. Park, J.Y. *et al.* Genetic engineering of a temperate phage-based delivery system for CRISPR/Cas9 antimicrobials against *Staphylococcus aureus*. *Scientific Reports* **7**, 44929 (2017).
89. Bikard, D. *et al.* Exploiting CRISPR-Cas nucleases to produce sequence-specific antimicrobials. *Nature Biotechnology* **32**, 1146-1150 (2014).
90. Dakheel, K.H. *et al.* Genomic analyses of two novel biofilm-degrading methicillin-resistant *Staphylococcus aureus* phages. *BMC Microbiology* **19**, 114 (2019).
91. Lu, T.K. & Collins, J.J. Dispersing biofilms with engineered enzymatic bacteriophage. *Proceedings of the National Academy of Sciences* **104**, 11197-11202 (2007).
92. Møller-Olsen, C. *et al.* Bacteriophage K1F targets *Escherichia coli* K1 in cerebral endothelial cells and influences the barrier function. *Scientific Reports* **10**, 8903 (2020).
93. Schmelcher, M. & Loessner, M.J. Application of bacteriophages for detection of foodborne pathogens. *Bacteriophage* **4**, e28137 (2014).
94. Schofield, D.A. & Westwater, C. Phage-mediated bioluminescent detection of *Bacillus anthracis*. *Journal of Applied Microbiology* **107**, 1468-1478 (2009).
95. Nguyen, C. *et al.* Detection of *Bacillus anthracis* spores from environmental water using bioluminescent reporter phage. *Journal of Applied Microbiology* **123**, 1184-1193 (2017).

96. Hinkley, T.C. *et al.* Reporter bacteriophage T7NLC utilizes a novel NanoLuc::CBM fusion for the ultrasensitive detection of: Escherichia coli in water. *Analyst* **143**, 4074-4082 (2018).

Article

Analysing Parallel Strategies to Alter the Host Specificity of Bacteriophage T7

Ákos Avramucz^{1,2,†}, Christian Møller-Olsen^{3,†}, Aurelija M. Grigonyte³, Yanahan Paramalingam³, Andrew Millard⁴, Antonia P. Sagona^{3,5,*}  and Tamás Fehér^{1,*} 

¹ Synthetic and Systems Biology Unit, Biological Research Centre, Eötvös Loránd Research Network (ELKH), 6726 Szeged, Hungary; avramucz.akos@brc.hu

² Doctoral School in Biology, University of Szeged, 6726 Szeged, Hungary

³ School of Life Sciences, University of Warwick, Coventry CV4 7AL, UK; C.Moller-Olsen@warwick.ac.uk (C.M.-O.); grigonyt@ualberta.ca (A.M.G.); yanahan.paramalingam.1@warwick.ac.uk (Y.P.)

⁴ Department Genetics and Genome Biology, University of Leicester, Leicester LE1 7RH, UK; adm39@leicester.ac.uk

⁵ Warwick Integrative Synthetic Biology Centre, University of Warwick, Coventry CV4 7AL, UK

* Correspondence: A.Sagona@warwick.ac.uk (A.P.S.); fehert@brc.hu (T.F.)

† These authors contributed equally to this work.

Simple Summary: The problem of antimicrobial resistance is prominent and new alternatives to antibiotics are necessary. Bacteriophages are viruses that target host bacteria and can be used efficiently for their antibacterial properties to solve the problem of antimicrobial resistance. In this study, we explore ways to genetically modify T7 bacteriophage and make its tropism broader, so that it can attack a higher variety of bacteria. We are using different methodologies to achieve this, among of those bacteriophage recombineering using electroporated DNA (BRED), which seems to be the most efficient.

Abstract: The recognition and binding of host bacteria by bacteriophages is most often enabled by a highly specific receptor–ligand type of interaction, with the receptor-binding proteins (RBPs) of phages being the primary determinants of host specificity. Specifically modifying the RBPs could alter or extend the host range of phages otherwise exhibiting desired phenotypic properties. This study employed two different strategies to reprogram T7 phages ordinarily infecting commensal K12 *Escherichia coli* strains to infect pathogen-associated K1-capsule-expressing strains. The strategies were based on either plasmid-based homologous recombination or bacteriophage recombineering using electroporated DNA (BRED). Our work pursued the construction of two genetic designs: one replacing the *gp17* gene of T7, the other replacing *gp11*, *gp12*, and *gp17* of T7 with their K1F counterparts. Both strategies displayed successful integration of the K1F sequences into the T7 genome, detected by PCR screening. Multiple methods were utilised to select or enrich for chimeric phages incorporating the K1F *gp17* alone, including *trxA*, host-specificity, and CRISPR-Cas-based selection. Irrespective of the selection method, the above strategy yielded poorly reproducible phage propagation on the new host, indicating that the chimeric phage was less fit than the wild type and could not promote continual autonomous reproduction. Chimeric phages obtained from BRED incorporating *gp11-12* and *gp17*, however, all displayed infection in a 2-stage pattern, indicating the presence of both K1F and T7 phenotypes. This study shows that BRED can be used as a tool to quickly access the potential of new RBP constructs without the need to engineer sustainably replicating phages. Additionally, we show that solely repurposing the primary RBP is, in some cases, insufficient to produce a viable chimeric phage.

Keywords: bacteriophage; phage; host specificity; host range; RBP; tail fibres; BRED



Citation: Avramucz, Á.; Møller-Olsen, C.; Grigonyte, A.M.; Paramalingam, Y.; Millard, A.; Sagona, A.P.; Fehér, T. Analysing Parallel Strategies to Alter the Host Specificity of Bacteriophage T7. *Biology* **2021**, *10*, 556. <https://doi.org/10.3390/biology10060556>

Academic Editor: Vladimir Kaberdin

Received: 20 May 2021

Accepted: 16 June 2021

Published: 20 June 2021

Publisher's Note: MDPI stays neutral with regard to jurisdictional claims in published maps and institutional affiliations.



Copyright: © 2021 by the authors. Licensee MDPI, Basel, Switzerland. This article is an open access article distributed under the terms and conditions of the Creative Commons Attribution (CC BY) license (<https://creativecommons.org/licenses/by/4.0/>).

1. Introduction

The acceleration and spread of bacterial antibiotic resistance have enabled phage therapy, the use of bacteriophages (phages) as therapeutics for resistant bacterial infections, to develop and mature as a technology over the last two decades. Clinical trials are in progress in both the U.S. and Europe [1] and procedures to access compassionate use of phage therapy are already in place in many countries [2].

A potential hindrance to the large-scale use of phage therapy compared to traditional antibiotics is the high host specificity of phages. Traditional antibiotics can often target and treat entire classes of non-resistant bacteria, whereas phages are generally limited to a smaller subset of closely related strains [3]. Thus, phage therapy is currently highly individualised and requires identification of the pathogenic strain and subsequent selection of a suitable phage strain. However, advancements in the field of molecular biology are enabling researchers to edit genomes more efficiently than ever. Hence, there is a potential to design and engineer recombinant phages with new phenotypic properties, such as an altered or expanded host tropism.

A variety of methodologies have been developed for genetic engineering, many of which rely on the well-established principles of homologous recombination. Possible phage genome editing approaches include CRISPR-Cas, whole-genome synthesis, and genome assembly in yeast or in cell-free TX-TL systems [4].

The phage specificity is primarily determined by the receptor-binding proteins (RBPs) located on either tail fibres or tail spikes. These RBPs are the main focus of phage engineering, aiming to alter or expand the host tropism. A modular approach was employed by Ando et al. [5] to reprogram wild-type *Escherichia coli* (*E. coli*) phage T7 to infect different bacterial species, including *Yersinia* and *Klebsiella*. This approach included the synthesis of the entire phage genome followed by Gibson assembly and expression in yeast cells [5]. Demonstrating a different approach, Yosef et al. [6] extended the host range of phage T7, intended for DNA transduction and not replication, potentially targeting bacterial species that would not normally support the propagation of phage T7. Individual recombinant phage particles were engineered by homologous recombination, incorporating a specific RBP gene into their genome. The recombinant phages showed susceptibility to multiple *Klebsiella pneumoniae* and *Salmonella enterica* strains [6].

The primary goal of this work was to test multiple strategies to reprogram the host specificity of the bacteriophage T7. The ease and safety of propagating phage T7 on *E. coli* K12 allowed the accumulation of a vast amount of knowledge and the development of numerous techniques for this phage. This could make phage T7 an ideal candidate system to develop general phage traits (e.g., altered virulence or immunogenicity, or fusion with fluorescent labels or tags) for basic research or biotechnological purposes. Such a collection of altered T7 phages could execute specific phage-related tasks on other bacterial strains after quickly modifying host specificity. We report here the application of two different groups of strategies to reprogram the specificity of phage T7 for K1-capsule-expressing *E. coli* hosts. We found that if multiple phage genome segments needed to be replaced, linear-DNA mediated recombineering could yield the most promising results, even if the complete gene set required for full phage viability was unknown.

2. Materials and Methods

2.1. Strains, Buffers, and Media

Two *Escherichia coli* strains were used for phage propagation: *E. coli* K-12 MG1655 [7] and *E. coli* EV36, a K12/K1 hybrid developed by conjugation of the Hfr *kps*⁺ strain, which was kindly provided by Dr Eric R. Vimr [8]. Phage T7 was obtained from Professor Ian Molineux, and phage K1F was kindly provided by Dr Dean Scholl [9]. *E. coli* BW25113 Δ *trx*A were obtained from the Keio collection and were kindly donated (from Professor Alfonso Jaramillo's lab). Bacteria were cultured in lysogeny broth (LB) [10]. Phage dilutions were made in buffer Φ 80+, containing 0.1 M NaCl, 0.01 M Tris (pH7.9), 0.01 M CaCl₂, and 0.01 M MgCl₂ [11]. The TBE buffer contained 45 mM Tris, 45 mM boric acid, and 1 mM

EDTA [10]. The TE buffer contained 10 mM Tris and 1 mM EDTA. Agar was used in a concentration of 1.5% in plates. SeaKem LE agarose (Lonza, Basel, Switzerland) used at 0.5% was applied as soft agarose overlay, always supplemented with 5 mM CaCl₂ and 5 mM MgSO₄. Antibiotics were used in the following end-concentrations: Ampicillin (Ap): 50 µg/mL, Chloramphenicol (Cm): 25 µg/mL, Kanamycin (Km): 25 µg/mL. If not indicated otherwise, chemicals were obtained from Sigma-Aldrich (St. Louis, MO, USA).

2.2. Plasmids

For plasmid-mediated phage engineering, the donor DNA encoding a chimeric *gp17*, constructed by Aurelija Grigonyte [12], was further synthesised as a G-block by Integrated DNA Technologies (Leuven, Belgium) and cloned into pSB6A1 (iGEM <http://parts.igem.org/Part:pSB6A1>, accessed on 4 March 2021) using a Gibson assembly to make pSB6A1_T7-K1Fgp17. The G-block sequence is available in Supplementary Table S1.

Recombineering of linear fragments was mediated by λ-Red recombinases expressed from the pORTMAGE2 plasmid after heat-induction [13]. The plasmid pORTMAGE2 was a kind gift of Dr Ákos Nyeges.

Plasmids pCas9_T7gp17 and pCas9_T7gp17-2, used for counterselection against wild-type T7 phages, were constructed as described elsewhere [14]. Briefly, two complementary oligonucleotides (listed in Table S1) encoding the spacers with appropriate overhangs were phosphorylated, hybridised, and ligated into BsaI-digested pCas9 plasmids. The plasmid pCas9 was a kind gift from Prof. Luciano Marraffini (Addgene plasmid # 42876).

2.3. General Phage Protocols

Phages T7 and K1F were routinely propagated on *E. coli* strains MG1655 and EV36, respectively, using the protocol described earlier [15]. During all cases of phage growth, the liquid medium and soft agarose contained 5 mM CaCl₂ and 5 mM MgSO₄. For phage titering, a log₁₀ serial dilution of the phage suspension was made and 10 µL of each dilution step was pipetted on top of solidified soft agarose, which contained the target bacterial strain at a 10⁷/mL initial concentration. Plaques were counted after incubating the plates (4 h for K1F, 16 h for T7) at 37 °C. For plaque PCR, plaques were aspirated with cut-off 200 µL pipette tips and resuspended in 100 µL of TBE buffer. After a 16 h incubation at 42 °C, 1 µL of the suspension was used in 10 µL PCR reactions to amplify various phage genome segments.

2.4. Phage DNA Preparation

Phage genome purification was carried out using a modification of earlier protocols [10,16]. First, a fresh T7 phage lysate was made from a 100 mL culture of *E. coli* MG1655 by infecting it with 4 × 10⁵ phages at OD₆₀₀ = 0.5. After lysis, DNAase (Promega, Madison, WI, USA) and RNAaseA (Thermo Fisher Scientific, Waltham, MA, USA) were added at a final concentration of 2 µg/mL each and incubated for 2 h at 37 °C. Next, NaCl was added to a final concentration of 1 M and incubated for 2 h at 4 °C. Afterwards, the cell debris was removed by centrifugation at 11,000 × g for 15 min at 4 °C. PEG8000 was added to the supernatant at a final concentration of 10%, and the solution was incubated at 4 °C overnight. The precipitated phage particles were recovered by pelleting at 11,000 × g for 15 min at 4 °C. The supernatant was discarded and the pellet was resuspended in 400 µL of TE. A quantity of 400 µL of buffered phenol was added, and the mixture was shaken for 10 min. After centrifugation at 10,000 × g for 3 min, the aqueous (top) layer was recovered and an equal amount of phenol was added for two more rounds of phenol extraction. After phenol treatment, 300 µL of chloroform was added, shaken, and centrifuged for 1 min at 10,000 × g. The aqueous (top) layer was recovered for another round of chloroform treatment. Next, 40 µL of 3 M sodium acetate was added to the recovered top phase, and phage DNA was precipitated with six volumes of 100% ethanol at room temperature. DNA was pelleted at 10,000 × g for 12 min at room temperature. The supernatant was removed,

and 1 mL of 70% ethanol was added and centrifuged for another 10 min. This step was repeated one more time. The pellet was dried and resuspended in 100 μ L of TE buffer.

2.5. Plasmid-Mediated Phage Editing

Recombinant phages were obtained by two consecutive rounds of homologous recombination. Each round consisted of adding the phage at an MOI of <1 to a log phase bacterial culture at an OD₆₀₀ of 0.3, previously transformed with the donor plasmid, and incubated at 37 °C with rotation (200 rpm). Following the bacterial clearance, the lysate was centrifuged at 3220 \times g for 15 min at 4 °C and subsequently passed through a 0.22 μ m pore size filter.

Selection for recombinant T7/K1F chimeric phages was performed using the standard double overlay method with multiple approaches: marker-based selection on a thioredoxin-deficient bacterial host, *E. coli* BW25113 Δ *trxA*; selection on a K1-capsule-expressing host; and selection on a host expressing pCas9 targeting phage T7 wild-type tail fibres. Candidate plaques were picked and screened by PCR using primers AS072 and AS081 to confirm the presence of recombinant phages. The phages were recovered from the plaques into the TBE buffer (as described above), were re-grown on the same host in a liquid medium, and were re-plated in successive rounds with the intent of confirming the genotype and obtaining pure phage clones.

2.6. Phage Selection Using pCas9

The phage mix obtained from the plasmid-mediated phage editing was grown on *E. coli* EV36 harbouring either the pCas9_T7gp17 or the pCas9_T7gp17-2 plasmid. The obtained phage lysates were titered and plated on *E. coli* EV36 in appropriate dilutions to obtain individual plaques. Plaques were screened by PCR using primers T7tailFW and K1FtailRev to detect recombinant phages.

2.7. BRED

Bacterial recombineering by electroporated DNA (BRED) [15] was used for the simultaneous modification of *gp11-12* and *gp17* genes of the T7 genome. The linear DNA used for this purpose was generated in three steps: first, PCR-amplification of the five segments shown in Figure 1; second, overlap-extension PCR-based fusion [17] of T7 left homology with *gp11-12* and *gp17* with T7 right homology; third, the NEBuilder (New England Biolabs, Ipswich, MA, USA) based assembly of three DNA fragments (T7 left homology + *gp11-12*; *gp13-16*; *gp17* + T7 right homology), each present at 0.18 pmol quantities (Figure 1). PCRs were carried out with Phusion DNA polymerase (Thermo Fisher Scientific, Waltham, MA, USA) at an annealing temperature of 58 °C. Primer sequences are listed in Table S1. The entire completed NEBuilder reaction was mixed with 50 μ L (ca. 110 μ g) of the purified T7 genomic DNA, and the mix was concentrated into 5 μ L of TE by ethanol precipitation. For BRED, 2 μ L of this concentrated mix was electroporated into thermally induced *E. coli* EV36/pORTMAGE2 electrocompetent cells. The electroporated cells were mixed with 3 mL of molten soft agarose, poured on LB + Ap plates, and incubated at 37 °C. The plaques that appeared were analysed by plaque-PCR using the following primer pairs to identify recombinants: gp10FWcheck + K1Fgp11Rev; K1Fgp12FW + T7gp13Rev; T7gp16FW + K1Fgp17Rev(check); and K1fgp17FW(check) + T7gp19Rev. The obtained agarose plugs were incubated at 42 °C overnight in 100 μ L of TE for the diffusion of phages into the buffer. A quantity of 50 μ L of this solution was added to 5 mL log phase culture of *E. coli* EV36pORTMAGE2 at 37 °C for phage propagation in an LB + Ap medium containing 5 mM CaCl₂ and 5 mM MgSO₄. After lysis, 1450 μ L of the lysate was mixed with 50 μ L of chloroform, pelleted, and the aqueous (top) layer was recovered and filtered sterile with a 0.22 μ m pore size PVDF filter. For the next cycle of phage growth, 10 μ L of this treated lysate was added to 5 mL of naive *E. coli* EV36pORTMAGE2 log phase culture, creating a 500 \times dilution.

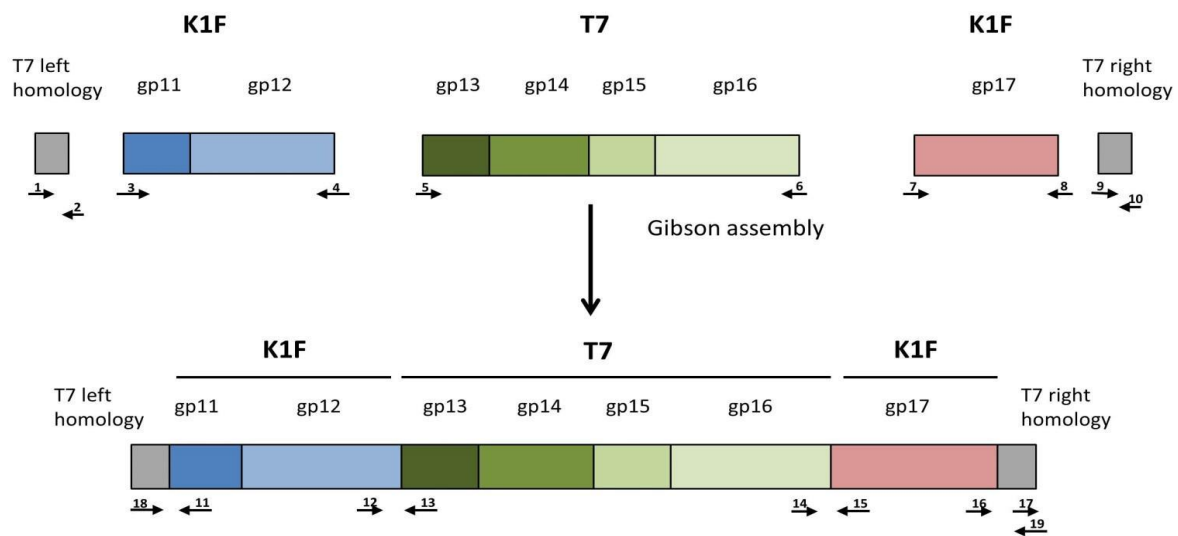


Figure 1. Construction of the genetic cassette designed to simultaneously alter *gp11*, *gp12*, and *gp17* of phage T7. The small arrows indicate the following primers used for cassette assembly: 1: T7gp10fw; 2: T7gp10rev; 3: K1Fgp11fw; 4: K1Fgp12rev; 5: T7gp13fw; 6: T7gp16rev; 7: K1Fgp17fw; 8: K1Fgp17rev; 9: T7gp18fw; 10: T7gp19revE. The following primers were used for joint verification: 11: K1Fgp11rev; 12: K1Fgp12fw; 13: T7gp13rev; 14: T7gp16fw; 15: K1Fgp17Rev(check); 16: K1fgp17fw(check); 17: T7gp19fw; 18: T7gp10fw(check); 19: T7gp19revE(check). Drawing not to scale.

In the alternative BRED protocol, 1 mL of electroporated culture from BRED was directly mixed with 5 mL of *E. coli* EV36 cells. After 2 h of shaking at 37 °C, the lysate was chloroform-treated and filtered sterile with a 0.22 µm pore size PVDF filter. For the next cycle of phage growth, either 5 or 500 µL of the lysate was mixed with *E. coli* EV36 corresponding to 1000× and 10× dilutions, respectively. Such growth cycles were repeated, as described in the Results.

3. Results

In this project, we tested multiple strategies to alter the host specificity of phage T7, to provide the capability of infecting K1-capsule-expressing *E. coli* cells. As a starting point, we analysed the growth and plaque-forming abilities of phage T7 and K1F on *E. coli* MG1655 and *E. coli* EV36 strains displaying the K12 and K1 capsules, respectively. The results, detailed in Table 1, indicated that the liquid-culture-mediated growth of T7 and K1F is only possible on *E. coli* MG1655 and EV36 strains, respectively. However, plaque formation in similar numbers was observed when switching the bacterial hosts (i.e., T7 on EV36 and K1F on MG1655), albeit yielding smaller plaque diameters. This indicated that the host specificities of the phages were not completely exclusive at the starting point of our experiments.

Table 1. Growth properties of phages T7 and K1F.

T7	MG1665	EV36	K1F	MG1665	EV36
canonical host	yes	no	canonical host	no	yes
able to lyse	yes	yes(!)	able to lyse	yes(!)	yes
plaque size *	large	small	plaque size *	small	large
able to clear liquid culture	yes	no	able to clear liquid culture	no	yes

* Small plaques: 1–2 mm, large plaques: 13–15 mm in diameter after 12–16 h of incubation.

In the case of phage T7, binding to the cell surface is ensured by the six tail fibres. Each tail fibre consists of three Gp17 proteins, all attached to the phage tail with their N-termini. The phage tail is made up of a dodecamer of the Gp11 and a hexamer of the Gp12 proteins. Gp7.3, an essential protein that is injected into the target cell, is also present

in the tail in about 30 copies at an unknown location [18]. Our first strategy to completely switch the specificity of phage T7 to K1 hosts targeted the tail fibre using plasmid-mediated phage engineering, i.e., the growth of T7 on *E. coli* K12 cells harbouring a donor plasmid (pSB6A1_T7-K1Fgp17) that carries a modified *gp17* gene (Strategy I). This plasmid was designed to include the 860 C-terminal residues of the K1F *gp17* (possessing endosialidase activity), thioredoxin (*trx*) for positive selection, and two flanking phage T7 homology regions (Figure 2). Sequence similarities between phage K1F and phage K1-5, another K1 capsule-targeting phage, showed that the 204 amino acids (AAs) of the N-terminal end of K1F Gp17 were not necessary for the correct folding of the enzymatic protein. We, therefore, designed homologies to obtain a fusion protein where the 165 AA N-terminal sequence of K1F *gp17* is replaced with the 162 AA N-terminal end of T7 *gp17*.

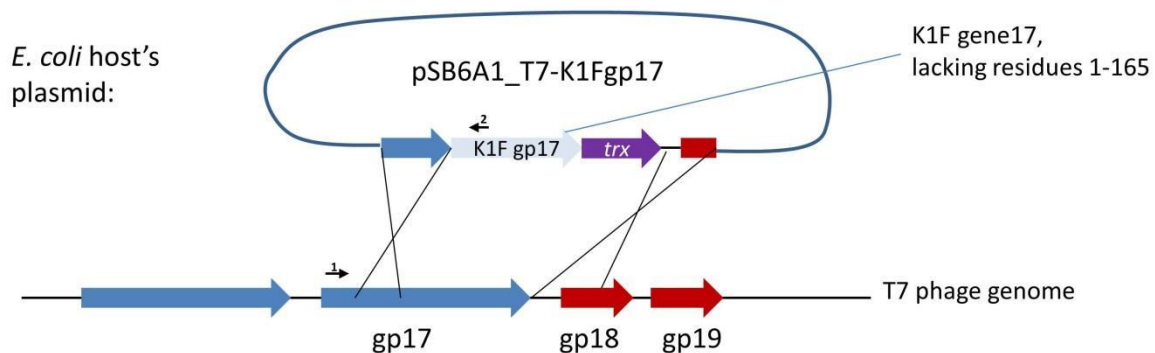


Figure 2. Strategy I, the genetic construct used for plasmid-mediated phage engineering. Large arrows depict genes. Small arrows represent the following primers: 1: AS072; 2: AS081.

Propagation of phage T7 on *E. coli* K-12 (MG1655)/pSB6A1_T7-K1Fgp17 yielded a phage lysate that contained detectable amounts of the fusion *gp17* gene, as verified by PCR using primers AS072 and AS081 (Figure 3). We applied three different strategies (IA-C) to select for or enrich the recombinants within the phage mix (Figure 4). Strategy IA consisted of phage growth on *E. coli* BW25113 Δ *trx*A, which lacks the thioredoxin gene. Since this gene is essential for phage replication, this host only allows the replication of phage genomes that have acquired a copy of the *trx*A gene. Unfortunately, PCR-detectability of the chimeric phage was lost over the first few rounds of phage propagation. The failure of this method can be, in part, attributed to the fact that our Δ *trx*A strain did not carry a K1 capsule and was, therefore, a suboptimal host for the propagation of the recombinant phage. Attempting to boost phage propagation by providing the Gp17 protein of T7 in trans did not solve this issue: the PCR signal also disappeared when growing the phages on *E. coli* BW25113 Δ *trx*A + pT7_*gp17*.

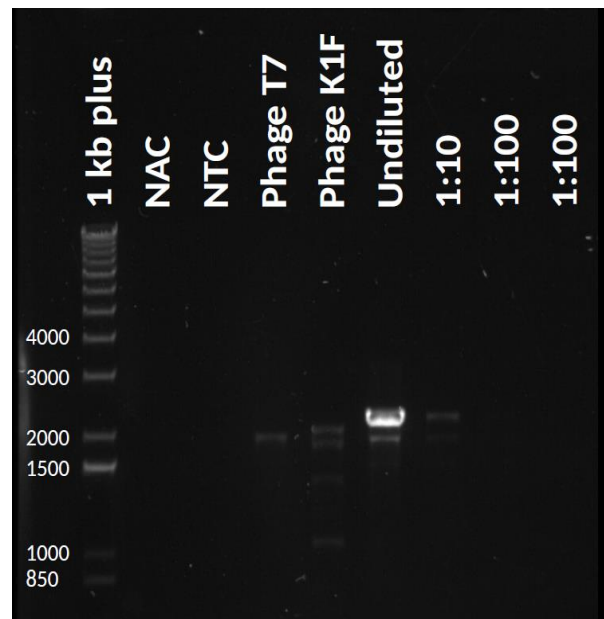


Figure 3. PCR analysis verifying the presence of the fusion *gp17* gene in the undiluted phage mix obtained by plasmid-mediated phage editing. An NAC (no amplification control) without taq polymerase and an NTC (no template control) without DNA template was included in each run. Marker: GeneRuler 1 kbp DNA Ladder Plus (Thermo Fisher Scientific, Waltham, MA, USA).

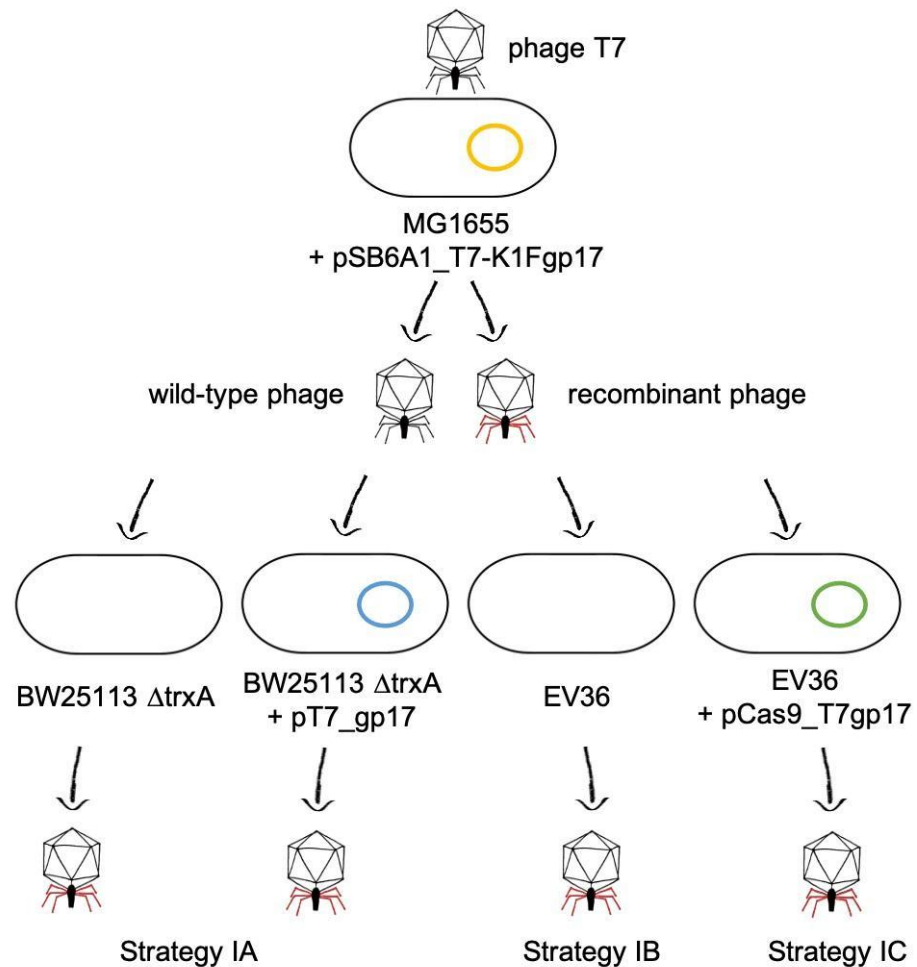


Figure 4. Plasmid-based homologous recombination and selection strategies used for phage editing.

Strategy IB was more straightforward; it relied on the potentially improved ability of the recombinant phage to lyse liquid cultures of *E. coli* EV36, a K1 capsule-expressing host. We propagated the phage mix on liquid cultures of *E. coli* EV36, measuring phage titers after every round of phage growth (even if no visible lysis occurred) using plated EV36. Overall, the phages displayed a weak and poorly reproducible ability to grow in liquid EV36 cultures. As apparent from Table 2, the titers measured in the course of three passages strongly fluctuated; furthermore, during the first and third steps, we only recovered the phages that we had mixed with the cells, indicating negligible phage propagation. A very similar titer pattern was observed when starting not with the complete phage lysate, but with a plaque obtained by plating the lysate on *E. coli* EV36. Importantly, in both series of propagations, the phage mix lost the PCR-positivity by the third passage. Overall, we concluded that propagating the phage mix on a K1-expressing host did not select for the recombinant phages and could not even maintain the fusion *gp17* genotype within the mix.

Table 2. Phage titers obtained by growing the recombinant phage mix (obtained via the recombination step shown on the top of Figure 4) on *E. coli* EV36.

	Titer	Titer after First Passage (I)	Titer after Second Passage (II)	Titer after Third Passage (III)
original K1F/T7 lysate (o)	1.6×10^{10}	8×10^4	6×10^6	4×10^4
plaque derived K1F/T7 (1)	—	2×10^4	6×10^6	1×10^4

In Strategy IC, we intended to further increase the pressure enriching recombinant phages by applying CRISPR-Cas selection. We grew the phage mix on K1 capsule-expressing hosts that carried the *S. pneumoniae* CRISPR-Cas machinery targeted against either of two loci in the T7 *gp17* gene, not present in the fusion *gp17*. Growth of the phage mix on *E. coli* EV36/pCas9_T7gp17 or EV36/pCas9_T7gp17-2 was carried out both in liquid culture and on plates, as described in the Methods. In both cases, the PCR-positivity of the obtained phages was lost already after the first round of phage growth, irrespective of the guide RNA used.

At this point, it became evident that the recombinant phage was not viable, or at least its selective disadvantage compared to T7 was greater than the selective pressure exerted by any of the three systems described above. A potential explanation and solution were provided by the work of Ando et al. [5], who made similar observations when replacing the *gp17* gene of T7 with that of *Klebsiella* phage K11. In their work, the recombinant phages were not viable unless *gp11* and *gp12* (the genes encoding the adaptor and the nozzle proteins of the phage tail, respectively) were also replaced by their K11 counterparts. The authors explained this requirement by the fact that the *gp17*-encoded tail fibres attach to the interface between the Gp11 and Gp12 proteins. In light of this information, we redesigned the donor plasmid to comprise the K1F derived *gp11*, *gp12*, and *gp17* genes, as well as the T7-derived *gp13*, *gp14*, *gp15*, and *gp16* genes, as shown in Figure 1. The gene set was to be flanked by two homologous ends allowing its entry into the T7 genome to replace the native *gp11-gp17* segment.

The donor plasmid was to be constructed as a four-way assembly (T7 left homology + *gp11-12*; *gp13-16*; *gp17* + T7 right homology; bacterial artificial chromosome segment) (Figure S1) using the method of Gibson et al. [19]. Gel electrophoresis of the reaction product and PCR of the assembly joints indicated that the 14.2 kbp-long linear cassette was most likely assembled (Figure S2). However, cloning it into pBeloBAC11 was not successful, irrespective of whether *E. coli* MDS42, MG1655, or EV36 was used as a host, possibly due to the toxicity of the construct. We, therefore, abandoned plasmid-mediated phage editing and switched to Strategy II (Figure 5), which relies on bacteriophage recombineering using electroporated DNA (BRED) [20]. This strategy builds on the fact that if purified phage DNA is electroporated into an *E. coli* cell expressing the λ -Red recombinases, complete phage genomes are assembled, yielding phage plaques within the bacterial lawn. If a linear

DNA fragment with appropriate homology arms is included in the electroporation mix, a certain fraction of the obtained plaques will contain recombinant phages, detectable by plaque-PCR.

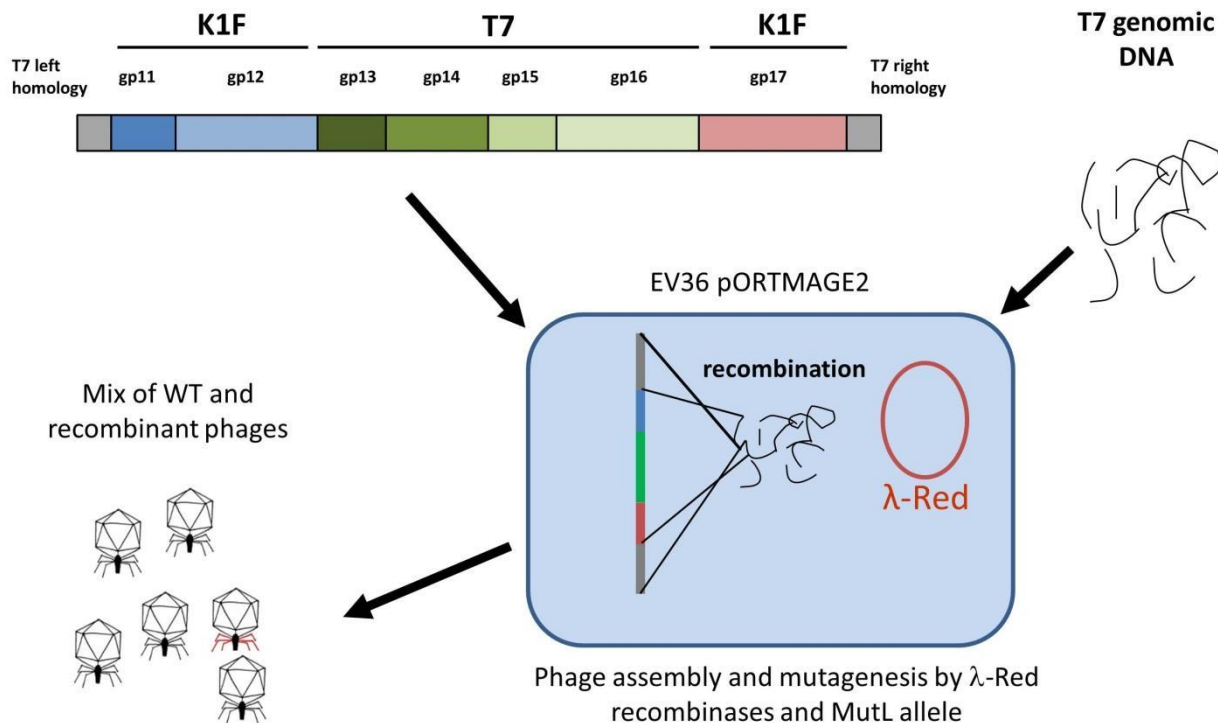


Figure 5. Strategy II, relying on bacteriophage recombineering using electroporated DNA. The linear DNA cassette comprising the planned genetic changes (**upper left**), is mixed with phage genomic DNA (**upper right**), and is electroporated into *E. coli* EV36 cells expressing the λ -Red recombinases from the pORTMAGE2 plasmid (**centre**). The recombinase assembles both WT genomes (yielding WT phage particles, **lower left**) and genomes incorporating the linear DNA cassette (yielding recombinant phages, **lower left**, marked with red tail fibres).

For strategy IIA, *E. coli* EV36/pORTMAGE2 cells were electroporated with a mix of T7 genomic DNA and the linear DNA fragment, as shown in Figure 5. After plating and overnight growth, a total of 14 large (>10 mm) clear plaques were observable. We analysed all plaques by four distinct PCR reactions (listed in Materials and Methods), screening for the presence of the four T7/K1F joints. We found that all of the plaques contained at least one of the two transgenic segments (i.e., *gp11-12* or *gp17*) and four of them contained both integrated into the T7 genome at the correct locus (Figure S3). Interestingly, small plaques formed by wild-type T7 did not emerge (otherwise seen when the phage genome is transformed without linear DNA). A double-positive plaque was picked, and the phages were recovered and further propagated on liquid *E. coli* EV36 culture to verify its growth ability and to enrich for virions containing the altered tail fibre. No lysis was observable in the liquid medium, and the obtained plaques displayed the absence of *gp17* and *gp11-12* genes, as analysed by PCR. As an alternative (Strategy IIB), the phages recovered from the plaque were grown on *E. coli* EV36/pORTMAGE2 to provide further possibilities of recombination (by the λ -Red recombinases) and an increased rate of point mutations (by the *mutL* allele). Growth on liquid *E. coli* EV36/pORTMAGE2 culture was possible, as the cells were consistently lysed. However, the transgenic segments of *gp17* and *gp11-12* were lost in the first and second round of phage growth, respectively. Genes of the T7 phage were readily detectable by PCR in all rounds of phage growth (Figure S4). The continued lysis of the non-corresponding host by phage T7 is explained by the presence of λ -Red recombinases. The expression of λ -Red in bacterial cells has recently been shown to provide sufficient genetic reorganisation to lyse non-canonical hosts [21] (in a control

experiment, we found that serial propagation of T7 on *E. coli* EV36/pORTMAGE2 liquid cultures led to full lysis starting from the second round, without any linear DNA fragment added; data not shown). The obtained phages nevertheless retained their ability to lyse *E. coli* MG1655, as well. The activity of the K1Fgp17 was still present after the end of the serial phage growth experiment in the form of two-stage plaques (Table 3, Figure 6), assuming some lasting genetic change did occur. The same could not be seen when wild-type T7 was assembled without K1F gene fragments.

Table 3. Summary of liquid bacterial lysis experiments with phages obtained by BRED.

	Isolated from Plaque; Grown without pORTMAGE (Strategy IIA)	Isolated from Plaque; Grown with pORTMAGE (Strategy IIB)	Directly from Electroporated Culture; Grown without pORTMAGE (Strategy IIC)
sustainable ¹	no	yes	yes
sustainable on pORTMAGE-free cells	no	no	yes
clearing liquid culture	no	yes	inconsistent ²
two-stage plaques	yes	yes	yes
T7 tail genes present	yes	yes	yes
K1F tail genes	lost	lost	lost

¹ Sustainability: capability of maintaining $\geq 10^6$ /mL phage titers during eight rounds of propagation on the indicated host. ² Inconsistency: phage propagation does not always result in the noticeable decrease of bacterial density.

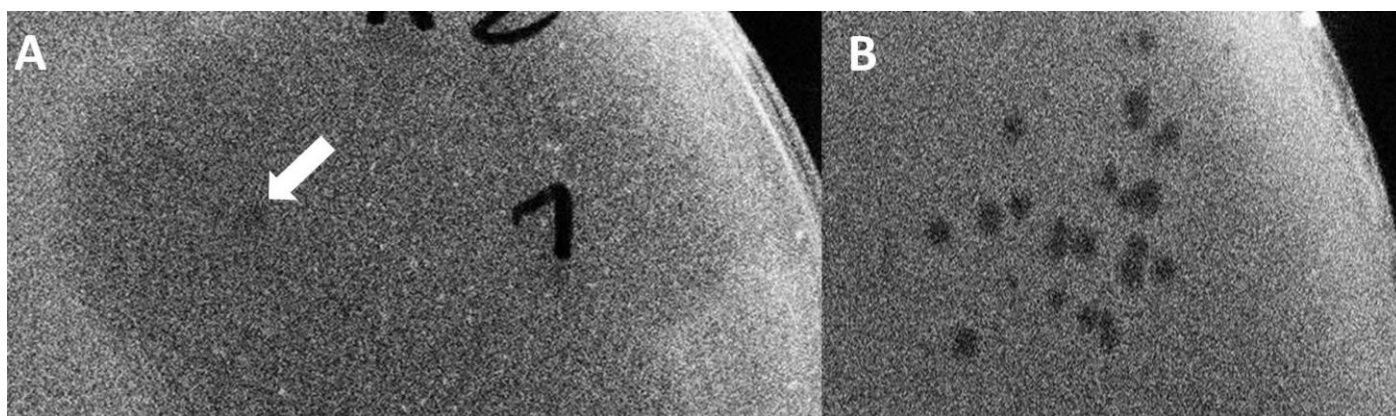


Figure 6. (A) A plaque of the recombinant phage displaying the two-stage phenotype on an *E. coli* EV36 host. The arrow marks the clear centre. (B) Plaques of phage T7 on *E. coli* EV36.

Finally, in Strategy IIC, we repeated the BRED, but instead of plating the transformed bacterial mix and picking a plaque, we grew the bacteria (and the emerging phages) directly in a liquid culture. This avoids the bottleneck introduced by randomly picking a plaque and allows the competition of all putative recombinant and wild-type T7 phages within a single mix. Growth took place without antibiotic selection to promote the quick loss of the pORTMAGE2 plasmid. In this case, although bacterial lysis was not always visible in the successive rounds of growth, phages were always detectable, despite the lack of pORTMAGE2. However, transgenic fragments were quickly lost from the phage genome. In all versions of Strategy II, the obtained plaques displayed a two-stage phenotype, usually starting from the second or third round of growth. This meant a small, clear centre surrounded by a turbid halo assuming the endosialidase activity of the K1F Gp17 protein [22] and the area of both kept increasing day-by-day (Figure 6). The observations made with BRED experiments are summarised in Table 3.

4. Discussion

Ever since the discovery of bacteriophages, knowledge concerning their host range has been vital for biomedical applications for at least two reasons. On the one hand, phage typing has long been used in microbial diagnostics to identify and classify the pathogens isolated from bacterial infections [23]. On the other hand, phage therapy requires the administration of phages capable of lysing the targeted pathogen. These needs explain the increased attention paid towards phages that display a broad host range [24] or a host range dependent on environmental factors, like temperature [25]. Later, spontaneously arising host range mutants were often described [26,27], and with the advent of DNA sequencing, the mutations responsible for the changes were also successfully identified [28,29]. With the accumulation of sequencing data, comparative genomic studies of phage sequences became possible. These revealed that in certain cases, exchanges of large genomic segments are responsible for host switching [30]. Such information, along with the development of phage engineering techniques, allowed the reprogramming of the host range of certain phages by replacing host-range-determinant DNA segments [5,31]. Recently, the structure-guided design of receptor-binding proteins has proven to offer an even more advanced method of redirecting phages towards new hosts [32].

Our work fits into this series by providing an example of transferring one or more large genomic segments between phages to alter the host tropism of the recipient phage. In the course of this project, we tested two groups of strategies and two different genetic constructs. Strategy I applied plasmid-based phage editing using either *trxA* (IA), host-specificity (IB), or CRISPR-Cas-based selection (IC). Strategy II relied on BRED, using a host-specificity-based selection of the recombinant phage. For Strategies IIA and IIB, a single positive plaque was picked for the outgrowth of the putative recombinants on cells either lacking or containing the λ -Red recombinase enzymes, respectively. Alternatively, outgrowth of the entire phage lysate was attempted in the absence of λ -Red recombinase enzymes for Strategy IIC.

To the best of our knowledge, this is the first published work aiming to tune phage T7 tropism towards a K1-capsule-expressing host. This type of specificity-change could bear clinical relevance in the future, when the rapid redirection of certain well-established phages towards novel bacterial pathogens is required. From the molecular genetic point of view, all six strategies accomplished the goal of producing detectable recombinant constructs. Since well-established techniques were used for their selection, we attribute the differences seen in the sustainability of the constructs not to differences of the selection methods themselves but instead to the differences in the genetic design. Strategy I only altered *gp17* and left the 5' end of the gene unchanged, while Strategy II applied the complete exchange of the *gp17* gene, along with that of *gp11* and *gp12*. Since the latter strategy yielded plaques that stood closest to the phenotype of completely lysing the new host, we conclude that modification of either *gp11* or *gp12*, or both, are required, in addition to that of *gp17* for the reprogramming of T7 to lyse K1-type hosts. The temporary nature of such lysis, however, indicates that these genetic changes were still not sufficient to develop a stable viable phage. Although this may be a shortcoming in some instances, it is satisfactory for numerous experimental setups. The most prominent example is the engineering of transducing phages or phage libraries, where efficient phage binding, DNA injection, and the overcoming of defence mechanisms without autonomous phage replication are enough to meet the requirements of practical applications [6].

Besides yielding unstable reprogrammed phages, our work also provides findings that may help design future host switching experiments. First, we observed that the presence of pORTMAGE is capable of allowing the growth of T7 on *E. coli* EV36 in liquid, irrespective of donor DNA. This is in line with recent observations reporting that λ -Red recombinase expression enables T7-like bacteriophages that do not normally propagate in *E. coli* to be recovered following genome transfection [21]. Including donor DNA in the transformation mix nevertheless exerted the temporary effect of yielding large clear plaques, which was eventually lost. This means that (a) the genes responsible for efficient lysis of *E. coli* EV36

are present; and (b) no pure, viable recombinant phage, which could pass on its genetic composition to its offspring, was made. A mixed infection (T7 + recombinant phages) or the integration of donor DNA into the bacterial host genome probably provided a genetic background that resulted in the formation of the large clear plaques seen in the first plating of Strategy IIA. Second, the observed two-stage plaques indicated the expression of the K1F *gp17* gene [22]. According to our hypothesis, *gp17* was transiently expressed, and Gp17 enzymatically broke down the capsule, forming the turbid halo. This allowed the access of T7 to the cell surface, which formed the clear centre of the two-stage plaques. However, the gene construct is unstable; the proteins encoded by the construct cannot assemble to yield viable phage particles alone. If a helper T7 is present, it can package the construct and transfer, but again, it will not form viable particles alone. Therefore, recombinant constructs are quickly lost from the phage mix. If the infected strain harbours λ -Red recombinases, it can protect the transformed *gp17* gene cassette and potentially integrate *gp17* transferred by the helper T7 phage into the bacterial genome. This allows transient production of endosialidase, which, upon cell lysis, will break down the capsule of neighbouring cells. The case of a mixed infection (T7 + recombinant phages) is supported by the fact that even when propagating phages derived from isolated plaques declared recombinant by PCR, wt T7 phages eventually become dominant and even exclusive after a few cycles of growth on EV36. BRED is known to produce mixed plaques [20], since both WT and recombinant phage genomes can be assembled in the same transformed host, which warrants that wt T7 is available as a helper phage during the initial growth of the recombinants. Transferring to liquid phase, however, lowers the chances of co-infection due to the effect of dilution, leading to the eventual cessation of the packaging of the recombinant phage genome into T7-virions.

Finally, although a stable phage displaying host switching was not assembled in this work, the large clear plaques are a strong indication that the necessary genes required for serial lysis of a non-canonical host were all present. The T7 engineered phage, even though it was not stable for the long term, still presented broader tropism and could efficiently target EV36 presenting the K1 capsule, which is normally a host for the K1F phage. The use of BRED for this purpose could be a quick way to test the potential use of a new tail fibre without the need to engineer a stable phage.

Concerning the future, the information collected to this point could provide a basis for the further enhancement of the hybrid construct, ultimately leading to a stable T7-K1F chimeric phage. The two most straightforward explanations of the instability of our chimera could be either the inadequate expression of genes present on the construct or the inappropriate assembly of the encoded proteins due to their potentially incompatible adjacent surfaces. Although we cannot completely exclude the former, earlier reports on reorganizing genes within a phage genome indicated a relatively high level of robustness [33,34]. Perhaps more likely is the incompatibility of neighbouring protein surfaces. This would suggest that modular phage reorganization, which works quite effectively in certain cases [5], is insufficient in others and demands sub-modular tuning for successful host-switching. The accumulation of protein structural data and the development of novel combinatorial genome editing techniques will certainly aid both the design-based and the selection-based strategies aiming to solve such issues in the future.

Supplementary Materials: The following are available online at <https://www.mdpi.com/article/10.3390/biology10060556/s1>: Table S1. Primers used in this study, Figure S1. Gel electrophoresis of PCR fragments generated to construct the pBeloBAC11-based donor plasmid, Figure S2. Verification of donor fragment assembly, Figure S3. PCR-validation of the genetic fusion between K1F and T7 genes, Figure S4. PCR-validation of the T7 *gp17* gene present in the phage lysate, Uncut gel photos list in the Supplementary Materials.

Author Contributions: Conceptualization, T.F. and A.P.S.; Methodology, C.M.-O., T.F., A.P.S., A.M.G., Y.P.; Validation, A.P.S. and T.F.; Investigation, Á.A., C.M.-O., Y.P.; Resources, A.P.S.; Writing—Original Draft Preparation, T.F., C.M.-O.; Writing—Review & Editing, A.P.S., Á.A., T.F., C.M.-O., A.M., A.M.G.; Visualization, Á.A., T.F., A.P.S.; Supervision, T.F., A.M., A.P.S.; Project Administration, A.P.S. and T.F.;

Funding Acquisition, T.F. and A.P.S. All authors have read and agreed to the published version of the manuscript.

Funding: This research was funded by the National Research, Development, and Innovation Office of Hungary (NKFIH) Grant No. K119298 (to T.F.), the Biotechnological National Laboratory of the National Research, Development and Innovation Office of Hungary (to T.F.), by the Biotechnology and Biological Sciences Research Council (BBSRC) Future Leader Fellowship (ref. BB/N011872/1) to A.P.S. and by the Biotechnology and Biological Sciences Research Council (BBSRC) and University of Warwick funded Midlands Integrative Biosciences Training Partnership (MIBTP) [grant number BB/M01116X/1] to C.M.O., Y.P. and A.P.S.

Institutional Review Board Statement: Not applicable.

Informed Consent Statement: Not applicable.

Data Availability Statement: All the data are available upon request.

Acknowledgments: This work was supported by the National Research, Development, and Innovation Office of Hungary (NKFIH) Grant No. K119298 (to T.F.), the Biotechnological National Laboratory of the National Research, Development and Innovation Office of Hungary (to T.F.), by the Biotechnology and Biological Sciences Research Council (BBSRC) Future Leader Fellowship (ref. BB/N011872/1) to A.P.S. and by the Biotechnology and Biological Sciences Research Council (BBSRC) and University of Warwick funded Midlands Integrative Biosciences Training Partnership (MIBTP) [grant number BB/M01116X/1] to C.M.O., Y.P. and A.P.S. The authors would like to thank Dean Scholl, AvidBiotics Corporation, for providing the bacteriophage K1F strain; Eric R. Vimr and Susan M. Steenbergen for providing the *E. coli* EV36 strain; and Alfonso Jaramillo, for donating the *E. coli* BW25113 $\Delta trxA$ strains.

Conflicts of Interest: The authors declare no conflict of interests.

References

1. McCallin, S.; Sacher, J.C.; Zheng, J.; Chan, B.K. Current State of Compassionate Phage Therapy. *Viruses* **2019**, *11*, 343. [[CrossRef](#)]
2. Fauconnier, A. Phage Therapy Regulation: From Night to Dawn. *Viruses* **2019**, *11*, 352. [[CrossRef](#)] [[PubMed](#)]
3. Nóbrega, F.; Vlot, M.; de Jonge, P.A.; Dreesens, L.L.; Beaumont, H.J.E.; Lavigne, R.; Dutilh, B.E.; Brouns, S.J.J. Targeting mechanisms of tailed bacteriophages. *Nat. Rev. Genet.* **2018**, *16*, 760–773. [[CrossRef](#)]
4. Pires, D.P.; Cleto, S.; Sillankorva, S.; Azeredo, J.; Lu, T.K. Genetically Engineered Phages: A Review of Advances over the Last Decade. *Microbiol. Mol. Biol. Rev.* **2016**, *80*, 523–543. [[CrossRef](#)]
5. Ando, H.; Lemire, S.; Pires, D.P.; Lu, T.K. Engineering Modular Viral Scaffolds for Targeted Bacterial Population Editing. *Cell Syst.* **2015**, *1*, 187–196. [[CrossRef](#)] [[PubMed](#)]
6. Yosef, I.; Goren, M.G.; Globus, R.; Molshanski-Mor, S.; Qimron, U. Extending the Host Range of Bacteriophage Particles for DNA Transduction. *Mol. Cell* **2017**, *66*, 721–728.e3. [[CrossRef](#)] [[PubMed](#)]
7. Blattner, F.R.; Plunkett, G.; Bloch, C.A.; Perna, N.T.; Burland, V.; Riley, M.; Collado-Vides, J.; Glasner, J.D.; Rode, C.K.; Mayhew, G.F.; et al. The Complete Genome Sequence of Escherichia coli K-12. *Science* **1997**, *277*, 1453–1462. [[CrossRef](#)] [[PubMed](#)]
8. Vimr, E.R.; A Troy, F. Regulation of sialic acid metabolism in Escherichia coli: Role of N-acetylneuraminidase pyruvate-lyase. *J. Bacteriol.* **1985**, *164*, 854–860. [[CrossRef](#)] [[PubMed](#)]
9. Scholl, D.; Merrill, C. The Genome of Bacteriophage K1F, a T7-Like Phage That Has Acquired the Ability to Replicate on K1 Strains of Escherichia coli. *J. Bacteriol.* **2005**, *187*, 8499–8503. [[CrossRef](#)]
10. Sambrook, J.; Fritsch, E.F.; Maniatis, T. *Molecular Cloning. A Laboratory Manual*; Cold Spring Harbor Laboratory Press: Cold Spring Harbor, NY, USA, 1987.
11. Blattner, F.; Fiandt, M.; Hass, K.; Twose, P.; Szybalski, W. Deletions and insertions in the immunity region of coliphage lambda: Revised measurement of the promoter-startpoint distance. *Virology* **1974**, *62*, 458–471. [[CrossRef](#)]
12. Grigonyte, A.M.; Harrison, C.; MacDonald, P.R.; Montero-Blay, A.; Tridgett, M.; Duncan, J.; Sagona, A.P.; Constantinidou, C.; Jaramillo, A.; Millard, A. Comparison of CRISPR and Marker-Based Methods for the Engineering of Phage T7. *Viruses* **2020**, *12*, 193. [[CrossRef](#)]
13. Nyerges, Ákos; Csörgő, B.; Nagy, I.; Bálint, B.; Bihari, P.; Lázár, V.; Apjok, G.; Umenhoffer, K.; Bogos, B.; Pósfai, G.; et al. A highly precise and portable genome engineering method allows comparison of mutational effects across bacterial species. *Proc. Natl. Acad. Sci. USA* **2016**, *113*, 2502–2507. [[CrossRef](#)] [[PubMed](#)]
14. Jiang, W.; Bikard, D.; Cox, D.; Zhang, F.; Marraffini, L.A. RNA-guided editing of bacterial genomes using CRISPR-Cas systems. *Nat. Biotechnol.* **2013**, *31*, 233–239. [[CrossRef](#)]
15. Fehér, T.; Karcagi, I.; Blattner, F.R.; Pósfai, G. Bacteriophage recombineering in the lytic state using the lambda red recombinases. *Microb. Biotechnol.* **2012**, *5*, 466–476. [[CrossRef](#)]

16. Lech, K. Making Phage DNA from Liquid Lysates. In *Current Protocols in Molecular Biology*; Ausubel, F.M., Brent, R., Kingston, R.E., Moore, D.D., Seidman, J.G., Smith, J.A., Struhl, K., Eds.; Greene Publishing Associates and Wiley-Interscience: Brisbane, Australia, 1987; pp. 1.13.1–1.13.6.
17. Horton, R.M.; Hunt, H.D.; Ho, S.N.; Pullen, J.K.; Pease, L.R. Engineering hybrid genes without the use of restriction enzymes: Gene splicing by overlap extension. *Gene* **1989**, *77*, 61–68. [[CrossRef](#)]
18. Molineux, I.J. The T7 group. In *The Bacteriophages*; Calendar, R., Ed.; Oxford University Press: Oxford, UK, 2006; p. 279.
19. Gibson, D.G.; Young, L.; Chuang, R.Y.; Venter, J.C.; Hutchison, C.A.; Smith, H.O. Enzymatic assembly of DNA molecules up to several hundred kilobases. *Nat. Methods* **2009**, *6*, 343–345. [[CrossRef](#)]
20. Marinelli, L.J.; Piuri, M.; Swigoňová, Z.; Balachandran, A.; Oldfield, L.M.; van Kessel, J.; Hatfull, G.F. BRED: A Simple and Powerful Tool for Constructing Mutant and Recombinant Bacteriophage Genomes. *PLoS ONE* **2008**, *3*, e3957. [[CrossRef](#)]
21. Jensen, J.D.; Parks, A.R.; Adhya, S.; Rattray, A.J. λ Recombineering Used to Engineer the Genome of Phage T7. *Antibiotics* **2020**, *9*, 805. [[CrossRef](#)]
22. Bessler, W.; Fehmel, F.; Freund-Mölbart, E.; Knüfermann, H.; Stirm, S. Escherichia coli capsule bacteriophages. IV. Free capsule depolymerase 29. *J. Virol.* **1975**, *15*, 976–984. [[CrossRef](#)]
23. Chirakadze, I.; Perets, A.; Ahmed, R. Phage Typing. *Methods Mol. Biol.* **2009**, *502*, 293–305. [[CrossRef](#)] [[PubMed](#)]
24. Lazarus, A.S.; Gunnison, J.B. The action of Pasteurella pestis bacteriophage on Pasteurella, Salmonella, and Shigella. *J. Bacteriol.* **1947**, *54*, 70. [[CrossRef](#)] [[PubMed](#)]
25. Gunnison, J.B.; Larson, A.; Lazarus, A.S. Rapid Differentiation Between Pasteurella Pestis and Pasteurella Pseudotuberculosis by Action of Bacteriophage. *J. Infect. Dis.* **1951**, *88*, 254–255. [[CrossRef](#)] [[PubMed](#)]
26. Iida, S. Bacteriophage P1 carries two related sets of genes determining its host range in the invertible c segment of its genome. *Virology* **1984**, *134*, 421–434. [[CrossRef](#)]
27. Morona, R.; Henning, U. Host range mutants of bacteriophage Ox2 can use two different outer membrane proteins of Escherichia coli K-12 as receptors. *J. Bacteriol.* **1984**, *159*, 579–582. [[CrossRef](#)]
28. Tétart, F.; Repoila, F.; Monod, C.; Krisch, H. Bacteriophage T4 Host Range is Expanded by Duplications of a Small Domain of the Tail Fiber Adhesin. *J. Mol. Biol.* **1996**, *258*, 726–731. [[CrossRef](#)] [[PubMed](#)]
29. Werts, C.; Michel, V.; Hofnung, M.; Charbit, A. Adsorption of bacteriophage lambda on the LamB protein of Escherichia coli K-12: Point mutations in gene J of lambda responsible for extended host range. *J. Bacteriol.* **1994**, *176*, 941–947. [[CrossRef](#)] [[PubMed](#)]
30. Garcia, E.; Elliott, J.M.; Ramanculov, E.; Chain, P.S.; Chu, M.C.; Molineux, I.J. The genome sequence of Yersinia pestis bacteriophage phiA1122 reveals an intimate history with the coliphage T3 and T7 genomes. *J. Bacteriol.* **2003**, *185*, 5248–5262. [[CrossRef](#)] [[PubMed](#)]
31. Chen, M.; Zhang, L.; Abdelgader, S.A.; Yu, L.; Xu, J.; Yao, H.; Lu, C.; Zhang, W. Alterations in gp37 Expand the Host Range of a T4-Like Phage. *Appl. Environ. Microbiol.* **2017**, *83*, e01576-17. [[CrossRef](#)] [[PubMed](#)]
32. Dunne, M.; Rupf, B.; Tala, M.; Qabrati, X.; Ernst, P.; Shen, Y.; Sumrall, E.; Heeb, L.; Plückthun, A.; Loessner, M.J.; et al. Reprogramming Bacteriophage Host Range through Structure-Guided Design of Chimeric Receptor Binding Proteins. *Cell Rep.* **2019**, *29*, 1336–1350. [[CrossRef](#)]
33. Chan, L.Y.; Kosuri, S.; Endy, D. Refactoring bacteriophage T7. *Mol. Syst. Biol.* **2005**, *1*, 1–10. [[CrossRef](#)]
34. Endy, D.; You, L.; Yin, J.; Molineux, I.J. Computation, prediction, and experimental tests of fitness for bacteriophage T7 mutants with permuted genomes. *Proc. Natl. Acad. Sci. USA* **2000**, *97*, 5375–5380. [[CrossRef](#)]